Abyssal barriers

Phylogeography, distribution and natural history of Asellota (Crustacea) in the deep sea

Dissertation

with the aim of achieving a doctoral degree (Dr. rer. nat)
at the Faculty of Mathematics,
Informatics and Natural Sciences
Department of Biology
of
Universität Hamburg

submitted by

Simon Bober

Hamburg, 2018

Disputation:
20.09.2018

First supervisor: Dr. Martin Schwentner

Second supervisor: Prof. Dr. Angelika Brandt

Contents

Chapter 3:

Chapter 4:

Chapter 1

Introduction

Introduction

The deep sea

A common non-scientific perception of the deep sea is that of a mysterious, dark and cold environment of exceptionally rare creatures. In fact, some of these conceptions are true. For instance the entire deep-sea environment lies within the aphotic zone and the majority of the deep sea is below the permanent thermocline, thus it is dark and cold, as presumed. But from an objective point of view the organisms inhabiting the deep sea are rather ordinary. The deep sea is and always has been the largest ecosystem on this planet (Ramirez-Llodra et al., 2010). About two thirds of this planet are water and 91.1 % of the worlds ocean are considered deep sea (Harris et al., 2014). The deep sea has a direct and fundamental impact on the global biosphere by storing atmospheric carbon, regulating the global temperature by storing heat, nutrient cycling in marine food webs and providing habitats for countless species (Armstrong et al., 2012). Even though the deep sea has been systematically sampled since the *Challenger Expedition* in 1872, still more than 99.0 % of the deep sea have not been sampled yet (Clark et al., 2016). Quintessentially, we achieved only a tiny fraction of knowledge about the largest ecosystem of our planet (Armstrong et al., 2012; Ramirez-Llodra et al., 2010; Raupach et al., 2004).

The deep sea is roughly partitioned in three depth ranges: the bathyal (200–3,000 m), the abyssal (3,000–6,000 m) and the hadal (6,000–12,000 m). The benthic fauna is confronted with differing challenges in these unlike habitats. The bathyal benthic zone typically encompasses the continental slope, mid-ocean ridges and seamounts; the hadal zone includes trenches deeper than 6,000 m. Due to their slopy nature, these two habitats usually include a serious proportion of hard substrata, which can affect the faunal composition considerably (Thistle, 2003). Compared to the abyssal zone these two habitats are heterogeneous with varying depth gradients and thus changes in hydrostatic pressure, temperature, salinity and food supply (Jamieson, 2015; Thistle, 2003). Within the deep sea, the abyssal zone is by far the most dominating depth zone (Smith et al., 2008; Vinogradova, 1997) with 84.7 % of the total mapped worlds ocean area (Harris et al., 2014). The abyssal is considered a homogeneous habitat of soft sediment, which is only interrupted by landmasses, seamounts, ocean ridges (bathyal) and

hadal trenches (Etter et al., 2005; Gage and Tyler, 1991; Smith et al., 2008). Physical parameters such as temperature, oxygen and salinity fluctuate little below the permanent thermocline (Etter et al., 2011; France and Kocher, 1996; Gage and Tyler, 1991; Lynn and Reid, 1968; Mantyla and Reid, 1983; Smith and Demopoulos, 2003) providing potentially a globally connected habitat. Except for hydrothermal vent and cold-seep sites, primary production is absent in the deep sea (Smith et al., 2008; Smith and Demopoulos, 2003; Zardus et al., 2006). This makes the deep-sea ecosystem almost entirely dependent on primary production within the euphotic zone. The reduced nutrition accessibility is considered the most significant restriction for the deep-sea fauna (Etter et al., 2005; Smith and Demopoulos, 2003; Snelgrove and Smith, 2003). However, despite many limitations, the abyss shows a remarkable species diversity (Brandt, 2012; Brandt et al., 2007a, 2007b; Chase et al., 1998; Elsner et al., 2015; Grassle and Maciolek, 1992; Hessler and Sanders, 1967; Jumars, 1976; McClain and Schlacher, 2015; Snelgrove and Smith, 2003; Wilson, 1998), which even today is hardly explored (Bouchet, 2006; Danovaro et al., 2008; Glover et al., 2002; Glover and Smith, 2003; Martínez Arbizu and Schminke, 2005; Priede et al., 2013).

Deep-sea Asellota

Isopoda Latreille, 1817 is one of the most successful crustacean orders and has successfully adapted to marine, freshwater and terrestrial environments. As land-living crustaceans, isopods are lacking an effective protection against desiccation and are bound to humid habitats (Edney, 1968). As an exception, *Hemilepistus reaumuri* (H. Milne-Edwards, 1840) for instance manages to survive in the desert by being monogamous and providing parental care (Linsenmair, 1984; Linsenmair and LinsenMair, 1971). Isopoda are found at altitudes above 2,200 m in Ladakh (India; *Protracheoniscus nivalis* Verhoeff, 1936) (Beron, 1997) as well as at the greatest depth in the Mariana Trench (*Macrostylis mariana* (Mezhov, 1993)). In the abyssal deep sea, isopods are a common and abundant taxon (Brandt, 1991; Frutos et al., 2016; Thistle and Wilson, 1987). The most dominating suborder is Asellota Latreille, 1802 (Brandt, 2004; Brandt et al., 2007a; Elsner et al., 2015; Hessler et al., 1979; Hessler and Wilson, 1983) and among these the Janiroidea G.O. Sars, 1897 represents the most diverse superfamily in the deep sea with several endemic families (Hessler et al., 1979; Wilson, 1999, 1998). Although faunal invasion of the deep sea from shallow waters is possibly a continuous process (Held, 2000; Wilson, 1998), the asellote diversity and high endemism in the

deep sea is best explained with an *in situ* radiation (Hessler and Thistle, 1975; Thistle and Hessler, 1976; Wilson, 1999).

Many deep-sea asellote families are highly specialized. Therefore, asellotes serve as the perfect model organisms for deep-sea faunal and biogeographic analyses. Four different families with different habitat adaptations were involved in this research: Macrostylidae Hansen, 1916, a burrowing inbenthic family; Munnopsidae Lilljeborg, 1864, a suprabenthic family with pronounced natatory adaptations; Desmosomatidae G.O. Sars, 1897 and Nannoniscidae Hansen, 1916, two epibenthic families, which mainly walk on the sediment, but especially within Desmosomatidae, a swimming and burrowing behavior was observed (Hessler and Strömberg, 1989).

Asellote larvae have a direct development; their eggs are directly placed into a brood pouch, the marsupium, which is a characteristic feature of the superorder Peracarida Calman, 1904. The marsupium is formed by oostegites, which are coxal plates formed by a varying number (usually 2-4) of anterior pereopods in the Janiroidea (Riehl, 2014; Riehl et al., 2014). The direct development and hence limited dispersal ability (Wilson and Hessler, 1987) is advantageous for biogeographic studies. A plankto- or lecithotrophic larva will drift with currents and might possibly also pass and survive more unfavorable habitats. The asellote offspring on the contrary is released by its mother as almost fully developed adults with similar dispersal mechanisms as the adult. For such organisms, even a short strip of unfavorable habitat (e.g. fracture zones) might be a strong physical dispersal barrier, if the adult is not able to swim for extended periods of time.

Distribution barriers in the deep sea

The abyssal deep sea is considered a widely connected habitat (Etter et al., 2005). For a long time abyssal species were considered to be cosmopolitans due to the perceived lack of barriers within the abyssal habitat (Bruun, 1957). However, physical barriers are present in all oceans such as landmasses, seamounts, hadal trenches or mid-oceanic ridges (Fig. 1); but there is still little knowledge about the effect of such barriers on the benthic fauna. Most biogeographical studies on abyssal barriers were performed in the Atlantic.

Previously, two prominent geographic barriers were analyzed regarding their impact on the macrofauna in the North Atlantic. The Greenland-Iceland-Scotland Ridge (GIS-Ridge) in the North Atlantic is a considerable barrier that disconnects the Nordic Seas

from the North Atlantic and therefore the GIS-Ridge was proposed to be a geographical barrier for the abyssal fauna (Brix et al., 2014; Brix and Svavarsson, 2010; Schnurr et al., 2014). The effect of the GIS-Ridge was analyzed in multiple publications (Brix and Svavarsson, 2010; Jennings et al., 2018; Negoescu and Svavarsson, 1997; Schnurr et al., 2018, 2014; Stransky and Svarvarsson, 2006; Weisshappel, 2001, 2000). The distribution range of most therein-analyzed peracarid crustaceans was affected by the GIS-Ridge as a barrier and only bathyal species and few eurybath abyssal species were found on both sides of the ridge. Another investigated ridge in the Atlantic that, however, turned out to be no distribution barrier for benthic peracarids is the Walvis Ridge in the Southeast Atlantic, which separates the Angola Basin from the Cape Basin (Brix et al., 2011; Brökeland, 2010a) (Fig. 1).

The most substantial barrier in the Atlantic is the Mid-Atlantic Ridge (MAR), which topographically separates the abyssal benthic zone of the Atlantic into an eastern and a western region (Murray et al., 1912). However, the MAR is not a continuous mountain range, it is regularly interrupted by fracture zones, which potentially are abyssal gateways for the abyssobenthic fauna to pass the MAR. The Vema Fracture Zone (VFZ) is distinctive among Atlantic fracture zones due to a narrow and almost flat west-east trough, the Vema Transform Fault (VTF), between 41°10´ and 44°30´ W with a thick sediment layer at approximately 5,000 m depth (Bader et al., 2007; Eittreim and Ewing, 1975; Heezen et al., 1964; Van Andel et al., 1971). Since the VTF is a true extension of the adjacent Demerara Abyssal Plain in the western Atlantic, a connectivity of abyssal benthic fauna through the VTF is theoretically possible. Therefore, in 2014/2015 the Vema-TRANSIT expedition (bathymetry of the Vema-Fracture-Zone and Puerto Rico TRench and Abyssal AtlaNtic BiodiverSITy Study) onboard R/V Sonne sampled an abyssal east-west transect at roughly 11° N across the MAR through the VTF. This expedition was the basis for most of the herein presented research.

Previous studies found no sufficient barrier to gene flow across the MAR in the deep sea (Brix et al., 2015, 2014; Etter et al., 2011; France and Kocher, 1996; Havermans et al., 2013; Knutsen et al., 2012; Lins et al., 2018; Pawlowski et al., 2007; Priede et al., 2013; Shields et al., 2013; Shields and Blanco-Perez, 2013; van der Heijden et al., 2012; White et al., 2011; Zardus et al., 2006). Most of the trans-MAR species known today, were either sampled at bathyal depth (Brix et al., 2014; Knutsen et al., 2012; Priede et al., 2013; Shields et al., 2013; Shields and Blanco-Perez, 2013; White et al., 2011) or do have planktonic larvae, which will drift with currents (Etter et al., 2011;

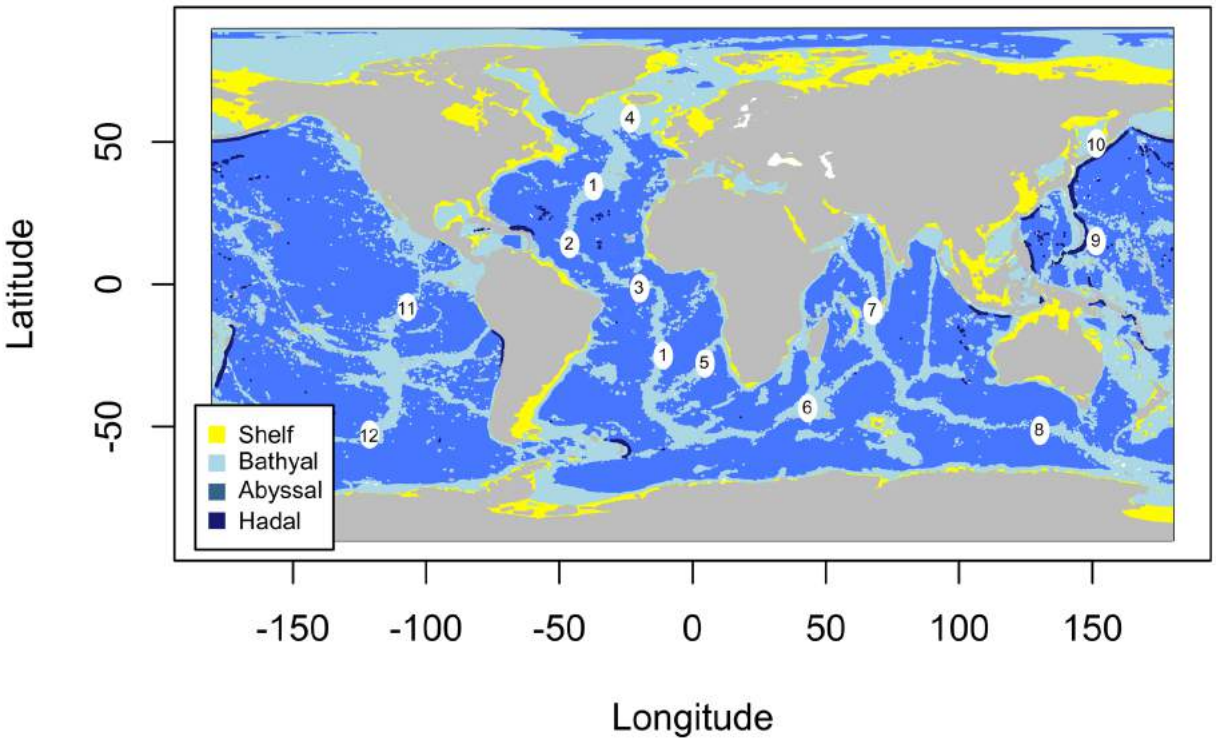

Fig. 1: Simplified map of the World Ocean, the Oceanic Ridge (global mid-oceanic ridge system) and a selcetion of geographic feratures treated in this study. Different depth ranges are color coded. Shelf (<200 m), bathyal (200–3,000 m), abyssal (3,000–6,000 m), hadal (6,000–12,000 m).
1 = Mid-Atlantic Ridge; 2 = Vema Fracture Zone; 3 = Romanche Fracture Zone; 4 = Greenland-Iceland-Scotland-Ridge; 5 = Walvis Ridge; 6 = SW Indian Ridge; 7 = Central Indian Ridge; 8 = SE Indian Ridge; 9 = Mariana Trench; 10 = Kuril Kamchatka Trench; 11 = East Pacific Rise; 12 = Pacific Antarctic Ridge

van der Heijden et al., 2012; Zardus et al., 2006).

Thus biogeographic information on abyssobenthic fauna across the MAR is scarce. Until today only the cosmopolitan species *Eurythenes maldoror* d´Udekem d´Acoz Havermans, 2015 (D'Acoz and Havermans, 2015; France and Kocher, 1996; Havermans et al., 2013) and the epibenthic species *Parvochelus russus* Brix and Kihara, 2015 (Brix et al., 2015) were described with an abyssal trans-MAR distribution. For *P. russus* a connectivity through the Romanche Fracture Zone was proposed (Brix et al., 2015), which is a fracture zone approximately 1,000 km south of the VFZ (Fig. 1).

Cosmopolitism in the deep sea

Many deep-sea species were considered cosmopolitan or at least widespread (Brandt, 1991; Wägele, 1986). This general perception changed with the emergence of genetic analyses. Quickly the term "cryptic species" was regularly mentioned in conjunction with deep-sea speciation. Indeed, genetic research revealed high genetic diversity in

combination with high genetic differentiation among populations in the deep sea. Such diversity was attested to most taxa (Brasier et al., 2016; Chase et al., 1998; Held, 2003; Janssen et al., 2015; Miyamoto et al., 2010; Moura et al., 2008; Quattro J. et al., 2001; Raupach et al., 2007; Vrijenhoek, 2009; Wilson et al., 2007; Zardus et al., 2006) and cryptic species were found to be rather common within deep-sea peracarids (Brandt et al., 2014; Brix et al., 2015, 2014, 2011; Brökeland, 2010b; Bucklin et al., 1987; Eustace et al., 2016; France and Kocher, 1996; Held, 2003; Held and Wägele, 2005; Krapp-Schickel and De Broyer, 2014; Larsen, 2003; Leese and Held, 2008; Raupach and Wägele, 2006; Schnurr et al., 2018). Cryptic species are two or more distinct species that were delimitated as one species based on morphological characters. The distribution of cryptic species is thought to be homogenous across taxa (Pfenninger and Schwenk, 2007). In the recent past, cryptic species were so commonly found in deep-sea peracarids that the mere existence of cosmopolitans is challenged. (Raupach et al., 2007) wrote (p. 1826): "*We hypothesize that most, if not all, widespread asellote species and many other Peracarida with benthic life styles are in reality widespread groups of closely related but distinct species that also can appear in sympatry.*" their hypothesis is called the *patchwork theory*. Some records, however, challenge the hypothesis by Raupach et al. (2007): *Eurythenes gryllus* (Lichtenstein in Mandt, 1822) was considered for a long time one of the "true" abyssal species with a pan-oceanic distribution. *Eurythenes gryllus sensu lato* is a large, necrophagous, natatory and abyssopelagic amphipod species mostly found at depth below 3,500 m (Baldwin and Smith, 1987; Bucklin et al., 1987; Smith and Baldwin, 1984) and was repeatedly caught down to hadal depths (Fujii et al., 2013; Thurston et al., 2002). It is a highly motile amphipod and was repeatedly sampled hundreds of meters above the seafloor (Baldwin and Smith, 1987; Smith et al., 1979), which supposedly supports an enhanced dispersability (Ingram and Hessler, 1983). With that said, also for *E. gryllus* multiple molecular studies suggest rather a species complex (Bucklin et al., 1987; France and Kocher, 1996; Havermans et al., 2013) and the most recent analyses revealed nine species–level lineages with partly overlapping geographic ranges (Havermans et al., 2013). Within this complex, the clade *Eg3* (Havermans et al., 2013), which is today accepted as *Eurythenes maldoror* has a cosmopolitan distribution at abyssal depths, and hence proofed that cosmopolitism is possible in the abyssal deep sea.

Natural history of deep-sea isopods

Unfortunately, we know very little about the behavior of deep-sea asellotes. Due to their small size and occurrence in the deep sea, life observations are scarce (but see Hessler and Strömberg, 1989; Hult, 1941; Jamieson et al., 2012; Marshall and Diebel, 1995). Specimens sampled in the deep sea with trawled gear usually die during the process of sampling and therefore most assumptions on behavior are inferred from morphological features (Hessler and Sanders, 1967; Wägele, 1989).

Nevertheless, it is possible to gain natural history information from fixed material. Essential information such as feeding behavior can be retrieved from dead material by analyzing gut contents. Except for one baited trap observation by Jamieson et al. (2012), many studies recovered dietary data from gut contents (Brökeland et al., 2010; Gudmundsson et al., 2000; Menzies, 1962, 1956; Sokolova, 1972; Svavarsson et al., 1993; Sye, 1887; Wilson and Thistle, 1985; Wolff, 1956).

Already in 1887, Sye suggested an omnivorous to saprovorous diet for marine isopods and Wolff (1956) came to the same conclusion based on observations for the first analyzed deep-sea isopods. More recent research, however, rather proposed a foraminiferivory diet for some deep-sea isopods (Brökeland et al., 2010; Gudmundsson et al., 2000; Svavarsson et al., 1993; Wilson and Thistle, 1985). Brökeland et al. (2010) presumed that in the early dissections the high amount of mineral and calcareous particles in gut contents of isopods might have erroneously led to the conclusion that isopods are saprovore. They further identified stercomata of the poorly known but globally abundant (Gooday et al., 2004; Tendal and Hessler, 1977), soft walled Foraminifera d´Orbigny, 1826 of the superfamily Komokioidea Tendal and Hessler, 1977 (incorrect synonym: Komociacea) within the analyzed gut contents of munnopsid isopods. Soft walled Foraminifera are an additional food source that is easily overlooked and often classified as unidentifiable organic mucus. Komokioidea was an abundant Foraminifera also during the Vema-TRANSIT expedition.

By the examination of an animal, not only the feeding behavior, but furthermore its anatomy can be analyzed. The paddle-shaped posterior pereopods of Munnopsidae for instance are most likely involved in the swimming locomotion (Marshall and Diebel, 1995). Statocysts are a further good example, it is a common organ of equilibrium among crustaceans (Cohen, 1955; Dijkgraaf, 1956; Hertwig et al., 1991; Neil, 1975; Takahata and Hisada, 1979; Wittmann et al., 1993) and other marine taxa (Hopf and Kingsford, 2013; Stephens and Young, 1976), but are fairly unique among Isopoda.

Except for Macrostylidae only the families Anthuridae Leach, 1814 and Leptanthuridae Poore, 2001 of the superfamily Anthuroidea Leach, 1914 developed statocysts in the telson (Poore, 2001; Wägele, 1989, 1981). The anatomy of macrostylid statocysts was previously described in a 3D-reconstruction during a master thesis (Bober, 2014), yet the statolith remained unstudied. Many crustaceans and also Anthuridae build their statoliths from calcium salts (Rose and Stokes, 1981), Macrostylidae as deep-sea organisms are living below the carbonate compensation depth (CCD), at which depth the solution of carbonates exceeds the sedimentation rate and thus carbonates are absent (Pytkowicz, 1970). The CCD is variable among oceans but in the Atlantic for instance it lays at an approximate depth of 4,700-6,000 m (Emelyanov, 2005). Since Macrostylidae as deep-sea organisms are affected by the CCD, the statolith is expected to be built from a different material.

Aims and hypothesis

The abyssal deep sea is considered a homogenous global habitat. Many studies were performed on testing potential barriers in the deep sea. Nevertheless there is little knowledge about the isolating effect of physical geographic barriers on the abyssobenthic fauna.

Therefore the intention of this thesis is to analyze the barrier effect of the MAR on abyssobenthic isopods in the Atlantic, along with determining if there are widespread or even cosmopolitan isopod species in the abyssal deep sea. It is hypothesized that swimming species are more effective dispersers than non-swimmers and for this purpose the effect of different niche adaptations in isopods (inbenthic (burrowing), epibenthic (walking), suprabenthic (swimming)) on the distribution range and ability to cross barriers will be tested.

During the KuramBio expedition in the Northwest Pacific, the most abundant, widespread but formally unknown morphospecies of Macrostylidae is supposedly a species complex of two cryptic species. This complex is going to be illuminated in detail using integrative taxonomy. This complex was sampled on both sides of the Kuril-Kamchatka Trench (KKT); hence the connectivity across a hadal trench will be tested.

Previously unpublished data showed that Macrostylidae is one of only three families within Isopoda that possess statocysts. However, information on the statolith was still lacking, therefore it is a further aim to investigate the statoliths of Macrostylidae and possibly retrieve natural history information from this data.

Based on the aims the following hypotheses were formed:

- The Vema Fracture Zone is a passage across the Mid-Atlantic Ridge for the abyssobenthic fauna.
- Natatory isopods are more effective dispersers compared to epi- or inbenthic species.
- *Acanthocope galatheae* Wolff, 1962 is a cosmopolitan isopod species.
- Hadal trenches like the Kuril-Kamchatka Trench in the Northwest Pacific basin represent a distribution barrier for inbenthic isopods.
- The most abundant macrostylid morphospecies sampled during the KuramBio expedition in the Kuril-Kamchatka Trench region is in reality a species complex of multiple morphologically indistinguishable species.
- Due to the carbonate compensation depth it is unlikely that Macrostylidae form a statolith from calcium salts, as reported for the statocysts in Anthuridae.

Summary

Geographic barriers within the abyssal deep sea were analyzed in the course of three publications from six expeditions and on four isopod families (Chapter 2, 3, 4). Additionally in Chapter 5, 6 and 7 classical morphology was used to infer natural history information from fixed deep-sea isopods.

Chapter 2 and 3 are focused on the barrier effect of the MAR on the abyssal benthic fauna. Since the abyssal fauna has a wide range of adaptations to its habitat, ranging from sessile (Young et al., 2008), to inbenthic (infaunal) (Blazewicz-Paszkowycz et al., 2012) or abyssopelagic taxa (Havermans et al., 2013). The dispersal ability of a species was repeatedly held responsible for wide or small spatial distribution ranges (Brandt et al., 2012; Ingram and Hessler, 1983; Raupach et al., 2007; Schnurr et al., 2014; Wilson and Hessler, 1987). Therefore, the barrier effect of the MAR was tested on taxa with differing adaptations to their habitat. Since Isopoda is an abundant, highly diverse (Elsner et al., 2015; Hessler and Sanders, 1967; Thistle and Wilson, 1987) and relatively well-studied deep-sea taxon (Rex and Etter, 2010) it was focused on members of this order. Macrostylidae as inbenthic, burrowing family was hypothesized in Chapter 2 to have the geographically most restricted distribution, followed by the epibenthic families Desmosomatidae and Nannoniscidae. Furthermore, a supposedly

cosmopolitan species *Acanthocope galatheae* of the swimming, suprabenthic family Munnopsidae was included. The presumed cosmopolitism of this species (Brandt et al., 2012; Malyutina, 1999; Malyutina et al., 2017; Schmid et al., 2002) was further tested in Chapter 4, in which additional genetic material was extracted from museum material of previous expeditions.

Chapter 5 is predominantly a taxonomic and ecological chapter treating only Macrostylidae of the Northwestern Pacific. For the taxonomic desriptions a new shading method was used, which is presented in Chapter 8. The distribution of the in Chapter 5 described species across the Kuril-Kamchatka Trench (KKT) allowed to examine, whether hadal trenches represent a distribution barrier to inbenthic crustaceans.

In Chapter 7 a feeding munnopsid isopod is presented, which allows exceptional insights in the feeding behavior of deep-sea asellotes. Furthermore, the organ of equilibrium of Macrostylidae (statocyst) were examined in Chapter 6.

Chapter 2

Does the Mid-Atlantic Ridge affect the distribution of abyssal benthic crustaceans across the Atlantic Ocean?

Deep-Sea Research Part II 148 (2018) 91–104

Contents lists available at ScienceDirect

Deep-Sea Research Part II

journal homepage: www.elsevier.com/locate/dsr2

Does the Mid-Atlantic Ridge affect the distribution of abyssal benthic crustaceans across the Atlantic Ocean?

Simon Bober[a,*], Saskia Brix[b], Torben Riehl[c], Martin Schwentner[a], Angelika Brandt[c,d]

[a] University of Hamburg, Centre of Natural History (CeNak), Zoological Museum, Hamburg, Germany
[b] Senckenberg am Meer, German Centre for Marine Biodiversity Research (DZMB), c/o Biocenter Grindel, Martin-Luther-King-Platz 3, 20146 Hamburg, Germany
[c] Senckenberg Research Institute and Natural History Museum, Department Marine Zoology, Crustacea, Senckenberganlage 25, 60325 Frankfurt, Germany
[d] Goethe-University of Frankfurt, FB 15, Institute for Ecology, Evolution and Diversity, Max-von-Laue-Str. 13, 60439 Frankfurt am Main, Germany

A B S T R A C T

A trans-Atlantic transect along the Vema Fracture Zone was sampled during the Vema-TRANSIT expedition in 2014/15. The aim of the cruise was to investigate whether the Mid-Atlantic Ridge (MAR) isolates the abyssal fauna of the western and eastern abyssal basins.

Based on two genetic datasets of Macrostylidae and Desmosomatidae/Nannoniscidae studied by Riehl et al. and Brix et al. in this issue we found that most of the therein-delimitated species were found at only one side of the MAR. We analysed those species of Macrostylidae and Desmosomatidae that were sampled across the MAR and complemented these with one species of a third family: Munnopsidae. With these datasets we were further able to consider the effect of different niche adaptations: Macrostylidae are infaunal (burrowing), Munnopsidae are considered epifaunal with pronounced swimming capabilities and Desmosomatidae and Nannoniscidae are partly able to swim, but are not as well adapted to swimming as Munnopsidae. We concluded that the MAR seems to be a dispersal barrier for the non-swimming Macrostylidae as well as weakly-swimming Desmosomatidae and Nannoniscidae. However, four species of Macrostylidae and Desmosomatidae did cross the MAR, but evidence for regular unrestricted gene flow is still lacking. For the swimming Munnopsidae we were able to detect persistent gene flow across the MAR.

1. Introduction

The general perception of the abyssal deep sea is that of a homogeneous habitat, free of dispersal barriers (Etter et al., 2005, 2011; Rex and Etter, 2011), which theoretically allows cosmopolitan distributions of species. In fact, the abyss accounts for 84.7% of the ocean (Harris et al., 2014). The abyssal seafloor is subdivided by topographical challenges in form of seamounts, ocean ridges and hadal trenches (Etter et al., 2005; Smith et al., 2008) forming various habitats as outlined in Ramirez-Llodra et al. (2010). These habitats might have a considerable effect on the distribution range of species. Recent molecular studies revealed that in several cases presumably widespread species are in fact groups of multiple, morphologically very similar species each with a much narrower distribution (Bober et al., 2017; Havermans et al., 2013; Held, 2003; Raupach et al., 2007; Raupach and Wägele, 2006). The Atlantic Ocean is topographically separated into western and eastern basins by the Mid-Atlantic Ridge (MAR) (Murray et al., 1912). However, the MAR as a potential barrier is regularly interrupted by fracture zones, which are potential gateways for organisms to cross the MAR. One of these passages is the Vema Fracture Zone (VFZ), which is unique in its flat, gently sloping valley (Heezen et al., 1964a, 1964b; Van Andel et al., 1971), theoretically providing a continuous habitat, in terms of depth and sediment cover, from the Demerara Abyssal Plain west of the MAR to the Gambia Abyssal Plain east of the MAR.

The isolating effect of the MAR on deep-sea organisms was already investigated during previous scientific surveys (Brix et al., 2014a; Etter et al., 2011; Knutsen et al., 2012; Priede et al., 2013; Shields et al., 2013; Shields and Blanco-Perez, 2013; van der Heijden et al., 2012; Vecchione et al., 2010; White et al., 2010, 2011; Zardus et al., 2006). In these surveys it was concluded that the MAR is not a dispersal barrier. However, the desmosomatid isopod species, *Parvochelus russus* Brix and Kihara, 2015, has been the only known isopod with a distribution across the MAR so far. This species is apparently capable of swimming and, based on molecular and morphological analyses, the authors proposed connectivity between eastern and western populations through the Romanche Fracture Zone. We also analysed abyssal benthic Isopoda Latreille (1817), a common taxon in the abyssal deep sea (Brandt et al., 2007; Hessler and Jumars, 1974; Hessler and Sanders,

* Corresponding author.
E-mail address: simon.bober@uni-hamburg.de (S. Bober).

https://doi.org/10.1016/j.dsr2.2018.02.007

Available online 17 February 2018

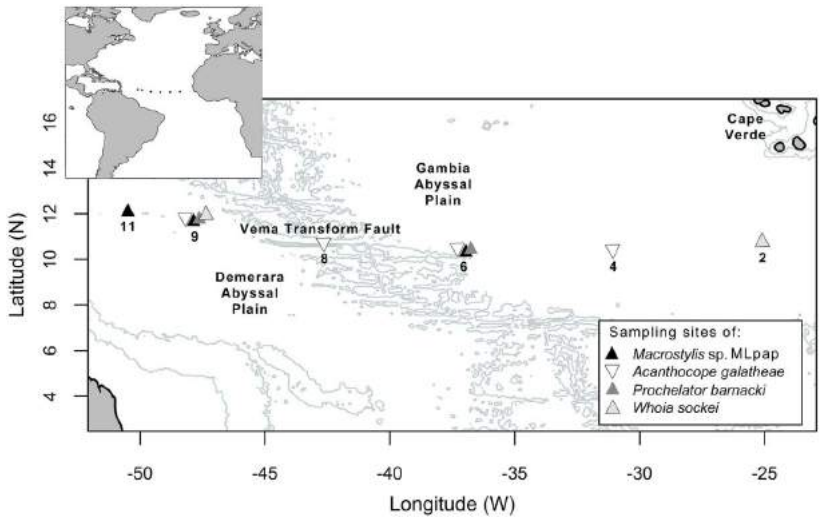

Fig. 1. Map of the sampling locations along the Vema Fracture Zone during the Vema-TRANSIT expedition in the Atlantic Ocean. 3000 m and 4000 m depth lines were plotted.

1967; Thistle and Wilson, 1987; Wolff, 1977) belonging to the Peracarida. Peracarids are brooders, which generally lack a planktonic larval stage. Thus, peracarids are assumed to have a reduced dispersal capability compared to organisms with larval stages (Wilson and Hessler, 1987) and the MAR may represent a strong barrier to their dispersal. However, isopods exhibit a wide range of life strategies and adaptations (Brandt et al., 2011). We investigated four abundant families with different adaptations to their habitat and differing dispersal capabilities. Three of these four families were distributed across the MAR. These are Munnopsidae Lilljeborg, 1864, an epifaunal family with pronounced adaptations to swimming (Hessler and Strömberg, 1989; Marshall and Diebel, 1995) of which we targeted the species *Acanthocope galatheae* Wolff, 1962. In addition, we analysed Macrostylidae Hansen (1916), a non-swimming, burrowing family (Harrison, 1989; Hessler and Sanders, 1967; Hessler and Strömberg, 1989; Hessler and Wilson, 1983; Wägele, 1989). A dataset regarding all macrostylid species along the VFZ is part of the paper by Riehl et al., (this issue). Based on the latter study, two macrostylid species were sampled on both sides of the MAR and we took a closer look at these. Desmosomatidae Sars (1897) is an epifaunal family with less pronounced adaptations to swimming compared to Munnopsidae (Brix et al., 2014b; Hessler and Strömberg, 1989), while some Nannoniscidae Hansen (1916) are capable of facultative swimming with elongated setae, other Nannoniscidae genera (e.g. *Austroniscus* Vanhöffen, 1914) seem to lack such natatorial adaptations (Kaiser and Brandt, 2007; Siebenaller and Hessler, 1981; Wilson, 2008). There has been little doubt about the close relationship of Desmosomatidae and Nannoniscidae (Wägele, 1989) and thus, they are treated together in the species delimitation dataset of Brix et al., (this issue) for the VFZ, which provides the background data for our approach outlined here. However, species of both families were geographically rather restricted. In the Brix et al., (this issue) dataset, eleven (ten desmosomatid and one nannoniscid) species out of a total of 72 species (53 desmosomatid, 19 nannoniscid) were collected at more than one sampling site and two of these (both desmosomatids) were collected on both sides of the MAR. We focused on these eleven widespread species only.

We hypothesize that swimming species have an enhanced capability to cross barriers either by active swimming or by passive drifting as "facultative plankton". Furthermore, we expect a more restricted distribution for the non-swimming Macrostylidae and a broader distribution for the Munnopsidae and Desmosomatidae along the sampled transect. Our approach highlights widely distributed deep-sea species within Munnopsidae and three more families from one trans-Atlantic expedition (see Riehl et al., this issue for Macrostylidae, Brix et al. (this issue) for Desmosomatidae and Nannoniscidae).

2. Material and methods

2.1. Study area

The VFZ offsets the crest of the MAR by 320 km (Van Andel et al., 1968, 1971; van Andel, 1969). Between 41°10´and 44°30`W there is a narrow west-east trending trough at approximately 5000 m depth (Van Andel et al., 1971). The Vema Transform Fault (VTF) valley is fringed by steep walls of 15° inclination and has a narrow passage of 3 km width at 45°W. The valley ground is a virtual extension of the Demerara Abyssal Plain in the west, with a thick continuous sediment layer (Bader et al., 2007; Eittreim and Ewing, 1975; Heezen et al., 1964b; Van Andel et al., 1971). The continuity to the Gambia Abyssal Plain in the east is disrupted by a sill area with a depth deviation of approximately 550–850 m (Vangriesheim, 1980). The sill area has a measureable influence on the currents within the VTF. An inflow of cold bottom water from the western basins through the VTF was repeatedly observed (Eittreim et al., 1983; Fischer et al., 1996; Heezen et al., 1964b; McCartney et al., 1991; Vangriesheim, 1980). The western Atlantic basins are dominated by the Lower Circumpolar Deep Water (LCDW), which is a component of the Antarctic Bottom Water (Eittreim et al., 1983; Fischer et al., 1996; Reid et al., 1977). The eastern Atlantic basins are dominated by the southward flowing North Atlantic Deep Water (NADW) (Fischer et al., 1996; Smethie and Swift, 1989). The different water masses were identifiable with a CTD during the Vema-TRANSIT expedition; the LCDW is colder and less saline compared to the NADW, but generally the differences are within a narrow range (Devey, this issue).

2.2. Sampling

A trans-Atlantic transect through the VFZ was sampled during the Vema-TRANSIT (Bathymetry of the Vema-Fracture Zone and Puerto Rico TRench and Abyssal AtlaNtic BiodiverSITy Study) expedition from 14. December 2014–26. January 2015 with research Vessel Sonne (SO237). Samples were obtained using a camera-epibenthic sledge (C-EBS) (Brandt et al., 2013; Brenke, 2005) along 11° N across the Atlantic Ocean (Fig. 1). For the C-EBS a mesh size of 500 µm was used and the cod ends were equipped with a 300 µm mesh. In total six sites were sampled with eleven EBS-hauls (stations) during this part of the

Table 1
All material used for this study.

Species	Collection-no. (ZMH K-)	GenBank accession no.			Haplotypes 16 S	Haplotypes COI	Haplotypes concatenated	Field-ID.
		COI	16 S	18 S				
Munnopsidae								
Acanthocope galatheae	47061	MG721979	MG721988		A4	A11	A21	VTMup19
Acanthocope galatheae	47062	MG721973	MG721990		A4	A9	A20	VTMup20
Acanthocope galatheae	47063	MG721975	MG721992		A2	A10	A23	VTMup21
Acanthocope galatheae	47064	MG721966			N/A	A14	A28	VTMup22
Acanthocope galatheae	47065	MG721976	MG721987		A4	A10	A22	VTMup23
Acanthocope galatheae	47066	MG721977	MG721993		A4	A10	A22	VTMup24
Acanthocope galatheae	47067	MG721971	MG721994		A4	A13	A25	VTMup25
Acanthocope galatheae	47068	MG721980	MG721989		A4	A11	A21	VTMup26
Acanthocope galatheae	47069	MG721962	MG721998		A6	A15	A29	VTMup27
Acanthocope galatheae	47070	MG721967	MG721999		A5	A14	A28	VTMup28
Acanthocope galatheae	47071	MG721963	MG722000		A5	A16	A30	VTMup29
Acanthocope galatheae	47072	MG721974	MG721991		A4	A12	A26	VTMup30
Acanthocope galatheae	47073		MG722004		A5	N/A	A27	VTMup31
Acanthocope galatheae	47074	MG721983	MG722001		A5	A11	A27	VTMup32
Acanthocope galatheae	47075	MG721981	MG721995		A4	A11	A21	VTMup33
Acanthocope galatheae	47076	MG721982	MG721997		A4	A11	A21	VTMup34
Acanthocope galatheae	47077	MG721964	MG721985		A7	A17	A31	VTMup35
Acanthocope galatheae	47078	MG721968	MG722002		A5	A14	A28	VTMup36
Acanthocope galatheae	47079	MG721972	MG721986		A3	A8	A19	VTMup37
Acanthocope galatheae	47080	MG721978	MG721996		A4	A10	A22	VTMup38
Acanthocope galatheae	47081	MG721965	MG722003		A5	A18	A32	VTMup39
Acanthocope galatheae	47082	MG721969	MG722005		A5	A14	A28	VTMup40
Acanthocope galatheae	47083	MG721970	MG722006		A5	A14	A28	VTMup42
Acanthocope galatheae	47084		MG721984		A1	N/A	A24	VTMup69
Macrostylidae								
Macrostylis sp. MLpap	45165		LT909287		M5	N/A	N/A	VTMac134
Macrostylis sp. MLpap	45166		LT909290		M5	N/A	N/A	VTMac137
Macrostylis sp. MLpap	45146		LT909293		M5	N/A	N/A	VTMac140
Macrostylis sp. MLpap	45147		LT909294		M5	N/A	N/A	VTMac141
Macrostylis sp. MLpap	45148		LT909298		M5	N/A	N/A	VTMac145
Macrostylis sp. MLpap	45149		LT909299		M5	N/A	N/A	VTMac147
Macrostylis sp. MLpap	45150		LT909300		M5	N/A	N/A	VTMac148
Macrostylis sp. MLpap	45167		LT909301		M5	N/A	N/A	VTMac149
Macrostylis sp. MLpap	45151		LT909302		M5	N/A	N/A	VTMac150
Macrostylis sp. MLpap	45168		LT909303		M5	N/A	N/A	VTMac151
Macrostylis sp. MLpap	45152		LT909308		M5	N/A	N/A	VTMac156
Macrostylis sp. MLpap	45153		LT909309		M5	N/A	N/A	VTMac157
Macrostylis sp. MLpap	45154		LT909318		M5	N/A	N/A	VTMac166
Macrostylis sp. MLpap	45155		LT909319		M5	N/A	N/A	VTMac167
Macrostylis sp. MLpap	45156		LT909333		M1	N/A	N/A	VTMac182
Macrostylis sp. MLpap	45157		LT909334		M3	N/A	N/A	VTMac183
Macrostylis sp. MLpap	45158		LT909335		M3	N/A	N/A	VTMac184
Macrostylis sp. MLpap	45145		LT909337		M3	N/A	N/A	VTMac186
Macrostylis sp. MLpap	45169		LT909338		M3	N/A	N/A	VTMac187
Macrostylis sp. MLpap	45159		LT909340		M3	N/A	N/A	VTMac189
Macrostylis sp. MLpap	45160		LT909341		M3	N/A	N/A	VTMac190
Macrostylis sp. MLpap	45161		LT909343		M3	N/A	N/A	VTMac192
Macrostylis sp. MLpap	45162		LT909344		M4	N/A	N/A	VTMac194
Macrostylis sp. MLpap	45163		LT909347		M2	N/A	N/A	VTMac197
Macrostylis sp. MLpap	45164		LT909348		M3	N/A	N/A	VTMac198
Desmosomatidae								

(*continued on next page*)

Table 1 (*continued*)

Species	Collection-no. (ZMH K-)	GenBank accession no.			Haplotypes 16 S	Haplotypes COI	Haplotypes concatenated	Field-ID.
		COI	16 S	18 S				
Prochelator barnacki	46202	MF325543		MF325760	P2	N/A	N/A	VTDes108
Prochelator barnacki	46201	MF325540			P1	N/A	N/A	VTDes147
Prochelator barnacki	46203	MF325541		MF325759	P2	N/A	N/A	VTDes115
Prochelator cf. *barnacki*	46324	MF325542			P2	N/A	N/A	VTDes138
Whoia sockei	46204	MF325578		MF325782				VTDes014
Whoia sockei	46205	MF325515						VTDes155
Chelator sp. A	46291	MF325436	MF325599					VTDes091
Chelator sp. A	46374	MF325462	MF325624					VTDes415
Chelator sp. A	46287	MF325454	MF325617					VTDes087
Chelator sp. A	46285	MF325449	MF325612					VTDes085
Chelator sp. A	46268	MF325435	MF325598	MF325704				VTDes068
Chelator sp. A	46262	MF325440	MF325603	MF325706				VTDes061
Chelator sp. A	46255	MF325430	MF325593	MF325699				VTDes053
Chelator sp. A	46253	MF325464	MF325626	MF325717				VTDes051
Chelator sp. A	46247	MF325415	MF325579	MF325693				VTDes045
Chelator sp. A	46290	MF325453	MF325616	MF325711				VTDes090
Chelator sp. A	46254	MF325446	MF325609					VTDes052
Chelator sp. A	46257	MF325433	MF325596	MF325702				VTDes056
Chelator sp. A	46264	MF325416	MF325580	MF325694				VTDes063
Chelator sp. A	46289	MF325448	MF325611					VTDes089
Chelator sp. A	46288	MF325457	MF325620	MF325712				VTDes088
Chelator sp. A	46250	MF325456	MF325619					VTDes048
Chelator sp. A	46283	MF325466	MF325628	MF325719				VTDes083
Chelator sp. A	46235	MF325441	MF325604	MF325707				VTDes033
Chelator sp. A	46246	MF325461	MF325623					VTDes044
Chelator sp. A	46245	MF325444	MF325607	MF325709				VTDes043
Chelator sp. A	46293	MF325428	MF325591					VTDes093
Chelator sp. B	46333	MF325431	MF325594	MF325700				VTDes148
Chelator sp. B	46334	MF325427	MF325590	MF325697				VTDes149
Chelator sp. B	46337	MF325438	MF325601	MF325705				VTDes153
Chelator sp. B	46368	MF325458	MF325621	MF325713				VTDes187
Chelator sp. B	46372	MF325452	MF325615	MF325710				VTDes200
Chelator sp. C	46366	MF325564	MF325686	MF325773				VTDes184
Chelator sp. C	46309	MF325432	MF325595	MF325701				VTDes117
Chelator sp. C	46327	MF325463	MF325625	MF325716				VTDes141
Chelator sp. C	46330	MF325460	MF325622	MF325715				VTDes144
Parvochelus russus (sp. E)	46341	MF325536	MF325670	MF325755				VTDes158
Parvochelus russus (sp. E)	46233	MF325537	MF325671	MF325756				VTDes031
Mirabilicoxa sp. F	46220	MF325508	MF325651					VTDes018
Mirabilicoxa sp. F	46219	MF325510	MF325653					VTDes017
Mirabilicoxa sp. F	46230	MF325519	MF325659					VTDes028
Mirabilicoxa sp. F	46243	MF325512	MF325655					VTDes041
Mirabilicoxa sp. G	46357	MF325521	MF325661					VTDes175
Mirabilicoxa sp. G	46339	MF325514	MF325657					VTDes156
Chelator sp. X	46348	MF325421	MF325585					VTDes165
Chelator sp. X	46349	MF325420	MF325584					VTDes166
Chelator sp. X	46350	MF325425	MF325588					VTDes167
Chelator sp. X	N/A		MF325646	MF325739				VTDes136
Eugerdella sp. H	46343	MF325483	MF325642					VTDes160
Eugerdella sp. H	45790	MF325499	MF325647	MF325740				VTDes135
Nannoniscidae								
Regabellator sp. K	46241	MF325566		MF325775				VTDes039
Regabellator sp. K	46375	MF325569						VTDes419

(*continued on next page*)

Table 1 (*continued*)

Species	Collection-no. (ZMH K-)	GenBank accession no. COI	GenBank accession no. 16 S	GenBank accession no. 18 S	Haplotypes 16 S	Haplotypes COI	Haplotypes concatenated	Field-ID.
Regabellator sp. K	46272	MF325568						VTDes072
Regabellator sp. K	46270	MF325573						VTDes070
Regabellator sp. K	46265	MF325570	MF325688	MF325776				VTDes064
Regabellator sp. K	46271	MF325571		MF325777				VTDes071
Regabellator sp. K	46353	MF325565						VTDes170

Species	Expedition	Site	Station	Start trawl (DD) latitude (N)	Start trawl (DD) longitude (W)	End trawl (DD) latitude (N)	End trawl (DD) longitude (W)	Trawl depth (m)	Sampling date (d.m.y)
Munnopsidae									
Acanthocope galatheae	Vema TRANSIT	6	6–7	10.36366667	36.91766667	10.36383333	36.91766667	5079	1/2/2015
Acanthocope galatheae	Vema TRANSIT	6	6–7	10.36366667	36.91766667	10.36383333	36.91766667	5079	1/2/2015
Acanthocope galatheae	Vema TRANSIT	6	6–7	10.36366667	36.91766667	10.36383333	36.91766667	5079	1/2/2015
Acanthocope galatheae	Vema TRANSIT	6	6–7	10.36366667	36.91766667	10.36383333	36.91766667	5079	1/2/2015
Acanthocope galatheae	Vema TRANSIT	6	6–8	10.3775	36.9225	10.37766667	36.9225	5127	1/2/2015
Acanthocope galatheae	Vema TRANSIT	6	6–8	10.3775	36.9225	10.37766667	36.9225	5127	1/2/2015
Acanthocope galatheae	Vema TRANSIT	6	6–8	10.3775	36.9225	10.37766667	36.9225	5127	1/2/2015
Acanthocope galatheae	Vema TRANSIT	6	6–8	10.3775	36.9225	10.37766667	36.9225	5127	1/2/2015
Acanthocope galatheae	Vema TRANSIT	4	4–8	10.427	31.07333333	10.427	31.07283333	5725	12/26/2014
Acanthocope galatheae	Vema TRANSIT	4	4–8	10.427	31.07333333	10.427	31.07283333	5725	12/26/2014
Acanthocope galatheae	Vema TRANSIT	4	4–8	10.427	31.07333333	10.427	31.07283333	5725	12/26/2014
Acanthocope galatheae	Vema TRANSIT	4	4–8	10.427	31.07333333	10.427	31.07283333	5725	12/26/2014
Acanthocope galatheae	Vema TRANSIT	8	8–4	10.71666667	42.66216667	10.71666667	42.66216667	5178	1/6/2015
Acanthocope galatheae	Vema TRANSIT	8	8–4	10.71666667	42.66216667	10.71666667	42.66216667	5178	1/6/2015
Acanthocope galatheae	Vema TRANSIT	8	8–4	10.71666667	42.66216667	10.71666667	42.66216667	5178	1/6/2015
Acanthocope galatheae	Vema TRANSIT	8	8–4	10.71666667	42.66216667	10.71666667	42.66216667	5178	1/6/2015
Acanthocope galatheae	Vema TRANSIT	4	4–9	10.4275	31.04966667	10.42766667	31.04966667	5733	12/27/2014
Acanthocope galatheae	Vema TRANSIT	4	4–9	10.4275	31.04966667	10.42766667	31.04966667	5733	12/27/2014
Acanthocope galatheae	Vema TRANSIT	4	4–9	10.4275	31.04966667	10.42766667	31.04966667	5733	12/27/2014
Acanthocope galatheae	Vema TRANSIT	4	4–9	10.4275	31.04966667	10.42766667	31.04966667	5733	12/27/2014
Acanthocope galatheae	Vema TRANSIT	9	9–2	11.67883333	47.96716667	11.67416667	47.98333333	4986	1/11/2015
Acanthocope galatheae	Vema TRANSIT	9	9–2	11.67883333	47.96716667	11.67416667	47.98333333	4986	1/11/2015
Acanthocope galatheae	Vema TRANSIT	9	9–2	11.67883333	47.96716667	11.67416667	47.98333333	4986	1/11/2015
Acanthocope galatheae	Vema TRANSIT	9	9–8	11.656	47.89983333	11.656	47.8995	5001	1/12/2015
Macrostylidae									
Macrostylis sp. MLpap	Vema TRANSIT	6	6–7	10.36366667	36.91766667	10.36383333	36.91766667	5079	1/2/2015
Macrostylis sp. MLpap	Vema TRANSIT	6	6–7	10.36366667	36.91766667	10.36383333	36.91766667	5079	1/2/2015
Macrostylis sp. MLpap	Vema TRANSIT	6	6–7	10.36366667	36.91766667	10.36383333	36.91766667	5079	1/2/2015
Macrostylis sp. MLpap	Vema TRANSIT	6	6–7	10.36366667	36.91766667	10.36383333	36.91766667	5079	1/2/2015
Macrostylis sp. MLpap	Vema TRANSIT	6	6–7	10.36366667	36.91766667	10.36383333	36.91766667	5079	1/2/2015
Macrostylis sp. MLpap	Vema TRANSIT	6	6–7	10.36366667	36.91766667	10.36383333	36.91766667	5079	1/2/2015
Macrostylis sp. MLpap	Vema TRANSIT	6	6–7	10.36366667	36.91766667	10.36383333	36.91766667	5079	1/2/2015
Macrostylis sp. MLpap	Vema TRANSIT	6	6–7	10.36366667	36.91766667	10.36383333	36.91766667	5079	1/2/2015
Macrostylis sp. MLpap	Vema TRANSIT	6	6–7	10.36366667	36.91766667	10.36383333	36.91766667	5079	1/2/2015
Macrostylis sp. MLpap	Vema TRANSIT	6	6–7	10.36366667	36.91766667	10.36383333	36.91766667	5079	1/2/2015
Macrostylis sp. MLpap	Vema TRANSIT	6	6–7	10.36366667	36.91766667	10.36383333	36.91766667	5079	1/2/2015
Macrostylis sp. MLpap	Vema TRANSIT	6	6–7	10.36366667	36.91766667	10.36383333	36.91766667	5079	1/2/2015
Macrostylis sp. MLpap	Vema TRANSIT	6	6–7	10.36366667	36.91766667	10.36383333	36.91766667	5079	1/2/2015
Macrostylis sp. MLpap	Vema TRANSIT	6	6–7	10.36366667	36.91766667	10.36383333	36.91766667	5079	1/2/2015
Macrostylis sp. MLpap	Vema TRANSIT	9	9–8	11.656	47.89983333	11.656	47.8995	5001	1/12/2015
Macrostylis sp. MLpap	Vema TRANSIT	9	9–8	11.656	47.89983333	11.656	47.8995	5001	1/12/2015
Macrostylis sp. MLpap	Vema TRANSIT	9	9–8	11.656	47.89983333	11.656	47.8995	5001	1/12/2015

(*continued on next page*)

Table 1 (*continued*)

Species	Expedition	Site	Station	Start trawl (DD)		End trawl (DD)		Trawl depth (m)	Sampling date (d.m.y)
				latitude (N)	longitude (W)	latitude (N)	longitude (W)		
Macrostylis sp. MLpap	Vema TRANSIT	9	9–8	11.656	47.89983333	11.656	47.8995	5001	1/12/2015
Macrostylis sp. MLpap	Vema TRANSIT	11	11–1	12.09733333	50.46616667	12.09683333	50.466	5088	1/14/2015
Macrostylis sp. MLpap	Vema TRANSIT	11	11–1	12.09733333	50.46616667	12.09683333	50.466	5088	1/14/2015
Macrostylis sp. MLpap	Vema TRANSIT	11	11–1	12.09733333	50.46616667	12.09683333	50.466	5088	1/14/2015
Macrostylis sp. MLpap	Vema TRANSIT	9	9–8	11.656	47.89983333	11.656	47.8995	5001	1/12/2015
Macrostylis sp. MLpap	Vema TRANSIT	11	11–4	12.0805	50.469	12.08033333	50.469	5108	1/14/2015
Macrostylis sp. MLpap	Vema TRANSIT	11	11–4	12.0805	50.469	12.08033333	50.469	5108	1/14/2015
Macrostylis sp. MLpap	Vema TRANSIT	11	11–4	12.0805	50.469	12.08033333	50.469	5108	1/14/2015
Desmosomatidae									
Prochelator barnacki	Vema TRANSIT	6	6–7	10.36366667	36.91766667	10.36383333	36.91766667	5079	1/2/2015
Prochelator barnacki	Vema TRANSIT	9	9–8	11.656	47.89983333	11.656	47.8995	5001	1/12/2015
Prochelator barnacki	Vema TRANSIT	6	6–7	10.36366667	36.91766667	10.36383333	36.91766667	5079	1/2/2015
Prochelator cf. *barnacki*	Vema TRANSIT	6	6–8	10.3775	36.9225	10.37766667	36.9225	5127	1/2/2015
Whoia sockei	Vema TRANSIT	2	2–6	10.72966667	25.062	10.72983333	25.06216667	5520	12/20/2014
Whoia sockei	Vema TRANSIT	9	9–8	11.656	47.89983333	11.656	47.8995	5001	1/12/2015
Chelator sp. A	Vema TRANSIT	4	4–9	10.72966667	25.062	10.72983333	25.06216667	5733	12/27/2014
Chelator sp. A	Vema TRANSIT	4	4–8	10.427	31.07333333	10.427	31.07283333	5725	12/26/2014
Chelator sp. A	Vema TRANSIT	4	4–9	10.72966667	25.062	10.72983333	25.06216667	5733	12/27/2014
Chelator sp. A	Vema TRANSIT	4	4–9	10.72966667	25.062	10.72983333	25.06216667	5733	12/27/2014
Chelator sp. A	Vema TRANSIT	4	4–8	10.427	31.07333333	10.427	31.07283333	5725	12/26/2014
Chelator sp. A	Vema TRANSIT	4	4–9	10.72966667	25.062	10.72983333	25.06216667	5733	12/27/2014
Chelator sp. A	Vema TRANSIT	4	4–8	10.427	31.07333333	10.427	31.07283333	5725	12/26/2014
Chelator sp. A	Vema TRANSIT	4	4–8	10.427	31.07333333	10.427	31.07283333	5725	12/26/2014
Chelator sp. A	Vema TRANSIT	4	4–8	10.427	31.07333333	10.427	31.07283333	5725	12/26/2014
Chelator sp. A	Vema TRANSIT	4	4–9	10.72966667	25.062	10.72983333	25.06216667	5733	12/27/2014
Chelator sp. A	Vema TRANSIT	4	4–8	10.427	31.07333333	10.427	31.07283333	5725	12/26/2014
Chelator sp. A	Vema TRANSIT	4	4–8	10.427	31.07333333	10.427	31.07283333	5725	12/26/2014
Chelator sp. A	Vema TRANSIT	4	4–9	10.72966667	25.062	10.72983333	25.06216667	5733	12/27/2014
Chelator sp. A	Vema TRANSIT	4	4–9	10.72966667	25.062	10.72983333	25.06216667	5733	12/27/2014
Chelator sp. A	Vema TRANSIT	4	4–9	10.72966667	25.062	10.72983333	25.06216667	5733	12/27/2014
Chelator sp. A	Vema TRANSIT	4	4–8	10.427	31.07333333	10.427	31.07283333	5725	12/26/2014
Chelator sp. A	Vema TRANSIT	4	4–9	10.72966667	25.062	10.72983333	25.06216667	5733	12/27/2014
Chelator sp. A	Vema TRANSIT	2	2–7	10.71485	25.0535	10.71533333	25.05278333	5507	12/20/2014
Chelator sp. A	Vema TRANSIT	4	4–8	10.427	31.07333333	10.427	31.07283333	5725	12/26/2014
Chelator sp. A	Vema TRANSIT	4	4–8	10.427	31.07333333	10.427	31.07283333	5725	12/26/2014
Chelator sp. A	Vema TRANSIT	4	4–9	10.72966667	25.062	10.72983333	25.06216667	5733	12/27/2014
Chelator sp. B	Vema TRANSIT	9	9–8	11.656	47.89983333	11.656	47.8995	5001	1/12/2015
Chelator sp. B	Vema TRANSIT	9	9–8	11.656	47.89983333	11.656	47.8995	5001	1/12/2015
Chelator sp. B	Vema TRANSIT	9	9–8	11.656	47.89983333	11.656	47.8995	5001	1/12/2015
Chelator sp. B	Vema TRANSIT	11	11–1	12.09733333	50.46616667	12.09683333	50.466	5088	1/14/2015
Chelator sp. B	Vema TRANSIT	11	11–4	12.0805	50.469	12.08033333	50.469	5108	1/14/2015
Chelator sp. C	Vema TRANSIT	8	8–4	10.71666667	42.66216667	10.71666667	42.66216667	5178	1/6/2015
Chelator sp. C	Vema TRANSIT	6	6–7	10.36366667	36.91766667	10.36383333	36.91766667	5079	1/2/2015
Chelator sp. C	Vema TRANSIT	6	6–8	10.3775	36.9225	10.37766667	36.9225	5127	1/2/2015
Chelator sp. C	Vema TRANSIT	6	6–8	10.3775	36.9225	10.37766667	36.9225	5127	1/2/2015
Parvochelus russus (sp. E)	Vema TRANSIT	8	8–4	10.71666667	42.66216667	10.71666667	42.66216667	5178	1/6/2015
Parvochelus russus (sp. E)	Vema TRANSIT	2	2–7	10.71485	25.0535	10.71533333	25.05278333	5507	12/20/2014
Mirabilicoxa sp. F	Vema TRANSIT	2	2–6	10.72966667	25.062	10.72983333	25.06216667	5520	12/20/2014
Mirabilicoxa sp. F	Vema TRANSIT	2	2–6	10.72966667	25.062	10.72983333	25.06216667	5520	12/20/2014
Mirabilicoxa sp. F	Vema TRANSIT	2	2–6	10.72966667	25.062	10.72983333	25.06216667	5520	12/20/2014
Mirabilicoxa sp. F	Vema TRANSIT	4	4–8	10.427	31.07333333	10.427	31.07283333	5725	12/26/2014
Mirabilicoxa sp. G	Vema TRANSIT	8	8–4	10.71666667	42.66216667	10.71666667	42.66216667	5178	1/6/2015
Mirabilicoxa sp. G	Vema TRANSIT	9	9–8	11.656	47.89983333	11.656	47.8995	5001	1/12/2015

(*continued on next page*)

Table 1 (*continued*)

Species	Expedition	Site	Station	Start trawl (DD)		End trawl (DD)		Trawl depth (m)	Sampling date (d.m.y)
				latitude (N)	longitude (W)	latitude (N)	longitude (W)		
Chelator sp. X	Vema TRANSIT	8	8–4	10.71666667	42.66216667	10.71666667	42.66216667	5178	1/6/2015
Chelator sp. X	Vema TRANSIT	8	8–4	10.71666667	42.66216667	10.71666667	42.66216667	5178	1/6/2015
Chelator sp. X	Vema TRANSIT	8	8–4	10.71666667	42.66216667	10.71666667	42.66216667	5178	1/6/2015
Chelator sp. X	Vema TRANSIT	6	6–8	10.3775	36.9225	10.37766667	36.9225	5127	1/2/2015
Eugerdella sp. H	Vema TRANSIT	8	8–4	10.71666667	42.66216667	10.71666667	42.66216667	5178	1/6/2015
Eugerdella sp. H	Vema TRANSIT	6	6–8	10.3775	36.9225	10.37766667	36.9225	5127	1/2/2015
Nannoniscidae									
Regabellator sp. K	Vema TRANSIT	4	4–8	10.427	31.07333333	10.427	31.07283333	5725	12/26/2014
Regabellator sp. K	Vema TRANSIT	4	4–8	10.427	31.07333333	10.427	31.07283333	5725	12/26/2014
Regabellator sp. K	Vema TRANSIT	4	4–8	10.427	31.07333333	10.427	31.07283333	5725	12/26/2014
Regabellator sp. K	Vema TRANSIT	4	4–8	10.427	31.07333333	10.427	31.07283333	5725	12/26/2014
Regabellator sp. K	Vema TRANSIT	4	4–9	10.72966667	25.062	10.72983333	25.06216667	5733	12/27/2014
Regabellator sp. K	Vema TRANSIT	4	4–8	10.427	31.07333333	10.427	31.07283333	5725	12/26/2014
Regabellator sp. K	Vema TRANSIT	8	8–4	10.71666667	42.66216667	10.71666667	42.66216667	5178	1/6/2015

expedition (2–6, 2–7, 4–8, 4–9, 6–7, 6–8, 8–4, 9–2, 9–8, 11–1, 11–4: Fig. 1, Table 1). Except for one site in the VTF (site 8), each site was sampled with two hauls separated by only a few kilometres (1.9–7.8 km). In favour of more robust analyses we combined the sampled individuals of both hauls as one putative population.

In *Macrostylis* sp. MLpap (Riehl et al., this issue) the distribution across the MAR was balanced with 14 individuals in the east and eleven individuals in the west. *Macrostylis* sp. MLpap was collected at site 6, 9,and 11 (maximum geographic distance between sampling locations = 1492 km). Within the family Munnopsidae 24 individuals of *Acanthocope galatheae* were found with a trans-Atlantic distribution of 16 specimens sampled in the eastern sites (site 4 and 6), four sampled within the VTF (site 8) and four specimens sampled in the western site 9 (maximum geographic distance between sampling locations = 1843 km).

For *Prochelator barnacki* Bober & Brix, this issue two individuals were collected at site 6 and one individual at site 9. (maximum geographic distance between sampling locations = 1203 km).

Whoia sockei Brix & Kihara, this issue were sampled at site 2 and 9 (geographic distance between sampling locations = 2498 km). All material used herein is listed in Table 1.

2.3. Sample treatment and genetic analyses

The samples from the C-EBS were sieved with filtered seawater, bulk-fixed in 96% precooled, denatured ethanol and stored at − 20 °C for 24–48 h on board. Sorting and species identification, as well as dissections for genetic analyses were performed on ice. The munnopsid isopods were handled in the laboratory of the Center of Natural History (CeNak) at the University of Hamburg. The whole specimens were transferred from 96% EtOH into TAE-buffer via a dilution series and then placed into 30 µl Chelex (6% Chelex resin). The specimens were incubated for 30 min at 56 °C and 10 min at 99 °C for extraction. The specimens were recovered after extraction and transferred back into 96% EtOH via a dilution series. The polymerase chain reactions (PCR) were performed with a total volume of 20 µl consisting of 2.0 µl DNA (diluted 1:10), 2.0 µl DreamTaq buffer, 0.4 µl dNTPs, 0.1 µl DreamTaq, 1.0 µl of each Primer (10 mmol) and 13.5 µl millipore H_2O. For COI the primers LCO1490 (5´-GGTCAACAAATCATAAAGATATTGG-3´) and HCO2198 (5´-TAAACTTCAGGGTGACCAAAAAATCA-3´) (Folmer et al., 1994) and for 16 S the primers 16Sbr (5´-CCGGTCTGAACTCAGATCACGT-3´) and 16Sar (5´-CGCCTGTTTATCAAAAACAT-3´) (Palumbi et al., 1991) were used. The PCR protocol had an initial denaturation step at 94 °C for 3 min, followed by 35 cycles of 30 s at 94 °C, 45 s at 48 °C and 1 min at 72 °C, followed by a final elongation step of 72 °C for 10 min. The final product was purified using FastAP and Exonuclease I and sent to Macrogen Europe, Inc. (Amsterdam-Zuidoost, Netherlands) for sequencing. The tissue samples for genetic analysis of Macrostylidae (see Riehl et al., this issue), Desmosomatidae and Nannoniscidae (see Brix et al., this issue) were treated following standard laboratory protocols as outlined in those publications. The 16 S and COI mitochondrial genes were analysed in both publications, Riehl et al. furthermore analysed the 18 S gene fragment.

For all families our main focus was on those species that exhibited cross-MAR distributions, e.g. only those genetically delimitated species present east and west of the MAR.

For this study 24 Munnopsidae were genetically analysed for the 16 S and COI genes. *Acanthocope galatheae* was directly targeted and identified on board. Furthermore we included selected data of other isopod families (Macrostylidae, Desmosomatidae, Nannoniscidae), which were analysed in whole with a different research question.

The complete datasets of Macrostylidae and Desmosomatidae/Nannoniscidae were treated in this issue by Riehl et al. (this issue) (in total 221 macrostylid specimens) and Brix et al. (this issue) (in total 195 desmosomatid and nannoniscid specimens). Species were identified in these studies using an integrative approach: first they were sorted into

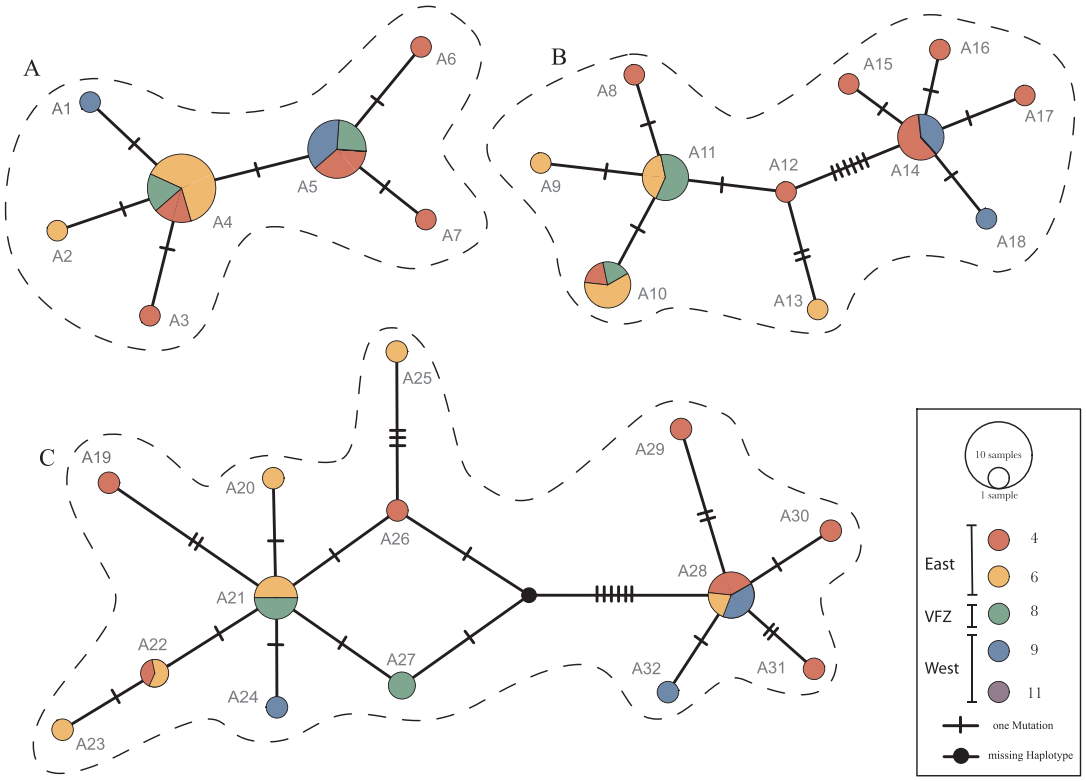

Fig. 2. Haplotype network (Median Joining): Each circle corresponds to a sampled haplotype and the size of the circle to the number of samples. The different haplotypes were tagged (A1–A32). A. *Acanthocope galatheae* Wolff, 1962 (Munnopsidae) haplotype network for the 16 S gene fragment. B. *A. galatheae* haplotype network for the COI gene. C. *A. galatheae* haplotype network of the concatenated COI + 16 S alignment.

phenotypic clusters based on morphological similarity and these clusters were evaluated using species delimitation models. Among 221 analysed individuals of Macrostylidae 19 putative species were identified; only two unknown species had a trans-Atlantic distribution: *Macrostylis* sp. MLpap (currently in the process of formal description, N. Heitland & T. Riehl, pers. comm.) and *Macrostylis* sp. ML08. We did not analyse *M.* sp. ML08 because with only a single individual sampled in the western stations the dataset was insufficient for population structure analyses. Within the Desmosomatidae and Nannoniscidae 195 individuals were analysed genetically and several species delimitation models were run with all specimens in Brix et al. (this issue) resulting in 53 desmosomatid and 19 nannoniscid species, most of which are new to science.

The obtained sequences of all species were further processed in the software package Geneious 8.1.7 (Kearse et al., 2012) and aligned using MUSCLE (Edgar, 2004), the resulting alignment was manually checked for possible errors.

To visualize the expansion of species across the MAR, haplotype networks were generated for the swimming Munnopsidae (Fig. 2) as well as the weakly- or non-swimming Macrostylidae, Desmosomatidae and Nannoniscidae (Fig. 3). For Desmosomatidae and Nannoniscidae all species recognized in both genes that were sampled at more than one site were taken into account. A median joining network was calculated in *Network 5* (Bandelt et al., 1999; http://fluxus-engineering.com/) and based on the alignments double checked by hand. The haplotype networks were calculated separately for the fast evolving genes 16 S and/or COI. For *A. galatheae* both genes were available, so a network from a concatenated alignment is presented as well (Fig. 2C). For two individuals (ZMH K-47064, 47084) only one gene was sequenced, the nucleotides of the missing gene were treated as missing data in the concatenated alignment. Furthermore individual ZMH K-47073 lacked 181 nucleotides in the middle of the COI sequence; therefore this sequence was not used in the COI network but included in the concatenated alignment.

To determine if the populations are structured by the MAR, population structure and diversity analyses were performed in Arlequin 3.5 (Excoffier and Lischer, 2010). These analyses were performed only on *Macrostylis* sp. MLpap and *Acanthocope galatheae* for which sufficiently high numbers of specimens were collected at both sides of the MAR (at least three specimens per group and population). We ran an AMOVA, which detects population differentiation within and among predefined groups within species. Two main groups were defined: “East” (site 2, 4, 6) and “West” (9, 11). *Acanthocope galatheae* was also collected at site 8 and therefore a third group “VFZ” was defined for this species to test whether the station within the VFZ was genetically divergent.

In contrast to a traditional F_{ST}, the pairwise Φ_{ST} considers the mutational differences among haplotypes when calculating the degree of population differentiation. Furthermore, we tested whether populations were isolated by distance with a Mantel test in Arlequin 3.5, which measures a correlation between the pairwise Φ_{ST} and geographic distance in kilometres. The AMOVA, pairwise Φ_{ST} and Mantel test ran with 1000 permutations.

The population genetic analyses were performed twice, once with each station as one population (Appendix 1–3) and once with each sampling site as one population, combining the two nearest stations, with the goal of having at least three individuals in each population. The 16 S dataset of *A. galatheae* for instance had only one individual at station 9–8, and three at station 9–2 resulting in four individuals at site 9. The results of the “sites model” did not differ much from the “stations model”, the sites model was used in favour of more stability and better comparability for all species and genes. These analyses were not performed for the 18 S gene fragment. The 18 S gene was not sequenced for

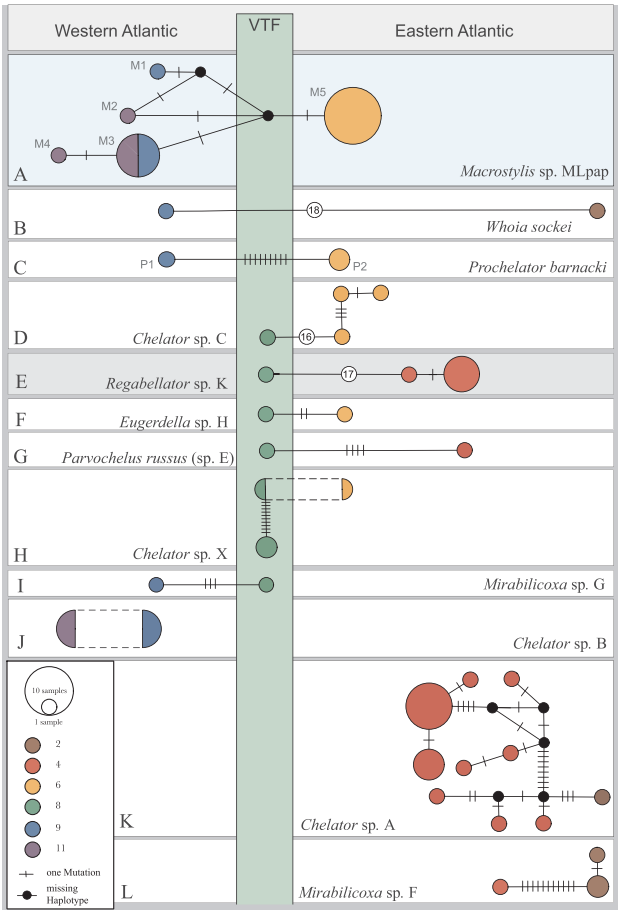

Fig. 3. Haplotype networks of Macrostylidae (blue), Desmosomatidae (white) and Nannoniscidae (grey) based on the comprehensive dataset presented by Riehl et al. (this issue) and Brix et al. (this issue). We selected only those species that occurred at more than one station and we prepared haplotype networks (Median Joining) for each species and plotted these roughly on the sampled transect. *Macrostylis* sp. MLpap (Macrostylidae) is based on a 16 S alignment. The different haplotypes were tagged (M1–M5). Two Desmosomatidae (*Prochelator barnacki* Bober & Brix, this issue, *Whoia sockei* Brix & Kihara, this issue) had a distribution across the Mid-Atlantic Ridge. All networks are based on COI sequences except for *Chelator* sp. X, for which only the 16 S gene was available. Each circle corresponds to a sampled haplotype and the size of the circle to the number of samples.

A. galatheae and the sequences obtained for *Macrostylis* sp. MLpap were identical among all specimens, offering no structure to test.

2.4. Alignment data

In Munnupsidae the 16 S alignment consisted of 23 sequences and had a length of 522 bp of which 515 positions were conserved, five positions variable, four positions singletons, and one position parsimony informative.

The COI alignment for Munnopsidae consisted of 22 sequences and had a length of 686 bp of which 669 positions were conserved, 14 positions variable, five positions singletons and nine positions parsimony informative. The gene fragment was free of stop codons and except for one single amino acid change from alanine to threonine in specimen ZMH K-47077 all mutations were neutral.

In Macrostylidae the 16 S alignment consisted of 25 sequences and had a length of 405 bp of which 398 positions were conserved, six positions variable, four positions singletons and 2 positions parsimony informative.

The COI alignment of *Prochelator barnacki* consisted of four sequences excluding the outgroup and had a length of 655 bp of which 585 positions were conserved, 57 positions variable, 53 positions singletons, and four positions parsimony informative. The gene fragments of *Prochelator barnacki* were free of stop codons and had no amino acid changes, except for the specimen *P.* cf. *barnacki* (ZMH K-46324), which had five amino acid changes.

Table 2
Results of the AMOVA calculated in Arlequin 3.5. Results are shown for the 16 S gene of *Macrostylis* sp. MLpap (Macrostylidae), the 16 S + COI gene separate and concatenated of *Acanthocope galatheae* Wolff, 1962 (Munnopsidae). The calculations were performed for sampling sites as populations (one site consists of two nearby sampled stations). The populations were grouped in eastern and western groups, for *A. galatheae* a third group in the middle the VTF = Vema Transform Fault was erected. Significant *P*-values were marked with asterisks. < 0.05 *; < 0.001 **; < 0.0001 ***.

Source of Variation	Sampling site = population					
		Percentage of variation	FCT	FSC	FST	P
Between East and West	1	78.02	0.78			0.33
Among sites in East or West	1	1.02		0.05		0.83
Among sites	22	20.96			0.79***	0.00
Macrostylis sp. MLpap 16 S						
Between East and West	2	−29.00	−0.29			0.84
Among sites in East or West	1	38.14		0.30*		0.03
Among sites	19	90.86			0.09*	0.05
Acanthocope galatheae 16 S						
Between East and West	2	12.88	0.13			0.50
Among sites in East or West	1	27.19		0.31		0.06
Among sites	18	59.92			0.40*	0.01
Acanthocope galatheae COI						
Between East and West	2	2.74	0.03			0.50
Among sites in East or West	1	34.06		0.35*		0.04
Among sites	20	63.19			0.37*	0.01
Acanthocope galatheae concatenated						

3. Results

Except for the swimming munnopsid species *A. galatheae*, none of the analysed species shared a haplotype across the MAR (Figs. 2 and 3). The AMOVAs for each of the swimming *A. galatheae* and burrowing *Macrostylis* sp. MLpap found no significant Φ_{CT} values (among groups of populations), so there was no significant genetic differentiation between the predefined groups “East” and “West”, plus “VFZ” for *A. galatheae* (Table 2). However, in *M.* sp. MLpap the percentage of variation from the AMOVA indicated that most of the genetic variation (78.0%) occurred between groups (East and West, i.e. across the barrier). The Φ_{CT} derived from the AMOVA and pairwise Φ_{CT} was similarly high but only significant for the pairwise Φ_{CT} (Table 4: 16 S, Φ_{CT} = 0.78, P = 0.33; pairwise Φ_{CT} = 0.78793, P < 0.000), suggesting a genetic differentiation between East and West in *M.* sp. MLpap. This finding is further emphasized by seemingly little variance among populations within each group (Table 2). However, the number of mutations underlying the genetic differences estimated by AMOVA and pairwise Φ_{CT} are low, which is visualized in the haplotype network (Fig. 3A). For *M.* sp. MLpap the genetic distances observed among western sites (9, 11) exceeded the distances observed between the eastern and western sites. The individuals from the eastern basin were genetically more conserved with all 14 individuals sharing the same haplotype (Fig. 3A; Haplotype M5). The samples from the western basin appeared to be genetically more diverse with four haplotypes.

Both species *A. galatheae* and *M.* sp. MLpap had a significantly high

Table 3
Genetic indices, parameters of demographic history and a Mantel test for the COI gene of *Macrostylis* sp. MLpap (Macrostylidae), the 16 S + COI gene separate and concatenated of *Acanthocope galatheae* Wolff, 1962 (Munnopsidae). Significant *P*-values were marked with asterisks. < 0.05*; < 0.001**; < 0.0001***.

Species	Marker	Group	Station	n	No. Of haplotypes	Haplotype diversity (h) ± SD	Nucleotide diversity (π_n) ± SD	Mantel Test	
								rY1 correlation coefficient (P-value)	Determination of Y1 (Φ_{ST}) by X1 (distance in km) (%)
Macrostylis sp. MLpap	16 S	East	6	14	1	0	0		
		West	9	5	3	0.7000 ± 0.2184	0.003478 ± 0.003078		
			11	3	1	0	0		
			Total	11	4	0.4909 ± 0.1754	0.003004 ± 0.002438		
		All	Total	25	5	0.6033 ± 0.0751	0.003797 ± 0.002732	0.975 (0.181)	0.95
Acanthocope galatheae	16 S	East	4	8	5	0.8571 ± 0.1083	0.002577 ± 0.002047		
			6	7	2	0.2857 ± 0.1964	0.000571 ± 0.000781		
			Total	15	6	0.7048 ± 0.1139	0.002019 ± 0.001608		
		VTF	8	4	2	0.6667 ± 0.2041	0.001336 ± 0.001499		
		West	9	4	2	0.5000 ± 0.2652	0.002004 ± 0.001985		
		All	Total	23	7	0.7115 ± 0.0679	0.001897 ± 0.001502	−0.298 (0.559)	0.089
	COI	East	4	8	7	0.9643 ± 0.0772	0.007482 ± 0.004681		
			6	8	5	0.8571 ± 0.1083	0.004885 ± 0.003207		
			Total	16	11	0.9167 ± 0.0493	0.007529 ± 0.004369		
		VTF	8	3	1	0	0		
		West	9	3	2	0.6667 ± 0.3143	0.001013 ± 0.001264		
		All	Total	22	11	0.8874 ± 0.0418	0.006921 ± 0.003946	−0.230 (0.670)	0.05
	Concatenated	East	4	8	7	0.9643 ± 0.0772	0.0052301 ± 0.003184		
			8	6	3	0.9286 ± 0.0844	0.004885 ± 0.003207		
			Total	16	12	0.9583 ± 0.0363	0.007529 ± 0.004369		
		VTF	8	4	2	0.6667 ± 0.204	0.000675 ± 0.000758		
		West	9	4	2	0.8333 ± 0.2224	0.002004 ± 0.001985		
		All	Total	24	15	0.9420 ± 0.0286	0.004917 ± 0.002790	−0.399 (0.961)	0.15

Φ_{ST} (within populations) in common (Table 2). They exhibited high genetic variation within populations (sampling sites) in 16 S (*A. galatheae* 16 S: 90.9%, Φ_{ST} = 0.09, P = 0.05; *M.* sp. MLpap 16 S: 21.0%, Φ_{ST} = 0.79, P < 0.000) and for *A. galatheae* also in COI (COI: 59.9%, Φ_{ST} = 0.40, P < 0.01). The concatenated 16 S and COI alignment of A. galatheae gives as expected similar results (*concatenated*: 63.9%, Φ_{ST} = 0.37, P < 0.01). Due to the high Φ_{ST} and the vast sampling area, Mantel tests were conducted for *A. galatheae* and *M.* sp. MLpap, which revealed no significant correlation between Φ_{ST} and geographic distance (Table 3), indicating that there is no isolation-by-distance in these sampled populations.

Population analyses were not feasible due to insufficient specimen numbers for the facultative-swimming Desmosomatidae, but the COI haplotype network of species *Prochelator barnacki* (Fig. 3C) allows some insights. Two of four individuals were collected at site 6 (haplotype P2) and one individual at site 9 (P1). The individuals (ZMH K-46202, ZMH K-46203) at site 6 shared one haplotype, while the individual (ZMH-46201) from site 9 across the MAR was separated by nine mutational steps.

We further used the sequences from Brix et al. (this issue) to estimate the haplotype diversity of all eleven widespread species in the haplotype networks (Fig. 3B–L). None of these species were sampled at more than two sites and six were sampled only at adjacent sites. However haplotypes shared among sites were found within *Chelator* sp. X and *Chelator* sp. B.

Prochelator barnacki and *Whoia sockei* do not share haplotypes across the MAR, but compared to the other species the number of mutations is similar to *Chelator* sp. C, which was collected at adjacent sites.

4. Discussion

In three of the four studied families, few species were able to cross the MAR. However, in a broader context an extended distribution range across the MAR is not the norm but rather the exception. The comprehensive datasets of Riehl et al. (this issue) and Brix et al. (this issue) revealed only two species of 19 putative macrostylid species and two of 53 desmosomatid species occurring on both sides of the MAR. All other species were restricted to one side of the MAR and the MAR thus seems to constitute a considerable dispersal barrier for most benthic isopods and possibly other organisms with a similar mode of life. This conclusion is, however, not congruent with the outcome of prior studies.

Prior research has demonstrated for multiple taxa that the MAR is no barrier to gene flow. This was found to be true for deep-sea fish (Knutsen et al., 2012; Priede et al., 2013; White et al., 2011), polychaetes (Shields et al., 2013; Shields and Blanco-Perez, 2013), bivalves (Etter et al., 2011; van der Heijden et al., 2012; Zardus et al., 2006), holothurians (Shields et al., 2013), and isopods (Brix et al., 2014a). However, it is important to emphasize that all previous analyses were based on specimens sampled at bathyal depths above 2800 m, except for the bivalves and isopods. The bathyal is a structurally diverse, heterogeneous habitat with depth gradients and resulting changes in hydrostatic pressure, temperature, and salinity. The abyss on the contrary is a mostly homogenous, continuous habitat (Etter et al., 2005; France and Kocher, 1996; Lynn and Reid, 1968; Mantyla and Reid, 1983; Smith et al., 2008; Smith and Demopoulos, 2003). Furthermore, the previously studied groups are free swimming and/or feature a planktonic larva during their development. Bivalves, for example, were studied from abyssal depth as well (Etter et al., 2011; van der Heijden et al., 2012; Zardus et al., 2006), but their free-swimming larvae drift with currents (Etter and Bower, 2015).

For the only isopod species studied so far, *Parvochelus russus*, which does hence not have a planktonic larva, little genetic divergence was observed and sporadic dispersal across the MAR was assumed by Brix et al. (2014a), through the Romanche Fracture Zone. However, *P. russus* has until recently been the only abyssal isopod species known from literature to have a distribution across the MAR.

Table 4
These tables show the pairwise Φ_{ST} calculated for the 16 S gene of *Macrostylis* sp. MLpap (Macrostylidae), the 16 S + COI gene separate and concatenated of *Acanthocope galatheae* Wolff, 1962 (Munnopsidae). The calculations were performed for sampling sites as populations (one site consists of two nearby sampled stations). Significant *P*-values were marked with asterisks. < 0.05 *; < 0.001 **; < 0.0001 ***.

Macrostylis sp. MLpap 16 S - FST				
site	6	9	11	
6	0			
9	0.85624***	0		
11	0.86074***	−0.09701	0	
Eastern vs. Western populations				
Group	East	West		
East	0			
West	0.78793***	0		
Acanthocope galatheae 16 S - FST				
Site	4	6	8	9
4	0			
6	0.29660*	0		
8	−0.15033	0.31450	0	
9	−0.09091	0.50877***	−0.11111	0
Eastern vs. Western vs. VTF populations				
Group	East	VTF	West	
East	0			
VTF	−0.12401	0		
West	0.08557	−0.11111	0	
Acanthocope galatheae COI - FST				
Site	4	6	8	9
4	0			
6	0.25146	0		
8	0.36916	−0.10092	0	
9	0.06190	0.64673*	0.95455	0
Eastern vs. Western vs. VTF populations				
Group	East	VTF	West	
East	0			
VTF	0.08826	0		
West	0.32034*	0.95455	0	
Acanthocope galatheae concatenated - FST				
Site	4	6	8	9
4	0			
6	0.27950*	0		
8	0.36705	0.04636	0	
9	−0.06325	0.61322*	0.84	0
Eastern vs. Western vs. VTF populations				
Group	East	VTF	West	
East	0			
VTF	0.10380	0		
West	0.18925*	0.84***	0	

4.1. Distribution range of four families

Following the 16 S data, *Acanthocope galatheae* is seemingly unaffected by the MAR, whereas in COI significant levels of differentiation between the eastern and western basins were observed. This apparent conflict is possibly due to sampling bias. Since whole mitochondrial genome is always inherited without recombination form the mother, the population genetic history of the mitochondrial genes should be identical. Relatively few specimens were available west of the MAR and from one of these specimens only the 16 S gene was successfully sequenced (from site 9) (Fig. 2A, haplotype A1). Given the 16 S haplotype A1 - which is nested among haplotypes recovered only east of the MAR and in the VFZ - it seems possible that the corresponding COI haplotype would have nested similarly and would have reduced the observed genetic differentiation between east and west in COI as well. This would imply that *A. galatheae* is hardly affected by a barrier as pronounced as the MAR. One should keep in mind that this species was selected specifically in this study because of its wide distribution and that this is potentially not a common pattern observed within Munnopsidae. Thus, no general trend for Munnopsidae can be drawn from this particular species.

For *Macrostylis* sp. MLpap the low number of mutational steps between eastern and western populations suggests at least one relatively recent successful dispersal event within Macrostylidae across the MAR. Due to the high number of individuals sharing one haplotype in the eastern population and because of the higher genetic diversity within the western populations (Fig. 3A), we propose a west to east dispersal event. Such a dispersal direction would also be in line with observed cold bottom water flowing through the VTF from the west (Eittreim et al., 1983; Fischer et al., 1996; Heezen et al., 1964b; McCartney et al., 1991; Vangriesheim, 1980).

Riehl et al. (this issue) also presented an AMOVA as well as a haplotype network for *Macrostylis* sp. MLpap, albeit with different results. First of all, Riehl et al. (this issue) scored an additional haplotype (haplotype 6 in their network) for the eastern population (site 6); however, this haplotype is based on an erroneous base call, which we fixed herein resulting in a genetically invariant eastern population. Furthermore, Riehl et al. (this issue) calculated their AMOVA and network with *PopArt* (Leigh and Bryant, 2015), which inferred high and significant levels of genetic differentiation on all hierarchical levels in their AMOVA. Conversely, our AMOVA computed in Arlequin suggested different and mostly insignificant levels of differentiation. The difference may in part be explained by the additional haplotype included in Riehl et al. (this issue) and in part by different treatment of the data by the two programs (e.g., PopArt shortens all sequences to the shortest sequence included in the alignment). So, for a better comparability to *A. galatheae* and other publications we repeated population genetical analysis on *Macrostylis* sp. MLpap.

The ten widespread desmosomatid isopod species – which were included in this study – are adapted to swimming as well as burrowing (Brix et al., this issue; Hessler and Strömberg, 1989) and therefore represent an interesting link between the two previously mentioned families examined in this study. The desmosomatid *Prochelator barnacki* is distributed across the MAR, but there is relatively large genetic differentiation within the 16 S gene (nine mutational steps; Fig. 3C), so a constant unhindered gene exchange across the MAR is uncertain. Nevertheless, the genetic distance is small enough (uncorrected *p*-distance: 1.1%) to assume at least relatively recent dispersal and gene exchange among populations such as observed for *Parvochelus russus* (Brix et al., 2014a). Also the desmosomatid *Whoia sockei* is distributed across the MAR with a p-distance of 3.8% in the sequence of the COI gene (Fig. 3B: *W. sockei*) between the two studied specimens. This leaves potential to argue whether the genetic distance is still within the range of one species. Brix et al. (this issue) however identified these two individuals to be of the same species based on morphological characters. Since we only have two individuals to compare and the genetic distance is above the 3% threshold (the ABGD analysis of Brix et al. (this issue) detected a barcode gap of 3–6% at COI in the whole dataset), we would consider the assumption of an occasional genetic exchange across the MAR with caution. Still, compared to other species the 3.8% are relatively “low” genetic distances among such far geographic distances (2498 km) (Fig. 3). Taken together, none of the 53 desmosomatid species differentiated by Brix et al. (this issue) shows evidence of regular or repeated gene flow across the MAR. As discussed for *Acanthocope galatheae*, the inclusion of more specimens may reveal some instances of gene flow missed herein, but it is unlikely that dispersal and gene flow across the MAR occurs regularly in species of this family.

Within the Nannoniscidae treated by Brix et al. (this issue) no species was sampled across the MAR. Nevertheless we included one

widespread species with a haplotype network (Fig. 3F: *Regabellator* sp. K). Nannoniscidae is mostly an epifaunal family that lives on the sediment without swimming adaptations (Wägele, 1989). The species shown here was the only species of 19 determined nannoniscid species that was found at more than one sampling site in the COI gene. Swimming adaptions in this genus are more pronounced in male specimens as sexual dimorphism. In general, swimming adaptations in desmosomatids and nannoniscids are more pronounced in males and thus represent sexual dimorphic characters (compare Brix et al., this issue).

Assuming limited distribution ranges in isopods we have to furthermore consider geographical distance as a possible barrier to gene flow (isolation-by-distance). This isolation seems to be obvious for the Desmosomatidae and Nannoniscidae, but is not as clear for the Munnopsidae or Macrostylidae. The individuals of these families were collected at sites at least 284 km and at most 1843 km apart across the MAR, representing a wide range for one species. The Mantel test of correlation between Φ_{ST} and geographic distance was not significant in both species and genes. This indicates that the geographic distances between stations alone have no measureable effect on the observed population structure.

Interestingly, several species have identical or at least very similar haplotypes in the VTF as in their "main" distribution east or west of the MAR (e.g., *Regabellator* sp. K; *Eugerdella* sp. H, *Parvochelus russus* (sp. E), *Chelator* sp. X, *Mirabilicoxa* sp. G), but without indication of trans-MAR dispersal. This implies that dispersal into and successfully establishing a population in the VTF from the east and west is possible and probably not a limiting factor to trans-MAR dispersal and distribution. The VTF could act as stepping-stone for species to cross the MAR, apparently providing suitable habitats for abyssal species. However, the observed lack of trans-MAR distributions suggests that dispersal out of the VTF and especially successful colonization of the respective other side of the MAR occurs only rarely and may be the limiting factor for trans-MAR dispersal. Either competitive exclusion (Waters, 2011) by resident species or differences in the available habitat restrict successful colonization of newly immigrating species after dispersal. Indeed, the studied habitats on either side of the MAR differed markedly (Devey, this issue). The VFZ itself may offer a mix of different (micro)habitats allowing species with the various specializations to co-exist at relatively small geographic scales.

In relation to the results on the swimming Munnopsidae, natatory Desmosomatidae/Nannoniscidae and non-swimming Macrostylidae the inherent lifestyle seems to have a considerable effect on the distribution range of species in the abyss. Macrostylidae and Desmosomatidae were both found across the MAR with two species respectively, but a regular exchange between eastern and western populations was not detected for these families. A persistent gene flow was only detected for the swimming munnopsid *A. galatheae*, indicating that pronounced swimming capabilities facilitate the dispersal across barriers like the MAR in the abyss.

4.2. Limitations to consider

The results on migrations especially within the Macrostylidae have to be regarded with caution. In this study, we considered mitochondrial genes only, which might introduce a misleading and faulty conclusion on population structure. The mitochondrial genome is always inherited as a whole from the mother without recombination. Therefore, the mitochondrial inheritance is haploid and asexual (Avise, 2009). This is critical for the conclusions we might draw from our data. Little is known about the behaviour of deep-sea asellotes (see Hessler and Strömberg, 1989). Especially for sexually dimorphic Macrostylidae, a change to a more epifaunal lifestyle with sexually mature males reproducing with probably stationary females was proposed before (Bober et al., 2017; Kniesz et al., 2017) and is potentially driven by sexually selective pressure (Riehl et al., 2012). If males are the more active dispersers, they might cross the MAR more often than females, and such male-based dispersal would have been missed by our mitochondrial gene based analyses. The easiest way to eliminate this potential error is the incorporation of nuclear genes (we tested a relatively fast-evolving region of 18 S but it did not yield any intraspecific variation). We furthermore tried to sequence the relatively fast evolving internal-transcribed-spacer 2 (ITS2), but the available primers (Innis et al., 2012; Wagstaff and Garnock-Jones, 1998; White et al., 1990), which worked for other crustaceans (Schwentner et al., 2014) have not worked with asellote DNA, so far. Sex-specific differences in dispersal capacities are more likely to occur (and thus to have been missed potentially) in Macrostylidae than in Munnopsidae for which to our knowledge no dispersal effecting sexual dimorphisms are apparent. In desmosomatids and nannoniscids, sexual dimorphism is more pronounced than in munnopsids and males more often show adaptations to swimming than females in various species, which might also have an effect on population genetic analyses.

4.3. The potential role of Fracture Zones for the distribution of abyssal benthos

Fracture zones like the VFZ are the most likely landscapes for benthic abyssal organisms to disperse across the MAR. Even for organisms that are less affected by currents, like infaunal Macrostylidae, the habitat within the VFZ could potentially provide a continuation of the abyssal soft-sediment habitat, from one side of the MAR to the other. As found previously (Brix et al., 2014a) and in this study, a complex habitat structure within the transform valleys is apparently not an insuperable barrier for some species of the abyssal benthos. The MAR is a complex habitat (see 2.1 Study area) compared to an abyssal plain. Especially the prevailing currents may influence distribution patterns for some deep-sea inhabitants. Probably caused by the easterly currents, the habitat (e.g. sediment, temperature) at site 8 within the transform fault resembled more the habitat of the western stations (Devey, this issue). Easterly currents might enhance the dispersal ability of organisms from the western to the eastern basin, but also decrease the potential for genetic exchange in the other direction. Within the western VFZ rather slow easterly currents were measured with a mean velocity of 2.9–3.7 cm s^{-1} and a maximum velocity of 12 cm s^{-1}; those currents are strongest near the bottom (Vangriesheim, 1980) where they may affect the benthos. Hence, the topography as well as the currents within the VFZ bears considerable potential to disrupt populations and our data on Macrostylidae suggest rather an easterly migration from the western Demerara Abyssal Plain. Interestingly, the haplotype networks of Desmomsomatidae and Nannoniscidae and the distribution of *M.* sp. ML08 (Riehl et al., this issue) indicate the opposite trend, a westerly migration. Except for *Mirabilicoxa* sp. G all five species sampled within the VFZ were found at eastern sites but not the western sites and ML08 was sampled at all eastern sites and only one individual was sampled in the western basin. Regarding these contradictory patterns, migrations in both directions seem to be possible.

5. Conclusions

The three isopod families Macrostylidae, Desmosomatidae and Nannoniscidae analysed here are part of a more comprehensive dataset, which was analysed elsewhere (Brix et al., this issue; Riehl et al., this issue). The majority of species were limited to a single side of the MAR, and only a few species were found to cross it. Therefore, we conclude that the MAR is a considerable dispersal barrier for most of the non-swimming Macrostylidae and facultative-swimming Desmosomatidae/Nannoniscidae.

The genetic structure observed in the trans-Atlantic species *Macrostylis* sp. MLpap shows a distinction between eastern and western populations, which may be caused by restricted connectivity across the MAR. The population structure of the swimming munnopsid species

Acanthocope galatheae, however, is seemingly unaffected by the MAR, having individuals from the eastern and western basins as well as from the connecting Vema Transform Fault which share identical haplotypes. We assume a persistent gene flow across the MAR over a vast geographic distance of 1843 km for this species. Thus, we hypothesize that benthic organisms with swimming capabilities are more likely to cross barriers in the abyss compared to infaunal burrowers, independent of their brooding lifestyle. We were able to confirm a genetic exchange across the barrier for burrowing and swimming isopods. However, gene flow across the MAR seems to be restricted or non-existent for non- and facultative-swimmers like Macrostylidae, Desmosomatidae and Nannoniscidae, but seems to be unhindered in the swimming isopod *A. galatheae*.

Acknowledgements

The project was undertaken with financial support of the PTJ (German Ministry for Science and Education), grant 03G0227A. Special thanks go to Marina Malyutina for the identification of the Munnopsidae and Robert M. Jennings for his help in finalizing this manuscript. Furthermore Captain Oliver Mayer and crew of R/V Sonne during cruise SO237 are thanked for their great job and guaranteeing a successful campaign. Nils Brenke, Enrico Schwabe, Inmaculada Frutos, Theresa Guggolz, GRG, Kathrin Linse and all involved in EBS deployment, sieving, and sample sorting are acknowledged for their efforts. Furthermore we kindly acknowledge the work of two anonymous reviewers and the editors Stefanie Kaiser and Javier Arístegui.

Formatting of funding sources

Funding: This study was supported by the German Federal Ministry of Education and Research with a grant to Angelika Brandt & Colin Devey (03G0237A).

Appendix A. Supporting information

Supplementary data associated with this article can be found in the online version at http://dx.doi.org/10.1016/j.dsr2.2018.02.007.

References

Avise, J.C., 2009. Phylogeography: retrospect and prospect. J. Biogeogr. 36, 3–15. http://dx.doi.org/10.1111/j.1365-2699.2008.02032.x.

Bader, R.G., Gerard, R.D., Benson, W.E., Bolli, H.M., Hay, W.W., Rothwell Jr., W.T., Ruef, M.H., Riedel, W.R., Sayles, F.L., 2007. Deep Sea Drill. Proj. -Introd. DSDP IV, 1–15. http://dx.doi.org/10.2973/dsdp.proc.4.1970.

Bandelt, H.J., Forster, P., Röhl, A., 1999. Median-joining networks for inferring intraspecific phylogenies. Mol. Biol. Evol. 16, 37–48.

Bober, S., Riehl, T., Henne, S., Brandt, A., 2017. New Macrostylidae (Isopoda) from the Northwest Pacific Basin described by means of integrative taxonomy with reference to geographical barriers in the abyss. Zool. J. Linn. Soc. 1–53. http://dx.doi.org/10.1093/zoolinnean/zlx042.

Brandt, A., Gooday, A.J., Brandão, S.N., Brix, S., Brökeland, W., Cedhagen, T., Choudhury, M., Cornelius, N., Danis, B., De Mesel, I., Diaz, R.J., Gillan, D.C., Ebbe, B., Howe, J.A., Janussen, D., Kaiser, S., Linse, K., Malyutina, M., Pawlowski, J., Raupach, M., Vanreusel, A., 2007. First insights into the biodiversity and biogeography of the Southern Ocean deep sea. Nature 447, 307–311. http://dx.doi.org/10.1038/nature05827.

Brandt, A., Bathmann, U., Brix, S., Cisewski, B., Flores, H., Göcke, C., Janussen, D., Krägefsky, S., Kruse, S., Leach, H., Linse, K., Pakhomov, E., Peeken, I., Riehl, T., Sauter, E., Sachs, O., Schüller, M., Schrödl, M., Schwabe, E., Strass, V., van Franeker, J.A., Wilmsen, E., 2011. Maud rise – a snapshot through the water column. Deep Sea Res. Part II: Top. Stud. Oceanogr., South. Ocean Biodivers. — Pelagic Process. Deep-Sea Response 58, 1962–1982. http://dx.doi.org/10.1016/j.dsr2.2011.01.008.

Brandt, A., Elsner, N., Brenke, N., Golovan, O., Malyutina, M.V., Riehl, T., Schwabe, E., Würzberg, L., 2013. Epifauna of the Sea of Japan collected via a new epibenthic sledge equipped with camera and environmental sensor systems. Deep Sea Res. Part II: Top. Stud. Oceanogr. 86–87, 43–55. http://dx.doi.org/10.1016/j.dsr2.2012.07.039.

Brenke, N., 2005. An epibenthic sledge for operations on marine soft bottom and bedrock. Mar. Technol. Soc. J. 39, 10–21. http://dx.doi.org/10.4031/002533205787444015.

Brix, S., Leese, F., Riehl, T., Kihara, T.C., 2015. A new genus and new species of Desmosomatidae Sars, 1897 (Isopoda) from the eastern South Atlantic abyss described by means of integrative taxonomy. Mar. Biodiv 1–55. http://dx.doi.org/10.1007/s12526-014-0218-3.

Brix, S., Svavarsson, J., Leese, F., 2014b. A multi-gene analysis reveals multiple highly divergent lineages of the isopod *Chelator insignis* (Hansen, 1916) south of Iceland. Pol. Polar Res. 35, 225–242.

Brix, S., Bober, S., Tschesche, C., Kihara, T.C., Driskell, A., Jennings, R.M., 2018. Molecular species delimitation and its implications for species descriptions using desmosomatid and nannoniscid isopods from the VEMA fracture zone as example taxa. Deep Sea Res. Part II: Top. Stud. Oceanogr (In this issue).

Devey, C.W., Augustin, N., Brandt, A., Brenke, N., Köhler, J., Lins, L., Schmidt, C., Yeo, I.A., 2018. Habitat characterization of the Vema Fracture Zone and Puerto Rico Trench. Deep Sea Res. Part II: Top. Stud. Oceanogr. http://dx.doi.org/10.1016/j.dsr2.2018.02.003. (In this issue).

Edgar, R.C., 2004. MUSCLE: multiple sequence alignment with high accuracy and high throughput. Nucleic Acids Res. 32, 1792–1797. http://dx.doi.org/10.1093/nar/gkh340.

Eittreim, S., Ewing, J., 1975. Vema fracture zone transform fault. Geology 3, 555–558.

Eittreim, S.L., Biscaye, P.E., Jacobs, S.S., 1983. Bottom-water observations in the Vema fracture zone. J. Geophys. Res. 88, 2609–2614. http://dx.doi.org/10.1029/JC088iC04p02609.

Etter, R., Rex, M.A., Chase, M.R., Quattro, J.M., 2005. Population differentiation decreases with depth in deep-sea bivalves. Evolution 59, 1479–1491.

Etter, R.J., Bower, A.S., 2015. Dispersal and population connectivity in the deep North Atlantic estimated from physical transport processes. Deep Sea Res. Part I: Oceanogr. Res. Pap. 104, 159–172. http://dx.doi.org/10.1016/j.dsr.2015.06.009.

Etter, R.J., Boyle, E.E., Glazier, A., Jennings, R.M., Dutra, E., Chase, M.R., 2011. Phylogeography of a pan-Atlantic abyssal protobranch bivalve: implications for evolution in the Deep Atlantic: evolution in the Deep Atlantic. Mol. Ecol. 20, 829–843. http://dx.doi.org/10.1111/j.1365-294X.2010.04978.x.

Excoffier, L., Lischer, H.E.L., 2010. Arlequin suite ver 3.5: a new series of programs to perform population genetics analyses under Linux and Windows. Mol. Ecol. Resour. 10, 564–567. http://dx.doi.org/10.1111/j.1755-0998.2010.02847.x.

Fischer, J., Rhein, M., Schott, F., Stramma, L., 1996. Deep water masses and transports in the Vema Fracture Zone. Deep Sea Res. Part I: Oceanogr. Res. Pap. 43 1067–1074. http://dx.doi.org/10.1016/0967-0637(96)00044-1.

Folmer, O., Black, M., Hoeh, W., Lutz, R., Vrijenhoek, R., 1994. DNA primers for amplification of mitochondrial cytochrome c oxidase subunit I from metazoan invertebrates. Mol. Mar. Biol. Biotechnol. 3, 294–299.

France, S.C., Kocher, T.D., 1996. Geographic and bathymetric patterns of mitochondrial 16S rRNA sequence divergence among deep-sea amphipods, *Eurythenes gryllus*. Mar. Biol. 126, 633–643.

Hansen, H.J., 1916. Crustacea Malacostraca: the order Isopoda. Dan. Ingolf Exped. 3, 1–262.

Harris, P.T., Macmillan-Lawler, M., Rupp, J., Baker, E.K., 2014. Geomorphology of the oceans. Mar. Geol. 50th Anniv. Spec. Issue 352, 4–24. http://dx.doi.org/10.1016/j.margeo.2014.01.011.

Harrison, K., 1989. Are deep-sea asellote isopods infaunal or epifaunal. Crustaceana 56, 317–319.

Havermans, C., Sonet, G., d'Udekem d'Acoz, C., Nagy, Z.T., Martin, P., Brix, S., Riehl, T., Agrawal, S., Held, C., 2013. Genetic and morphological divergences in the Cosmopolitan deep-Sea amphipod *Eurythenes gryllus* reveal a diverse Abyss and a bipolar species. PLoS ONE 8, e74218. http://dx.doi.org/10.1371/journal.pone.0074218.

Heezen, B.C., Bunce, E.T., Hersey, J.B., Tharp, M., 1964a. Chain and romanche fracture zones. Deep Sea Res. Oceanogr. Abstr. 11, 11–33. http://dx.doi.org/10.1016/0011-7471(64)91079-4.

Heezen, B.C., Gerard, R.D., Tharp, M., 1964b. The Vema fracture zone in the equatorial Atlantic. J. Geophys. Res. 69, 733–739. http://dx.doi.org/10.1029/JZ069i004p00733.

Held, C., 2003. Molecular evidence for cryptic speciation within the widespread Antarctic crustacean *Ceratoserolis trilobitoides* (Crustacea, Isopoda). Antarct. Biol. a Glob. Context 135–139.

Hessler, R.R., Jumars, P.A., 1974. Abyssal community analysis from replicate cores in the central North Pacific. Deep Sea Res. Oceanogr. Abstr. 21, 185–209. http://dx.doi.org/10.1016/0011-7471(74)90058-8.

Hessler, R.R., Sanders, H., 1967. Faunal diversity in the deep-sea. Deep Sea Res. Oceanogr. Abstr. 14, 65–78. http://dx.doi.org/10.1016/0011-7471(67)90029-0.

Hessler, R.R., Strömberg, J.-O., 1989. Behavior of janiroidean isopods (Asellota), with special reference to deep sea genera. Sarsia 74, 145–159.

Hessler, R.R., Wilson, G.D.F., 1983. The origin and biogeography of malacostracan crustaceans in the deep sea. In: Sims, R.W., Price, J.H., Whalley, P.E.S. (Eds.), Evolution, Time, and Space: The Emergence of the Biosphere. Academic Press, London, pp. 227–254.

Innis, M.A., Gelfand, D.H., Sninsky, J.J., White, T.J., 2012. PCR Protocols: A Guide to Methods and Applications. Academic Press.

Kaiser, S., Brandt, A., 2007. Two new species of the genus Austroniscus Vanhoeffen, 1914 (Isopoda: Asellota: Nannoniscidae) from the Antarctic shelf. Zootaxa 1394, 47–68.

Kearse, M., Moir, R., Wilson, A., Stones-Havas, S., Cheung, M., Sturrock, S., Buxton, S., Cooper, A., Markowitz, S., Duran, C., Thierer, T., Ashton, B., Meintjes, P., Drummond, A., 2012. Geneious Basic: an integrated and extendable desktop software platform for the organization and analysis of sequence data. Bioinformatics 28, 1647–1649. http://dx.doi.org/10.1093/bioinformatics/bts199.

Kniesz, K., Brandt, A., Riehl, T., 2017. Peritrich epibionts on the hadal isopod species Macrostylis marionae n. sp. from the Puerto Rico Trench used as indicator for sex-specific behaviour. Deep Sea Res. Part II: Top. Stud. Oceanogr. http://dx.doi.org/10.1016/j.dsr2.2017.10.007.

Knutsen, H., Jorde, P.E., Bergstad, O.A., Skogen, M., 2012. Population genetic structure in a deepwater fish *Coryphaenoides rupestris*: patterns and processes. Mar. Ecol. Prog. Ser. 460, 233–246. http://dx.doi.org/10.3354/meps09728.

Latreille, P.A., 1817. Les Crustaces, les Arachnides, et les Insectes., In: Le Regne Animal, Distribue D'apres Son Organisation, Pour Servrir de Base a L'histoire Naturelle Des Animaux et D'introduction a L'anatomie Comparee. Paris.

Leigh, J.W., Bryant, D., 2015. Popart: full-feature software for haplotype network construction. Methods Ecol. Evol. http://dx.doi.org/10.1111/2041-210X.12410.

Lynn, R.J., Reid, J.L., 1968. Characteristics and circulation of deep and abyssal waters. Deep Sea Res. Oceanogr. Abstr. 15, 577–598. http://dx.doi.org/10.1016/0011-7471(68)90064-8.

Mantyla, A.W., Reid, J.L., 1983. Abyssal characteristics of the World Ocean waters. Deep Sea Res. Part A. Oceanogr. Res. Pap. 30, 805–833. http://dx.doi.org/10.1016/0198-0149(83)90002-X.

Marshall, N., Diebel, C., 1995. "Deep-sea spiders" that walk through the water. J. Exp. Biol. 198, 1371–1379.

McCartney, M.S., Bennett, S.L., Woodgate-Jones, M.E., 1991. Eastward flow through the Mid-atlantic ridge at 11°N and its influence on the abyss of the Eastern Basin. J. Phys. Oceanogr. 21, 1089–1121. http://dx.doi.org/10.1175/1520-0485(1991)021<1089:EFTTMA>2.0.CO;2.

Murray, J., Appellöf, J.J.A., Gran, H.H., Helland-Hansen, B., Hjort, J., 1912. The Depths of the Ocean: A General Account of the Modern Science of Oceanography Based Largely on the Scientific Researches of the Norwegian Steamer Michael Sars in the North Atlantic / by Sir John Murray and Dr. Johan Hjort; with contributions from Professor A. Appellöf, Professor H. H. Gran and Dr. B. Helland-Hansen. Macmillan, London.

Palumbi, S.R., Martin, A., Romano, S., McMillan, W.O., Stice, L., Grabowski, G., 1991. Simple Fool's Guide PCR. University of Hawaii Press (45 pp).

Priede, I.G., Bergstad, O.A., Miller, P.I., Vecchione, M., Gebruk, A., Falkenhaug, T., Billett, D.S.M., Craig, J., Dale, A.C., Shields, M.A., Tilstone, G.H., Sutton, T.T., Gooday, A.J., Inall, M.E., Jones, D.O.B., Martinez-Vicente, V., Menezes, G.M., Niedzielski, T., Sigurðsson, Þ, Rothe, N., Rogacheva, A., Alt, C.H.S., Brand, T., Abell, R., Brierley, A.S., Cousins, N.J., Crockard, D., Hoelzel, A.R., Høines, Å., Letessier, T.B., Read, J.F., Shimmield, T., Cox, M.J., Galbraith, J.K., Gordon, J.D.M., Horton, T., Neat, F., Lorance, P., 2013. Does presence of a mid-ocean ridge enhance biomass and biodiversity? PLOS ONE 8, e61550. http://dx.doi.org/10.1371/journal.pone.0061550.

Ramirez-Llodra, E.Z., Brandt, A., Danovaro, R., De Mol, B., Escobar, E., German, C.R., Narayanaswamy, B.E., 2010. Deep, diverse and definitely different: unique attributes of the world's largest ecosystem. Biogeosciences 9.

Raupach, M.J., Wägele, J.-W., 2006. Distinguishing cryptic species in Antarctic Asellota (Crustacea: Isopoda) – a preliminary study of mitochondrial DNA in *Acanthaspidia drygalskii*. Antarct. Sci. 18, 191. http://dx.doi.org/10.1017/S0954102006000228.

Raupach, M.J., Malyutina, M., Brandt, A., Wägele, J.-W., 2007. Molecular data reveal a highly diverse species flock within the munnopsoid deep-sea isopod *Betamorpha fusiformis* (Barnard, 1920) (Crustacea: Isopoda: Asellota) in the Southern Ocean. Deep Sea Res. Part II: Top. Stud. Oceanogr. 54, 1820–1830. http://dx.doi.org/10.1016/j.dsr2.2007.07.009.

Reid, J.L., Nowlin, W.D., Patzert, W.C., 1977. On the characteristics and circulation of the southwestern Atlantic Ocean. J. Phys. Oceanogr. 7, 62–91. http://dx.doi.org/10.1175/1520-0485(1977)007<0062:OTCACO>2.0.CO;2.

Rex, M., Etter, R., 2011. Deep-sea biodiversity: pattern and scale. Oceanography 24, 183–185.

Riehl, T., Wilson, G.D.F., Hessler, R.R., 2012. New Macrostylidae Hansen, 1916 (Crustacea: Isopoda) from the Gay head-Bermuda transect with special consideration of sexual dimorphism. Zootaxa 1–26.

Riehl, T., Lins, L., Brandt, A., 2018. The effects of depth, distance, and the Mid-Atlantic Ridge on genetic differentiation of abyssal and hadal isopods (Macrostylidae). Deep Sea Res. Part II: Top. Stud. Oceanogr. http://dx.doi.org/10.1016/j.dsr2.2017.10.005. (In this issue).

Sars, G.O., 1897. Parts 7, 8. Desmosomidae, Munnopsidae, In: An Account of the Crustacea of Norway with Short Descriptions and Figures of All the Species. Vol. 2, Isopoda. Bergen: Bergen Museum, pp. 117–144, NaN–64.

Schwentner, M., Timms, B.V., Richter, S., 2014. Evolutionary systematics of the Australian *Eocyzicus* fauna (Crustacea: Branchiopoda: Spinicaudata) reveals hidden diversity and phylogeographic structure. J. Zool. Syst. Evolut. Res. 52, 15–31. http://dx.doi.org/10.1111/jzs.12038.

Shields, M.A., Blanco-Perez, R., 2013. Polychaete abundance, biomass and diversity patterns at the Mid-Atlantic Ridge, North Atlantic Ocean. Deep Sea Res. Part II: Top. Stud. Oceanogr., ECOMAR: Ecosyst. -Atl. Ridge Sub-Polar Front Charlie-Gibbs Fract. Zone 98 (Part B), 315–325. http://dx.doi.org/10.1016/j.dsr2.2013.04.010.

Shields, M.A., Glover, A.G., Wiklund, H., 2013. Polynoid polychaetes of the Mid-Atlantic Ridge and a new holothurian association. Mar. Biol. Res. 9, 547–553. http://dx.doi.org/10.1080/17451000.2012.749992.

Siebenaller, J.F., Hessler, R.R., 1981. The Genera of the Nannoniscidae (Isopoda, Asellota). San Diego Society of Natural History.

Smethie, W.M., Swift, J.H., 1989. The tritium:krypton-85 age of Denmark Strait overflow water and Gibbs fracture zone water just south of Denmark Strait. Tritium-Krypto.-85 Age Den. Strait Overflow Water Gibbs Fract.-Zone Water Just South Den. Strait 94, 8265–8275. http://dx.doi.org/10.1029/JC094iC06p08265.

Smith, C.R., Demopoulos, A.W., 2003. The deep Pacific ocean floor. Ecosyst. World 179–218.

Smith, C.R., De Leo, F.C., Bernardino, A.F., Sweetman, A.K., Arbizu, P.M., 2008. Abyssal food limitation, ecosystem structure and climate change. Trends Ecol. Evol. 23, 518–528. http://dx.doi.org/10.1016/j.tree.2008.05.002.

Thistle, D., Wilson, G.D.F., 1987. A hydrodynamically modified, abyssal isopod fauna. Deep-Sea Res. Part A Oceanogr. Res. Pap. 34, 73–87.

van Andel, T.H., 1969. Recent uplift of the Mid-Atlantic Ridge south of the Vema fracture zone. Earth Planet. Sci. Lett. 7, 228–230.

Van Andel, T.H., Phillips, J.D., Von Herzen, R.P., 1968. Rifting origin for the vema fracture in the North Atlantic. Earth Planet. Sci. Lett. 5, 296–300. http://dx.doi.org/10.1016/S0012-821X(68)80055-X.

Van Andel, T.H., Von Herzen, R.P., Phillips, J.D., 1971. The Vema fracture zone and the tectonics of transverse shear zones in oceanic crustal plates. Mar. Geophys. Res. 1, 261–283.

van der Heijden, K., Petersen, J.M., Dubilier, N., Borowski, C., 2012. Genetic connectivity between North and South Mid-Atlantic Ridge chemosynthetic bivalves and their symbionts. PLoS ONE 7, e39994. http://dx.doi.org/10.1371/journal.pone.0039994.

Vangriesheim, A., 1980. Antarctic bottom water flow through the Vema fracture zone. Oceanol. Acta 3, 199–207.

Vecchione, M., Bergstad, O.A., Byrkjedal, I., Falkenhaug, T., Gebruk, A.V., Godø, O.R., Gislason, A., Heino, M., Høines, A.S., Menezes, G., others, 2010. Biodiversity patterns and processes on the Mid-Atlantic Ridge. In: McIntyre, A. (Eds.), Life in the World's Oceans: Diversity, Distribution, and Abundance, pp. 103–121.

Wägele, J.W., 1989. Evolution und phylogenetisches System der Isopoda: Stand der Forschung und neue Erkenntnisse [Evolution and phylogeny of isopods. New data and the state of affairs]. E. Schweizerbart'sche Verlagsbuchhandlung, Stuttgart.

Wagstaff, S.J., Garnock-Jones, P.J., 1998. Evolution and biogeography of the Hebe complex (Scrophulariaceae) inferred from its sequences. N.Z. J. Bot. 36, 425–437. http://dx.doi.org/10.1080/0028825X.1998.9512581.

Waters, J.M., 2011. Competitive exclusion: phylogeography's "elephant in the room"? Mol. Ecol. 20, 4388–4394. http://dx.doi.org/10.1111/j.1365-294X.2011.05286.x.

White, T.A., Stamford, J., Rus Hoelzel, A., 2010. Local selection and population structure in a deep-sea fish, the roundnose grenadier (*Coryphaenoides rupestris*). Mol. Ecol. 19, 216–226. http://dx.doi.org/10.1111/j.1365-294X.2009.04446.x.

White, T.A., Fotherby, H.A., Stephens, P.A., Hoelzel, A.R., 2011. Genetic panmixia and demographic dependence across the North Atlantic in the deep-sea fish, blue hake (*Antimora rostrata*). Heredity 106, 690–699. http://dx.doi.org/10.1038/hdy.2010.108.

White, T.J., Bruns, T., Lee, S., Taylor, J.L., 1990. Amplification and direct sequencing of fungal ribosomal RNA genes for phylogenetics. PCR Protoc.: Guide Methods Appl. 18, 315–322.

Wilson, G.D.F., 2008. A review of taxonomic concepts in the Nannoniscidae (Isopoda, Asellota), with a key to the genera and a description of *Nannoniscus oblongus* Sars. Zootaxa 1680, 1–24.

Wilson, G.D.F., Hessler, R.R., 1987. Speciation in the deep sea. Annu. Rev. Ecol. Syst. 185–207.

Wolff, T., 1977. Diversity and faunal composition of the deep-sea benthos. Nat. Lond. 267, 780–785.

Zardus, J.D., Etter, R.J., Chase, M.R., Rex, M.A., Boyle, E.E., 2006. Bathymetric and geographic population structure in the pan-Atlantic deep-sea bivalve *Deminucula atacellana*(Schenck, 1939): genetic structure in a deep-sea bivalve. Mol. Ecol. 15, 639–651. http://dx.doi.org/10.1111/j.1365-294X.2005.02832.x.

Author contributions

The study was designed and conducted by Simon Bober.

Munnopsidae were handled in the laboratory of the CeNak by S. Bober. Macrostylidae, Desmosomatidae and Nannoniscidae were prepared externally by a professional laboratory. Genetic analyses were concducted by S. Bober and the population genetic analyses were performed by S. Bober with contributions of Martin Schwentner. Saskia Brix had the idea for Figure 3, which was then realized by S. Bober. All other figures were made by S. Bober. The first draft of the manuscript was written by S. Bober with subsequent contributions of Saskia Brix, Torben Riehl, Martin Schwentner and Angelika Brandt. Angelika Brandt had the idea for the project (Vema-TRANSIT) and wrote the proposals, she was the leader of the expedition.

Chapter 3

Molecular species delimitation and its implications for species descriptions using desmosomatid and nannoniscid isopods from the VEMA fracture zone as example taxa

Deep-Sea Research Part II 148 (2018) 180–207

Contents lists available at ScienceDirect

Deep-Sea Research Part II

journal homepage: www.elsevier.com/locate/dsr2

Molecular species delimitation and its implications for species descriptions using desmosomatid and nannoniscid isopods from the VEMA fracture zone as example taxa

Saskia Brix[a,*], Simon Bober[b], Claudia Tschesche[b], Terue-Cristina Kihara[c], Amy Driskell[d], Robert M. Jennings[e]

[a] Senckenberg am Meer, German Centre for Marine Biodiversity Research (DZMB), c/o CeNak, Biocenter Grindel, Martin-Luther-King-Platz 3, 20146 Hamburg, Germany
[b] University of Hamburg, Centre of Natural History (CeNak), Zoological Museum, Hamburg, Germany
[c] Senckenberg am Meer, German Centre for Marine Biodiversity Research (DZMB), Südstrand 44, 26382 Wilhelmshaven, Germany
[d] Smithsonian Institution, Laboratories of Analytical Biology, National Museum of Natural History, Smithsonian Institution, Washington DC, USA
[e] Biology Department, Temple University, Philadelphia, PA, USA

ARTICLE INFO

Keywords:
Asellota
Reverse taxonomy
DNA barcoding
Peracarida
Deep sea
Atlantic Ocean
Distribution

ABSTRACT

We found 72 species for COI and 45 for 16 S by species delimitation among 186 (from 195 extracted) desmosomatid (144) and nannoniscid (42) sequenced specimens of a total of > 400 specimens for both families. Multiple "discovery"-type species delimitation methods were used, so that consistency across methods could be assessed: The ABGD analysis detected a barcode gap of 3–6% for COI and 4–6% for 16 S, in the whole dataset. Most putative species have a horizontally limited distribution along the Vema fracture zone, although the details depend in part on the interpretation of species delimitation analyses. Putative species were mostly restricted to the eastern or western Vema fracture zone, with only eight crossing the complete Vema fracture zone. Our data suggest that even robustly-sampled species exhibited small ranges; the range estimates calculable from present data were around 500 km, and three were on the order of 1000–2500 km. We chose an abundant, but geographically restricted species (*Eugerdella egoni* Tschesche and Brix sp. nov.) collected at a single site in the Vema transform fault, and two species (*Prochelator barnacki* Bober and Brix sp. nov. and *Whoia sockei* Brix and Kihara sp. nov.) with a broad, but disjunct distribution in the Vema fracture zone for taxonomic description.

1. Introduction

A common taxon in the benthic fauna are the peracarid crustaceans. Among these, isopods are frequently encountered in marine benthic samples of the North Atlantic (Hessler and Sanders, 1967; Svavarsson et al., 1993; Brix and Svavarsson, 2010). This highly diverse group contains more than 10.000 species known worldwide to date and especially in the deep oceans the suborder Asellota is numerous and diverse (Hessler and Thistle, 1975; Poore and Bruce, 2012). Janiroidean asellotes comprise 25 families plus 8 genera incertae sedis (Riehl et al., 2014). The deep-sea families Desmosomatidae Sars, 1897 and Nannoniscidae Hansen, 1916 are ubiquitous, small macrofaunal isopods with a wide geographic and bathymetric distribution. Species from these two families have been sampled throughout the world's oceans: in the Arctic and North Atlantic (Malyutina and Kussakin, 1996), South Atlantic (Brix, 2006a), North (Birstein, 1971; Golovan, 2007) and South Pacific (Brix, 2007; Janssen et al., 2015; Kaiser et al., In this Issue) and Southern Ocean (Kaiser and Brix, 2005; Brix, 2006b).

Species delimitation was dominated by morphology for centuries, but nowadays integrative approaches to species delimitation that include morphological, genetic and ecological data can increase the accuracy of species delimitations (Brix et al., 2015; Dayrat, 2005; Sites and Marshall, 2004). Several recent species descriptions (Brix et al., 2015; Brandt et al., 2014) combined Confocal Laser Scanning Microscopy, Scanning electron Microscopy, light microscopy, life photographs and molecular markers for species delimitation (SD). While the different microscopy techniques provide more information also about inner structure of the organisms (for example muscle orientation visible in CLSM), so far "barcoding approaches" were used to differentiate species in peracarid crustaceans (Brix at al, 2011; Jażdżewska et al. in press) or species level identifications were imbedded into phylogenetic trees (Osborn, 2009). Riehl et al., (In this Issue) did apply the Poisson tree processes (PTP) molecular model for Macrostylidae Hansen, 1916. Only the approach in Kaiser et al., (In this Issue), is comparable to our

* Corresponding author.
E-mail address: sbrix@senckenberg.de (S. Brix).

https://doi.org/10.1016/j.dsr2.2018.02.004

Available online 09 February 2018

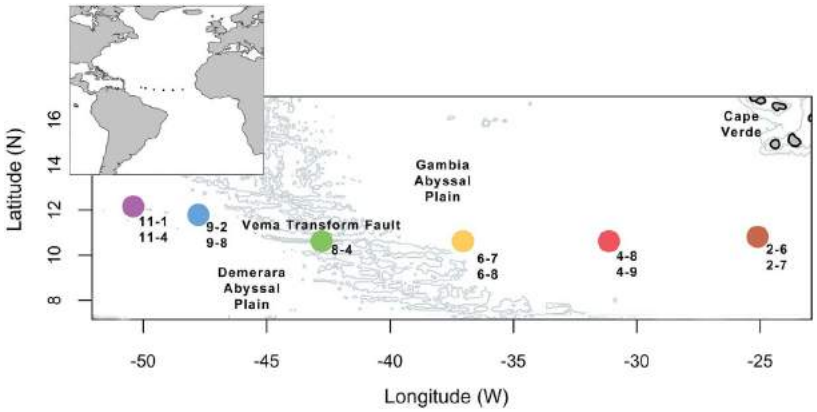

Fig. 1. Map with VEMA sites colored the way as shown in the circle trees in Figs. 2 and 3.

approach as Kaiser et al., (In this Issue) put the focus on two genera within the Nannoniscidae Hansen, 1916 - a family also included herein. They did also run the same molecular models for a much smaller dataset (bPTP: Bayesian Poisson tree process, Zhang et al., 2013; GMYC: general mixed Yule coalescent, Pons et al., 2006; ABGD: automated barcode gap discovery, Puillandre et al., 2011) as outlined in our methods below. ABGD is used as standard in DNA barcoding.

We used a combined morphological and genetic approach for species delimitation within desmosomatid and nannoniscid isopods in the VFZ. After *a priori* morphological determination on family and genus level, we tested, whether species delimitation models like the ABGD algorithm, GMYC, and bPTP recognize the same species on both sides of the Mid Atlantic Ridge (MAR) using the Vema fracture zone (VFZ) as an example area (Fig. 1) and the isopod families Desmosomatidae Sars, 1897 and Nannoniscidae Hansen, 1916 as example taxa. The sampling area (Fig. 1) is described in detail in Bober et al., (In this issue): the VFZ is unique in its flat gently sloping valley providing theoretically a continuous habitat from the Demerara Abyssal Plain west of the MAR to the Gambia Abyssal Plain east of the MAR. The Vema Fracture transform crossing the MAR could serve as a passage for the migration of organisms across the MAR as has been seen in the Romane Fracture Zone (RF, Brix et al., 2015).

Based on the SD results and adding morphological data from light-, scanning electron-, and confocal laser scanning- microscopy as well as on mitochondrial (COI, 16 S) markers, we differentiate and describe three new species. We chose a locally abundant, but geographically restricted species (*Eugerdella egoni* sp. nov.) collected at one site in the VEMA transform fault (VTF), and two species (*Whoia sockei* sp. nov. and *Prochelator barnacki* sp. nov.) with a broad, but disjunct distribution (compare Bober et al., In this issue) in the VFZ for description.

2. Methods

Sampling took place along a transect of the entire length of the Vema-Fracture Zone on board of RV *Sonne* (SO-237) between December 2014 and January 2015. For a complete station list, and for details on EBS data of the sited used for the present study see Brandt et al. (In this issue) and Devey et al. (In this issue).

In total, our dataset contained about 400 specimens, of which 186 specimens were sequenced successfully. All were sorted on board during the expedition and identified on genus level prior to molecular analysis. Only intact specimens allowing future morphological species identification were used for genetics to allow later morphological species identification and description; damaged specimens were excluded. Each specimen was used for DNA extraction and we choose two mitochondrial markers (COI and 16 S) for species delimitation. Relevant voucher information, taxonomic classifications, and sequences are accessible through the public data set "SDEL" on the Barcode of Life Data Systems (BoLD; www.boldsystems.org) and are from BoLD submitted to GenBank receiving accession numbers (Table 1).

2.1. Molecular methods

2.1.1. DNA extraction, PCR amplification, and sequencing

Extraction of DNA, PCR amplification, and sequencing of specimens was performed at the Laboratories of Analytical Biology, National Museum of Natural History, Smithsonian Institution, Washington, D.C. USA. A single posterior leg was removed from each specimen for DNA extraction, which was performed as described in Riehl et al. (2014). Amplification of two mitochondrial markers, the mitochondrial ribosomal large subunit (16 S), and cytochrome *c* oxidase subunit I (COI), as well as the nuclear small ribosomal subunit (18 S) were performed separately for each specimen using primers and protocols described in Riehl et al. (2014). Amplicons were prepared for sequencing with ExoSap-IT (USB), and sequenced bidirectionally on an ABI 3730xl capillary sequencer. For each specimen, gene sequences were edited in Geneious v9.1.6 to resolve disagreements and ambiguities and to remove primer regions. Sequences of 18 S were obtained for future work, but were not aligned or analyzed here because this marker evolves too slowly to be of use in species delimitation. Alignment of 16 S was performed with the online MAFFT server v7 (Katoh and Standley, 2013) and ambiguously aligned portions were removed using the online Gblocks server (Talavera and Castresana, 2007), employing all three criteria for less-stringent selection. The COI alignment was performed on DNA codons using the Clustal X algorithm (Larkin et al., 2007) as implemented in BioEdit. All alignments were edited for consistency by hand, and ends were trimmed to avoid large blocks of gaps. Sequences of COI were translated to amino acids to ensure proper coding. The nuclear small ribosomal subunit (18 S) was amplified

2.1.2. Phylogenetic and species delimitation (SD) analyses

Multiple "discovery"-type species delimitation methods (*sensu* Carstens et al., 2013) were used, so that consistency across methods could be assessed: the ABGD algorithm (automated barcode gap discovery; Puillandre et al., 2011), GMYC (general mixed Yule coalescent; Pons et al., 2006), and bPTP (Bayesian Poisson tree process; Zhang et al., 2013).

The ABGD algorithm takes aligned sequences from a single gene as input, and requires no phylogentic tree or *a priori* species hypotheses. Because several genera of desmosomatids are thought to be para- or polyphyletic and poorly delimited by current morphological characters (e.g. *Eugerda* Meinert, 1890 vs. *Desmosoma* G.O. Sars 1864 or *Eugerdella* Kussakin 1965, *Disparella* Hessler 1970, and *Mirabilicoxa* Hessler 1970 as one group); (compare Brix 2007; Brix, Kaiser and Jennings personal

Table 1
List of voucher specimens used for the genetic study located at the Zoological Museum Hamburg (ZMH) including Field ID (BoLD) and GenBank accession numbers per gene. Generally, genus identification is given, described species are listed with cf., but the full name. Specimens with type status listed first indicating also species names. Further listed voucher specimens ordered by Field ID, not indicating species allocation except species described in Kaiser et al. (In this Issue). For exact positions for each station see Devey et al. (In this issue).

Field ID (BoLD)	Family	Genus	Sex	Station	Collection code	GenBank accession numbers			BIN	type status	species name (if applicable)
					ZMH K-	COI	16 S	18 S			
VTDes134	Desmosomatidae	*Eugerdella*	female	6–8	45783	MF325488			BOLD: ADG2983	holotype	*Eugerdella egoni*
VTDes131	Desmosomatidae	*Eugerdella*	female	6–8	45788	MF325485		MF325733	BOLD: ADG2983	paratype	*E. egoni*
VTDes132	Desmosomatidae	*Eugerdella*	female	6–8	45789	MF325497			BOLD: ADG2983	paratype	*E. egoni*
VTDes133	Desmosomatidae	*Eugerdella*	female	6–8	45792					paratype	*E. egoni*
VTDes135	Desmosomatidae	*Eugerdella*	female	6–8	45790	MF325499	MF325647	MF325740	BOLD: ADG2692	paratype	*E. egoni*
VTDes136	Desmosomatidae	*Eugerdella*	female	6–8	45791		MF325646	MF325739		paratype	*E. egoni*
VTDes097	Desmosomatidae	*Eugerdella*	male	6–7	45784	MF325494			BOLD: ADG2983	paratype	*E. egoni*
VTDes098	Desmosomatidae	*Eugerdella*	female	6–7	45785	MF325496		MF325738	BOLD: ADG2983	paratype	*E. egoni*
VTDes099	Desmosomatidae	*Eugerdella*	female	6–7	45786	MF325493		MF325737	BOLD: ADG2983	paratype	*E. egoni*
VTDes100	Desmosomatidae	*Eugerdella*	n.a.	6–7	45787	MF325492			BOLD: ADG2983	paratype	*E. egoni*
VTDes147	Desmosomatidae	*Prochelator*	female	9–8	46201	MF325540			BOLD: ADG0009	holotype	*Prochelator barnacki* = sp. I
VTDes108	Desmosomatidae	*Prochelator*	male	6–7	46202	MF325543		MF325760	BOLD: ADG0009	paratype	*Prochelator barnacki* = sp. I
VTDes115	Desmosomatidae	*Prochelator*	female	6–7	46203	MF325541		MF325759	BOLD: ADG0009	paratype	*Prochelator barnacki* = sp. I
VTDes014	Desmosomatidae	*Whoia*	female	2–6	46204	MF325578		MF325782	BOLD: ADG3380	paratype	*Whoia sockei* = sp. D
VTDes155	Desmosomatidae	*Whoia*	female	9–8	46205	MF325515			BOLD: ADG2296	holotype	*Whoia sockei* = sp. D
VTDes013	Nannoniscidae	*Ketosoma*	male	2–6	46140	MF040892	KY951730	KY951737	BOLD: ADG0809	holotype	*Ketosoma vemae* Brix & Kihara 2017
VTDes569	Nannoniscidae	*Ketosoma*	female	6–7	46141		KY951729			holotype	*Ketosoma hessleri* Kaiser & Brix 2017
VTDes001	Desmosomatidae	*Disparella*	male	2–6	46206	MF325479	MF325639	MF325728	BOLD: ADG0960	voucher	*Disparella* cf. *valida* Hessler (1970)
VTDes003	Nannoniscidae	*Exiliniscus*	female	2–6	46207	MF325501			BOLD: ADG3415	voucher	
VTDes004	Nannoniscidae	*Exiliniscus*	female	2–6	46208	MF325506			BOLD: ADG3415	voucher	
VTDes005	Nannoniscidae	*Exiliniscus*	male	2–6	46209	MF325504	MF325650		BOLD: ADG3418	voucher	
VTDes006	Desmosomatidae	*Desmosoma*	female	2–6	46210		XXXXXXXX			voucher	
VTDes007	Desmosomatidae	*Torwolia*	female	2–6	46211	MF325577	MF325692	MF325781	BOLD: ADG0799	voucher	*Torwolia* cf. *creper* Hessler (1970)
VTDes008	Desmosomatidae	*Pseudomesus*	female	2–6	46212	MF325557	MF325684	MF325770	BOLD: ADG2271	voucher	*Pseudomesus* cf. *pitombo* Kaiser & Brix, 2007
VTDes009	Desmosomatidae	*Chelator*	female	2–6	46213	MF325450	MF325613		BOLD: ADG2083	voucher	sp. A (Figs. 2,3)
VTDes010	Desmosomatidae	*Desmosoma*		2–6	46214	MF325476			BOLD: ADF9662	voucher	*Desmosoma* cf. *renatae* Brix, 2007
VTDes011	Desmosomatidae	*Eugerdella*	female	2–6	ZMH K 46215	MF325489		MF325735	BOLD: ADG2985	voucher	
VTDes012	Desmosomatidae	*Eugerdella*	female	2–6	ZMH K 46216	MF325490		MF325736	BOLD: ADG2689	voucher	
VTDes015	Desmosomatidae	*Eugerda*	female	2–6	ZMH K 46217	MF325480				voucher	
VTDes016	Desmosomatidae	*Mirabilicoxa*	male	2–6	ZMH K 46218	MF325522			BOLD: ADG2546	voucher	
VTDes017	Desmosomatidae	*Mirabilicoxa*		2–6	ZMH K 46219	MF325510	MF325653		BOLD: ADG2549	voucher	sp. F (Figs. 2,3)
VTDes018	Desmosomatidae	*Mirabilicoxa*	male	2–6	ZMH K 46220	MF325508	MF325651		BOLD: ADG2549	voucher	sp. F (Figs. 2,3)
VTDes019	Desmosomatidae	*Pseudomesus*	female	2–6	ZMH K 46221	MF325554	MF325681	MF325768	BOLD: ADG2271	voucher	*Pseudomesus* cf. *pitombo* Kaiser & Brix, 2007
VTDes020	Desmosomatidae	*Pseudomesus*	male	2–6	ZMH K 46222	MF325550	MF325678	MF325765	BOLD: ADG2271	voucher	*Pseudomesus* cf. *pitombo* Kaiser & Brix, 2007
VTDes021	Desmosomatidae	*Pseudomesus*	male	2–6	ZMH K 46223	MF325552			BOLD: ADG1980	voucher	
VTDes022	Nannoniscidae	*Exiliniscus*	male	2–6	ZMH K 46224	MF325505			BOLD: ADG3418	voucher	
VTDes023	Desmosomatidae	*Eugerdella*	female	2–6	ZMH K 46225	MF325498	MF325645		BOLD: ADG2690	voucher	
VTDes024	Desmosomatidae	*Torwolia*	female	2–6	ZMH K 46226	MF325576	MF325691	MF325780	BOLD: ADG0798	voucher	
VTDes026	Nannoniscidae	*Exiliniscus*	female	2–6	ZMH K 46228	MF325503	MF325649		BOLD: ADG3417	voucher	sp. Y (Figs. 2,3)
VTDes028	Desmosomatidae	*Mirabilicoxa*	female	2–6	ZMH K 46230	MF325519	MF325659		BOLD: ADG2549	voucher	sp. F (Figs. 2,3)
VTDes029	Nannoniscidae	*Ketosoma*		2–7	ZMH K 46231	MF325507		MF325742	BOLD: ADG0195	voucher	
VTDes031	Desmosomatidae	*Parvochelus*	female	2–7	ZMH K 46233	MF325537	MF325671	MF325756	BOLD: ADG1435	voucher	*Parvochelus russus* Brix & Kihara, 2015 = sp. E (Figs. 2,3)
VTDes032	Desmosomatidae	*Pseudomesus*	female	2–7	ZMH K 46234	MF325548			BOLD: ADG1980	voucher	
VTDes033	Desmosomatidae	*Chelator*	female	2–7	ZMH K 46235	MF325441	MF325604	MF325707	BOLD: ADG0336	voucher	sp. A (Figs. 2,3)
VTDes034	Desmosomatidae	*Chelator*	female	2–7	ZMH K 46236	MF325473	MF325635	MF325723	BOLD: ADG0651	voucher	
VTDes035	Desmosomatidae	*Eugerdella*	female	2–7	ZMH K 46237	MF325487			BOLD: ADG2985	voucher	
VTDes036	Desmosomatidae	*Disparella*		2–7	ZMH K 46238	MF325478		MF325727	BOLD: ADG0959	voucher	
VTDes038	Nannoniscidae	*Nannoniscus*	female	4–8	ZMH K 46240	MF325529	MF325664	MF325749	BOLD: ADG3529	voucher	
VTDes039	Nannoniscidae	*Regabellator*	female	4–8	ZMH K 46241	MF325566		MF325775	BOLD: ADG3760	voucher	sp. K (Figs. 2,3)
VTDes041	Desmosomatidae	*Mirabilicoxa*	female	4–8	ZMH K 46243	MF325512	MF325655		BOLD: ADG2301	voucher	sp. F (Figs. 2,3)

(*continued on next page*)

Table 1 (*continued*)

Field ID (BoLD)	Family	Genus	Sex	Station	Collection code	GenBank accession numbers			BIN	type status	species name (if applicable)
					ZMH K-	COI	16 S	18 S			
VTDes042	Desmosomatidae	*Chelator*	male	4–8	ZMH K 46244	MF325471	MF325633	MF325721	BOLD: ADF9117	voucher	*Chelator* cf. *aequabilis* Brix & Leese, 2014
VTDes043	Desmosomatidae	*Chelator*	male	4–8	ZMH K 46245	MF325444	MF325607	MF325709	BOLD: ADG0336	voucher	sp. A (Figs. 2,3)
VTDes044	Desmosomatidae	*Chelator*	male	4–8	ZMH K 46246	MF325461	MF325623		BOLD: ADG0336	voucher	sp. A (Figs. 2,3)
VTDes045	Desmosomatidae	*Chelator*	female	4–8	ZMH K 46247	MF325415	MF325579	MF325693	BOLD: ADG0337	voucher	sp. A (Figs. 2,3)
VTDes046	Desmosomatidae	*Chelator*	female	4–8	ZMH K 46248	MF325451	MF325614		BOLD: ADF9117	voucher	*Chelator* cf. *aequabilis* Brix & Leese, 2014
VTDes047	Desmosomatidae	*Chelator*	female	4–8	ZMH K 46249	MF325475	MF325637	MF325725	BOLD: ADF9117	voucher	*Chelator* cf. *aequabilis* Brix & Leese, 2014
VTDes048	Desmosomatidae	*Chelator*	female	4–8	ZMH K 46250	MF325456	MF325619		BOLD: ADG0338	voucher	sp. A (Figs. 2,3)
VTDes049	Desmosomatidae	*Chelator*	female	4–8	ZMH K 46251	MF325474	MF325636	MF325724	BOLD: ADF9117	voucher	*Chelator* cf. *aequabilis* Brix & Leese, 2014
VTDes050	Desmosomatidae	*Chelator*	male	4–8	ZMH K 46252	MF325469	MF325631		BOLD: ADF9117	voucher	*Chelator* cf. *aequabilis* Brix & Leese, 2014
VTDes051	Desmosomatidae	*Chelator*	male	4–8	ZMH K 46253	MF325464	MF325626	MF325717	BOLD: ADG0337	voucher	sp. A (Figs. 2,3)
VTDes052	Desmosomatidae	*Chelator*	female	4–8	ZMH K 46254	MF325446	MF325609		BOLD: ADG0337	voucher	sp. A (Figs. 2,3)
VTDes053	Desmosomatidae	*Chelator*	female	4–8	ZMH K 46255	MF325430	MF325593	MF325699	BOLD: ADG0337	voucher	sp. A (Figs. 2,3)
VTDes055	Desmosomatidae	*Chelator*	male	4–8	ZMH K 46256	MF325467	MF325629		BOLD: ADF9117	voucher	*Chelator* cf. *aequabilis* Brix & Leese, 2014
VTDes056	Desmosomatidae	*Chelator*	female	4–8	ZMH K 46257	MF325433	MF325596	MF325702	BOLD: ADG0337	voucher	sp. A (Figs. 2,3)
VTDes057	Desmosomatidae	*Pseudomesus*	female	4–9	ZMH K 46258	MF325553	MF325680	MF325767		voucher	
VTDes058	Nannoniscidae	*Exiliniscus*	female	4–9	ZMH K 46259	MF325502	MF325648			voucher	sp. Y (Fig. 3)
VTDes059	Nannoniscidae	*Rapaniscus*	female	4–9	ZMH K 46260	MF325561	MF325685	MF325772	BOLD: ADF9377	voucher	
VTDes060	Desmosomatidae	*Parvochelus*	female	4–9	ZMH K 46261		MF325669	MF325754		voucher	
VTDes061	Desmosomatidae	*Chelator*	male	4–9	ZMH K 46262	MF325440	MF325603	MF325706	BOLD: ADG0337	voucher	sp. A (Figs. 2,3)
VTDes062	Desmosomatidae	*Chelator*	male	4–9	ZMH K 46263	MF325418	MF325582		BOLD: ADF9117	voucher	*Chelator* cf. *aequabilis* Brix & Leese, 2014
VTDes063	Desmosomatidae	*Chelator*	male	4–9	ZMH K 46264	MF325416	MF325580	MF325694	BOLD: ADG0337	voucher	sp. A (Figs. 2,3)
VTDes064	Nannoniscidae	*Regabellator*	female	4–9	ZMH K 46265	MF325570	MF325688	MF325776	BOLD: ADG3760	voucher	sp. K (Figs. 2,3)
VTDes065	Desmosomatidae	*Mirabilicoxa*	female	2–7	ZMH K 46266	MF325517			BOLD: ADG2546	voucher	
VTDes066	Desmosomatidae	*Pseudomesus*	female	4–8	ZMH K 46267	MF325547	MF325676	MF325763	BOLD: ADG1981	voucher	
VTDes068	Desmosomatidae	*Chelator*	female	4–8	ZMH K 46268	MF325435	MF325598	MF325704	BOLD: ADG0337	voucher	sp. A (Figs. 2,3)
VTDes070	Nannoniscidae	*Regabellator*	female	4–8	ZMH K 46270	MF325573			BOLD: ADG3760	voucher	sp. K (Figs. 2,3)
VTDes071	Nannoniscidae	*Regabellator*	female	4–8	ZMH K 46271	MF325571		MF325777	BOLD: ADG3760	voucher	sp. K (Figs. 2,3)
VTDes072	Nannoniscidae	*Regabellator*	female	4–8	ZMH K 46272	MF325568			BOLD: ADG3760	voucher	sp. K (Figs. 2,3)
VTDes073	Desmosomatidae	*Pseudomesus*	male	4–8	ZMH K 46273	MF325549	MF325677	MF325764	BOLD: ADG1981	voucher	
VTDes074	Desmosomatidae	*Pseudomesus*	male	4–8	ZMH K 46274	MF325556	MF325683	MF325769	BOLD: ADG1981	voucher	
VTDes075	Nannoniscidae	*Panetela*	female	4–8	ZMH K 46275	MF325531			BOLD: ADG3669	voucher	
VTDes076	Nannoniscidae	*Panetela*	female	4–8	ZMH K 46276	MF325530		MF325750	BOLD: ADG3669	voucher	
VTDes077	Desmosomatidae	*Chelator*	male	4–8	ZMH K 46277	MF325459		MF325714	BOLD: ADF9117	voucher	*Chelator* cf. *aequabilis* Brix & Leese, 2014
VTDes078	Desmosomatidae	*Disparella*	female	6–7	ZMH K 46278	MF325477	MF325638	MF325726	BOLD: ADG0957	voucher	
VTDes079	Desmosomatidae	*Parvochelus*	male	4–9	ZMH K 46279	MF325535	MF325668		BOLD: ADG1434	voucher	
VTDes080	Desmosomatidae	*Parvochelus*	female	4–9	ZMH K 46280	MF325534	MF325667	MF325753	BOLD: ADG3077	voucher	
VTDes081	Desmosomatidae	*Pseudomesus*	male	4–9	ZMH K 46281	MF325555	MF325682		BOLD: ADG1981	voucher	
VTDes082	Desmosomatidae	*Pseudomesus*	male	4–9	ZMH K 46282	MF325551	MF325679	MF325766	BOLD: ADG1981	voucher	
VTDes083	Desmosomatidae	*Chelator*	male	4–9	ZMH K 46283	MF325466	MF325628	MF325719	BOLD: ADG0338	voucher	sp. A (Figs. 2,3)
VTDes084	Desmosomatidae	*Chelator*	male	4–9	ZMH K 46284	MF325470	MF325632		BOLD: ADF9117	voucher	*Chelator* cf. *aequabilis* Brix & Leese, 2014
VTDes085	Desmosomatidae	*Chelator*	male	4–9	ZMH K 46285	MF325449	MF325612		BOLD: ADG0337	voucher	sp. A (Figs. 2,3)
VTDes086	Desmosomatidae	*Chelator*	male	4–9	ZMH K 46286	MF325472	MF325634	MF325722	BOLD: ADF9117	voucher	*Chelator* cf. *aequabilis* Brix & Leese, 2014
VTDes087	Desmosomatidae	*Chelator*	female	4–9	ZMH K 46287	MF325454	MF325617		BOLD: ADG0337	voucher	sp. A (Figs. 2,3)
VTDes088	Desmosomatidae	*Chelator*	female	4–9	ZMH K 46288	MF325457	MF325620	MF325712	BOLD: ADG0338	voucher	sp. A (Figs. 2,3)
VTDes089	Desmosomatidae	*Chelator*	female	4–9	ZMH K 46289	MF325448	MF325611		BOLD: ADG0337	voucher	sp. A (Figs. 2,3)
VTDes090	Desmosomatidae	*Chelator*	female	4–9	ZMH K 46290	MF325453	MF325616	MF325711	BOLD: ADG0337	voucher	sp. A (Figs. 2,3)
VTDes091	Desmosomatidae	*Chelator*	female	4–9	ZMH K 46291	MF325436	MF325599		BOLD: ADG0337	voucher	sp. A (Figs. 2,3)
VTDes092	Desmosomatidae	*Chelator*	female	4–9	ZMH K 46292	MF325468	MF325630	MF325720	BOLD: ADF9117	voucher	*Chelator* cf. *aequabilis* Brix & Leese, 2014
VTDes093	Desmosomatidae	*Chelator*	female	4–9	ZMH K 46293	MF325428	MF325591		BOLD: ADG0336	voucher	sp. A (Figs. 2,3)
VTDes096	Desmosomatidae	*Eugerdella*	female	6–7	ZMH K 46294	MF325491			BOLD: ADG2983	voucher	*Eugerdella egoni* Tschesche & Brix sp. nov.
VTDes101	Nannoniscidae	*Nannoniscus*	female	6–7	ZMH K 46295	XXXXXXXX				voucher	
VTDes104	Nannoniscidae	*Rapaniscus*	male	6–7	ZMH K 46298	MF325562				voucher	
VTDes105	Nannoniscidae	*Regabellator*	female	6–7	ZMH K 46299	MF325567			BOLD: ADG3527	voucher	

(*continued on next page*)

Table 1 (*continued*)

Field ID (BoLD)	Family	Genus	Sex	Station	Collection code	GenBank accession numbers			BIN	type status	species name (if applicable)
					ZMH K-	COI	16 S	18 S			
VTDes106	Nannoniscidae	*Regabellator*	female	6–7	ZMH K 46300	MF325572			BOLD: ADG3527	voucher	
VTDes107	Desmosomatidae	*Mirabilicoxa*	female	8–4	ZMH K 46301	MF325524	MF325662		BOLD: ADG2300	voucher	
VTDes109	Desmosomatidae	*Chelator*	female	6–7	ZMH K 46302	MF325419	MF325583		BOLD: ADF9120	voucher	
VTDes110	Desmosomatidae	*Chelator*	female	6–7	ZMH K 46303	MF325434	MF325597	MF325703	BOLD: ADF9120	voucher	
VTDes111	Desmosomatidae	*Prochelator*	female	6–7	ZMH K 46304	MF325544	MF325674		BOLD: ADG2373	voucher	
VTDes112	Desmosomatidae	*Prochelator*	male	6–7	ZMH K 46305	MF325545		MF325761		voucher	
VTDes113	Desmosomatidae	*Chelator*	female	6–7	ZMH K 46306	MF325447	MF325610		BOLD: ADG2693	voucher	
VTDes114	Desmosomatidae	*Chelator*	female	6–7	ZMH K 46307	MF325442	MF325605	MF325708	BOLD: ADG2693	voucher	
VTDes116	Desmosomatidae	*Chelator*	male	6–7	ZMH K 46308	MF325424			BOLD: ADG3198	voucher	
VTDes117	Desmosomatidae	*Chelator*	female	6–7	ZMH K 46309	MF325432	MF325595	MF325701	BOLD: ADG2084	voucher	sp. C (Figs. 2,3)
VTDes118	Desmosomatidae	*Chelator*		6–7	ZMH K 46310	MF325443	MF325606		BOLD: ADG2693	voucher	
VTDes119	Desmosomatidae	*Chelator*	female	6–7	ZMH K 46311	MF325417	MF325581	MF325695	BOLD: ADG2693	voucher	
VTDes120	Desmosomatidae	*Chelator*	female	6–7	ZMH K 46312	MF325437	MF325600		BOLD: ADG2693	voucher	
VTDes121	Desmosomatidae	*Chelator*	female	6–7	ZMH K 46313	MF325423	MF325587		BOLD: ADG2693	voucher	
VTDes122	Desmosomatidae	*Chelator*	female	6–8	ZMH K 46314	MF325495	MF325644		BOLD: ADG2693	voucher	
VTDes123	Nannoniscidae		male	6–8	ZMH K 46315	XXXXXXXX				voucher	
VTDes124	Desmosomatidae	*Mirabilicoxa*	female	6–8	ZMH K 46316	MF325516	MF325658		BOLD: ADG2545	voucher	
VTDes125	Desmosomatidae	*Prochelator*	female	6–8	ZMH K 46317	MF325539	MF325673	MF325758	BOLD: ADG2373	voucher	
VTDes126	Desmosomatidae	*Chelator*	male	6–8	ZMH K 46318	MF325429	MF325592	MF325698	BOLD: ADG2693	voucher	
VTDes127	Desmosomatidae	*Chelator*	female	6–8	ZMH K 46319	MF325445	MF325608		BOLD: ADG2693	voucher	
VTDes128	Desmosomatidae	*Prochelator*	female	6–8	ZMH K 46320	MF325546	MF325675	MF325762	BOLD: ADG0010	voucher	
VTDes129	Nannoniscidae	Ketosoma	male	6–8	ZMH K 46321	MF325574	MF325689	MF325778	BOLD: ADG0196	voucher	
VTDes130	Desmosomatidae	*Parvochelus*	female	6–8	ZMH K 46322	MF325538	MF325672	MF325757	BOLD: ADG1433	voucher	*Parvochelus russus* Brix & Kihara, 2015 = sp. E (Fig. 3)
VTDes135	Desmosomatidae	*Eugerdella*		6–7	ZMH K 46323	MF325499	MF325647	MF325740	BOLD: ADG2692	voucher	sp. H (Figs. 2,3)
VTDes136a	Desmosomatidae	*Chelator*		6–7	ZMH K 46324		MF325646	MF325739		voucher	sp. X (Fig. 3)
VTDes137	Desmosomatidae	*Disparella*	female	6–8	ZMH K 46325	MF325422	MF325586	MF325696	BOLD: ADF9119	voucher	
VTDes138	Desmosomatidae	*Prochelator*	female	6–8	ZMH K 46326	MF325542			BOLD: ADG0011	voucher	
VTDes140	Desmosomatidae	*Mirabilicoxa*	female	6–8	ZMH K 46327	MF325513	MF325656			voucher	
VTDes141	Desmosomatidae	*Chelator*	female	6–8	ZMH K 46328	MF325463	MF325625	MF325716	BOLD: ADG2084	voucher	sp. C (Figs. 2,3)
VTDes142	Desmosomatidae	*Chelator*	female	6–8	ZMH K 46329	MF325455	MF325618		BOLD: ADG2693	voucher	
VTDes143	Desmosomatidae	*Chelator*		6–8	ZMH K 46330	MF325465	MF325627	MF325718	BOLD: ADG2693	voucher	
VTDes144	Desmosomatidae	*Chelator*		6–8	ZMH K 46331	MF325460	MF325622	MF325715	BOLD: ADG2084	voucher	sp. C (Figs. 2,3)
VTDes145	Desmosomatidae	*Chelator*		6–8	ZMH K 46332	MF325426	MF325589		BOLD: ADG2693	voucher	
VTDes146	Desmosomatidae	*Mirabilicoxa*		9–8	ZMH K 46333	MF325518		MF325744	BOLD: ADG2548	voucher	
VTDes148	Desmosomatidae	*Chelator*		9–8	ZMH K 46334	MF325431	MF325594	MF325700	BOLD: ADF9118	voucher	sp. B (Figs. 2,3)
VTDes149	Desmosomatidae	*Chelator*		9–8	ZMH K 46335	MF325427	MF325590	MF325697	BOLD: ADF9118	voucher	sp. B (Figs. 2,3)
VTDes150	Desmosomatidae	*Mirabilicoxa*		9–8	ZMH K 46336	MF325523			BOLD: ADG2548	voucher	
VTDes151	Desmosomatidae	*Mirabilicoxa*		9–8	ZMH K 46337	MF325525		MF325746	BOLD: ADG2553	voucher	
VTDes153	Desmosomatidae	*Chelator*	female	9–8	ZMH K 46338	MF325438	MF325601	MF325705	BOLD: ADF9118	voucher	sp. B (Figs. 2,3)
VTDes154	Desmosomatidae	*Eugerda*	male	9–8	ZMH K 46339	MF325482	MF325641	MF325731	BOLD: ADG3651	voucher	
VTDes156	Desmosomatidae	*Mirabilicoxa*	female	9–8	ZMH K 46340	MF325514	MF325657		BOLD: ADG2552	voucher	sp. G (Figs. 2,3)
VTDes158	Desmosomatidae	*Parvochelus*	female	8–4	ZMH K 46341	MF325536	MF325670	MF325755		voucher	*Parvochelus russus* Brix & Kihara, 2015 = sp. E (Figs. 2,3)
VTDes159	Desmosomatidae	*Torwolia*	female	8–4	ZMH K 46342	MF325575	MF325690	MF325779		voucher	
VTDes160	Desmosomatidae	*Eugerdella*	female	8–4	ZMH K 46343	MF325483	MF325642		BOLD: ADG2692	voucher	sp. H (Figs. 2,3)
VTDes161	Desmosomatidae	*Eugerdella*	female	8–4	ZMH K 46344	MF325484		MF325732	BOLD: ADG2688	voucher	
VTDes162	Desmosomatidae	*Parvochelus*	female	8–4	ZMH K 46345	MF325486	MF325643	MF325734	BOLD: ADG3076	voucher	
VTDes163	Desmosomatidae	*Eugerdella*	female	8–4	ZMH K 46346	XXXXXXXX				voucher	sp. H (Fig. 3)
VTDes164	Desmosomatidae	*Parvochelus*		8–4	ZMH K 46347	MF325533	MF325666	MF325752	BOLD: ADG3076	voucher	
VTDes165	Desmosomatidae	*Chelator*	female	8–4	ZMH K 46348	MF325421	MF325585		BOLD: ADF9115	voucher	sp. X (Fig. 3)
VTDes166	Desmosomatidae	*Chelator*		8–4	ZMH K 46349	MF325420	MF325584		BOLD: ADF9115	voucher	sp. X (Fig. 3)
VTDes167	Desmosomatidae	*Chelator*	female	8–4	ZMH K 46350	MF325425	MF325588		BOLD: ADF9116	voucher	sp. X (Fig. 3)
VTDes168	Desmosomatidae	*Eugerda*	male	8–4	ZMH K 46351		MF325640	MF325729		voucher	
VTDes169	Desmosomatidae	*Eugerda*	female	8–4	ZMH K 46352	MF325481		MF325730	BOLD: ADG3653	voucher	

(*continued on next page*)

Table 1 (*continued*)

Field ID (BoLD)	Family	Genus	Sex	Station	Collection code	GenBank accession numbers			BIN	type status	species name (if applicable)
					ZMH K-	COI	16 S	18 S			
VTDes170	Nannoniscidae	*Regabellator*	female	8–4	ZMH K 46353	MF325565			BOLD: ADG2522	voucher	sp. K (Figs. 2,3)
VTDes171	Desmosomatidae	*Mirabilicoxa*	female	8–4	ZMH K 46354	MF325520	MF325660	MF325745	BOLD: ADG3087	voucher	
VTDes172	Desmosomatidae	*Mirabilicoxa*	female	8–4	ZMH K 46355	MF325509	MF325652	MF325743	BOLD: ADG2300	voucher	
VTDes173	Desmosomatidae	*Mirabilicoxa*	female	8–4	ZMH K 46356	MF325511	MF325654		BOLD: ADG3086	voucher	
VTDes175	Desmosomatidae	*Mirabilicoxa*	male	8–4	ZMH K 46357	MF325521	MF325661		BOLD: ADG2552	voucher	sp. G (Figs. 2,3)
VTDes176	Desmosomatidae	*Chelator*		6–8	ZMH K 46358	MF325439	MF325602		BOLD: ADG2693	voucher	
VTDes177	Nannoniscidae	*Nannoniscus*		9–8	ZMH K 46359	MF325532	MF325665	MF325751	BOLD: ADG3757	voucher	
VTDes178	Nannoniscidae	*Regabellator*		6–7	ZMH K 46360	MF325559			BOLD: ADG3527	voucher	
VTDes179	Nannoniscidae	*Rapaniscus*		6–7	ZMH K 46361		MF325687	MF325774		voucher	
VTDes181	Nannoniscidae	*Exiliniscus*		9–8	ZMH K 46362	MF325500		MF325741	BOLD: ADG3419	voucher	
VTDes182	Nannoniscidae	*Ketosoma*		8–4	ZMH K 46363	MF325563				voucher	
VTDes184	Nannoniscidae	*Rapaniscus*		8–4	ZMH K 46364	MF325564	MF325686	MF325773		voucher	sp. C (Figs. 2,3)
VTDes186	Nannoniscidae	*Nannoniscus*		8–4	ZMH K 46365	MF325527		MF325748		voucher	
VTDes187	Desmosomatidae	*Chelator*		11–1	ZMH K 46366	MF325458	MF325621	MF325713	BOLD: ADF9118	voucher	sp. B (Figs. 2,3)
VTDes188	Desmosomatidae	*Pseudomesus*		6–8	ZMH K 46367	MF325558		MF325771	BOLD: ADG2272	voucher	
VTDes189	Nannoniscidae	*Nannoniscus*		6–8	ZMH K 46368	MF325528			BOLD: ADG3758	voucher	
VTDes199	Nannoniscidae	*Nannoniscus*		11–4	ZMH K 46369	MF325526	MF325663	MF325747	BOLD: ADG3759	voucher	
VTDes200	Desmosomatidae	*Chelator*		11–4	ZMH K 46370	MF325452	MF325615	MF325710	BOLD: ADF9118	voucher	sp. B (Figs. 2,3)
VBTDes201	Desmosomatidae	*Chelator*		11–4	ZMH K 46371	XXXXXXXX				voucher	sp. B (Figs. 2,3)
VTDes415	Desmosomatidae	*Chelator*	female	4–8	ZMH K 46372	MF325462	MF325624		BOLD: ADG0337	voucher	sp. A (Figs. 2,3)
VTDes419	Nannoniscidae	*Regabellator*	female	4–8	ZMH K 46373	MF325569			BOLD: ADG3760	voucher	sp. K (Fig. 2)

communication about unpublished results of a phylogeny dataset in preparation), ABGD was performed on uncorrected *p*-distances using the entire dataset, under the assumption that the smallest gap in the pairwise distance histogram reflected the boundary between intraspecific variation (smaller values) and interspecific variation (larger values).

The GMYC and bPTP algorithms require ultrametric phylogenetic trees built from single genes; these trees were estimated in BEAST2 v 2.4.4 (Bouckaert et al., 2014). Each gene was given a four-category gamma-distributed model of sequence mutation, with the gamma shape parameter and equilibrium base pair frequencies estimated. For COI, the HKY model was employed, whereas for 16 S the GTR model was employed. Strict clocks and Yule tree priors were used for both genes. To speed convergence, all gamma priors were replaced with lognormal priors, and all 1/X priors were replaced with exponential priors. Convergence of BEAST2 runs was assessed with Tracer v1.6 (Rambaut et al., 2014) to choose a burn-in such that all effective sample sizes (ESSs) were at least 200. The trees were produced and annotated with Bayesian posterior probabilities (PP) using TreeAnnotator in the BEAST2 package. The resulting gene trees were analyzed with GMYC and bPTP via their online servers; the single threshold model of GMYC was chosen over the multiple, as the former has been shown to outperform the latter (Fujisawa and Barraclough, 2013). To explore the effects of using these SD models on such a large dataset containing 1) deeper divergences than are typical and 2) numerous singleton specimens, the above SD analyses were also performed on two subclades: the genus *Chelator* Hessler 1970, and the closely related genera *Disparella, Eugerda, Eugerdella,* and *Mirabilicoxa* (results not shown as they mirror exactly the results shown in Figs. 2 and 3).

We decided to assign a species when minimum two of the three models applied decided for one species. As we used the BoLD database to store our data, we also retrieved Barcode Index Numbers (BIN) for each putative species, a fourth model decision. The BoLD system compares newly submitted sequences with the sequences already available in BoLD (Ratnasingham and Hebert, 2013) and worked fine in parallel to ABGD in amphipod custaceans (Jażdżewska et al. in press). Here, we indicate the BINs in Table 1, but do not include them into our species decisions because they were entirely congruent to the other methods. They match perfectly (usually with ABGD), and always match one of the other methods and are thus redundant).

2.2. Morphology

The specimen handling for light microscopy followed the methods described in Brix et al. (2015). Measurements were done according to Hessler (1970). Slides were prepared following Riehl et al. (2012) using the same protocol for Euparal. For the species description, we compared the following type material from different museum collections (ZMH = Zoological Museum, Hamburg; USNM = United States National Museum of Natural History, Washington; ZMUC or NHMD = Zoological Museum, University of Copenhagen):

Eugerdella serrata Brix, 2006, —Holotype, ZMH K – 41004; —Paratypes, ZMH K – 40106 and ZMH K – 40105; *Eugerdella falklandica* (Nordenstam, 1933), —Holotype, SMNH – type 766 (described as *Desmosoma falklandicum*); *Eugerdella margaretae* Zemko and Brix 2011—Holotype, adult female (ZMH K – 42701); *Eugerdella celata* Zemko and Brix 2011 —Holotype, adult female (ZMH K – 42711); *Prochelator sarsi*,—Holotype, female (USNM 138731), *Prochelator angolensis* Brenke, Brix and Knuschke, 2005—Holotype, female (ZMH K–40331A – K); *Prochelator angolensis* Brenke, Brix and Knuschke, 2005, —Paratypes female (ZMH K–40322 – K-40323); *Prochelator abyssalis* Hessler, 1970, —Holotype female (USNM 125107), *Prochelator hampsoni* Hessler, 1970, —Holotype female (USNM 125108), *Prochelator incomitatus* Hessler, 1970, —Holotype female (USNM 125109), *Thaumastosoma platycarpus* Hessler 1970, —Holotype, female (USNM

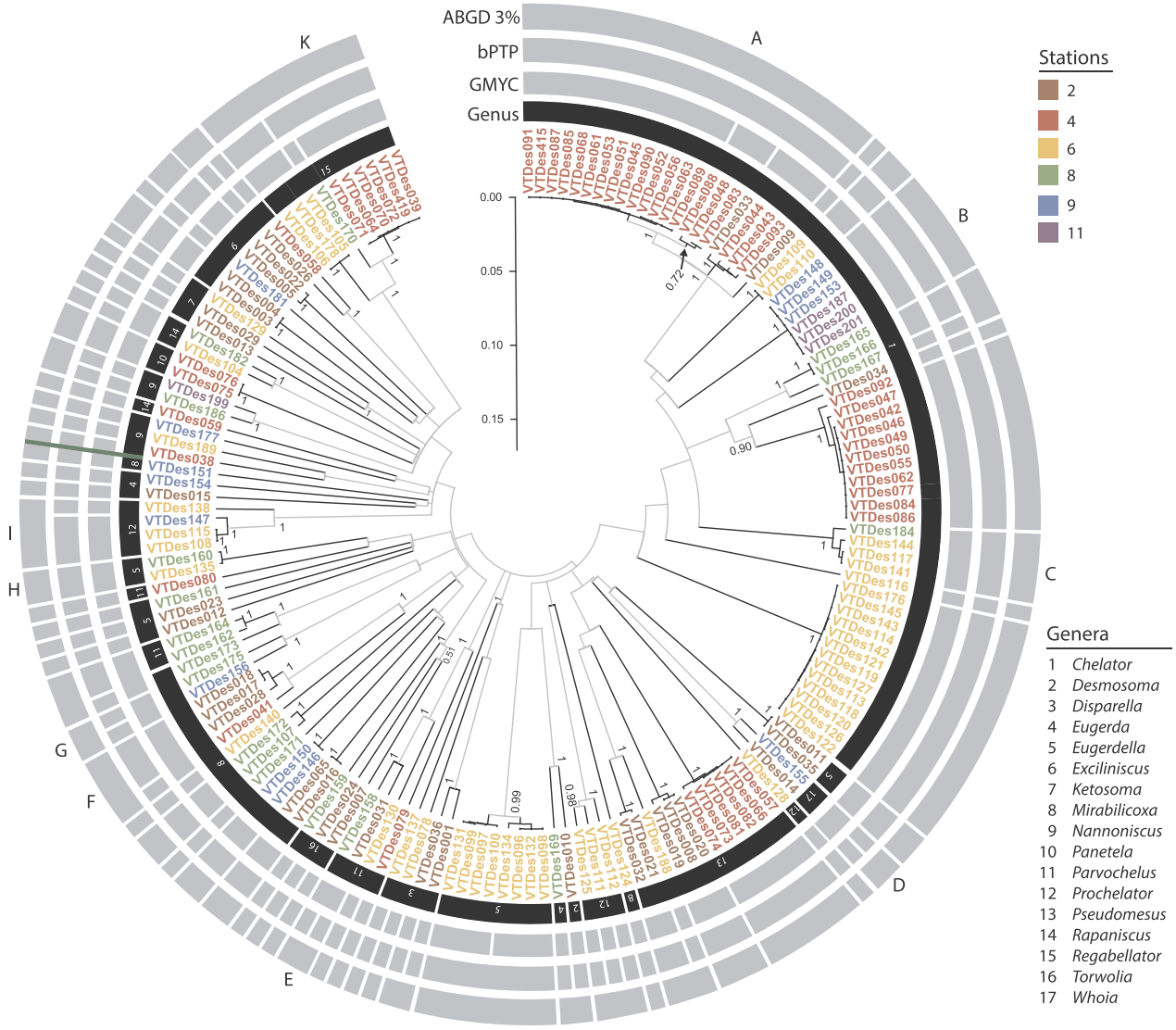

Fig. 2. Ultrametric, unrooted circle tree for COI. Numbers at nodes indicate Bayesian posterior probabilities and are shown only for nodes relevant to species delimitations (black branches; deeper tree structure is in grey). Color of specimen label denotes sampling station as in Fig. 1, listed in the upper legend. Numbers in the inner black ring denote morphological determination of genus, listed in the lower legend. Grey wedges in the outer rings indicate species delimitation results with method indicated at the top of each ring. The green line denotes the phylogenetic separation between desmosomatids (larger group) and nannoniscids (smaller group).

125112), *Balbidocolon atlanticum* Hessler, 1970, —Holotype female (USNM 125088)

2.2.1. Confocal laser scanning microscopy (CLSM)

Five specimens were used for CLSM as indicated in the descriptions below. An adult female specimen of *Eugerdella* Kussakin, 1965 (VTDes134), two specimens of *Whoia* Hessler, 1970 (VTDes014 and VTDes155), two adult specimens of *Prochelator* Hessler, 1970 (VTDes147 female and VTDes108 male), were stained with 1:1 solution of Congo Red and Acid Fuchsin overnight using procedures adapted from Michels and Büntzow (2010). The whole specimen was temporarily mounted onto a slide with glycerine; self-adhesive plastic reinforcement rings were used to support the coverslip (Kihara and Rocha, 2009; Michels and Büntzow, 2010). To mount the specimens in lateral view, Karo® light corn syrup was used as mounting medium and double sided tape pieces were combined in appropriate thickness, between the slide and coverslip to avoid a mechanical stress on the sample. The material was scanned using a Leica TCS SP5 (Leica, Wetzlar, Germany) equipped with a Leica DM5000 B upright microscope (Leica, Wetzlar, Germany) and three visible-light lasers (DPSS 10 mW 561 nm; HeNe 10 mW 633 nm; Ar 100 mW 458 nm, 476 nm, 488 nm and 514 nm) at the DZMB in Wilhelmshaven and a Leica TCS SPE with a Leica DM2500 upright microscope with four visible-light lasers (405, 488, 532, 635 nm) at the CeNak in Hamburg. The TCS units were used with the software LAS AF 2.2.1. - Leica Application Suite Advanced Fluorescence (Leica, Wetzlar, Germany). Series of stacks were obtained, collecting overlapping optical sections throughout the whole preparation; the imaging settings according to the software, are given in Table 2. Final images were obtained by maximum projection in Leica Application Suite or Fiji (Schneider et al., 2012; Schindelin et al., 2015). To obtain a three-dimensional representation from selected body parts, the data produced during the CLSM scanning was processed with the free software Drishti (Kamanli et al., 2017). Final plates were composed and adjusted for contrast and brightness using the software Adobe Photoshop CS4 and CS5.

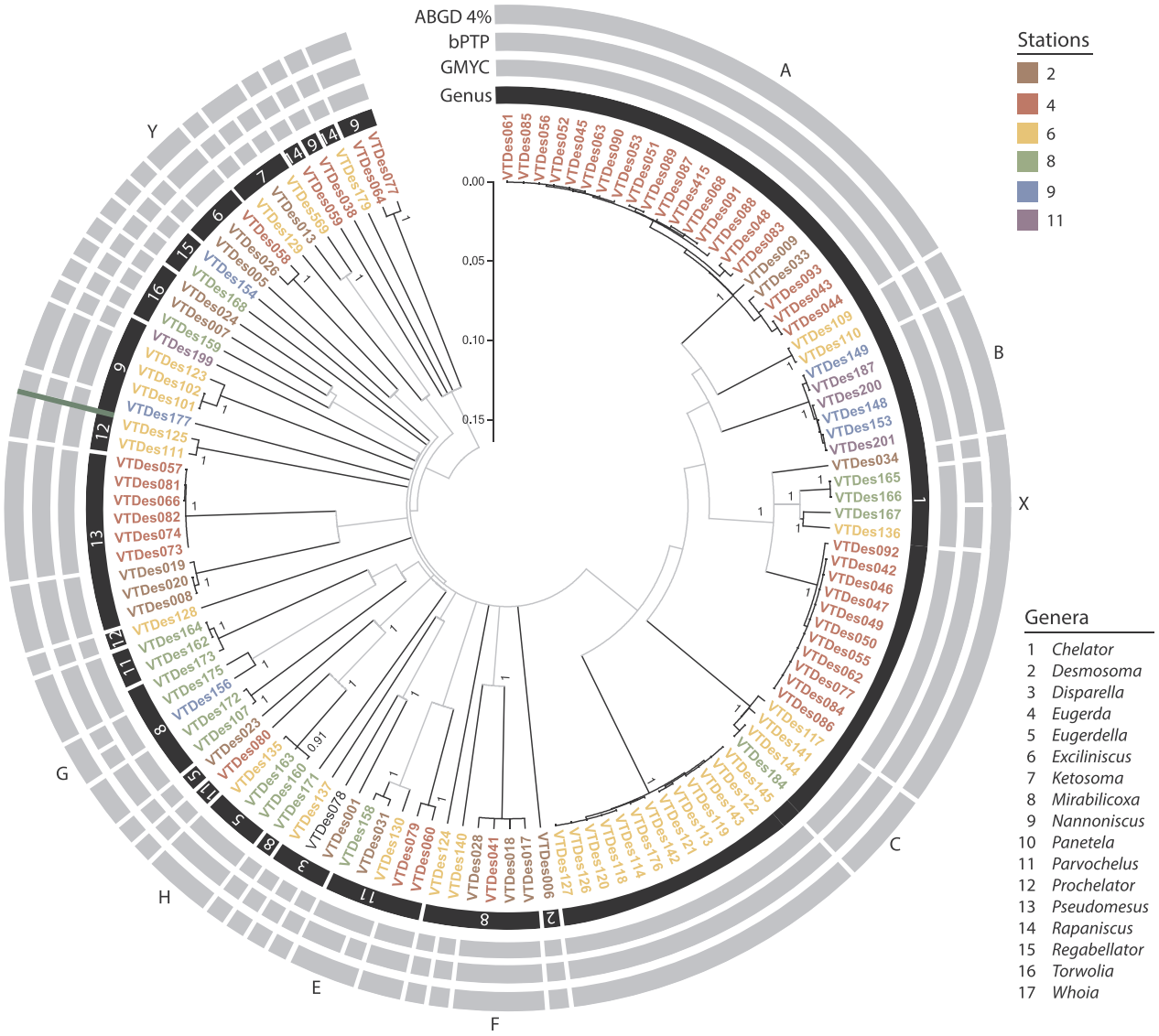

Fig. 3. Ultrametric, unrooted circle tree for 16 S. Tree depiction, symbols, and SD delimitations are as in Fig. 2.

2.2.2. Scanning Electron Microscopy (SEM)

Only specimens of the new *Eugerdella* species were treated for SEM because enough specimens were available. Three specimens were used for SEM. They were cleaned in an ultrasonic bath for 10 s, dehydrated in a series of ethanol concentrations, transferred to 100% acetone and critical point dried. Afterwards they were attached to the slide and sputter coated with graphite. Pictures were taken in a Leo 1525 SEM.

2.2.3. Digital drawing and manual inking

The material used for taxonomic illustrations was gently transferred into glycerine. The illustrations were drawn by hand with a *camera lucida* on a Leica DM2500. The pencil drawings were scanned at 600 dpi, these were either manually traced using a vector-graphic software (Adobe Illustrator CS5) following the methods of Coleman (2003, 2009) or alternatively a clean pencil drawing was scanned and directly converted into a line drawing using the "live trace" tool in Adobe Illustrator CS5. For best results we found the following settings to be useful: *Tracing Options > Adjustments: Mode (Black and White), Threshold (200), Blur (0); Trace Settings: Fills (no), Strokes (yes), Max Stroke Weight (100 px), Min Stroke Length (20 px), Path Fitting (2 px), Minimum Area (10 px), Corner Angle (20), Ignore White (yes)*. After tracing all lines were set to a stroke weight of 1 pt and then adjusted as needed. Setae were added as described by Coleman (2009). To increase the visual content of the black and white line drawings stippling was applied to some illustrations (Bober and Riehl, 2014). Figure plates were prepared using Adobe Photoshop CS5. The drawings were calibrated using a stage micrometre and the measurements were taken from the line drawings after Hessler (1970).

2.3. Abbreviations used in this study

A1 = antennula; A2 = antenna; Ip = Incisior process; lMd = left mandible; rMd = right mandible; lm = lacinia mobilis; mp = molar process; Op = operculum; PI-PVII = pereopods I-VII; Plt = pleotelson; Prn1–7 = pereonites 1–7; Up = uropods; ZMH = Zoological Museum, Hamburg; NADW = North Atlatic Deep Water; AABW = Antarctic Bottom Water; RF = Romanche Fracture Zone, VFZ = Vema Fracture Zone; VTF = Vema Transform Fault

Table 2
List of figures with information on microscope lenses and confocal laser scanning microscopy (CLSM) settings; Ch1 and Ch2 = detection channels 1 and 2.

Figure	Objective/ numerical aperture	Detected emission wavelength (nm)	Detector gain (V)/ nmplitude offset(%)	Electronic zoom	Pinhole aperture (µm)
Fig. 1A, B	HCX APO U-V-I 40.0 × 0.75 DRY UV	Ch1: 570 – 629 Ch2: 629 – 717	Ch 1: 667.0/ −1.7 Ch 2: 605.0/ −0.8	1.0X	113.2
Fig. 2A	HCX PL APO CS 63.0 × 1.40 OIL UV	Ch1: 570 – 629 Ch2: 629 – 717	Ch 1: 688.0/ −1.7 Ch 2: 667.0/ −0.8	2.0X	95.5
Fig. 2B	HCX PL APO CS 63.0 × 1.40 OIL UV	Ch1: 570 – 629 Ch2: 629 – 717	Ch 1: 701.0/ −1.7 Ch 2: 680.0/ −0.8	2.0X	95.5
Fig. 2C	HCX PL APO CS 63.0 × 1.40 OIL UV	Ch1: 570 – 629 Ch2: 629 – 717	Ch 1: 723.0/ −1.7 Ch 2: 702.0/ −0.8	2.0X	95.5
Fig. 2D	HCX PL APO CS 63.0 × 1.40 OIL UV	Ch1: 570 – 629 Ch2: 629 – 717	Ch 1: 731.0/ −1.7 Ch 2: 675.0/ −0.8	2.0X	110.0
Fig. 2E	HCX PL APO CS 63.0 × 1.40 OIL UV	Ch1: 570 – 629 Ch2: 629 – 717	Ch 1: 681.0/ −1.7 Ch 2: 643.0/ −0.8	1.6X	95.5
Fig. 2F	HCX APO U-V-I 40.0 × 0.75 DRY UV	Ch1: 570 – 629 Ch2: 629 – 717	Ch 1: 667.0/ −1.7 Ch 2: 656.0/ −0.8	3.1X	113.2
Fig. 3A	HCX PL APO CS 63.0 × 1.40 OIL UV	Ch1: 570 – 629 Ch2: 629 – 717	Ch 1: 681.0/ −1.7 Ch 2: 643.0/ −1.6	1.1X	95.5
Fig. 3B	HCX PL APO CS 63.0 × 1.40 OIL UV	Ch1: 570 – 629 Ch2: 629 – 717	Ch 1: 684.0/ −1.7 Ch 2: 662.0/ −1.6	2.0X	95.5
Fig. 3C	HCX PL APO CS 63.0 × 1.40 OIL UV	Ch1: 570 – 641 Ch2: 641 – 717	Ch 1: 695.0/ −1.7 Ch 2: 719.0/ −1.6	3.0X	95.5
Fig. 3D	HCX PL APO CS 63.0 × 1.40 OIL UV	Ch1: 570 – 641 Ch2: 641 – 717	Ch 1: 735.0/ −1.7 Ch 2: 700.0/ −1.6	2.2X	95.5
Fig. 3E	HCX PL APO CS 63.0 × 1.40 OIL UV	Ch1: 570 – 641 Ch2: 641 – 717	Ch 1: 669.0/ −1.7 Ch 2: 648.0/ −1.6	1.5X	95.5
Fig. 3F	HCX PL APO CS 63.0 × 1.40 OIL UV	Ch1: 570 – 641 Ch2: 641 – 717	Ch 1: 691.0/ −1.7 Ch 2: 662.0/ −1.6	2.0X	95.5

Table 3
Species (12: A-Y, marked in Figs. 2 and 3) occurring at more than one station indicating their distribution range along the VFZ. E, present in the eastern basin, Tr, present in the VFZ, W, present in the western basin.

Multi-station species	Span distance (km)	Distribution
A	660	E only
B	280	W only
C	630	Tr and E
D	2490	W, Tr, E
E	1920	Tr and E
F	660	E only
G	580	W and Tr
H	630	Tr and E
I	1210	W, Tr, E
K	1270	Tr and E
X	630	Tr and E
Y	660	E only

3. Results

3.1. Species delimitation

The ABGD analysis detected a barcode gap of 3–6% for COI and 4–6% for 16 S, in the whole dataset. For COI there were a very few *p*-distances occurring between 7% and 17%, but as the simplest criterion the species threshold was taken to be the beginning of the barcode gap (i.e. smallest value). Applying these 3% and 4% thresholds to the Bayesian COI and 16 S trees (Figs. 2 and 3), respectively, 72 species of desmosomatid and nannoniscid isopods were delimited. Most of them are new to science, after comparing them morphologically with described species from the Atlantic Ocean. Delimitations were largely consistent across genes (accounting for differences in sequencing success) and SD methods, though some differences did occur. A few of these differences consisted of a single specimen included in vs. excluded from a larger, consistently-delimited species. For COI, 29 species were delimited from a single specimen (single-specimen delimitation, SSD), and for 16 S there were 22 SSDs (the remaining COI singletons were not

Fig. 4. *Eugerdella egoni* sp. nov. holotype ZMH K–45783 (VTDes134), adult ovigerous female. CLSM micrograph. A. dorsal habitus; B. pereopod, surface rendering based on CLSM images; C. pleotelson, surface rendering based on CLSM images. Scale = 500 µm (A); 350 µm (B, C).

Fig. 5. CLSM *Eugerdella egoni* sp. nov. paratype ZMH K–44788 (VTDes131), adult non-ovigerous female, mouthparts. CLSM micrograph. A. left mandible; B. right mandible; C. maxillula; D. maxilliped. Scale = 100 µm.

successfully sequenced for 16 S so no determination could be made). All new sequences were deposited in GenBank, and alignments were deposited to TreeBASE (treebase.org).

When the geographical site of specimen collection was considered, it could be seen that the majority of delimited species' ranges do not cross the transform fault of the VFZ. In addressing putative species that occurred at multiple sites, we considered only those delimited by at least two SD methods. For COI, there were 10 delimited species occurring at multiple stations (Fig. 2 labelled A–K, Table 3). Seven of these were also present in 16 S (labelled with the same letters), and there were two additional multi-station species (MSSs) delimited in 16 S that were absent or differently delimited for COI (Fig. 3 labelled X and Y, Table 3). Ignoring SSDs and low-occurrence species (delimited from ten specimens or fewer), the most specimen-rich species in which all specimens came from a single sampling site were delimited from 14, 13, and 11. Six MSSs occurred in the transform fault and on one side of it, and two occurred in the transform fault and on both sides (D and I). Span distances, where they could be calculated as a rough estimate of species' ranges, are also given in Table 3.

From species occurring in the eastern VFZ five were potentially described species (see Table 1), mostly known from the DIVA-2 expedition (Brix, 2006b; Kaiser and Brix, 2005; Brix et al., 2015) plus one potential *Disparella* species (cf. *valida*) described by Hessler (1970). From species occurring in the western VFZ, two species were described, *Parvochelus russus* and *Eugerda* cf. *fulcimandibulata* Hessler 1970; *Parvochelus russus* known from the DIVA-2 and 3 expedition (Brix et al., 2015) occurring in the Guinea and Brazilian Basin. In total, seven species have been previously described (4.83%) and 62 are new to science (95.17%).

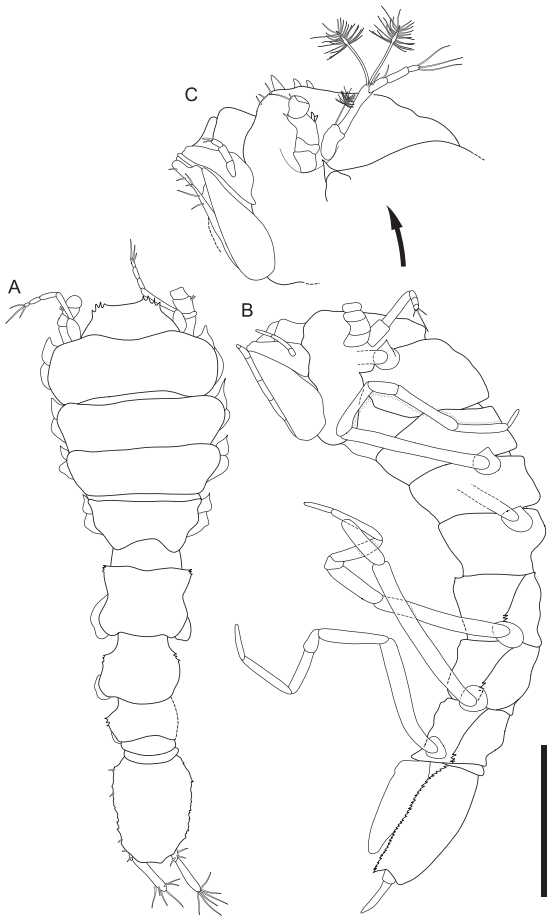

Fig. 6. *Eugerdella egoni* sp. nov. holotype ZMH K–45783, female. A. dorsal habitus; B. lateral habitus; C. cephalothorax and mouthparts, detail. Scale = 500 µm (A, B), 350 µm (C).

3.2. Species descriptions

Taxonomy
Family Desmosomatidae Sars, 1897
Subfamily Eugerdellatinae Hessler, 1970

3.2.1. Genus *Eugerdella* Kussakin, 1965

Diagnosis see Brix (2006) & Zemko & Brix (2011)
Synonymy *Desmosomella* Kussakin, 1965 (junior synonym)
Composition *Eugerdella armata* (Sars G.O., 1864); *Eugerdella celata* Zemko & Brix, 2011; *Eugerdella coarctata* (Sars G.O., 1899); *Eugerdella falklandica* (Nordenstam, 1933); *Eugerdella hessleri* Just, 1980

Eugerdella huberti Schnurr & Brix, 2012; *Eugerdella ischnomesoides* Hessler, 1970; *Eugerdella margaretae* Zemko & Brix, 2011; *Eugerdella minutula* Mezhov, 1986; *Eugerdella natator* (Hansen, 1916); *Eugerdella ordinaria* Mezhov, 1986; *Eugerdella polita* (Hansen, 1916); *Eugerdella pugilator* Hessler, 1970; *Eugerdella serrata* Brix, 2006; *Eugerdella theodori* Brix, 2007

***Eugerdella egoni* sp. nov. Tschesche and Brix (Figs. 4–13)**
Material
Holotype: Female, adult, 1.8 mm; ZMH K–45783 (VTDes134); designated here

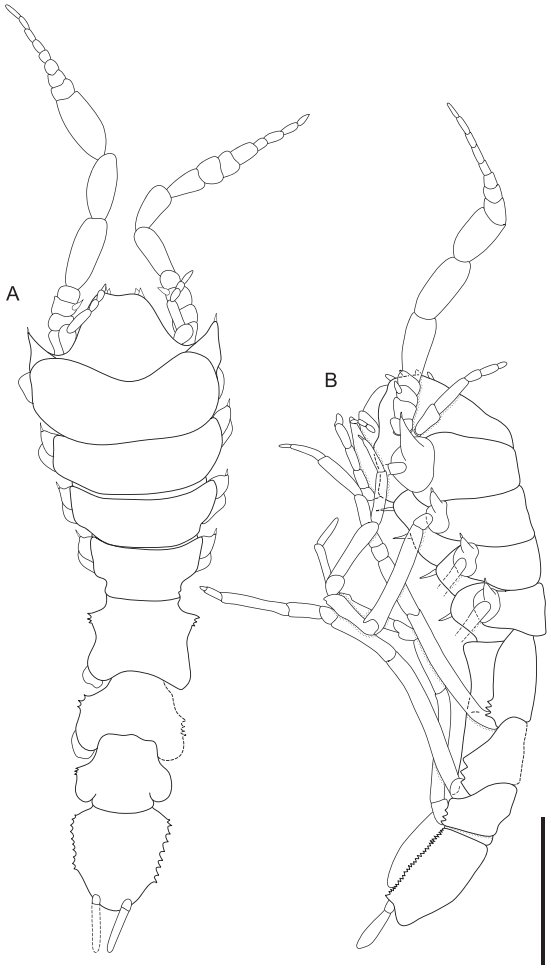

Fig. 7. Habitus *Eugerdella egoni* sp. nov. paratype ZMH K–45783, adult male (type 1). A. dorsal habitus; B. lateral habitus. Scale = 500 µm.

Type locality: VFZ, position: 10°22.293' N 36°55.852' W, depth 5127 m; RV Sonne So237; station 6–8; gear: C-EBS; January 2nd, 2015.

Paratypes: 1 male, adult, 2.24 mm; ZMH K–45784 (VTDes097) and 1 female ZMH K-46294 (VTDes096); January 2nd, 2015; VFZ; position: 10°21.547' N 36°55.585' W, depth 5079 m; RV Sonne So237; station 6–7; gear: C-EBS. 1 female, preparatory, ZMH K-45785 (VTDes098), VEMA-Transit, station 6–7; 1 female, preparatory, ZMH K-45786 (VTDes099), VEMA-Transit, station 6–7; 1 female, ZMH K-45787 (VTDes100), VEMA-Transit, station 6–7; 1 female, 2.2 mm; ZMH K–45788 (VTDes131); same locality as holotype. 1 female, preparatory, ZMH K-45789 (VTDes132), VEMA-Transit, station 6–8; 1 female, preparatory, ZMH K-45790 (VTDes135), VEMA-Transit, station 6–8; 1 female, adult, ZMH K-45791 (VTDes136), VEMA-Transit, station 6–8; 1 female, preparatory, ZMH K-45792 (VTDes133), VEMA-Transit, station 6–8; 1 female, preparatory, ZMH K-45793 (VTDes666-4), VEMA-Transit, station 6; 1 female, adult, ZMH K-45794 (VTDes666-5), VEMA-Transit, station 6. 3 SEM specimens: 1 male, adult, ZMH K-45798 (VTDes666-1), VEMA-Transit, station 6; 1 female, adult, ZMH K-44799 (VTDes666-2), VEMA-Transit, station 6.

Etymology

The species name refers to the grandfather of Claudia Tschesche, Egon.

Diagnosis

Body length 3.3 times longer than the body width. Lateral margins of Prn 5–7 with 4 anterolateral spines more prominent in male than in female. Prn 1–4 with one ventral spine each. Head tipped with row of eight spines like a crown. Lm of rMd with 3 teeth, lm of lMd distally serrated; Carpus of PI with ventral row of nine robust unequally bifid setae of irregular size. Lateral margin of Plt serrated. A1 of five articles.

Description of female

Habitus (ZMH K–45788/VTDes131 Figs. 4, 6) body 1.8 mm long, 3.2 longer than width of Prn2. Cephalon free, with cuticular folds arranged as ring of four small "horns" from dorsal view. Plt 1.2 longer than wide. Prn1 length 1.2 length Prn2. Lateral margins of Prn1–4 without spines. Prn5 width 0.8 length, anterior corners serrated (3 "spines"). Coxae 1–4 anteriorly produced, tipped with stout setae. Plt length 1.3 width. Posterolateral spines absent. Lateral margins serrated.

Antennula (ZMH K–45788/VTDes131 Fig. 9) with 5 articles, 0.2 body length. Article 1 with 4 broom setae and 2 simple setae. Article 2 length 6.3 width, 1.8 article 1 length; distally with 2 small and 2 large broom seta. Article 4 distally with 1 small broom seta. Article 5 with 1 broom seta, 1 slender seta and 2 aestetascs.

Antenna (ZMH K–45788/VTDes131 Fig. 9) with 15 articles, 0.5 body length. Article 5 distally with 1 simple seta and 3 broom setae, marginally with 1 simple seta. Article 6 distally with 3 broom setae, 2 short simple setae and 2 slender setae. Flagellar articles distally with few simple slender setae, distal flagellar article terminally with 4 long slender setae and 1 short simple seta. Relative length of articles: 1: 1.14: 2.29: 1: 5.71: 8.21: 4.14: 2.14: 2.29: 2.43: 1.71: 1.29: 1.

Mandibles (ZMH K–45788/VTDes131 Figs. 5, 8) with palpus, first article of Md palp without setae, second article marginally fringed with numerous fine setae, apical article marginally with many small simple setae and 2 longer terminal setae. Ip with 3 teeth. Lm of rMd with 3 teeth, lm of lMd distally serrated. RMd spine row containing six spines. LMd spine row containing five spines. Mp with 16 (lMd) and 15 (rMd) setae.

Maxillula (ZMH K–45788/VTDes131 Figs. 5, 8) Inner lobe smaller than outer lobe (0.6 times of outer lobe length), with 3 rows of five simple setae each. Outer lobe terminally with 12 strong spines, marginally with 10 pairs of setae. Outer lobe terminally with 9 strong spines, 5 small simple setae and 2 serrated setae.

Maxilla (ZMH K–45788/VTDes131 Figs. 5, 8) with 3 lobes. Medial lobe slightly shorter than outer lobes, terminally with 4 setae. Outer lobes length 7.1 width, terminally with 4 long seta. Inner lobes length 5.5 width dorsolaterally and ventrolaterally numerous simple setae.

Maxilliped (ZMH K–45788/VTDes131 Figs. 5, 8) epipodite length 5.2 width, length 1 endite length, distolaterally with comb of 8 fine setae. Endite with 2 coupling hooks, terminally with several simple setae and 3 star-shaped setae. On distolateral margin with 5 pairs of fine setae. Ventrolaterally with numerous small simple setae. Distomedially with several simple setae. Outer margins of palp articles 1 and 2 fringed with numerous fine setae. Palp article 1 without setae on inner margin. Palp article 2 with 2 setae on inner margin and palp article 3 with 3 setae on inner margin and several fine setae on outer margin. Article 4 and 5 terminally with 2 setae. Palp article 4 with 6 small simple setae on inner margin and article 5 with 1 simple seta on outer margin.

Pereopod I (ZMH K–45788/VTDes131 Fig. 11) basis terminally with 1 seta. Ischium length 1.3 width, distodorsally with 5 distally setulate setae, distoventrally with 2 distally setulate setae. Merus length 0.6 width, distodorsally with 1 unequally bifid seta and 1 small simple seta, distoventrally with 2 unequally bifid setae, 1 slender seta and 2 fine setae. Carpus with dias between base of propodus insertion and end of ventral setal row, length 1.9 width, distoventrally with a row of 8 unequally bifid setae of irregular length and ventromedially with one slender seta. Propodus length 2.3 width, ventrally fringed with combs

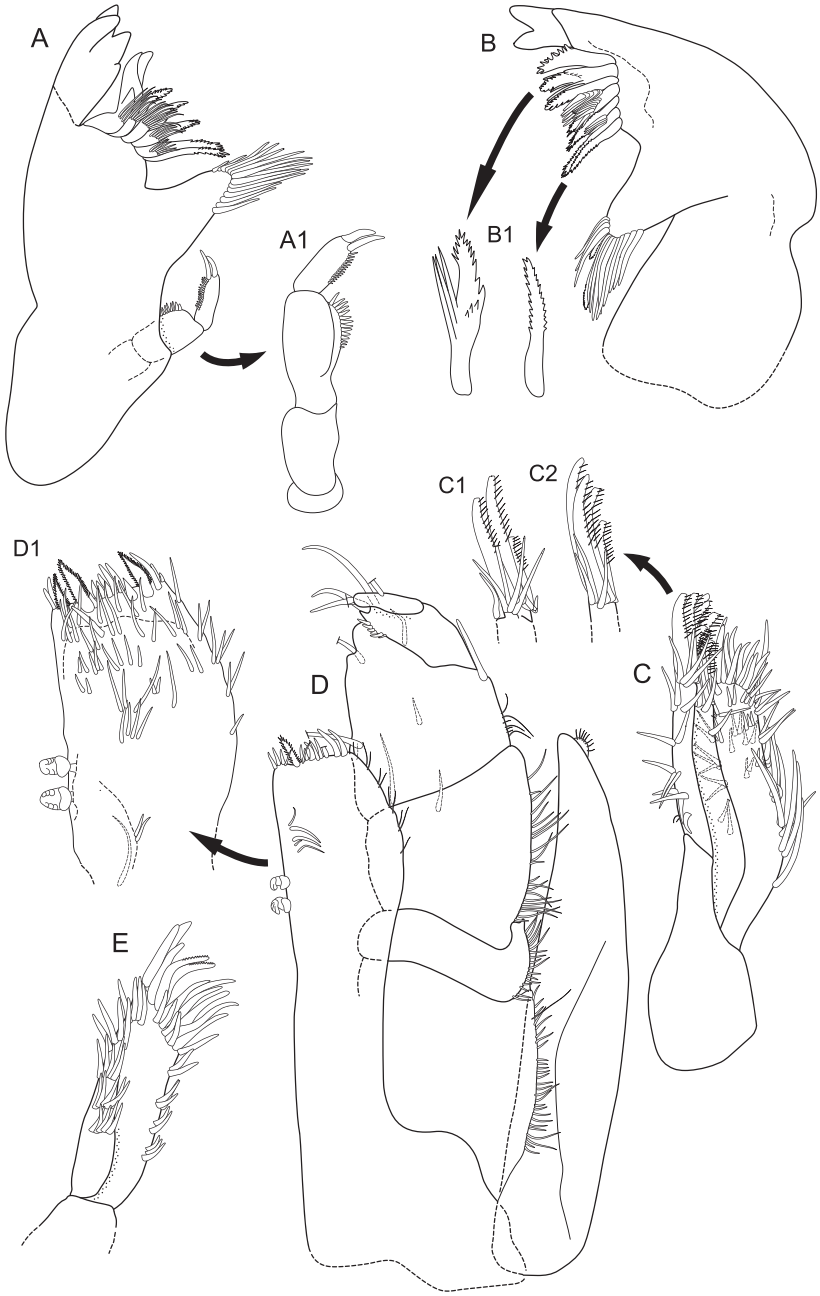

Fig. 8. *Eugerdella egoni* sp. nov. paratype VTDes131 ZMH K–45788, mouthparts. A. left mandible; A1. mandible palpus, detail; B. right mandible; B1. mandible setae, detail; C. maxilla; C1. maxilla lateral lobe; C2. maxilla, medial lobe; D. maxilliped; D1. maxilliped, detail; E. maxillula. Scale = 100 µm (A–E); 70 µm (A1, C1 + 2, D1); 50 µm (B1).

of 6 unequally bifid setae in a cuticular membrane, distodorsally with 4 unequally bifid setae and medially with 4 unequally bifid setae. Dactylus distomedially with 3 simple slender setae and terminally with 3 simple slender setae. Claw of dactylus consisting of 1 conate seta.

Pereopod II (ZMH K–45788/VTDes131 Fig. 11) basis length 7.55 width, dorsally with 2 small setae and 1 broom seta. Ischium length 2.2 width, dorsally and ventrally with one fine seta. Dorsomedially with one seta and distoventrally with one simple seta. Ischium length 5 times width, distodorsally with 1 small simple seta, ventrally with 2 distally setulate setae. Merus length 1.7 width, distodorsally with 1 seta and ventrally with 2 distally setulate seta. Carpus length 5.2 width, dorsally row of 4 distally setulate setae, ventrally with row of 7 distally setulate setae. Propodus length 4.3 width, dorsally with row of 4 setae, ventrally combs with fine setae and 4 small unequally bifid setae. Distally with 1 broom seta. Dactylus with two simple setae. Claw of dactylus consisting of 1 large simple conate seta, with 2 slender setae ventrally.

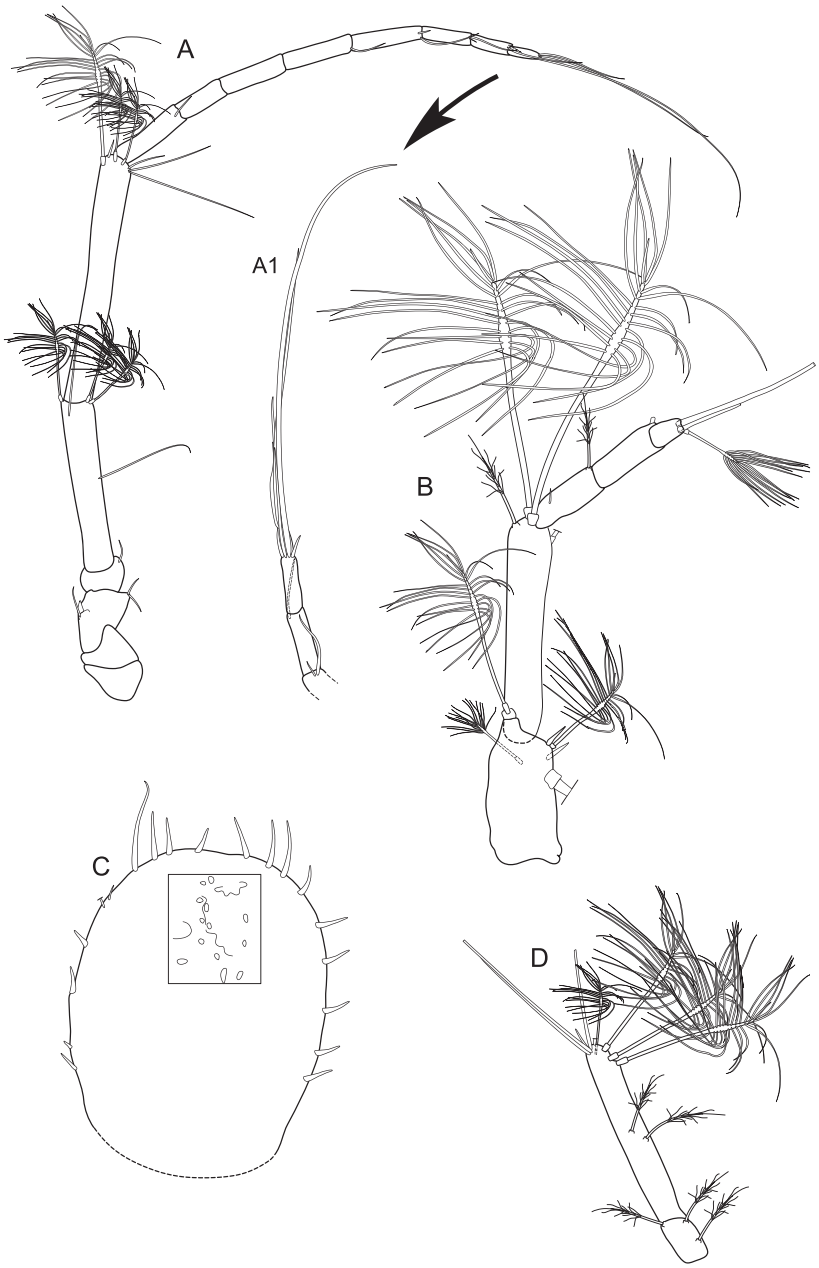

Fig. 9. *Eugerdella egoni* sp. nov. paratype VTDes131 ZMH K–45788, female appendages. A. antenna; A1. antenna, detail; B. antennula; C. operculum; D. uropod. Scale = 100 μm (A–C); 70 μm (A1, B).

Pereopod III (ZMH K–45788/VTDes131 Fig. 11) basis length 11.7 width. Ischium length 5.4 width, distoventrally with 2 distally setulate setae, dorsally with 2 distally setulate setae. Merus length 4.7 width, dorsally with 1 distally setulate seta, distolaterally with 3 distally setulate setae and 1 small seta. Carpus length 6.2 width, dorsally with row of 6 distally setulate setae and 1 simple seta, distodorsally with 1 broom seta. Propodus length 5.1 width, dorsally with 1 distally setulate setae, ventrally with 2 and distolaterally with 4 distally setulate setae. Dactylus distolaterally 3 three small slender setae and 1 long slender seta close to claw. Claw of dactylus consisting of 1 simple conate seta.

Pereopod IV (ZMH K–45788/VTDes131 Fig. 12) basis length 7.9 width, ventrally with 3 boom setae, dorsally with 1 broom seta and 3 simple seta, distodorsally with 1 slender distally setulate seta. Ischium length 3.7 width, distolaterally with 2 setae. Merus length 1.7 width, distolaterally with 3 setae. Carpus length 4.9 width, mediodorsally with row of 6 distally setulate setae, ventrally with 2 distally setulate ad 2 small setae. Propodus length 3.8 width, dorsally with 4 distally setulate setae, ventrally with 1 simple seta and distolaterally with 2 distally setulate setae and a comb with fine setae. Dactylus with 1 distally setulate seta in cuticular membrane and 1 small seta close to claw. Claw

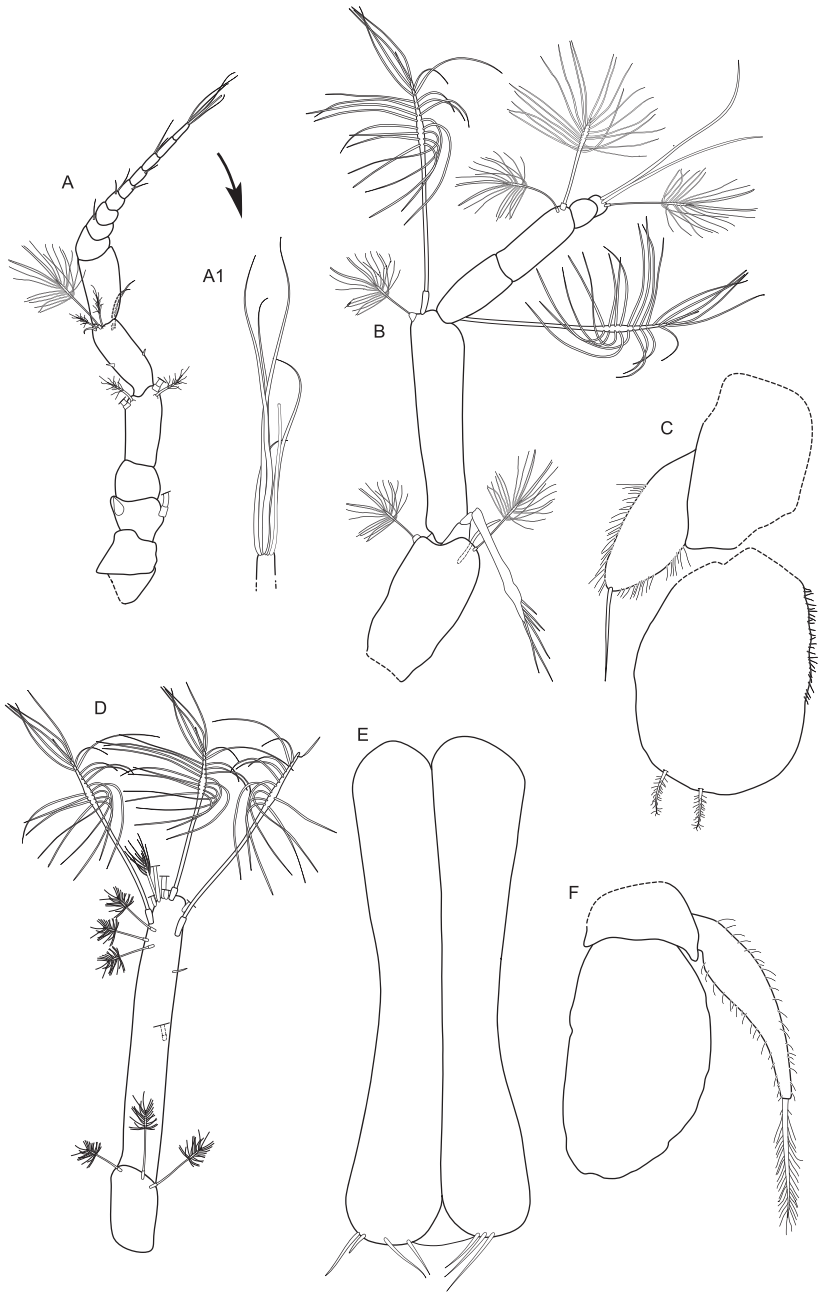

Fig. 10. *Eugerdella egoni* sp. nov. paratype VTDes097 ZMH K–45784, male appendages (type 1). A. antenna; A1. antenna, detail; B. antennula; C. pleopod 3; D. uropod; E. pleopod 1; F. pleopod 4. Scale = 100 µm (B–F); 400 µm (A).

of dactylus consisting of 2 simple conate seta and 2 long simple slender setae.

Pereopod V (ZMH K–45788/VTDes131 Fig. 12) basis length 9.5 width, with 3 broom setae. Ischium length 3.4 width, distodorsally with 1 simple seta, distoventrally with 1 seta. Merus length 0.9 width, dorsally with 2 setae close to ischium, distoventrally with 1 composed seta. Carpus length 3.9 width, dorsally with 2 distally setulate setae and 1 simple slender seta. Ventrally with row of 4 slender distally setulate setae. Propodus length 4.8 width, dorsally with row of 3 distally setulate setae. Ventrally with 1 long slender seta, 2 distally setulate setae, 2 long unequally bifid seta and 1 fine seta. Dactylus with 1 simple seta and 1 long slender seta close to claw. Claw of dactylus consisting of 2 slender and 1 conate seta.

Pereopod VII (ZMH K–45788/VTDes131 Fig. 12) basis length 7.5 width, with 4 small broom setae. Ischium length 3.5 width, dorsally with 1 long slender seta, ventrally with 2 setae. Merus length 1.1 width, distodorsally with 2 simple setae, distoventrally with 1 simple seta. Carpus length 6.1 width, dorsally 2 small setae, ventrally with 3 long simple slender setae. Propodus length 6.4 width, distodorsally with 3 slender setae and 1 small broom seta, ventrally with row of 4 long slender setae and 1 small seta. Claw of dactylus consisting of 2 long simple setae and 1 long conate seta.

Pleopod 2, operculum (ZMH K–45788/VTDes131 Figs. 9, 13) length 1.3 width. Lateral margins slightly convex. Lateral margins with 5 small simple setae each and distal margin with 8 simple setae. Surface structure present.

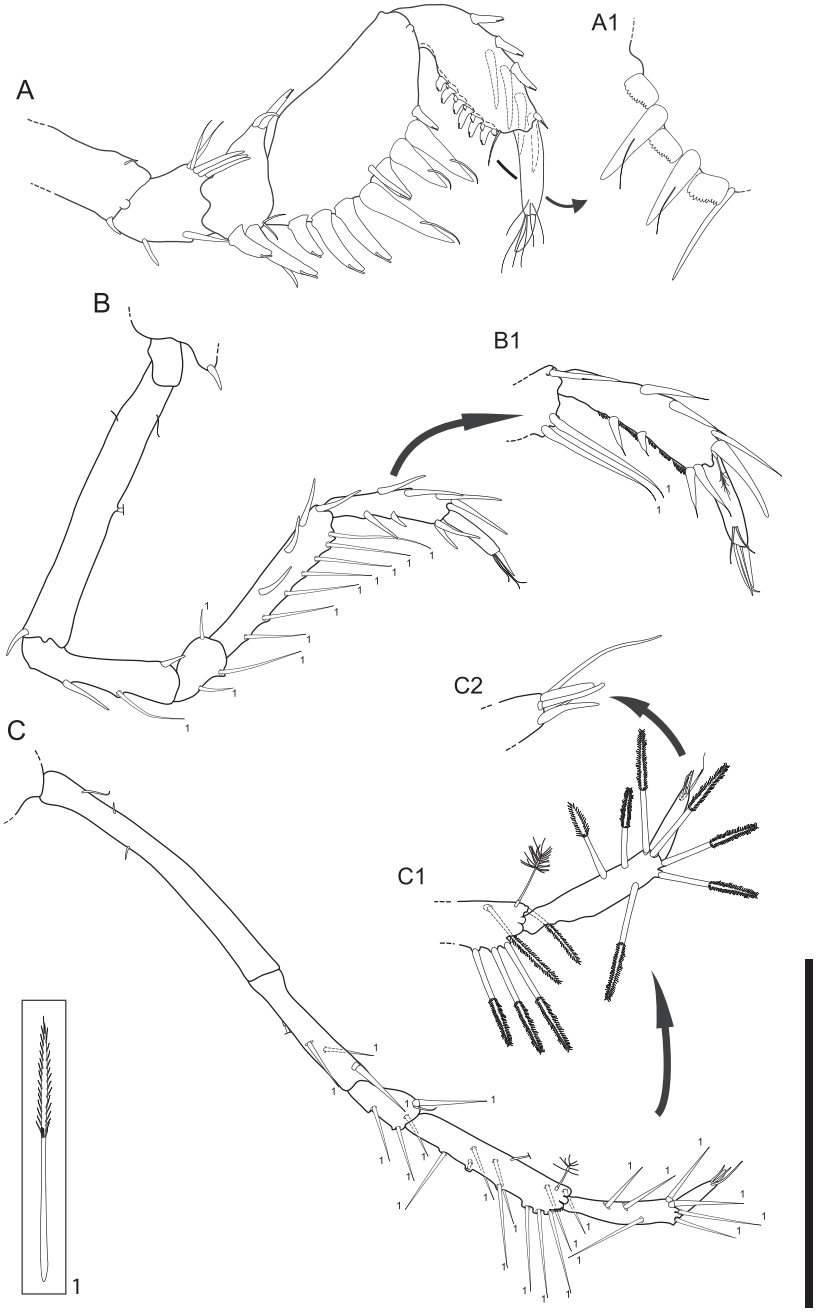

Fig. 11. *Eugerdella egoni* sp. nov. paratype VTDes131 ZMH K–45788, anterior pereopods. A. pereopod 1; A1. pereopod I, propodus detail; B. pereopod II; B1. pereopod II, propodus + dactylus detail; C. pereopod III; C1. pereopod III, propodus + dactylus detail; C2. pereopod III, dactylus, detail. Scale = 500 µm (B, C); 350 µm (A, B1, C1); 125 µm (A1, C2).

Pleopod 3 (ZMH K–45788/VTDes131 Fig. 9) endopod length 1.4 width, distally with 2 plumose setae. Outer margin with numerous fine setae. Exopod length 0.5 endopod length, terminally with several small fine setae and 1 long slender seta.

Pleopod 4 (ZMH K–45788/VTDes131 Fig. 9) endopod oval, length 1.7 width. Exopod length 5.5 width, 0.9 endopod length, lateral margins fringed with fine setae, terminally with 1 plumose seta.

Uropods (ZMH K–45788/VTDes131 Figs. 9, 13) biramous. Protopod with 3 broom setae. Endopod length 3.9 protopod length, endopod length 6.6 width, with 9 broom setae, 4 long simple setae and 1 fine seta on outer margin.

Sexual dimorphism of male

Habitus (ZMH K–45784/VTDes097 Figs. 7, 10) length 2.2 mm, 3.3 Prn2 width. Cephalon with cuticular folds arranged as ring of four small "horns" from dorsal view. Prn1 width 1.3 cephalon width. Prn1 length 1.2 Prn2 length, 1.1 Prn2 width. Prn5 length 0.8 width. Prn 1–4 with one ventromedial spine each. Coxae 1–4 more produced than female coxae, tipped with stout setae. Plt length 1.0 width. Posterolateral spines absent. Lateral margins serrated. The pleotelson shape varies between two different male types (compare Fig. 13).

Antenna (ZMH K–45784/VTDes097 3 Figs. 7, 10) length 0.6 body length, with 16 articles. Article 5 distally with 4 small broom setae,

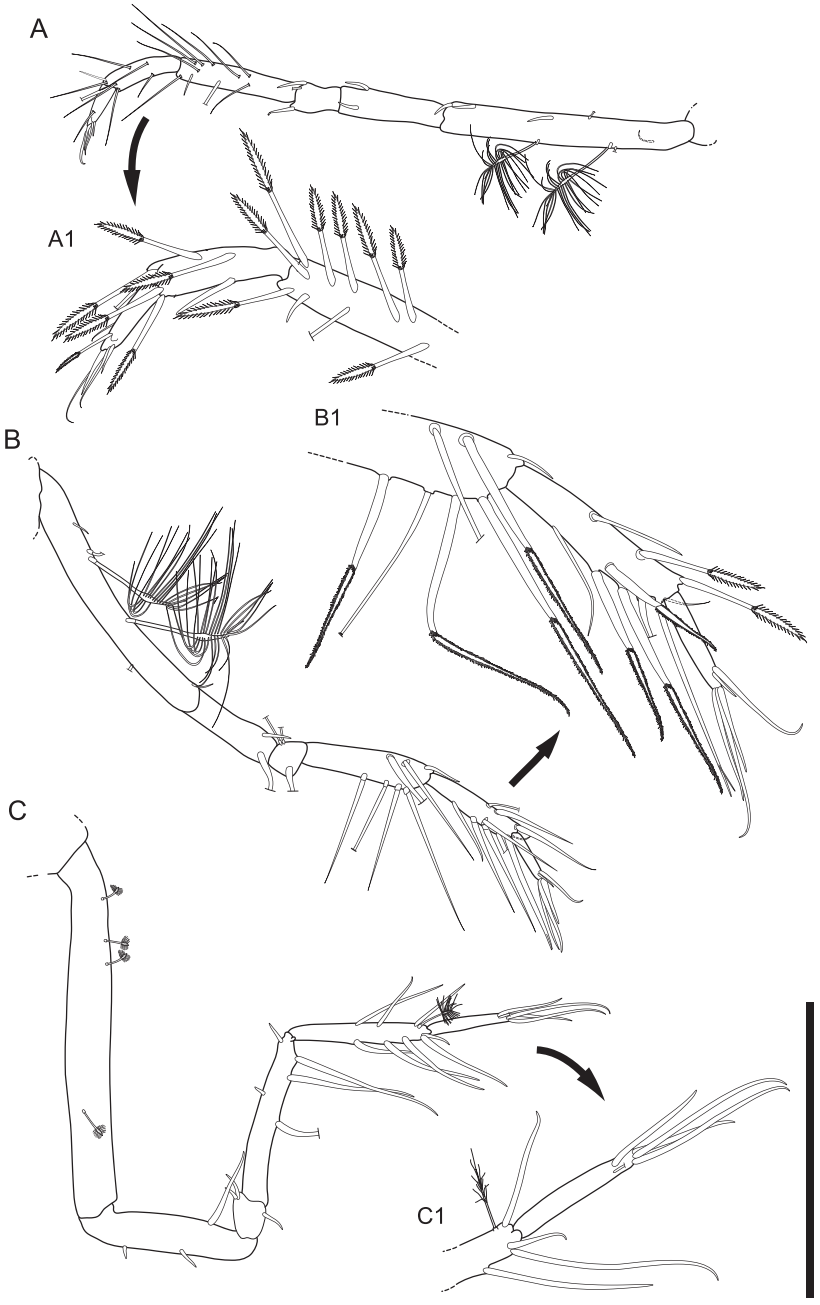

Fig. 12. *Eugerdella egoni* sp. nov. paratype ZMH K–45784, posterior pereopods. A. pereopod IV; A1. pereopod IV, carpus–dactylus detail; B. pereopod V; B1. pereopod V, carpus–dactylus detail; C. pereopod VII; C1. pereopod VII, propodus + dactylus detail. Scale = 500 μm (A–C); 350 μm (detail).

article 6 distally with 1 long broom seta, 2 small broom setae and 2 simple setae and 1 lateral fine setae. Flagellar articles distally with few setae, distal flagellar article terminally with 5 long slender setae and 1 aesthetasc.

Pleopod 1 (ZMH K–45784/VTDes097 783 Fig. 10) illustrated in situ, adult condition. Length 7.4 width. Lateral margins slightly concave, distal margin convex on each half with each ending with 4 small slender setae.

Remarks

Eugerdella egoni sp. nov. resembles most *E. pugilator* Hessler, 1970 or *E. serrata* Brix, 2007, but differing from both in the ventral setation of PI. Like the new species, in *E. serrata* the lateral margins of Plt are serrated as well as parts of the Prns. It differs from *E. serrata* by the head tipped with row of eight spines like a crown and the carpus of PI bearing a ventral row of nine robust unequally bifid setae of irregular size. Like *E. serrata*, *E. egoni* has ventral spines ventrally on the first four Prns. Ventral spines are present in some species of Desmosomatidae, but also Nannoniscidae and Macrostylidae Hansen, 1916. A detailed overview about the location of spines in the three families is given in Kaiser et al., (In this Issue) as in some genera spines also function as sexually dimorphic characters. In *E. egoni*, the ventral spines are present in both sexes. Nevertheless, we may see two different types of males: a more “female looking male” (type 1) with a fully developed pleopod I and a male differing in body shape, especially the pleotelson, from the female habitus (type 2: Fig. 13). The serration of the margins may be

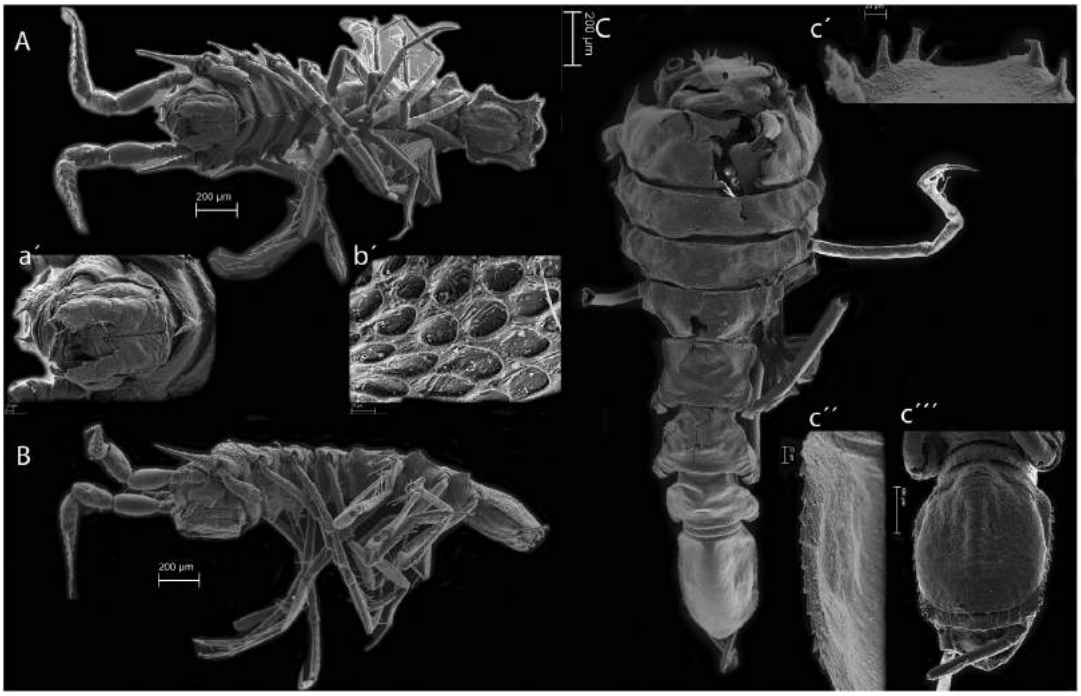

Fig. 13. SEM of *Eugerdella egoni* female and male (type 2) arranged different views: ZMH K-45794 (VTDes666-5), ZMH K-45798 (VTDes666-1), ZMH K-44799 (VTDes666-2).

Fig. 14. *Prochelator barnacki* sp. nov. holotype ZMH K-46201 (VTDes147), adult female, and paratype VTDes108, adult male. CLSM micrographs. A. dorsal habitus (ZMH K-46201); B. lateral habitus (ZMH K-46201); C. ventral habitus (ZMH K-46201); D. dorsal habitus (ZMH K-46202; VTDes108); E. lateral habitus (ZMH K-46202); F. ventral habitus (ZMH K-46202). Scale: 500 µm.

Fig. 15. *Prochelator barnacki* sp. nov. paratype ZMH K-46203 (VTDes115), adult non-ovigerous female, mouthparts. CLSM micrograph. A. mandible; B. maxilla; C. maxilliped; D. maxillula. Scale = 50 µm.

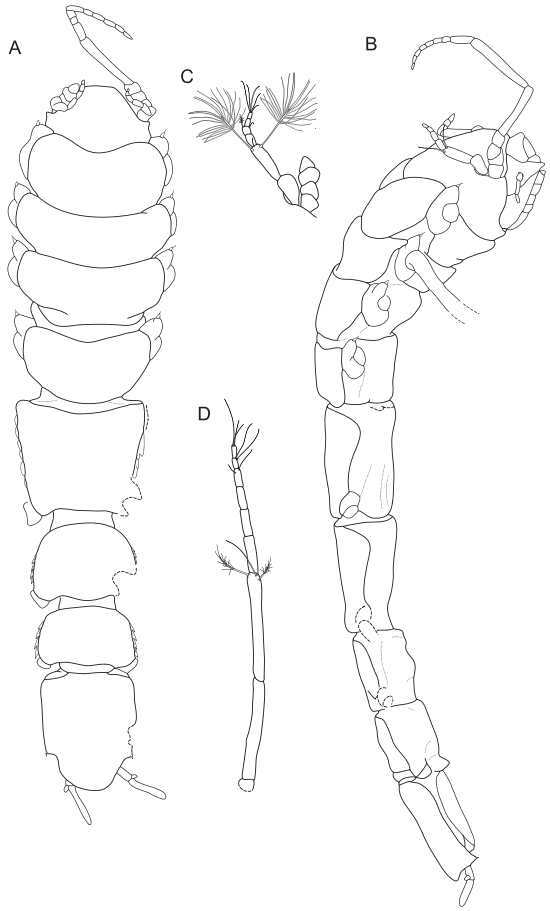

Fig. 16. *Prochelator barnacki* sp. nov. holotype ZMH K-46201, female. A. dorsal habitus; B. lateral habitus; C. antennula; D. antenna. Scale: 500 µm (A–B), 200 µm (C–D).

part of the sexual dimorphism together with the enlarged antenna and the more pronounced swimming legs. Different male types are already known from asellote isopods and occur for example in some macrostylid species were a different body shape of males allows them a different lifestyle from the females within a species and thus may enlarge the distribution range of males compared to females (Bober et al., 2017; Kniesz et al., 2018, In this issue). For Desmosomatidae, the sexual dimorphism is normally less pronounced than in the macrostylid examples cited. In *E. egoni* male type 2 was only observed from formalin fixed material and not included into the genetic analysis. However, the occurrence at the same station, the high similarity in setation of PI and diagnositic features of the body (serration of pereonites) does allow a morphological species allocation of male type 2 to *E. egoni*.

3.2.2. Genus Prochelator Hessler, 1970

Diagnosis see Brix and Bruce 2008

Synonymy see Golovan (2015)

Composition *Prochelator abyssalis* Hessler, 1970; *Prochelator angolensis* Brenke, Brix and Knuschke, 2005; *Prochelator hampsoni* Hessler, 1970; *Prochelator incomitatus* Hessler, 1970; *Prochelator keenani* Golovan, 2015; *Prochelator kussakini* Mezhov, 1986; *Prochelator lateralis* (Sars G.O., 1899); *Prochelator litus* Hessler, 1970; *Prochelator sarsi* George, 2001; *Prochelator tupuhi* Brix & Bruce, 2008; *Prochelator uncatus* Hessler, 1970

***Prochelator barnacki* sp. nov. Bober and Brix (Figs. 14–21)**

Material

Three specimens from two stations were determined and compared for the species description.

Holotype: Female, preparatory, 2,9 mm; ZMH K–46201 (VTDes147); designated here.

Type locality: VFZ, position: 11°39.201' N 47°54.697' W, depth 5001 m; RV Sonne So237; station 9–8; gear: C-EBS; January 12th, 2015.

Paratypes: 1 male ZMH K–46202 (VTDes108) and 1 female ZMH K–46203 (VTDes115), VFZ, position: 10°21.547' N 36°55.585' W; 5079 m; station 6–7; C-EBS; January 2nd, 2015.

Etymology

Prochelator barnacki sp. nov. is named in honour of Oscar Barnack (November 1, 1879 – January 16, 1936), the head of development department at Ernst Leitz in Wetzlar (today LEICA) who invented the first 35 mm camera in 1914.

Diagnosis

Body widest at Prn 2; body length 4.5 times longer than width of Prn 2. Form of Prn 5 trapezoid. Lateral margins of Prn 5–7 serrated in female. Coxae 1 – 4 anteriorly produced, each with robust acute setae. Pereopod 1 carpus not produced at base of claw-seta, mid-ventral unequally bifid seta more close to claw-seta than to merus. Pleotelson with posterolateral spines located at 3.1 of pleotelson length. Uropods biramous, exopod 1/3 of endopod length.

Description of female

Habitus (ZMH K–46201 Figs. 15, 17)

body length 6.0 width; body length 4.5 Prn2 width. Crephalothorax. Length 0.81 width, 0.12 body length, clypeus in dorsal view convex,

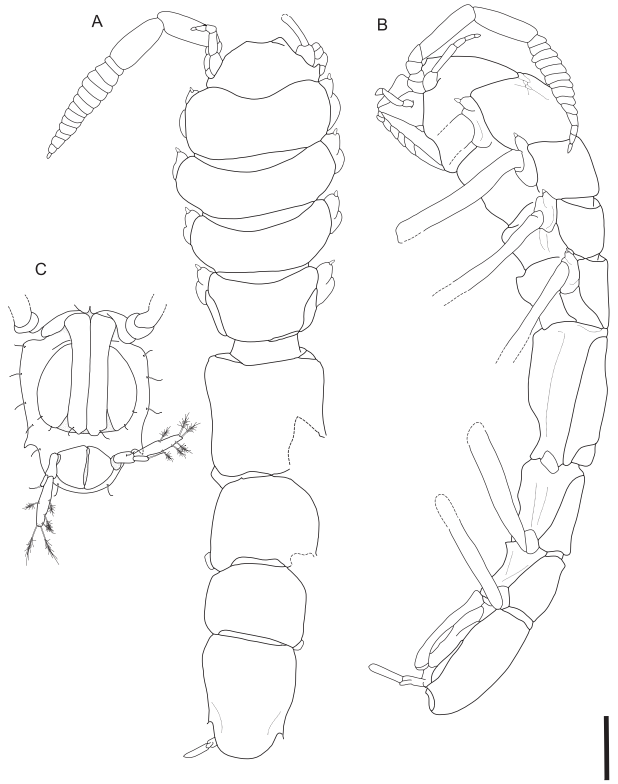

Fig. 17. *Prochelator barnacki* sp. nov. paratype ZMH K-46202, adult male. A. dorsal habitus; B. lateral habitus, C. pleotelson ventral. Scale: 500 µm (A–B), 0.125 µm (C).

frontal furrow present, straight. Lateral margins of Prn1–4 rounded. Coxae of Prn 1–4 produced anteriorly with 1 sensulate stout seta. Prn 1 length 0.46 width, 0.09 body length, Prn1 length 1.3 Prn2 length; anterior margin convex, wide "V" shape. Prn 2 length 0.33 width, length 0.07 body length. Prn 3 length 0.38 width, length 0.08 body length. Prn 4 length 0.51 width, 0.10 body length, width 1.1 Prn5 width. Prn 5 length 0.87 width, trapezoid posteriorly tapering, lateral margins serrated; length 1.7 Prn4 length. Prn 6 length 0.78 width, 0.72 Prn5 length. Prn 7 length 0.65 width. Pleotelson length 1.4 width, 0.16 body length; posterolateral spines at 0.76 Plt length; Plt slightly tapering till posterolateral spines, Plt apex semicircular

Antennula (ZMH K–46201 Fig. 16) with 6 articles, length 0.42 head width; width 0.57 Antenna width. Article 1 longer than wide. Article 2 distinctly longer than wide, longest article, longer than Article 3–6 together. Article 4 with 1 broom and 1 simple seta. Article 6 with 1 aesthestasc and 4 asensillate setae. Relative length ratios of articles 1.0, 1.2, 0.41, 0.27, 0.25, 0.18; L/W ratios of articles 1.8, 3.3, 1.6, 1.2, 1.4, 1.4.

Mandibles (ZMH K–46201 Figs. 15, 18) first article of Md palp with 1 seta each, second article with 2 setulate setae, marginally fringed with numerous fine setae, apical article with 2 setulate setae and combs of fine setae. Ip with 3 teeth. Lm of lMd with 4 teeth, lm like structure of rMd distally serrated, spine row with 5 spines. Mp with 10–17 setae.

Maxillula (ZMH K–46201 Fig. 18) Outer lobe terminally with 12 strong spines, marginally with several small setae.

Maxilla (ZMH K–46201 Figs. 15, 18) with 3 lobes. Medial lobe as long as outer lobes, slightly broader, ventrobasally with 3 long slender setae and marginally with numerous fine setae, terminally with 8 serrated setae and several simple setae. Outer lobes terminally with 3 long, serrated setae.

Maxilliped (ZMH K–46201 Figs. 15, 18) epipodite fringed with fine setae, distally 2 slender seta on inner margin. Endite with 2 coupling hooks, terminally with fine setae, 1 fan setae and several simple setae. Outer margins of palp article 2 fringed with fine setae. Palp article 2 with 3 setae on inner margin. Article 3 with 1 seta on inner margin and 1 seta on outer margin. Article 4 with 2 setae, article 5 with 3 setae.

Pereopod II (ZMH K–46201 Fig. 19) length 0.47 body length, relative article length ratios 1.0, 0.35, 0.21, 0.51, 0.38, 0.32; article L/W ratios 7.7, 3.1, 1.9, 3.9, 4.1, 6.0. Merus distodorsally with 1 distally setulate seta, ventrally with 1 distally setulate seta, medioventral 1 simple seta. Carpus dorsomedially with row of 4 setae and distodorsally with 1 broom seta, ventrally with row of 5 composed (unequally bifid distally setulate) setae increasing in size towards propodus. Propodus dorsally with row of 4 distally setulate setae, medioventrally with 1 composed (unequally bifid, distally setulate) and distoventrally with 1 composed and 1 simple seta. Dactylus distomedially 3 small slender setae close to claw. Claw of dactylus consisting of 1 large and 1 small simple conate seta, with 2 slender setulate setae inserting in between.

Pereopod V (ZMH K–46201 Fig. 20) Length 0.45 body length; article L/W ratios missing, 3.3, 1.5, 3.6, 3.9, 5. Basis dorsally with 1 broom seta and fine cuticular combs, ventrally with 6 broom setae and 2 slender setae. Ischium ventrally with 1 small seta. Merus distodorsally with 1 small seta, distoventrally with 1 seta. Carpus dorsally with 1 seta, ventrally with row of 4 long slender distally setulate setae. Propodus dorsally with row of 2 slender setae, ventrally with row of 6 long slender setae. Dactylus with 3 small simple setae inserting close to claw. Claw of dactylus consisting of 1 long simple conate seta and 2 slender setae, which are slightly longer than the conate seta.

Pereopod VII (ZMH K–46201 Fig. 20) Length 0.49 body length; relative article length ratios 1.0, 0.38, 0.18, 0.47, 0.43, 0.27; article L/W ratios 7.7, 2.9, 1.6, 4.8, 5.5, 7.2. Basis dorsally with 3 broom seta and fine cuticular combs, ventrally with row of 6 setae and 1 broom seta medioventrally. Ischium with 1 seta medioventrally. Merus distodorsally and distoventrally with 1 seta each. Carpus with one seta mediodorsally and distodorsally, a row of 3 distally setulate seta distoventrally. Propodus mediodorsally and medioventrally with 1 seta each, distodorsally with 1 broom seta and a row of 4 distally setulate seta distoventrally. Dactylus claw of dactylus consisting of 1 long simple conate seta and 3 slender setae, which are shorter than the conate seta.

Operculum (ZMH K–46201 Fig. 21) length 1.1 width. Lateral margins slightly convex, distal margin straight. Lateral margins without seta and distal margin with 4 small setae. Surface structure (folds) present.

Pleopod III (ZMH K–46201 Fig. 21) length 1.9 width, protopod length 0.95 width, 0.34 total length. Exopod length 0.45 total length.

Uropods (ZMH K–46201) biramous, length 0.33 plt length. Protopod length 0.11 plt length. Endopod 2.1 protopod length. Protopod with 3 simple setae. Endopod with 6 broom setae. Exopod with 1 seta terminally, exopod length 0.26 endopod length.

Description of male

Habitus (ZMH K–46202 Figs. 15, 17)

body length 6.1 width; body length 4.6 Prn2 width. Cephalothorax. Length 0.62 width, 0.09 body length, clypeus in dorsal view concave, frontal furrow present, convex, rounded. Lateral margins of Prn1–4 and coxae of Prn 1–4 as in female. Prn 1 length 0.42 width, 0.09 body length, Prn1 length 1.1 Prn2 length; anterior margin convex, not as wide "V" shape as in female. Prn 2 length 0.29 width, length 0.06 body length. Prn 3 length 0.33 width, length 0.07 body length. Prn 4 length 0.51 width, 0.08 body length, width 1.1 Prn5 width. Prn 5 length 1.1 width, trapezoid, slightly tapering posteriorly, lateral margins serrated;

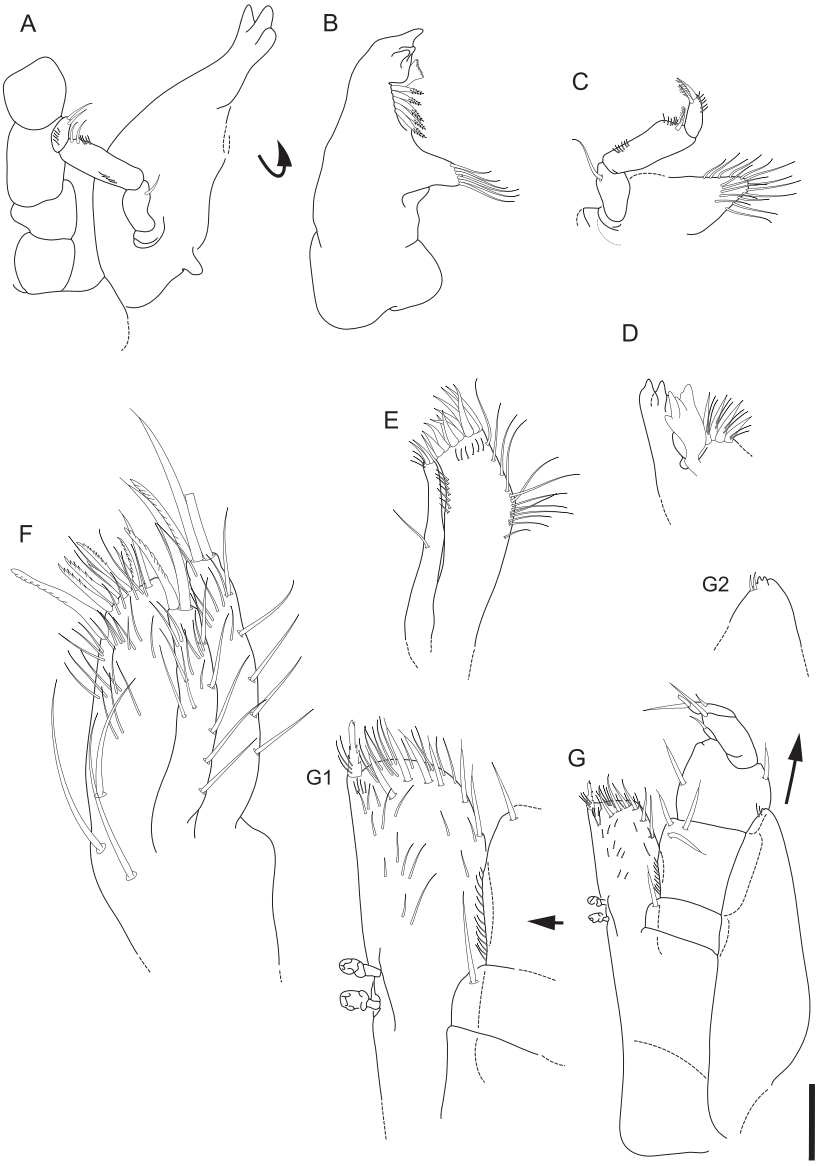

Fig. 18. *Prochelator barnacki* sp. nov. paratype ZMH K-46203, female, mouthparts. A. right mandible, in situ; B. right mandible; C. left mandible palpus, detail; D. left mandible, lacina mobilis + spine row detail; E. maxillula; F. maxilla; G. maxilliped; G1. maxilliped, endite detail; G2. maxilliped, epipodit detail.

length 2.1 Prn4 length. Prn 6 length 1.2 width, 0.80 Prn5 length. Prn 7 length 0.65 width. Pleotelson length 1.2 width, 0.15 body length; posterolateral spines at 0.77 Plt length; Plt slightly tapering till posterolateral spines, Plt apex semicircular

Antennula (ZMH K–46202 Fig. 14) with 6 articles, length 0.83 head width; width 0.83 Antenna width. Article 1 longer than wide. Article 2 distinctly longer than wide, longest article, longer than article 3–6 together. Relative length ratios of articles 1.0, 1.7, 0.48, 0.66, 0.26, 0.18; L/W ratios of articles 1.4, 3.9, 1.8, 2.7, 1.6, 3.4.

Antenna (ZMH K–46202 Fig. 14) Length 0.42 body length. Coxa–Merus squat, wider than long. Carpus elongate, longer than coxa, basis, ischium and merus together. Propodus subequal Carpus length. Flagellum enlarged with 12 articles, articles decreasing in size from proximal to distal, first flagellomere distinctly longer than following articles.

Remarks

Prochelator barnacki is easy to distinguish from *P. incomitatus* and *P. angolensis* by having biramous uropods. The body of *P. barnacki* is not as compact as both of the latter species. *Prochelator tupuhi* also posseses biramous uropods, but in contrast to *P. barnacki* also spine-like ventral elongations on Prns 1–4 (as in *P. lateralis*, *P. uncatus* and *P. hampsoni*). While *Prochelator keenani* Golovan, 2015 and *P. hampsoni* Hessler, 1970 are showing a long Prn 5 with acutely produced anterolateral corners, characters distinguishing *P. barnacki* from other species of the genus with biramous uropods are: Lateral margins of Prns 5–7 serrated, shape of Prn5 trapezoid. The carpus of pereopod 1 is not produced at the base

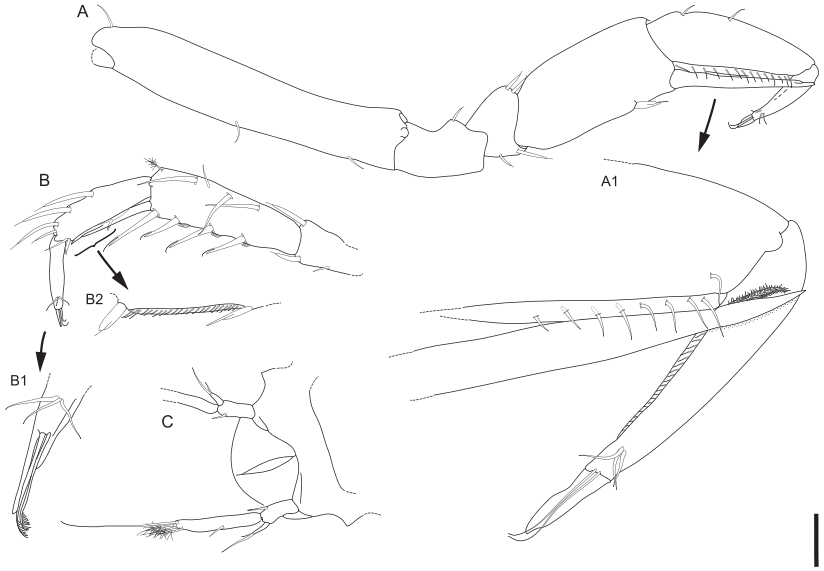

Fig. 19. *Prochelator barnacki* sp. nov. holotype ZMH K-46201, female, anterior pereopods. A. pereopod I; A1. pereopod I, porpodus + dactylus detail; B. pereopod II; B1. pereopod II, dactylus detail; B2. pereopod II, propodus detail; C. pleotelson + uropod ventral. Scale = 100 µm (A–C); 40 µm (A1, B1, B2).

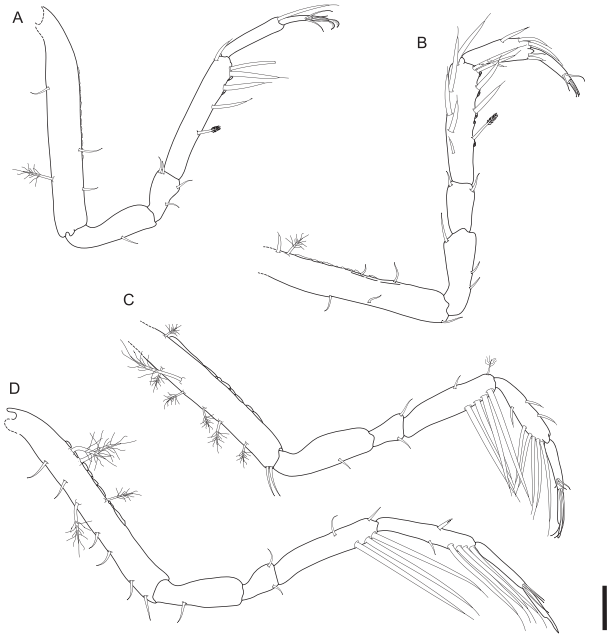

Fig. 20. *Prochelator barnacki* sp. nov. holotype ZMH K-46201, female, posterior pereopods. A. pereopod III; B. pereopod IV; C. pereopod V; D. pereopod VII. Scale = 100 µm.

of the claw-seta and the mid-ventral unequally bifid setae is located more close to the claw seta than towards the merus, the propodus dorsally with 2 setae. The sexual dimorphism is not strong in *P. barnacki* (Fig. 14), a serration of the lateral margins of Prn5-7 is not visible in male.

3.2.3. Genus Whoia Hessler, 1970

Diagnosis see Hessler, 1970

Synonymy see Kussakin (1999)

Composition *Whoia angusta* (G.O. Sars, 1899), *Whoia dumbshafensis* Svavarsson, 1988, *Whoia variabilis* Hessler, 1970, *Whoia victoriensis* Brix, 2006

***Whoia sockei* sp. nov. Brix and Kihara (Figs. 22–27)**

Material

Holotype: Female, preparatory, 2,9 mm; ZMH K–46204 (VTDes014); designated here

Type locality: VFZ, position: 10°43.69' N25°3.83' W, depth 5502 m; RV Sonne So237; station 2–6; gear: C-EBS; December 20th, 2014.

Paratypes: 1 female, 2,2 mm; ZMH K–46205 (VTDes155); position: 11°39.201'N 47°54.697'W, depth 5001 m; RV Sonne So237; station 9–8; gear: C-EBS; January 12th, 2015.

Etymology

The species name refers to the German child story of a raven called “Socke”, the favorite story books of the first authors children in the age of 4 and 7 wishing mommy to name a species who is as lovable cheeky as the litte raven “Socke”.

Diagnosis

Prn1 widest point of body. Prn5 second widest Prn of body, lateral margins anteriorly strongly convex in female, more straight in male, Plt without posterolateral spines in female and male. A1 of five articles. Lm with three teeth, PI with four strong unequally bifid setae ventrally on carpus, carpus 1,7 times width, propodus 2.8 times width, dactylus 3.2 times width.

Description of female

Habitus (ZMH K–46204 Figs. 22, 24) body 4.9 longer than width of Prn2. Head free, 1.2 longer than wide. Prn1 of similar size of Prn2. Lateral margins of Prn1–3 rounded, Prn 4 lateral margins straight. Prn5 width equal length, lateral margins of Prn5 convex, widest in anterior part giving a bulbous impression. Coxae 1–4 anteriorly produced, tipped with stout setae. Plt length 1.5 width. Posterolateral spines absent.

Antennula (ZMH K–46204 Figs. 22, 24 in situ) with 5 articles, 0.2 body length. Article 1 with 3 slender setae, article 2 length 4 times width, distally 2 large broom setae, article 3 with 1 slender seta, article 4 with 2 slender and 1 broom seta, article 5 tipped with 1 small broom seta, 3 slender setae and 1 aestethasc.

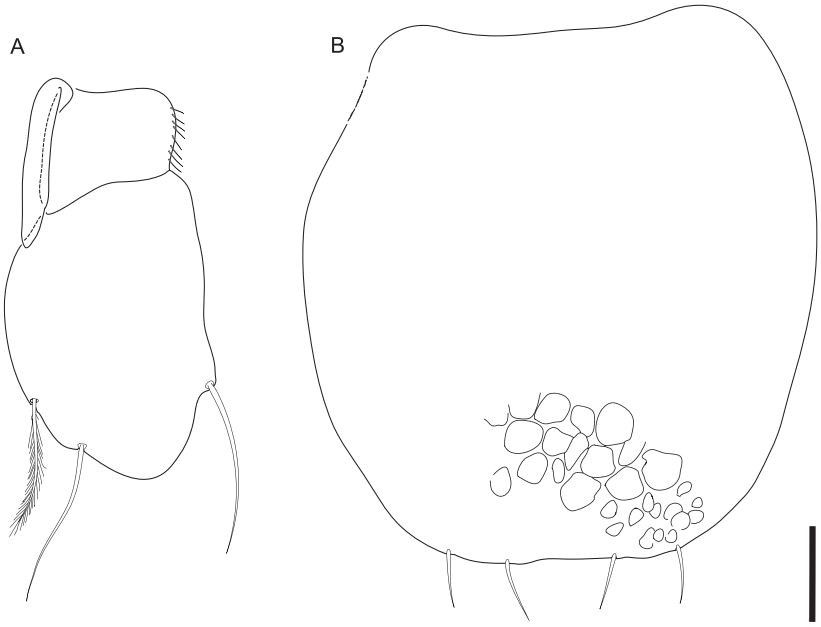

Fig. 21. *Prochelator barnacki* sp. nov. paratype ZMH K-46203, adult non-ovigerous female, pleopods. A. pleopod III; B. operculum. Scale = 50 μm.

Antenna (ZMH K–46204 Fig. 24 in situ) length 0.4 body length, with 21 articles. To avoid damage of the specimen, we did not measure the relative length of articles.

Mandibles (ZMH K–46204 Figs. 23, 26) Ip with five teeth. Lm of lMd with 3 teeth (2 small ones and 1 prominent one), spine row with 7 serrated spines with setules inserting between them. Mp with 14 distally setulate setae. Palpus of MdL broken off.

Maxillula (ZMH K–46204 Fig. 23) Outer lobe terminally with 12 strong spines, marginally with 6 pairs of small setae, inner lobe terminally with numerous setae (three of them strong), upper margin with eight pairs of fine setae.

Maxilla (ZMH K–46204 Fig. 23) with three lobes. Medial lobe slightly broader and shorter than outer lobes. Dorsally outer lobed with 5 pairs of slender setae, distally 4 long setulate each.

Maxilliped (ZMH K–46204 Fig. 26) Endite with two coupling hooks. Palp with 5 articles. Outer margin of scale fringed with cuticular membrane. Palpus article 1 outer margin fringed with numerous fine setae and tipped with 1 slender seta, ventral margin tipped with 1 slender seta, palp article 2 outer margin distally with 3 setae, article 3 with 5 setae, article 4 with 5 setae as well and article 5 tipped with 3 setae.

Pereopod I (ZMH K–46204 Fig. 25) Basis and Ischium not drawn. Merus length 0.97 width, distodorsally with 2 setae (1 unequally bisfid, 1 slender), distoventrally with 3 setae (2 unequally bifid, 1 slender). Carpus length 1.7 width, ventrally with row of 4 strong unequally bifid setae increasing in size towards propodus, dorsally with row of 4 setae. Propodus length 2.8 width, distoventrally with 2 setae, dorsally with row of four setae. Dactylus distomedially with 3 simple slender setae close to claw. Claw of dactylus consisting of 2 conate setae with 2 slender setae inserting in between them.

Pereopod II (ZMH K–46204 Fig. 25) basis length 2.7 width, dorsally with 1 broom seta, ventrally with 1 distally setulate setae. Ischium length 1.7 width, dorsally with 1 seta, medioventrally with 2 setae, ventrally fringed with cuticular combs. Merus length 1.1 width, distodorsally with 2 setae, ventrally with 2 composed setae and fringed with cuticular combs. Carpus length 1.4 width, dorsomedially with 2 setae, ventrally with row of 3 composed setae increasing in size towards propodus. Propodus length 4.6 width, dorsally with 1 seta, distoventrally with 3, medially 1 slender seta. Dactylus distomedially with 3 small slender setae close to claw. Claw of dactylus consisting of 1 large conate seta, with 2 slender setulate setae inserting below.

Pereopod V (ZMH K–46204 Fig. 25) basis length 5.9 width, dorsally with 1 broom seta. Ischium length 3 width, without setae. Merus length 1,3 width, distodorsally 1 composed seta, distoventrally 1 composed seta. Carpus length 2.6 width, distodorsally with 1 composed seta, ventrally with 2 long slender distally setulate setae. Propodus length 3.7 width, dorsally with 2 slender distally setulate setae, distoventrally with 1 long slender setae. Dactylus with 3 small simple setae inserting close to claw. Claw of dactylus consisting of 1 long simple conate seta and 2 slender setae, which are slightly longer than the conate seta.

Operculum (Fig. 27) rounded, distal margin with 4 simple setae. Upper margin with 2 prominent lines remembering in shape of male pleopod 1 visible as surface structure.

Pleopod 3 (Fig. 27) endopod with 3 plumose setae, exopod 0,2 size of endopod, tipped with on slender seta.

Pleopod 4 (Fig. 27) endopod as long as exopod, endopod width 0.5 length, exopod width 0.1 length and tipped with 1 plumose seta.

Uropods. Missing.

Remarks

Whoia sockei sp. nov. is the most widely distributed species in the complete dataset. Although facing the deep-sea phenomenon “rarity”, VTDes155, and VTDes014, are delimited as one species by ABGD and GMYC for COI (though they were actually delimited as separate species by bPTP, Fig. 2. Unfortunately 16 S sequences were not available for these two specimens. Thus, it is not 100% congruent, but 2 out of 3 molecular SD methods do support the morphological conclusion. The species defining characters are found in both specimens as there are: PI carpus ventrally with row of four strong unequally bifid setae instead of three in *W. angusta* and *W. variabilis*, Prn 5 margin anteriorly convex while more straight in *W. angusta* female. Prn 5 margin also convex in

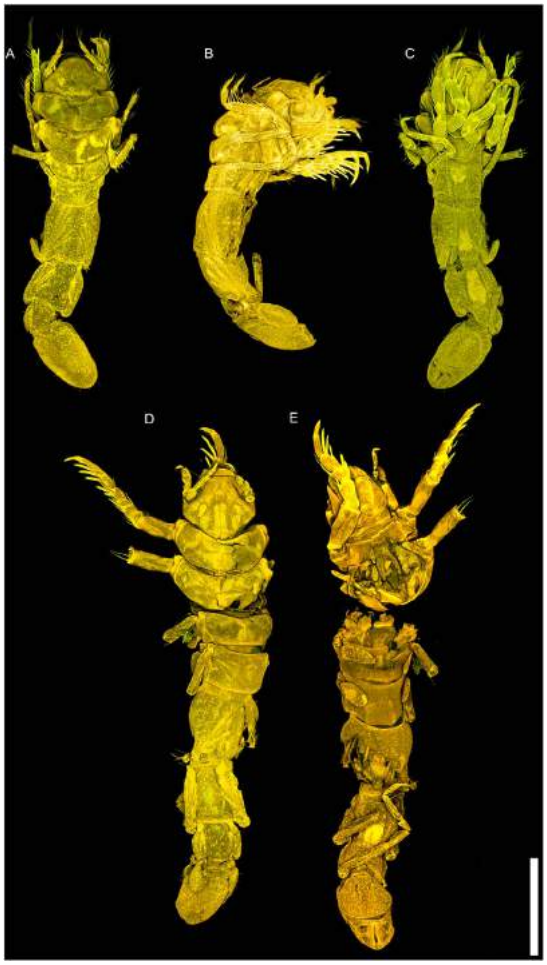

Fig. 22. *Whoia sockei* sp. nov. holotype ZMH K-46204 (VTDes014) and paratype ZMH K-46205 (VTDes155), adult non-ovigerous female. CLSM micrographs. A. dorsal habitus (ZMH K-46205); B. lateral habitus (ZMH K-46205); C. ventral habitus (ZMH K-46205); D. dorsal habitus (ZMH K-46204); E. ventral habitus (ZMH K-46204). Scale = 500 μm.

W. variabilis, but not as strong. Cuticular folds are not obviously recognizable.

4. Discussion

Assessing species' range size and population connectivity at abyssal depths is challenging (Janssen et al., 2015) because benthic communities are diverse, many species occur as singletons and most species are new to science (Tyler et al., 2016) resulting from under sampling coupled with high diversity. In the VFZ and transform fault alone, more than 95% of desmosomatid and nannoniscid species were new to science, in total over 60 species of 72 delimited species. The taxonomic effort required to describe all these species new to science would be immense; with a rough estimate of 4 weeks per description for an experienced taxonomist, it would probably take about 248 weeks (5 years!). Combining morphological analysis with molecular species delimitation therefore has the potential to inform, and perhaps speed, the process of formal species identification, by identifying putative species groups whose validity can be assessed by further analysis.

Our analysis shows that most species have a limited distribution, although the details depend in part on the interpretation of SD analyses and are complicated by many delimitations comprising just one or a few specimens. However, even ignoring SSDs, most species were sampled from a single station or a pair of neighboring stations on one side of the transform fault, and few species' estimated ranges (just eight of 72) included or spanned the fault (12 MSSs total: three only in the east, one only in the west, the remaining eight in the transform plus at least one side.). Bober et al., (this issue; Fig. 4) show the haplotype network for those species defined as one species by 2 of the applied SD models. Also the single sites sampled along the VFZ comprise a variety of habitats (Devey et al., this issue).

An increasing number of morphological and molecular analyses of deep-sea invertebrate taxa have documented genetic discontinuities within seemingly homogeneous populations; however, these studies often find that species are broadly distributed horizontally across thousands of kilometers while exhibiting strong genetic differentiation vertically along mere hundreds of meters (Jennings et al., 2013; Havermans et al., 2013; Quattrini et al., 2013; Cowart et al., 2014; Brix et al., 2014). It is important to note that most of these studies have focused on areas with less complex topography. The patterns of combined geological barriers and associated hydrographic circulation in the VEMA region likely present a very different environment through

Fig. 23. *Whoia sockei* sp. nov. holotype ZMH K-46204, adult non-ovigerous female, mouthparts. CLSM micrograph. A. mandible; B. maxilla; C. maxillula. Scale = 100 μm.

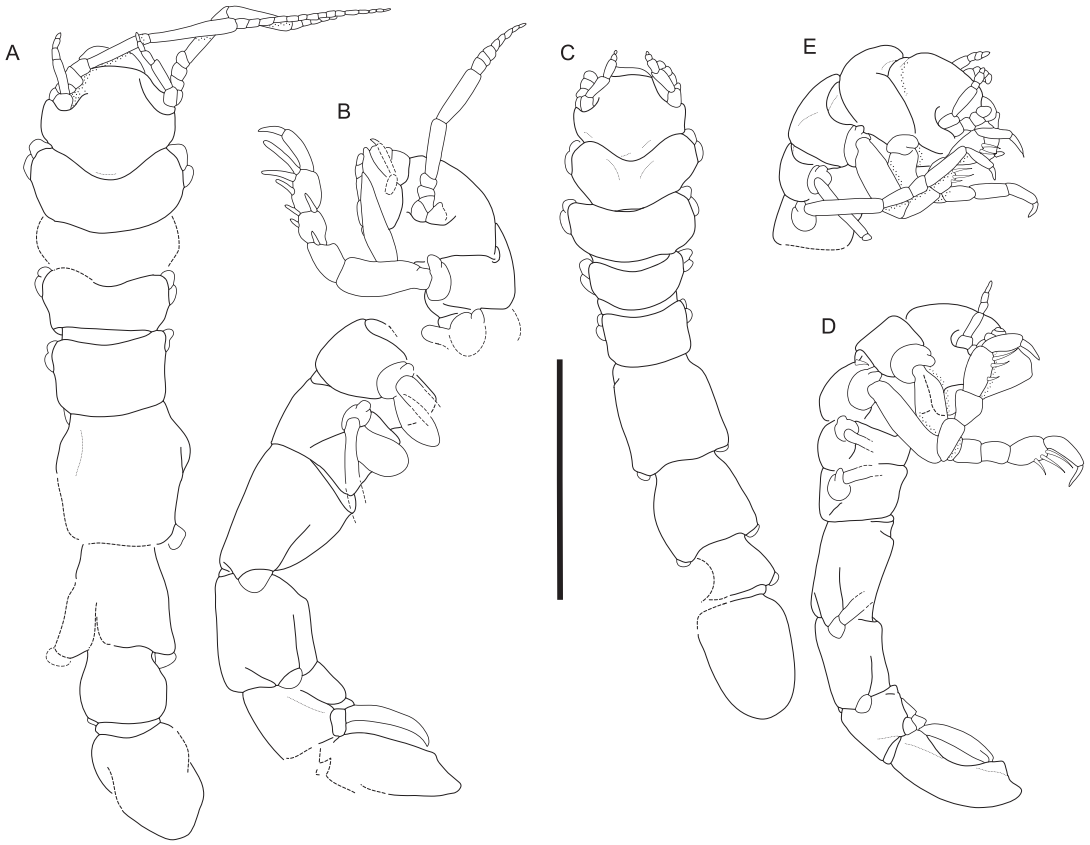

Fig. 24. *Whoia sockei* sp. nov. holotype ZMH K-46204 and paratype ZMH K-46205, adult non-ovigerous female. A. dorsal habitus (VT014); B. lateral habitus (VT014); C. dorsal habitus (ZMH K-46205); D. lateral habitus (ZMH K-46205); E. lateral cephalothorax and anterior segments, detail (ZMH K-46205). Scale 1 mm.

which species must disperse to maintain genetic cohesion. A recent study of the highly topologically complex abyssal and hadal trench regions of the Pacific did uncover both, strong horizontal and strong vertical, genetic differentiation among lysianassoid amphipods (Ritchie et al., 2015).

The morphological species concept is the most commonly applied, approach in deep-sea isopod taxonomy. DNA barcoding (Hebert et al., 2003) as an alternative approach is based on strict application of a distinct gap between intraspecific variability and interspecific variation in genetic distances of cytochrome *c* oxidase subunit I (COI). It was complemented in this study by inclusion of other "barcoding" markers such as 16 S. While Hebert et al. (2003) proposed a 3% threshold value to delineate species in general, Radulovici et al. (2009) found intraspecific divergence greater than > 13% in amphipods (which are peracarids like isopods), although this includes likely mophologically-cryptic species. For branchiopods, Schwentner et al. (2011) identified a 5–6% threshold between intra- and interspecific divergence. The application of a general threshold has its shortcomings due to the not particularly uncommon findings of overlap between interspecific and intraspecific nucleotide variability (e.g. Meier et al., 2006, Schwentner et al., 2011). Threshold estimates calculated at one taxonomic scale or for one taxonomic group are sometimes not applicable to other scales or groups. Many examples of high interspecific divergence and low intraspecific divergence (< 2%) have been discovered in asellote isopods (intraspecific uncorrected p-distances of as little as 7% and as much as 34%). For example, in *Haploniscus,* Richardson, 1908 distances were 9–20% interspecific, 25–28% intergeneric, < 1.8% intraspecific (Brix et al., 2011). Other examples exist in the Munnopsidae (CO1 data; Osborn, 2009), the Macrostylidae (16 S data; Riehl and Brandt, 2013), the desmosomatids *Chelator* and *Parvochelus* (both CO1 and 16 S data; Brix et al., 2015), and other isopod groups (Wetzer, 2001). It all describes the same pattern: high interspecific distances, but low intraspecific variability.

The species delimitation analyses performed here relied not only on pairwise difference thresholds (whose ease of comparison among studies is nonetheless advantageous), but employed more recently developed methods invoking multispecies coalescent models, using sequence data in a more complex and integrative manner, and producing not just species clusters but estimates of statistical confidence on them. For these reasons the coalescent-based delimitations could be assumed to be less susceptible to missing sequence data, and more reliable in cases of SSDs. In the present case both distributional (i.e. ABGD) and model-based (bPTP and GMYC) analyses converged on highly similar delimitations with only relatively minor discrepancies, which also matched well with our *a priori* morphological determination on genus level. In total, we see 24 discrepancies between the single models mostly reflecting the basic taxonomic uncertainty and thus gives no more information than knowing that these discrepancies need to be discussed comparing them to a morphological species determination. As in Kaiser et al., (This Issue) SD analyses of the molecular data were mostly

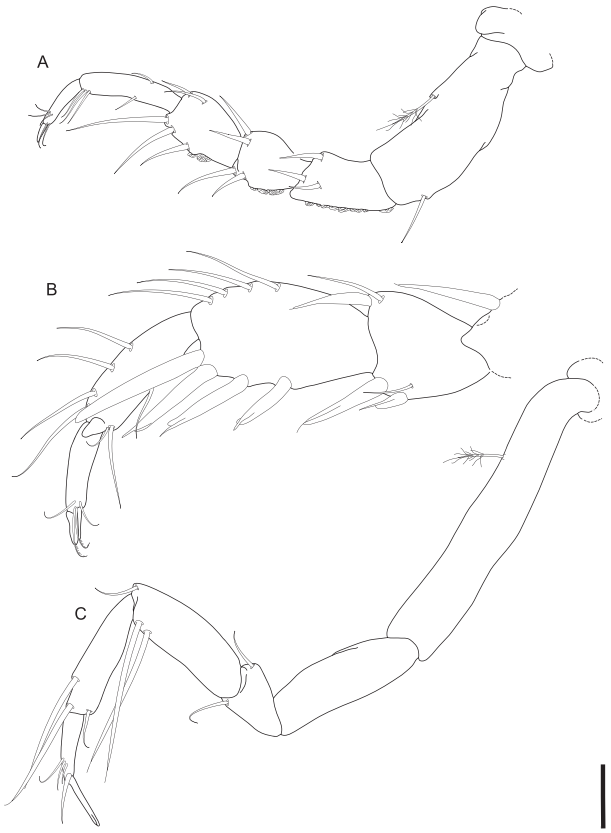

Fig. 25. *Whoia sockei* sp. nov. holotype ZMH K-46204 and paratype ZMH K-46205, adult non-ovigerous females, pereopods. A. pereopod I (ZMH K-46204); B. pereopod II, in situ (ZMH K-46205); A. pereopod VII, in situ (ZMH K-46204). Scale = 100 µm (A, C); 50 µm (B).

congruent with morphological assumptions to differentiate species within genera, but morphological species identifications were performed *a posteriori,* examining only the incongruent results among SD models. In several cases the different results reflected difficulties in the morphoplogical determination. Looking at the Kaiser et al., (This Issue) example of the *Ketosoma vemae/hessleri* clade, the dilemma was that neither morphological nor molecular examination provided unequivocal evidence for species differentiation and furthermore *K. vemae* and *K. hessleri* are singletons representing only male or female and thus a sexual dimorphism should be discussed in species description despite the assumption of undersampling. In our data, also represented by only two specimens, but in this case of only one sex but comparable genetic distance to the *Ketosoma vemae/hessleri* clade, we describe *Whoia sockei* as one species (compare Fig. 4 in Bober et al., this issue). These two examples show that morphological discussion of characters and comparing different SD models of molecular data can result in different taxonomic decisions.

Our analysis shows that most species have a limited distribution, although the details depend in part on the interpretation of SD analyses and are complicated by many delimitations comprising just one or a few specimens. Also the single sites sampled along the VFZ show a variety of habitats (Devey et al., In this issue). It is interesting that more species were present in the transform fault and at sites to its east than were present in the transform fault and to its west (5 vs. 1). This finding, while tentative, is surprising given the circulation patterns in and near the VFZ, which represents one of the most important pathways by which the cold waters of the deep western Atlantic basins cross the Mid-Atlantic Ridge and penetrate into the deep eastern Atlantic basins (McCartney et al., 1991). Approximately one fourth to one third of the Antarctic Bottom Water (AABW) moving northwards in the deep western Atlantic passes through Vema from about 3600 m depth down to the floor of the passage > 4500 m depth (McCartney et al., 1991; Fischer et al., 1996; Morozov et al., 2015), and a fraction of the cold, southward-moving North Atlantic Deep Water (NADW) passes through Vema from west to east as well. This predominant and significant west-to-east flow is complicated by three main factors: a series of sills at the eastern end of Vema at about 4700 m depth, a weaker east-to-west flow concentrated along the southern wall above 3800 m depth, and strong vertical mixing caused by the convergence of the large water masses in a region of complex topography (Fischer et al., 1996; Morozov et al., 2015). Thus, the predominant currents would seem to facilitate the eastward, not westward, spread of any species whose range included the transform fault itself.

In addition, although strong mixing and counter-currents might be expected to promote wider dispersal of species, our data suggest that even robustly-sampled species exhibited small ranges. For most multiple-station species, the best range estimates calculable from present data were around 500 km, and three were on the order of 1000–2500 km, which is remarkable for an isopod with limited swimming abilities. However, it has to be noted that large distance between the sampling locations and the likely patchiness of faunal distributions (Kaiser and Barnes, 2008; Kaiser et al., 2009) cannot be sufficiently inferred based on our analysis, although our dataset represents one of the most comprehensive ones for the deep sea. Thus, we are still facing the problem of undersampling. Not undesampled were some genera like *Chelator* (62 specimens) or *Eugerdella* (19 specimens), both desmosomatid genera with highly similar species inside and especially Chelator has been proven to be tricky and species differ by minor characters while showing high genetic distance (Brix et al., 2015) or reflecting a bathymetry related pattern along with a uniform morphology (Brix et al., 2014). This phenomenon was also observed by Brandt et al. (2014) in the case of deep-sea serolids.

Brix et al. (2015) outlined that both, the Guinea and Angola basins, are influenced by the southward current of North Atlantic Deep Water (NADW). Following Kröncke and Türkay (2003) and Brix et al. (2015), AABW and NADW may function as potential vectors for species dispersal. While Brix et al. (2015) found some substantial genetic variation within *Parvochelus russus* (1.5 – 11.9% p-distances), the close relatedness of some specimens from either side of the MAR suggests sporadic connectivity (DIVA-2 and 3 samples). The *Parvochelus* species found in our dataset indicate the presence of nine *Parvochelus* species in the VFZ, only one of them (*P. russus*) was also present in the DIVA material and some Vema specimens have joined in while the remaining species are new to science and were unknowable from the DIVA material.

5. Conclusion

We observe horizontal limitation of species distribution in the VFZ. SD results have to deal with singletons and do mirror morphological difficulties to delineate species as also observed by Kaiser et al., (In this Issue). It therefore seems that, for most situations where species delimitation is unclear, morphological and molecular data must be used in concert for the most likely species hypothesis. Although the species delimitation analyses chosen here employ a range of models and methods, their congruence to each other and to morphological species designation suggest that the combined molecular and morphological approach is a powerful technique to understand and improve our understanding of species boundaries, even in taxonomically complex groups like the asellote isopods. Our conservative criterion for

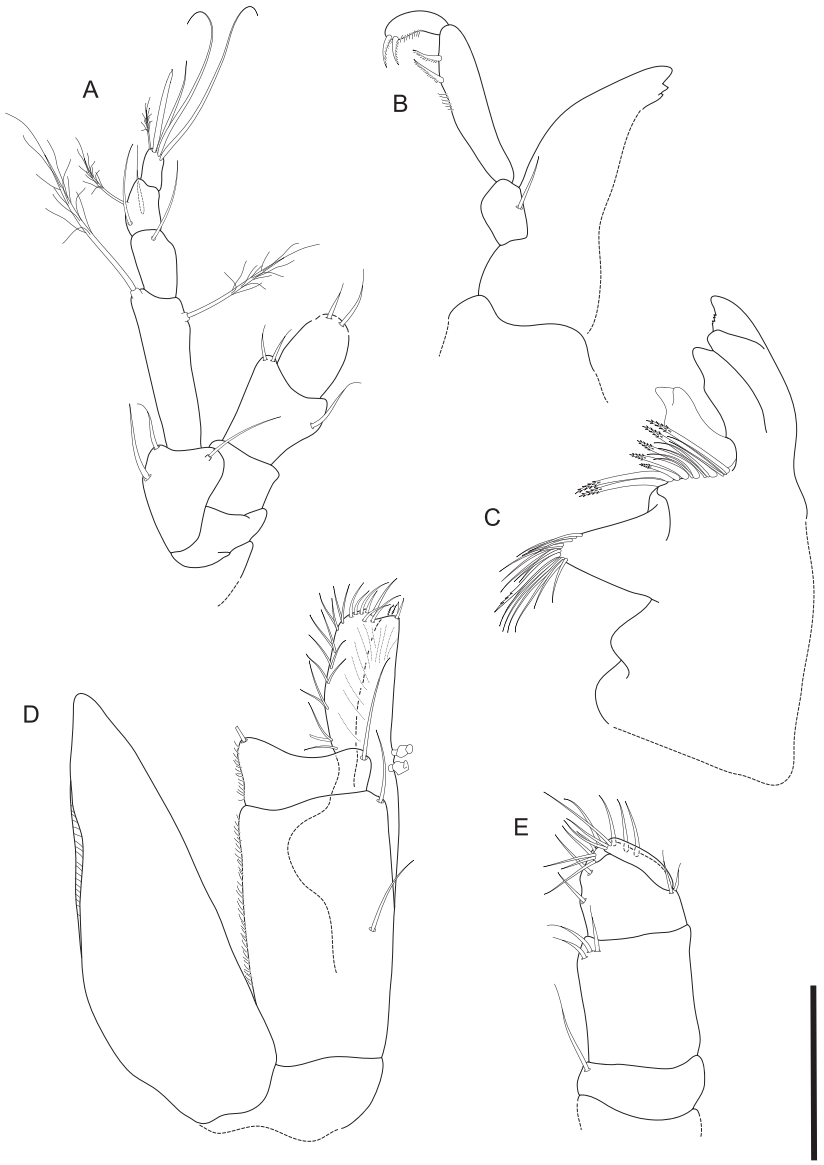

Fig. 26. *Whoia sockei* sp. nov. paratype ZMH K-46204, adult female, antennula and mouthparts. A. antennula and basal segments of antenna; B. right mandible palpus (in situ); C. left mandible; D. right maxilliped (palpus missing); E. left maxilliped palpus. Scale = 100 µm.

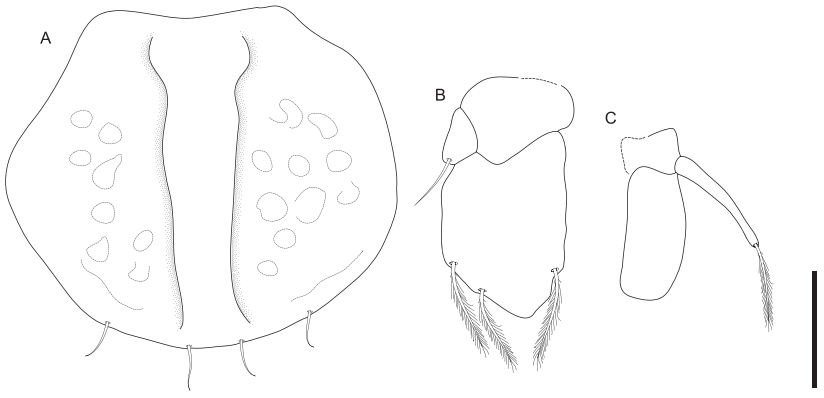

Fig. 27. *Whoia sockei* sp. nov. paratype ZMH K-46204, adult female, pleopods. A. operculum; B. pleopod 3; pleopod 4. Scale = 100 µm.

considering species as robustly delimited, combined with the relative simplicity of some models (e.g. ABGD) imply that we may be underestimating the true species diversity of this group. Moreover, the high frequency of species delimited from one or a few specimens, from a relatively large dataset of almost 200 sequences, highlights the likelihood of as yet undetected diversity.

Acknowledgements

We thank all pickers and sorters on board of RV Sonne during SO237 as well as captain and crew for all their support, Angelika Brandt and Colin Devey for organizing the Vema-TRANSIT project, Inmaculata Frutos and Tanja Springer for handling the project database at home and on bord, Renate Walter for her help with the SEM pictures. Inmaculata Frutos did manage the sample sorting and making specimens available. The “DNA barcoding deep-sea Peracardia” project is hosted at the Smithsonian Institution, we kindly thank Karen Osborn for her support. Sarah Schnurr helped with her labwork during her visit at the Smithsonian in November 2015 and Karen Jeskulke supported the project with her lab work in our home laboratory. Financial support war given by the DFG grant to the first author BR3843/6-1 enabling us to work together in the different institutions (Smithsonian, Senckenberg, University of Massachusetts and Temple University) contributing to our American-German cooperation and having a great time together with great isopod data. The Vema-TRANSIT (Bathymetry of the Vema-Fracture Zone and Puerto Rico TRench and Abyssal AtlaNtic BiodiverSITy Study) project was funded by the German federal ministry (03G0237A).

References

Birstein, J.A., 1971. Fauna of the Kurile-Kamchatka Trench. Additions to the fauna of isopods (Crustacea, Isopoda) of the Kurile-Kamhcatka Trench. Part II. Asellota 2 92. Trudy Instituta Okeaonogiya, Akademiya Nauk SSSR, Moscow, pp. 162–238.

Bober, S., Riehl, T., Henne, S., Brandt, A., 2017. New Macrostylidae (Isopoda) from the Northwest Pacific Basin described by means of integrative taxonomy with reference to geographical barriers in the abyss. Zool. J. Linn. Soc. zlx042. http://dx.doi.org/10.1093/zoolinnean/zlx042.

Bober, S., Riehl, T., 2014. Adding depth to line artwork by digital stippling—a step-by-step guide to the method. Org. Divers. Evol. http://dx.doi.org/10.1007/s13127-014-0173-7.

Bober, S., Brix, S., Riehl, T., Schwentner, M., Brandt, A., 2018. Does the Mid-Atlantic Ridge affect the distribution of abyssal benthic crustaceans across the Atlantic Ocean? Deep Sea Res. II (In this issue).

Bouckaert, R., Heled, J., Kühnert, D., Vaughan, T., Wu, C.-H., Xie, D., et al., 2014. BEAST 2: a software platform for Bayesian evolutionary analysis. PLoS Comput. Biol. 10 (4), e1003537. http://dx.doi.org/10.1371/journal.pcbi.1003537.

Brandt, A., Brix, S., Held, C., Kihara, T.C., 2014. Molecular differentiation in sympatry despite morphological stasis: deep-sea *Atlantoserolis* Wägele, 1994 and *Glabroserolis* Menzies, 1962 from the south-west Atlantic (Crustacea: Isopoda: Serolidae). Zool. J. Linn. Soc. 2014 (172), 318–359.

Brandt, A., Devey, C.W., Arndt, H., Riehl, T., 2018. Introduction to the bathymetry of the Vema-Fracture Zone and Puerto Rico TRench and Abyssal AtlaNtic BiodiverSITy Study (Vema-TRANSIT). Deep Sea Res. II (In this issue).

Brix, S., 2006a. A New Species of Desmosomatidae (Isopoda: Crustacea) from the Deep Southern Ocean: *Eugerdella serrata* sp. nov. Including Remarks to the Morphological Variability within *Eugerdella* Hessler, 1970 103. Mitteilungen aus dem hamburgischen Zoologischen Museum und Institut, pp. 69–84.

Brix, S., 2006b. A new genus and new species of Desmosomatidae (Crustacea: isopoda: Asellota) from the deep sea of south-eastern Australia. Mem. Mus. Vic. 63 (2), 175–205.

Brix, S., 2007. Four new species of Desmosomatidae Sars, 1847 (Crustacea, Isopoda) from deep sea of Angola Basin. Mar. Biol. Res. 3 (4), 205–230.

Brix, S., Leese, F., Riehl, T., Kihara, T.C., 2015. A new genus and new species of Desmosomatidae Sars, 1897 (Isopoda) from the eastern South Atlantic abyss described by means of integrative taxonomy. Mar. Biodivers. 45 (1), 7–61.

Brix, S., Leese, F., Svavarsson, J., 2014. A multi−gene analysis reveals multiple highly divergent lineages of the isopod *Chelator insignis* (Hansen, 1916) south of Iceland. Pol. Polar Res. 35 (2), 225–242. http://dx.doi.org/10.2478/popore−2014−0015.

Brix, S., Riehl, T., Leese, F., 2011. First genetic data for species of the genus *Haploniscus* Richardson, 1908 (Isopoda: Asellota: Haploniscidae) from neighbouring deep-sea basins in the South Atlantic. Zootaxa 2838, 79–84.

Brix, S., Svavarsson, J., 2010. Distribution and diversity of desmosomatid and nannoniscid isopods (Crustacea) on the Greenland–Iceland–Faeroe Ridge. Polar Biol. 33, 515–530.

Carstens, B.C., Pelletier, T.A., Reid, N.M., Satler, J.D., 2013. How to fail at species delimitation. Mol. Ecol. 22 (17), 4369–4383. http://dx.doi.org/10.1111/mec.12413.

Coleman, C.O., 2003. "Digital inking": how to make perfect line drawings on computers. Org. Divers. Evol. 3 (Electronic Supplement 14), 1–14.

Coleman, O., 2009. Drawing the setae the digital way. Zoosystematics Evol. 85 (2), 305–310. http://dx.doi.org/10.1002/zoos.200900008.

Cowart, D.A., Halanych, K.M., Schaeffer, S.W., Fisher, C.R., 2014. Depth-dependent gene flow in Gulf of Mexico cold seep *Lamellibrachia* tubeworms (Annelida, Siboglinidae). Hydrobiologia 736 (1), 139–154. http://dx.doi.org/10.1007/s10750-014-1900-y.

Dayrat, B., 2005. Towards integrative taxonomy. Biol. J. Linn. Soc. 85 (3), 407–415.

Devey, C., Augustin, N., Brandt, A., Brenke, N., Köhler, J., Lins, L., Schmidt, C., Yeo, I., 2018. Habitat characterization of the Vema Fracture Zone and Puerto Rico Trench. Deep Sea Res. II (In this issue).

Fischer, J., Rhein, M., Schott, F., Stramma, L., 1996. Deep water masses and transports in the Vema Fracture Zone. Deep-Sea Res. Part I 43 (7), 1067–1074.

Fujisawa, T., Barraclough, T.G., 2013. Delimiting species using single-locus data and the generalized mixed Yule coalescent approach: a revised method and evaluation on simulated data sets. Syst. Biol. 62 (5), 707–724.

Golovan, O.A., 2007. *Mirabilicoxa kussakini* sp. nov., a new species of Desmosomatidae (Crustacea, Isopoda, Asellota) from the Sea of Japan. Russ. J. Mar. Biol. 33, 365. http://dx.doi.org/10.1134/S1063074007060028.

Golovan, O., 2015. Desmosomatidae (Isopoda: asellota)from the abyssal plain to the east of the Kuril–Kamchatka Trench: new data on diversity with the description of two New species. Deep-Sea Res. Part II 111, 256–278.

Hansen, H.J., 1916. Crustacea Malacostraca: The Order Isopoda 3. The Danish Ingolf Expedition, pp. 1–262.

Havermans, C., Sonet, G., d'Acoz, C.U., Nagy, Z.T., Martin, P., Brix, S., et al., 2013. Genetic and morphological divergences in the cosmopolitan deep-Sea amphipod *Eurythenes gryllus* reveal a diverse Abyss and a bipolar species. PLoS One.

Hebert, P.D.N., Ratnasingham, S., deWaard, J.R., 2003. Barcoding animal life: cytochrome c oxidase subunit 1 divergences among closely related species. Proc. R. Soc. B: Biol. Sci. 270 (Suppl 1), S96–S99.

Hessler, R.R., 1970. The Desmosomatidae (Isopoda, Asellota) of the Gay Head-Bermuda Transect. University of California Press, Berkeley.

Hessler, R.R., Sanders, H.L., 1967. Faunal diversity in the deep-sea. Deep-Sea Res. 14, 65–78.

Hessler, R.R., Thistle, D., 1975. On the place of origin of deep-sea Isopods. Mar. Biol. 32 (2), 155–165.

Janssen, A., Kaiser, S., Meißner, K., Brenke, N., Menot, L., Arbizu, P.M., 2015. A reverse taxonomic approach to assess macrofaunal distribution patterns in abyssal Pacific polymetallic nodule fields. PLoS One 10 (2), e0117790.

Jażdżewska, A.M., Corbari, C., Driskell, A., Frutos, I., Havermans, C., Hendrycks, E., Hughes, L., Lörz, A.-N., Stransky, B., Tandberg, A.H.S., Vader, W., Brix, S., In press. A genetic fingerprint of Amphipoda from Icelandic waters - an urgent need for integrating morphological and molecular methods in taxonomy. Zookeys IceAGE SI Amphipoda.

Jennings, R.M., Etter, R.J., Ficarra, L., 2013. Population differentiation and species formation in the deep sea: the potential role of environmental gradients and depth. PLoS One. http://dx.doi.org/10.1371/journal.pone.0077594.

Kaiser, S., Brix, S., 2005. A New Isopod Species from the Southern Ocean: *Disparella maiuscula* sp. nov. (Isopoda: Asellota: Desmosomatidae) 102. Mitteilungen aus dem Hamburgischen Zoologischen Museum und Institut, pp. 153–165.

Kaiser, S., Barnes, D.K.A., 2008. Southern Ocean deep-sea biodiversity: sampling strategies and predicting responses to climate change. Clim. Res. 37, 165–179.

Kaiser, S., Barnes, D.K.A., Sands, C.J., Brandt, A., 2009. Biodiversity of an unknown Antarctic Sea: assessing isopod richness and abundance in the first benthic survey of the Amundsen continental shelf. Mar. Biodivers. 39 (1), 27–43.

Kaiser, S., Brix, S., Kihara, T.C., Janssen, A., Jennings, R.M., 2018. Integrative species delimitation in the deep-sea genus *Thaumastosoma* Hessler, 1970 (Isopoda, Asellota, Nannoniscidae) reveals a new genus and species from the Atlantic and central Pacific abyss. Deep Sea Res. II (In this issue).

Kamanli, S.A., Kihara, T.C., Ball, A.D., Morrit, D., Clark, P.F., 2017. A 3D imaging and visualization workflow, using confocal microscopy and advanced image processing for brachyuran crab larvae. J. Microsc. 266 (3), 307–323. http://dx.doi.org/10.1111/jmi.12540.

Katoh, K., Standley, D.M., 2013. MAFFT Multiple Sequence Alignment Software Version 7: Improvements in Performance and Usability. Mol. Biol. Evol. 30 (4), 772–780. http://dx.doi.org/10.1093/molbev/mst010.

Kihara, T.C., Rocha, C., 2009. Técnicas para o estudo taxonômico de copépodes harpacticóides da meiofauna marinha. Asterisco, Porto Alegre.

Kniesz, K., Brandt, A., Riehl, T., 2018. Peritrich epibionts on the hadal isopod species *Macrostylis marionae* n. sp. from the Puerto Rico Trench used as indicator for sex-specific behavior. Deep Sea Res. II. http://dx.doi.org/10.1016/j.dsr2.2017.10.007. (In this issue).

Kröncke, I., Türkay, M., 2003. Structural and functional aspects of the benthic communities in the deep Angola Basin. Mar. Ecol. Prog. Ser. 260, 43–53.

Larkin, M.A., Blackshields, G., Brown, N.P., Chenna, R., McGettigan, P.A., McWilliam, H., et al., 2007. Clustal W and Clustal X version 2.0. Bioinformatics 23 (21), 2947–2948.

Malyutina, M.V., Kussakin, O.G., 1996. Addition to the polar Sea bathyal and abyssal Isopoda (Crustacea). Part 1. Anthuridea, Valvifera, Asellota (Ischnomesidae, Macrostylidae, Nannoniscidae). Zoosyst. Ross. 4, 49–62.

McCartney, M.S., Bennett, S.L., Woodgate-Jones, M.E., 1991. Eastward flow through the Mid-Atlantic Ridge at 11-degrees-N and its influence on the Abyss of the Eastern Basin. J. Phys. Oceanogr. 21 (8), 1089–1121.

Meier, R., Shiyang, K., Vaidya, G., Ng, P.K.L., 2006. DNA barcoding and taxonomy in Diptera: a tale of high intraspecific variability and low identification success. Syst. Biol. 55, 715–728.

Michels, J., Büntzow, M., 2010. Assessment of Congo red as a fluorescence marker for the exoskeleton of small crustaceans and the cuticle of polychaetes. J. Microsc. 238 (2), 95–101.
Morozov, E.G., Tarakanov, R.Y., Makarenko, N.I., 2015. Flows of Antarctic bottom water through fractures in the southern part of the North Mid-Atlantic Ridge. Oceanology 55 (6), 796–800. http://dx.doi.org/10.1134/S0001437015060120.
Osborn, K.J., 2009. Relationships within the Munnopsidae (Crustacea, Isopoda, Asellota) based on three genes. Zool. Scr. 38 (6), 617–635.
Poore, G.C.B., Bruce, N.L., 2012. Global Diversity of Marine Isopods (Except Asellota and Crustacean Symbionts). PLoS One 7 (8), e43529. http://dx.doi.org/10.1371/ journal.pone.0043529.
Pons, J., Barraclough, T., Gomez-Zurita, J., Cardoso, A., Duran, D., Hazell, S., et al., 2006. Sequence-based species delimitation for the dna taxonomy of undescribed insects. Syst. Biol. 55 (4), 595–609. http://dx.doi.org/10.1080/10635150600852011.
Puillandre, N., Lambert, A., Brouillet, S., Achaz, G., 2011. ABGD, automatic barcode gap discovery for primary species delimitation. Mol. Ecol. 21 (8), 1864–1877.
Quattrini, A.M., Georgian, S.E., Byrnes, L., Stevens, A., Falco, R., Cordes, E.E., 2013. Niche divergence by deep-sea octocorals in the genus *Callogorgia* across the continental slope of the Gulf of Mexico. Mol. Ecol. http://dx.doi.org/10.1111/mec.12370.
Radulovici, A.E., Bernard, S.-M., Dufresne, F., 2009. DNA barcoding of marine crustaceans from the Estuary and Gulf of St Lawrence: a regional-scale approach. Mol. Ecol. Resour. 9, 181–187.
Rambaut, A., Suchard, M.A., Xie, D., Drummond, A.J., 2014. Tracer v1. 6.
Ratnasingham, S., Hebert, P.D.N., 2013. A DNA-based Registry for all animal species: the barcode index number (BIN) system (doi.org/). PLoS One 8 (7), e66213. http://dx.doi.org/10.1371/journal.pone.0066213.
Riehl, T., Wilson, G.D., Hessler, R.R., 2012. New Macrostylidae Hansen, 1916 (Crustacea: Isopoda) from the Gay head-Bermuda transect with special consideration of sexual dimorphism. Zootaxa 1–26.
Riehl, T., Brandt, A., 2013. Southern Ocean Macrostylidae reviewed with a key to the species and new descriptions from Maud Rise. Zootaxa 3692 (1), 160–203.
Riehl, T., Brenke, N., Brix, S., Driskell, A., Kaiser, S., Brandt, A., 2014. Field and Laboratory Methods for DNA Studies on Deep-sea Isopod Crustaceans. Retrieved from ⟨http://www.degruyter.com/view/j/popore.2014.35.issue-2/popore-2014-0018/popore-2014-0018.xml⟩.
Riehl, T., Lins, L., Brandt, A., 2018. The effects of depth, distance, and the Mid-Atlantic Ridge on genetic differentiation of abyssal and hadal isopods (Macrostylidae). Deep Sea Res. II (In this issue).
Ritchie, H., Jamieson, A.J., Piertney, S.B., 2015. Phylogenetic relationships among hadal amphipods of the Superfamily Lysianassoidea: implications for taxonomy and biogeography. Deep-Sea Res. Part I-Oceanogr. Res. Pap. 105, 119–131. http://dx.doi.org/10.1016/j.dsr.2015.08.014.
Sars, G.O., 1897. Isopoda. Part VII, VIII. Desmosomidae, Munnopsidae. An account of the Crustacea of Norway with short descriptions and figures of all the species: 117–144.
Schindelin, J., Rueden, C.T., Hinder, M.C., Eliceiri, K.W., 2015. Fiji: an open-source platform for biological-image analysis. Nat. Methods. http://dx.doi.org/10.1002/mrd.22489.
Schneider, Rasband, Eliceiri, 2012. NIH Image to ImageJ: 25 years of image analysis, Nature Methods.
Schwentner, M., Timms, B.V., Richter, S., 2011. An integrative approach to species delineation incorporating different species concepts: a case study of *Limnadopsis* (Branchiopoda: Spinicaudata). Biol. J. Linn. Soc. 104 (3), 575–599.
Sites, J.W., Marshall, J.C., 2004. Operational criteria for delimiting species. Annu. Rev. Ecol., Evol., Syst. 35, 199–227.
Svavarsson, J., Strömberg, J.O., Brattegard, T., 1993. The deep-Sea Asellote (Isopoda, Crustacea) fauna of the northern Seas: species composition, distributional patterns and origin. J. Biogeogr. 20 (5), 537–555.
Talavera, G., Castresana, J., 2007. Improvement of phylogenies after removing divergent and ambiguously aligned blocks from protein sequence alignments. Syst. Biol. 56 (4), 564–577. http://dx.doi.org/10.1080/10635150701472164.
Tyler, P.A., Baker, M., Ramirez-Llodra, E., 2016. Deep-Sea Benthic habitats. In: Clark, Malcolm R., Consalvey, Mireille, Rowden, Ashley A. (Eds.), Biological Sampling in the Deep Sea, First ed. John Wiley & Sons, pp. 1–13.
Wetzer, R., 2001. Hierarchical analysis of mtDNA variation and the use of mtDNA for isopod (Crustacea: Peracarida: Isopoda) systematics. Contrib. Zool. 70, 23–39.
Zhang, J., Kapli, P., Pavlidis, P., Stamatakis, A., 2013. A general species delimitation method with applications to phylogenetic placements. Bioinformatics. http://dx.doi.org/10.1093/bioinformatics/btt499/-/DC1.

Author contributions

The study was designed and conducted by Saskia Brix.

The map (Fig. 1) was made by Simon Bober. The CLSM micrographs (Fig. 4, 5, 14, 15, 22, 23) were made and arranged with captions by S. Bober with contributions of Terue-Cristina Kihara. S. Brix and Claudia Tschesche prepared taxonomic sketches, which S. Bober transformed into digital vector graphics and arranged as final plates with captions (Fig. 6–12, 16–21, 24–27). The description of *Prochelator barnacki* was conducted by S.Bober with contributions of S. Brix. The manuscript was prepared by S. Brix with contributions of S. Bober, C.Tschesche, T.C. Kihara, Amy Driskell and Robert Jennings.

Angelika Brandt had the idea for the project (Vema-TRANSIT) and wrote the proposals, she was the leader of the expedition.

Chapter 4

Is *Acanthocope galatheae* Wolff, 1962 (Crustacea, Isopoda, Munnopsidae) a deep-sea cosmopolitan?

Manuscript

Is *Acanthocope galatheae* Wolff, 1962 (Crustacea, Isopoda, Munnopsidae) a deep-sea cosmopolitan?

Abstract

During this preliminary study, 81 specimens of the suprabenthic natatory asellote *Acanthocope galatheae* from the Atlantic and Pacific were genetically analyzed.

Based on this dataset we propose an early state of speciation into two geographically isolated species and reject the assumed cosmopolitism of *A. galatheae*, the Atlantic and Pacific Ocean is inhabited by two distinct lineages. For the Atlantic however we confirm a pan-Atlantic distribution. Our assumptions are supported by population genetic analyses and the Automatic Barcoding Gap Discovery (ABGD) method.

Introduction

For a long time it had been assumed that deep-sea species are widespread and probably cosmopolitan (Bruun, 1957; Vinogradova, 1997). This was mainly based on the morphological uniformity observed for many species and the assumption that the abyssal deep sea constitutes a vast continuous ecosystem without barriers to dispersal (Danovaro et al., 2008; Ramirez-Llodra et al., 2010). However, the abyssal benthal is partially separated by land masses, seamounts, deep-sea trenches and mid-ocean ridges (Smith et al., 2008), and also molecular genetic analyses have challenged these assumptions, showing that many species, which were assumed to be cosmopolitan, comprise several genetically (and often morphologically) differentiated species, each with a much narrower distribution range (Brandt et al., 2014; Brix et al., 2015, 2014, 2011; Brökeland, 2010; Bucklin et al., 1987; Eustace et al., 2016; France and Kocher, 1996; Held, 2003; Held and Wägele, 2005; Krapp-Schickel and De Broyer, 2014; Larsen, 2003; Leese and Held, 2008; Miyamoto et al., 2010; Raupach and Wägele, 2006; Schnurr et al., 2018; Wilson et al., 2007).

Even nowadays some cosmopolitan deep-sea species are (Brandt et al., 2012). One of which is *Acanthocope galatheae* Wolff, 1962 (unaccepted synonym: *A. galathea*), a munnopsid isopod that has been sampled in all world oceans (Malyutina et al., 2017; Schmid et al., 2002).

Munnopsid isopods, like all peracarid crustaceans, are suprabenthic brooders without a free-swimming larval stage, therefore a limited dispersal ability is generally assumed (Wilson and Hessler, 1987). However, Munnopsidae are facultative but capable swimmers (Hessler and Strömberg, 1989; Marshall and Diebel, 1995). And geographically wide, up to cosmopolitan distributions were attested for Peracarida before (France and Kocher, 1996; Havermans et al., 2013; Leese et al., 2010; Riehl and Kaiser, 2012). However all knowledge

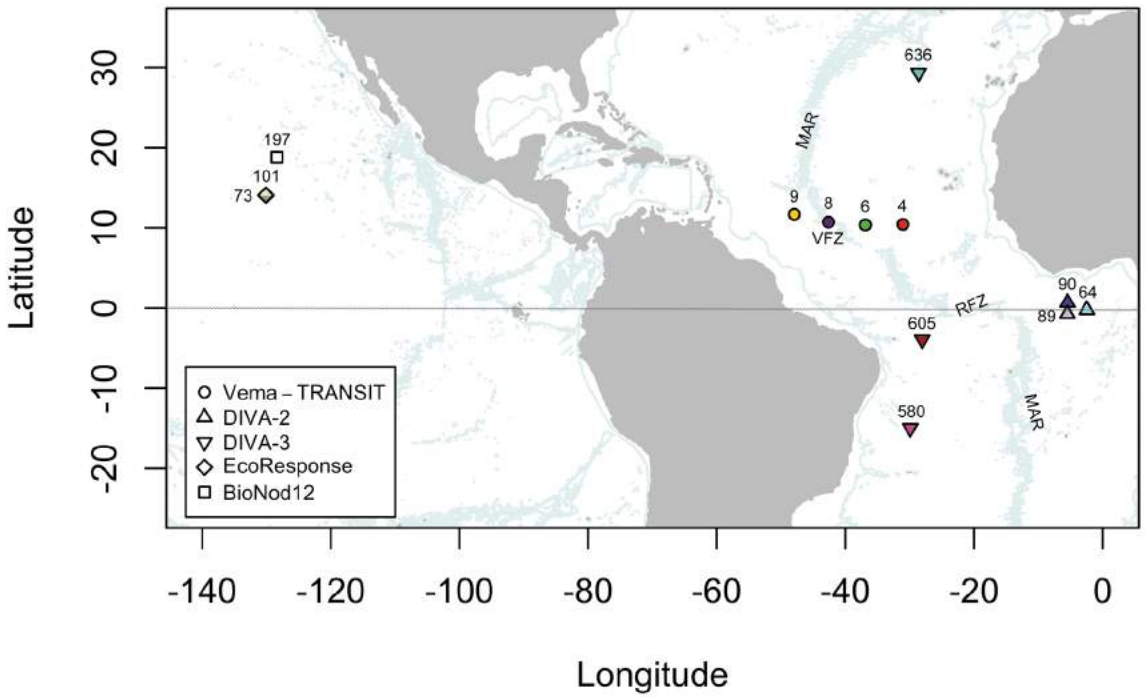

Fig. 1: Map of the sampling regions. Expeditions are indicated with unique symbols and station number. The stations are color coded to match the haplotype networks. 3,000 m depth lines were plotted. MAR = Mid-Atlantic Ridge, VFZ = Vema Fracture Zone, RFZ= Romanche Fracture Zone

about the distribution of *A. galatheae* is based on morphological similarities (Malyutina, 1999; Schmid et al., 2002; Wolff, 1962) and the consistency of characters is not without a doubt (Malyutina, 1999). Furthermore, widespread peracarid morphospecies were repeatedly revealed as multiple cryptic species (Brökeland and Raupach, 2008; France and Kocher, 1996; Havermans et al., 2013; Held, 2003; Raupach et al., 2007; Raupach and Wägele, 2006).

To assess the presumed cosmopolitism of *A. galatheae,* we herein analyzed 81 individuals from multiple expeditions sampled in the Atlantic and Pacific Ocean based on two mitochondrial genetic markers.

Material and Methods

Sampling

The material used for this study was sampled during the Vema-TRANSIT, EcoResponse, BioNod12, DIVA-2 and DIVA-3 expeditions (Fig. 1, Tab. 1).

In total we have 74 individuals from twelve sampling sites in the Atlantic and seven individuals from three sampling sites in the Pacific. Additionally, one individual from GenBank was included in the COI phylogram: *Acanthocope* sp. (EF682286.1) from Monterey Bay, California.

The samples were obtained using a (camera-) epibenthic sledge (C-EBS) (Brandt et al., 2013; Brenke, 2005) with a mesh size of 500 µm, the cod ends (thermally insulated since DIVA-3 expedition) had a mesh size of 300 µm. The samples were sieved with filtered seawater, bulk-fixed in

96 % precooled, denatured ethanol and stored at -20° C for 24–48 h on board.

Genetic analyses

To preserve the material in good condition, whole specimens were incubated in 30µl Chelex (6 % Chelex resin) for extraction. The lab protocol we used was described in (Bober et al., 2018a). We were able to retrieve 55 16S and 32 COI sequences of 56 individuals from Vema-TRANSIT and DIVA-3 material (Tab. 1). This protocol was unsuccessful with DIVA-1 and DIVA-2 museum material, but 17 COI sequences from the DIVA-2 expedition were available as unpublished data from Saskia Brix (DZMB), which are included herein. In the Pacific Ocean four individuals of *A. galatheae* were sampled in the Clarion-Clipperton Zone (CCZ) in 2015 during the EcoResponse expedition. The lab work was performed in the Smithsonian Lab in Washington following a standard lab protocol (pers. comm. Saskia Brix). Three further COI sequences of *A. galatheae* from the Pacific are available online at GenBank (KJ736109.1, KJ736110.1, KJ736111.1), which were also sampled in the CCZ during the BioNod 12 expedition by (Janssen et al., 2015).

Unfortunately, the two genes were not successfully amplified or sequenced for all specimens. The COI dataset lacks 23 individuals from the DIVA-3 expedition and two individuals from the Vema-TRANSIT expedition. The 16S dataset on the other hand lacks the DIVA-2 material (18 individuals) and the BioNod12 material from the Pacific (3 individuals) and one individual from DIVA-3. Only 33 of 81 individuals yielded both genes. To retrieve as much information as possible, we analyzed both genes separately as well as concatenated (the latter including only these 33 specimens with both genes available). Specimens for which only one gene sequence is available were excluded from the concatenated alignment.

The raw-data was processed in Geneious 9.0.5 (Kearse et al., 2012) and aligned using MUSCLE (Edgar, 2004), the resulting alignments were manually checked for errors.

All specimens were morphologically determined as *A. galatheae*. Furthermore the Automatic Barcoding Gap Detection (ABGD) analysis was used to identify species boundaries within the COI, 16S and the concatenated dataset. We used a *p*-distance matrix exported from MEGA 7 (Kumar et al., 2016) and simple distances with no evolution model applied with the following settings: Pmin= 0.005, Pmax=0.1, X=0.05, nbins=20, steps=100. For phylogenetic analyses the best model of nucleotide substitution (GTR with no invariable sites and equal rates for all sites) was selected by Hierarchical Likelihood Ratio Tests (hLRT) with MrModeltest 2.3 (Nylander, 2004) implemented in PAUP*4.0a147 (Swofford, 2001). CIPRES (Miller et al., 2010) was used to calculate the phylogenetic trees with MrBayes on XSEDE (3.2.6) (Huelsenbeck and Ronquist, 2001; Ronquist and Huelsenbeck, 2003). The analyses were running for 10,000,000 generations with a sample frequency of 1,000 and the first 25 % were discarded as burnin. For the COI alignment *Betamorpha fusiformis* (Barnard, 1920) (EF682291.1) (Munnopsidae) was used as outgroup. Furthermore, *Acanthocope* sp. (EF682286.1) from Monterey Bay,

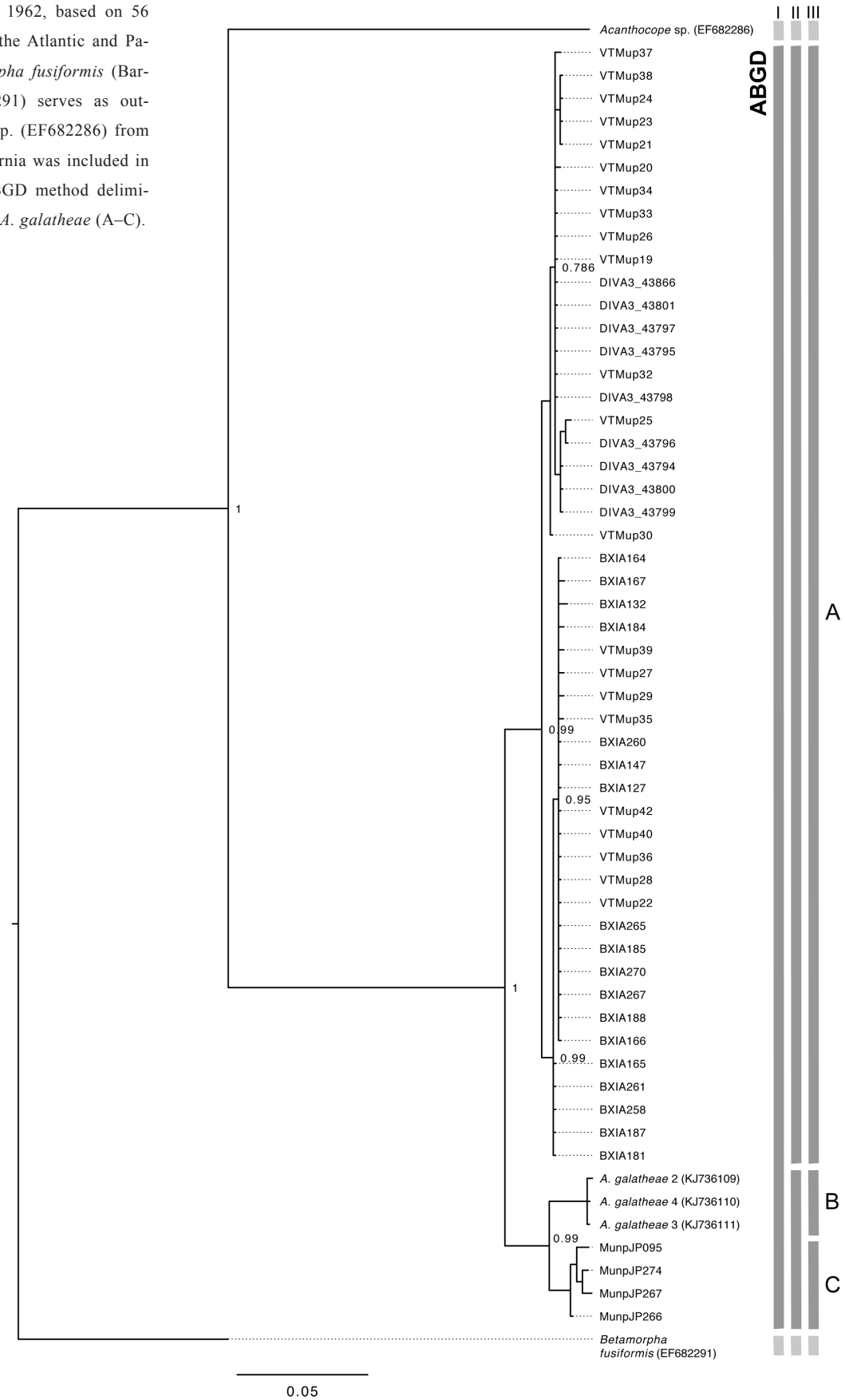

Fig. 2: Bayesian phylogram of *Acanthocope galatheae* Wolff, 1962, based on 56 COI sequences from the Atlantic and Pacific Ocean. *Betamorpha fusiformis* (Barnard, 1920) (EF682291) serves as outgroup. *Acanthocope* sp. (EF682286) from Monterey Bay, California was included in the analyses. The ABGD method delimitated 1–3 lineages for *A. galatheae* (A–C).

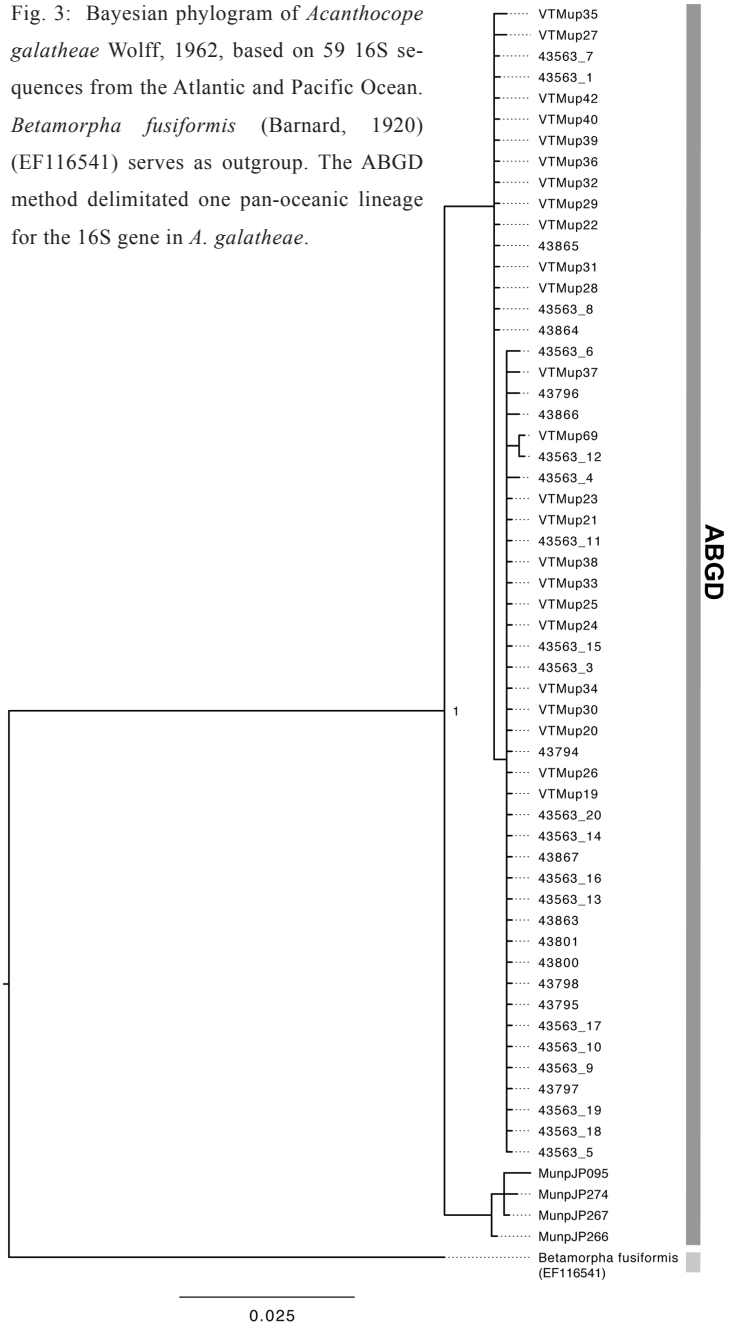

Fig. 3: Bayesian phylogram of *Acanthocope galatheae* Wolff, 1962, based on 59 16S sequences from the Atlantic and Pacific Ocean. *Betamorpha fusiformis* (Barnard, 1920) (EF116541) serves as outgroup. The ABGD method delimitated one pan-oceanic lineage for the 16S gene in *A. galatheae*.

California was included. One COI sequence of *A. galatheae* (EF682285.1) is available on GenBank, but was accidentally uploaded and had to be excluded from the analyses due to an insufficient quality (pers. comm. Karen Osborn). For the 16S alignment a GenBank record of *B. fusiformis* (EF116541.1) was used as outgroup.

From the previously described alignments without outgroup a median joining network was calculated in PopArt (Leigh and Bryant, 2015). The haplotype networks were also calculated separately for the genes COI and 16S and together as a concatenated alignment. PopArt crops all sequences to equal length, therefore the haplotype network lacks mutations found in the beginning or end of an alignment.

Population structure and diversity analyses were performed in Arlequin 3.5 (Excoffier and Lischer, 2010). We ran an AMOVA, which measures genetic divergence among and within predefined groups. For the whole dataset we defined an Atlantic and Pacific group. For the Atlantic we tested the eastern against the western Atlantic to evaluate a possible barrier effect induced by the MAR in the COI gene. The sampling site 8 within the MAR was excluded from this analysis.

Additionally we used the pairwise Φ_{ST} to measure the degree of population differentiation among haplotypes and ran a Mantel test, which tested a correlation between pairwise Φ_{ST} and geographic distance in kilometres. All Arlequin analyses ran with 1,000 permutations.

Results

Alignment data

The COI alignment consisted of 56 sequences and had a length of 673 bp of which 614 positions were conserved, 58 positions variable, 8 positions singletons, and 50 position parsimony informative.

Tab. 1: All material used during this study.

Field-ID	Species	Station	Area	Expedition	latitude (DD)	longitude (DD)	COI	16S	Collection-no. (ZMHK-)	GenBank accession no.	
										COI	16S
VTMup021	*Acanthocope galatheae sensu stricto*	6	NE-Atlantic	Vema-TRANSIT	N10.35000°	W36.91767°	x	x	47063	MG721975	MG721992
VTMup023	*Acanthocope galatheae sensu stricto*	6	NE-Atlantic	Vema-TRANSIT	N10.35000°	W36.91767°	x	x	47065	MG721976	MG721987
VTMup030	*Acanthocope galatheae sensu stricto*	4	NE-Atlantic	Vema-TRANSIT	N10.42700°	W31.07333°	x	x	47072	MG721974	MG721991
VTMup032	*Acanthocope galatheae sensu stricto*	8	Vema	Vema-TRANSIT	N10.71667°	W42.66217°	x	x	47074	MG721983	MG722001
VTMup037	*Acanthocope galatheae sensu stricto*	4	NE-Atlantic	Vema-TRANSIT	N10.42700°	W31.07333°	x	x	47079	MG721972	MG721986
VTMup027	*Acanthocope galatheae sensu stricto*	4	NE-Atlantic	Vema-TRANSIT	N10.42700°	W31.07333°	x	x	47069	MG721962	MG721998
VTMup028	*Acanthocope galatheae sensu stricto*	4	NE-Atlantic	Vema-TRANSIT	N10.42700°	W31.07333°	x	x	47070	MG721967	MG721999
VTMup029	*Acanthocope galatheae sensu stricto*	4	NE-Atlantic	Vema-TRANSIT	N10.42700°	W31.07333°	x	x	47071	MG721963	MG722000
VTMup035	*Acanthocope galatheae sensu stricto*	4	NE-Atlantic	Vema-TRANSIT	N10.42700°	W31.07333°	x	x	47077	MG721964	MG721985
VTMup036	*Acanthocope galatheae sensu stricto*	4	NE-Atlantic	Vema-TRANSIT	N10.42700°	W31.07333°	x	x	47078	MG721968	MG722002
VTMup038	*Acanthocope galatheae sensu stricto*	4	NE-Atlantic	Vema-TRANSIT	N10.42700°	W31.07333°	x	x	47080	MG721978	MG721996
VTMup019	*Acanthocope galatheae sensu stricto*	6	NE-Atlantic	Vema-TRANSIT	N10.35000°	W36.91767°	x	x	47061	MG721979	MG721988
VTMup020	*Acanthocope galatheae sensu stricto*	6	NE-Atlantic	Vema-TRANSIT	N10.35000°	W36.91767°	x	x	47062	MG721973	MG721990
VTMup022	*Acanthocope galatheae sensu stricto*	6	NE-Atlantic	Vema-TRANSIT	N10.35000°	W36.91767°	x	x	47064	MG721966	NA
VTMup024	*Acanthocope galatheae sensu stricto*	6	NE-Atlantic	Vema-TRANSIT	N10.35000°	W36.91767°	x	x	47066	MG721977	MG721993
VTMup025	*Acanthocope galatheae sensu stricto*	6	NE-Atlantic	Vema-TRANSIT	N10.35000°	W36.91767°	x	x	47067	MG721971	MG721994
VTMup026	*Acanthocope galatheae sensu stricto*	6	NE-Atlantic	Vema-TRANSIT	N10.35000°	W36.91767°	x	x	47068	MG721980	MG721989
VTMup031	*Acanthocope galatheae sensu stricto*	8	Vema	Vema-TRANSIT	N10.71667°	W42.66217°	bad	x	47073	NA	MG722004
VTMup033	*Acanthocope galatheae sensu stricto*	8	Vema	Vema-TRANSIT	N10.71667°	W42.66217°	x	x	47075	MG721981	MG721995
VTMup034	*Acanthocope galatheae sensu stricto*	8	Vema	Vema-TRANSIT	N10.71667°	W42.66217°	x	x	47076	MG721982	MG721997
VTMup039	*Acanthocope galatheae sensu stricto*	9	NW-Atlantic	Vema-TRANSIT	N11.67883°	W47.96717°	x	x	47081	MG721965	MG722003
VTMup040	*Acanthocope galatheae sensu stricto*	9	NW-Atlantic	Vema-TRANSIT	N11.67883°	W47.96717°	x	x	47082	MG721969	MG722005
VTMup042	*Acanthocope galatheae sensu stricto*	9	NW-Atlantic	Vema-TRANSIT	N11.67883°	W47.96717°	x	x	47083	MG721970	MG722006
VTMup069	*Acanthocope galatheae sensu stricto*	9	NW-Atlantic	Vema-TRANSIT	N11.67883°	W47.96717°	bad	x	47084	NA	MG721984
43563-1	*Acanthocope galatheae sensu stricto*	636	NE-Atlantic	DIVA 3	N29.32067°	W28.63233°	NA	x	NA	NA	NA
43863	*Acanthocope galatheae sensu stricto*	605	SW-Atlantic	DIVA 3	S3.95817°	W28.07783°	NA	x	NA	NA	NA
43864	*Acanthocope galatheae sensu stricto*	605	SW-Atlantic	DIVA 3	S3.95817°	W28.07783°	NA	x	NA	NA	NA
43865	*Acanthocope galatheae sensu stricto*	605	SW-Atlantic	DIVA 3	S3.95817°	W28.07783°	NA	x	NA	NA	NA
43866	*Acanthocope galatheae sensu stricto*	605	SW-Atlantic	DIVA 3	S3.95817°	W28.07783°	x	x	NA	NA	NA
43867	*Acanthocope galatheae sensu stricto*	605	SW-Atlantic	DIVA 3	S3.95817°	W28.07783°	NA	x	NA	NA	NA

43794	*Acanthocope galatheae sensu stricto*	580	SW-Atlantic	DIVA 3	S14.98183°	W29.94150°	x	x	NA	NA	NA
43795	*Acanthocope galatheae sensu stricto*	580	SW-Atlantic	DIVA 3	S14.98183°	W29.94150°	x	x	NA	NA	NA
43796	*Acanthocope galatheae sensu stricto*	580	SW-Atlantic	DIVA 3	S14.98183°	W29.94150°	x	x	NA	NA	NA
43797	*Acanthocope galatheae sensu stricto*	580	SW-Atlantic	DIVA 3	S14.98183°	W29.94150°	x	x	NA	NA	NA
43798	*Acanthocope galatheae sensu stricto*	580	SW-Atlantic	DIVA 3	S14.98183°	W29.94150°	x	x	NA	NA	NA
43799	*Acanthocope galatheae sensu stricto*	580	SW-Atlantic	DIVA 3	S14.98183°	W29.94150°	x	NA	NA	NA	NA
43800	*Acanthocope galatheae sensu stricto*	580	SW-Atlantic	DIVA 3	S14.98183°	W29.94150°	x	x	NA	NA	NA
43801	*Acanthocope galatheae sensu stricto*	580	SW-Atlantic	DIVA 3	S14.98183°	W29.94150°	x	x	NA	NA	NA
43563-3	*Acanthocope galatheae sensu stricto*	636	NE-Atlantic	DIVA 3	N29.32067°	W28.63233°	NA	x	NA	NA	NA
43563-4	*Acanthocope galatheae sensu stricto*	636	NE-Atlantic	DIVA 3	N29.32067°	W28.63233°	NA	x	NA	NA	NA
43563-5	*Acanthocope galatheae sensu stricto*	636	NE-Atlantic	DIVA 3	N29.32067°	W28.63233°	NA	x	NA	NA	NA
43563-6	*Acanthocope galatheae sensu stricto*	636	NE-Atlantic	DIVA 3	N29.32067°	W28.63233°	NA	x	NA	NA	NA
43563-7	*Acanthocope galatheae sensu stricto*	636	NE-Atlantic	DIVA 3	N29.32067°	W28.63233°	NA	x	NA	NA	NA
43563-8	*Acanthocope galatheae sensu stricto*	636	NE-Atlantic	DIVA 3	N29.32067°	W28.63233°	NA	x	NA	NA	NA
43563-9	*Acanthocope galatheae sensu stricto*	636	NE-Atlantic	DIVA 3	N29.32067°	W28.63233°	NA	x	NA	NA	NA
43563-10	*Acanthocope galatheae sensu stricto*	636	NE-Atlantic	DIVA 3	N29.32067°	W28.63233°	NA	x	NA	NA	NA
43563-11	*Acanthocope galatheae sensu stricto*	636	NE-Atlantic	DIVA 3	N29.32067°	W28.63233°	NA	x	NA	NA	NA
43563-12	*Acanthocope galatheae sensu stricto*	636	NE-Atlantic	DIVA 3	N29.32067°	W28.63233°	NA	x	NA	NA	NA
43563-13	*Acanthocope galatheae sensu stricto*	636	NE-Atlantic	DIVA 3	N29.32067°	W28.63233°	NA	x	NA	NA	NA
43563-14	*Acanthocope galatheae sensu stricto*	636	NE-Atlantic	DIVA 3	N29.32067°	W28.63233°	NA	x	NA	NA	NA
43563-15	*Acanthocope galatheae sensu stricto*	636	NE-Atlantic	DIVA 3	N29.32067°	W28.63233°	NA	x	NA	NA	NA
43563-16	*Acanthocope galatheae sensu stricto*	636	NE-Atlantic	DIVA 3	N29.32067°	W28.63233°	NA	x	NA	NA	NA
43563-17	*Acanthocope galatheae sensu stricto*	636	NE-Atlantic	DIVA 3	N29.32067°	W28.63233°	NA	x	NA	NA	NA
43563-18	*Acanthocope galatheae sensu stricto*	636	NE-Atlantic	DIVA 3	N29.32067°	W28.63233°	NA	x	NA	NA	NA
43563-19	*Acanthocope galatheae sensu stricto*	636	NE-Atlantic	DIVA 3	N29.32067°	W28.63233°	NA	x	NA	NA	NA
43563-20	*Acanthocope galatheae sensu stricto*	636	NE-Atlantic	DIVA 3	N29.32067°	W28.63233°	NA	x	NA	NA	NA
BXIA164	*Acanthocope galatheae sensu stricto*	89	equatorial E Atlantic	DIVA 2	S0.71583°	W5.52150°	x	x	NA	NA	NA
BXIA165	*Acanthocope galatheae sensu stricto*	89	equatorial E Atlantic	DIVA 2	S0.71583°	W5.52150°	x	NA	NA	NA	NA
BXIA167	*Acanthocope galatheae sensu stricto*	89	equatorial E Atlantic	DIVA 2	S0.71583°	W5.52150°	x	NA	NA	NA	NA
BXIA132	*Acanthocope galatheae sensu stricto*	90	equatorial E Atlantic	DIVA 2	N0.67483°	W5.49517°	x	NA	NA	NA	NA
BXIA184	*Acanthocope galatheae sensu stricto*	89	equatorial E Atlantic	DIVA 2	S0.71583°	W5.52150°	x	NA	NA	NA	NA
BXIA261	*Acanthocope galatheae sensu stricto*	64	equatorial E Atlantic	DIVA 2	S0.22117°	W2.49850°	x	NA	NA	NA	NA

BXIA258	*Acanthocope galatheae sensu stricto*	64	equatorial E Atlantic	DIVA 2	S0.22117°	W2.49850°	x	NA	NA	NA	NA
BXIA187	*Acanthocope galatheae sensu stricto*	89	equatorial E Atlantic	DIVA 2	S0.71583°	W5.52150°	x	NA	NA	NA	NA
BXIA181	*Acanthocope galatheae sensu stricto*	89	equatorial E Atlantic	DIVA 2	S0.71583°	W5.52150°	x	NA	NA	NA	NA
BXIA267	*Acanthocope galatheae sensu stricto*	64	equatorial E Atlantic	DIVA 2	S0.22117°	W2.49850°	x	NA	NA	NA	NA
BXIA188	*Acanthocope galatheae sensu stricto*	89	equatorial E Atlantic	DIVA 2	S0.71583°	W5.52150°	x	NA	NA	NA	NA
BXIA270	*Acanthocope galatheae sensu stricto*	64	equatorial E Atlantic	DIVA 2	S0.22117°	W2.49850°	x	NA	NA	NA	NA
BXIA265	*Acanthocope galatheae sensu stricto*	64	equatorial E Atlantic	DIVA 2	S0.22117°	W2.49850°	x	NA	NA	NA	NA
BXIA185	*Acanthocope galatheae sensu stricto*	89	equatorial E Atlantic	DIVA 2	S0.71583°	W5.52150°	x	NA	NA	NA	NA
BXIA260	*Acanthocope galatheae sensu stricto*	64	equatorial E Atlantic	DIVA 2	S0.22117°	W2.49850°	x	NA	NA	NA	NA
BXIA147	*Acanthocope galatheae sensu stricto*	90	equatorial E Atlantic	DIVA 2	N0.67483°	W5.49517°	x	NA	NA	NA	NA
BXIA127	*Acanthocope galatheae sensu stricto*	90	equatorial E Atlantic	DIVA 2	N0.67483°	W5.49517°	x	NA	NA	NA	NA
BXIA166	*Acanthocope galatheae sensu stricto*	89	equatorial E Atlantic	DIVA 2	S0.71583°	W5.52150°	x	NA	NA	NA	NA
MunpJP095	*Acanthocope galatheae sensu lato*	197	CCZ / NE Pacific	EcoResponse	N18.81083°	W128.37916°	x	x	NA	NA	NA
MunpJP274	*Acanthocope galatheae sensu lato*	197	CCZ / NE Pacific	EcoResponse	N18.81083°	W128.37916°	x	x	NA	NA	NA
MunpJP266	*Acanthocope galatheae sensu lato*	197	CCZ / NE Pacific	EcoResponse	N18.81083°	W128.37916°	x	x	NA	NA	NA
MunpJP267	*Acanthocope galatheae sensu lato*	197	CCZ / NE Pacific	EcoResponse	N18.81083°	W128.37916°	x	x	NA	NA	NA
Acanthocope galathea 2	*Acanthocope galatheae sensu lato*	73	CCZ / NE Pacific	BioNod12	N14.05125°	W130.09426°	x	NA	NA	KJ736109.1	NA
Acanthocope galathea 3	*Acanthocope galatheae sensu lato*	101	CCZ / NE Pacific	BioNod12	N15.15405°	W127.05992°	x	NA	NA	KJ736111.1	NA
Acanthocope galathea 4	*Acanthocope galatheae sensu lato*	73	CCZ / NE Pacific	BioNod12	N14.05125°	W130.09426°	x	NA	NA	KJ736110.1	NA
Acanthocope sp. MB H2	*Acanthocope sp.*		Monterey Bay, California				x	NA	NA	EF682286	NA

The 16S alignment consisted of 59 sequences and had a length of 514 bp of which 489 positions were conserved, 24 positions variable, 10 positions singletons, and 14 position parsimony informative.

The concatenated alignment consisted of 33 sequences and had a length of 1,187 bp of which 1,115 positions were conserved, 69 positions variable, 15 positions singletons, and 54 position parsimony informative. The gene fragment was free of stop codons and except for one single amino acid change from alanine to threonine in specimen ZMH K-47077 and one mutation from Glycine to Valine in MunpJP267 all mutations were neutral.

Genetic analyses

The ABGD found one (Fig. 2ABC) to three groups (Fig. 2A, B, C) (hypothetical species) in the COI gene, one group in the 16S gene (Fig. 3) and two groups in the concatenated dataset (Fig. 4).

Within the COI gene the ABGD barcode thresholds were for three groups 0.5–0.6 % (Fig. 2-3), here all Atlantic specimens were considered one lineage and in the Pacific two more lineages were detected. These two Pacific lineages were

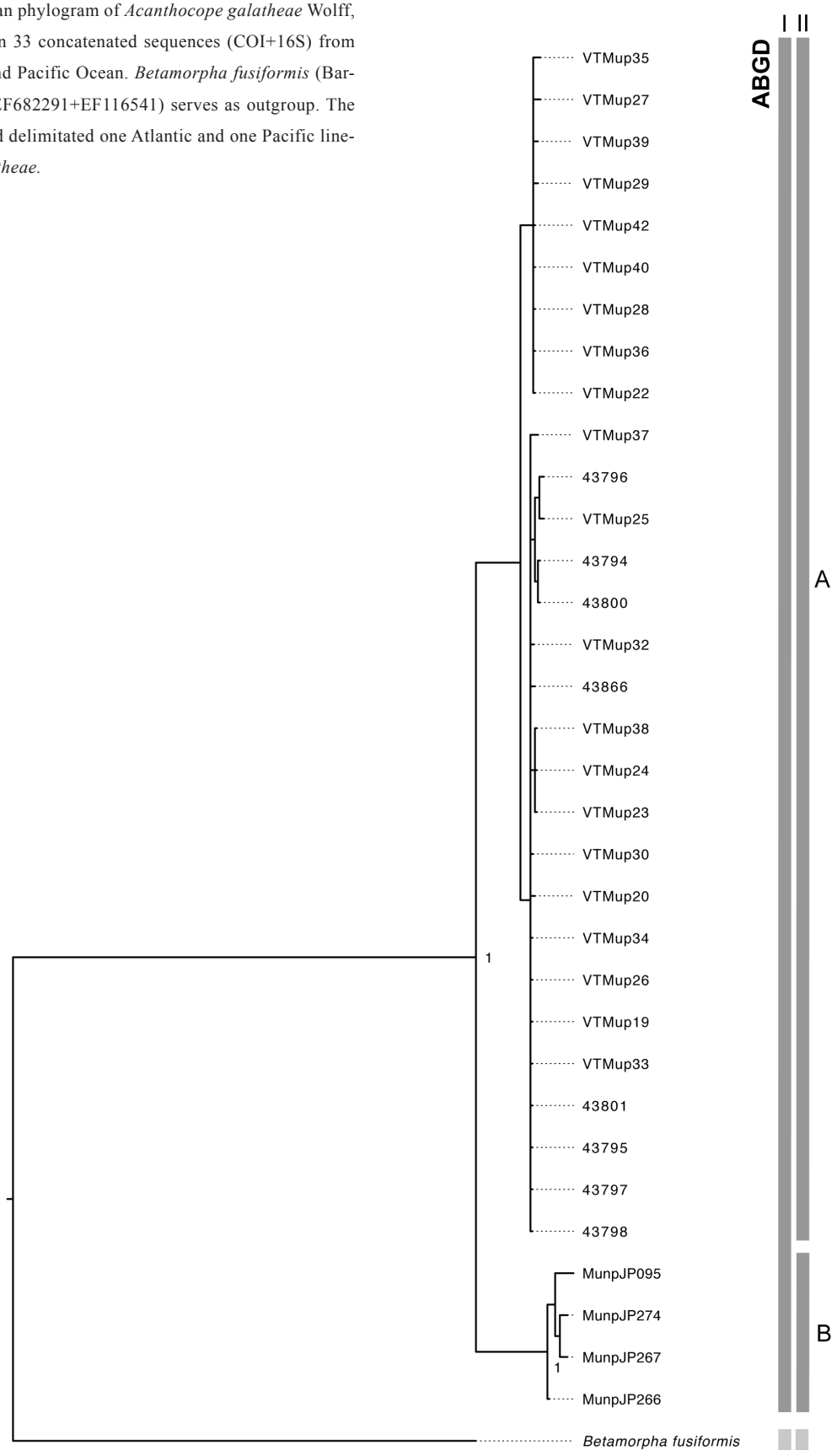

Fig. 4: Bayesian phylogram of *Acanthocope galatheae* Wolff, 1962, based on 33 concatenated sequences (COI+16S) from the Atlantic and Pacific Ocean. *Betamorpha fusiformis* (Barnard, 1920) (EF682291+EF116541) serves as outgroup. The ABGD method delimitated one Atlantic and one Pacific lineage in *A. galatheae.*

sampled only 428–558 km apart in the CCZ region, but during two different expeditions (Eco-Response, BioNod 12). The barcode threshold for two groups was 0.7–1.5 % (Fig. 2-2). Here, a barcoding gap was found between Atlantic and Pacific populations. With a barcode threshold of ≥1.6 % (Fig. 2-1), the model recognizes one cosmopolitan species.

In the concatenated subsample the ABGD detected two species-like lineages separated in an Atlantic and a Pacific population with a threshold of 0.5–3.7 % (Fig. 4 II) or one cosmopolitan species with a threshold of ≥3.8 % (Fig. 4 I).

For the 16S genetical marker a pan-oceanic genetical distance of 2.18–3.72 % and for the COI marker a distance of 4.58–6.99 % uncorrected pairwise-distance (*p*-distance) was measured. The concatenated dataset had a pan-oceanic *p*-distance of 3.83–8.58 %.

The genetic variance was in both genes highest between Atlantic and Pacific populations (AMOVA: 82.9 % (COI) and 92.2 % (16S)) but the Φ_{CT} (between groups) derived from the AMOVA was only significant within the COI gene (AMOVA Φ_{CT} = 0.829, *P* = 0.002) (Tab. 2). The pairwise Φ_{CT} however was significant for both genes (pairwise $\Phi_{CT\ (COI)}$ =0.84527, *P* = 0.000; pairwise $\Phi_{CT\ (16S)}$ =0.92519, *P* = 0.000).

The Mantel test was significant for both genes, suggesting correlation between geographic and genetic distance, which indicates isolation-by-distance (Tab. 3).

The ABGD detected only one group in the Atlantic for both markers (Fig. 2A). However, regarding the haplotype network (Fig. 5C) there is a geographical trend noticeable. The haplotype group 1 (Fig. 5C, HG1) consists of individuals from the Vema Fracture Zone (VFZ) and the SW Atlantic. The haplotype group 2 (HG2) consists of individuals from the VFZ and eastern equatorial Atlantic. In the Southern Atlantic eastern and western populations seem to be separated, an AMOVA however found no significant divergence between both groups (Tab. 4), but the pairwise Φ_{CT} found a significant genetic variance between the Eastern and Western Atlantic (pairwise $\Phi_{CT\ (COI)}$ =0.25997, *P* = 0.000). The 16S gene showed no differentiation

Tab. 2: Results of the AMOVA calculated in Arlequin 3.5. Results are shown for the 16S and COI gene of *Acanthocope galatheae* Wolff, 1962 and a concatenated alignment of both genes. The populations were grouped in Atlantic and Pacific populations. Significant *P*-values were marked with asterisks. < 0.05*; < 0.001**; < 0.0001***.

Source of Variation	d.f.	Percentage of variation	FCT	FSC	FST	*P*
Between Atlantic and Pacific	1	82.90	0.829 ***			0.002
Among stations in Atlantic or Pacific	10	10.50		0.934 ***		0.000
Within stations	42	6.60			0.829 ***	0.000
Acanthocope galatheae COI						
Between Atlantic and Pacific	1	92.22	0.922			0.125
Among stations in Atlantic or Pacific	6	1.15		0.148*		0.010
Within stations	48	6.63			0.934 ***	0.000
Acanthocope galatheae 16S						
Between Atlantic and Pacific	1	88.39	0.884			0.132
Among stations in Atlantic or Pacific	5	4.08		0.351**		0.003
Within stations	26	7.53			0.925 ***	0.000
Acanthocope galatheae concatenated						

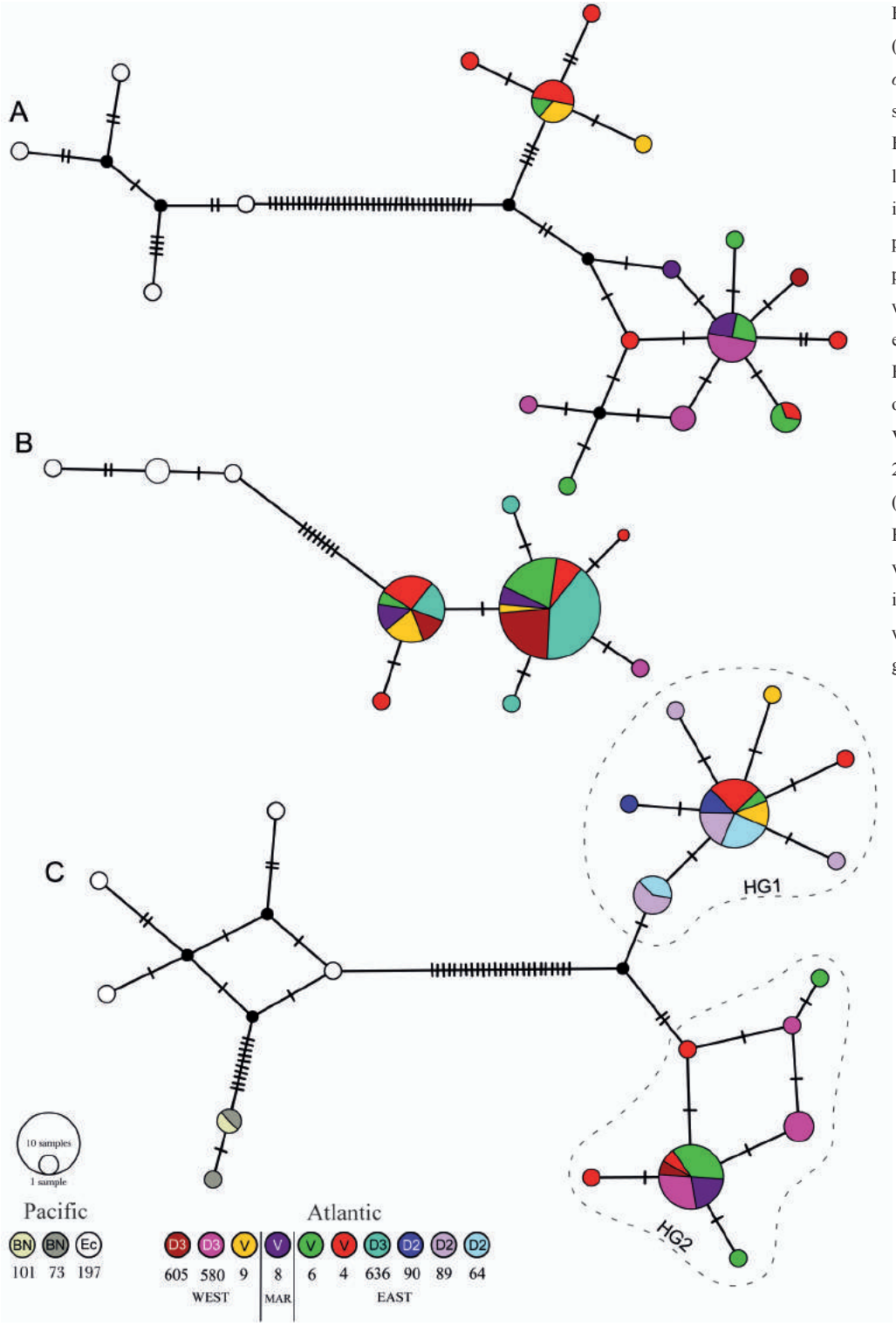

Fig. 5: Haplotype networks (Median Joining) of *Acanthocope galatheae* Wolff, 1962, sampling sites are color-coded. Each circle is one sampled haplotype and the size to the circle indicates the number of samples per haplotype. The sampling sites were sorted from west to east and the respective expeditions were abbreviated: Ec =EcoResponse, BN= BioNod12, D3 = DIVA-3, V = Vema-TRANSIT, D2 = DIVA-2. A. Concatenated alignment (COI+16S) of 33 individuals B. 16S alignment of 59 individuals C. COI alignment of 56 individuals, the Atlantic Ocean was sorted into two haplotype groups (HG1 and HG2).

in the Atlantic (Fig. 5B). In contrast to the pan-oceanic dataset the Mantel test is insignificant for the Atlantic sector in both genetical markers indicating no correlation between Φ_{ST} and geographic distance.

Discussion

Is *Acanthocope galatheae* a cosmopolitan species?

Due to a homogenous habitat in the abyss the occurrence of cosmopolitans in the deep sea was expected (Vinogradova, 1997). Genetic analyses consequently revealed that many previously assumed widespread deep-sea species are often species complexes (Brandt et al., 2014; Brix et al., 2015, 2014, 2011; Brökeland, 2010; Bucklin et al., 1987; Eustace et al., 2016; France and Kocher, 1996; Held, 2003; Held and Wägele, 2005; Larsen, 2003; Leese and Held, 2008; Miyamoto et al., 2010; Raupach and Wägele, 2006; Wilson et al., 2007). Nevertheless, *Acanthocope galatheae* was considered a deep-sea cosmopolitan until today (Brandt et al., 2012; Malyutina et al., 2017; Schmid et al., 2002). Cosmopolitism is

Tab. 3: Genetic indices, parameters of demographic history and a Mantel test for the COI and 16S gene of *Acanthocope galatheae* Wolff, 1962 and a concatenated alignment of both genes.

Species	Marker	Group	Expedition	Station	n	No. Of haplotypes	Haplotype diversity (h) ± SD	Nucleotide diversity (πn) ± SD	Mantel Test	
									rY1 correlation coefficient (*P*-value)	Determination of Y1 (ΦST) by X1 (distance in km) (%)
Acanthocope galatheae	COI	Atlantic	Vema	4	8	6	0.8929 ± 0.1113	0.007482 ± 0.004681	0.618218 (0.000)	0.382193
				6	7	5	0.9048 ± 0.1033	0.005355 ± 0.003545		
				8	3	1	0	0		
				9	3	2	0.6667 ± 0.3143	0.001013 ± 0.001264		
			DIVA-3	636	NA	NA	NA	NA		
				605	1	1	0	0		
				580	8	4	0.7500 ± 0.1391	0.001281 ± 0.001160		
			DIVA-2	64	6	2	0.5333 ± 0.1721	0.000929 ± 0.001021		
				90	3	2	0.6667 ± 0.3143	0.002303 ± 0.002366		
				89	8	5	0.8571 ± 0.1083	0.001925 ± 0.001624		
			All		47	23	0.9315 ± 0.0227	0.007620 ± 0.004283		
		Pacific	BioNod12	73	2	2	1.0000 ± 0.5000	0.001828 ± 0.002585		
				101	1	1	0	0		
			EcoResponse	197	4	4	1.0000 ± 0.1768	0.006876 ± 0.005142		
			All		7	7	1.0000 ± 0.0764	0.017671 ± 0.010622		
		Total	All		54	30	0.9483 ± 0.0181	0.019436 ± 0.009977		
	16S	Atlantic	Vema	4	8	4	0.7857 ± 0.1127	0.002035 ± 0.001716	0.779456 (0.049)	0.607551
				6	7	3	0.5238 ± 0.2086	0.001118 ± 0.001167		
				8	3	2	0.6667 ± 0.3143	0.001307 ± 0.001630		
				9	3	1	0	0		
			DIVA-3	636	19	5	0.5263 ± 0.1266	0.001189 ± 0.001191		
				605	5	3	0.8000 ± 0.1640	0.002004 ± 0.001866		
				580	7	2	0.2857 ± 0.1964	0.000561 ± 0.000767		
			All		52	14	0.8341 ± 0.0325	0.001661 ± 0.001424		
		Pacific	EcoResponse	197	4	4	1.0000 ± 0.1768	0.004167 ± 0.003495		
		Total	All		56	18	0.8571 ± 0.0299	0.004727 ± 0.003016		
	Concatenated	Atlantic	Vema	4	8	7	0.9643 ± 0.0772	0.005230 ± 0.003184	0.642943 (0.038)	0.413376
				6	7	5	0.9048 ± 0.1033	0.003262 ± 0.002136		
				8	3	2	0.6667 ± 0.3143	0.000572 ± 0.000713		
				9	3	2	0.6667 ± 0.3143	0.000571 ± 0.000712		
			DIVA-3	605	1	1	0	0		
				580	7	4	0.7143 ± 0.1809	0.001028 ± 0.000861		
			All		52	14	0.8341 ± 0.0325	0.001661 ± 0.001424		
		Pacific	EcoResponse	197	4	4	1.0000 ± 0.1768	0.005678 ± 0.004079		
		Total	All		33	23	0.9678 ± 0.0168	0.012885 ± 0.006590		

Tab. 4: Results of the AMOVA calculated in Arlequin 3.5. Results are shown for the COI gene of *Acanthocope galatheae* Wolff, 1962. The populations were grouped in Eastern and Western Atlantic populations. Significant *P*-values were marked with asterisks. < 0.05*; < 0.001**; < 0.0001***.

Source of Variation	d.f.	Percentage of variation	FCT	FSC	FST	*P*
Between East and West Atlantic	1	11.65	0.117			0.256
Among stations in East and West Atlantic	6	46.58		0.527 ***		0.000
Within stations	36	41.76			0.582 ***	0.000

generally not unlikely for natatory deep-sea species like *A. galatheae*, the suprabenthic amphipods *Eurythenes maldoror* d´Udekem d´Acoz & Havermans, 2015 and *E. magellanicus* (H. Milne Edwards, 1848) have a comparable mode of life and were found to be true abyssal cosmopolitans (France and Kocher, 1996; Havermans et al., 2013; Ritchie et al., 2015).

Our analyses on *A. galatheae* suggest a pan-Atlantic distribution with a potentially unrestricted gene flow, but the Pacific population is genetically distinct. The ABGD method splits the Atlantic and Pacific populations into independent groups (Fig. 2 II–III; 4). Generally, the assumption of one cosmopolitan species is imaginable and justifiable with the ABGD method (Fig. 2 I, 3). A barcode threshold between 1.0–3.0 % was found to be adequate for most metazoans (Puillandre et al., 2012). Thus, both thresholds: two groups 0.7–1.5 % or one group ≥1.6 % are acceptable. It is likely that the observed structure results from recent speciation, which is difficult to detect with the ABGD method (Puillandre et al., 2012).

The genetic distances are generally not too high for intraspecific variability. (Brix et al., 2018) for instance detected for Desmosomatidae a barcoding gap of 3.00–6.00 % in COI and 4.00–6.00 % in 16S, these were however rather high distances, (Bober et al., 2018b) presents intraspecific *p*-distance of 0.00–0.80 % and interspecific *p*-distances of 7.70–8.00 % for Macrostylidae in 16S. But regarding the genetic variance of the Atlantic (COI: 0.00–2.33 %; 16S: 0.00–0.66 %) the pan-oceanic p-distances are rather high (COI: 4.58–6.99 %). But still, the lowest geographic distance connecting the Pacific and Atlantic sampling sites is higher (8,528–14,602 km) than the highest geographic distances within the Atlantic (5,195 km). The measured distances are straight lines and do not incorporate barriers animals have to overcome, therefore in reality the distances from one ocean to the other are considerably higher. The Mantel test indicated a significant correlation between geographical and genetic distance in both genes. Therefore, isolation-by-distance is one further explanation for the high genetic distances between both oceans. Nevertheless, the pan-oceanic amphipods *Eurythenes maldoror* and *E. magellanicus* for instance are sharing identical haplotypes in the Atlantic and Pacific (Havermans et al., 2013; Ritchie et al., 2015), demonstrating

that such distances and barriers are not necessarily impeding gene flow. However, we assume a split between the Atlantic and Pacific populations. Since the original description of *A. galatheae* by Wolff (1962) was performed in the Atlantic, we consider the Atlantic population as *A. galatheae sensu stricto* and due to the lack of a formal revision of this species complex, the morphospecies as *A. galatheae sensu lato*.

The ABGD method indicated in the COI gene a further split of the Pacific lineage into the two lineages B and C (Fig. 2 III). The two resulting groups include individuals from either the BioNod12 or EcoResponse expedition from the CCZ.

Both sampling locations are separated by 428–558 km geographic distance and 2.34–3.52 % *p*-distance in the COI gene. Compared to the Atlantic the Pacific lineage seems to have a higher genetic diversity. But due to the small sample size in the Pacific conclusions remain uncertain. The 16S gene was not available for the BioNod12 samples, thus this information is missing for the 16S and concatenated analyses, but a similar topography here is not unlikely.

We applied a molecular clock with substitution rates established by (Schubart et al., 1998), which were set to an average rate of pairwise sequence divergence of 0.65 % for 16S and 1.66 % for COI or 1.17 % for concatenated sequences per million years. The time of divergence between both lineages is 3.35–5.72 million years ago (mya) in 16S, 2.76–4.21 mya in COI or 3.31–7.33 mya for the concatenated dataset.

The molecular clock we used was calibrated on transisthmian species of intertidal and supratidal crabs of the *Sesarma* species group. This species group got most likely not split up before the formation of the Isthmus of Panama 3.1 mya and was therefore used to determine the divergence time by (Schubart et al., 1998). We think the divergence rate is generally applicable for crustaceans, but possibly not accurate for deep-sea peracarids. Etter et al. (2011) for instance suggested a generally lower genetic divergence in the abyssal deep sea, but based on crustacean phylogenies Peracarida seem to have a faster divergence time compared to other crustacean groups (Jarman et al., 2000; Meland and Willassen, 2007; Schwentner et al., under Review). Therefore, the molecular clock approach used herein in only an approximation.

The time of divergence seems to approximately coincide with the formation of the Isthmus of Panama approximately 3.0 mya (O'Dea et al., 2016). There has been many studies on transisthmian sister species and divergence times based on the closure of the isthmus (Collins et al., 1996; Knowlton et al., 1993; Knowlton and Weigt, 1998; Lessios, 1979; Schubart et al., 1998). A relatively sudden isolation of species in shallow waters by the formation of the isthmus is imaginable, but it is generally difficult to estimate the time of isolation in offshore species like *A. galatheae* (Knowlton and Weigt, 1998).

Before the formation of the isthmus a semi-emergent island chain existed since at least 30.0 mya (O'Dea et al., 2016). The passages connecting the Pacific and Atlantic were at least 1,800 m deep

(Osborne et al., 2014), theoretically allowing an exchange of deep-sea fauna. But these deep passages vanished around 9.2 mya (Newkirk and Martin, 2009; O'Dea et al., 2016; Osborne et al., 2014), which most likely caused an earlier isolation for deep-sea fauna than for shallower water or coastal species.

We propose that the relatively low levels of trans-isthmian divergence are hardly explained by the formation of the Isthmus of Panama due to a presumably earlier isolation of the deep-sea fauna. However, the formation of the isthmus had a considerable effect on global ocean circulations (Maier-Reimer et al., 1990) and therefore the Isthmus might have indirectly provoked an isolation by altering ocean currents.

Acanthocope galatheae in the Atlantic

The Atlantic population is statistically not structured, but regarding the COI haplotype network (Fig. 5C), which is the only dataset that includes material from all geographic regions (Tab. 1), we can observe a geographical pattern, possibly induced by the MAR.

In (Bober et al., 2018a; Brix et al., 2018) and by (Guggolz et al., 2017; Riehl et al., 2018) the connectivity and possible gene flow across the MAR was detected for multiple species. However, the MAR was a strong dispersal barrier for multiple different taxa, with most species occurring on only one side of the MAR (Bober et al., 2018a; Brandt et al., 2018; Schmidt et al., 2017). The VFZ was found to be a possible passage for *A. galatheae* (Bober et al., 2018a), but data on the MAR as potential barrier was lacking. In the herein treated dataset we have two haplotype groups in the Atlantic, which are separated by only few mutations (Fig. 5C, HG1 + HG2). One group consists of individuals solely from the VFZ and Southwestern Atlantic and the other group consists of individuals from the VFZ and eastern equatorial Atlantic), emphasizing that these groups are not strictly geographically separated. Indeed, gene flow across the MAR seems to be occurring in the north Atlantic.

The geographic distance from the Southwestern Atlantic to the eastern equatorial Atlantic stations is 2,534–3,115 km across the MAR with a *p*-distance of 0.91–2.33 % in the COI gene. Identical haplotypes were however found between the SW Atlantic and the VFZ (2,813 km) and eastern equatorial Atlantic and the VFZ (5,195 km) (Fig. 5C). These geographic distances are mostly higher, indicating that the MAR is possibly compromising gene flow in the Southern Atlantic and the VFZ is a passage for dispersal across the MAR. The SW Atlantic and eastern equatorial Atlantic regions are theoretically connected by the Romanche Fracture Zone (RFZ) and the study of (Brix et al., 2015) for instance showed that the RFZ is connecting desmosomatid populations in the eastern and western Atlantic. The RFZ is structurally more complex and the trench is deeper than its adjacent abyssal plains (Heezen et al., 1964a). In opposite to the RFZ the VFZ is a virtual continuation of the abyssal habitat (Heezen et al., 1964a, 1964b; Van Andel et al., 1971), possibly facilitating a trans-MAR expansion.

Currents might further shape the observed distri-

bution pattern in the Atlantic. The eastern Atlantic abyssal basins are dominated by the southward flowing North Atlantic Deep Water (NADW) (Fischer et al., 1996; Smethie and Swift, 1989) and the western Atlantic is dominated by the Lower Circumpolar Deep Water (LCDW), which is a component of the Antarctic Bottom Water (Eittreim et al., 1983; Fischer et al., 1996; Reid et al., 1977). The VFZ is a continuous connection between the Demerara Abyssal Plain in the west and the Gambia Abyssal Plain in the east. The cold water derived from the LCDW was repeatedly reported to flow easterly through the Vema fracture zone (Eittreim et al., 1983; Fischer et al., 1996; Heezen et al., 1964b; McCartney et al., 1991; Vangriesheim, 1980). If these bottom currents disperse suprabenthic fauna, we should be able to detect a west to east expansion. But we find genetically identical individuals in the eastern equatorial Atlantic and across the MAR in the NW Atlantic. Most individuals are genetically identical across these stations (Fig. 5). Intuitively, the observed panmixia rejects a unidirectional dispersal. Since we have a seemingly unrestricted gene flow here we conclude that *A. galatheae* as a suprabenthic isopod is most likely not affected by bottom currents. The same is true for the specimens of the VFZ and the SW Atlantic. If there is a directional distribution, a migration into the VFZ area from the surrounding areas is the most likely. The herein treated already comprehensive dataset is, however, by no means complete and therefore our conclusions remain vague. Especially samples from fracture zones in the Southern Atlantic like the Chain Fracture Zone are needed to evaluate the significance of the VFZ as trans-Atlantic passage for *A. galatheae*.

Conclusions

Acanthocope galatheae has a pan-Atlantic distribution with a good connectivity of all haplotypes. The gene flow between SE and SW Atlantic individuals is possibly reduced by the MAR, but the major haplotype groups occur in sympatry at the Vema Fracture Zone, where the transform fault potentially acts as passage across the MAR.

Based on this dataset *A. galatheae* is no cosmopolitan, we assume a historic isolation of Atlantic and Pacific lineages. The connectivity of Atlantic and Pacific populations remains unclear due to insufficient sampling at potential areas of exchange in the SE Pacific, SW Atlantic and Southern Ocean.

Acknowledgements

I thank the following persons for providing me with material and expertise: Angelika Brandt, Nils Brenke, Saskia Brix, Inmaculada Frutos, Stefanie Kaiser, Terue Cristina Kihara, Sarah Schnurr and Martin Schwenter.

References

Bober, S., Brix, S., Riehl, T., Schwentner, M., Brandt, A., 2018a. Does the Mid-Atlantic Ridge affect the distribution of abyssal benthic crustaceans across the Atlantic Ocean? Deep Sea Research Part II: Topical Studies in Oceanography, Bathymetry of the Vema-Fracture Zone and Puerto Rico TRench Abyssal AtlaNtic BiodiverSITy Study (Vema-TRANSIT) 148,

91–104. https://doi.org/10.1016/j.dsr2.2018.02.007

Bober, S., Riehl, T., Henne, S., Brandt, A., 2018b. New Macrostylidae (Isopoda) from the Northwest Pacific Basin described by means of integrative taxonomy with reference to geographical barriers in the abyss. Zoological Journal of the Linnean Society 182, 549–603. https://doi.org/10.1093/zoolinnean/zlx042

Brandt, A., Błażewicz-Paszkowycz, M., Bamber, R., Mühlenhardt-Siegel, U., Malyutina, M., Kaiser, S., De, B.C., Havermans, C., 2012. Are there widespread peracarid species in the deep sea (Crustacea: Malacostraca)? Polish Polar Research 33, 139–162. https://doi.org/10.2478/v10183-012-0012-5

Brandt, A., Brix, S., Held, C., Kihara, T.C., 2014. Molecular differentiation in sympatry despite morphological stasis: deep-sea *Atlantoserolis* Wägele, 1994 and *Glabroserolis* Menzies, 1962 from the south-west Atlantic (Crustacea: Isopoda: Serolidae): Deep-Sea Serolidae. Zoological Journal of the Linnean Society 172, 318–359. https://doi.org/10.1111/zoj.12178

Brandt, A., Elsner, N., Brenke, N., Golovan, O., Malyutina, M.V., Riehl, T., Schwabe, E., Würzberg, L., 2013. Epifauna of the Sea of Japan collected via a new epibenthic sledge equipped with camera and environmental sensor systems. Deep Sea Research Part II: Topical Studies in Oceanography 86–87, 43–55. https://doi.org/10.1016/j.dsr2.2012.07.039

Brandt, A., Frutos, I., Bober, S., Brix, S., Brenke, N., Guggolz, T., Heitland, N., Malyutina, M., Minzlaff, U., Riehl, T., Schwabe, E., Zinkann, A.-C., Linse, K., 2018. Composition of abyssal macrofauna along the Vema Fracture Zone and the hadal Puerto Rico Trench, northern tropical Atlantic. Deep Sea Research Part II: Topical Studies in Oceanography, Bathymetry of the Vema-Fracture Zone and Puerto Rico TRench Abyssal AtlaNtic BiodiverSITy Study (Vema-TRANSIT) 148, 35–44. https://doi.org/10.1016/j.dsr2.2017.07.014

Brenke, N., 2005. An Epibenthic Sledge for Operations on Marine Soft Bottom and Bedrock. Marine Technology Society Journal 39, 10–21. https://doi.org/10.4031/002533205787444015

Brix, S., Bober, S., Tschesche, C., Kihara, T.-C., Driskell, A., Jennings, R.M., 2018. Molecular species delimitation and its implications for species descriptions using desmosomatid and nannoniscid isopods from the VEMA fracture zone as example taxa. Deep Sea Research Part II: Topical Studies in Oceanography, Bathymetry of the Vema-Fracture Zone and Puerto Rico TRench Abyssal AtlaNtic BiodiverSITy Study (Vema-TRANSIT) 148, 180–207. https://doi.org/10.1016/j.dsr2.2018.02.004

Brix, S., Leese, F., Riehl, T., Kihara, T.C., 2015. A new genus and new species of Desmosomatidae Sars, 1897 (Isopoda) from the eastern South Atlantic abyss described by means of integrative taxonomy. Mar Biodiv 45, 7–61. https://doi.org/10.1007/s12526-014-0218-3

Brix, S., Riehl, T., Leese, F., 2011. First genetic data for species of the genus *Haploniscus* Richardson, 1908 (Isopoda: Asellota: Haploniscidae) from neighbouring deep-sea basins in the South Atlantic. Zootaxa 2838, 79–84.

Brix, S., Svavarsson, J., Leese, F., 2014. A multi-gene analysis reveals multiple highly divergent lineages of the isopod *Chelator insignis* (Hansen, 1916) south of Iceland. Polish Polar Research 35, 225–242.

Brökeland, W., 2010. Description of four new species from the *Haploniscus unicornis* Menzies, 1956 complex (Isopoda: Asellota: Haploniscidae). Zootaxa 2536.

Brökeland, W., Raupach, M.J., 2008. A species complex within the isopod genus *Haploniscus* (Crustacea: Malacostraca: Peracarida) from the Southern Ocean deep sea: a morphological and molecular approach. Zoological Journal of the Linnean Society 152, 655–706.

Bruun, A.F., 1957. Chapter 22: Deep Sea and Abyssal Depths, in: Geological Society of America Memoirs. Geological Society of America, pp. 641–673.

Bucklin, A., Wilson Jr, R.R., Smith Jr, K.L., 1987. Genetic differentiation of seamount and basin populations of the deep-sea amphipod *Eurythenes gryllus*. Deep Sea Research Part A. Oceanographic Research Papers 34, 1795–1810.

Collins, L.S., Budd, A.F., Coates, A.G., 1996. Earliest evolution associated with closure of the Tropical American Seaway. Proc Natl Acad Sci U S A 93, 6069–6072.

Danovaro, R., Gambi, C., Dell'Anno, A., Corinaldesi, C., Fraschetti, S., Vanreusel, A., Vincx, M., Gooday, A.J., 2008. Exponential Decline of Deep-Sea Ecosystem Functioning Linked to Benthic Biodiversity Loss. Current Biology 18, 1–8. https://doi.org/10.1016/j.cub.2007.11.056

Edgar, R.C., 2004. MUSCLE: multiple sequence alignment with high accuracy and high throughput. Nucleic Acids Research 32, 1792–1797. https://doi.org/10.1093/nar/gkh340

Eittreim, S.L., Biscaye, P.E., Jacobs, S.S., 1983. Bottom-water observations in the Vema fracture zone. J. Geophys. Res. 88, 2609–2614. https://doi.org/10.1029/JC088iC04p02609

Etter, R.J., Boyle, E.E., Glazier, A., Jennings, R.M., Dutra, E., Chase, M.R., 2011. Phylogeography of a pan-Atlantic abyssal protobranch bivalve: implications for evolution in the Deep Atlantic: EVOLUTION IN THE DEEP ATLANTIC. Molecular Ecology 20, 829–843. https://doi.org/10.1111/j.1365-294X.2010.04978.x

Eustace, R.M., Ritchie, H., Kilgallen, N.M., Piertney, S.B., Jamieson, A.J., 2016. Morphological and ontogenetic stratification of abyssal and hadal *Eurythenes gryllus sensu lato* (Amphipoda: Lysianassoidea) from the Peru–Chile Trench. Deep Sea Research Part I: Oceanographic Research Papers 109, 91–98. https://doi.org/10.1016/j.dsr.2015.11.005

Excoffier, L., Lischer, H.E.L., 2010. Arlequin suite ver 3.5: a new series of programs to perform population genetics analyses under Linux and Windows. Molecular Ecology Resources 10, 564–567. https://doi.org/10.1111/j.1755-0998.2010.02847.x

Fischer, J., Rhein, M., Schott, F., Stramma, L., 1996. Deep water masses and transports in the Vema Fracture Zone. Deep Sea Research Part I: Oceanographic Research Papers 43, 1067–1074. https://doi.org/10.1016/0967-0637(96)00044-1

France, S.C., Kocher, T.D., 1996. Geographic and bathymetric patterns of mitochondrial 16S rRNA sequence divergence among deep-sea amphipods, *Eurythenes gryllus*. Marine Biology 126, 633–643.

Guggolz, T., Lins, L., Meißner, K., Brandt, A., 2017.

Biodiversity and distribution of polynoid and spionid polychaetes (Annelida) in the Vema Fracture Zone, tropical North Atlantic. Deep Sea Research Part II: Topical Studies in Oceanography. https://doi.org/10.1016/j.dsr2.2017.07.013

Havermans, C., Sonet, G., d'Udekem d'Acoz, C., Nagy, Z.T., Martin, P., Brix, S., Riehl, T., Agrawal, S., Held, C., 2013. Genetic and Morphological Divergences in the Cosmopolitan Deep-Sea Amphipod *Eurythenes gryllus* Reveal a Diverse Abyss and a Bipolar Species. PLoS ONE 8, e74218. https://doi.org/10.1371/journal.pone.0074218

Heezen, B.C., Bunce, E.T., Hersey, J.B., Tharp, M., 1964a. Chain and romanche fracture zones. Deep Sea Research and Oceanographic Abstracts 11, 11–33. https://doi.org/10.1016/0011-7471(64)91079-4

Heezen, B.C., Gerard, R.D., Tharp, M., 1964b. The Vema fracture zone in the equatorial Atlantic. J. Geophys. Res. 69, 733–739. https://doi.org/10.1029/JZ069i004p00733

Held, C., 2003. Molecular evidence for cryptic speciation within the widespread Antarctic crustacean *Ceratoserolis trilobitoides* (Crustacea, Isopoda). Antarctic biology in a global context 135–139.

Held, C., Wägele, J.-W., 2005. Cryptic speciation in the giant Antarctic isopod Glyptonotus antarcticus (Isopoda: Valvifera: Chaetiliidae). Scientia Marina 69, 175–181.

Hessler, R.R., Strömberg, J.-O., 1989. Behavior of janiroidean isopods (Asellota), with special reference to deep sea genera. Sarsia 74, 145–159.

Huelsenbeck, J.P., Ronquist, F., 2001. MRBAYES: Bayesian inference of phylogenetic trees. Bioinformatics 17, 754–755.

Janssen, A., Kaiser, S., Meißner, K., Brenke, N., Menot, L., Martínez Arbizu, P., 2015. A Reverse Taxonomic Approach to Assess Macrofaunal Distribution Patterns in Abyssal Pacific Polymetallic Nodule Fields. PLoS ONE 10, e0117790. https://doi.org/10.1371/journal.pone.0117790

Jarman, S.N., Nicol, S., Elliott, N.G., McMinn, A., 2000. 28S rDNA Evolution in the Eumalacostraca and the Phylogenetic Position of Krill. Molecular Phylogenetics and Evolution 17, 26–36. https://doi.org/10.1006/mpev.2000.0823

Kearse, M., Moir, R., Wilson, A., Stones-Havas, S., Cheung, M., Sturrock, S., Buxton, S., Cooper, A., Markowitz, S., Duran, C., Thierer, T., Ashton, B., Meintjes, P., Drummond, A., 2012. Geneious Basic: An integrated and extendable desktop software platform for the organization and analysis of sequence data. Bioinformatics 28, 1647–1649. https://doi.org/10.1093/bioinformatics/bts199

Knowlton, N., Weigt, L., Solorzano, L., Mills, D., Bermingham, E., 1993. Divergence in proteins, mitochondrial DNA, and reproductive compatibility across the isthmus of Panama. Science 260, 1629–1632. https://doi.org/10.1126/science.8503007

Knowlton, N., Weigt, L.A., 1998. New dates and new rates for divergence across the Isthmus of Panama. Proc Biol Sci 265, 2257. https://doi.org/10.1098/rspb.1998.0568

Krapp-Schickel, T., De Broyer, C., 2014. Revision of *Leucothoe* (Amphipoda, Crustacea) from the Southern Ocean: a cosmopolitanism concept is va-

nishing. European Journal of Taxonomy 0. https://doi.org/10.5852/ejt.2014.80

Kumar, S., Stecher, G., Tamura, K., 2016. MEGA7: Molecular Evolutionary Genetics Analysis Version 7.0 for Bigger Datasets. Mol. Biol. Evol. 33, 1870–1874. https://doi.org/10.1093/molbev/msw054

Larsen, K., 2003. The Tanaidacean Fauna (Peracarida) from a Deep-Sea Cold-Seep in the Gulf of Mexico. J Crustacean Biol 23, 777–794. https://doi.org/10.1651/C-2395

Leese, F., Agrawal, S., Held, C., 2010. Long-distance island hopping without dispersal stages: transportation across major zoogeographic barriers in a Southern Ocean isopod. Naturwissenschaften 97, 583–594. https://doi.org/10.1007/s00114-010-0674-y

Leese, F., Held, C., 2008. Identification and characterization of microsatellites from the Antarctic isopod *Ceratoserolis trilobitoides*: nuclear evidence for cryptic species. Conserv Genet 9, 1369–1372. https://doi.org/10.1007/s10592-007-9491-z

Leigh, J.W., Bryant, D., 2015. popart: full-feature software for haplotype network construction. Methods in Ecology and Evolution n/a-n/a. https://doi.org/10.1111/2041-210X.12410

Lessios, H.A., 1979. Use of Panamanian sea urchins to test the molecular clock. Nature 280, 599–601. https://doi.org/10.1038/280599a0

Maier-Reimer, E., Mikolajewicz, U., Crowley, T., 1990. Ocean General Circulation Model Sensitivity Experiment with an open Central American Isthmus. Paleoceanography 5, 349–366. https://doi.org/10.1029/PA005i003p00349

Malyutina, M.V., 1999. New Species of *Acanthocope* (Isopoda, Munnopsidae). Russian Journal of Marine Biology 25, 320–329.

Malyutina, M.V., Frutos, I., Brandt, A., 2017. Diversity and distribution of the deep-sea Atlantic *Acanthocope* (Crustacea, Isopoda, Munnopsidae), with description of two new species. Deep Sea Research Part II: Topical Studies in Oceanography. https://doi.org/10.1016/j.dsr2.2017.11.003

Marshall, N., Diebel, C., 1995. "Deep-sea spiders" that walk through the water. Journal of experimental biology 198, 1371–1379.

McCartney, M.S., Bennett, S.L., Woodgate-Jones, M.E., 1991. Eastward Flow through the Mid-Atlantic Ridge at 11°N and Its Influence on the Abyss of the Eastern Basin. J. Phys. Oceanogr. 21, 1089–1121. https://doi.org/10.1175/1520-0485(1991)021<1089:EFTTMA>2.0.CO;2

Meland, K., Willassen, E., 2007. The disunity of "Mysidacea" (Crustacea). Molecular Phylogenetics and Evolution 44, 1083–1104. https://doi.org/10.1016/j.ympev.2007.02.009

Miller, M.A., Pfeiffer, W., Schwartz, T., 2010. Creating the CIPRES Science Gateway for inference of large phylogenetic trees. Presented at the Proceedings of the Gateway Computing Environments Workshop (GCE), IEEE, New Orleans, pp. 1–8. https://doi.org/10.1109/GCE.2010.5676129

Miyamoto, H., Machida, R.J., Nishida, S., 2010. Genetic diversity and cryptic speciation of the deep sea chaetognath *Caecosagitta macrocephala* (Fowler, 1904). Deep Sea Research Part II: Topical Studies in Oceanography 57, 2211–2219. https://doi.

org/10.1016/j.dsr2.2010.09.023

Newkirk, D.R., Martin, E.E., 2009. Circulation through the Central American Seaway during the Miocene carbonate crash. Geology 37, 87–90. https://doi.org/10.1130/G25193A.1

Nylander, J.J.A., 2004. MrModeltest v2. Program distributed by the author, Evolutionary Biology Centre, Uppsala.

O'Dea, A., Lessios, H.A., Coates, A.G., Eytan, R.I., Restrepo-Moreno, S.A., Cione, A.L., Collins, L.S., de Queiroz, A., Farris, D.W., Norris, R.D., Stallard, R.F., Woodburne, M.O., Aguilera, O., Aubry, M.-P., Berggren, W.A., Budd, A.F., Cozzuol, M.A., Coppard, S.E., Duque-Caro, H., Finnegan, S., Gasparini, G.M., Grossman, E.L., Johnson, K.G., Keigwin, L.D., Knowlton, N., Leigh, E.G., Leonard-Pingel, J.S., Marko, P.B., Pyenson, N.D., Rachello-Dolmen, P.G., Soibelzon, E., Soibelzon, L., Todd, J.A., Vermeij, G.J., Jackson, J.B.C., 2016. Formation of the Isthmus of Panama. Science Advances 2, e1600883–e1600883. https://doi.org/10.1126/sciadv.1600883

Osborne, A.H., Newkirk, D.R., Groeneveld, J., Martin, E.E., Tiedemann, R., Frank, M., 2014. The seawater neodymium and lead isotope record of the final stages of Central American Seaway closure: CAS CLOSURE ND AND PB. Paleoceanography 29, 715–729. https://doi.org/10.1002/2014PA002676

Puillandre, N., Lambert, A., Brouillet, S., Achaz, G., 2012. ABGD, Automatic Barcode Gap Discovery for primary species delimitation: ABGD, AUTOMATIC BARCODE GAP DISCOVERY. Molecular Ecology 21, 1864–1877. https://doi.org/10.1111/j.1365-294X.2011.05239.x

Ramirez-Llodra, E., Brandt, A., Danovaro, R., De Mol, B., Escobar, E., German, C.R., Levin, L.A., Martínez Arbizu, P., Menot, L., Buhl-Mortensen, P., Narayanaswamy, B.E., Smith, C.R., Tittensor, D.P., Tyler, P.A., Vanreusel, A., Vecchione, M., 2010. Deep, diverse and definitely different: unique attributes of the world's largest ecosystem. Biogeosciences 7, 2851–2899. https://doi.org/10.5194/bg-7-2851-2010

Raupach, M.J., Malyutina, M., Brandt, A., Wägele, J.-W., 2007. Molecular data reveal a highly diverse species flock within the munnopsoid deep-sea isopod *Betamorpha fusiformis* (Barnard, 1920) (Crustacea: Isopoda: Asellota) in the Southern Ocean. Deep Sea Research Part II: Topical Studies in Oceanography 54, 1820–1830. https://doi.org/10.1016/j.dsr2.2007.07.009

Raupach, M.J., Wägele, J.-W., 2006. Distinguishing cryptic species in Antarctic Asellota (Crustacea: Isopoda) - a preliminary study of mitochondrial DNA in *Acanthaspidia drygalskii*. Antarctic Science 18, 191. https://doi.org/10.1017/S0954102006000228

Reid, J.L., Nowlin, W.D., Patzert, W.C., 1977. On the Characteristics and Circulation of the Southwestern Atlantic Ocean. J. Phys. Oceanogr. 7, 62–91. https://doi.org/10.1175/1520-0485(1977)007<0062:OTCACO>2.0.CO;2

Riehl, T., Kaiser, S., 2012. Conquered from the Deep Sea? A New Deep-Sea Isopod Species from the Antarctic Shelf Shows Pattern of Recent Colonization. PLoS ONE 7, e49354. https://doi.org/10.1371/journal.pone.0049354

Riehl, T., Lins, L., Brandt, A., 2018. The effects of depth, distance, and the Mid-Atlantic Ridge on ge-

netic differentiation of abyssal and hadal isopods (Macrostylidae). Deep Sea Research Part II: Topical Studies in Oceanography, Bathymetry of the Vema-Fracture Zone and Puerto Rico TRench Abyssal AtlaNtic BiodiverSITy Study (Vema-TRANSIT) 148, 74–90. https://doi.org/10.1016/j.dsr2.2017.10.005

Ritchie, H., Jamieson, A.J., Piertney, S.B., 2015. Phylogenetic relationships among hadal amphipods of the Superfamily Lysianassoidea: Implications for taxonomy and biogeography. Deep Sea Research Part I: Oceanographic Research Papers 105, 119–131. https://doi.org/10.1016/j.dsr.2015.08.014

Ronquist, F., Huelsenbeck, J.P., 2003. MrBayes 3: Bayesian phylogenetic inference under mixed models. Bioinformatics 19, 1572–1574.

Schmid, C., Brenke, N., Wägele, J.W., 2002. On abyssal isopods (Crustacea: Isopoda: Asellota) from the Angola Basin: *Eurycope tumidicarpus* n. sp. and redescription of *Acanthocope galathea* Wolff, 1962. Organisms Diversity & Evolution 2, 87–88. https://doi.org/10.1078/1439-6092-00030

Schmidt, C., Escobar Wolf, K., Lins, L., Martínez Arbizu, P., Brandt, A., 2017. Meiofauna abundance and community patterns along a transatlantic transect in the Vema Fracture Zone and in the hadal zone of the Puerto Rico trench. Deep Sea Research Part II: Topical Studies in Oceanography. https://doi.org/10.1016/j.dsr2.2017.12.021

Schnurr, S., Osborn, K.J., Malyutina, M., Jennings, R., Brix, S., Driskell, A., Svavarsson, J., Arbizu, P.M., 2018. Hidden diversity in two species complexes of munnopsid isopods (Crustacea) at the transition between the northernmost North Atlantic and the Nordic Seas. Mar Biodiv 1–31. https://doi.org/10.1007/s12526-018-0877-6

Schubart, C.D., Diesel, R., Hedges, S.B., 1998. Rapid evolution to terrestrial life in Jamaican crabs. Nature 393, 363–365. https://doi.org/10.1038/30724

Schwentner, M., Richter, S., Rogers, C., Giribet, G., under Review. Tetraconatan phylogeny with special focus on Malacostraca and Branchiopoda—Designing taxon-specific matrices increases accuracy in phylogenomics. Proceedings of the Royal Society.

Smethie, W.M., Swift, J.H., 1989. The tritium:krypton-85 age of Denmark Strait Overflow Water and Gibbs Fracture Zone Water just south of Denmark Strait. The Tritium-Krypton-85 Age of Denmark Strait Overflow Water and Gibbs Fracture-Zone Water Just South of Denmark Strait 94, 8265–8275. https://doi.org/10.1029/JC094iC06p08265

Smith, C.R., De Leo, F.C., Bernardino, A.F., Sweetman, A.K., Arbizu, P.M., 2008. Abyssal food limitation, ecosystem structure and climate change. Trends in Ecology & Evolution 23, 518–528. https://doi.org/10.1016/j.tree.2008.05.002

Swofford, D.L., 2001. PAUP*: Phylogenetic Analysis Using Parsimony (and other methods) 4.0.b5.

Van Andel, T.H., Von Herzen, R.P., Phillips, J.D., 1971. The Vema fracture zone and the tectonics of transverse shear zones in oceanic crustal plates. Marine Geophysical Researches 1, 261–283.

Vangriesheim, A., 1980. Antarctic bottom water flow through the Vema fracture zone. Oceanologica Acta 3, 199–207.

Vinogradova, N.G., 1997. Zoogeography of the Abys-

sal and Hadal Zones, in: Gebruk, A.V., Southward, E.C., Tyler, P.A. (Eds.), The Biogeography of the Oceans, Advances in Marine Biology. Academic Press, San Diego, Calif, pp. 325–387.

Wilson, G.D.F., Hessler, R.R., 1987. Speciation in the deep sea. Annual Review of Ecology and Systematics 185–207.

Wilson, N.G., Hunter, R.L., Lockhart, S.J., Halanych, K.M., 2007. Multiple lineages and absence of panmixia in the "circumpolar" crinoid *Promachocrinus kerguelensis* from the Atlantic sector of Antarctica. Mar Biol 152, 895–904. https://doi.org/10.1007/s00227-007-0742-9

Wolff, T., 1962. The systematics and biology of bathyal and abyssal Isopoda Asellota. Galathea Report 6, 1–320.

Authors contributions

The study was designed and conducted by Simon Bober.

The Munnopsidae from the Vema-TRANSIT, DIVA-3 expeditions were handled in the laboratory of the CeNak by S. Bober. All analyses and figures were made by S. Bober. The first draft of the manuscript was written by Simon Bober with subsequent contributions of Martin Schwentner.

The COI sequences from DIVA-2 are unpublished sequences from Saskia Brix. The sequences from the EcoResponse expedition were provided by Sarah Schnurr. Angelika Brandt had the idea for the project (Vema-TRANSIT) and wrote the proposals, she was the leader of the expedition.

Chapter 5

New Macrostylidae (Isopoda) from the Northwest Pacific Basin described by means of integrative taxonomy with reference to geographical barriers in the abyss

Zoological Journal of the Linnean Society, 2018, **182**, 549–603. With 40 figures.

New Macrostylidae (Isopoda) from the Northwest Pacific Basin described by means of integrative taxonomy with reference to geographical barriers in the abyss

SIMON BOBER[1]*, TORBEN RIEHL[2], STEPHAN HENNE[1] and ANGELIKA BRANDT[2]

[1]*University of Hamburg, Center of Natural History (CeNak), Zoological Museum, Hamburg, Germany*
[2]*Department Marine Zoology, Senckenberg Research Institute and Natural History Museum, Crustacea, Senckenberganlage 25, 60325 Frankfurt, Germany*

Received 12 January 2017; revised 6 June 2017; accepted for publication 22 June 2017

During the KuramBio expedition in 2012, previously unknown Macrostylidae (Crustacea, Isopoda) were collected from the Northwest Pacific Basin near the Kuril–Kamchatka Trench. Three of these species are described herein, ***Macrostylis amaliae* sp. nov.**, ***M. daniae* sp. nov.** and ***M. sabinae* sp. nov.**, using a combination of morphological and molecular–genetic approaches. The use of confocal laser scanning microscopy was evaluated and found to be a valuable, non-destructive method to visualize precious type material, as opposed to scanning electron microscopy, which renders material useless for other purposes. In the KuramBio samples two species of Macrostylidae (***M. sabinae* sp. nov.**, ***M. amaliae* sp. nov**.) dominated. Moreover, their females are morphologically indistinguishable and have thus been delineated by means of DNA data. The adult males, however, are distinguishable by their antennula and the type of aesthetascs. This is the first time that a new type of aesthetasc has been assigned to this family. For these two species evidence for sexual size dimorphism, in which the females are significantly larger than the males, was found. ***Macrostylis sabinae* sp. nov.** was widely distributed, so a biogeographical approach was followed and the dispersibility of benthic infaunal isopods across deep-sea trenches in the abyssal deep sea is discussed.

ADDITIONAL KEYWORDS: adaptation – evolution, adult modifications – evolution, sibling species – evolution, sympatric speciation – evolution, speciation – evolution, mtDNA – genetics, population genetics – genetics, biogeography – geography, deep sea – geography, distribution.

INTRODUCTION

During the KuramBio (Kuril Kamchatka Biodiversity Studies) project of 2012, 207 species of isopod crustaceans belonging to 19 families and 73 genera were collected from the Northwest Pacific Abyssal Plain in the Kuril Kamchatka Trench (KKT) region (Fig. 1) (Elsner *et al.*, 2015). The KKT reaches hadal depths of up to 9717 m (Brandt *et al.*, 2015) and is formed where the Pacific Plate subducts beneath the Okhotsk Plate (Apel *et al.*, 2006). All stations from which individuals are reported herein lie within the depth range attributed to the abyss (here 4500–5500 m). The joint German/Russian deep-sea expedition KuramBio was inspired by a history of comprehensive Russian investigations on board RV *Vityaz* from 1949 to 1966. Nine deep-sea expeditions were conducted during that time, which greatly contributed to a deeper understanding of the deep-sea fauna. Based on these expeditions, for example, more than 100 isopod species were described (Birstein, 1957, 1960, 1961, 1962a, b, 1963, 1970, 1971; Kussakin, 1971, 1990; Mezhov, 1980, 1981; Brandt & Malyutina, 2015). The KuramBio expedition was the first expedition in that area to use internationally standardized sampling equipment and particularly target small size classes, such as macrofauna and meiofauna (Brandt & Malyutina, 2015; Elsner *et al.*, 2015).

Isopoda Latreille, 1817 (Crustacea, Peracarida) is generally a common, abundant and diverse group among the macrofaunal taxa inhabiting abyssal soft-bottoms (Thistle & Wilson, 1987). Isopods are also often

*Corresponding author. E-mail: simon.bober@uni-hamburg.de
[Version of Record, published on 8 November 2017; http://zoobank.org/urn:lsid:zoobank.org:pub:F86A4E12-3343-4729-83B7-1AA214929A56]

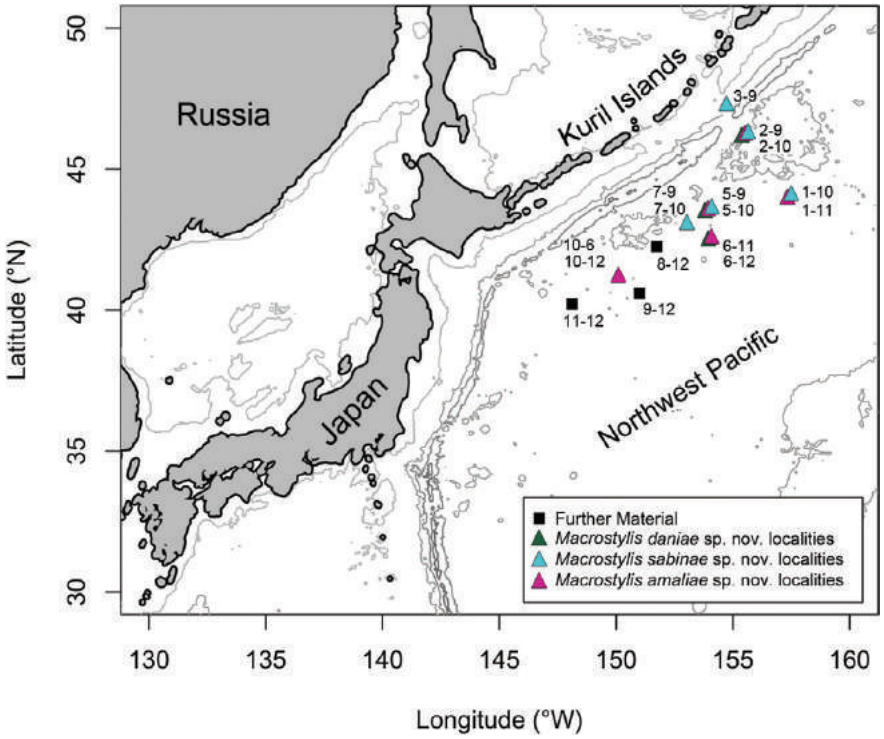

Figure 1. KuramBio stations in the Northwest Pacific Basin at which material for the here presented new species of Macrostylidae was collected. The 1000-, 5000-, 7000- and 9000-m depth contours were plotted. The localities at which genetic material was gathered are highlighted for each species. The type localities for ***Macrostylis daniae* sp. nov.**, ***M. sabinae* sp. nov.** and ***M. amaliae* sp. nov.** are stations 2–9, 2–9 and 10–6. All three species occur sympatrically at stations 2–9 and 5–9. For more detailed information see Supporting Information S1.

numerically dominant among crustaceans (Hessler & Sanders, 1967; Hessler & Jumars, 1974; Wolff, 1977). Among deep-sea macrofauna collected by the camera-equipped epibenthic sledge during the KuramBio expedition, peracarid crustaceans were the most diverse and most abundant taxon and Isopoda was the most diverse and most abundant taxon within the peracarids (Golovan *et al.*, 2013). The macrostylid genus *Macrostylis* Sars, 1864 was one of the most species-rich genera of peracarids collected during this campaign.

The monotypic isopod family Macrostylidae Hansen, 1916 is widely distributed across all depths and oceans (Riehl & Brandt 2010) and is regularly abundant and diversely represented (Wilson, 2008b; Elsner *et al.*, 2015; Janssen *et al.*, 2015). This highly derived and specialized family is characterized particularly by its fossosome, a partial fusion of tergites 1–3, amongst multiple further derived characters (Wägele, 1989; Riehl, Wilson, & Malyutina, 2014b). The family consists of 86 formally described species (Table 1) all of which are assigned to the genus *Macrostylis*. Little is known about this family's mode of life, but species of Macrostylidae are thought to follow an infaunal lifestyle (Hessler & Sanders, 1967; Hessler & Wilson, 1983; Harrison, 1989; Hessler & Strömberg, 1989; Wägele, 1989). Ten species of Macrostylidae have previously been described from the Kuril–Kamchatka region (Table 2), all of which originated from RV *Vityaz* material (Birstein, 1963, 1970). During the KuramBio expedition additional species were found. The genus *Macrostylis* was one of the two most abundant genera, represented by 18 species, 12 of which were undescribed (Elsner *et al.*, 2015). Three species new to science are described by means of integrative taxonomy in this paper.

One of these new species, *Macrostylis daniae* sp. nov., has a blunt, rounded first ventral projection and a tiny ventral projection on the seventh sternite. It can be distinguished from other species known from this region by its relatively large size and robust body. The only similarly sized or larger congeners from this area have clearly distinct morphologies; *M. curticornis* (Birstein, 1963) reached > 1 cm in the KuramBio samples but is easily distinguishable (see Results). Another two medium- to large-sized species in the size range of *M. daniae* sp. nov. are *M. grandis* Birstein, 1970 and *M. ovata* Birstein, 1970, but they exhibit an oval habitus and conspicuously protruding posterolateral margins of the posterior pereonites (Birstein, 1970).

Table 1. Macrostylidae Hansen, 1916 family composition and distribution, based on the matrix provided by Riehl & Brandt (2010)

Species	Locality	Depth (m)
Genus: *Macrostylis* Sars, 1864		
abyssalis Brandt, 2004	S Atlantic, Angola Basin	5389
abyssicola Hansen, 1916	NW Atlantic, Davis Strait	698–3921
affinis Birstein, 1963	NW Pacific	4690–5554
***amaliae* sp. nov.**	NW Pacific, Kuril–Kamchatka Trench	5251–5429
amplinexa Mezhov, 1989	Indian Ocean	2385–4221
angolensis Brandt, 2004	SE Atlantic, Angola Basin	5395
angulata Mezhov, 1999	NE Atlantic	5420–6051
antennamagna Riehl & Brandt, 2010	Southern Ocean, NW Weddell Sea	4698–4760
***daniae* sp. nov.**	NW Pacific, Kuril–Kamchatka Trench	4830–5380
belyaevi Mezhov, 1989	N Pacific	8540–8780
bifurcatus Menzies, 1962	SE Atlantic	4588–4960
bipunctatus Menzies, 1962	SW Atlantic	3954–5024
birsteini Mezhov, 1993	S Pacific	1200
capito Mezhov, 1989	Indian Ocean	2218–4737
caribbicus Menzies, 1962	W Atlantic, Caribbean, Columbia	2875–941
carinifera carinifera Mezhov, 1988	Indian Ocean	3074–4458
carinifera dilatata Mezhov, 1988	Indian Ocean	2540
cerritus Vey & Brix, 2009	Southern Ocean, Weddell Sea	2149
compactus Birstein, 1963	W Pacific, Bougainville Trench	6920–7954
confinis Mezhov, 2003	NW Indian Ocean	3617
curticornis Birstein, 1963	NW Pacific	5680–6670
dellacrocei Aydogan, Wägele & Park, 2000	SE Pacific, Atacama Trench	7800
diatona Mezhov, 2004	E Indian Ocean	6433
dorsaetosa Riehl, Wilson & Hessler, 2012	N Atlantic, Long Island	2469–2500
elongata Hansen, 1916	N Atlantic, Iceland	1591
emarginata Mezhov, 2000	N Atlantic	5420
expolita Mezhov, 2003	N Indian Ocean, Arabian Sea	2478–2519
foveata Mezhov, 2000	W Atlantic, Puerto Rico Trench	5060–6650
fragosa Mezhov, 2004	E Indian Ocean	5410
galatheae Wolff, 1956	W Pacific, Philippine Trench	8440–10000
gerdesi (Brandt, 2002) comb. nov.	Southern Ocean, Maud Rise	238
gestuosa Mezhov, 1993	W Pacific	5526
grandis Birstein, 1970	NW Pacific, Kuril–Kamchatka Trench	7265–7295
hadalis Wolff, 1956	W Pacific, Banda Trench	7270
hirsuticaudis Menzies, 1962	SE Atlantic	2997
lacunosa Mezhov, 2003	N Indian Ocean	4706–4737
latifrons Beddard, 1886	N Pacific	3749
latiuscula Mezhov; 2003	Central Indian Ocean	4730–4808
longifera Menzies & George, 1972	E Pacific, Peru–Chile Trench	4823–6134
longipedis Brandt, 2004	S Atlantic, Angola Basin	5389
longipes Hansen, 1916	N Atlantic, Iceland	325–1412
longiremis (Meinert, 1890)	N Atlantic, Skagerrak	149–228
longispinis Brandt, 2004	S Atlantic, Angola Basin	5415
longissima Mezhov, 1981	N Central Pacific	6043–6051
longiuscula Mezhov, 1981	N Central Pacific	4400
longula Birstein, 1970	N Pacific	5005–5045
magnifica Wolff, 1962	NW Atlantic, Davis Strait	3521
matildae Riehl & Brandt, 2013	Southern Ocean, Maud Rise	2152–2153
mariana Mezhov, 1993	W Pacific	10223–10730

Table 1. *Continued*

Species	Locality	Depth (m)
marionae Kniesz, accepted	Puerto Rico Trench, W Atlantic	8317
medioxima Mezhov, 2003	NW Indian Ocean	4458
meteorae Brandt, 2004	S Atlantic, Angola Basin	5387–5390
minuscularia Mezhov, 2003	NW Indian Ocean	3617
minutus Menzies, 1962	W Atlantic, Puerto Rico Trench	5163–5494
obscurus (Brandt, 1992) comb. nov.	Southern Ocean, Weddell Sea	4335
ovata Birstein, 1970	NW Pacific, Kuril–Kamchatka Trench	6435–6710
papillata Riehl, Wilson & Hessler, 2012	N Atlantic	4800–4833
pectorosa Mezhov, 2004	E Indian Ocean	2807
polaris Malyutina & Kussakin, 1996	Arctic Ocean	325–400
porrecta Mezhov, 1988	Indian Ocean	6433
profundissima Birstein, 1970	NW Pacific, Kuril–Kamchatka Trench	8185–9530
prolixa Mezhov, 2003	NW Indian Ocean	4458
pumicosa Mezhov, 2004	E Indian Ocean	2917
quadratura Birstein, 1970	NW Pacific, Kuril–Kamchatka Trench	3175–3250
rectangulata Mezhov, 1989	Indian Ocean	5220
reticulata Birstein, 1963	NW Pacific	5502
roaldi Riehl & Kaiser, 2012	Southern Ocean, Amundsen Sea	478–1486
robusta Brandt, 2004	S Atlantic, Angola Basin	5497–5398
***sabinae* sp. nov.**	NW Pacific, Kuril–Kamchatka Trench	4830–5429
sarsi Brandt, 1992	Southern Ocean, Weddell Sea	4335
sensitiva Birstein, 1970	NW Pacific, Kuril–Kamchatka Trench	5005–5100
setulosa Mezhov, 1992	Southern Ocean, Scotia Sea	757–2705
scotti Riehl & Brandt, 2013	Southern Ocean, Maud Rise	2152–2153
setifer Menzies, 1962	W Atlantic, Puerto-Rico Trench	5477–5494
spiniceps Barnard, 1920	S Atlantic, South Africa	1280
spinifera Sars, 1864	N Atlantic, Norwegian Sea	27–1710
squalida Mezhov, 2000	Central Atlantic, Romanche Trench	6380–6430
subinermis Hansen, 1916	N Atlantic, Norwegian Sea	5420
strigosa Mezhov, 1999	NE Atlantic	830–3474
truncatex Menzies, 1962	NW Atlantic	3950–3963
tumulosa Mezhov, 1989	W Pacific, Izu–Bonin Trench	8900
uniformis Riehl & Brandt, 2010	Southern Ocean, Weddell Sea	4651–4975
urceolata Mezhov, 1989	Indian Ocean	2596
vemae Menzies, 1962	W Atlantic, Puerto Rico Trench	5410–5684
vigorata Mezhov, 1999	NE Atlantic	2655–2667
vinogradovae Mezhov, 1992	Southern Ocean, Weddell Sea	2705–4335
viriosa Mezhov, 1999	NE Atlantic	4050
vitjazi Birstein, 1963	W Pacific, Bougainville Trench	6920–7954
wolffi Mezhov, 1988	Indian Ocean	2385–3717
zenkevitchi Birstein, 1963	NW Pacific	4690–6135

Among the Macrostylidae collected during the KuramBio expedition, another species was dominant in abundance (i.e. *Macrostylis* sp. #2 *sensu* Elsner *et al.*, 2015). However, genetic analyses revealed two distinct species which are described here as *Macrostylis sabinae* sp. nov. and *Macrostylis amaliae* sp. nov. Both species are distinguishable morphologically by their adult males only. As opposed to adult males of *M. amaliae* sp. nov., *M. sabinae* sp. nov. males lack the ventral projections on pereonites 5 and 6. Moreover, the shape of the antennula differs between the adult males of both species; in particular, the fifth segment is distinctly longer in *M. sabinae* sp. nov. Furthermore, *M. sabinae* sp. nov. has two different types of aesthetascs on the first antenna, one of which has not been described for this family before.

Sexual dimorphism among Macrostylidae is known (Riehl *et al.*, 2012). In this study, however, we were able to confirm a sexual size dimorphism in Macrostylidae for the first time. The males of *M. sabinae* sp. nov. and

Table 2. All species known from the sampling area in the Northwest Pacific, today; *Macrostylis profundissima* Birstein, 1970, *M. quadratura* Birstein, 1970 and *M. ovata* Birstein, 1970 were excluded from the analyses due to insufficient descriptions

Species	Author	
Macrostylis longula	Birstein, 1970	
Macrostylis grandis	Birstein, 1970	
Macrostylis affinis	Birstein, 1973	
Macrostylis curticornis	Birstein, 1973	
Macrostylis reticulata	Birstein, 1973	
Macrostylis zenkevitchi	Birstein, 1973	
Excluded		Notes
Macrostylis profundissima	Birstein, 1970	based on male characters
Macrostylis quadratura	Birstein, 1970	based on male characters
Macrostylis ovata	Birstein, 1970	possibly juvenile of *M. grandis*
Macrostylis sensitiva	Birstein, 1973	based on male characters

M. amaliae sp. nov. are significantly smaller than the females. Due to a sufficient number of individuals (N = 196) of *M. sabinae* sp. nov. and *M. amaliae* sp. nov. from multiple stations, a rather vague size determination for adult female individuals was attested to. The definitive body size of an ovigerous female varied across stations and furthermore seems to correlate with sampling locations.

With the sampled specimens of *M. sabinae* sp. nov. we were able to follow a biogeographical approach and compare the dispersibility of benthic infaunal isopods in the abyssal deep sea. One station was located north of the KKT (3–9), while all other stations were located south of the trench allowing us to test for connectivity of abyssal species across the KKT.

MATERIAL AND METHODS

Sampling and type localities

All specimens used for species description were collected during the joint German–Russian KuramBio expedition onboard RV *Sonne* (SO223) from July to September 2012 at the KKT and the adjacent abyssal Northwest Pacific Basin (Brandt & Malyutina, 2015) (Fig. 1). The collection equipment used primarily on this campaign was a camera-equipped epibenthic sledge (C-EBS) (Brenke, 2005; Brandt *et al.*, 2013) and a Multicorer (MUC). For the C-EBS a mesh size of 500 µm was used; the cod ends, however, were equipped with a 300-µm mesh. All recorded material of the three described species is listed in Supporting Information S1.

Sample treatment and genetic analyses

On board the samples were sieved with filtered seawater, bulk-fixed in 96% precooled ethanol and stored at –20 °C for 24–48 h during which the containers were regularly moved to ensure sediment penetration by the ethanol. Sorting, species identification and dissections for genetic analyses were performed on ice. All genetic samples were treated and handled following the protocol for fixation of genetic deep-sea samples by Riehl *et al.* (2014a). Tissue samples were sent to LGC Genomics Germany (Berlin) for extraction, amplification and sequencing. Standard universal laboratory protocols as described by Riehl *et al.* (2014a) were applied. The resulting data were further processed in the software package Geneious 8.1.7 (Kearse *et al.*, 2012). Both strands were proofread and the contigs were assembled. For the alignments, multiple methods yielded similar results so the contigs of the 16S sequences were aligned using MAFFT (Katoh & Standley, 2013) with default parameters. *Chelator vulgaris* Hessler, 1970 [GenBank accession number: KJ630813 (Brix, Svavarsson, & Leese, 2014)] served as the outgroup. All the 16S sequences for Macrostylidae available on GenBank were used for the ingroup: *Macrostylis roaldi* Riehl & Kaiser, 2012 (accession numbers: JX260314–JX260348); *Macrostylis matildae* Riehl & Brandt, 2013 (accession numbers: KC715761–KC715768; KC715770–KC715775; KC715777–KC715780); *Macrostylis scotti* Riehl & Brandt, 2013 (accession number: KC715769); *Macrostylis* sp. (accession numbers: KC715776; KC715781; KC715783); and *Macrostylis* sp. (accession number: KC715782). The contigs of the 18S sequences were aligned using MUSCLE (Edgar, 2004) with default parameters. *Chelator vulgaris* Hessler, 1970 (accession number: KJ630816) served as the outgroup. All the 18S sequences for Macrostylidae available on GenBank were used for the ingroup: *Macrostylis roaldi* Riehl & Kaiser, 2012 (accession numbers: JX603349–JX603351); *Macrostylis* sp. [accession number: AY461476 (Raupach, Held, & Wägele, 2004)]; *Macrostylis* sp. [accession number: AY461477 (Raupach *et al.*, 2004)]; and *Macrostylis* sp. [accession number:

EU414442 (Raupach *et al.*, 2009)]. With MrModeltest 2.3 (Nylander, 2004) and in PAUP*4.0a147 (Swofford, 2001) a likelihood ratio test was performed and the best model of nucleotide substitution was chosen. Following the Akaike Information Criterion (AIC) and the Hierarchical Likelihood Ratio Test (hLRT), GTR+G was used for the 16S dataset and GTR+I+G for the 18S dataset.

Based on the alignments, a consensus tree was inferred in MrBayes 3.2.5 (Huelsenbeck & Ronquist, 2001; Ronquist & Huelsenbeck, 2003). The 16S dataset was run for 3 000 000 generations with a sampling frequency of 1000, and the 18S dataset was run for 2 000 000 generations with a sampling frequency of 1000 until the split frequencies dropped below 0.01. For a better visualization of genetic distances, a haplotype network was calculated from the 16S MAFFT alignment. The TCS Network was built using PopART (Leigh & Bryant, 2015).

With a Mantel test in R (mantel.rtest(), package: 'ade4') an assumed correlation between genetic and geographical distance was tested. Furthermore, a three-dimensional genetic landscape shapes interpolation was performed using the software Alleles in Space (Miller, 2005). The genetic landscape was plotted on geographical station data (x = longitude, y = latitude) and the z-values represent the genetic pairwise distances between individuals. The interpolation results were plotted on a 80 × 80 grid with a distance weight of 1.0 (default setting). Monmonier's algorithm (Monmonier, 1973) implemented in the software tested for possible genetic barriers in the dataset.

Prior to statistical tests the data were tested for normality with a Shapiro–Wilk Normality test in Rstudio (R Development Core Team, 2008; RStudio, 2015). For non-parametric data the Wilcoxon–Mann–Whitney U test or the Kruskall–Wallis test was performed in RStudio. For parametrical data the Welch Two-Sample t-test was used.

Taxonomy

For the taxonomic descriptions, six individuals each of *Macrostylis daniae* sp. nov. and *M. sabinae* sp. nov. as well as five individuals of *M. amaliae* sp. nov. were examined and illustrated in detail (Table 3). Adult non-ovigerous females were chosen as holotypes for all three species. DNA data were also available for these species. DNA vouchers were stored at –80 °C in 96% EtOH; the material used for description was separated from the vouchers but kept in 96% EtOH. For illustrations and dissections the specimens were transferred to glycerine. For habitus illustrations the specimens were temporarily mounted on concavity microscope slides (Wilson, 2008a) and drawn by hand with a camera lucida on a Leica DM2500 microscope with interference-contrast optics. The drawings were digitally traced using vectorgraphic software (Adobe Illustrator CS5) following the methods of Coleman (2003, 2009). To increase the visual content of the black and white line drawings, stippling was applied to some illustrations (Bober & Riehl, 2014). Figure plates were prepared using Adobe Photoshop CS5. The drawings were calibrated using a stage micrometer and the measurements were taken from the line drawings after Hessler (1970) with the Measuring Tool in Adobe Reader XI (vers. 11.0.07).

The holotypes were illustrated in dorsal and lateral views without dissections except for DNA tissue. Furthermore, the pleotelson was illustrated in detailed ventral view, also without causing damage to the specimens. Appendages were illustrated *in situ* from the holotypes where possible. All additional views and further appendages were illustrated from the paratypes after dissections were made.

Diagnostic characters (potential autapomorphies of the respective species and synapomorphies suitable for species delineation) were extracted from identification keys generated with the software Key as implemented in DELTA (Dallwitz, 1974). Terms specific for Janiroidea were adopted from Wilson (1989), and setal terminology follows Riehl & Brandt (2010). Macrostylid-specific terminology follows Riehl (2014). For reasons of homology with the proposed sister taxon Urstylidae, the articles of the antenna are named rather than numbered (Riehl *et al.*, 2014b).

The description was exported from DELTA (Dallwitz, 1980) and is based upon a previously established macrostylid data matrix (Riehl *et al.*, 2012; Riehl & Kaiser, 2012). For the measurements the term 'subequal' means 'within 5% of the measurement' as described by Kavanagh & Wilson (2007). All sequences of ratios and setal descriptions provided in the descriptions are ordered from proximal to distal. Setae were excluded from segment and article measurements except for the claws of the anterior pereopods I–III where the claw articulations are not expressed and hence the delimitation of dactylus and claw is ambiguous. Comparisons with previously described species from the area were limited to the original description texts and drawings, as well as new material collected for most of these species during the KuramBio expedition. The type material apparently has been lost and was not available from the collections in St. Petersburg, Moscow or Vladivostok upon request. Nevertheless, important characters could be extracted from the available sources and were coded in the DELTA database.

Confocal laser scanning microscopy (CLSM)

To preserve the good condition of the only male of *M. sabinae* sp. nov., a non-invasive method was chosen. Staining with Congo Red as a fluorescence marker for CLSM was previously described by Michels & Büntzow (2010) and successfully established by Kihara & Arbizu (2012), Kottmann *et al.* (2013) and Brix *et al.* (2014).

Table 3. The taxonomic descriptions are based on the material listed

Species	Type	Genbank accession no.		ZMH-ID	sex	Developing stage	Size (mm)	Station	Depth (m)	Sampling date (d.m.y)	Gear
		16S	18S								
Macrostylis sabinae n. sp.	Holotype, CLSM	MF071237	-	45908	♀	non-ovigerous	2.36	223-2-9	4830–4864	02.-03.08.2012	EBS
Macrostylis sabinae n. sp.	Paratype	MF071234	-	45909	♀	non-ovigerous	2.57	223-2-9	4830–4864	02.-03.08.2012	EBS
Macrostylis sabinae n. sp.	Paratype	MF071225	-	45910	♂	adult	1.75	223-1-10	5418–5429	30.07.2012	EBS
Macrostylis sabinae n. sp.	Paratype, SEM	MF071228	-	45911	♀	non-ovigerous	1.84	223-2-9	4830–4864	02.-03.08.2012	EBS
Macrostylis sabinae n. sp.	Paratype	MF071260	MF071278	45912	♂	juvenile	1.31	223-5-9	5376–5379	11.08.2012	EBS
Macrostylis sabinae n. sp.	Paratype, CLSM	-	-	45913	♂	adult	1.67	223-2-10	4859–4863	03.08.2012	EBS
Macrostylis amaliae n. sp.	Holotype, CLSM	MF071254	-	45914	♀	non-ovigerous	2.11	223-10-6	5251	26.08.2012	MUC
Macrostylis amaliae n. sp.	Paratype	MF071223	-	45915	♂	adult	1.72	223-1-10	5418–5429	30.07.2012	EBS
Macrostylis amaliae n. sp.	Paratype, SEM	MF071230	-	45916	♀	non-ovigerous	2.10	223-2-9	4830–4864	02.-03.08.2012	EBS
Macrostylis amaliae n. sp.	Paratype, CLSM	MF071249	-	45917	♂	adult	1.54	223-6-7	5297	13.08.2012	MUC
Macrostylis amaliae n. sp.	Paratype, CLSM	-	-	45918	♂	adult	1.50	223-10-12	5249–5262	27.08.2012	EBS
Macrostylis daniae n. sp.	Holotype	MF071253	MF071277	45919	♀	non-ovigerous	2.70	223-2-9	3117	02.-03.08.2012	EBS
Macrostylis daniae n. sp.	Paratype	MF071251	-	45920	♀	non-ovigerous	3.10	223-2-9	3117	02.-03.08.2012	EBS
Macrostylis daniae n. sp.	Paratype	-	-	45921	♂	adult	2.80	223-2-9	3117	02.-03.08.2012	EBS
Macrostylis daniae n. sp.	Paratype	-	-	45922	♀	non-ovigerous		223-6-11	2624	15.01.2012	EBS
Macrostylis daniae n. sp.	Paratype	-	-	45923	♂	adult	2.70	223-2-9	3117	02.-03.08.2012	EBS
Macrostylis daniae n. sp.	Paratype	-	-	45924	♀	non-ovigerous	2.80	223-2-9	3117	02.-03.08.2012	EBS

One adult male of *M. sabinae* sp. nov. (ZMH K K-45913) and two adult males of *M. amaliae* sp. nov. (ZMH K-45917, ZMH K-45918) were stained in Congo Red solution for CLSM. Furthermore, the female holotypes of both species were stained and scanned for comprehensive investigation (ZMH K-45908, ZMH K-45914). The staining, mounting and scanning were performed following the guidelines of Michels & Büntzow (2010). However, due to the absence of a 561 nm laser line, the Congo Red-stained chitinous exoskeleton parts were excited by 532 nm laser light and emitted light was detected with a bandpass filter set to 539–670 nm. To gain further autofluorescence of the exoskeleton, both the 405 and 488 nm laser lines were applied with emission filters set to 420–480 and ≥ 490 nm, respectively (Michels & Gorb, 2012). The specimens were scanned in dorsal, ventral and lateral views using a Leica DM2500 with a Leica TCS SPE at a resolution of 2480 × 2480 pixels with a 10× lens or an APO 40×/1.15 oil-immersion CS lens. Two scans per individual and view were necessary to capture each entire animal. The software package LEICA LAS AF was used for recording the image from the scans. The image stacks were further processed in Fiji (Schneider *et al.*, 2012; Schindelin *et al.*, 2012) and finalized in Adobe Photoshop CS5.

Scanning electron microscopy

The specimens were stored in 70% EtOH and were dehydrated in a dilution series of ethanol and amyl acetate and subsequently critically point dried with carbon dioxide as an intermediate medium and finally sputter-coated with graphite. The specimens were glued to the tip of a needle, which was glued to a sample holder. Specimens were scanned utilizing a LEO 1525 (Zeiss) scanning electron microscope at 5 kV acceleration voltage.

RESULTS

Taxonomy

Family: Macrostylidae Hansen, 1916

Genus: *Macrostylis* Sars, 1864

Type species: *Macrostylis spinifera* Sars, 1864

Macrostylis daniae sp. nov.

(Figs 2–12)

urn:lsid:zoobank.org:act:41A76D5C-0B56-4C7B-ACAD-E5531A723028

Diagnosis

Ventral projections on pereonites 1 and 7 present, blunt and keeled in pereonite 1, spine-shaped in pereonite 7. Pereonite 7 with posterolateral tergite protrusions, similar to pereonites 5 and 6. Pleotelson narrower than pereonite 7; waist present; ventrolateral setal ridges present and not visible in dorsal view; posterior apex in male slightly concave. Pereopod III ischium dorsal lobe triangular, with one outstanding apical seta, seta spine-like, straight, bifid. Operculum elongate and ventrally roundedly keeled. Pereopod VII dorsal (posterior) margin row of elongate setae absent. Pleopod III exopod biarticulate. Uropod protopod and endopod of female of similar lengths.

Etymology

Macrostylis daniae sp. nov. is named after the first author's wife Daniela Bober.

Type fixation

Holotype: adult female, 2.7 mm (ZMH K-45919), designated here.

Type material examined

Table 3, Supporting Information S1.

Type locality

North-west Pacific, abyssal plain south-east from KKT; RV *Sonne* stations SO223–2–9, 02–03. August 2012, 46.2268° N, 155.5567° E, 4830–4864 m depth

Further records

SO223–2–10, 03. August 2012, 46.226° N, 155.5595° E, 4859–4863 m depth; SO223–5–9, 11. August 2012, 43.5913° N, 153.9647° E, 5376–5379 m depth; SO223–5–10, 11. August 2012, 43.5912° N, 153.9635° E, 5375–5379 m depth; SO223–6–11, 15. August 2012, 42.4927° N, 154.0005° E, 5291–5305 m depth; SO223–6–12, 15. August 2012, 42.4915° N, 153.9989° E, 5291–5307 m depth.

Description of female

Body: (Figs 2, 3) Broadest in anterior half, narrowing posteriorly. Length 2.7–3.1 mm, 5.1 width, subcylindrical, paucisetose; with furry cuticular hair.

Ventral projections: Pereonite 1 projection prominent and blunt, directed ventrally. Pereonites 2–6 projections absent. Pereonite 7 projection small and acute.

Imbricate ornamentation (IO): Pereonite 4 IO scarce (Fig. 3D); pereonite 5 IO covering whole tergite and collum (Fig. 3D). No ornamentation on posterior margin of each tergal plate in a semicircular arrangement,

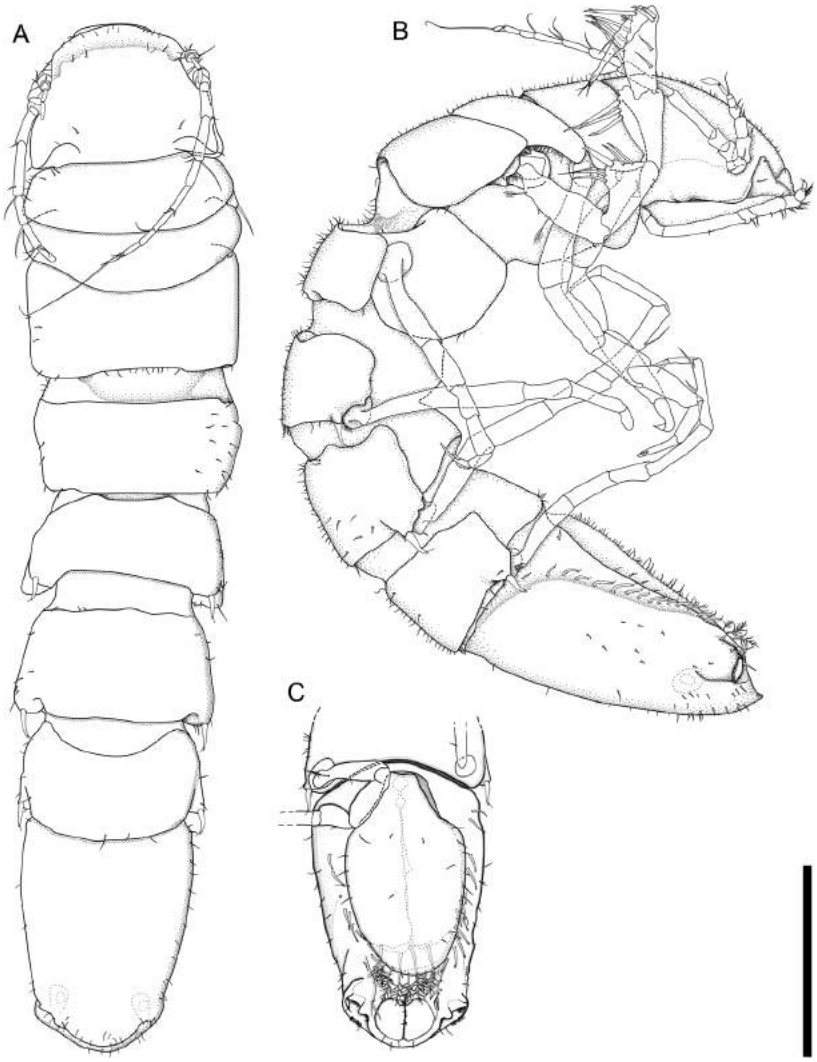

Figure 2. ***Macrostylis daniae*** **sp. nov.**, holotype ZMH K-45919, adult non-ovigerous female. A, dorsal habitus; B, lateral habitus; C, ventral pleotelson. Scale = 0.5 mm (A, B); 0.25 mm (C).

as seen in pereonites 5 and 7 (compare Fig. 3B, D); pereonites 6 and 7 IO depressions less developed than in male, covering whole tergite and collum (compare Fig. 3B–C); pleotelson IO prominent (Fig. 3A–B, K).

Cephalothorax: Length 0.69–0.81 width, 0.13–0.15 body length; clypeus in dorsal view convex and smooth; frontal furrow present, straight, weakly expressed a shallow, rounded ditch, dorsal surface with setae. Posterolateral setae minute. Posterolateral margins blunt.

Fossosome: Tergite articulations present (Fig. 2A, B), sternite articulations absent (Fig. 2B), ventral surface without keel, length 0.94–1.0 width, length 0.20–0.22 body length, lateral tergite margins confluent.

Pereonite 1: Posterolaterally with long, asensillate setae (Fig. 2A, B).

Pereonite 4: Width 1.0 pereonite 5 width, length 0.59 width; pereonal collum present. Laterally expressed, segment anteriorly constricted. Shape clearly distinct from both anterior and posterior pereonites. Lateral margins anteriorly widest, narrowing gradually towards posterior. Posterolateral margins contracting laterally, rounded and posterolateral setae absent.

Pereonite 5: Length 0.43–0.53 width, 0.70 pereonite 4 length. Posterolateral margins rounded. Tergite posterolateral setae sensillate, robust, flexibly articulated.

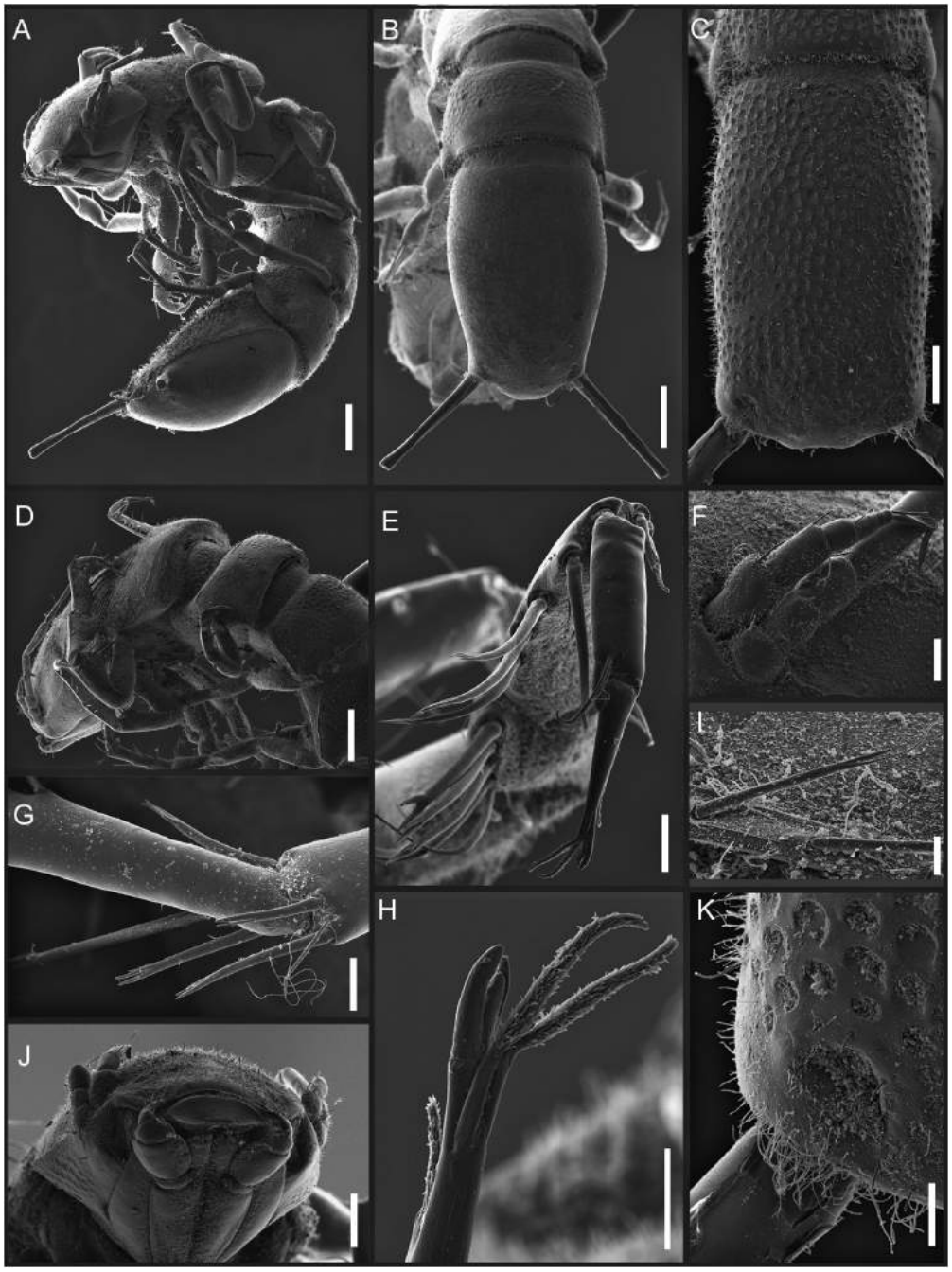

Figure 3. ***Macrostylis daniae*** **sp. nov.**, non-ovigerous female paratype ZMH K-45924, SEM micrographs. A, lateral habitus, 200 μm; B, dorsal pleotelson, 200 μm; C, dorsal pleotelson, male (ZMH K-45923), 100 μm; D, lateral anterior habitus, 200 μm; E, detail of propodus and dactylus pereopod III (right); 20 μm; F, lateral detail of antennula, 40 μm, G, detail of pereopod VII, 20 μm; H, detail of pereopod III (right), 20 μm; I, detail of ventrolateral setae (right), 20 μm; J, anteroventral cephalothorax, 100 μm; K, dorsal statocyst opening and uropod, male (ZMH K-45923), 30 μm.

Pereonite 6: Length 0.72–0.73 width, 1.5–1.7 pereonite 5 length. Posterolateral margin produced posteriorly, rounded. Tergite posterolateral setae sensillate and robust, flexibly articulated.

Pereonite 7: Length 0.55–0.64 width. Posterolateral margin produced posteriorly, rounded. Tergite posterolateral setae sensillate, robust, flexibly articulated.

Pleonite 1: Sternal articulation with pleotelson absent.

Pleotelson: Ovoid, lateral margins convex. Length 0.21–0.23 body length, 1.2–1.5 width; narrower than pereonite 7. Posterior margin concave at uropod insertions; apex convex, slightly rounded, almost straight, apex length 0.10 pleotelson length. Posterior apex setae absent. Pleopodal cavity width 0.70 pleotelson width; setal ridges present (Fig. 3I), visible in dorsal view. Statocysts present, with dorsal concave slot-like apertures, diagonal across longitudinal axis (Fig. 3K); longitudinal trough width 0.36 pleotelson width. Anal opening subterminal, exposed and superficial, tilted posteriorly relative to frontal plane.

Antennula: (Figs 2B, 3F) Length 0.57 head width, 0.25 antenna length, width 1.0 antenna width; articles decreasing in size from proximal to distal; relative length ratios of articles 1.0, 0.86, 0.43, 0.29, 0.29; length/width (L/W) ratios of articles 1.4, 1.5, 1.0, 1.0, 1.0. Article 1 longest and widest, distinctly longer than wide, with 2 asensillate setae and 1 broom seta. Article 2 distinctly longer than wide, with 1 asensillate seta and 2 broom setae. Article 3 length subequal width, with 1 asensillate seta. Article 4 length subequal width, with 1 asensillate seta. Terminal article length subequal width, with 1 asensillate seta and 1 aesthetasc with intermediate belt of constrictions.

Antenna: (Fig. 2A, B) Length 0.29 body length. Coxa squat, with one simple seta. Basis not longer than wide, longer than coxa. Ischium elongate, longer than coxa. Merus longer than coxa, basis and ischium combined, distally with 1 asensillate seta. Carpus subequal merus length, longer than coxa, basis and ischium combined, distally with 1 asensillate seta and 3 broom setae. Flagellum with 6 articles.

Mandible: (Figs 4D–F, 10G) With lateral seta; molar process length less than incisor length; left mandible incisor process oligodentate with dorsal and ventral subdistal teeth that partly enclose lacinia, with 3 cusps; lacinia mobilis robust, similar to incisor process, with 3 denticles; right mandible incisior process simplified, mono- or bidentate rounded, blunt, with 2 cusps; dorsally with projecting cutting edge with 1 acute distal cusp and 1 blunt intermediate cusp; lacinia mobilis spine-like, clearly smaller than left *lacinia*, with 5 or 6 denticles.

Maxillula: (Fig. 4B) Lateral lobe terminally with 12 robust and 4 slender setae.

Maxilla: (Fig. 4C) Lateral lobe with 4 setae terminally: one lateral serrate, robust seta followed by three simple slender setae; middle lobe with 5 robust to slender setae terminally; medial lobe terminally with 8 simple, slender setae.

Maxilliped: (Figs 3J, 4A) Basis length 4.2 width; endite distally with 2 or 3 fan setae, medioventrally with seta present; palp wider than endite, article 2 wider than article 1, palp article 1 distomedially with 1 seta, article 1 shorter than article 3; epipod length 3.8 width, 0.92 coxa-basis length.

Pereopod I: (Fig. 5A) Length 0.30 body length; article L/W ratios 3.8, 2.8, 1.9, 1.9, 3.0, 5.5; relative article length ratios 1.0, 0.65, 0.50, 0.38, 0.35, 0.32. Ischium dorsal margin with 3 simple setae. Merus dorsal margin with 3 simple setae and ventrally with 3 distally fringe-like sensillae and 1 bifurcate seta. Carpus dorsally with 1 bifurcate seta. Dactylus medial cuticle subdistally with 3 sensillae, terminal claw length 0.11 dactylus length.

Pereopod II: (Figs 5B, 6B) Longer than pereopod I, length 0.37–0.43 body length; article L/W ratios 4.2–5.0, 3.25–3.3, 1.7–2.0, 2.6–2.7, 3.6–4.0, 5.5–6.0; relative article length ratios 1.0, 0.66–0.68, 0.40–0.46, 0.47–0.54, 0.32–0.37, 0.31–0.32. Ischium dorsally with 3 simple setae. Merus dorsally with 4 simple setae, ventrally with 3 distally fringe-like sensillae. Carpus dorsally with 3 setae: simple, broom and bifurcate, ventrally with 4 distally fringe-like sensillae. Dactylus medial cuticle subdistally with 3 sensillae.

Pereopod III: (Figs 5C, 6A) Length 0.39–0.43 body length; article L/W ratios 2.9–3.1, 1.9–2.2, 1.6–1.7, 2.7–2.9, 3.0–3.7, 6.5; relative article length ratios 1.0, 0.77–0.86, 0.56–0.66, 0.71–0.79, 0.32–0.41, 0.38–0.45. Ischium dorsal lobe triangular; proximally with 2 bisetulate setae; apex apical with 1 prominent robust, sensillate, bifid, straight, spine-like seta; distally with 2 bisetulate setae. Merus dorsally with 5 setae: 1 serrate, slender, 4 bifurcate; ventrally with 4 distally fringe-like sensillae. Carpus dorsally with 5 bifurcate, pappose setae; ventrally with 3 distally fringe-like sensillae and 1 bifurcate seta (Fig. 3E). Dactylus medial cuticle subdistally with 3 sensillae (Fig. 3H).

Pereopod VI: (Figs 6D, 7A) Length 0.33–0.44 body length; article L/W ratios 4.1–5.3, 2.7–3.2, 1.9–2.7, 4.4–5.2, 6.7–7.0, 4.0–4.5; relative article length ratios 1.0, 0.55–0.59, 0.45–0.50, 0.76–0.81, 0.63–0.72, 0.25–0.31. Ischium distodorsally and mid-ventrally with 1 simple seta; distoventrally with 2 simple setae. Merus distodorsally with 3, distoventrally with 3 bifurcate, pappose setae. Carpus mid-dorsally with 2 bifurcate, pappose setae; distodorsally with

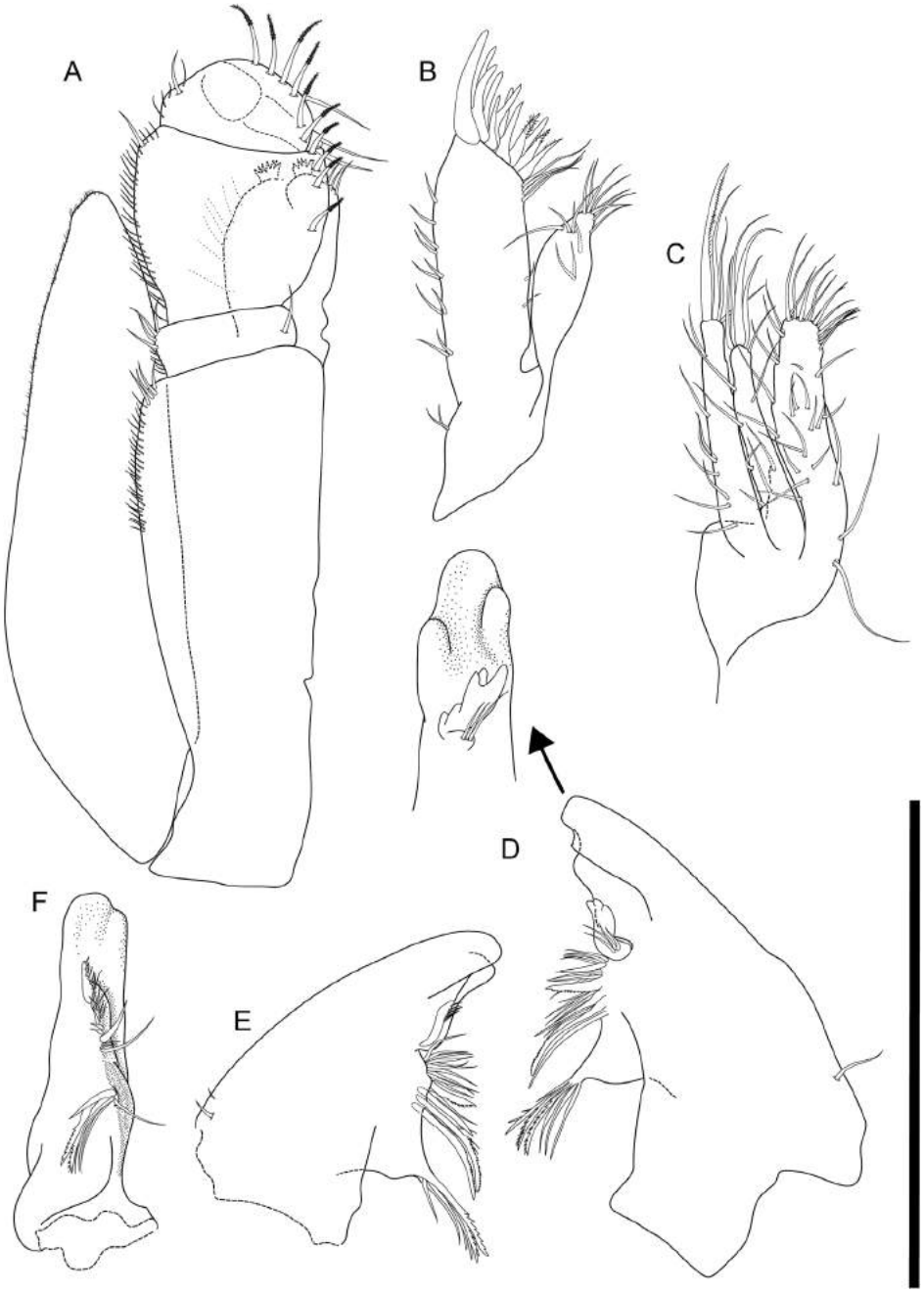

Figure 4. ***Macrostylis daniae*** **sp. nov.**, non-ovigerous female paratype ZMH K-45920 mouthparts. A, maxilliped; B, maxillula; C, maxilla; D, left mandible; E, right mandible, defective proximal; F, medial view of right mandible, defective proximal. Scale = 0.25 mm; 0.2 mm (D detail).

3 bifurcate, pappose setae; mid-ventrally with 2 bifurcate, pappose setae, paired; distoventrally with 3 bifurcate, pappose setae.

Pereopod VII: (Figs 3G, 6C, 7B) 0.26 body length; relative article length ratios 1.0, 0.65, 0.57, 0.78, 0.65, 0.26; basis length 4.6 width, dorsal and ventral margin rows of elongate setae absent. Ischium length 3.0 width, mid-ventrally with 1 simple seta; distoventrally with 2 simple setae. Merus length 3.3 width, distodorsally with 3 bifurcate, pappose setae; mid-ventrally with 1 seta; distoventrally with 2 bifurcate setae. Carpus length 6.0 width, mid-dorsally with 2 bifurcate pappose setae, in a row; distodorsally with 3

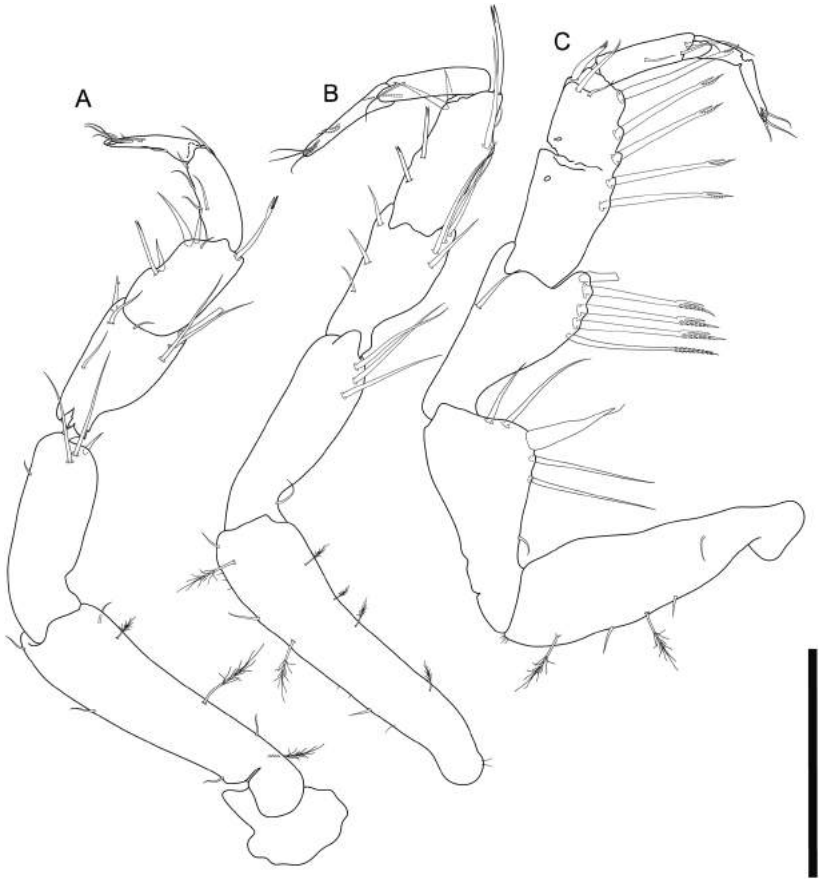

Figure 5. ***Macrostylis daniae*** **sp. nov.**, non-ovigerous female paratype ZMH K-45920 anterior pereopods. A, pereopod I; B, pereopod II; C, pereopod III. Scale = 0.25 mm.

bifurcate setae: 2 pappose bifurcate and 1 broom seta; mid-ventrally with 2 paired bifurcate, pappose setae and one single bifurcate seta; distoventrally with 3 bifurcate, pappose setae. Propodus length 7.5 width. Dactylus length 6.0 width.

Operculum: (Figs 2C, 8C) Elongate, ovoid; length 1.61–1.66 width, 0.74–0.94 pleotelson dorsal length; apical width 0.52–0.63 operculum width; not reaching anus. Distal margin broadly rounded, ventrally with oblate keel. Longitudinal furrow absent. With lateral fringe consisting of 8 or 9 undivided setae; with continuous transition to apical row of setae, apical row comprising 10–12 short pappose setae, extending to anal opening.

Pleopod III: (Fig. 8E) Length 3.7 width; protopod length 3.0 width, 0.55 pleopod III length, endopodal plumose setae subequal endopod length; exopod length 0.70 pleopod III length, biarticulated, with fluent outline transition, articulation hardly visible, one conspicuous subterminal seta present.

Pleopod IV: (Fig. 8F) Length 2.3 width, endopod length 1.7 width, exopod length 6.0 width, 0.60 endopod length; exopod lateral fringe of setae present.

Pleopod V: (Fig. 8G) Present.

Uropod: (Fig. 7C) Inserting on posterior margin; protopod of subequal width over its complete length, distal margin blunt, endopod insertion terminal, uropod length 1.2 pleotelson length; protopod length 14.7 width, 0.61 pleotelson length; endopod width at articulation subequal protopod width, length 11.0 width; 1.0 protopod length.

Description of terminal male

Body: (Figs 9, 10) More elongate than female, subcylindrical, length 2.8 mm, 6.4 width.

Ventral projections: (Fig. 9A) Pereonite 1 projection blunt, bulbous and prominent (Fig. 10H). Pereonite

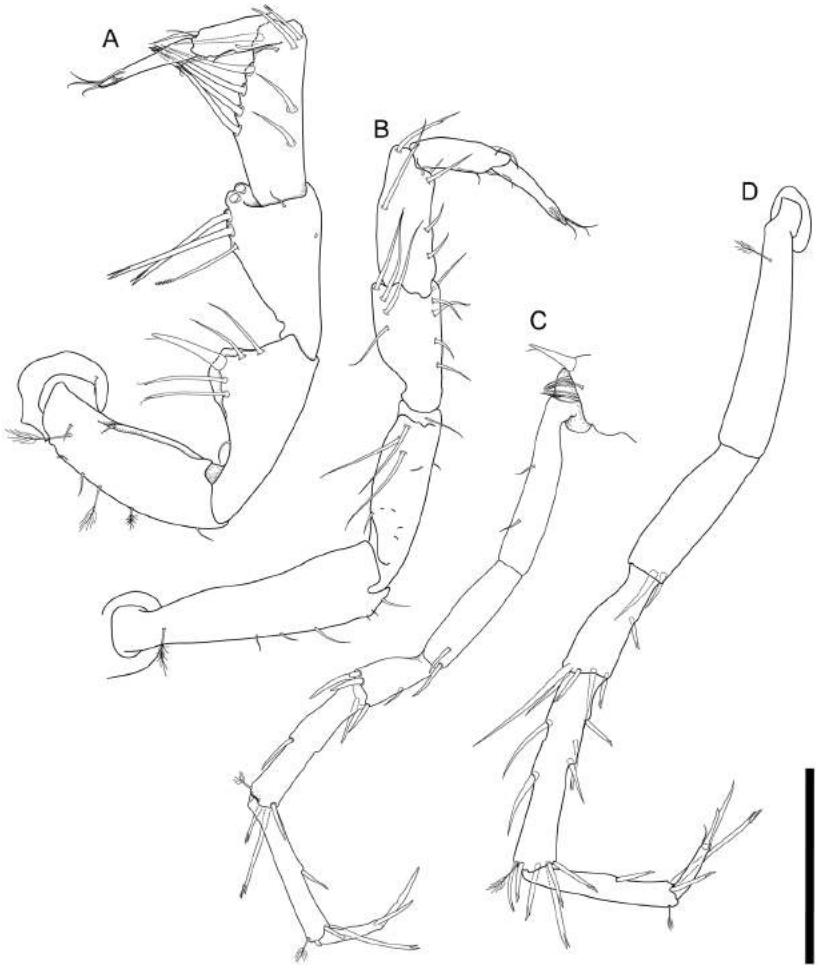

Figure 6. ***Macrostylis daniae*** **sp. nov.**, non-ovigerous female holotype ZMH K-45919 appendages drawn *in situ*. A, pereopod III; B, pereopod II; C, pereopod VII; D, pereopod VI. Scale = 0.25 mm.

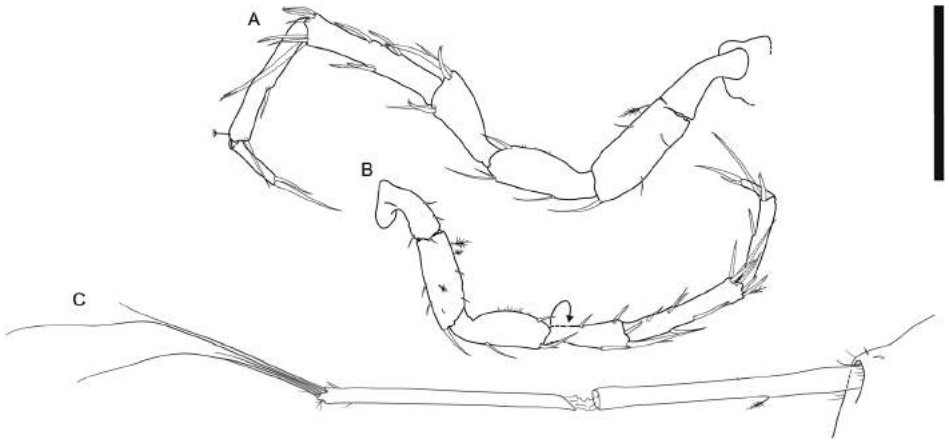

Figure 7. ***Macrostylis daniae*** **sp. nov.**, non-ovigerous female paratype ZMH K-45920 posterior appendages. A, pereopod VI; B, pereopod VII – pereopod twisted at merus; C, uropod from ventral side (damaged). Scale = 0.25 mm.

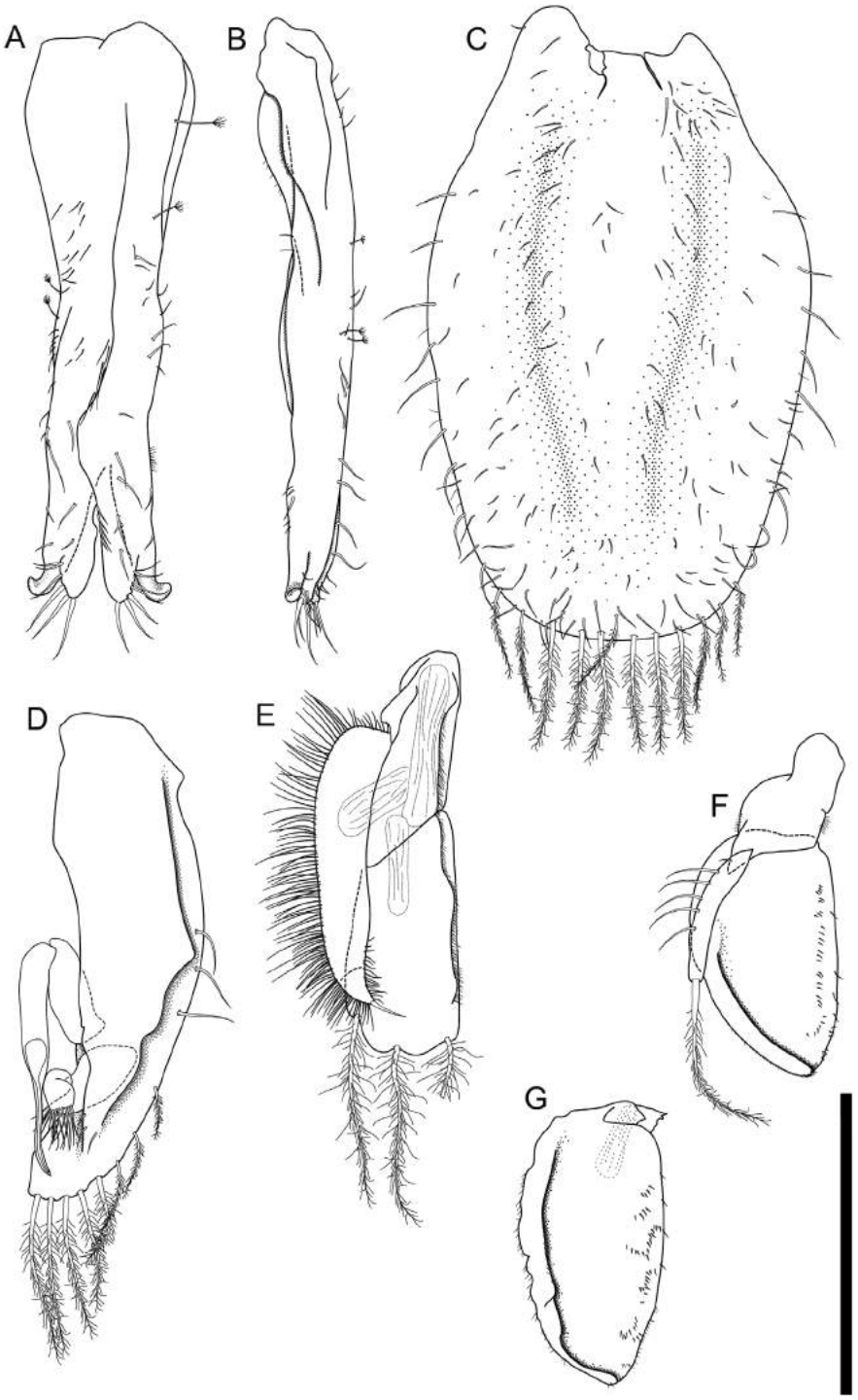

Figure 8. ***Macrostylis daniae*** **sp. nov.**, pleopods of terminal male (ZMH K-45921; A, B, D) and non-ovigerous female (ZMH K-45920; C, E–G) paratypes. A, pleopod I ventral, slightly damaged; B, pleopod I lateral; C, operculum; D, pleopod II; E, pleopod III; F, pleopod IV; G, pleopod V. Scale = 0.25 mm.

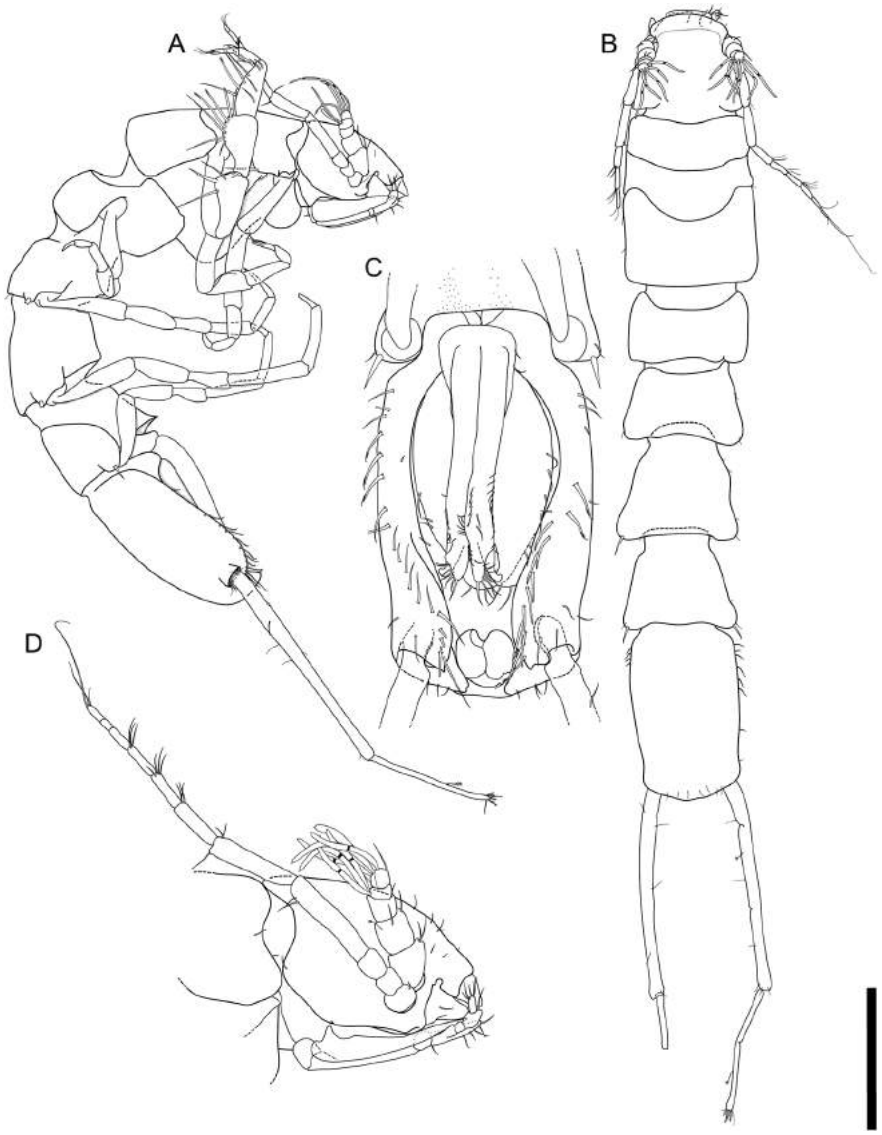

Figure 9. ***Macrostylis daniae*** **sp. nov.**, terminal male paratype ZMH K-45921. A, lateral habitus; B, dorsal habitus; C, ventral pleotelson (pleopod I + II misaligned); D, lateral cephalothorax. Scale = 0.5 mm (A, B); 0.25 mm (C, D).

2–6 projections absent. Pereonite 7 projection spine-shaped, small (Fig. 9I).

Imbricate ornamentation (IO): Pereonite 3 IO on posterior and posterolateral margin (Fig. 10A, C), pereonite 4–7 and pleotelson IO more prominent than in female (Figs 3B, C, 10B, C).

Cephalothorax: Frontal furrow present, smooth and straight; L/W ratio larger than in female, length 2.1 width, 0.34 body length; dorsal surface with setae; posterolateral corners rounded, posterolateral setae present.

Fossosome: L/W ratio greater than in female, length 1.3 width, length/body-length ratio subequal to female.

Pereonite 4: Pereonal collum present, medially concave. Lateral margins in dorsal view convex, almost parallel; integration with other segments clearly distinct from both anterior and posterior segments; posterolateral margins not produced posteriorly.

Pereonite 5: Length 0.64 width, length 1.1 pereonite 4 length. Posterolateral setae on tergite as in female.

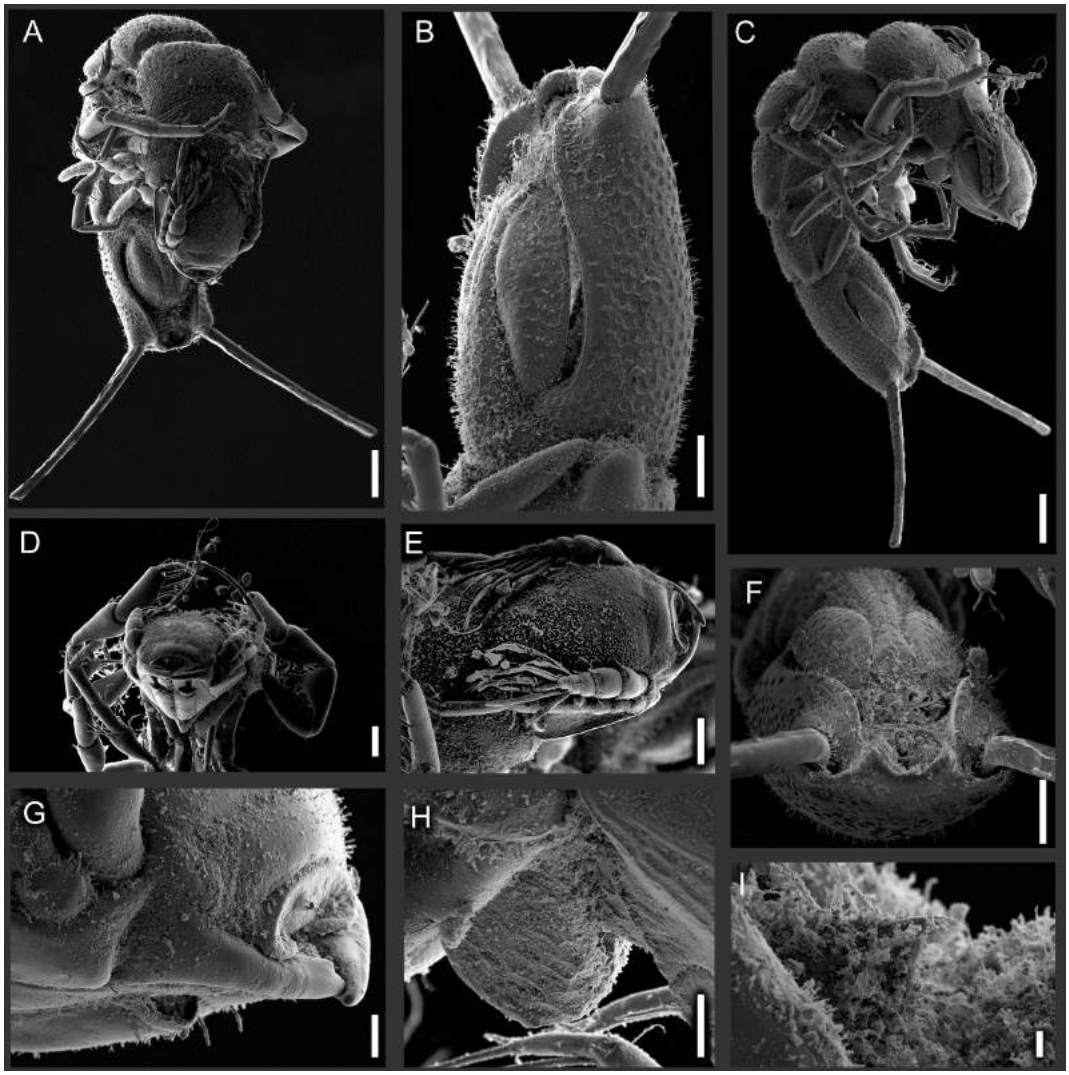

Figure 10. ***Macrostylis daniae*** **sp. nov.**, terminal male paratype ZMH K-45921. A, dorsal habitus, 200 μm; B, lateral pleotelson, with ciliate epibionts, 100 μm; C, lateral habitus, 200 μm; D, frontal cephalothorax, 100 μm; E, dorsal cephalothorax, with ciliate epibionts on aesthetascs and antenna, 100 μm; F, posterioventral pleotelson, 100 μm; G, lateral mandibles, maxilliped palp broken, 30 μm; H, lateral pereonite 1 ventral projection, 40 μm; I, lateral pereonite 7 ventral projection, 10 μm.

Pereonite 6: Length 0.81 width, clearly larger pereonite 5 length, length 1.3 pereonite 5 length. Posterolateral setae on tergite as in female.

Pereonite 7: As in female.

Pleonite 1: Sternal articulation with pleotelson present.

Pleotelson: In dorsal view sexually dimorphic, minimally constricted anteriorly to uropod articulation, rectangular, lateral margins straight and almost parallel, width maximum anterior to waist; L/W ratio in male greater than in female, length 1.6 width, 0.22 body length, width less than pereonite 7 width. Posterior apex medially and at uropod insertions concave and rounded, length 0.08 pleotelson length, without setae on margin. Pleopodal cavity width 0.68 pleotelson width, longitudinal trough width 0.29 pleotelson width.

Antennula: (Figs 9D, 10E) Length 0.55 head width, width 1.4 antenna width; article L/W ratios 1.0, 1.0, 1.0, 0.50, 1.0; relative article length ratios 1.0, 0.86, 0.57, 0.29, 0.43; terminal article with 4 aesthetascs, penultimate article with 5 aesthetascs. Aesthetascs with intermediate belt of constrictions, length shorter antennula length. Article 1 squat, longest and widest, with 4 asensillate setae. Article 2 squat, shorter than article 1, with 2 asensillate

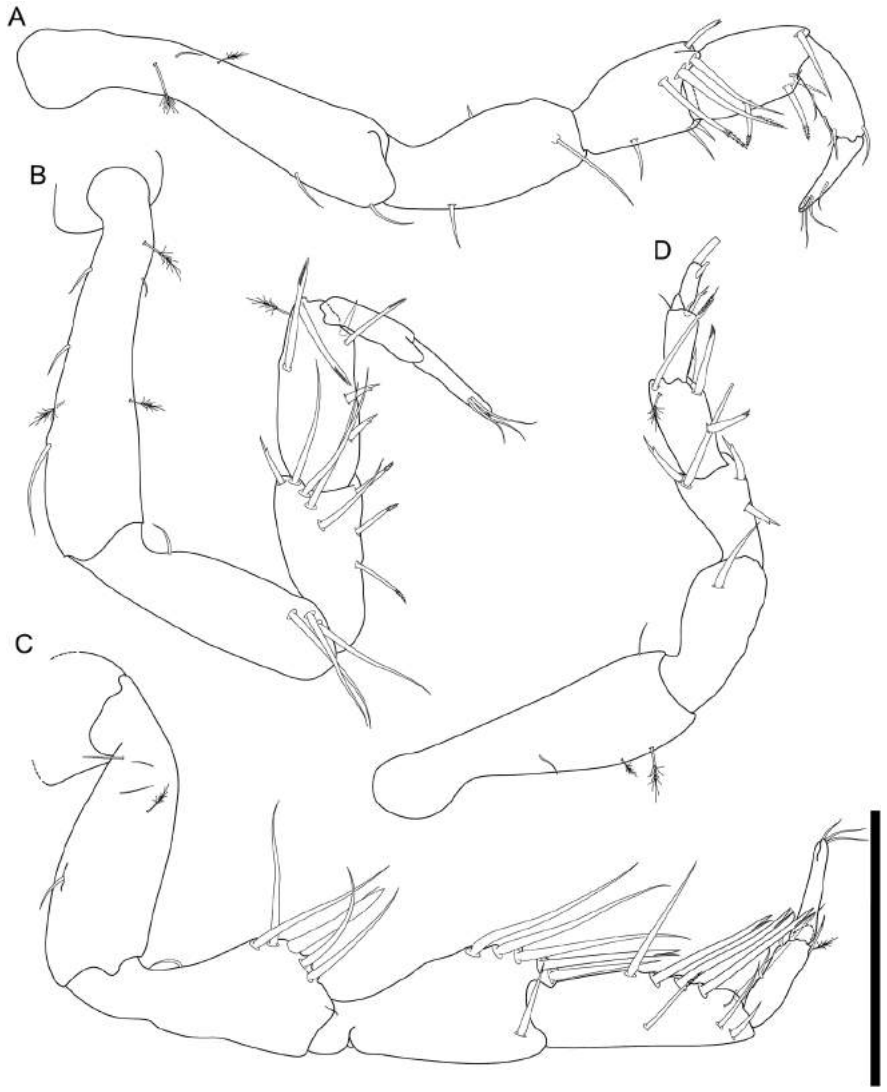

Figure 11. ***Macrostylis daniae*** **sp. nov.**, terminal male paratype ZMH K-45921 anterior appendages. A, pereopod I; B, pereopod II; C, pereopod III; D, pereopod IV. Scale = 0.25 mm.

setae and 1 broom seta. Article 3 squat, shorter than article 1, with 2 asensillate setae. Article 4 squat, minute. Article 5 squat, shorter than article 1.

Antenna: (Fig. 9D) Length 0.28 body length, flagellum of 5 articles, coxa and basis squat, basis length subequal coxa length. Ischium elongate, cylindrical, longer than coxa. Merus longer than coxa, basis and ischium together, distally with 2 simple setae. Carpus shorter than merus, distally with 1 asensillate seta and 3 broom setae.

Pereopod I: (Fig. 11A) Length 0.32 body length; article L/W ratios 4.5, 2.1, 1.4, 1.7, 2.8, 4.0; relative article length ratios 1.0, 0.47, 0.31, 0.33, 0.31, 0.22. Ischium dorsally with 1 seta submarginally. Merus and carpus setation as in female.

Pereopod II: (Fig. 11B) Length 0.38 body length; article L/W ratios 4.0, 3.3, 1.9, 2.6, 3.0, 5.0; relative article length ratios 0.72, 0.42, 0.50, 0.25, 0.28. Ischium, merus and carpus setation as in female.

Pereopod III: (Fig. 11C) Length 0.37 body length; article L/W ratios 2.6, 2.5, 1.8, 3.0, 3.0, 4.5; relative article length ratios 0.96, 0.77, 0.81, 0.35, 0.35.

Pereopod IV: (Fig. 11D) Length 0.25 body length; article L/W ratios 3.2, 2.1, 1.3, 1.8, 2.3, 2.0; relative article length ratios 1.0, 0.52, 0.28, 0.31, 0.24, 0.14.

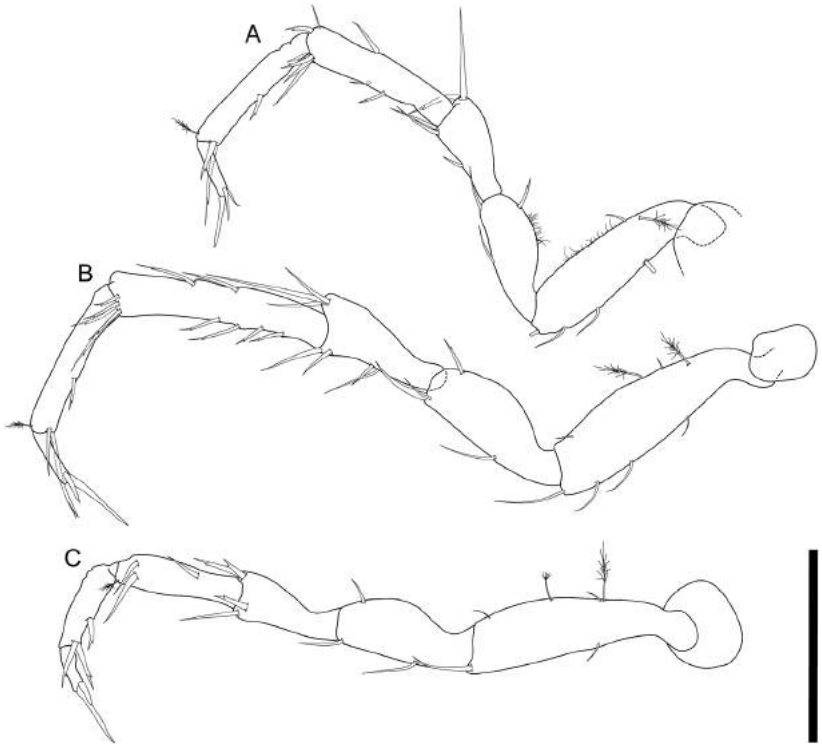

Figure 12. ***Macrostylis daniae*** **sp. nov.**, terminal male paratype ZMH K-45921 posterior appendages. A, pereopod V; B, pereopod VI; C, pereopod VII. Scale = 0.25 mm.

Pereopod V: (Fig. 12A) 0.34 body length; article L/W ratios 3.6, 2.3, 2.2, 4.0, 3.3, 3.0, relative article length ratios 1.0, 0.62, 0.45, 0.55, 0.45, 0.21. Ischium distodorsally with 1 simple seta; mid-ventrally with 1 simple seta; distoventrally with 1 simple seta. Merus distodorsally with 2 bifurcate setae; distoventrally with 2 bifurcate setae. Carpus distodorsally with 1 simple seta; distoventrally with 2 setae: 1 simple and 1 broom seta.

Pereopod VI: (Fig. 12B) Length 0.44 body length; article L/W ratios 3.7, 2.6, 2.0, 5.8, 5.3, 4.0; relative article length ratios 1.0, 0.64, 0.49, 0.88, 0.64, 0.24. Ischium and merus setation as in female. Carpus setation, mid-dorsally with 2 bifurcate setae; distodorsally with 4 setae: 3 bifurcate and 1 broom; mid-ventrally with 4 bifurcate setae; distoventrally with 4 simple setae.

Pereopod VII: (Fig. 12C) Length/body-length ratio sexually dimorphic, distinctly longer than in female, length 0.37 body length, shorter than pereopod VI; relative article length ratios 1.0, 0.61, 0.46, 0.75, 0.71, 0.29; segment L/W ratios sexually dimorphic. Basis length 4.0 width; dorsal margin with row of 3 elongate setae. Ischium length 2.8 width; mid-ventrally with 1 simple seta; distoventrally with 1 simple seta. Merus length 2.2 width; distodorsally with 2 setae; mid-ventrally with 1 simple seta; distoventrally with 2 bifurcate setae. Carpus length 5.3 width; mid-dorsally with 1 simple seta; distodorsally with 3 bifurcate setae and 1 broom seta; mid-ventrally with 2 bifurcate setae; distoventrally with 3 bifurcate setae. Propodus length 6.7 width. Dactylus length 4.0 width.

Operculum: (Fig. 10B) Male operculum vaulted.

Pleopod I: (Fig. 8A, B) Length 0.77 pleotelson length, subequal pleopod II length. Lateral lobes projecting lateroventrally to form horns, clearly extending distally beyond medial lobes; medial lobes distally with 7 asetulate setae, ventrally with simple and pappose setae. Pleopods I and II distally level, in the same plane.

Pleopod II: (Fig. 8D) Protopod apex rounded; distally not enclosing pleopods I; with 3 setae along entire lateral margin and 8 pappose setae distally. Endopod distance of insertion from protopod distal margin 0.33 protopod length. Stylet weakly curved, extending near to distal margin of protopod, length 0.48 protopod length.

Uropod: (Fig. 9A, B) Length 2.0 pleotelson length; protopod L/W ratio less than in female, protopod length 9.4 width. Endopod/protopod length ratio less than in female, endopod length 0.94 protopod length, 22.0 width, width smaller protopod width.

Remarks

This species features a set of character states that are unique amongst Macrostylidae. It shares with *M. curticornis* a blunt first ventral projection and a tiny ventral projection on tergite 7. In contrast to *M. curticornis* this species has the plesiomorphic state of a five-segmented antennula, it lacks a dorsal row of setae on pereopod VII and has a clearly visible pleotelson waist; the pleotelson is narrower than pereonite 7 and the operculum is elongated, amongst further differences. *Macrostylis daniae* sp. nov. shares many character states with the species described below in this article, but the blunt ventral projection of the first sternite, its distinctly larger body size as well as relative length of the pleotelson allow for delimitation.

Macrostylis sabinae sp. nov.

(Figs 13–24)

urn:lsid:zoobank.org:act:F3936020-7319-42D1-825F-F3F97291DCC5

Diagnosis

Ventral projection 1, and 3–7 present in females; ventral projections in males: pereonite 5 and 6 ventral projection absent. Pereonite 4 widest anteriorly and continuously narrowing towards posterior, not produced posteriorly, posterolateral setae absent; pleotelson waist present; operculum elongate; pleotelson L/W ratio in males greater than in females; male pleotelson of hourglass-like shape, with an anterior and a posterior convex outline separated by a concave waist; posterior apex short, laterally slightly convexly curved and medially truncate. Male aesthetascs of two types: (1) aesthetasc with intermediate belt of constriction, (2) aesthetasc with intermediate belt of constriction and additional single constriction in distal half. Pereopod III ischium dorsal lobe triangular; apex with 1 prominent seta; apical seta robust, sensillate, bifid and curved proximally, spine-like. Prominent coxal seta on pereopod VII. Pleopod I lateral horns clearly projecting distally beyond medial lobes.

Etymology

Macrostylis sabinae sp. nov. was named after the first author's mother Sabine Bober.

Type fixation

Holotype: Adult female, 2.4 mm (ZMH K-45908), designated here.

Type material examined

Table 3, Supporting Information S1.

Nineteen specimens of various stages and both genders used for DNA extraction.

Type locality

North-west Pacific, abyssal plain south-east from KKT; RV *Sonne* stations SO223–2–9, 03. August 2012, 46.2268° N, 155.5567° E, 4830–4864 m depth.

Further records

SO223–1–10, 30. July 2012, 43.9710° N, 157.3278° E, 5418–5429 m depth; SO223–2–10, 03. August 2012, 46.226° N, 155.5595° E, 4859–4863 m depth; SO223–3–9, 05. August 2012, 47.2307° N, 154.6982° E, 4859–4863 m depth; SO223–5–9, 11. August 2012, 43.5913° N, 153.9647° E, 5376–5379 m depth; SO223–7–9, 17. August 2012, 43.0473° N, 152.9905° E, 5216–5223 m depth. Specimens found at other stations with no genetic data available were excluded from this series to avoid potential errors due to the close similarity of *Macrostylis amaliae* sp. nov. and *M. sabinae* sp. nov. These are listed only in Supporting Information S1.

Description of female

Body: (Fig. 13; Supporting Information S2, S3) Body shape broadest in anterior half, narrowing posteriorly. Length 1.8–2.6 mm, 4.5 width, subcylindrical, paucisetose.

Ventral projections: Pereonite 1 projection prominent and acute. Reduced or minimally expressed at anterior overlapping of oostegites in ovigerous females. Pereonite 3 projection absent. Pereonite 4 projection directed posteriorly; small, acute and closer to posterior segment border. Pereonite 5 and 6 projection acute, prominent and closer to posterior segment border. Pereonite 7 projection prominent and acute.

Imbricate ornamentation (IO): absent on all pereonites.

Cephalothorax: Length 0.79 width, 0.16 body length; clypeus in dorsal view convex and smooth, frontal furrow present and straight. Posterolateral setae absent, posterolateral margins blunt.

Fossosome: (Fig. 13A, B) Tergite articulations present, sternite articulations absent (Fig. 14A), ventral

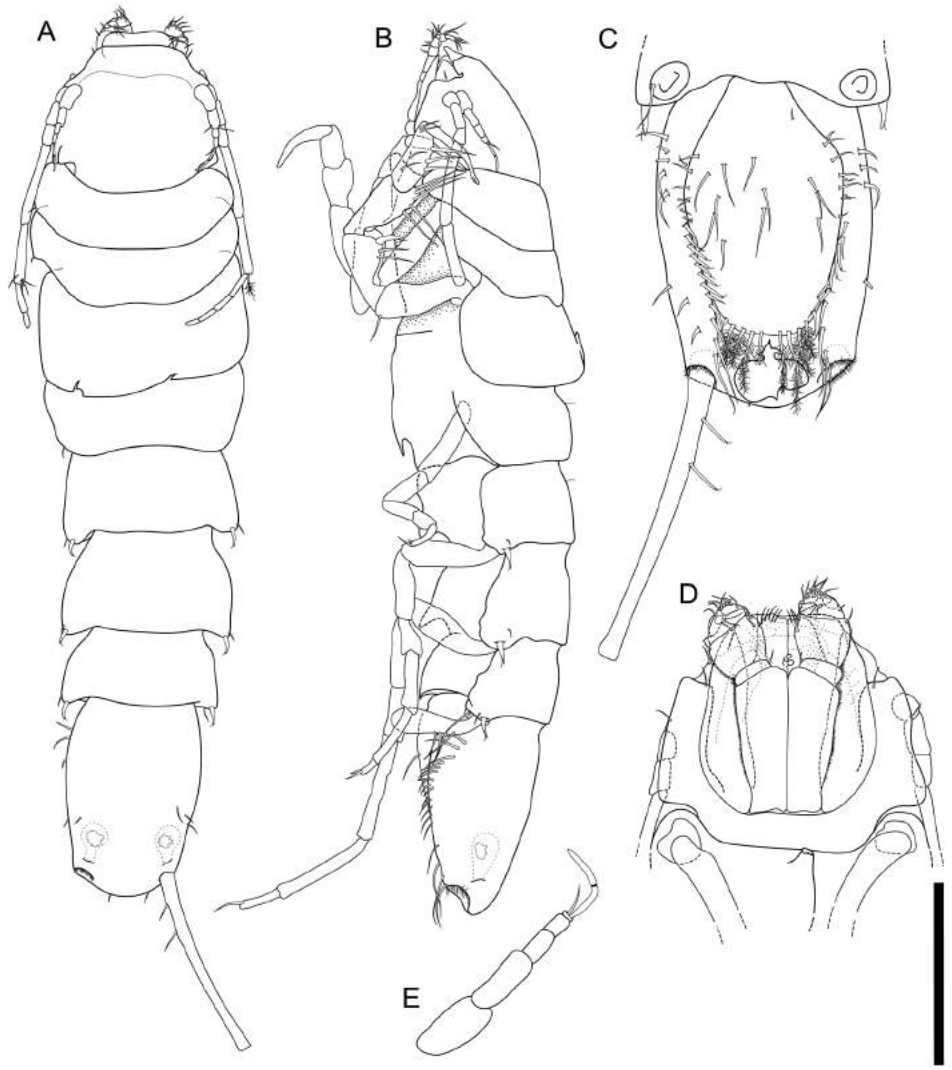

Figure 13. ***Macrostylis sabinae*** **sp. nov.**, non-ovigerous female holotype ZMH K-45908, damaged on posterior pereonite 3 and pereonite 1 ventral projection. A, dorsal habitus; B, lateral habitus; C, ventral pleotelson; D, lateral cephalothorax; E, antennula (antenna I). Scale = 0.5 mm (A, B); 0.25 mm (C, D); 0.4 mm (E).

surface rounded, length 0.81–0.97 width, 0.21–0.23 body length, lateral tergite margins confluent.

Pereonite 4: (Fig. 13A, B) Width 1.1–1.2 pereonite 5 width, length 0.27–0.32 width; pereonal collum present. Shape clearly distinct from both anterior and posterior segments. Lateral margins anteriorly widest, narrowing gradually towards posterior. Posterolateral margin width relative to max. width contracting laterally; posterolateral margins rounded and posterolateral setae minute.

Pereonite 5: (Fig. 13A, B) Length 0.48–0.49 width, 1.3–1.6 pereonite 4 length. Posterolateral margins rounded. Posterolateral setae sensillate, robust, flexibly articulated. Coxal setae absent.

Pereonite 6: (Fig. 13A, B) Length 0.51–0.58 width, 1.0–1.2 pereonite 5 length. Posterolateral margin produced posteriorly, rounded. Tergite posterolateral setae sensillate, robust, spine-like.

Pereonite 7: (Fig. 13A, B) Length 0.43–0.48 width. Posterolateral margin produced posteriorly, rounded. Tergite posterolateral setae sensillate, robust, spine-like. Coxal bisetulate setae present.

Pleonite 1: (Fig. 13A–C) Sternal articulation with pleotelson present.

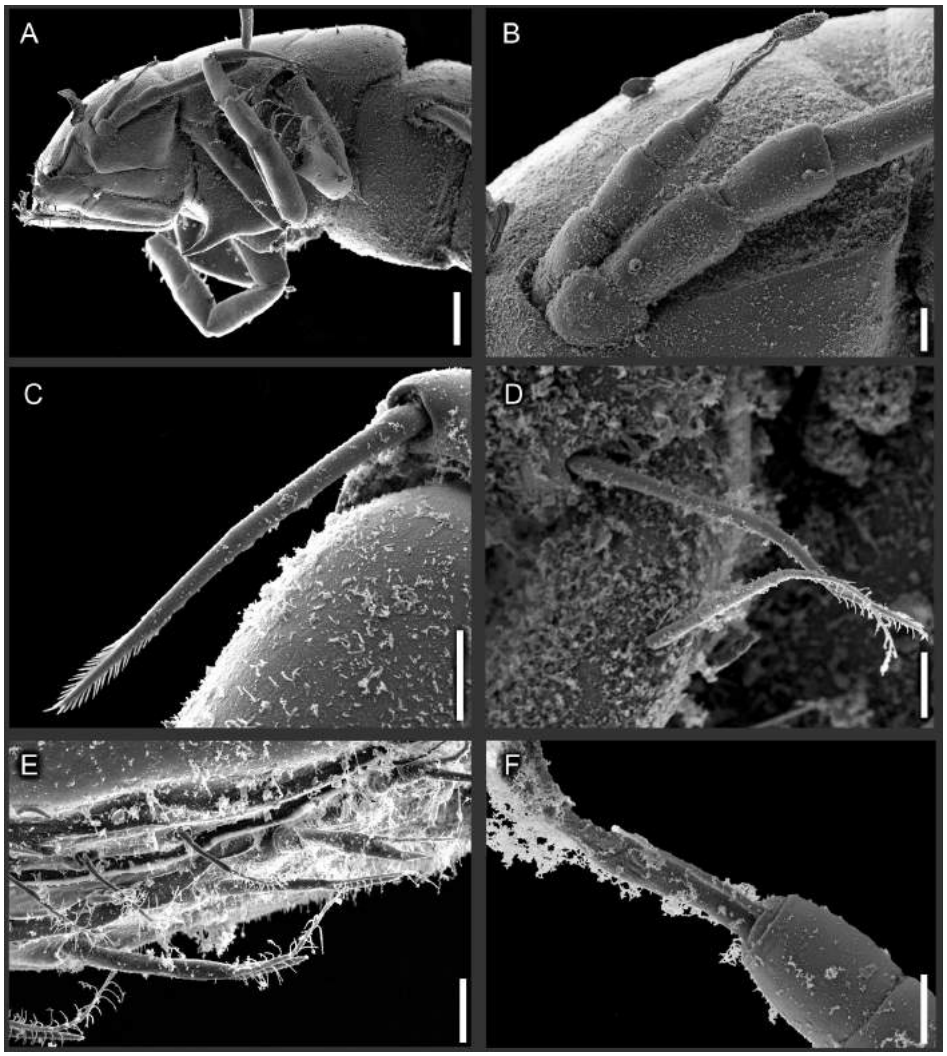

Figure 14. ***Macrostylis sabinae*** **sp. nov.**, non-ovigerous female paratype ZMH K-45909 and ***Macrostylis amaliae*** **sp. nov.**, non-ovigerous female paratype ZMH K-45916, SEM micrographs. A, ***M. amaliae*** **sp. nov.**, lateral, 100 µm; B, ***M. amaliae*** **sp. nov.**, antennula, 20 µm; C, bisetulate setae of ***M. amaliae*** **sp. nov.** on basis of pereopod V, 10 µm; D, coxal seta and seta of ***M. amaliae*** **sp. nov.** on basis of pereopod VII, 10 µm; E, operculum lateral fringe of pappose setae (top) and pleotelson ventrolateral setal ridges with row of bifid, pappose setae (bottom) of ***Macrostylis sabinae*** **sp. nov.**, 10 µm; F, detail of antennula, articles 3–5 including disc-like terminal article and aesthetasc articulation in ***M. sabinae*** **sp. nov.**, 4 µm.

Pleotelson: (Fig. 13C) Ovoid, lateral margins convex. Length 0.23–0.26 body length, 1.4 width; narrower than pereonite 7. Posterior margin concave at uropod insertions; apex convex, rounded, length 0.11–0.12 pleotelson length, apical setae 2–4 altogether, positioned laterally to apex. Pleopodal cavity width 0.66 pleotelson width, setal ridges present (Fig. 14E), not visible in dorsal view; statocysts present with dorsal concave slot-like apertures, diagonal across longitudinal axis (Supporting Information S2C); longitudinal trough width 0.47 pleotelson width. Anal opening terminal exposed and superficial, tilted posteriorly relative to frontal plane.

Antennula: (Figs 13E, 14F) Length 0.31 head width, width 0.53–0.66 antenna width; articles decreasing in size from proximal to distal; relative length ratios of articles 1.0, 0.71–0.75, 0.38, 0.27–0.38, 0.07–0.09; L/W ratios of articles 2.1–2.6, 1.7–2.0, 1.2–1.4, 1.2–1.6, 0.44–0.70. Articles 1–4 distinctly longer than wide; article 1 longest and widest, with 1 asensillate seta and 1 broom seta. Article 2 with 2 broom setae. Article 4 shorter than article 1. Terminal article minute, 'disc-like' (Fig. 14F), with 1 asensillate seta and 1 aesthetasc with intermediate belt of constrictions.

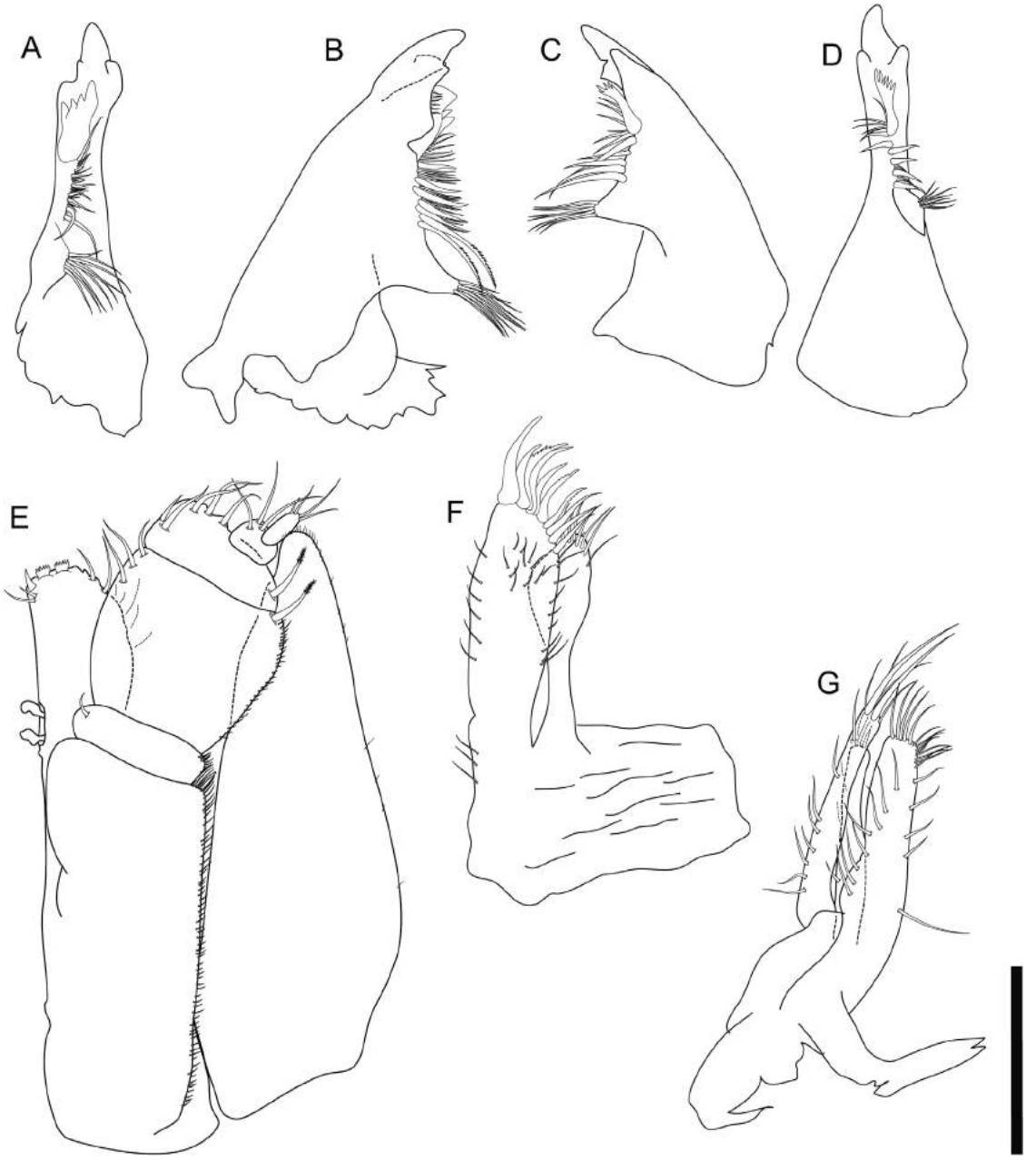

Figure 15. ***Macrostylis sabinae*** **sp. nov.**, non-ovigerous female paratype ZMH K-45909. A, left mandible medial; B, left mandible dorsal; C, right mandible dorsal; D, right mandible medial; E, maxilliped; F, maxillula; G, maxilla. Scale = 0.1 mm.

Antenna: (Fig. 13B, Supporting Information S3B) Coxa squat. Basis elongate, twice coxal length. Ischium elongate, about as long as coxa. Merus longer than coxa, basis and ischium combined, distally with 1 broom seta. Carpus shorter than merus, subequal or shorter than coxa, basis and ischium combined, distally with 5 asensillate setae and 2 broom setae.

Mandible: (Fig. 15A–D) With lateral seta; molar process length less than incisor length; mandible incisor processes oligodentate with dorsal and ventral subdistal teeth that partly enclose lacinia, left incisor with 4 cusps; lacinia mobilis robust, similar to incisor process, with 4 denticles; right incisior with 3 cusps; lacinia mobilis spine-like, clearly smaller than left lacinia, with 4–7 denticles.

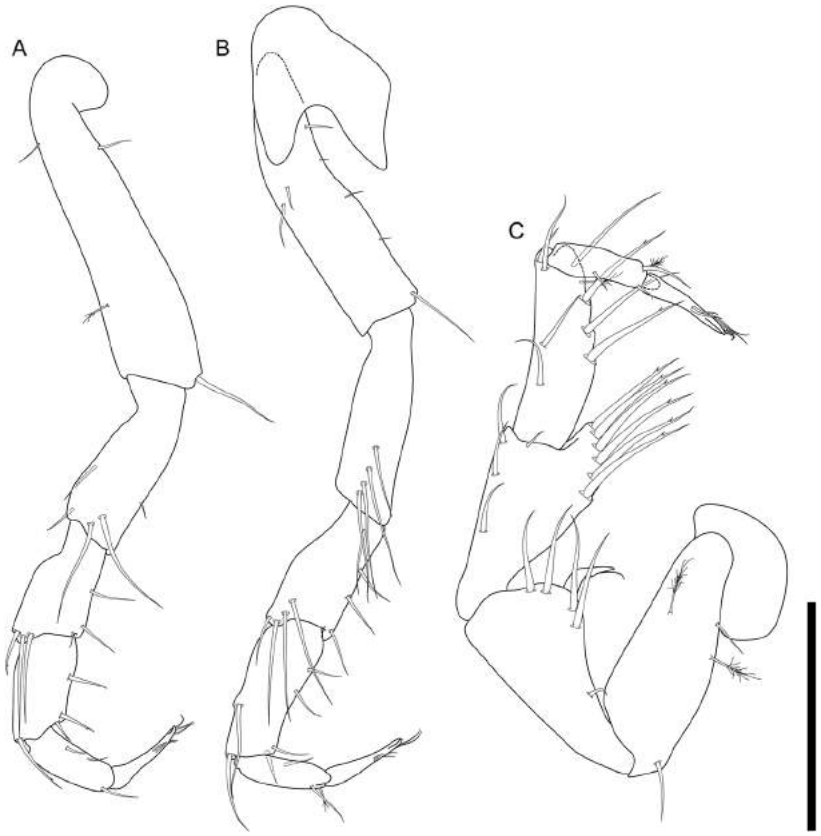

Figure 16. ***Macrostylis sabinae*** **sp. nov.**, non-ovigerous female paratype ZMH K-45909 anterior appendages. A, pereopod I; B, pereopod II; C, pereopod III. Scale = 0.25 mm.

Maxillula: (Fig. 15F) Lateral lobe terminally with 10 robust and 2 slender setae.

Maxilla: (Fig. 15G) Lateral lobe with 6 simple setae terminally; middle lobe with 6 simple setae terminally; medial lobe terminally with 7 simple setae.

Maxilliped: (Figs 13D, 15E) Basis length 3.4 width; distally with 2 fan setae, medioventral setae present. Palp wider than endite; article 2 wider than article 1, distomedially with 1 seta, article 1 shorter than article 3; epipod length 2.9 width, 1.0 basis length.

Pereopod I: (Fig. 16A) Length 0.38 body length; article L/W ratios 4.3, 2.9, 1.9, 2.2, 2.3, 5.0; relative article length ratios 1.0, 0.51, 0.38, 0.33, 0.23, 0.26; ischium dorsal margin with 4 bisetulate setae on dorsal margin. Merus dorsal margin with 3 simple, bifurcate setae on dorsal margin, ventral margin with 3 simple setae. Carpus dorsally with 1 bifurcate seta. Dactylus medial cuticle subdistally with 2 sensillae, terminal claw length 0.10 dactylus length.

Pereopod II: (Fig. 16B) Longer than pereopod I, length 0.40 body length; article L/W ratios 4.0, 3.4, 2.3, 2.4, 3.3, 5.0; relative article length ratios 1.0, 0.75, 0.50, 0.53, 0.31, 0.31. Ischium dorsally with 4 simple setae. Merus dorsally with 4 simple setae, ventrally with 4 distally fringe-like sensillae. Carpus dorsally with 2 simple setae, ventrally with 4 distally fringe-like sensillae. Dactylus medial cuticle subdistally with 2 sensillae.

Pereopod III: (Figs 16C, 17A) Length 0.35–0.43 body length; article L/W ratios 2.8–3.0, 2.1, 2.0–2.2, 2.7–3.1, 2.8–3.0, 5.0–5.5; relative article length ratios 1.0, 0.81–0.89, 0.86–0.93, 0.76–0.79, 0.39–0.43, 0.39–0.48. Ischium dorsal lobe triangular; proximally and distally with 2 bisetulate setae respectively; apex with 1 prominent seta; apical seta robust, bifid, curved proximally, spine-like. Merus dorsally with 6 bifurcate, serrate setae, ventrally with 3 distally fringe-like sensillae. Carpus dorsally with 4 bifurcate setae, ventrally with 4 distally fringe-like sensillae. Dactylus medial cuticle subdistally with 3 sensillae.

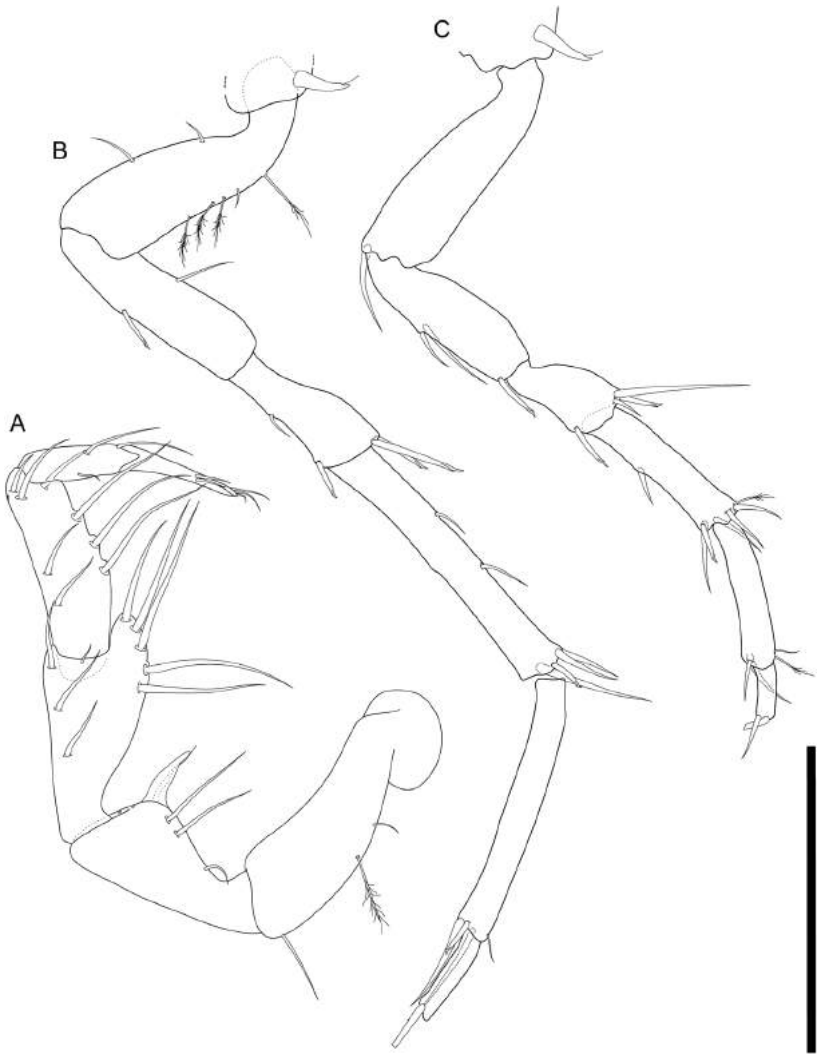

Figure 17. ***Macrostylis sabinae*** **sp. nov.**, non-ovigerous female holotype ZMH K-45908, appendages drawn *in situ*. A, pereopod III; B, pereopod VI; C, pereopod V. Scale = 0.25 mm.

Pereopod IV: (Fig. 18A) Length 0.12 body length; article L/W ratios 5.2, 2.8, 2.3, 3.0, 3.0, 4.0; relative article length ratios 1.0, 0.54, 0.35, 0.35, 0.23, 0.15. Carpus oval in cross section.

Pereopod V: (Figs 17C, 18B) Length 0.31–0.41 body length; article L/W ratios 3.5–5.0, 3.2–3.5, 1.8–2.1, 3.3–4.5, 4.3–6.0, 2.0–3.0; relative article length ratios 1.0, 0.60–0,76, 0.43, 0.51–0.62, 0.17–0.19. Ischium mid-dorsally with 1 bisetulate seta; distodorsally setae absent; mid-ventrally with 2 or 3 bisetulate setae; distoventrally with 2 bisetulate setae. Merus distodorsally with 3 setae: 2 short bisetulate and 1 long bisetulate; mid-ventrally with 2 setae; distoventrally with 2 bifurcate setae. Carpus mid-dorsally setae absent. Carpus distodorsally with 2 bifurcate setae and 1 broom seta; distoventrally with 3 bifurcate setae.

Pereopod VI: (Fig. 17B) Length 0.43 body length; article L/W ratios 3.1, 3.6, 2.4, 6.0, 7.3, 4.0; relative article length ratios 1.0, 0.82, 0.55, 1.1, 1.0, 0.36. Ischium dorsally with 1 seta; mid-ventrally with 1 bifurcate seta; distoventrally setae absent. Merus mid-dorsally setae absent; distodorsally with 2 bifurcate setae; mid-ventrally with 1 simple seta; distoventrally with 1 bifurcate seta. Carpus mid-dorsally with 2 simple setae; distodorsally with 3 bifurcate setae; mid-ventrally with 2 setae; distoventrally with 1 simple seta.

Pereopod VII: (Fig. 18C) Length 0.58 body length; relative article length ratios 1.0, 0.76, 0.55, 1.0, 0.97,

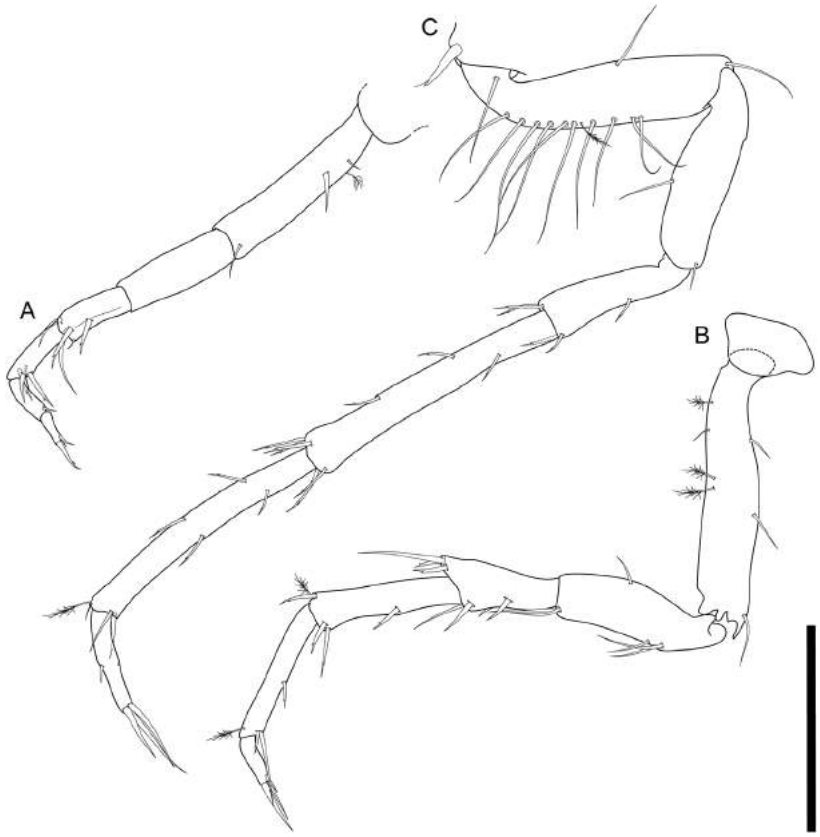

Figure 18. ***Macrostylis sabinae*** **sp. nov.**, non-ovigerous female paratype ZMH K-45909, posterior appendages. A, pereopod IV; B, pereopod V; C, pereopod VII. Scale = 0.25 mm.

0.39; basis length 4.7 width, dorsal margin row of 10 elongate setae present, setae longer basis width, exceeding beyond proximal half of article, ventral margin row of elongate setae absent. Ischium length 3.6 width, mid-dorsally with 1 simple seta; mid-ventrally with 1 seta; distoventrally with 1 simple seta. Merus length 3.0 width; distodorsally with 2 bifurcate setae; mid-ventrally with 0 or 1 bifurcate seta; distoventrally with 2 bifurcate setae. Carpus length 5.5 width; mid-dorsally with 2 bifurcate setae; distodorsally with 3 bifurcate setae; mid-ventrally with 1 bifurcate seta; distoventrally with 2 bifurcate setae. Propodus length 8.0 width. Dactylus length 6.5 width.

Operculum: (Fig. 19A) Elongate, ovoid; length 1.7 width, 0.53–0.78 pleotelson dorsal length; apical width 0.52 operculum width; not reaching anus. Distal margin broadly rounded. Ventrally roundedly keeled. Longitudinal furrow absent. With lateral fringe consisting of 9 pappose setae (Fig. 14E), distinctly separate from apical row of setae. Apex with 12 pappose setae, completely covering anal opening.

Pleopod III: (Fig. 19B) Length 3.7 width; protopod length 2.8 width, 0.59 pleopod III length, setae length subequal endopod length; exopod length 0.70 pleopod III length, exopod biarticulate.

Pleopod IV: (Fig. 19C) Length 1.9 width, endopod length 1.6 width, exopod length 4.0 width, 0.62 endopod length, exopod lateral fringe of setae present.

Pleopod V: Present.

Uropod: (Fig. 13A, C; Supporting Information S2C, D, S3) Length greater than pleotelson length; inserting on pleotelson posterior margin. Protopod over its complete length of subequal width, distal margin blunt, endopod insertion terminal, length 12.2 width, 0.91 pleotelson length. Endopod broken, lost in all specimens.

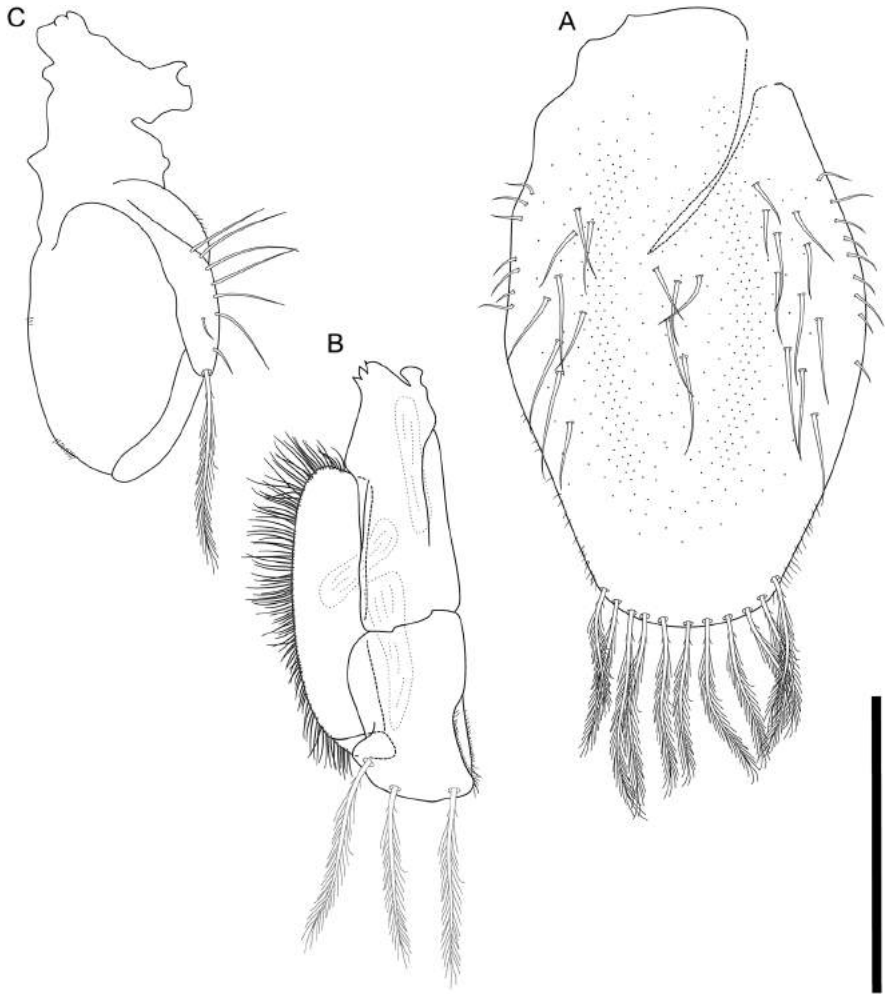

Figure 19. ***Macrostylis sabinae*** **sp. nov.**, non-ovigerous female paratype ZMH K-45909, pleopods. A, operculum, damaged; B, pleopod III; C, pleopod IV. Scale = 0.25 mm.

Description of terminal male

Body: (Figs 20A, B, 21) More elongate than female, subcylindrical, elongate, length 1.7–1.8 mm, 5.8–6.1 width.

Ventral projections: (Figs 20B, 21B, C) Pereonite 1 projection prominent, acute. Pereonites 2 and 3 projection absent. Pereonite 4 projection directed posteriorly, prominent and acute, located closer to posterior segment border. Pereonites 5 and 6 projection absent. Pereonite 7 projection prominent.

Imbricate ornamentation (IO): (Fig. 21) Present on pereonites 4 and 5 tergites, in collum depressions.

Cephalothorax: (Figs 20A, B, 21, 22A) Frons smooth, frontal furrow present; L/W ratio larger than in female, length 0.9 width, 0.15 body length; without setae dorsally, posterolateral corners rounded, without posterolateral setae.

Fossosome: (Figs 20A, B, 21) L/W ratio subequal to female, length 1.1 width, length/body-length ratio subequal to female.

Pereonite 1: (Figs 20A, B, 21) Length 0.31–0.33 width, 0.06 body length.

Pereonite 2: (Figs 20A, B, 21) Length 0.33–0.38 width, 0.06–0.07 body length.

Pereonite 3: (Figs 20A, B, 21) Length 0.39–0.45 width, 0.07–0.08 body length; posterolateral setae absent.

Pereonite 4: (Figs 20A, B, 21) Length 0.44–0.47 width; pereonal collum present, medially concave. Lateral

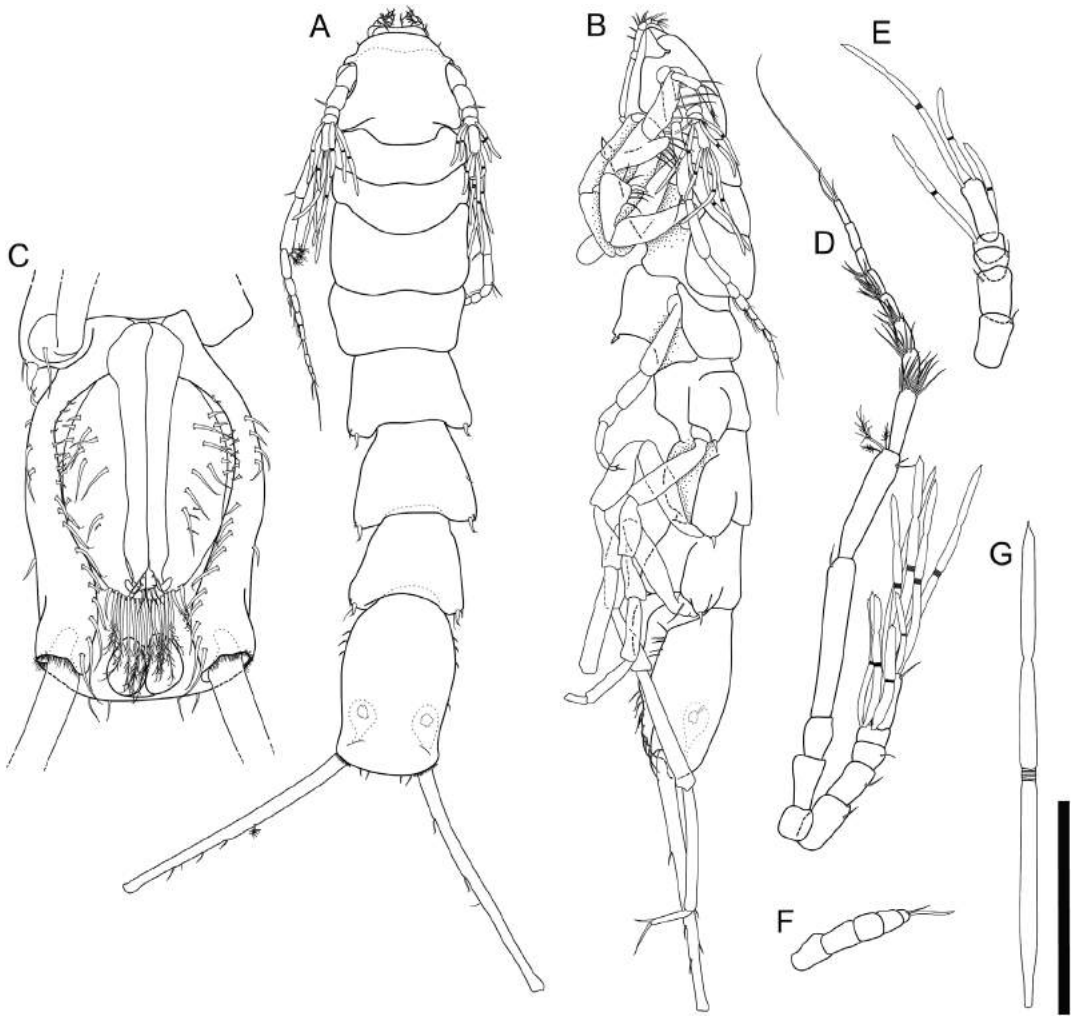

Figure 20. ***Macrostylis sabinae*** **sp. nov.**, terminal male paratype ZMH K-45910, ZMH K-45913 and juvenile male ZMH K-45912. A, dorsal habitus; B, lateral habitus; C, ventral pleotelson; D, antenna and antennula; E, antennula of morphologically identified terminal male ZMH K-45913, most aesthetascs were not illustrated for a better view on the segments; F, antennula of juvenile male (ZMH K-45912); G, aesthetasc with intermediate belt of constrictions and additional single constriction in distal half (no scale). Scale = 0.5 mm (A, B); 0.25 mm (C, F).

margins in dorsal view widest anteriorly, gradually narrowing posteriorly; integration with other segments clearly distinct from both anterior and posterior segments; width maximum anteriorly; posterolateral margins not produced posteriorly.

Pereonite 5: (Figs 20A, B, 21) Length 0.59–0.62 width. Posterolateral setae on tergite sensillate and robust, flexibly articulated.

Pereonite 6: Length 0.72–0.73 width, 1.2 pereonite 5 length. Posterolateral setae on tergite sensillate, robust, flexibly articulated.

Pereonite 7: (Figs 20A, B, 21) Posterolateral setae on tergite sensillate, robust, flexibly articulated. Coxal setae bisetulate.

Pleonite 1: Sternal articulation with pleotelson present.

Pleotelson: (Fig. 20C) In dorsal view sexually dimorphic, constricted anteriorly to uropod articulation, of hourglass-like shape, with an anterior and a posterior convex outline separated by a concave waist, width maximum anterior to waist; L/W ratio in male greater than in female, length 1.6–1.8 width, 0.24–0.25 body length, width less than pereonite 7

Figure 21. ***Macrostylis sabinae*** **sp. nov.**, terminal male paratype (ZMH K-45913), CLSM micrograph. A, dorsal habitus; B, lateral habitus; C, ventral habitus. Scale = 0.5 mm.

width. Posterior apex length 0.07–0.08 pleotelson length, with 4 setae on posterior margin laterally to apex, pleopodal cavity width 0.68–0.74 pleotelson width, longitudinal trough width 0.36–0.37 pleotelson width.

Appendages

Antennula: (Fig. 20D, E) Length 0.77–0.85 head width, 0.29–0.31 antenna length, width 1.2–1.3 antenna width; article L/W ratios 1.6–1.8, 1.5–1.6, 0.57–0.66, 0.54–0.79, 2.8–2.9; relative article length ratios 1.0, 0.71–0.97, 0.35–0.36, 0.29–0.45, 1.0–1.2. Articles 1, 2 and 5 elongate, tubular; articles 3 and 4 noticeably shorter. Terminal article with 6 or 7 aesthetascs, penultimate article with 4 or 5 aesthetascs, antepenultimate article without aesthetascs; aesthetascs of multiple types (Fig. 22A): with intermediate belt of constrictions, as well as with intermediate belt of constrictions and additional single constriction in distal half (Fig. 20G). Common aesthetasc length shorter than antennula length, new aesthetasc type subequal antennula length. Article 1 elongate, longest and widest, with 1 asensillate seta. Article 2 elongate, shorter than article 1, with 1 asensillate seta. Article 3 squat, shorter than article 1, with 1 asensillate seta. Article 4 squat, minute. Article 5 elongate, length subequal article 1 length, with 1 asensillate seta.

Antenna: (Fig. 20D) Length 0.45 body length, flagellum of 8 articles. Coxa squat, basis elongate, cylindrical, distally widening, longer than coxa. Ischium elongate, cylindrical, shorter than coxa length. Merus longer than coxa, basis and ischium together, distally with 1 simple seta. Carpus shorter than merus, distally with 2 asensillate setae and 3 broom setae.

Mouthparts: Identical with female. (Supporting Information S4).

Pereopod II: (Fig. 23A) Length/body-length ratio sexually dimorphic, length 0.43 body length; article L/W ratios 4.2, 3.6, 2.2, 2.6, 3.0, 4.0; relative article length ratios 1.0, 0.72, 0.44, 0.52, 0.24, 0.32. Ischium setation as in female, dorsally with 4 bisetulate setae. Merus setation as in female, dorsally with 3 bifurcate

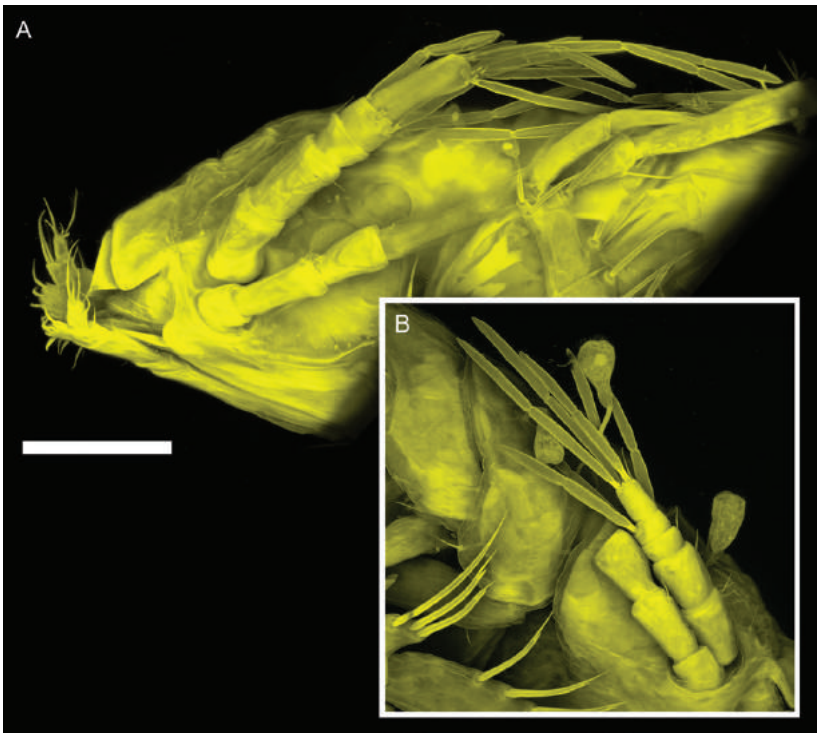

Figure 22. ***Macrostylis sabinae*** **sp. nov.**, terminal male paratype (ZMH K-45913) and ***Macrostylis amaliae*** **sp. nov.**, terminal male paratype (ZMH K-45917), detailed CLSM micrographs of antennula. A, detail of cephalothorax with two types of aesthetascs on antennula [***Macrostylis sabinae*** **sp. nov.** (ZMH K-45913)]; B, detail of antennula with only one type of aesthetasc [***Macrostylis amaliae*** **sp. nov.** (ZMH K-45917)]. Scale = 0.1 mm.

and simple setae; ventrally with 2 simple setae. Carpus setation as in female, dorsally with 3 setae: 2 simple and 1 broom; ventrally with 2 simple setae.

Pereopod III: (Fig. 23B) Length 0.44 body length; article L/W ratios 3.0, 2.3, 2.3, 2.5, 3.0, 3.5; relative article length ratios 1.0, 0.86, 0.86, 0.71, 0.29, 0.33. Ischium setation similar to female.

Pereopod IV: (Fig. 23C) Length 0.26 body length; article L/W ratios 3.4, 2.5, 2.3, 2.0, 2.0, 3.0; relative article length ratios 1.0, 0.59, 0.41, 0.35, 0.24, 0.18.

Pereopod VII: (Fig. 23D) Length/body-length ratio sexually dimorphic: distinctly longer than in female, length 0.70 body length; relative article length ratios 1.0, 0.91, 0.64, 0.41, 1.3, 0.46. Segment L/W ratios sexually dimorphic; basis length 3.7 width; dorsal (posterior) margin row of elongate setae sexually dimorphic, 1 or 2 simple setae. Ventral (anterior) margin row of elongate setae absent. Ischium length 3.3 width; mid-dorsally with 1 simple seta; mid-ventrally 1 simple seta; distoventrally with 2 simple setae. Merus length 2.8 width; distodorsally with 1 simple seta; mid-ventrally with 1 simple seta; distoventrally with 1 simple seta. Carpus length 7.8 width; setation as in female; mid-dorsally with 1 simple seta; distodorsally with 3 bifurcate setae; mid-ventrally with 1 simple seta; distoventrally with 3 bifurcate setae. Propodus length 9.7 width. Dactylus length 5.0 width.

Operculum: Male operculum vaulted.

Pleopod I: (Fig. 24A, B) Length 0.70 pleotelson length. Length clearly shorter pleopod II, with pleopods II projecting beyond pleopods I. Lateral lobes projecting lateroventrally to form horns, lateral lobes clearly extending distally beyond medial lobes, medial lobes distally with 8 asetulate setae; ventrally loosely arranged setae present. Pleopods I and II distally level, in the same plane.

Pleopod II: (Fig. 24C, D) Protopod apex tapering; distally enclosing pleopod I; with 11 setae on proximolateral margin and 8 pappose setae distally. Endopod distance of insertion from protopod distal margin 0.25 protopod length. Stylet weakly curved, not extending to distal margin of protopod, length 0.43 protopod length.

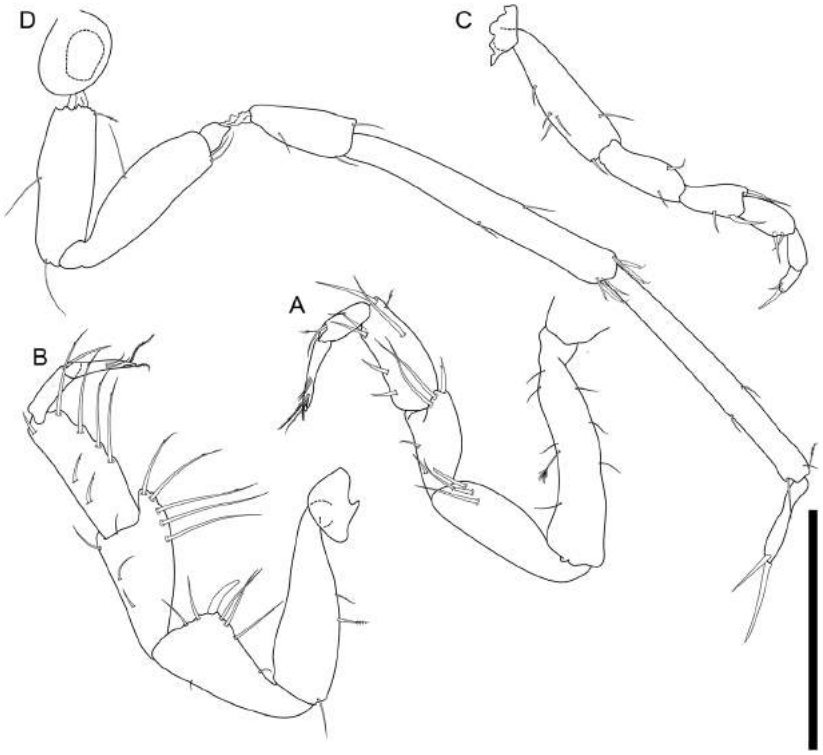

Figure 23. ***Macrostylis sabinae*** **sp. nov.**, terminal male paratype (ZMH K-45910) appendages. A, pereopod II; B, pereopod III; C, pereopod IV; D, pereopod VII (damaged). Scale = 0.25 mm.

Pleopod III: (Fig. 24E) As in female.

Pleopod IV: (Fig. 24F) As in female.

Pleopod V: (Fig. 24G) Identical with female.

Uropod: (Fig. 20A, B) Protopod L/W ratio greater than in female, length 20.0 width, longer pleotelson.

Remarks

The distribution of *M. sabinae* sp. nov. overlaps with the occurrences of the other two species described in this paper, *M. amaliae* sp. nov. and *M. daniae* sp. nov. As this species is remarkably similar to *M. amaliae* sp. nov. described below, morphological affinities are discussed jointly in the remarks paragraph of the latter species.

MACROSTYLIS AMALIAE SP. NOV.

(FIGS 25–33)

urn:lsid:zoobank.org:act:3A7E5E92-28BE-41FB-9CD4-D8FF3BF7FE68

Diagnosis

Similar to *M. sabinae* sp. nov. with some exceptions: Ventral projections 1, 3–7 present in females and males; pleotelson L/W ratio in males subequal to females. In contrast to adult males of *M. sabinae* sp. nov., the fifth segment of the first antenna is distinctly shorter with only one type of aesthetasc. Pereopod VII length to body-length ratio in females less than in *M. sabinae* sp. nov. Male pleotelson subrectangular, pleuropodal constriction weakly expressed. Pleopod I lateral horns not projecting distally beyond medial lobes.

Etymology

Macrostylis amaliae sp. nov. is named after the grandmother of the first author's wife, Amalie Blume.

Type fixation

Holotype: Adult female, 2.1mm, (ZMH K-45914), designated here.

Type material examined

Table 3, Supporting Information S1.

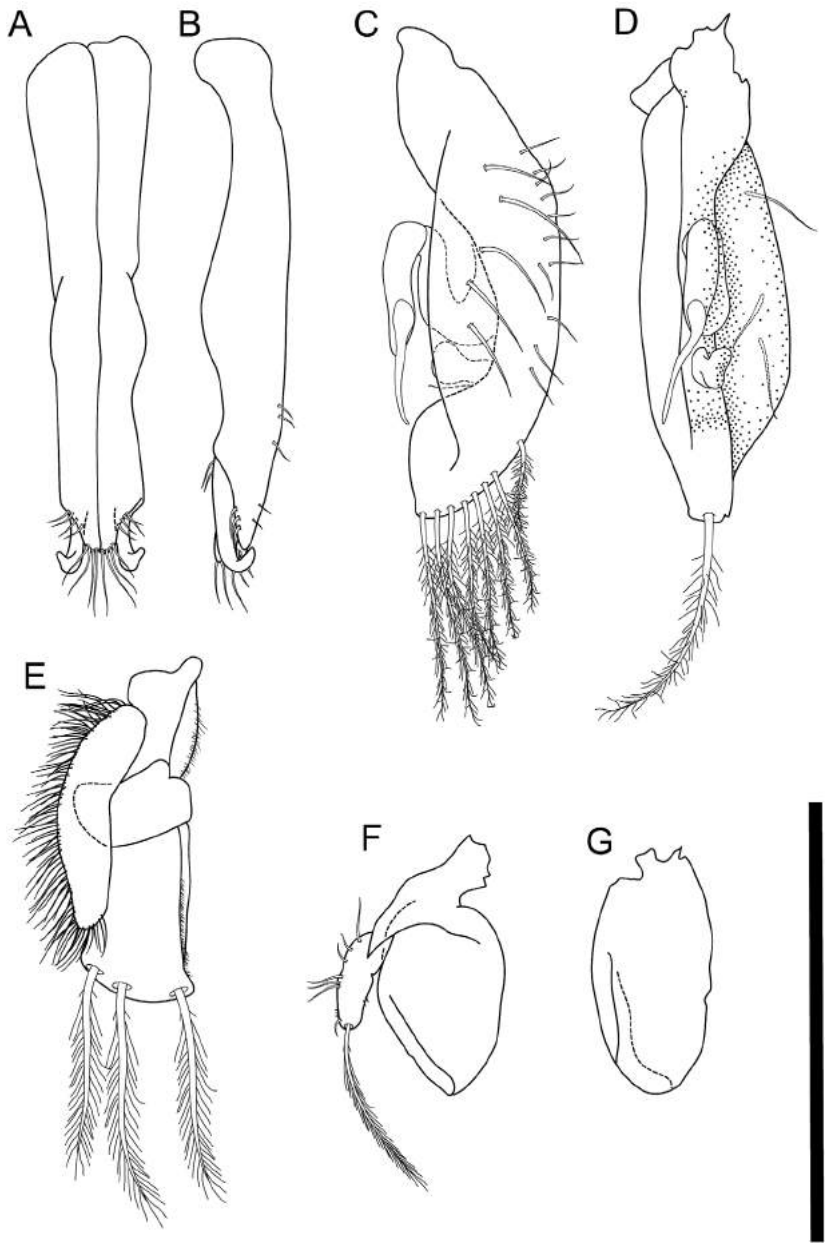

Figure 24. ***Macrostylis sabinae*** **sp. nov.**, terminal male paratype (ZMH K-45910) pleopods. A, pleopod I ventral; B, pleopod I lateral; C, pleopod II; D, pleopod II medial; E, pleopod III; F, pleopod IV; G, pleopod V. Scale = 0.25 mm.

Eight specimens of various age and both genders used for DNA extraction.

Type locality

North-west Pacific, abyssal plain south-east from KKT; 31.40 RV *Sonne* stations SO223–10–6, 03 August 2012, 41°11.99′N, 150°5.72′E, 5251 m depth.

Further records

SO223–1–10, 30. July 2012, 43.9710° N, 157.3278° E, 5418–5429 m depth; SO223–2–9, 03. August 2012, 46.2268° N, 155.5567° E, 4830–4864 m depth; SO223–5–9, 11. August 2012, 43.5913° N, 153.9647° E, 5376–5379 m depth; SO223–6–7, 13. August 2012, 47.4838°′N, 153.9833° E, 5297 m depth; SO223–10–6, 26. August 2012, 41.1998° N,

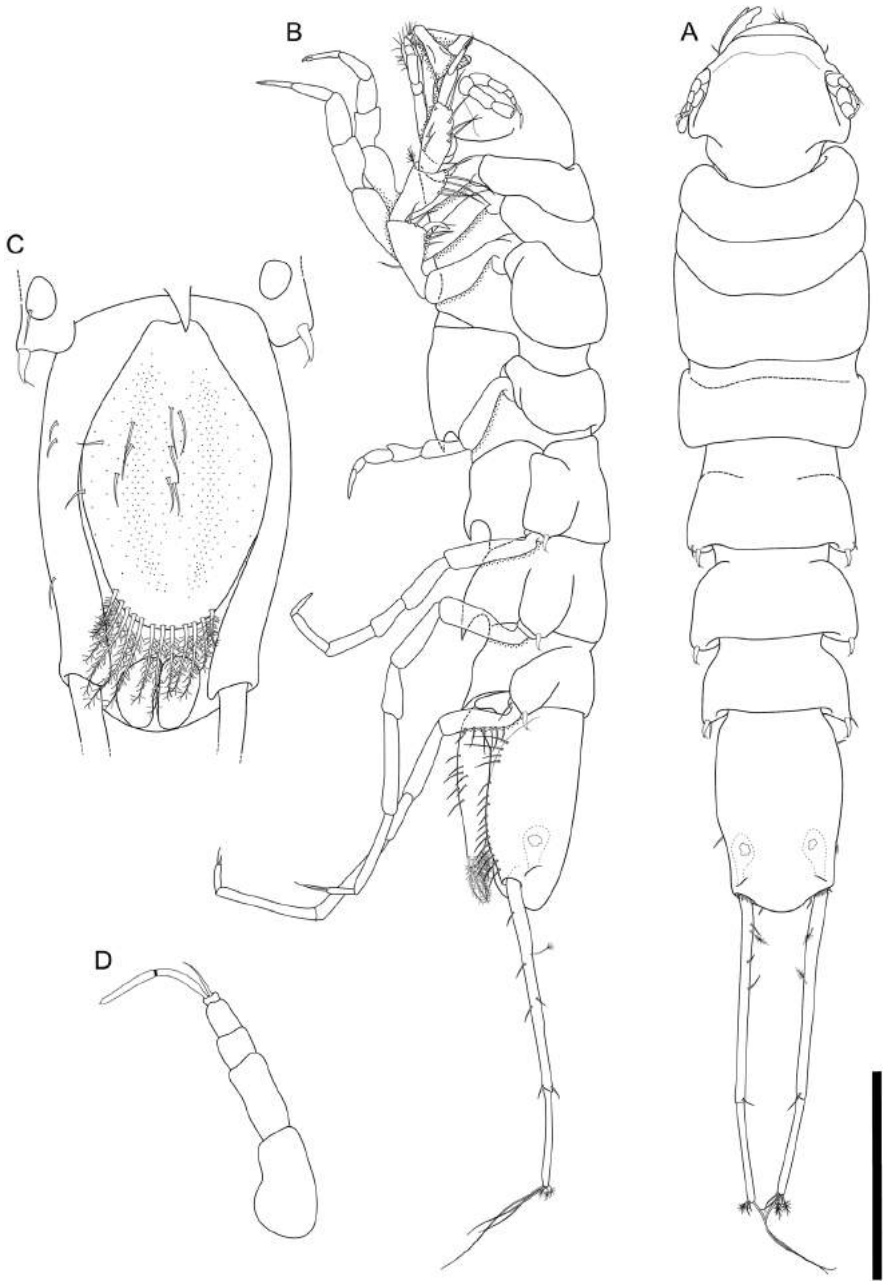

Figure 25. ***Macrostylis amaliae*** **sp. nov.**, non-ovigerous female holotype (ZMH K-45914). A, dorsal habitus; B, lateral habitus; C, ventral pleotelson; D, antennula. Scale = 0.5 mm (A, B); 0.25 mm (C, D).

150.0958° E, 5251m depth; SO223–10–12, 27. August 2012, 41.1939° N, 150.0942° E, 5249–5262 m depth. Specimens found at other stations with no genetic data available were excluded from this series to avoid potential errors due to the close similarity of *Macrostylis amaliae* sp. nov. and *M. sabinae* sp. nov. These are listed only in Supporting Information S1.

Description of female

Body: (Fig. 25A, B, Supporting Information S2A, B) Body shape broadest in anterior half, narrowing posteriorly. Length 2.1 mm, 5.2 width, subcylindrical, without setation.

Ventral projections: (Fig. 25B, Supporting Information S2B) Pereonite 1 projection prominent and acute

(Fig. 14A). In ovigerous female reduced at anterior overlapping of oostegites. Pereonite 3 projection absent. Pereonite 4 projection directed posteriorly; small, acute and closer to posterior segment border. Pereonites 5–7 projections acute, prominent and closer to posterior segment border.

Imbricate ornamentation (IO): Absent on all pereonites.

Cephalothorax: (Fig. 14A) Length 0.72 width, 0.13 body length; clypeus in dorsal view convex and smooth, frontal furrow present and straight. Posterolateral setae absent, posterolateral margins blunt.

Fossosome: Tergite articulations present, sternite articulations absent, ventral surface rounded, length 0.93 width, length 0.20 body length, lateral tergite margins confluent.

Pereonite 4: Width 1.1 pereonite 5 width, length 0.40 width; pereonal collum present. Shape generally resembling more anterior segments. Lateral margins almost parallel, anteriorly widest, narrowing gradually towards posterior. Posterolateral margin width relative to max. width contracting laterally; posterolateral margins rounded and posterolateral setae absent.

Pereonite 5: Length 0.66 width, 1.5 pereonite 4 length. Posterolateral margins rounded. Posterolateral setae sensillate, robust, flexibly articulated. Coxal setae absent.

Pereonite 6: Length 0.55 width, 0.82 pereonite 5 length. Posterolateral margin produced posteriorly, rounded. Tergite posterolateral setae sensillate, robust, flexibly articulated.

Pereonite 7: Length 0.51 width. Posterolateral margin produced posteriorly, rounded. Tergite posterolateral setae sensillate, robust, flexibly articulated. Coxal bisetulate setae present (Fig. 14D).

Pleonite 1: Sternal articulation with pleotelson present.

Pleotelson: (Fig. 25C) Ovoid, lateral margins convex. Length 0.23 body length, 1.6 width; narrower than pereonite 7. Posterior margin concave at uropod insertions; apex convex, rounded, apex length 0.10 pleotelson length. Posterior apex setae 2 and 3 altogether, positioned on and around apex. Pleopodal cavity width 0.77 pleotelson width, setal ridges present and not visible in dorsal view; statocysts present with concave dorsal slot-like apertures, diagonal across longitudinal axis; longitudinal trough width 0.39 pleotelson width. Anal opening terminal, exposed and superficial, tilted posteriorly relative to frontal plane.

Antennula: (Figs 14B, 25D) Length 0.33 head width, width 0.55 antenna width; articles decreasing in size from proximal to distal; relative length ratios of articles 1.0, 0.64–0.81, 0.42, 0.32–0.42, 0.10–0.14; L/W ratios of articles 1.9, 1.5, 1.1, 1.1–1.4, 0.56–0.86. Article 1 longest and widest, distinctly longer than wide, with 1 asensillate seta. Article 2 distinctly longer than wide, but shorter than article 1, with 1 broom seta. Article 3 distinctly longer than wide, shorter than article 1. Article 4 distinctly longer than wide. Terminal article minute, 'disc-like', with 1 asensillate seta and 1 aesthetasc with intermediate belt of constrictions.

Antenna: (Fig. 25B, Supporting Information S2B) Coxa squat. Basis elongate, more than twice coxal length. Ischium length elongate, longer coxal length. Rest of the antenna broken and missing.

Mandible: (Fig. 26A–D) With lateral setae; molar process length less than incisor length; mandible incisor processes oligodentate with dorsal and ventral subdistal teeth that partly enclose lacinia, left incisor with 4 cusps; lacinia mobilis robust, similar to incisor process, with 4 denticles; right incisior with 3 cusps; lacinia mobilis spine-like, clearly smaller than left lacinia, with 4–7 denticles.

Maxillula: (Fig. 26F) Lateral lobe terminally with 10 robust setae and 2 slender setae.

Maxilla: (Fig. 26G) Lateral lobe with 3 simple setae terminally; middle lobe with 6 simple setae terminally; medial lobe terminally with 3 simple setae.

Maxilliped: (Figs 14A, 26E) Basis length 3.8 width; distally with 2 fan setae, medioventral setae present; article 2 wider than article 1, distomedially with 1 seta, article 2 wider than article 3, article 1 shorter than article 3; epipod length 3.3 width, 1.1 basis length.

Pereopod I: (Fig. 27A) Length 0.37 body length; article L/W ratios 4.1, 2.6, 1.7, 1.8, 3.0, 4.5; relative article length ratios 1.0, 0.62, 0.35, 0.31, 0.31, 0.31; ischium dorsal margin with 4 bisetulate setae. Merus dorsal margin with 3 simple and bifurcate setae, ventral margin with 3 simple setae. Carpus dorsally with 1 bifurcate seta. Dactylus medial cuticle subdistally with 3 sensillae, terminal claw length 0.09 dactylus length.

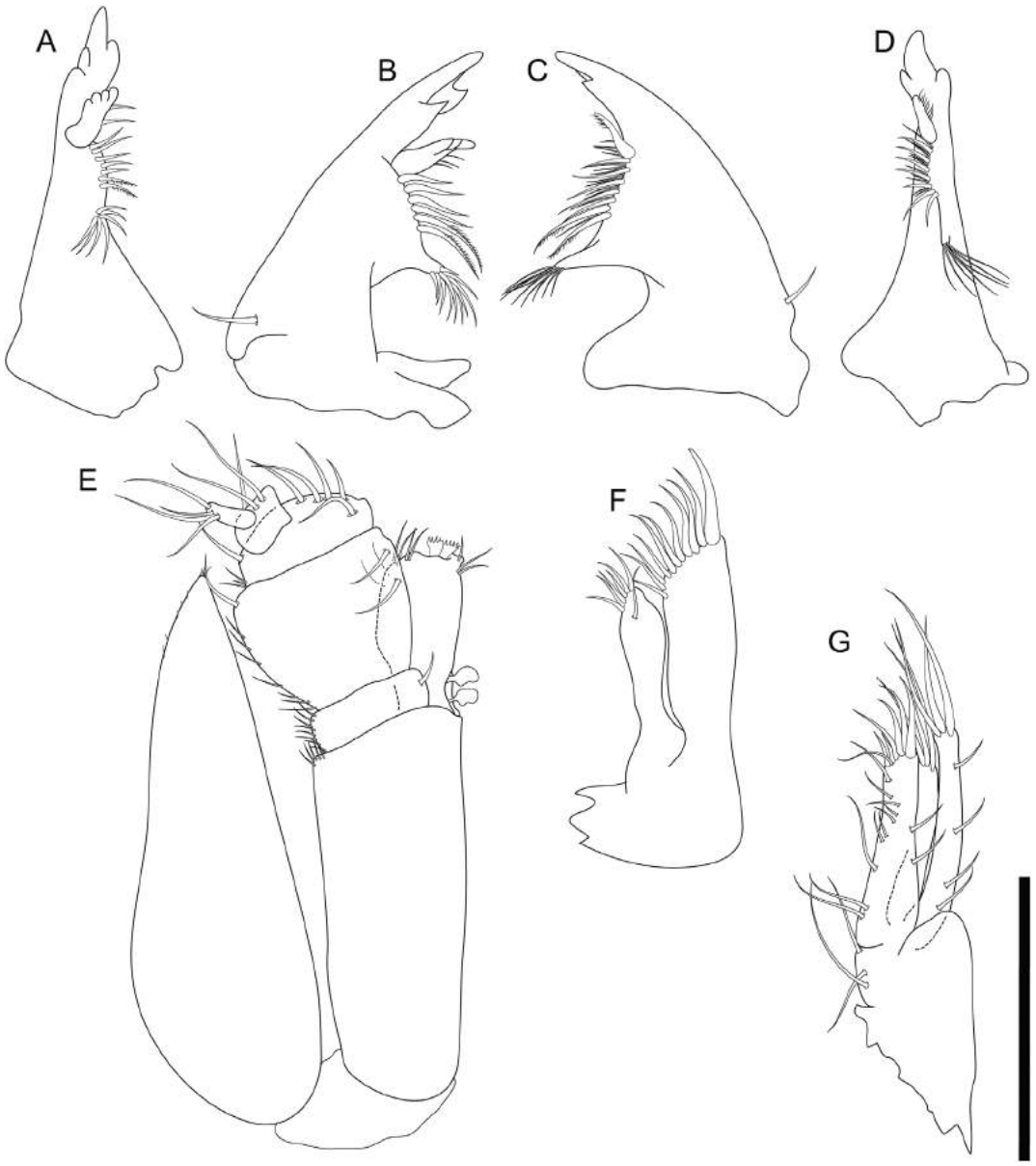

Figure 26. ***Macrostylis amaliae*** **sp. nov.**, terminal male paratype (ZMH K-45915) mouthparts. A, left mandible medial; B, left mandible dorsal; C, right mandile dorsal; D, right mandible medial; E, maxilliped; F, maxillula; G. maxilla. Scale = 0.1 mm.

Pereopod II: (Fig. 27B) Longer than pereopod I, length 0.41 body length; article L/W ratios 3.6, 3.2, 2.2, 2.2, 2.7, 4.5; relative article length ratios 1, 0.66, 0.45, 0.45, 0.28, 0.31. Ischium dorsally with 5 simple setae and 1 proximodorsal seta. Merus dorsally with 2 simple setae and 1 broom seta, ventrally with 2 simple setae. Carpus dorsally with 2 simple setae and 1 broom seta, ventrally with 4 simple setae. Dactylus medial cuticle subdistally with 3 sensillae.

Pereopod III: (Fig. 27C) Length 0.43 body length; article L/W ratios 2.8, 2.2, 2.0, 2.4, 2.3, 5.5; relative article length ratios 1.0, 0.80, 0.72, 0.68, 0.36, 0.44. Ischium dorsal lobe triangular; proximally with 2 bisetulate setae; apex with 1 prominent seta; apical seta robust, bifid, curved proximally, spine-like; distally with 2 bisetulate setae. Merus dorsally with 5 bifurcate, serrate setae, ventrally with 1 simple seta. Carpus dorsally with 4 bifurcate setae, ventrally with 4 simple setae. Dactylus medial cuticle subdistally with 3 sensillae.

Pereopod IV: (Fig. 28A) Length 0.24 body length; article L/W ratios 3.3, 2.8, 1.8, 2.0, 2.5, 4.0; relative article

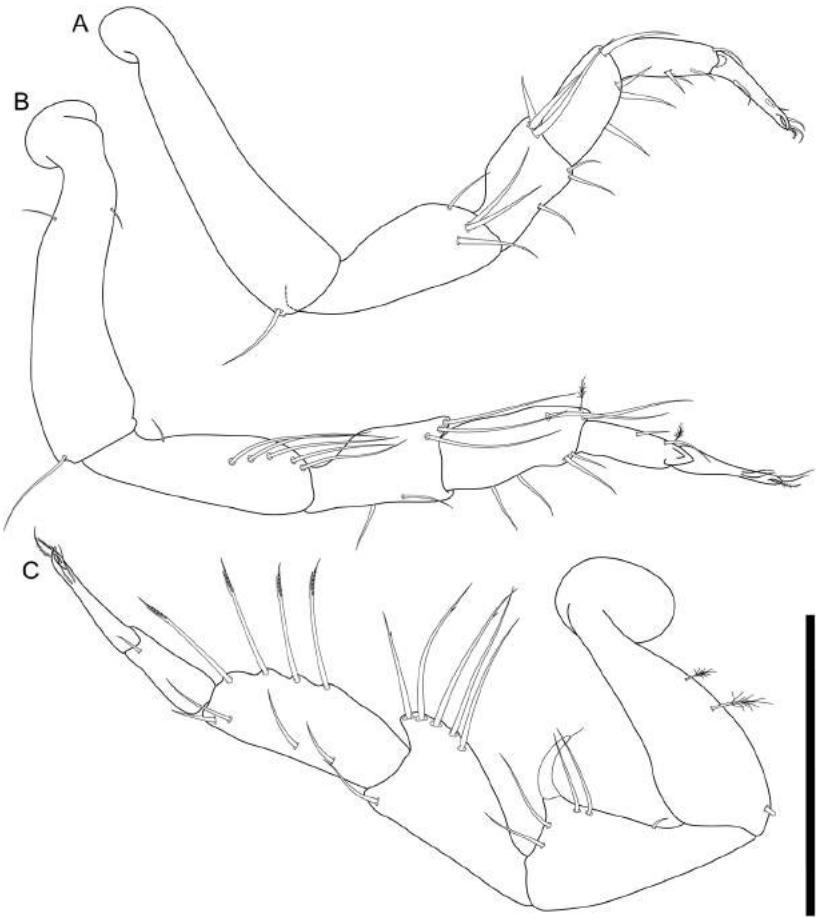

Figure 27. ***Macrostylis amaliae*** **sp. nov.**, non-ovigerous female holotype (ZMH K-45914) anterior appendages, holotype. A, pereopod I; B, pereopod II; C, pereopod III. Scale = 0.25 mm.

length ratios 1.0, 0.55, 0.35, 0.30, 0.25, 0.20. Carpus oval in cross section.

Pereopod V: (Fig. 28B) Length 0.35 body length; article L/W ratios 4.0, 3.2, 2.2, 4.0, 4.0, 2.5; relative article length ratios 1.0, 0.67, 0.46, 0.50, 0.50, 0.21. Ischium distodorsally setae absent; mid-ventrally with 3 bisetulate setae (see Fig. 14C); distoventrally with 2 bisetulate setae. Merus distodorsally with 3 setae: 2 short and 1 long bisetulate; mid-ventrally with 2 setae; distoventrally with 2 setae. Carpus distodorsally with 2 setae; distoventrally with 1 seta.

Pereopod VI: Broken, missing.

Pereopod VII: (Fig. 28C) 0.51 body length; relative article length ratios 1.0, 0.78, 0.52, 1.0, 0.10, 0.39; basis length 4.6 width, dorsal margin row of 7 elongate setae present, setae longer basis width, exceeding beyond proximal half of article, ventral margin row of elongate setae absent. Ischium length 3.6 width, mid-dorsally with 1 seta; mid-ventrally with 2 setae; distoventrally with 1 seta. Merus length 3.0 width, mid-ventrally with 1 seta; distoventrally with 1 seta. Carpus length 8.0 width, mid-dorsally with 2 setae; distodorsally with 4 setae; mid-ventrally with 2 setae; distoventrally with 2 setae. Propodus length 8.0 width. Dactylus length 4.5 width.

Operculum: (Fig. 25C) Elongate, ovoid; length 1.7 width, 0.79 pleotelson dorsal length; apical width 0.64 operculum width; not reaching anus. Distal margin broadly rounded. Ventrally roundedly keeled. Longitudinal furrow absent. With lateral fringe consisting of 9 pappose setae, distinctly separate from apical row of setae; 12 apical setae, completely covering anal opening.

Uropod: (Fig. 25A, B, Supporting Information S2A, B) Length 1.5 pleotelson length, protopod length 17.3 width,

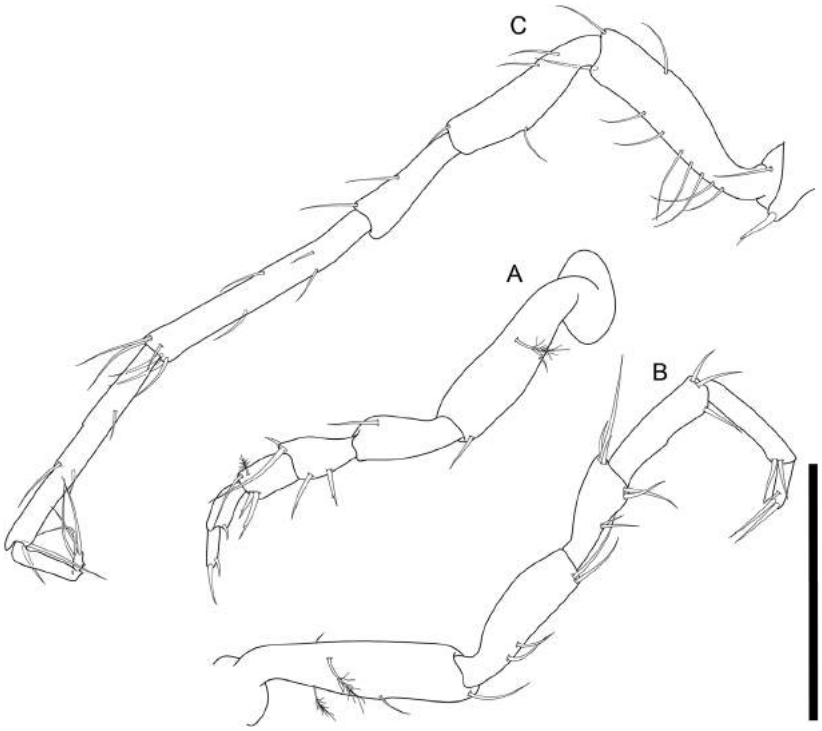

Figure 28. ***Macrostylis amaliae*** **sp. nov.**, non-ovigerous female holotype (ZMH K-45914) posterior appendages. A, pereopod IV; B, pereopod V; C, pereopod VII. Scale = 0.25 mm.

1.1 pleotelson length; inserting on pleotelson posterior margin; protopod of subequal width over its complete length, distal margin blunt, endopod insertion terminal; uropod endopod width at articulation subequal protopod width; endopod length 12.0 width, 0.46 protopod length.

Description of terminal male

Body: (Figs 29A, B, 30, Supporting Information S5) More elongate than female, subcylindrical, elongate, length 1.56 mm, 6.4 width.

Ventral projections: Pereonite 1 projection prominent and acute. Pereonites 2 and 3 projection absent. Pereonite 4 and 5 projections directed posteriorly, small and acute, located closer to posterior segment borders. Pereonite 6 projection prominent and acute, located closer to posterior segment border. Pereonite 7 projection prominent.

Imbricate ornamentation (IO): (Fig. 30, Supporting Information S5) Present on tergites 4 and 5 in the collum depressions.

Cephalothorax: Frons smooth, frontal furrow present; L/W ratio larger than in female, length 0.97 width, 0.19 body length; without setae dorsally, posterolateral corners rounded, without posterolateral setae.

Fossosome: L/W ratio subequal to female, length 0.97 width, length/body-length ratio subequal to female.

Pereonite 1: Length 0.30 width, 0.06 body length.

Pereonite 2: Length 0.32 width, 0.06 body length.

Pereonite 3: Length 0.40 width, 0.08 body length; posterolateral setae absent.

Pereonite 4: Length 0.48 width; pereonal collum present, medially concave. Lateral margins in dorsal view widest anteriorly, gradually narrowing posteriorly; integration with other segments generally resembling anterior segments; width maximum anteriorly; posterolateral margins not produced posteriorly.

Pereonites 5–7: With sensillate, robust, spine-like posterolateral setae.

Pereonite 5: Length 0.64 width.

Pereonite 6: Length 0.80 width, length 1.3 pereonite 5 length.

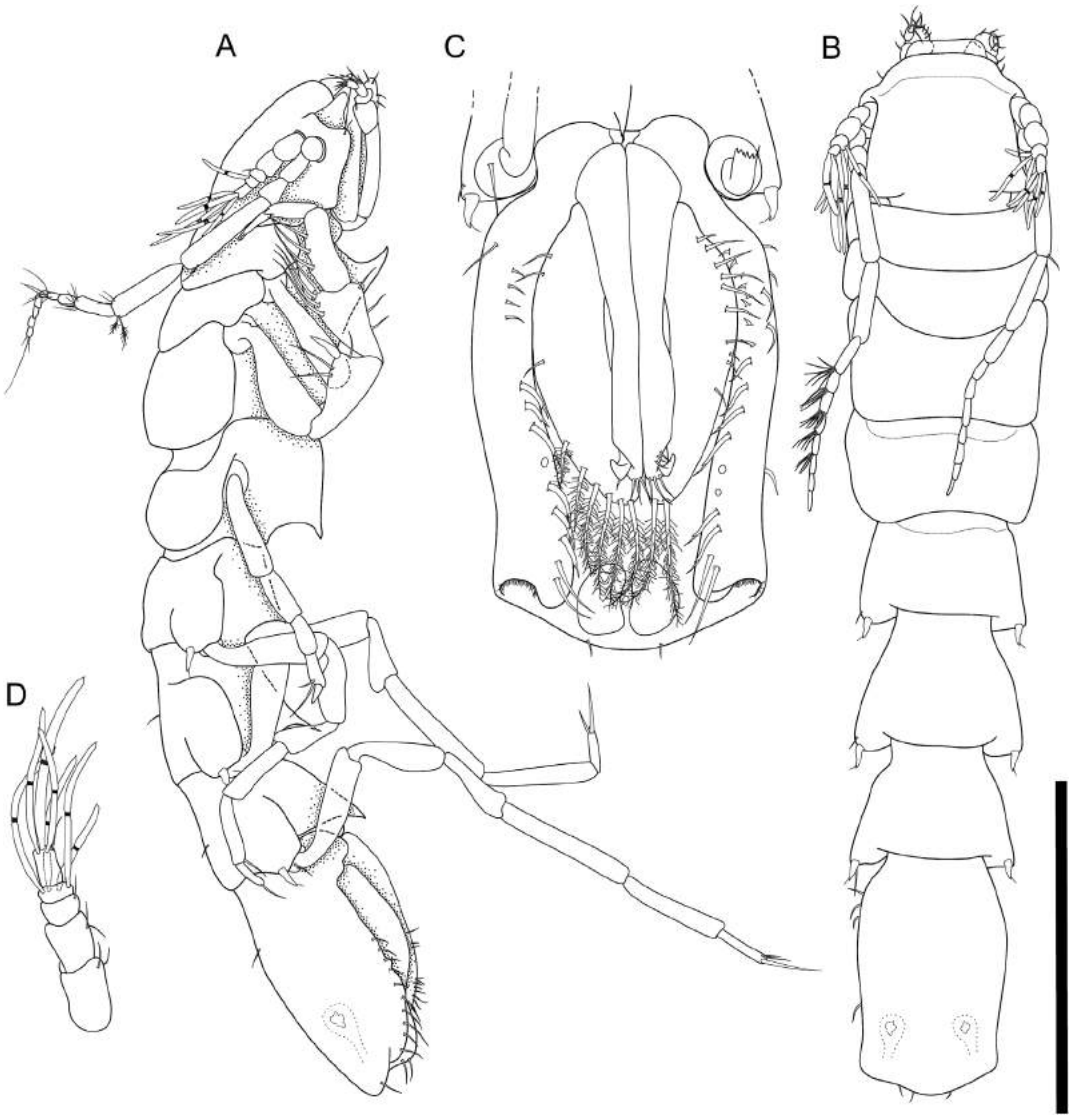

Figure 29. ***Macrostylis amaliae*** **sp. nov.**, terminal male paratype (ZMH K-45915). A, lateral habitus; B, dorsal habitus; C, ventral pleotelson; D, antennula. Scale = 0.5 mm (A, B); 0.25 mm (C, D).

Pereonite 7: With bisetulate coxal seta.

Pleonite 1: Sternal articulation with pleotelson absent.

Pleotelson: (Fig. 29C) In dorsal view similar to female, constricted anteriorly to uropod articulation, of hourglass-like shape, with an anterior and a posterior convex outline separated by a concave waist, width maximum anterior to waist; L/W ratio in male subequal to female, 0.22 body length, width less than pereonite 7.0 width. Posterior apex length 0.09 pleotelson length, with 2–4 setae on margin laterally to apex; pleopodal cavity width 0.70 pleotelson width, longitudinal trough width 0.39 pleotelson width.

Antennula: (Figs 22B, 29D) Length 0.50 head width, 0.20 antenna length, width 1.0 antenna width; article L/W ratios 1.3–1.5, 1.2–1.3, 0.54–0.67, 0.50–0.60, 1.5; relative article length ratios 1.0, 0.80–0.86, 0.33–0.40, 0.20–0.33, 0.60–0.64; articles 1, 2 and 5 elongate, tubular; articles 3 and 4 squat or noticeably shorter. Terminal article with 3 or 4 aesthetascs, penultimate article with 4 aesthetascs, aesthetascs with intermediate belt of constrictions. Aesthetasc length subequal antennula length or shorter. Article 1 elongate, longest and widest, with 3 asensillate setae. Article 2 elongate, shorter than article 1, with 2 asensillate setae. Article 3 squat, shorter than article 1, with 1 asensillate seta. Article 4 squat, minute.

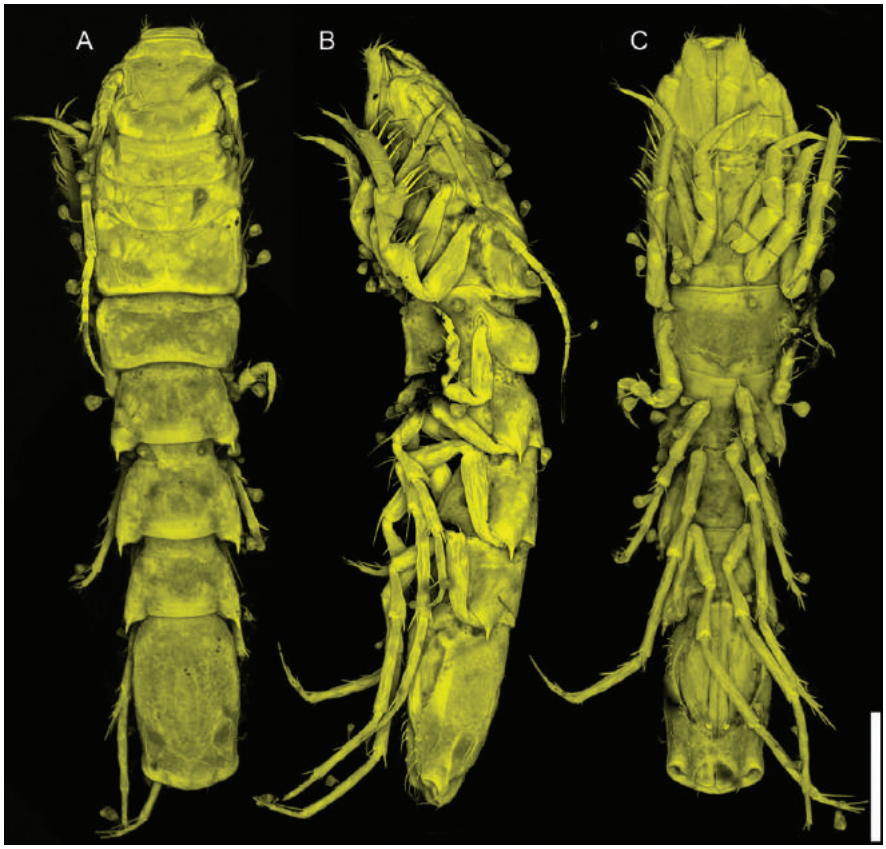

Figure 30. ***Macrostylis amaliae*** **sp. nov.**, terminal male paratype (ZMH K-45917), CLSM micrographs. A, dorsal habitus; B, lateral habitus; C, ventral habitus. Scale = 0.5 mm.

Article 5 elongate, length subequal article 1 length, with 1 asensillate seta.

Antenna: (Fig. 29A, B) Length 0.44 body length, flagellum of 8 articles, coxa squat, basis elongate, cylindrical and longer than coxa. Ischium elongate, cylindrical and subequal coxa length. Merus longer than coxa, basis and ischium together, distally with 1 simple seta. Carpus shorter than merus, distally with 3 asensillate setae and 2 broom setae.

Pereopod I: (Fig. 31A) Length 0.39 body length; article L/W ratios 0, 2.0, 1.8, 1.8, 2.3, 7.0. Ischium dorsally with 1 seta. Merus setation as in female, dorsally with 1 seta, ventrally with 2 setae. Carpus setation as in female, dorsally with 1 seta, ventrally with 3 setae.

Pereopod II: (Fig. 31B) Dactylus broken and lost. Article L/W ratios 3.8, 3.2, 1.8, 2.2, 3.0, 0; relative article length ratios 1.0, 0.70, 0.48, 0.48, 0.26, 0. Ischium setation as in female, dorsally with 3 setae. Merus setation as in female, dorsally with 4 setae, ventrally with 2 setae. Carpus setation as in female, dorsally with 2 setae, ventrally with 4 setae.

Pereopod III: (Fig. 31C) Length 0.48 body length; article L/W ratios 3.2, 2.3, 2.0, 2.5, 3.0, 4.0; relative article length ratios 1.0, 0.84, 0.84, 0.79, 0.32, 0.42.

Pereopod IV: (Fig. 31D) Length 0.28 body length; article L/W ratios 3.2, 2.3, 1.5, 2.0, 2.5, 3.0; relative article length ratios 1.0, 0.56, 0.38, 0.38, 0.31, 0.19.

Pereopod V: (Fig. 32A) 0.44 body length; article L/W ratios 4.2, 3.3, 2.5, 4.0, 6.0, 2.5; relative article length ratios 1.0, 0.62, 0.48, 0.57, 0.57, 0.24. Ischium mid-dorsally setae absent; distodorsally setae absent; mid-ventrally with 2 setae; distoventrally with 2 setae. Merus setation as in female; distodorsally with 2 bifurcate setae and 1 broom seta; mid-ventrally without setae; distoventrally with 2 bifurcate setae. Carpus setation as in female; distodorsally with 2

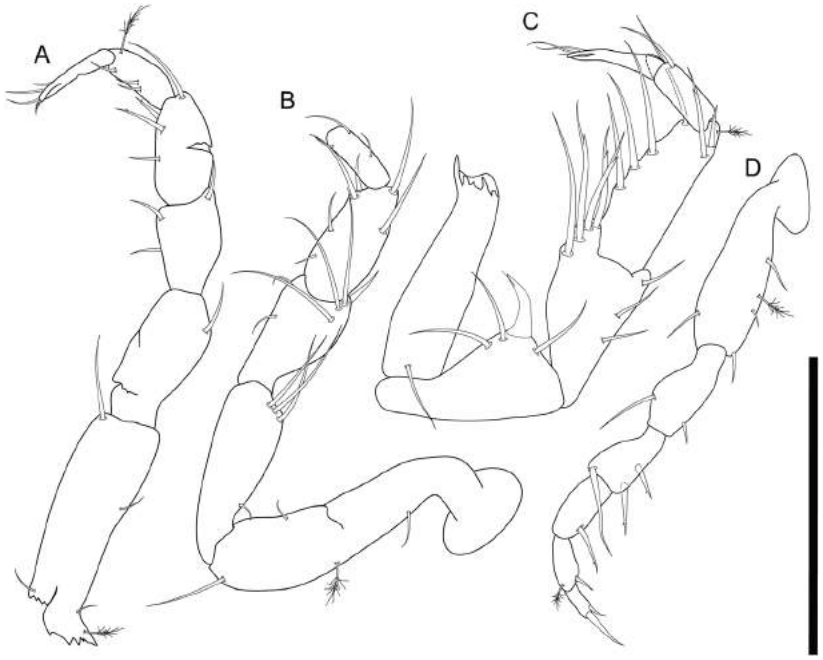

Figure 31. ***Macrostylis amaliae*** **sp. nov.**, terminal male paratype (ZMH K-45915), anterior appendages. A, pereopod I, basis damaged; B, pereopod II, dactylus missing; C, pereopod III, basis damaged; D, pereopod IV. Scale = 0.25 mm.

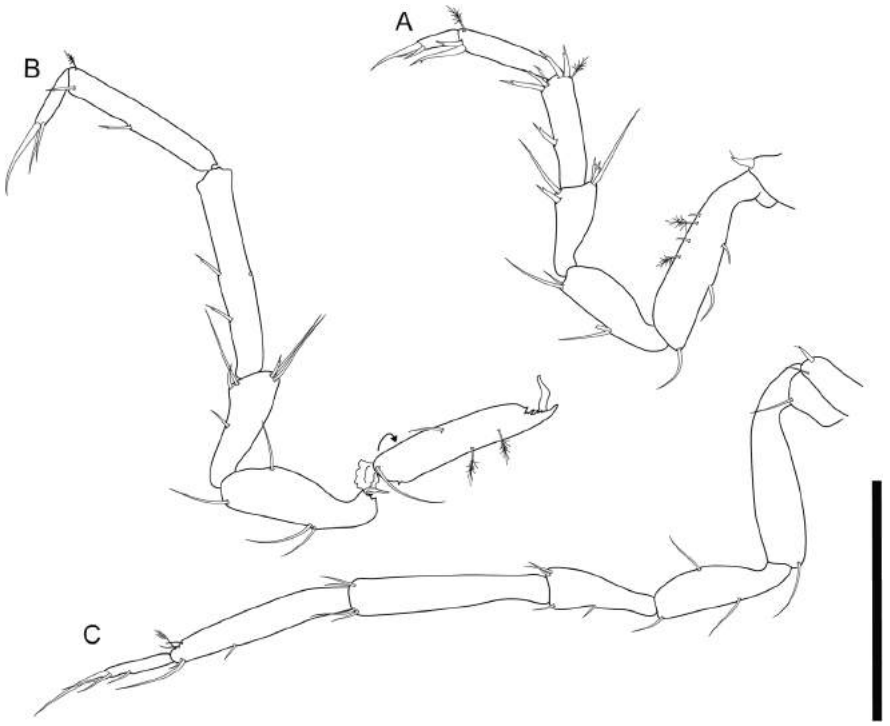

Figure 32. ***Macrostylis amaliae*** **sp. nov.**, terminal male paratype (ZMH K-45915), posterior appendages. A, pereopod V; B, pereopod VI (damaged); C, pereopod VII. Scale = 0.25 mm.

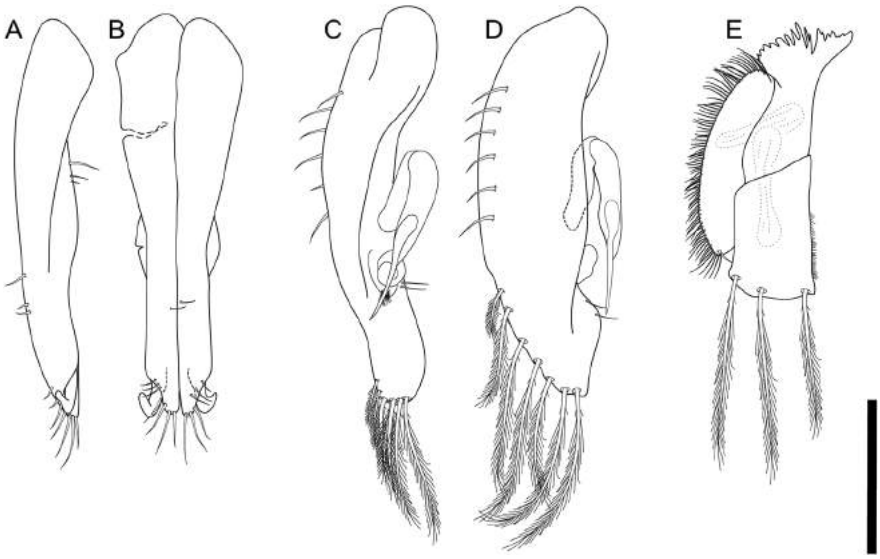

Figure 33. ***Macrostylis amaliae*** **sp. nov.**, terminal male paratype (ZMH K-45915), pleopods. A, pleopod I, lateral; B, pleopod I, ventral; C, pleopod II, medial; D, pleopod II, ventral; E, pleopod III. Scale = 0.1 mm.

bifurcate setae and 1 broom seta; mid-ventrally with 1 bifurcate seta; distoventrally with 3 bifurcate setae.

Pereopod VI: (Fig. 32B) Length 0.60 body length; article L/W ratios 5.0, 3.2, 2.6, 5.5, 5.0, 3.5; relative article length ratios 1.0, 0.80, 0.65, 1.1, 0.90, 0.35. Ischium setation as in female; dorsally with 1 seta; mid-ventrally with 2 setae; distoventrally with 1 seta. Merus distodorsally with 3 setae: 2 long and 1 short bifurcate setae; mid-ventrally with 1 seta; distoventrally with 2 setae: 1 long and 1 short bifurcate seta. Mid-ventrally with 2 bifurcate setae.

Pereopod VII: (Fig. 32C) Length/body-length ratio distinctly longer than in female, length 0.60 body length, length subequal to pereopod VI length; relative article length ratios 1.0, 0.71, 0.57, 1.0, 0.95, 0.33; segment L/W ratios sexually dimorphic; basis length 4.2 width. Ventral (anterior) margin row of elongate setae absent. Ischium length 3.8 width; setation as in female; mid-dorsally with 1 seta; mid-ventrally with 1 seta. Merus length 3.0 width; setation as in female; distodorsally with 2 setae; mid-ventrally with 1 seta; distoventrally with 1 seta. Carpus length 5.3 width; setation as in female; distodorsally with 2 setae. Propodus length 6.7 width. Dactylus length 7 width.

Operculum: Male operculum vaulted.

Pleopod I: (Fig. 33A, B) Length 0.74 pleotelson length. Length clearly shorter pleopod II with the latter projecting beyond pleopod I distally. Lateral lobes

Figure 34. Two morphotypes of ***Macrostylis amaliae*** **sp. nov.**, scale = 0.5 mm. A, ovigerous female with almost absent pereonal collum on pereonite 4, dorsal habitus (ZMH K-45940); B, adult female with distinct pereonal collum on pereonite 4, dorsal habitus (ZMH K-45943).

projecting lateroventrally to form horns, lateral lobes not extending distally beyond medial lobes, medial lobes distally with 7 asetulate setae; ventrally loosely arranged setae present. Distally pleopods I and II level, in the same plane.

Pleopod II: (Fig. 33C, D) Protopod apex tapering; distally enclosing pleopods I; with 6 setae on proximolateral margin and 7 pappose setae distally. Endopod distance of insertion from protopod distal margin 0.44 protopod length. Stylet weakly curved, not extending to distal margin of protopod, length 0.28 protopod length.

Pleopod III: (Fig. 33E) Length 3.0 width; protopod length 2.5 width, 0.56 pleopod III length, setae length subequal endopod length; exopod length 0.67 pleopod III length, exopod biarticulate.

Pleopod IV: Length 2.3 width, endopod length 2.0 width, exopod length 9.0 width, 0.75 endopod length, exopod lateral fringe of setae present.

Pleopod V: Present.

Remarks for *Macrostylis sabinae* sp. nov. and *Macrostylis amaliae* sp. nov.

The females of *Macrostylis sabinae* sp. nov. and *M. amaliae* sp. nov. are remarkably similar to each other. The coxal seta only on pereopod VII seems to be a synapomorphic character for these sister species. Coxal setae on pereopods V–VII are found in *M. wolffi* Mezhov, 1988 from the Pacific Ocean. Apart from the shared coxal seta on pereopod VII the species have no further similarities.

The distributions of the morphologically indistinguishable (in the case of females, mancas and subadult male stages) *M. sabinae* sp. nov. and *M. amaliae* sp. nov. are sympatric but they are genetically distinct (Fig. 35). However, the adult males of both species are morphologically distinct. While subadult males and the females have ventral projections on pereonites 5 and 6 (Figs 13B; 25B, 29A; 30B, C; Supporting Information S2B, D, S3B, S5), they are absent in the adult male of *M. sabinae* sp. nov. (Figs 20B, 21B, C). Furthermore, in *M. sabinae* sp. nov. the lateral lobes of pleopod I project beyond the medial lobes distally (Fig. 24A, B), which is not the case in *M. amaliae* sp. nov. (Fig. 33A, B). Another difference between the terminal males of both species is featured in the aesthetascs, which are different in length and structure (Fig. 22).

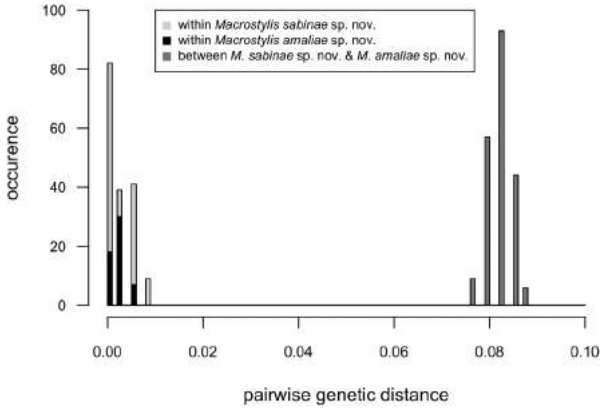

Figure 35. Frequency spectrum of uncorrected pairwise genetic distances, based on the 16S alignment: within ***M. amaliae* sp. nov.**, within ***M. amaliae* sp. nov.** and between ***M. sabinae* sp. nov.** and ***M. amaliae* sp. nov.**

The aesthetascs of *M. amaliae* sp. nov. extend up to the distal margin of the fourth segment of the antenna (merus) (Figs 22B, 29A, 30B, Supporting Information S5) while the aesthetascs of *M. sabinae* sp. nov. extend further until the distal margin of the fifth segment (carpus) (Figs 20A, B, 21A, B, 22A). Furthermore the aesthetascs of *M. sabinae* sp. nov. have a conspicuous constriction distally to the macrostylids' common belt of constriction, which is situated medially along the aesthetasc proximo-distal axis (Figs 20D, E, G, 22A). This additional constriction was present on the majority of aesthetascs. There was no interspecific difference found in the aesthetascs of juvenile males (Fig. 20F).

Identification key to the species of Macrostylidae from the Northwest Pacific

Remarks: Except where mentioned otherwise, the key is based on females. For the identification key all adequately described species known for the KKT region were included. However, four species were excluded. The descriptions of *Macrostylis profundissima* Birstein, 1970, *M. sensitiva* Birstein, 1970 and *M. quadratura* Birstein, 1970 are based on male specimens only and the females remain unknown. *Macrostylis ovata* Birstein, 1970 was excluded because we assume, based on the development of the seventh pereonite and the similarly weakly developed setation on the anterior pereopods, that the individual upon which the species was described may be a manca, possibly of *M. grandis* Birstein, 1970, which occurs sympatrically.

KEY TO THE NORTHWEST PACIFIC MACROSTYLIDAE

1. Pereonite 1 ventral projection directed ventrally, rounded or acute, spine-like 2
Pereonite 1 ventral projection spine-like, orientated anteriorly 5

2(1). Pereonite 6 posterolateral margin produced posteriorly; pereonite 7 with posterolateral protrusions, similar to pereonites 5 and 6; operculum ventrally roundedly keeled; pleotelson ventrolateral setal ridges present 3
Pereonite 6 posterolateral margin not produced posteriorly; pereronite 7 without or with weakly developed posterolateral protrusions; operculum without keel; pleotelson ventrolateral setal ridges absent . 4

3(2). Pleotelson waist absent, without lateral constriction anteriorly to uropod insertions; operculum elongate (length 1.8 width); pleotelson as wide as pereonite 7; pereopod VII dorsal (posterior) margin row of elongate setae present; pleotelson setal ridges not visible in dorsal view; pleotelson posterior apex acutely tapering; antennula (antenna 1) comprising one segment ..... *Macrostylis curticornis* Birstein, 1963
Pleotelson waist present, constricted anteriorly to uropod articulation; operculum elongate (length clearly more than 1.5 width); pleotelson narrower than pereonite 7; pereopod VII dorsal (posterior) margin row of elongate setae absent; pleotelson setal ridges visible in dorsal view; pleotelson posterior apex smoothly rounded; antennula (antenna 1) five segments ..... *Macrostylis daniae* sp. nov.

4(2). Pereronite 4 posterolateral setae present and segment widened in the middle; pleotelson waist present, constriction anteriorly to uropod articulation; operculum elongate (length clearly more than 1.5 width), acutely tapering posteriorly; pleotelson shape ovoid, lateral margins convex (outlines of anterior part in dorsal view); fossosome ventral surface with sharp keel; antennula (antenna 1) of three segments (unlike in the original description); distinctly elongate and slender body; uropod protopod 4.5 times the length of endopod ..... *Macrostylis longula* Birstein, 1970
Pereronite 4 posterolateral setae absent; waist absent; operculum stout (length 1.5 width or less), smoothly rounded posteriorly; pleotelson shape narrowing evenly towards uropodal insertions, lateral margins straight (outlines of anterior part in dorsal view); fossosome ventral surface without keel; antennula (antenna 1) of five segments; distinct by heavy imbricate ornamentation on all segments ..... *Macrostylis reticulata* Birstein, 1963

5(1). Pereonite 4 posterolateral margins produced posteriorly and posterolateral setae present; pleotelson waist absent, constriction anteriorly to uropod articulation; operculum stout (length 1.5 width or less); fossosome ventral surface without keel 6
Pereonite 4 posterolateral margins not produced posteriorly and posterolateral setae absent; pleotelson waist present, constricted anteriorly to uropod articulation; operculum elongate (length clearly more than 1.5 width); fossosome ventral surface with sharp keel 8

6(5). Distinct body shape: stout (L/W ratio < 3.0) and rather large (7.8 mm); pleotelson anteriorly much wider than posteriorly, convex, progressively narrowing towards uropod insertions (outlines of anterior part in dorsal view); pereonite 3 posterolateral margin with tapering posterior projection; pereonite 7 without or with weakly developed posterolateral protrusions (as in manca); pleotelson as wide as pereonite 7 ..... *Macrostylis grandis* Birstein, 1970
Body shape elongate (L/W ratio > 3.0); pleotelson ovoid, lateral margins convex (outlines of anterior part in dorsal view); pereonite 3 posterolateral margin not produced posteriorly, pereonite 7 with posterolateral protrusions, similar to pereonites 5 and 6; pleotelson narrower than pereonite 7 7

7(6). Pereonite 6 length clearly larger pereonite 5 length; pereonite 5 length smaller or subequal pereonite 4 length; pereonite 6 posterolateral margin rounded; pereonite 4 pereonal collum laterally expressed (segment anteriorly constricted); pereonite 4 shape generally resembling more posterior pereonites; posterolateral spine like setae and ventral projection present on pereonite 4; ventral and dorsal row of elongate setae present on pereopod VII ..... *Macrostylis zenkevitchi* Birstein, 1963
Pereonite 6 length smaller or subequal pereonite 5 length; pereonite 5 length clearly greater pereonite 4 length; pereonite 6 posterolateral margin tapering; pereonite 4 pereonal collum laterally not expressed (segment anteriorly not constricted); pereonite 4 shape clearly distinct from both anterior and posterior pereonites ..... *Macrostylis affinis* Birstein, 1963

8(5). In males ventral projections similar to female on all pereonites; in males aesthetascs all of same type; pleotelson L/W ratio in male subequal to female ..... *Macrostylis amaliae* sp. nov.
In males ventral projections differ from females, ventral projections on pereonites 5 and 6 absent; in males aesthetascs of multiple types; pleotelson L/W ratio in male greater than in female ..... *Macrostylis sabinae* sp. nov.

Species delimitation of known species from the Northwest Pacific which were excluded from the key

Macrostylis sensitiva Birstein, 1970: The adult males are distinguishable from *Macrostylis daniae* sp. nov. by the shape of the first antenna (antennula). *Macrostylis daniae* sp. nov. has a squat and not elongate terminal segment. In contast to *Macrostylis sabinae* sp. nov. and *Macrostylis amaliae* sp. nov., this species has a straight apex seta on the ischium of pereopod III. Furthermore, the shape of the pleotelson narrows continuously to the uropod insertion. The pleotelson is clearly wider anteriorly than posteriorly.
Macrostylis profundissima Birstein, 1970: In contrast to the three species described here the first antennula is composed of a single segment and the pleotelson waist is absent.
Macrostylis quadratura Birstein, 1970: The pleotelson is rectangular in form. The antennula is short, thick and composed of three segments only.

Genetic results, phylogenetic inference and molecular species delimitation

We were able to successfully amplify 50 sequences for the 16S gene fragment and nine sequences for the 18S gene fragment. Unfortunately, we were not able to amplify the barcoding marker *COI*. The 16S gene fragment varied between 384 and 493 base pairs (bp) in length and had a high AT content (66.4%) typical of this gene (Simon *et al.*, 1994). The MAFFT alignment for the 16S gene was made from 109 sequences including the outgroup and had a length of 519 bp of which 200 bp was conserved, 242 bp was variable and 210 bp was parsimony informative. Following the AIC and hLRT, the best substitution model was GTR+G with no invariable sites and a gamma distribution shape parameter of 0.3188. The nucleotide frequencies of the alignment were A = 0.3438, C = 0.1354, G = 0.1811 and T = 0.3397. The substitution rates were R[AC] = 0.9425, R[AG] = 7.3100, R[AT] = 3.0851, R[CG] = 0.3979, R[CT] = 9.4418 and R[GT] = 1.000. The 18S gene fragment amplified varied between 1766 and 2221 bp in length and had a balanced AT to GC content (AT = 50.5%). The MUSCLE alignment for the 18S gene was made from 16 sequences including the outgroup and had a length of 2369 bp of which 1931 bp was conserved, 402 bp was variable and 263 bp was parsimony informative. The AIC and the hLRTs suggested the same substitution model, which was GTR+I+G with a proportion of invariable sites of 0.6605 and a gamma distribution shape parameter of 0.4811. The nucleotide frequencies of the alignment were: A = 0.2387, C = 0.2229, G = 0.2706 and T = 0.2678. The substitution rates were: R[AC] = 0.4540, R[AG] = 1.3860, R[AT] = 0.7423, R[CG] = 0.3988, R[CT] = 2.5437 and R[GT] = 1.000. Considerably more sequences were amplified for the 16S genetic marker. However, the phylogenetic reconstructions of the two markers separately resulted in similar topologies.

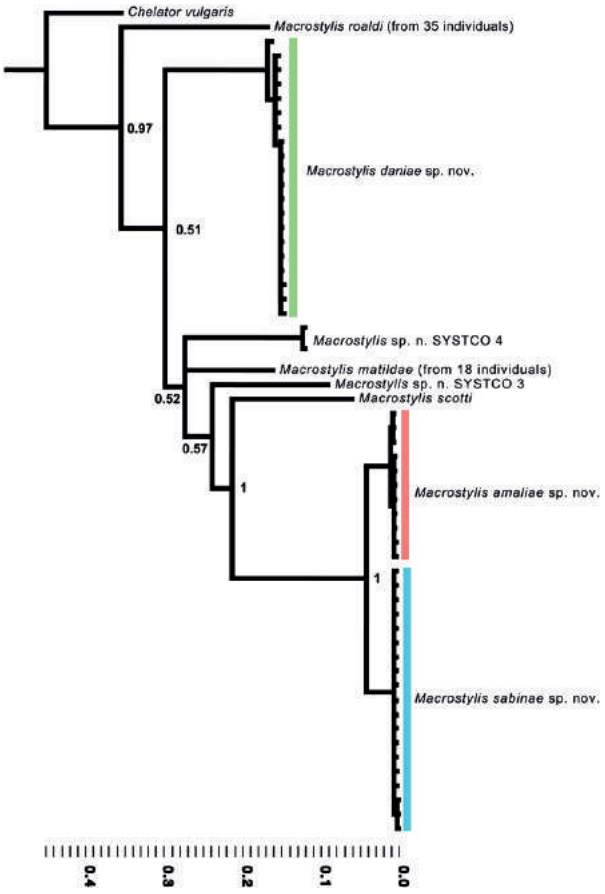

Figure 36. Consensus tree of 108 individuals based on a MAFFT alignment from 16S sequences; posterior probabilities are calculated for each node. The material of ***Macrostylis daniae* sp. nov.**, ***M. sabinae* sp. nov.** and ***M. amaliae* sp. nov.** was aligned with all 16S sequences of this family available online on GenBank. The clade of *Macrostylis roaldi* Riehl & Kaiser, 2012 and *Macrostylis matildae* Riehl & Brandt, 2013 was reduced in favour of greater clarity. *Chelator vulgaris* Hessler, 1970 served as the outgroup.

For both *M. sabinae* sp. nov. and *M. amaliae* sp. nov., the 16S gene showed a low maximum within-group divergence of 0.8% uncorrected *p*-distance (Fig. 35). The clades formed by the individuals of these two respective species divided into two monophyletic groups (Fig. 36, posterior probability = 1), representing the species proposed here. They are genetically distinct by 7.7–8.0 % without intermediate distances (Fig. 35). The most closely related species to *M. sabinae* sp. nov. and *M. amaliae* sp. nov. in the 16S dataset is *M. scotti*. This relatedness is statistically well supported (post. prob. = 1). The rest of the cladogram is not well supported and

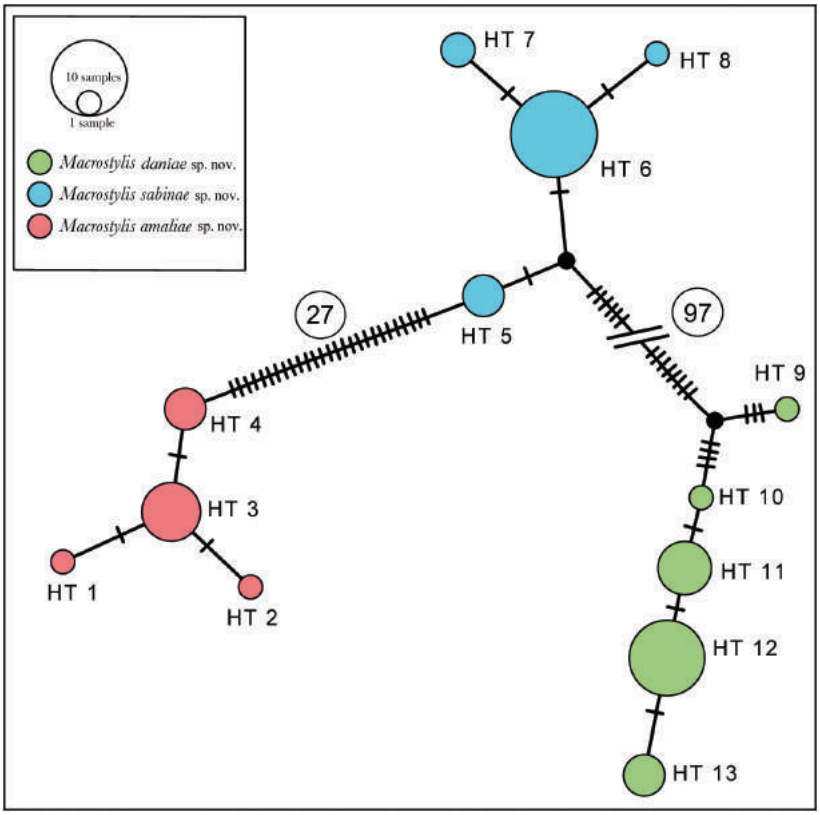

Figure 37. Haplotype network of ***Macrostylis daniae* sp. nov.**, ***M. sabinae* sp. nov.** and ***M. amaliae* sp. nov.**, ***M. sabinae* sp. nov.** and ***M. amaliae* sp. nov.** are separated by 27 mutations. ***Macrostylis daniae* sp. nov.** is separated from ***M. sabinae* sp. nov.** by 97 mutations. HT, haplotype.

not sufficiently resolved; for a better resolution more sequences from more species would be necessary. In the 16S cladogram, the species *M. roaldi* represents the well-supported sister taxon (post. prob. = 0.97) to all other tested Macrostylidae. *Macrostylis daniae* sp. nov. occupies one distinct clade (Fig. 36), but its position is not well supported (post. prob. = 0.51).

The 18S cladogram differs slightly from the 16S cladogram. Since 18S is a more slowly evolving gene than 16S and the species composition differed between the alignments, the 18S cladogram is better resolved and better supported. *Macrostylis sabinae* sp. nov. and *M. amaliae* sp. nov. remain in two monophyletic groups (Supporting Information S6, post. prob. = 1). However, *M. roaldi* does not sit opposite to all other Macrostylidae; here it is a rather 'recent' species forming a monophyletic group with *Macrostylis* sp. (EU414442) (post. prob. = 1). *Macrostylis daniae* sp. nov. forms a monophyletic group with *Macrostylis* sp. (AY461477) (post. prob. = 0.88). The species *Macrostylis* sp. (AY461476) is placed opposite to all other Macrostylidae for the 18S marker (post. prob. = 0.72). The genetic distinction of the three newly described species was apparent in the haplotype network as well (Fig. 37). In the haplotype network 13 haplotypes are represented. Haplotypes 1–4 represent *M. amaliae* sp. nov., haplotypes 5–8 represent *M. sabinae* sp. nov. and haplotypes 9–13 represent *M. daniae* sp. nov.

Macrostylis sabinae sp. nov. is separated from *M. amaliae* sp. nov. by 27 mutation steps (7.7% divergence), while there is a maximum of six mutations (0.8%) within these species. *Macrostylis daniae* sp. nov. is separated from *M. sabinae* sp. nov. by 97 mutations (28.6%) and from *M. amaliae* sp. nov. by 124 mutations (29.4%) and has a higher intraspecific variation than *M. sabinae* sp. nov. or *M. amaliae* sp. nov. with a maximum of 15 mutations (1.9%) within its clade. Those distances, however, are mainly caused by one individual which was the only specimen of this species sampled at station 6–11. KBMa120 is separated from the closest other specimens of *M. daniae* sp. nov. by nine mutations (1.6%).

Body-size variation between males and females of *M. sabinae* sp. nov. and *M. amaliae* sp. nov.

Variations in body length were found between adult conspecific males and females (Fig. 38). We were

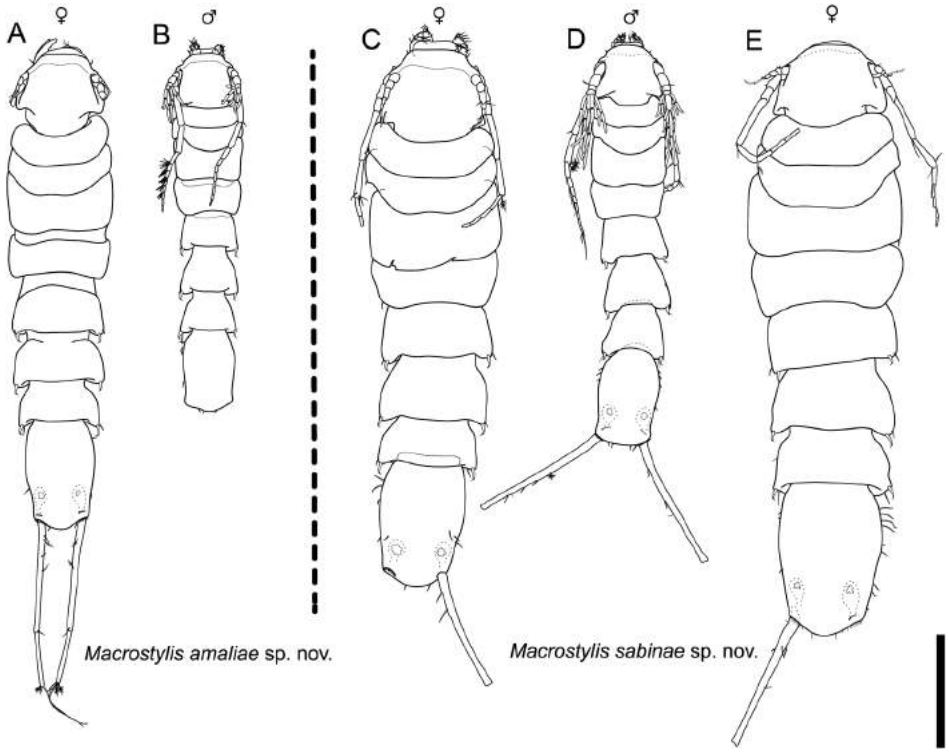

Figure 38. Females and males of ***Macrostylis sabinae* sp. nov.** and ***M. amaliae* sp. nov.** are presented to scale to illustrate the sexual size dimorphism. From left to right: ZMH K-45914, ZMH K-45915, ZMH K-45908, ZMH K-45910, ZMH K-45909. Scale = 0.5 mm.

interested in the size difference between males and females of comparable stages. To compare these, only ovigerous females and adult males were considered for analyses. The genetic dataset was unbalanced due to the low numbers of terminal males. As a result, it was not suitable for statistics, but a boxplot (Fig. 39A) provided an overview of the available data. Furthermore, this dataset confirms similar variations in both species.

To test whether the observed size variability between males and females among these two species was statistically significant, the formalin-fixed material was included in the analysis. The formalin-fixed animals of *M. sabinae* sp. nov. and *M. amaliae* sp. nov. were analysed together with the ethanol-fixed material, but all individuals were treated as one species (*Macrostylis sabinae-amaliae* complex). A Wilcoxon–Mann–Whitney *U* test was conducted to compare the body length of ovigerous females and adult males (Fig. 39B). The ovigerous females are significantly larger than the adult males ($W = 129.5$, $P < 0.0001$). While equally significant (Welch two-sample *t*-test, $M_{\text{females}} = 1.961, M_{\text{males}} = 1.632, t_{(35.66)} = 5.707, P < 0.0001$) the non-ovigerous but seemingly adult females may be of interest, but they represent a rather roughly defined group possibly comprising multiple developmental stages and are not a sufficient group for a size comparison.

A significant size difference was further found between ovigerous females among stations (Kruskal–Wallis test, $\chi^2_{(11)} = 20.985$, $P < 0.05$) (Fig. 39C). The effect of this incident on the present data was analysed in Fig. 39D. Based on the results (Fig. 39D) it is clear that the size difference between males and females was similarly distributed among all stations.

Dispersibility of *M. sabinae* sp. nov. in the abyss

Conspecific specimens were collected at abyssal depths from both sides of the hadal KKT. With its maximum depth of over 9700 m, the KKT may well represent a dispersal barrier for abyssal benthos. Station 3–9 was located north of the KKT, while all other stations were located south of the trench (Fig. 1). It was hence possible to test for connectivity of abyssal species across the KKT. Three individuals of *M. sabinae* sp. nov. of the same 16S haplotype were found north of the KKT (station 3–9) (ZMH K-45929,

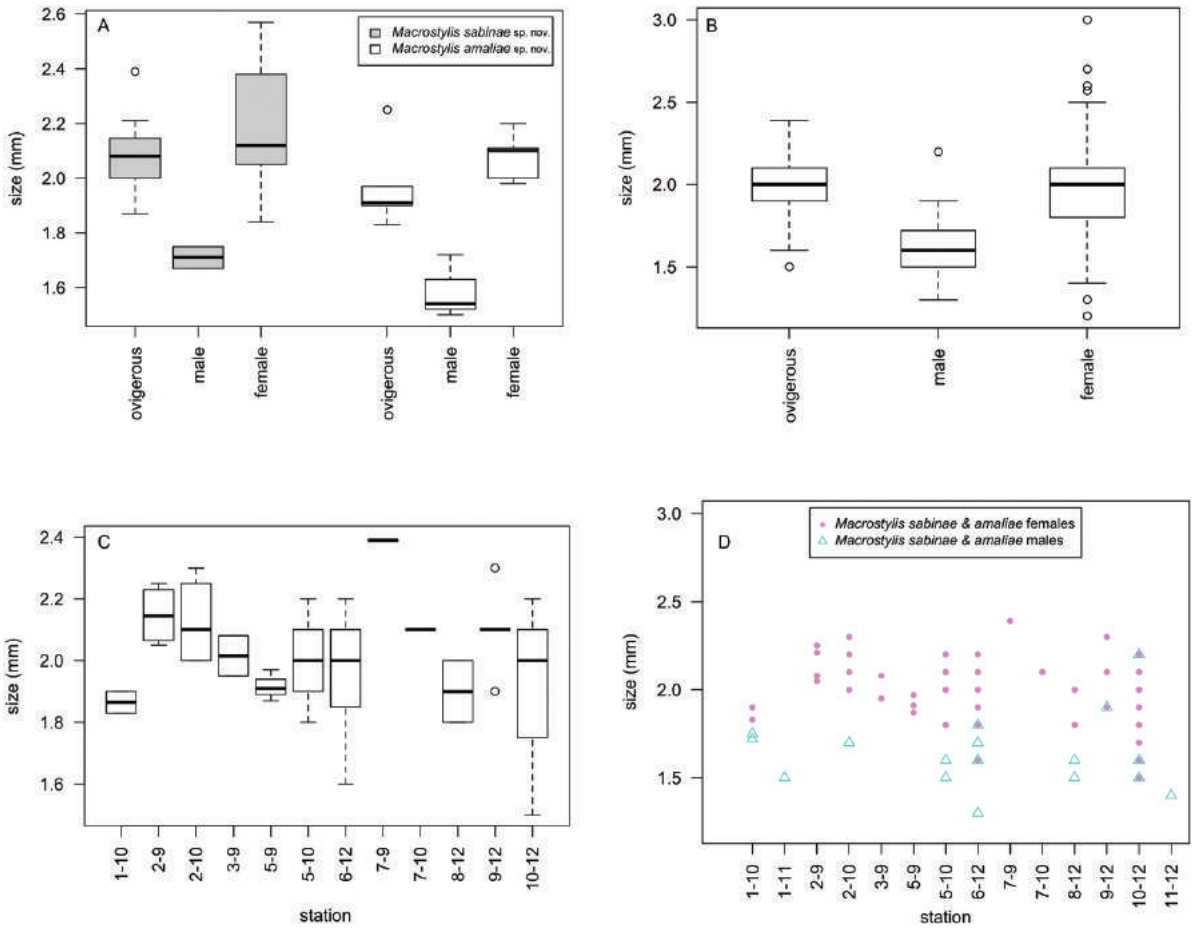

Figure 39. Body length variation within the ***M. amaliae–M. sabinae*** complex. All ovigerous females, adult females and males sampled (formalin and EtOH fixed material, N = 195) of ***M. sabinae* sp. nov.** and ***M. amaliae* sp. nov.** were measured in length. Due to the morphologically cryptic females, all individuals were treated as one species in B–D. A, the ovigerous females, adult females and males of both species (N = 30) were compared in body length. Only genetically verified material was used. The boxplot shows for both species that the males are significantly smaller than adult females and ovigerous females. B, the boxplot compares the body length of males, ovigerous females and adult females of all sampled material. Males are significantly smaller than ovigerous and adult females. C, the boxplot compares the body length of ovigerous females across stations (sampling locations). Ovigerous females are not equal in size among stations. D, in this scatterplot ovigerous females and males were sorted by station and plotted against body length. Except for station 10–12 the females are larger than the males. Males and females hardly overlap in size. At station 10–12, however, a particularly large male was found, so the sexes overlap in size.

ZMH K-45933, ZMH K-45926) (Fig. 37: haplotype 5). The closest station across the KKT was station 2–9 (Fig. 1), where 12 individuals of *M. sabinae* sp. nov., also sharing one haplotype, were found (Fig. 37: haplotype 6). Both haplotypes, geographically isolated by the KKT, were separated by four mutation steps equalling 0.5% uncorrected *p*-distance. All three haplotypes south of the KKT were separated by only one mutation step (0.3%) (Fig. 37: HT6 vs. HT7, HT8). No correlation was found between genetic and geographical distance (Mantel test, r = 0.191, 9999 replicates, P > 0.30). A possible genetic barrier was analysed using a 'genetic landscape shapes' interpolation (Miller, 2005) (Fig. 40). The three-dimensional genetic landscape presented high genetic *p*-distances across the KKT. The interpolation was based on a Delauney triangulation network (Watson, 1992; Brouns, Wulf & Constales, 2003) (Fig. 40: black lines). One high peak was found from station 3–9 to 7–9/5–9 and a further peak was found between 3–9 and 2–9, indicting high genetic distances. Among the stations south of the KKT, three low peaks for low genetic distances were found. Monmonier's algorithm implemented in Alleles in Space detected a barrier in the tested dataset

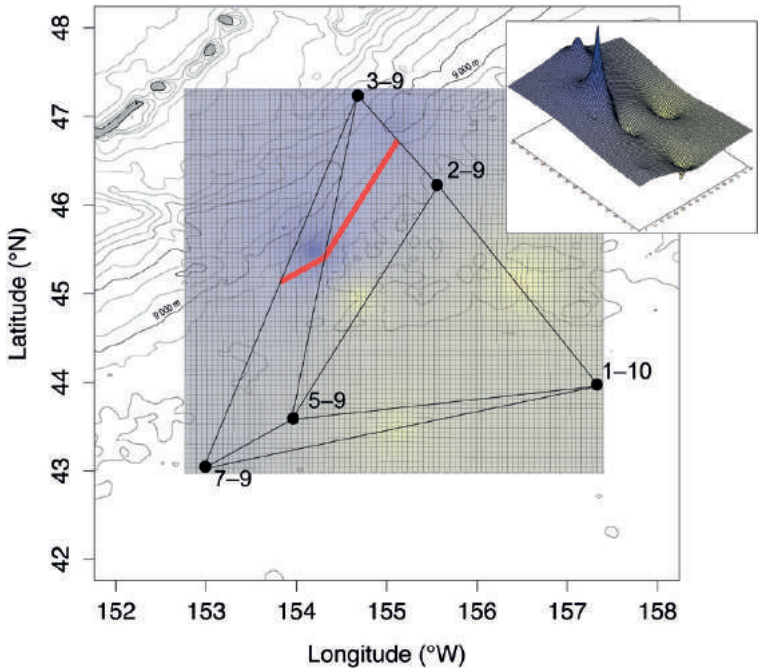

Figure 40. A genetic landscape shapes interpolation (Miller, 2005) was performed (top right). The *x*- and *y*-axes represent geographical coordinates and the *z*-axis shows the pairwise genetic distances between individuals of ***Macrostylis sabinae* sp. nov.** The genetic landscape was plotted on the sampling area from top view (blue/yellow: high/low pairwise genetic distance). Each station (black dots) and the underlying connectivity network (black lines) were plotted. Genetic barriers were obtained from Monmonier's algorithm (red line) and coincide with the extent of the Kuril–Kamchatka Trench.

(Fig. 40: red line). This suggested barrier overlapped with the extent of the KKT, indicating that hadal trenches represent a physical barrier to deep-sea benthic organisms.

DISCUSSION

Three new species of *Macrostylis* are described in this paper using an integrative approach. We also used a taxonomic feedback loop (Page, Choy & Hughes, 2005), also referred to as reciprocal illumination of the available evidence (Henning, 1966; Fitzhugh, 2016). However, in the case of cryptic females where the morphological signal was insufficient for species delimitation, the molecular data were used to compensate. Taking into account the rarity of deep-sea samples, CLSM was successfully evaluated as a non-destructive means of imaging. Regarding the detailed scans (Figs 21, 22, 30, Supporting Information S2, S5), this approach is a sufficient method to visualize delicate or rare material such as type material.

Including the three new species described in this article, the cosmopolitan isopod family Macrostylidae is today represented by 12 taxonomically described species from the region and 90 worldwide (Table 1).

Species delimitation and cryptic species

Macrostylis daniae sp. nov. can be distinguished morphologically based on female and male specimens, and hence the taxon fits the criteria for a phenotypic cluster approach (Hausdorf, 2011) of morphological species delimitation, as well as molecular cluster and lineage-based approaches (see below).

In *M. amaliae* sp. nov. and *M. sabinae* sp. nov., the commonly used phenotypic cluster concept does not apply due to the indistinct morphologies of the females. Accordingly, additional data and approaches are required for that purpose. As with *M. daniae* sp. nov., however, they fulfil the requirements of the phylogenetic species concept (Eldredge & Cracraft, 1980) given that both form monophyletic groups. Since they form clusters of individuals with no intermediates, the genotypic cluster definition (Sites & Marshall, 2004; Hausdorf & Hennig, 2010) of species applies here as well. This distinction between intra-cluster diversity and inter-group divergence reflects interspecific genetic variation that exceeds intraspecific variation and may therefore be seen as a 'barcoding gap' as established for the *COI* gene (Hebert *et al.*, 2003), which has mutation rates in other Janiroidea similar to those in 16S, the marker used in this study. Amongst morphologically similar specimens the persistence of distinct

genetic clusters without intermediates in sympatry has been interpreted as evidence for the existence of coexisting cryptic species in other Crustacea as well (France & Kocher, 1996; Held, 2003).

In the abyssal deep sea, organisms are thought to show a strong distribution heterogeneity, often referred to as patchiness (Wilson & Hessler, 1987; Grassle & Maciolek, 1992; De Broyer, Jazdewski & Dauby, 2003; Brandt *et al.*, 2004). Our sampling method with trawled gear integrated the samples over a certain distance (haul distance varied from 2,161 m at station 1–11 to 3117 m at station 2–9) (Brandt *et al.*, 2015). Following the conclusions of Grassle & Morse-Porteous (1987), we cannot assume a sympatric distribution of the sampled species with certainty (while close proximity of their occurrences within the trawled area can be safely assumed). Establishment of microhabitats is known to exist for foraminifera (Corliss, 1985), which are considered a food sources of deep-sea asellotes (Wolff, 1962; Svavarsson, Gudmundsson & Brattegard, 1993; Brandt, 1997; Gudmundsson, von Schmalensee & Svarvarsson, 2000; Brökeland, Guðmundsson & Svavarsson, 2010; Riehl *et al.*, 2016). Another likely food source for deep-sea isopods is detritus (Wolff, 1962; Hessler & Strömberg, 1989; Svavarsson *et al.*, 1993; Brökeland *et al.*, 2010). As detritus is also found in small patchy accumulations on the seafloor (Grassle & Morse-Porteous, 1987; Riemann, 1989; Grassle & Maciolek, 1992), the utilization of microhabitats by macrofaunal organisms is conceivable. A different feeding behaviour could in this case even lead to allopatry on a small scale, although we have no morphological evidence for that conclusion, given that no particular difference was found in the mouthparts of *M. sabinae* sp. nov. and *M. amaliae* sp. nov. However, morphology is not destiny (Gailer *et al.*, 2016), meaning that although morphological specialization was not observed, this does not necessarily imply similar preferred food sources for the two species. Since we cannot interpret the distribution of species within one EBS trawl at the moment, a sympatric distribution along one trawl or, respectively, one station is assumed.

Except for the terminal males, *M. sabinae* sp. nov. and *M. amaliae* sp. nov. would fulfil the following criteria for cryptic speciation postulated by Held (2003) and summarized by Raupach & Wägele (2006): (1) bimodal distribution of pairwise distance values without intermediates (Fig. 36), (2) differentiation at a level known for this gene from undisputed species pairs closely related to the studied species and (3) persistence of high levels of genetic differentiation in sympatry (Fig. 1). On the one hand, we could speak of cryptic species because none of the female or juvenile stages are morphologically distinguishable while genetically distinct. On the other hand, the adult males are distinguishable based on morphology. A similar state was described by Brökeland (2010b) for the species complex of *Haploniscus unicornis* Menzies, 1956 and was also previously mentioned for Macrostylidae (Riehl & Brandt, 2010). Due to the species-specific differences of the adult males we cannot speak of a fully cryptic species. However, given that adult males were rare in our samples compared to females and younger males and without genetic analyses the majority of specimens could not be identified as either of both species, we had to establish the '*Macrostylis sabinae-amaliae* complex' as a taxonomic unit. In these samples the male to female ratio was roughly 1:6 for *M. sabinae* sp. nov. and *M. amaliae* sp. nov. (these ratios might alter if the species were separated). Genetically for *M. sabinae* sp. nov. only one adult males was available, and for *M. amaliae* sp. nov. this was only two. Those, however, were morphologically unique (see remarks for *M. sabinae* sp. nov. and *M. amaliae* sp. nov.). With only three individuals to compare, the features that made them distinguishable could have caused misinterpretations. That is why the formalin-fixed material was decisively integrated in the analyses. Among 218 formalin-fixed individuals of *M. sabinae* sp. nov. and *M. amaliae* sp. nov., only 24 individuals were males, 23 of which were identified as *M. amaliae* sp. nov. However, one male was noticeably different and shared the same features with the genetically verified male of *M. sabinae* sp. nov. The genetically identified male was dissected for description, so the formalin-fixed male remains the only intact individual available to science today. This individual was handled with care and was only used for CLSM micrographs. The distinct differences between the males indicate sex-dependent selective forces. While the evolution of sexual dimorphisms in the deep sea can probably be best explained by either the low densities, the low food supply or a combination of both, we hypothesize that the sexual dimorphisms themselves, as featured in these species, may promote speciation in sympatry through increased morphospace.

Macrostylis sabinae sp. nov. and *M. amaliae* sp. nov. are difficult to delineate and delimit, but with 247 specimens sampled they were the most abundant macrostylid isopods during this survey. With 217 morphologically indistinguishable specimens it is, however, impossible to state whether one species is more abundant than the other.

Aesthetascs

Aesthetascs, special sensillae for chemoreception (Ache, 1982; Heimann, 1984) located on the first antenna (antennula), are found in all major crustacean groups (Wasserthal & Seibt, 1976; Rieder & Spaniol, 1980; Guse, 1983; Heimann, 1984; Lowry, 1986). Among other functions, aesthatascs serve in food and

mate recognition (Ache, 1982). The aesthetascs of *M. sabinae* sp. nov. adult males are particularly long and easily recognizable under a stereomicroscope. Interestingly, this is a type of aesthetasc that to our knowledge has not been described for this family or elsewhere before (Fig. 20G). The increased number of aesthetascs and an enlargement in adult males only indicate that perception for sexual pheromones may be amongst the main functions of these aesthetascs, as well as for macrostylids generally (Riehl *et al.*, 2012). The aesthetascs of juvenile males resemble more those of the females (Fig. 20F). A closer look at the adult males of *M. sabinae* sp. nov. and *M. amaliae* sp. nov. shows that not all aesthetascs are equally long (Figs 20E, 22). In both species the males carried aesthetascs that resemble those of the females in form, size and location.

This further encourages the assumption that most of the males' aesthetascs might serve in specialized perception for sexual pheromones, and 'regular' aesthetascs are preserved for general chemoreception. Yet, without a more detailed look into function, all this remains highly speculative.

Furthermore, the modified aesthetascs of *M. sabinae* sp. nov. males might indicate a different habitat preference. Macrostylidae are considered an infaunal, burrowing family (Harrison, 1989; Hessler & Strömberg, 1989; Wägele, 1989). The modified protruding aesthetascs combined with the reduced ventral projections might point towards a differing lifestyle. Prior studies on terrestrial and aquatic crustaceans have shown aesthetasc adaptations to certain environments (Ghiradella, Case & Cronshaw, 1968).

Sexual size dimorphism

During this study we found a significant body-size difference between conspecific males and females. Sexual dimorphism in macrostylids in general, expressed as morphological features of terminal males as opposed to females and non-adult male stages, has been extensively discussed before (Riehl *et al.*, 2012) and is applicable to *M. sabinae* sp. nov. and *M. amaliae* sp. nov. alike. Among these characters are a more slender body, elongated posterior pereopods and an anatomical change in the first antenna, making the third and fourth segments the shortest. Within the present set of data the size difference between the adult males and females was particularly conspicuous and may relate to sexual size dimorphisms, as was found for *Ischnomesus harrietae* Kavanagh, Frutos & Sorbe, 2015 from the bay of Biscay or *Haploniscus rostratus* (Menzies, 1962a) (Brökeland, 2010a). The size difference between males and females of comparable stages was of interest, and hence only ovigerous females and adult males were analysed. The adult males and ovigerous females are possibly still of multiple moulting stages but they are visibly sexually mature and therefore the most suitable group for comparison.

The sexual size difference is a noteworthy observation, but considering the small numbers of males available in the samples it might be a misleading coincidence due to an unrepresentative sample. Further tests were performed to minimize the possibility of a sampling-biased observation. It was necessary to confirm that the males were not just small individuals of their species. For instance, one male of each species (ZMH K-45910, ZMH K-45915) was sampled at station 1–10. Interstingly, two further ovigerous females of *M. amaliae* sp. nov. (ZMH K-45937, ZMH K-45938), which were the smallest females collected for the species, were also sampled from the same station. It is important to note that a considerable size difference was also found between ovigerous females (Fig. 39C). Also interesting is that body size seems to correlate with station; hence the sampling location seems to have an influence on the size of individuals (Fig. 39C). There may be multiple reasons for this correlation, ranging from the most obvious, i.e. food limitation, to more subtle environmental variations of, for example, oxygen or temperature limitation. However, a detailed investigation into the possible reasons for the observed size differences across stations was not part of this study. Furthermore, a significant difference (Wilcoxon–Mann–Whitney U, $W = 129.5$, $P < 0.0001$) between body lengths of males and ovigerous females across all stations was found (Fig. 39D), ruling out the effect of stations as seen in Fig. 39C; across and among stations the males are considerably smaller than the females. Thus we were able to confirm a sexual size dimorphism for the species *M. sabinae* sp. nov. and *M. amaliae* sp. nov. Our observations seem to correspond to the suggestions of Riehl *et al.* (2012), in which the sexual dimorphism was interpreted as a consequence of the different reproductive roles. The females are bigger due to resource storage and breeding. The males have an increased number of aesthetascs for sensing a mating partner and, compared to females, the body is more slender and the posterior pereopods are often elongated. In this case the sexual dimorphism goes even further. The male body is not only more slender, but is also reduced in size overall. As mentioned above in relation to the aesthetascs, the males might actually change from an infaunal mode of life to a more actively searching epifaunal lifestyle. In addition, the elongated posterior pereopods suggest a rather epifaunal life. In this scenario, the females remain locally restricted and passively 'wait' for an actively searching mating partner. This behaviour can connect populations across larger distances and males are independent from local female abundances. A smaller male seems to have an evolutionary advantage over a larger male. This might

be linked to food availability. An epifaunal male possibly has fewer food sources available, and therefore does not grow as large. Furthermore, a male does not necessarily need to store energy, which the females do need for breeding.

Morphological variation in females of *M. sabinae* sp. nov. and *M. amaliae* sp. nov.

During the description of *M. sabinae* sp. nov. and *M. amaliae* sp. nov., differences were observed between females of the same species. Non-ovigerous females tended to show a distinct pereonal collum on pereonite 4, and to some extent also on pereonite 5 (Fig. 34B). By contrast, this pereonal collum was almost absent in ovigerous females (Fig. 34A), resulting in a more condensed body shape. This condensed body may be beneficial for improved integrity of pereonites 1–4, which could favour more stability of the marsupium. The marsupium in macrostylids is composed of two pairs of oostegites growing out of the third and fourth pereonal coxae. The holotype of *M. sabinae* sp. nov. has no visible marsupium, but has the distinct body shape of an ovigerous female, so a secondary effect from the marsupium may be rejected. This observations might be completely explained by a tendency of the females to keep the body in a more straight position once they become ovigerous. However, in other species such radical changes have not yet been evaluated. After all, the females of both species remain virtually inseparable, despite the apparent differences in the holotypes. Considering the above-mentioned observations, it is important to emphasize that these differences illustrated between both holotypes are not interspecific differences.

These observations are quite critical to taxonomic descriptions, since the morphology of the same species may alter drastically depending on the extent to which the specimen is bent and extended. For future taxonomic work on the group, we highly recommend that extra effort is made to compare ovigerous and non-ovigerous females of one species for species delimitation. These observations have implications on how length–width measurements of the impacted pereonites and of the whole body are made and highlight that such measurements provided in previous studies (as well as those presented herein) represent only more or less precise estimates, rather than exact values. In future studies, pereonite 4 length should probably be measured excluding the collum so that the effects of stretching or retracting of the specimens are excluded. Similar observations have been made also in other species of Macrostylidae (T. Riehl, unpubl. data). However, interspecific comparisons are, as of now, still lacking.

Implications from biogeography for macrostylid locomotion

Macrostylidae are thought to live within the sediment (Thistle & Wilson, 1987, 1996; Hessler & Strömberg, 1989) and lack adaptations for swimming locomotion (Riehl, 2014; Riehl *et al.*, 2014b). Like all peracarid crustaceans, they are brooders without real, free-swimming larval stages. Macrostylids are therefore without a dispersing stage. This predicts a rather low dispersibility for Macrostylidae (Wilson & Hessler, 1987). However, *M. sabinae* sp. nov. had a rather large distribution range, even across the KKT, which may represent a physical barrier. The haplotypes of *M. sabinae* sp. nov. geographically isolated by the KKT are separated by four mutation steps equalling 0.2% uncorrected *p*-distance, which is well within the range of intraspecific variation of 16S in deep-sea Janiroidea (Raupach & Wägele, 2006; Raupach *et al.*, 2007; Brökeland & Raupach, 2008; Riehl & Brandt, 2013; Brix *et al.*, 2015). Given that no haplotype was shared between the northern and southern sides of the KKT, a restricted exchange associated with this physical barrier could be proposed. This may be supported by the geographical distribution of some southern haplotypes; haplotype 6 was found at stations 2–9 and 7–9, which are further apart from each other than the two closest stations across the KKT (Fig. 1), but apparently without restrictions to gene flow. Our assumption was confirmed by Monmonier's algorithm, which proposed a distribution barrier between populations across the KKT. This indicates that gene flow across the KKT may be reduced, thus confirming that it may contribute to differentiation between (sub-) populations.

ACKNOWLEDGEMENTS

The execution of this study was supported by the German Federal Ministry of Education and Research (03G0237A). The KuramBio expedition and sample treatment was supported by the German Federal Ministry of Education and Research (03G0223A).

Captain Oliver Mayer and crew of *R/V Sonne* during cruise SO223 are thanked for their help in guaranteeing a successful campaign. Nils Brenke, Enrico Schwabe, Nikolaus Elsner, Marina Malyutina and all involved in EBS deployment, sieving and sample sorting are acknowledged for their efforts. Special thanks go to Terue Cristina Kihara who shared her comprehensive knowledge about CLSM and staining with us. Further thanks go to Renate Walter, who kindly operated the SEM. We thank Fiona Kavanagh and one anonymous reviewer for their helpful reviews. This is KuramBio publication # 37.

REFERENCES

Ache B. 1982. Chemoreception and thermoreception. In: Atwood HL, Sandeman DC (eds) *The biology of Crustacea*. New York: Academic Press, 369–398.

Apel EV, Bürgmann R, Steblov G, Vasilenko N, King R, Prytkov A. 2006. Independent active microplate tectonics of northeast Asia from GPS velocities and block modeling. *Geophysical Research Letters* **33:** L11303.

Birstein JA. 1957. Certain peculiarities of the ultra-abyssal fauna at the example of the genus *Storthyngura* (Crustacea, Isopoda, Asellota). *Zoologicheskii Zhurnal* **36:** 961–985.

Birstein JA. 1960. The family Ischnomesidae (Crustacea, Isopoda, Asellota) in the north-western part of the Pacific and the problem of amphiboreal and bipolar distribution of the deep sea fauna. *Zoologik Zhurnal SSSR* **34:** 3–28.

Birstein JA. 1961. *Microthambema tenuis* n. gen., n. sp. (Isopoda, Asellota) and relations of some asellote isopods. *Crustaceana* **2:** 132–141.

Birstein JA. 1962a. Über eine neue Art der Gattung *Austroniscus* Vanhoffen (Crustacea, Isopoda, Asellota) aus Grossen Tiefen des nord-westlichen Teiles des Stillen Oceans. *Izdanija Posebna Zavoda Za Ribarstvo NRM* **3:** 33–38.

Birstein JA. 1962b. Palaeophreatoicus sojanensis *gen. et sp. nov. and some problems of phylogeny and distribution of Isopoda*. *Paleontol. Zhurnal*, Vol. 3, Moscow: Academy of Sciences of the USSR 86, P.P. Shirshov Institute of Oceanology, 65–80.

Birstein JA. 1963. *Deep sea isopod crustaceans of the northwestern part of the Pacific Ocean*. Moscow: Institute of Oceanology, Academy of Sciences, USSR.

Birstein JA. 1970. *Additions to the fauna of Isopods (Crustacea, Isopoda) of the Kurile-Kamchatka Trench. Part I*. Moscow: Academy of Sciences of the USSR 86, P.P. Shirshov Institute of Oceanology, 292–340.

Birstein J. 1971. Additions to the fauna of isopods (Crustacea : Isopoda) of the Kurile-Kamchatka trench. Part 2. Asellota-2. *Trudy Instituta okeanologii* **92:** 162–238.

Bober S, Riehl T. 2014. Adding depth to line artwork by digital stippling—a step-by-step guide to the method. *Organisms Diversity & Evolution* **14:** 327–337.

Brandt A. 1997. Redescription of *Munnopsurus giganteus* (Sars, 1879) (Isopoda, Asellota, Eurycopidae). *Crustaceana* **70:** 288–303.

Brandt A, Brökeland W, Brix S, Malyutina M. 2004. Diversity of Southern Ocean deep-sea Isopoda (Crustacea, Malacostraca) — a comparison with shelf data. *Deep-Sea Research Part II: Topical Studies in Oceanography* **51:** 1753–1768.

Brandt A, Elsner N, Brenke N, Golovan O, Malyutina MV, Riehl T, Schwabe E, Würzberg L. 2013. Epifauna of the Sea of Japan collected via a new epibenthic sledge equipped with camera and environmental sensor systems. *Deep-Sea Research Part II: Topical Studies in Oceanography* **86–87:** 43–55.

Brandt A, Elsner NO, Malyutina MV, Brenke N, Golovan OA, Lavrenteva AV, Riehl T. 2015. Abyssal macrofauna of the Kuril–Kamchatka Trench area (Northwest Pacific) collected by means of a camera–epibenthic sledge. *Deep-Sea Research Part II: Topical Studies in Oceanography* **111:** 175–187.

Brandt A, Malyutina MV. 2015. The German–Russian deep-sea expedition KuramBio (Kurile Kamchatka biodiversity studies) on board of the RV *Sonne* in 2012 following the footsteps of the legendary expeditions with RV Vityaz. *Deep-Sea Research Part II: Topical Studies in Oceanography* **111:** 1–9.

Brenke N. 2005. An epibenthic sledge for operations on marine soft bottom and bedrock. *Marine Technology Society Journal* **39:** 10–21.

Brix S, Leese F, Riehl T, Kihara TC. 2015. A new genus and new species of Desmosomatidae Sars, 1897 (Isopoda) from the eastern South Atlantic abyss described by means of integrative taxonomy. *Marine Biodiversity* **45:** 7–61.

Brix S, Svavarsson J, Leese F. 2014. A multi-gene analysis reveals multiple highly divergent lineages of the isopod *Chelator insignis* (Hansen, 1916) south of Iceland. *Polish Polar Research* **35:** 225–242.

Brökeland W. 2010a. Redescription of *Haploniscus rostratus* (Menzies, 1962) (Crustacea: Peracarida: Isopoda) with observations on the postmarsupial development, size ranges and distribution. *Zootaxa* **2521:** 1–25.

Brökeland W. 2010b. Description of four new species from the *Haploniscus unicornis* Menzies, 1956 complex (Isopoda: Asellota: Haploniscidae). *Zootaxa* **2536.** DOI: 10.5281/zenodo.196630.

Brökeland W, Guðmundsson G, Svavarsson J. 2010. Diet of four species of deep-sea isopods (Crustacea: Malacostraca: Peracarida) in the South Atlantic and the Southern Ocean. *Marine Biology* **157:** 177–187.

Brökeland W, Raupach MJ. 2008. A species complex within the isopod genus *Haploniscus* (Crustacea: Malacostraca: Peracarida) from the Southern Ocean deep sea: a morphological and molecular approach. *Zoological Journal of the Linnean Society* **152:** 655–706.

Brouns G, Wulf AD, Constales D. 2003. Delaunay triangulation algorithms useful for multibeam echosounding. *Journal of Surveying Engineering* **129:** 79–84.

Coleman CO. 2003. 'Digital inking': how to make perfect line drawings on computers. *Organisms Diversity & Evolution* **3:** 303–304.

Coleman CO. 2009. Drawing setae the digital way. *Zoosystematics and Evolution* **85:** 305–310.

Corliss BH. 1985. Microhabitats of benthic foraminifera within deep-sea sediments. *Nature* **314:** 435–438.

Dallwitz MJ. 1974. A flexible computer program for generating identification keys. *Systematic Zoology* **23:** 50–57.

Dallwitz MJ. 1980. A general system for coding taxonomic descriptions. *Taxon* **29:** 41–46.

De Broyer C, Jazdewski K, Dauby P. 2003. Biodiversity patterns in the Southern Ocean: lessons from Crustacea. In: Huiskes AHL, Gieskes WWC, Rozema J, Schorno RML, van der Vlies SM, Wolff WJ, eds. *Antarctica in a global context*. Leiden: Backhuys, 201–214

Edgar RC. 2004. MUSCLE: multiple sequence alignment with high accuracy and high throughput. *Nucleic Acids Research* **32:** 1792–1797.

Eldredge N, Cracraft J. 1980. *Phylogenetic patterns and the evolutionary process: method and theory in comparative biology.* New York: Columbia University Press.

Elsner NO, Malyutina MV, Golovan OA, Brenke N, Riehl T, Brandt A. 2015. Deep down: Isopod biodiversity of the Kuril–Kamchatka abyssal area including a comparison with data of previous expeditions of the RV Vityaz. *Deep-Sea Research Part II: Topical Studies in Oceanography* **111:** 210–219.

Fitzhugh K. 2016. Dispelling five myths about hypothesis testing in biological systematics. *Organisms Diversity & Evolution* **16:** 443–465.

France SC, Kocher TD. 1996. Geographic and bathymetric patterns of mitochondrial 16S rRNA sequence divergence among deep-sea amphipods, *Eurythenes gryllus*. *Marine Biology* **126:** 633–643.

Gailer JP, Calandra I, Schulz-Kornas E, Kaiser TM. 2016. Morphology is not destiny: discrepancy between form, function and dietary adaptation in bovid cheek teeth. *Journal of Mammalian Evolution* **23:** 369–383.

Ghiradella HT, Case JF, Cronshaw J. 1968. Structure of aesthetases in selected marine and terrestrial decapods: chemoreceptor morphology and environment. *American Zoologist* **8:** 603–621.

Golovan OA, Blazewicz-Paszkowycz M, Brandt A, Jażdżewska A, Jóźwiak P, Lavrenteva AV, Malyutina M, Petryashov VV, Riehl T, Sattarova VV. 2013. Diversity and distribution of peracarid crustaceans (Malacostraca) from the continental slope and the deep-sea basin of the Sea of Japan. *Deep-Sea Research Part II: Topical Studies in Oceanography* **86–87:** 66–78.

Grassle JF, Maciolek NJ. 1992. Deep-sea species richness: regional and local diversity estimates from quantitative bottom samples. *The American Naturalist* **139:** 313–341.

Grassle JF, Morse-Porteous LS. 1987. Macrofaunal colonization of disturbed deep-sea environments and the structure of deep-sea benthic communities. *Deep-Sea Research Part A. Oceanographic Research Papers* **34:** 1911–1950.

Gudmundsson G, von Schmalensee M, Svarvarsson J. 2000. Are foraminifers (Protozoa) important food for small isopods (Crustacea) in the deep sea? *Deep-Sea Research Part I: Oceanographic Research Papers* **47:** 2093–2109.

Guse GW. 1983. Ultrastructure, development, and moulting of the aesthetascs of *Neomysis integer* and *Idotea baltica* (Crustacea, Malacostraca). *Zoomorphology* **103:** 121–133.

Harrison K. 1989. Are deep-sea asellote isopods infaunal or epifaunal? *Crustaceana* **56:** 317–319.

Hausdorf B, Hennig C. 2010. Species delimitation using dominant and codominant multilocus markers. *Systematic Biology* **59:** 491–503.

Hausdorf B. 2011. Progress toward a general species concept. *Evolution* **65:** 923–931.

Hebert PD, Cywinska A, Ball SL, deWaard JR. 2003. Biological identifications through DNA barcodes. *Proceedings of the Royal Society of London B: Biological Sciences* **270:** 313–321.

Heimann P. 1984. Fine structure and molting of aesthetasc sense organs on the antennules of the isopod, *Asellus aquaticus* (Crustacea). *Cell and Tissue Research* **235:** 117–128.

Held C. 2003. Molecular evidence for cryptic speciation within the widespread Antarctic crustacean *Ceratoserolis trilobitoides* (Crustacea, Isopoda). In: Huiskes AHL, Gieskes WWC, Rozema J, Schorno RM, van der Vies SM,Wolff WJ, eds. *Antarctic biology in a global context*. Leiden: Backhuys Publishers, 135–139.

Henning W. 1966. *Phylogenetic systematics*. Urbana: University of Illinois Press.

Hessler RR. 1970. *The Desmosomatidae (Isopoda, Asellota) of the Gay Head-Bermuda Transect*. Berkeley: University of California Press.

Hessler RR, Jumars PA. 1974. Abyssal community analysis from replicate cores in the central North Pacific. *Deep Sea Research and Oceanographic Abstracts* **21:** 185–209.

Hessler RR, Sanders H. 1967. Faunal diversity in the deep-sea. *Deep Sea Research and Oceanographic Abstracts* **14:** 65–78.

Hessler RR, Strömberg JO. 1989. Behavior of janiroidean isopods (Asellota), with special reference to deep sea genera. *Sarsia* **74:** 145–159.

Hessler RR, Wilson GDF. 1983. The origin and biogeography of malacostracan crustaceans in the deep sea. In: Sims RW, Price JH, Whalley PES, eds. *Evolution, time, and space: the emergence of the biosphere*. London: Academic Press, 227–254.

Huelsenbeck JP, Ronquist F. 2001. MRBAYES: Bayesian inference of phylogenetic trees. *Bioinformatics* **17:** 754–755.

Janssen A, Kaiser S, Meißner K, Brenke N, Menot L, Martínez Arbizu P. 2015. A reverse taxonomic approach to assess macrofaunal distribution patterns in abyssal Pacific polymetallic nodule fields. *PLoS ONE* **10:** e0117790.

Katoh K, Standley DM. 2013. MAFFT multiple sequence alignment software version 7: improvements in performance and usability. *Molecular Biology and Evolution* **30:** 772–780.

Kavanagh FA, Frutos I, Sorbe JC. 2015. *Ischnomesus harrietae* sp. nov., a new benthic asellote (Crustacea: Isopoda: Ischnomesidae) from bathyal bottoms of the southern Bay of Biscay. *Zootaxa* **3911:** 201–217.

Kavanagh FA, Wilson GDF. 2007. Revision of the genus *Haplomesus* (Isopoda: Asellota: Ischnomesidae) with erection of four new genera. *Invertebrate Systematics* **21:** 487–535.

Kearse M, Moir R, Wilson A, Stones-Havas S, Cheung M, Sturrock S, Buxton S, Cooper A, Markowitz S, Duran C, Thierer T, Ashton B, Meintjes P, Drummond A. 2012. Geneious Basic: an integrated and extendable desktop software platform for the organization and analysis of sequence data. *Bioinformatics* **28:** 1647–1649.

Kihara TC, Arbizu PM. 2012. Three new species of *Cerviniella* Smirnov, 1946 (Copepoda: Harpacticoida) from the Arctic. *Zootaxa* **3345:** 1–33.

Kottmann J, Kihara TC, Glatzel T, Veit-Köhler G. 2013. A new species of *Wellsopsyllus* (Copepoda, Harpacticoida, Paramesochridae) from the deep Southern Ocean and remarks on its biogeography. *Helgoland Marine Research* **67:** 33–48.

Kussakin OG. 1971. Additions to the fauna of isopods (Crustacea, Isopoda) of the Kurile-Kamtschatka Trench. Part III. Flabellifera and Valvifera. *Trudy Instituta Oceanologii Akademiya Nauk USSR* **92:** 239–273.

Kussakin OG. 1990. Biogeography of isopod crustaceans in the Boreal Pacific. *Bulletin of Marine Science* **46:** 620–639.

Leigh JW, Bryant D. 2015. popart: full-feature software for haplotype network construction. In Nakagawa S, ed. *Methods in ecology and evolution*. Oxford: Wiley-Blackwell.

Lowry JK. 1986. The callynophore, a eucaridan/peracaridan sensory organ prevalent among the Amphipoda (Crustacea). *Zoologica Scripta* **15:** 333–349.

Mezhov BV. 1980. On the fauna of Isopoda (Crustacea) of the Japanese and Idzubonin Trough of the Pacific. *Zoologicheskii Zhurnal* **59:** 818–829.

Mezhov B. 1981. *Isopoda. Benthos of the Submarine mountains Marcus-Necker and adjacent Pacific regions*. Moscow: Academy of Sciences of the USSR 86, P.P. Shirshov Institute of Oceanology, 62–82.

Michels J, Büntzow M. 2010. Assessment of Congo red as a fluorescence marker for the exoskeleton of small crustaceans and the cuticle of polychaetes. *Journal of Microscopy* **238:** 95–101.

Michels J, Gorb SN. 2012. Detailed three-dimensional visualization of resilin in the exoskeleton of arthropods using confocal laser scanning microscopy. *Journal of Microscopy* **245:** 1–16.

Miller MP. 2005. Alleles in space (AIS): computer software for the joint analysis of interindividual spatial and genetic information. *Journal of Heredity* **96:** 722–724.

Monmonier MS. 1973. Maximum-difference barriers: an alternative numerical regionalization method. *Geographical Analysis* **5:** 245–261.

Nylander JJA. 2004. *MrModeltest v2*. Uppsala: Evolutionary Biology Centre. Program distributed by the author.

Page TJ, Choy SC, Hughes JM. 2005. The taxonomic feedback loop: symbiosis of morphology and molecules. *Biology Letters* **1:** 139–142.

R Development Core Team. 2008. *R: A Language and Environment for Statistical Computing*. Vienna: R Core Team.

Raupach MJ, Held C, Wägele JW. 2004. Multiple colonization of the deep sea by the Asellota (Crustacea: Peracarida: Isopoda). *Deep-Sea Research Part II: Topical Studies in Oceanography* **51:** 1787–1795.

Raupach MJ, Malyutina M, Brandt A, Wägele JW. 2007. Molecular data reveal a highly diverse species flock within the munnopsoid deep-sea isopod *Betamorpha fusiformis* (Barnard, 1920) (Crustacea: Isopoda: Asellota) in the Southern Ocean. *Deep-Sea Research Part II: Topical Studies in Oceanography* **54:** 1820–1830.

Raupach MJ, Mayer C, Malyutina M, Wägele JW. 2009. Multiple origins of deep-sea Asellota (Crustacea: Isopoda) from shallow waters revealed by molecular data. *Proceedings of the Royal Society B: Biological Sciences* **276:** 799–808.

Raupach MJ, Wägele JW. 2006. Distinguishing cryptic species in Antarctic Asellota (Crustacea: Isopoda) – a preliminary study of mitochondrial DNA in *Acanthaspidia drygalskii*. *Antarctic Science* **18:** 191.

Rieder N, Spaniol H. 1980. Die Rezeptoren an den ersten Antennen von *Leptestheria dahalacensis* Rüppel (Crustacea, Conchostraca). *Zoomorphologie* **95:** 169–179.

Riehl T. 2014. *A phylogenetic approach to the classification of macrostylid isopods and faunal linkages between the deep sea and shallow-water environments.* Unpublished Dissertation, University of Hamburg.

Riehl T, Bober S, Voltski I, Malyutina MV, Brandt A. 2016. Caught in the act: an abyssal isopod collected while feeding on Komokiaceae. *Marine Biodiversity*. DOI: 10.1007/s12526-016-0606-*y*

Riehl T, Brandt A. 2010. Descriptions of two new species in the genus *Macrostylis* Sars, 1864 (Isopoda, Asellota, Macrostylidae) from the Weddell Sea (Southern Ocean), with a synonymisation of the genus *Desmostylis* Brandt, 1992 with *Macrostylis*. *ZooKeys* **57:** 9–49.

Riehl T, Brandt A. 2013. Southern Ocean Macrostylidae reviewed with a key to the species and new descriptions from Maud Rise. *Zootaxa* **3692:** 160–203.

Riehl T, Brenke N, Brix S, Driskell A, Kaiser S, Brandt A. 2014a. Field and laboratory methods for DNA studies on deep-sea isopod crustaceans. *Polish Polar Research* **35:** 205–226.

Riehl T, Kaiser S. 2012. Conquered from the deep sea? A new deep-sea isopod species from the Antarctic shelf shows pattern of recent colonization. *PLoS ONE* **7:** e49354.

Riehl T, Wilson GDF, Hessler RR. 2012. New Macrostylidae Hansen, 1916 (Crustacea: Isopoda) from the Gay Head-Bermuda transect with special consideration of sexual dimorphism. *Zootaxa* **3277:** 1–26.

Riehl T, Wilson GDF, Malyutina MV. 2014b. Urstylidae – a new family of abyssal isopods (Crustacea: Asellota) and its phylogenetic implications: a new family of higher Janiroidea. *Zoological Journal of the Linnean Society* **170:** 245–296.

Riemann F. 1989. Gelatinous phytoplankton detritus aggregates on the Atlantic deep-sea bed. *Marine Biology* **100:** 533–539.

Ronquist F, Huelsenbeck JP. 2003. MrBayes 3: Bayesian phylogenetic inference under mixed models. *Bioinformatics* **19:** 1572–1574.

RStudio Team. 2015. *RStudio: integrated development for R.* Boston: RStudio, Inc.

Sars GO. 1864. Om en anomal Gruppe af Isopoder. In: *Forhandhlinger Videnskapsselskapet I Kristiania*, 205–221.

Schindelin J, Arganda-Carreras I, Frise E, Kaynig V, Longair M, Pietzsch T, Preibisch S, Rueden C, Saalfeld S, Schmid B, Tinevez JY, White DJ, Hartenstein V, Eliceiri K, Tomancak P, Cardona A. 2012. Fiji: an open-source platform for biological-image analysis. *Nature Methods* **9:** 676–682.

Schneider CA, Rasband WS, Eliceiri KW. 2012. NIH Image to ImageJ: 25 years of image analysis. *Nature Methods* **9:** 671–675.

Simon C, Frati F, Beckenbach A, Crespi B, Liu H, Flook P. 1994. Evolution, weighting, and phylogenetic utility of mitochondrial gene sequences and a compilation of conserved polymerase chain reaction primers. *Annals of the Entomological Society of America* **87:** 651–701.

Sites JW, Marshall JC. 2004. Operational criteria for delimiting species. *Annual Review of Ecology, Evolution, and Systematics* **35:** 199–227.

Svavarsson J, Gudmundsson G, Brattegard T. 1993. Feeding by asellote isopods (Crustacea) on

foraminifers (Protozoa) in the deep sea. *Deep-Sea Research Part I: Oceanographic Research* **40:** 1225–1239.

Swofford DL. 2001. *PAUP*: phylogenetic analysis using parsimony (and other methods) 4.0.b5*. Sunderland: Sinauer.

Thistle D, Wilson GDF. 1987. A hydrodynamically modified, abyssal isopod fauna. *Deep-Sea Research Part A. Oceanographic Research Papers* **34:** 73–87.

Thistle D, Wilson GDF. 1996. Is the HEBBLE isopod fauna hydrodynamically modified? A second test. *Deep-Sea Research Part I: Oceanographic Research Papers* **43:** 545–554.

Wägele JW. 1989. *Evolution und phylogenetisches System der Isopoda: Stand der Forschung und neue Erkenntnisse [Evolution and phylogeny of isopods. New data and the state of affairs].* Stuttgart: E. Schweizerbart'sche Verlagsbuchhandlung.

Wasserthal LT, Seibt U. 1976. Feinstruktur, Funktion und Reinigung der antennalen Sinneshaare der Garnele *Hymenocera picta* (Gnathophyllidae). *Zeitschrift für Tierpsychologie* **42:** 186–199.

Watson D. 1992. *Contouring: A guide to the analysis and display of spatial data*. Oxford: Pergammon.

Wilson GDF. 1989. A systematic revision of the deep-sea subfamily Lipomerinae of the Isopod Crustacean family Munnopsidae. In Cox CS, Fleminger A, Kooyman GL, Rosenblatt RH, eds. *Bulletin of the Scripps Institution of Oceanography 27(67).* San Diego: University of California, 1–151.

Wilson GDF. 2008a. A review of taxonomic concepts in the Nannoniscidae (Isopoda, Asellota), with a key to the genera and a description of *Nannoniscus oblongus* Sars. *Zootaxa* **1680:** 1–24.

Wilson GDF. 2008b. Local and regional species diversity of benthic Isopoda (Crustacea) in the deep Gulf of Mexico. *Deep-Sea Research Part II: Topical Studies in Oceanography* **55:** 2634–2649.

Wilson GDF, Hessler RR. 1987. Speciation in the deep sea. *Annual Review of Ecology and Systematics*: 185–207.

Wolff T. 1962. The systematics and biology of bathyal and abyssal Isopoda Asellota. *Galathea Report* **6:** 1–320.

Wolff T. 1977. Diversity and faunal composition of the deep-sea benthos. *Nature London* **267:** 780–785.

SUPPORTING INFORMATION

Additional Supporting Information may be found in the online version of this article at the publisher's web-site:

S1. Material of ***Macrostylis daniae* sp. nov.**, ***M. sabinae* sp. nov.** and ***M. amaliae* sp. nov.** *Morphologically indistinguishable individuals of the *M. sabinae–M. amaliae* complex.
S2. CLSM micrographs of the holotypes of ***M. amaliae* sp. nov.** (ZMH K-45914) and ***M. sabinae* sp. nov.** (ZMH K-45908). A, ***M. amaliae* sp. nov.**, dorsal habitus; B, ***M. amaliae* sp. nov.**, lateral habitus; C, ***M. sabinae* sp. nov.**, dorsal habitus; D, ***M. sabinae* sp. nov.**, lateral habitus. Scale = 0.5 mm.
S3. ***Macrostylis sabinae* sp. nov.**, non-ovigerous female paratype ZMH K-45909. A, dorsal habitus; B, lateral habitus. Scale = 0.5 mm.
S4. ***Macrostylis sabinae* sp. nov.**, terminal male paratype (ZMH K-45910) mouthparts. A, left mandible medial; B, left mandible dorsal; C, left mandile ventral; D, right mandible dorsal; E, right mandible medial; F, maxillula; G, maxilla; H, maxilliped. Scale = 0.1 mm.
S5. CLSM micrograph of ***Macrostylis amaliae* sp. nov.**, male paratype (ZMH K-45917). A, dorsal habitus; B, lateral habitus; C, ventral habitus. Scale = 0.5 mm.
S6. Consensus tree of 16 individuals based on a MUSCLE alignment from 18S data. The material of ***Macrostylis daniae* sp. nov.**, ***M. sabinae* sp. nov.** and ***M. amaliae* sp. nov.** was aligned with all 18S sequences of this family available online at GenBank. *Chelator vulgaris* Hessler, 1970 served as the outgroup.

The Additional Supporting Information are printed below.

S1 was due to its size not printed here, but can be downloaded from the publishers website.

S2. CLSM micrographs of the holotypes of ***Macrostylis amaliae*** **sp. nov.** (ZMH K-45914) and ***M. sabinae*** **sp. nov.** (ZMH K-45908). A, ***M. amaliae*** **sp. nov**., dorsal habitus; B, ***M. amaliae*** **sp. nov.**, lateral habitus; C, ***M. sabinae*** **sp. nov.**, dorsal habitus; D, ***M. sabinae*** **sp. nov**., lateral habitus. Scale = 0.5 mm.

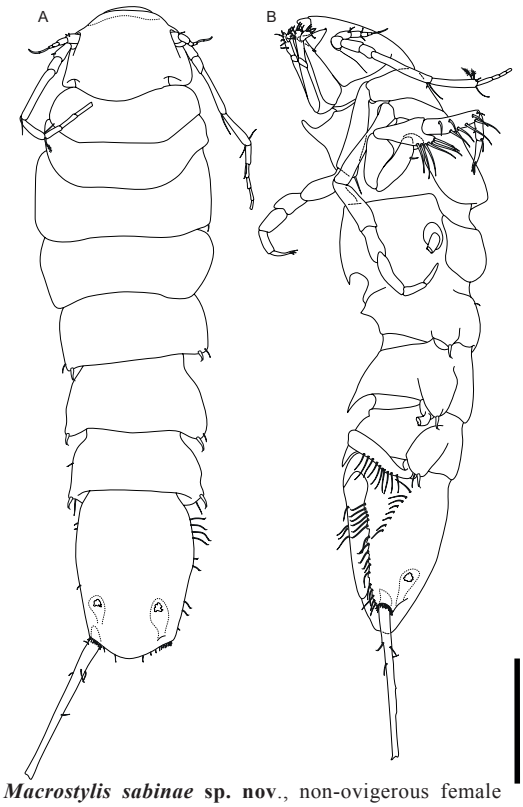

S3. ***Macrostylis sabinae*** **sp. nov**., non-ovigerous female paratype ZMH K-45909. A, dorsal habitus; B, lateral habitus. Scale = 0.5 mm.

S4. ***Macrostylis sabinae*** **sp. nov.**, terminal male paratype (ZMH K-45910) mouthparts. A, left mandible medial; B, left mandible dorsal; C, left mandile ventral; D, right mandible dorsal; E, right mandible medial; F, maxillula; G, maxilla; H, maxilliped. Scale = 0.1 mm.

S5. CLSM micrograph of ***Macrostylis amaliae* sp. nov.**, male paratype (ZMH K-45917). A, dorsal habitus; B, lateral habitus; C, ventral habitus. Scale = 0.5 mm.

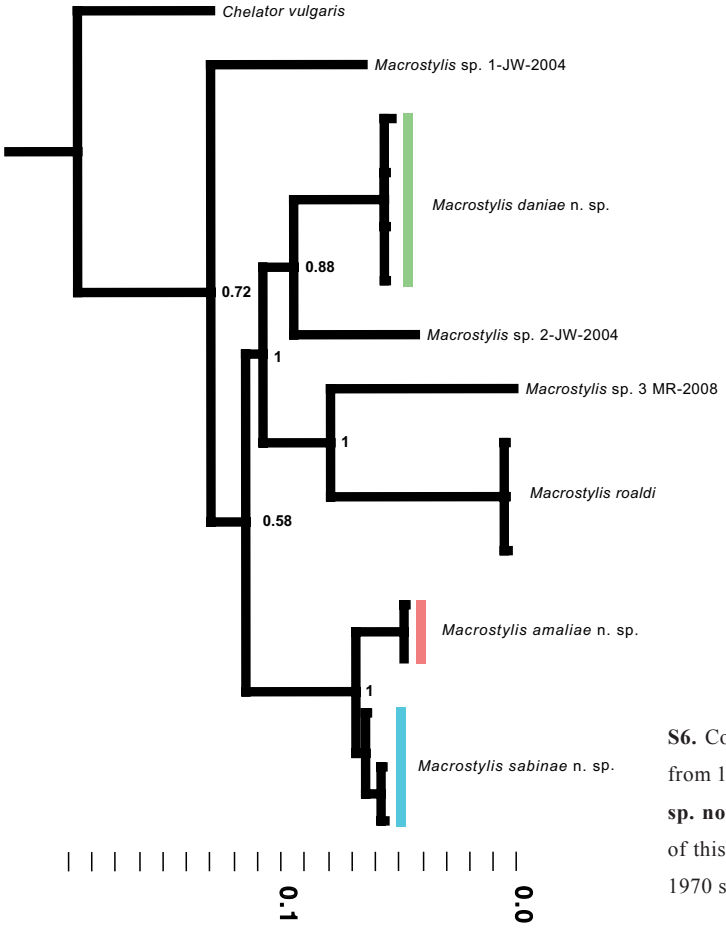

S6. Consensus tree of 16 individuals based on a MUSCLE alignment from 18S data. The material of ***Macrostylis daniae* sp. nov.**, ***M. sabinae* sp. nov.** and ***M. amaliae* sp. nov.** was aligned with all 18S sequences of this family available online at GenBank. *Chelator vulgaris* Hessler, 1970 served as the outgroup.

Author contributions

The study was designed and conducted by Simon Bober with subsequent contributions of Torben Riehl. Genetic sequences were obtained externally by a professional laboratory. Specimens were dissected and illustrated by S. Bober. The taxonomic descriptions and the key were made by S. Bober based on a taxonomic database built by T. Riehl with contributions of George D. F. Wilson. The genetical and statistical analyses were planned and conducted by S. Bober. The CLSM micrographs were made and arranged by S. Bober. The SEM micrographs were taken by S. Bober and T. Riehl with the assistance of Renate Walter. All figures were made by S. Bober. A preliminary description of *Macrostylis daniae* was part of S. Bobers master thesis.

The first draft of the manuscript was written by S. Bober with subsequent contributions of T. Riehl, Stephan Henne and Angelika Brandt.

A. Brandt had the idea for this project (KuramBio) and submitted the proposal, she was the expedition leader.

Chapter 6

An organ of equilibrium in deep-sea isopods revealed: the statocyst of Macrostylidae (Crustacea, Peracarida, Janiroidea)

Zoomorphology (2018) 137:71–82
https://doi.org/10.1007/s00435-017-0376-5

ORIGINAL PAPER

An organ of equilibrium in deep-sea isopods revealed: the statocyst of Macrostylidae (*Crustacea*, *Peracarida*, *Janiroidea*)

Simon Bober[1] · **Torben Riehl**[2] · **Angelika Brandt**[2]

Received: 14 March 2017 / Revised: 1 September 2017 / Accepted: 7 September 2017 / Published online: 21 September 2017

Abstract *Isopoda* (*Crustacea*, *Peracarida*) from the deep sea are relatively well studied but little is known about their lifestyles or the functional morphology and anatomy. The isopod family Macrostylidae, for example, is rather small in size, usually less than 1 cm in body length, and occurs mainly in the deep sea between 3000–6000 m. This family features a paired subepidermal structure on the posterior end of the pleotelson. It has been reported only in this family and was first mentioned by Hansen in 1916, who hypothesised that it represents a pair of statocysts. Nevertheless, neither the structure nor the function has been investigated until now. The shape of some related features, however, has already been used for species differentiation thus indicating that phylogenetically as well as systematically valuable information may be inherent in this feature. Here, the anatomy of this structure was studied based on four species of Macrostylidae from the North Pacific and Atlantic Oceans. It was digitally reconstructed from histological sections. The paired structure comprised two tergal invaginations, each with distinct muscular attachments and a modified seta that distally held a statocyst on the shaft. This resembles equilibrium organs reported from other organisms and thus the statocysts hypothesis seems reliable. Using energy-dispersive X-ray spectroscopy, the substance of the statolith could be determined as silicon dioxide. Based on these findings, the function of this organ and its potential phylogenetic and ecological implications are discussed.

Keywords Scanning electron microscopy (SEM) · 3D-Reconstruction · Histology · EDX · Asellota

Introduction

For a profound understanding of organisms in general, knowledge about their anatomy is fundamental. Such knowledge can aid to elucidate the evolutionary background and provide information about the general natural history and behaviour. This seems especially crucial for taxa, such as Macrostylidae Hansen, 1916 (*Peracarida*: *Isopoda*), about which almost no natural-history information is available (but see Hessler and Strömberg 1989) due to their main distribution in the deep-sea between 3000 and 6000 m (Hessler et al. 1979; Brandt et al. 2009; Riehl and Brandt 2010; Riehl 2014) and their small size between 2 and 3 mm. The isopod family Macrostylidae consist of 86 described species (Riehl and Brandt 2010, 2013; Riehl et al. 2012; Riehl and Kaiser 2012; Riehl 2014) which all belong to the genus *Macrostylis* Sars, 1864. Based on a single life observation, significant morphological similarities and sampling evidence all species of *Macrostylis* are thought to share an infaunal lifestyle (Hult 1941; Hessler and Sanders 1967; Hessler and Wilson 1983; Harrison 1989).

Macrostylidae features a unique paired subepidermal structure dorsally near the posterior end of the pleotelson and close to the uropod insertions. This feature occurs only in this family but has been identified in most species studied to date with a few exceptions (e.g. *Macrostylis setifer* Menzies, 1962b; *M. mariana* Mezhov, 1993). It is

The original version of this article was revised: Table 1 was incorrectly published in the original version and the same is corrected here.

✉ Simon Bober
simon.bober@yahoo.de

[1] Centre of Natural History (CeNak), Zoological Museum, University of Hamburg, Hamburg, Germany

[2] Department Marine Zoology, Crustacea, Senckenberg Research Institute and Natural History Museum, Senckenberganlage 25, 60325 Frankfurt, Germany

nevertheless considered, next to a long list of other character states, synapomorphic for this taxon (Riehl 2014; Riehl et al. 2014). This feature has been interpreted as "caudal organ" (Mezhov 1992), "sensory organ" (Menzies 1962b) and as a pair of statocysts (Hansen 1916; Wägele 1992) but without any morphological or physiological analyses undertaken so far that may support the hypothesis that it represents an equilibrium organ.

Statocysts are epidermal or subepidermal invaginations that contain statoliths (Purschke 1990). These may also comprise mechanoreceptive sensillae and secretory pores (Sekiguchi and Terazawa 1997). They are gravity-receptive organs (Espeel 1985) found in several aquatic animal taxa such as *Cnidaria* (Hopf and Kingsford 2013), *Cephalopoda* (Stephens and Young 1976), and *Crustacea* (Sekiguchi and Terazawa 1997). Crustacean statocysts were first mentioned in 1811, but misleadingly described as the olfactory organs (Rosenthal 1811). A static function was assigned to this organ in 1898 and the terms *statocyst* and *statolith* were established (Beer 1898). Crustacean statocysts have been described for many taxa (Cohen 1955; Dijkgraaf 1956; Neil 1975; Takahata and Hisada 1979; Hertwig et al. 1991; Wittmann et al. 1993) and for some the ultrastructure has been investigated (Kharkeevich 1983; Espeel 1985; Hertwig et al. 1991). Especially in more common species, in vivo analyses were performed (Schöne 1954, 1957; Neil 1975; Janse and Sandeman 1979; Hama et al. 2007) in order to analyse the physiological function or behavioural implications of statocysts. However, investigations on isopods are rare and virtually not existent for Macrostylidae.

Until today, neither the exact structure nor the function of this organ has been described, however, its potential homology with external cuticular features in the closely related Urstylidae has been proposed (Riehl et al. 2014). In several taxonomic descriptions, the form and orientation of a related feature has been employed in taxonomic works to delineate species (Mezhov 1992, 2003; Riehl and Brandt 2010). These "slot-like apertures" (Mezhov 2004; Riehl and Brandt 2010) or "fissure-shaped openings" (Mezhov 1992) may represent the openings of the proposed statocyst invaginations.

In vivo analyses, as performed on other crustacean taxa (Kreidl 1893; Alverdes 1926; Schöne 1954; Hama et al. 2007; Dijkgraaf 1956), are not practicable without disproportionate effort due to their deep-sea habitat. Alternatively, a morphological approach was used. The presence of this organ was analysed in the available material from museum collections of almost all described species of Macrostylidae. To clarify the anatomy of this organ, we used a classical histological sectioning approach with subsequent 3D reconstruction, scanning Electron microscopy (SEM) and energy-dispersive X-ray spectroscopy (EDX). Statocysts of five different macrostylid species were investigated in detail and compared to statocysts of other crustaceans.

Materials and methods

Samples

All 86 described species except those described by Malyutina and Kussakin (1996); Menzies and George (1972) and some of those described by Birstein (1963, 1970), which were not available at the collections in Washington DC and St. Petersburg) were studied to score the presence/absence of the paired morphological feature in each species.

Additionally, ten specimens of five species and one species complex were used for the morphological studies; this material is stored at the *Centre of Natural History* in Hamburg and is identifiable by a unique ZMH-ID. More detailed data are available in Table 1. Eight of these specimens were collected during the German/Russian KuramBio expedition (Kuril Kamchatka Biodiversity Studies) from July to September in 2012 on RV Sonne (SO223) (Brandt and Malyutina 2015; Elsner et al. 2015). One specimen was sampled in the Puerto Rico Trench during the Vema-TRANSIT (Bathymetry of the Vema-Fracture Zone and Puerto Rico TRench and Abyssal AtlaNtic BiodiverSITy Study) expedition in December 2014–January 2015. Another specimen of the species was collected in the North Atlantic during the BIOICE expedition in August 1995 (Brix et al. 2014b). The samples from the KuramBio and the Vema-TRANSIT expedition were obtained using a camera epibenthic sledge (C-EBS) (Brenke 2005; Brandt et al. 2013). During the BIOICE expedition, an R-P sledge (Rothlisberg and Pearcy 1977) was used. The samples were transferred into chilled (−20 °C) ethanol (96%) for genetic analyses or in 4% formalin solution. For sectioning, the formalin-fixed material was preferably used.

Histological sectioning

For the reconstruction of the statocyst, four individuals of three different species were investigated (Table 1). One adult female of *Macrostylis magnifica* Wolff, 1962 (ZMH-K 46401), the pleotelson of a female and a complete male of *Macrostylis curticornis* Birstein, 1963 (ZMH-K 46399, ZMH-K 46400) and one female of *Macrostylis daniae* Bober et al. in press (ZMH-K 46398) were treated for histology.

The specimens were embedded in Araldite® (Coulter 1967). After solidification, the Araldite block was mounted on a Leica RM2265 microtome with attached stereomicroscope. The specimens were cut into 1.0 µm slices using glass blades. Crustacean cuticle contains, among other compounds, amorphous calcium carbonate, calcite crystals, and magnesium calcites (Roer and

Table 1 Material examined for this study. The material is deposited at the collection of the Center of Natural History (CeNak) in Hamburg. (ZMH = collection number)

Species	ZMH-ID	Sex	Developing stage	Method	Comment	Expedition	Station	Depth (m)	Sampling date (d.m.y)	Gear	Start trawl (DD)		End trawl (DD)	
											Latitude	Longitude	Latitude	Longitude
Macrostylis daniae	ZMH-K 46398	♀	Non-ovigerous	Hist. sectioning	In Araldit, sections fixed on slides. 3D reconstruction based on this specimen	KuramBio	SO223-5-9	5376–5379	11/08/2012	C-EBS	43.5913°N	153.9647°E	43.5717°N	153.9693°E
Macrostylis curticornis	ZMH-K 46399	♀	–	Hist. sectioning	Pleotelson only, in Araldit, sections fixed on slides.	KuramBio	SO223-2-10	4859–4863	03/08/2012	C-EBS	46.226°N	155.5595°E	46.2499°N	155.5438°E
Macrostylis curticornis	ZMH-K 46400	♂	Adult	Hist. sectioning	In Araldit, sections fixed on slides.	KuramBio	SO223-10-12	5249–5262	27/08/2012	C-EBS	41.1939°N	150.0928°E	41.2169°N	150.0942°E
Macrostylis magnifica	ZMH-K 46401	♀	Non-ovigerous	Hist. sectioning	In Araldit, sections fixed on slides.	BIOICE	734	2400	30/08/1995	R-P sledge	61.1683°N	18.039°W	61.1705°N	18.0520°W
Macrostylis daniae	ZMH-K 46402	♀	–	EDX	Pleotelson only, statolith removed	KuramBio	SO223-5-10	5375–5379	11/08/2012	C-EBS	43.5912°N	153.9635°E	43.5699°N	153.9691°E
Macrostylis daniae	ZMH-K 46403	♀	Non-ovigerous	EDX	In lactic acid, statolith removed	KuramBio	SO223-5-10	5375–5379	11/08/2012	C-EBS	43.5912°N	153.9635°E	43.5699°N	153.9691°E
Macrostylis daniae	ZMH-K 46404	♀	–	EDX	Pleotelson only, in situ scan	KuramBio	SO223-2-10	4859–4863	03/08/2012	C-EBS	46.2260°N	155.5595°E	46.2499°N	155.5438°E
Macrostylis sabinae-amaliae complex	ZMH-K 46405	♀	Ovigerous	EDX	In LR-White, sections for EDX	KuramBio	SO223-10-12	5249–5262	27/08/2012	C-EBS	41.1939°N	150.0928°E	41.2169°N	150.0942°E
Macrostylis sabinae-amaliae complex	ZMH-K 46406	♀	Non-ovigerous	EDX	In LR-White, sections for EDX	KuramBio	SO223-10-12	5249–5262	27/08/2012	C-EBS	41.1939°N	150.0928°E	41.2169°N	150.0942°E
Macrostylis sp.	ZMH-K 46407	♂	Adult	EDX	w/o head, Pleotelson separated for in situ EDX	Vema TRANSIT	SO237-12-6	8336	21/01/2015	EBS	19.8100°N	66.7522°W	19.8101°N	66.7520°W
Macrostylis sabinae-amaliae complex	ZMH-K 46612	–	Manca	EDX	Statolith removed	KuramBio	SO223-11-12	2346	31/08/2012	C-EBS	40.2184°N	148.1088°E	40.2018°N	148.0923°E

Dillaman 1984; Neues et al. 2007); these materials are harmful to the glass blades. Therefore, the specimens were kept in slightly acidic milieu for 24 h. This treatment did not affect the specimens but reduced the blade abrasion. The intestine was filled up with hard substrate in all specimens. Cutting through the gut damaged the blade as well as the sections. This could be caused by foraminiferans which are thought to be a preferred diet for macrostylids and often have calcified shells (Menzies 1962a; Hessler and Strömberg 1989; Brökeland et al. 2010; Würzberg et al. 2011; Riehl et al. 2016). The crystalline statoliths were harmful for the highly sensitive glass blades of the microtome, but for most specimens cutting through the statoliths worked acceptably well. Each section was collected in a droplet aqua dest. on Histobond® adhesive microscope slides. These were subsequently dried for at least 2 h at 60 °C. The slides were stained with Tolonium chloride ((7-amino-8-methyl-phenothiazin-3-ylidene)-dimethyl-ammonium) for 1.5 min. The completely dried slides were permanently covered with coverslips using Roti®-Histokitt. The slides were digitised on a Leica DM6000B microscope using the software Leica MM AF (ver.: 1.5.0) for automated scanning and subsequent merging. *Macrostylis daniae* (ZMH-K 46398) was scanned with a 40 × lens, while the other three specimens were scanned with a 20 × lens. The digitised slides of *Macrostylis daniae* (ZMH-K 46398) were imported to Amira® (ver.: 5.2.2; Zuse Institute Berlin, FEI Visualization Sciences Group) to align the sections. All body structures relevant for this study were digitally selected in all 97 sections, to make each structure available as a volume stack. To smoothen the surfaces, these stacks were exported as object files (.obj), which served as a basic frame onto which a smooth polygon surface was modelled in Modo (ver.: 801 –service pack 2-73514; Luxology, LLC). Relevant views were rendered in Modo at a resolution of 3000 × 2000 pixels. The muscles, intestine and seta do not represent the actual colours. The anatomical measurements were accomplished with the measuring tool implemented in Amira. For mean values, at least four measurements were made and the standard deviation calculated. Measurements along the anterior–posterior axis were calculated from the number of sections and therefore have an accuracy of > 2.0 µm.

Energy-dispersive X-ray spectroscopy (EDX)

In total, six individuals were used for EDX on a Carl Zeiss Leo 1525 Scanning Electron Microscope (SEM) (Table 1).

Direct dissection of the statoliths

One specimen of *Macrostylis daniae* (ZMH-K 46403) was kept for several months in 70% EtOH with lactic acid to test if the statoliths are acid-soluble. The statoliths were dissected from this individual and another conspecific specimen (ZMH-K 46402) without the acetic treatment. Furthermore, the statolith of another individual from the *Macrostylis sabinae-amaliae* complex (Bober et al. in press) was dissected (ZMH-K 46612) (Table 1). The statolith fragments were directly placed on a carbon conductive tab. After graphite sputter-coating, the statolith fragments were analysed by EDX.

In situ dissections

The pleotelson of two specimens (*M. daniae* (ZMH-K 46404), *M.* sp. (ZMH-K 46407)) was critical point dried and directly placed on a conductive carbon tab. The statocysts were partly opened with a needle after this procedure and an EDX was performed.

In situ sections

Two individuals (*M. sabinae-amaliae* complex (ZMH-K 46405, ZMH-K 46406)) were embedded in LR-WHITE and cut in 2.0 µm sections with glass blades using a Reichert-Jung Ultracut E Ultramicrotome. The specimens were cut from posterior to anterior from the approximate position of the statocysts. The sections were collected in a droplet of aqua dest. and directly placed onto a conductive carbon tab sticking on a SEM stub. The samples were left to dry for at least 24 h, afterwards the samples were sputter-coated with graphite. The sections were investigated using a SEM. On sections comprising statolith crystals, an EDX was performed.

Results

Anatomical results

The investigations of type collections and other museum specimens revealed that the paired structure is present in all species that were studied, even those in which an absence had been claimed before (Fig. 1).

The investigated structures were found to be bilateral invaginations of the dorsal (tergal) cuticle. Each invagination formed a bulbous space with a narrow opening that was oriented posterolaterally. The statocyst cuticle and the general tergal cuticle were separated by layers of tissue in *Macrostylis daniae* (ZMH-K 46398) and *M. magnifica* (ZMH-K 46401) (Fig. 2b, d). This was not the case in *M.*

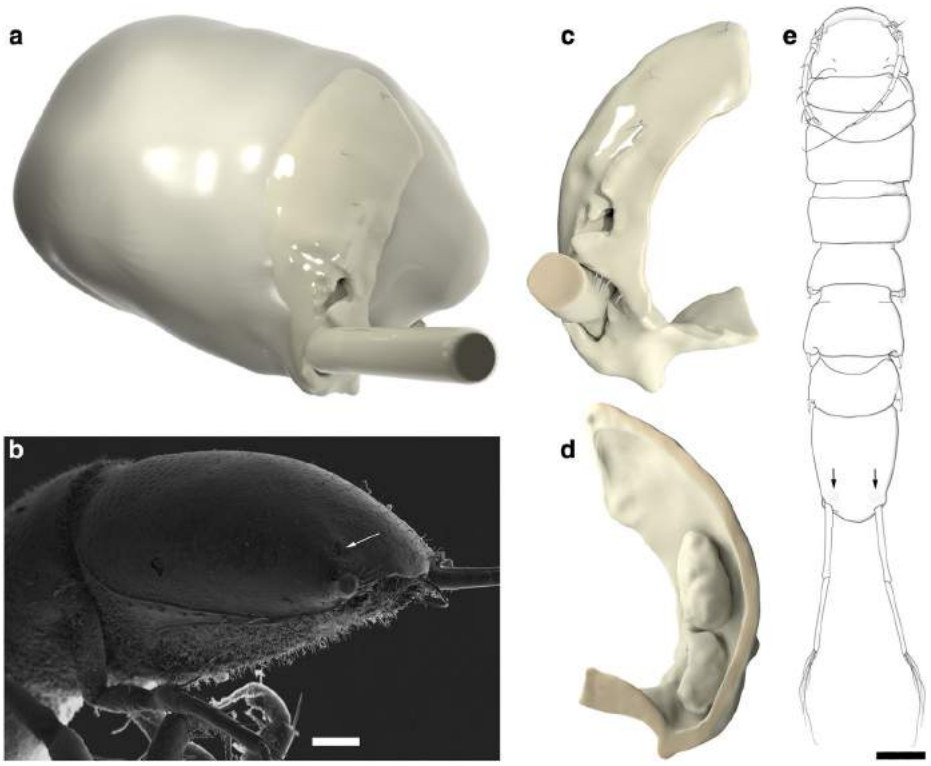

Fig. 1 *Macrostylis daniae* Bober et al. in press (ZMH-K 46398), non-ovigerous female used for 3D reconstruction. *M. daniae* (ZMH-K 45924) non-ovigerous female, SEM micrograph. **a** round the studied area for a better comparability with (**b**). **b** Pleotelson SEM scan as reference, from posterolateral. **c** Reconstruction of all cuticle parts, from posterior. The opening of the statocysts as well as the uropod is visible. **d** Reconstruction of all cuticle parts, from anterior. Statocyst invagination (upper) and uropod invagination (lower) are well visible. **e** Idealised taxonomic drawing of *M. daniae*. Scale = 75 µm (**a**, **b**); 50 µm (**c**, **d**); 25 µm (**e**)

curticornis (ZMH-K 46400), where the statocysts cuticle was found to be widely fused with the tergal cuticle (Fig. 2c). The cuticle is strong and inflexible at the opening canal, which does not comprise a closing mechanism. The lumen is consequently filled with the exterior medium. The opening of *M. curticornis* (ZMH-K 46400) featured a row of transverse setae (Fig. 2e). *Macrostylis daniae* (ZMH-K 46398) lacks these (Fig. 2f). Gland tissue that may alter the interior environment by secretion was not found. Each invagination contained a single crystalline object that was attached to the distal shaft of a seta (Fig. 3). The seta emerges dorsally and has a dorsoventral orientation. The statolith was highly fragile and collapsed easily. Dissections were thus difficult, and only small particles could be recovered. The statolith was composed of several crystalline particles cemented together, which were not acid-soluble. An EDX identified a high amount of silicon and oxygen in the particles (4b, d). Therefore, the results in all analysed species suggest silicon dioxide (SiO_2) as main component of the statolith. The cuticle of the invagination was of similar material as the external cuticle (Fig. 2), but except for the opening canal the cuticle was thinner. While the external tergal cuticle had a mean thickness of 7.79 (± 1.33) µm, the thickness of the statocyst cuticle averaged 1.69 (± 0.30) µm. The statocyst reached 85 µm anteriorly into the body. The main cavity, which holds the statolith, had an approximate dimension of 46.30 (± 5.54) µm in width and 76.84 (± 6.05) µm in height. The statolith itself was measured dorsoventrally with a maximum extent of 33.57 (± 4.30) µm and a maximal transversal diameter of 23 µm × 26.10 (± 4.31) µm. The seta had a length of approximately 31 µm and three quarters of the shaft were covered by the statolith (Figs. 2a–d; 3). The statocyst entrance had a maximum diameter of 11.36 µm at the opening, and a minimum diameter of 1.87 µm at the most narrow passage. The inner cuticle showed a few tiny outward pointed spike-like protrusions in multiple slides (Fig. 2f). The statocyst body was surrounded by a cell layer (Fig. 2a, b, d, f).

Muscles

In *Macrostylis daniae*, 14 muscles were found in close proximity or direct connection with one statocyst. This is a bilateral symmetric organ resulting in a total of 28 muscles in one individual. These muscles were sorted into three major groups according to their attachment positions:

Intestine-statocyst muscles M1–M9 (Fig. 3c)

This group includes nine muscles (M1–M9), which extent from the statocyst to the intestine. M2–M9 are directly connected with the statocyst and intestine, while M1 has only a connection to the intestine and inserts in M2. The muscles of this group are predominantly inserting at the basis of the statocysts cuticle. The cuticle is relatively thick

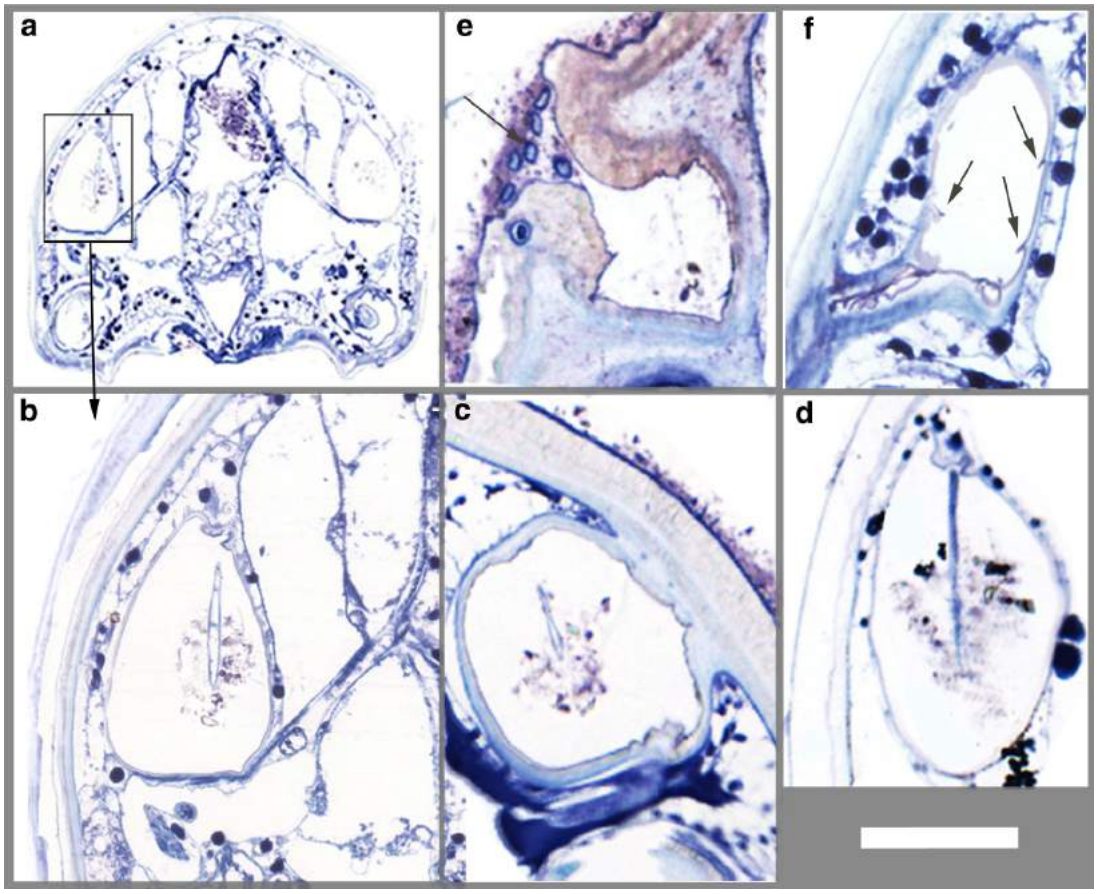

Fig. 2 Histological sections through the statocyst from various species. **a** Full section of *Macrostylis daniae* Bober et al. in press (ZMH-K 46398), the boxed area is seen in **b** with a higher magnification. **b** Detailed scan of the statocyst from *M. daniae,* the seta and statolith are visible. **c** Section of the statocyst from *M. curticornis* Birstein 1973 (ZMH-K 46400) at approximately the same position as *M. daniae* (ZMH-K 46398) (**b**); the seta and statolith are visible as well, but the statocysts cuticle is fused with the tergal cuticle. **d** Section of the statocyst from *M. magnifica* Wolff 1962 (ZMH-K 46401) at approximately the same position as **b** and **c**; the seta and statolith are visible. **e** Detail of the opening canal in *M. curticornis*, in opposite to *M. daniae* (ZMH-K 46398) a row of strong setae is covering the opening (arrow). **f** Detail of the statocyst from *Macrostylis daniae* (ZMH-K 46398) near its opening. Visible are the spike-like protrusions (arrows) and the double-layered cuticle. Scale = 50 µm (**b**–**f**); 130 µm (**a**)

in the region of muscular attachment and ranges from 3.57 to 5.33 µm. Close to the statocyst entrance, the ventrolateral statocyst cuticle walls lay on top of each other and provide a thickness of 8.52 µm.

Uropod-statocyst muscles M13–M14 (Fig. 3d)

Two muscles (M13, M14) contribute to this group. Only M14 is directly connecting the statocyst and the uropodal insertion. M13 is inserting into M2 and M14 fuses partly with M12.

Cuticle-statocyst muscles M10–M12 (Fig. 3e)

Three muscles (M10–M12) are connected with the tergal cuticle. Only M12 and M10 are directly connecting statocyst and cuticle. M11 inserts into M10 and is not directly attached to the statocyst. In contrast to the muscles of the former group, these muscles are attached to the ventromedial side of the statocyst where the cuticle is fairly thin. The tergal cuticle, on the other hand, is relatively thick in the region of muscular attachment (12.24 µm compared to an average tergal thickness of 7.79 (±1.33) µm).

Discussion

There have not been any studies on the ultrastructure or composition of macrostylid statocysts so far. This is surprising because of the unique organs location in Macrostylidae. In most other known crustaceans that have evolved statocysts, their position is either in the basis of the first antenna (e.g. *Astacidea*), the cephalon (e.g. *Amphipoda*) or in the uropods (e.g. *Mysidacea*) and may be an

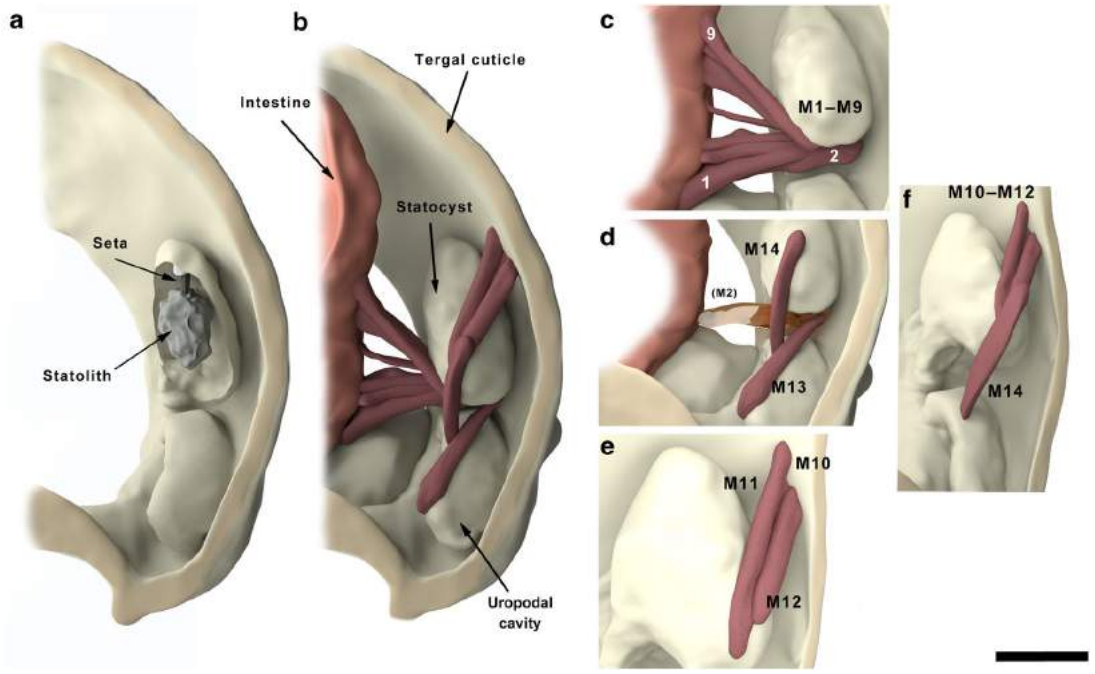

Fig. 3 3D reconstruction of the statocyst and all involved muscles; *Macrostylis daniae* Bober et al. in press (ZMH-K 46398), non-ovigerous female. The colours do not reflect actual colours. **a** The statocyst was opened to see the statoliths internal organisation. **b** Overview of the whole reconstruction and all 14 muscles involved. **c** Intestine-statocyst muscle group, M1–M9 emerge on the base of the statocyst and attach on the intestine. **d** Uropod-statocyst muscle group, M13 is terminally attached to the uropod invagination and inserts in M2 (transparent). M14 is basally attached on the uropod invagination and attaches on the statocyst. **e** The cuticle-statocyst muscle group (M10–M12) ranges from the statocyst to the tergal cuticle. **f** The statocyst-muscle complex that might directly influence the statocyst. Scale = 50 µm (**a**–**d**, **f**); 35 µm (**e**)

ectodermal invagination with a persisting opening to the surrounding environment (e.g. Cohen 1955) as in macrostylidae or an internal closed vacuole-like structure (e.g. Espeel 1985). In every case, the statocysts contain statoliths, which may be formed from a single crystalline structure, or from several such crystals (Sekiguchi and Terazawa 1997) this was found to be true for macrostylidae. The statolith can either be comprised of external material (Milne Edwards 1837), such as sediment particles (see Discussion: Statoliths), or is excreted by the animal itself (Neil 1975). Mixed forms may exist as well.

For isopod statocysts, only two detailed publications are available to date. These were performed on the cymothoid family Anthuridae Leach 1814 (Langenbuch 1928; Rose and Stokes 1981). Anthuridae are not closely related to Macrostylidae, but the general appearance and location of the macrostylid statocysts are similar to those found in the anthurid isopod *Cyathura polita* Stimpson, 1886, yet there are some major differences (Rose and Stokes 1981) that contradict a common origin. *C. polita* have three setae, whereas Macrostylidae have one seta in their statocysts. The statoliths of Macrostylidae are composed of silicon dioxide crystals glued together by an unidentified agent and not of calcium salt crystals as in *C. polita*. The position of the statolith setae is different in both taxa. In *C. polita*, the setae articulate ventrally and point towards dorsally. The opposite is the case in Macrostylidae where the seta is articulating dorsally and points downwards. The setae in *C. polita* are bifurcate which could not be verified for any of the tested Macrostylidae where the shaft seems to be simple. However, this information might have been lost during the sectioning and needs further investigation. The attached musculature is different in these two families as well. Only one muscle that is attached to the statocyst has been identified in Anthuridae (Rose and Stokes 1981). This muscle was described as the third tail flexor muscle and might be used for relocating the statocyst within the body and modify the signal from the statocyst (Rose and Stokes 1981). For Macrostylidae, fourteen different muscles were found. The exact function of these muscles could not be clarified during this study.

We assume that statocysts as gravity-receptive organs assist Macrostylidae to maintain spatial orientation, for instance within the sediment or in the water column. Next to the hypothesised predominant endobenthic lifestyle that macrostylids lead (Hessler and Strömberg 1989; Wägele 1989; Riehl et al. 2014), it has been proposed that drifting along with deep-sea currents may provide means of long-

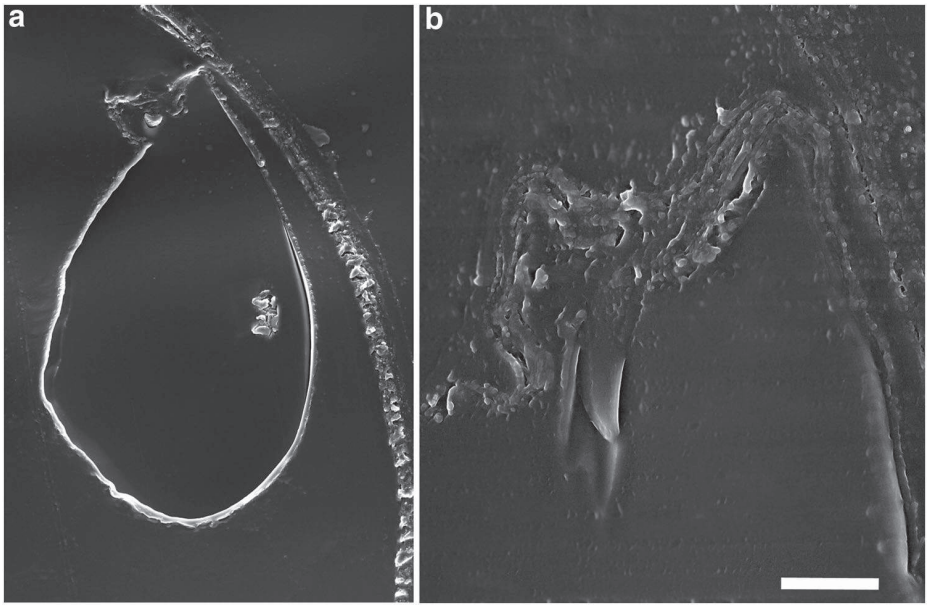

Fig. 4 Statocyst of one specimen from the *Macrostylis sabinae-amaliae* complex, non-ovigerous female (ZMH-K 46406), histological sagittal sections; SEM micrograph. **a** section through the statocyst, statolith and seta articulation. **b** Section through the statocyst seta. Scale = 10 µm (**a**); 3 µm (**b**)

range dispersal in these and other isopod groups (Brix et al. 2011, 2014a; Riehl and Kaiser 2012). While adaptations to active means of swimming have not been discovered, the statocysts may play a role for gravity perception in the water column as well.

Muscles of the macrostylid statocysts

The ethanol fixation used for the analysed specimens is thought to optimise the possibility for genetic analyses; it, however, affects the soft tissues by dehydration and thereby causes shrinking. Especially, the muscle tissue may have changed in volume from this fixation and therefore the volume of the muscles shown may not reflect their natural extend. However, the attachment points were comprehensible. The function of the muscles M1–M9 (Fig. 3c) is potentially limited to manipulating the intestine. M2–M9 are attached basally near the opening of the statocyst, where the cuticle is relatively thick and thus probably inflexible. The intestine on the other hand is of soft tissue and therefore likely to be the moving part. M13–M14 (Fig. 3d) and M10–M12 (Fig. 3e) are probably interacting actively with the statocyst. However, M13 is an exception, it is probably not manipulating the statocyst as it has no direct connection to it but instead emerges from M2 (Fig. 3d) and is attached to the terminal soft part of the uropod articulation. It is, therefore, more likely involved in the movement of the uropod. M14 is also attached to the uropod insertion but as opposed to M13 (Fig. 3d), it is basally attached, where the cuticle is strong and inserts terminally on the statocyst, where the cuticle is thin. This implies that the statocyst itself might be relocated or deformed by the muscles tension. But a functional unit between the statocyst and uropod is imaginable. A direct linkage between statocyst and uropod function was shown in the freshwater crayfish species *Procambarus clarkii* Girard, 1852 by (Yoshino et al. 1980). The contraction of M14 (Fig. 3d) might cause a posteroventral movement or a contraction of the statocyst. M10–M12 (Fig. 3e) seem to be solely interacting with the statocyst. All three muscles are attached to the tergal cuticle anterolaterally to the statocyst itself. The cuticle is noticeably thicker (>30%) where these muscles attach compared to its average thickness. M10 is inserting into M11 (Fig. 3e). M10–M12 are attached to the same area on the statocyst to which M14 is attached (Fig. 3f). M12 seems to fuse with M14 at the point of attachment (Fig. 3f). While M14 might perform a posteroventral manipulation, M10–M12 could perform an anterolateral manipulation. The concept of a moveable non-static statocyst was already mentioned by Rose and Stokes (1981) for Anthuridae. However except for the possible relocation of the statocyst for extended sensing, the muscles might furthermore become relevant as a deforming movement for statolith forming or during moulting when the statolith, the seta and the cuticle are replaced.

Statoliths

Due to a difficult process of statolith dissections, the origin of the particles was not perfectly traceable. An EDX "blind shot" into a violently opened statocyst was

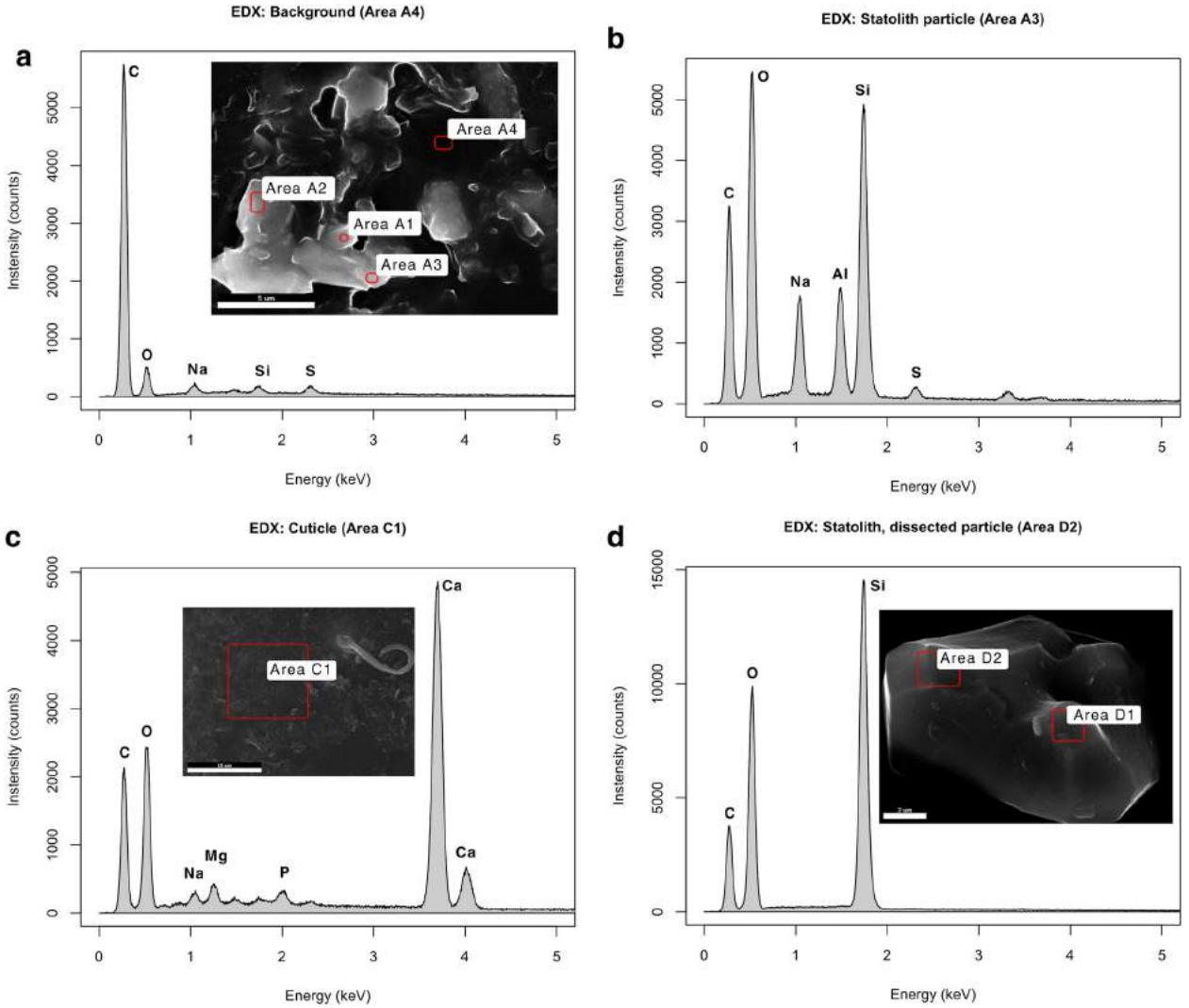

Fig. 5 EDX analyses of the statolith from one specimen of the *Macrostylis sabinae-amaliae* complex non-ovigerous female (ZMH-K 46406). **a** Background EDX scan as reference (Area A4), carbon (C) is dominating the sample due to the carbon coating necessary for this analysis. **b** EDX analysis of a statolith particle from **a** Area A3. Silicon (Si) and oxygen (O) are clearly dominating the sample. **c** EDX analysis of the outer cuticle as a reference. A high amount of calcium (Ca) was detected; *Macrostylis* sp. (ZMH-K 46407). **d** EDX analysis of a dissected statolith particle; apart from the carbon coating, only silicon (Si) and oxygen (O) were detected. Note the crystalline structure; *M.* sp. (ZMH-K 46403)

consistent with previous results, but still the origin of the signal was uncertain. The histological sections used for the 3D reconstruction revealed single crystals in situ, perfectly preserved by the fixation in araldite resin (Fig. 2a–d). Based on that observation, two further specimens (ZMH-K 46405, ZMH-K 46406) were fixed in LR-White resin and cut in 2-µm sections. In multiple sections, the crystals (Fig. 4a) and also the seta were found, which seems to have an internal canal (Fig. 4b). An EDX was now used to identify the statolith particles in situ. The composite statolith of Macrostylidae is composed of small silicon-dioxide particles that are bond by an unidentified agent. Silicon-dioxide is commonly found in nature as quartz and is usually the main component of sand. In crustacean that actively excretes the statolith, it was repeatedly observed to be build from calcium (Rose and Stokes 1981; Steele 1984). Macrostylidae as a predominantly deep-sea family can be affected by the carbonate compensation depth, which would affect the excretion of calcium salts. The main component of the cuticle, however, is calcium (Fig. 5c). As a reference only the background (carbon conductive tab) was measured with an expected high amount of carbon (Fig. 5a) from the process of carbon coating and

the carbon conductive tab itself. We conclude that the statolith of Macrostylidae is made of external materials, cemented together. In all seven specimens of multiple species and from globally different locations, the statolith was built from presumably sand grains. With seven specimens, it is difficult to state whether they are specifically targeting sand grains or if in the absence of sand other hard structures are alternatively taken. But for now, it seems convincing that sand grains are preferably taken. As an epidermal invagination, the statolith should have to be replaced after each moult. Our investigations imply that Macrostylidae after every moult are actively collecting particles (sand grains in this case) from its environment to build a new statolith; this behaviour was observed in other crustacean groups before (Milne Edwards 1837; Kreidl 1893; Hertwig et al. 1991). The particles are probably replaced immediately after each moult when the cuticle is still soft. With the methods used it was not possible to identify the substance used to cement the particles together. After this successful approach, analysing sections with an EDX seems to be a valuable method for future scientific issues as well. But it should be stated here that soft tissues are almost invisible after the carbon coating of the section.

Phylogenetic an taxonomic implications

The statocyst might serve as a valuable character for the phylogeny of Macrostylidae. In this study, the statocysts of five species were compared. In *M. curticornis,* the statocyst body is widely fused with the tergal cuticle (Fig. 2c). This is unique among all investigated species and is an evidence for alternate organisations in macrostylid statocysts. Furthermore, the statocyst opening is covered by strong setae, which was not found in the other species investigated. Also the statocysts differed strongly by their shape in cross sections, but this could be affected by the animal itself, depending on the muscle tension. And it might be a secondary effect from dehydration in ethanol, too. However, the observations show that statocysts are not identically organised in all macrostylid isopods and therefore potentially harbour characters useful for phylogenetic investigations. Due to the internal location, a proper inspection of statocysts is time consuming and therefore probably not conceivable as a source of standard taxonomic characters, but it adds a further aspect to evaluate the evolution of Macrostylidae and should therefore be considered a valuable phylogenetic character.

The recently described family Urstylidae is the sister taxon to Macrostylidae (Riehl et al. 2014). Statocysts have not been described for this family. *Urstylis zapiola* Riehl et al. 2014, however, have cuticular tubercles filled with crystalline structure, which might be statocysts as well. *Urstylis solicopia* Riehl et al. 2014, on the other hand, has conspicuous setae at the positions where Macrostylidae have statocysts. This could give an indication on the evolution of macrostylid statocysts or this kind of statocysts in general. The last common ancestor of both families might have had a similar state as *Urstylis solicopia* Riehl et al. 2014 has, to date. The exposed elevated broom setae of *Urstylis solicopia* are most likely involved in detecting water movements. A shift to a less exposed seta for living within the sediment is imaginable. The fully protected seta within a statocyst lumen is an evolutive consequence. The ancestor of Macrostylidae might have developed an invagination of that region, and the external seta became an internal statocyst seta. This shift might have been induced by a shift to a more infaunal mode of life.

Acknowledgements The captain and crew of R/V Sonne and R/V Bjarni Sæmundssonduring during the cruises SO223, SO237 and BIOICE B-13-95 are thanked for their great job and guaranteeing successful campaigns. Nils Brenke, Enrico Schwabe, Nikolaus Elsner, Marina Malyutina, Saskia Brix, Sarah Schnurr, Jörundur Svavarsson, and all involved in gear deployment, sieving, and sample sorting are acknowledged for their efforts. Macrostylid material was made available to Torben Riehl by Chad T. Walter if the National Museum of Natural History of the Smithsonian Institution, Washington D.C., by Christine Lebeau of the American Museum of Natural History, New York City, C. Oliver Coleman of the Museum für Naturkunde, Berlin, Miranda Lowe of the Natural History Museum, London, Åse Wilhelmsen of the Natural History Museum, Oslo, Jørgen Olesen of the Natural History Museum of Denmark, Copenhagen, Gerdes Research Group, Kathrin Phillips Bussau and Petra Wagner of the Center of Natural History Hamburg, George D.F. (Buz) Wilson and Stephen Keable, Australian Museum, Sydney, Dmitry Ivanov of the Zoological Museum of the Moscow State University with the kind help of Nataliya Budaeva, and by Sadie Mills, NIWA, Wellington. Very special thanks goes to Renate Walter who kindly operated the SEM and Sabine Gaude who prepared the histological sections for the EDX. The work of two anonymous reviewers is kindly acknowledged. This work was realised within the project Vema-TRANSIT, which received funding from the German Federal Ministry for Education and Research (BMBF) under grant no 03G0237A.

References

Alverdes F (1926) Stato-, Photo- und Tangoreaktionen bei zwei Garneelenarten. Z F vergl Physiologie 4:699–765. doi:10.1007/BF00342381

Beer DT (1898) Vergleichend-physiologische Studien zur Statocystenfunction. Pflüger, Arch 73:1–41. doi:10.1007/BF01666178

Birstein JA (1963) Deep Sea Isopod Crustaceans of the Northwestern Part of the Pacific Ocean. Institute of Oceanology, Academy of Sciences, USSR, Moscow

Birstein JA (1970) New Crustacea Isopoda from the Kurile-Kamchatka Trench area. In: Bogorov VG (ed) Fauna of the Kurile-Kamchatka Trench and its environment. Academy of Sciences of the USSR, Moscow, pp 308–356

Birstein JA (1973) Deep water isopods (Crustacea. Isopoda) of the north-western part of the Pacific Ocean—Translated from Birstein 1963. Akademiya Nauk, SSSR, Moscow

Bober S, Riehl T, Henne S, Brandt A (in press) New Macrostylidae (Isopoda) from the Northwest Pacific Basin described by means of integrative taxonomy with reference to geographical barriers in the abyss. Zool J Linn Soc 1–53. doi:10.1093/zoolinnean/zlx042

Brandt A, Malyutina MV (2015) The German-Russian deep-sea expedition KuramBio (Kurile Kamchatka biodiversity studies) on board of the RV Sonne in 2012 following the footsteps of the legendary expeditions with RV Vityaz. Deep Sea Res Part II 111:1–9. doi:10.1016/j.dsr2.2014.11.001

Brandt A, Linse K, Schüller M (2009) Bathymetric distribution patterns of Southern Ocean macrofaunal taxa: bivalvia, Gastropoda, Isopoda and Polychaeta. Deep Sea Res Part I 56:2013–2025. doi:10.1016/j.dsr.2009.06.007

Brandt A, Elsner N, Brenke N et al (2013) Epifauna of the Sea of Japan collected via a new epibenthic sledge equipped with camera and environmental sensor systems. Deep Sea Res Part II 86–87:43–55. doi:10.1016/j.dsr2.2012.07.039

Brenke N (2005) An epibenthic sledge for operations on marine soft bottom and bedrock. Mar Technol Soci J 39:10–21. doi:10.4031/002533205787444015

Brix S, Riehl T, Leese F (2011) First genetic data for *Haploniscus rostratus* and *Haploniscus unicornis* from neighbouring deep-sea basins in the South Atlantic. Zootaxa. doi 2838:79–84

Brix S, Leese F, Riehl T, Kihara TC (2014a) A new genus and new species of Desmosomatidae Sars, 1897 (Isopoda) from the eastern South Atlantic abyss described by means of integrative taxonomy. Mar Biodivers 45:7–61

Brix S, Meißner K, Stransky B, et al (2014b) The IceAGE Project—a follow up of BIOICE

Brökeland W, Guðmundsson G, Svavarsson J (2010) Diet of four species of deep-sea isopods (Crustacea: malacostraca: Peracarida) in the South Atlantic and the Southern Ocean. Mar Biol 157:177–187. doi:10.1007/s00227-009-1308-9

Cohen MJ (1955) The function of receptors in the statocyst of the lobster *Homarus americanus*. J Physiol 130:9–34

Coulter HD (1967) Rapid and improved methods for embedding biological tissues in Epon 812 and Araldite 502. J Ultrastruct Res 20:346–355. doi:10.1016/S0022-5320(67)80104-7

Dijkgraaf S (1956) Structure and functions of the statocyst in crabs. Experientia 12:394–396. doi:10.1007/BF02157289

Elsner NO, Malyutina MV, Golovan OA et al (2015) Deep down: isopod biodiversity of the Kuril-Kamchatka abyssal area including a comparison with data of previous expeditions of the RV Vityaz. Deep Sea Res Part II 111:210–219. doi:10.1016/j.dsr2.2014.08.007

Espeel M (1985) Fine structure of the statocyst sensilla of the mysid shrimp *Neomysis integer* (Leach, 1814) (Crustacea, Mysidacea). J Morphol 186:149–165. doi:10.1002/jmor.1051860203

Hama N, Tsuchida Y, Takahata M (2007) Behavioral context-dependent modulation of descending statocyst pathways during free walking, as revealed by optical telemetry in crayfish. J Exp Biol 210:2199–2211. doi:10.1242/jeb.002865

Hansen HJ (1916) Crustacea Malacostraca: the order Isopoda. Dan Ingolf Exped 3:1–262

Harrison K (1989) Are deep-sea asellote isopods infaunal or epifaunal. Crustaceana (Leiden) 56:317–319

Hertwig I, Schneider H, Hentschel J (1991) Light- and electron-microscopic analysis of the statocyst of the American crayfish *Orconectes limosus* (Crustacea, Decapoda). Zoomorphology 110:189–202. doi:10.1007/BF01633003

Hessler RR, Sanders H (1967) Faunal diversity in the deep-sea. Deep Sea Res Oceanogr Abstr 14:65–78. doi:10.1016/0011-7471(67)90029-0

Hessler RR, Strömberg J-O (1989) Behavior of janiroidean isopods (Asellota), with special reference to deep sea genera. Sarsia 74:145–159

Hessler RR, Wilson GDF (1983) The origin and biogeography of malacostracan crustaceans in the deep sea. In: Sims RW, Price JH, Whalley PES (eds) Evolution, time, and space: the emergence of the biosphere. Academic Press, London, pp 227–254

Hessler RR, Wilson GDF, Thistle D (1979) The deep-sea isopods: a biogeographic and phylogenetic overview. Sarsia 64:67–75. doi:10.1080/00364827.1979.10411365

Hopf JK, Kingsford MJ (2013) The utility of statoliths and bell size to elucidate age and condition of a scyphomedusa (*Cassiopea* sp.). Mar Biol (Berlin) 160:951–960

Hult J (1941) On soft-bottom Isopods of the Skager Rak. Zoologiska Bidrag fran Uppsala 1–236

Janse C, Sandeman DC (1979) The role of the fluid-filled balance organs in the induction of phase and gain in the compensatory eye reflex of the crab Scylla serrata. J Comp Physiol 130:95–100. doi:10.1007/BF00611044

Kharkeevich TA (1983) Ultrastructure du statocyste de *Mysis oculata* (Mysidacea Crustacea) Ultrastructure of the statocyst of *Mysis oculata* (Mysidacea, Crustacea). Citologiâ 25:1145–1152

Kreidl A (1893) Versuche an Krebsen. In: Weitere Beitrage zur Physiologie der Ohrlabyrinthes. Sitzungsberichte Akademie Wien, pp 149–174

Langenbuch R (1928) Ueber die Statocysten einiger Crustaceen. I. Cyathura. II. Ampelisca. Zoologische Jahrbuecher Jena Allgemeine Zoologie 575–622

Leach WE (1814) Crustaceology. Brewster's Edinburgh Encyclopedia 7:383–437

Malyutina MV, Kussakin OG (1996) Addition to the Polar Sea bathyal and abyssal Isopoda (Crustacea). Part 1. Anthuridea, Valvifera, Asellota (Ischnomesidae, Macrostylidae, Nannoniscidae). Zoosystematica Rossica 4:49–62

Menzies RJ (1962a) On the food and feeding habits of abyssal organisms as exemplified by the *Isopoda*. Int Revue ges Hydrobiol Hydrogr 47:339–358. doi:10.1002/iroh.19620470303

Menzies RJ (1962b) The isopods of abyssal depths in the Atlantic Ocean. In: Barnard JL, Menzies RJ, Bacescu MC (eds) Abyssal Crustacea. Columbia University Press, New York, pp 79–206

Menzies RJ, George RY (1972) Isopod Crustacea of the Peru-Chile Trench. Anton Bruun Report 9:1–124

Mezhov BV (1992) Two new species of the genus *Macrostylis* G.O.Sars, 1864 (Crustacea Isopoda Asellota Macrostylidae from the Antarctic. Arthropoda Selecta 1:83–87

Mezhov B (1993) Three new species of Macrostylis GO Sars, 1864 (Crustacea Isopoda Asellota Macrostylidae) from the Pacific Ocean. Arthropoda Selecta 2:3–9

Mezhov B (2003) Three new species of the genus *Macrostylis* GO SARS, 1864 (Crustacea: isopoda: Macrostylidae) from the Indian Ocean. Arthropoda Selecta 12:95–100

Mezhov BV (2004) New species of the genus *Macrostylis* G.O. Sars, 1864 (Crustacea: Isopoda: Macrostylidae) from the abyssal and ultraabyssal zones of the Indian Ocean

Milne Edwards H (1837) Histoire naturelle des Crustacés, comprenant l'anatomie, la physiologie et la classification de ces animaux. Librairie encyclopédique de Roret, Paris

Neil DM (1975) The mechanism of statocyst operation in the mysid shrimp *Praunus flexuosus*. J Exp Biol 62:685–700

Neues F, Ziegler A, Epple M (2007) The composition of the mineralized cuticle in marine and terrestrial isopods: a comparative study. CrystEngComm 9(12):1245–1251

Purschke G (1990) Ultrastructure of the "statocysts" in *Protodrilus* species (Polychaeta): reconstruction of the cellular organization with morphometric data from receptor cells. Zoomorphology 110:91–104. doi:10.1007/BF01632815

Riehl T (2014) A phylogenetic approach to the classification of macrostylid isopods and faunal linkages between the deep sea

and shallow-water environments. Unpublished Dissertation, University of Hamburg
Riehl T, Brandt A (2010) Descriptions of two new species in the genus *Macrostylis* Sars, 1864 (Isopoda, Asellota, Macrostylidae) from the Weddell Sea (Southern Ocean), with a synonymisation of the genus *Desmostylis* Brandt, 1992 with *Macrostylis*. ZooKeys 57:9–49. doi:10.3897/zookeys.57.310
Riehl T, Brandt A (2013) Southern Ocean Macrostylidae reviewed with a key to the species and new descriptions from Maud Rise. Zootaxa 3692:160–203
Riehl T, Kaiser S (2012) Conquered from the deep sea? a new deep-sea isopod species from the antarctic shelf shows pattern of recent colonization. PLoS ONE 7:e49354. doi:10.1371/journal.pone.0049354
Riehl T, Wilson GDF, Hessler RR (2012) New Macrostylidae Hansen, 1916 (*Crustacea: isopoda*) from the Gay Head-Bermuda transect with special consideration of sexual dimorphism. Zootaxa 3277(1):1–26
Riehl T, Wilson GDF, Malyutina MV (2014) Urstylidae—a new family of abyssal isopods (*Crustacea: asellota*) and its phylogenetic implications: A New Family of Higher Janiroidea. Zoolog J Linn Soci 170:245–296. doi:10.1111/zoj.12104
Riehl T, Bober S, Voltski I et al (2016) Caught in the act: an abyssal isopod collected while feeding on Komokiaceae. Mar Biodivers. doi:10.1007/s12526-016-0606-y
Roer R, Dillaman R (1984) The structure and calcification of the crustacean cuticle. AmerZool 24:893–909
Rose RD, Stokes DR (1981) A crustacean statocyst with only three hairs: light and scanning electron microscopy. J Morphol 169:21–28. doi:10.1002/jmor.1051690103
Rosenthal (1811) Über den Geruchssinn der Insekten ARCHIV FUR DIE PHYSIOLOGIE
Rothlisberg PC, Pearcy WG (1977) An epibenthic sampler used to study the ontogeny of vertical migration of *Pandalus jordani* (*Decapoda*, *Caridea*—Fishery Bulletin. National Oceanographic and Atmospheric Administration of the United States 74:994–997
Sars GO (1864) Om en anomal Gruppe af Isopoder. In: Forhandhlinger Videnskapsselskapet I Kristiania. 205–221
Schöne H (1954) Statozystenfunktion und statische Lageorientierung bei dekapoden Krebsen. Z Vergl Physiol 36:241–260. doi:10.1007/BF00298215
Schöne H (1957) Kurssteuerung Mittels der Statocysten (Messungen an Krebsen). Zeitschrift für vergleichende Physiologie 39:235–240. doi:10.1007/BF00340427
Sekiguchi H, Terazawa T (1997) Statocyst of *Jasus edwardsii pueruli* (Crustacea, Palinuridae), with a review of crustacean statocysts. Mar Freshw Res 48:715. doi:10.1071/MF97131
Steele VJ (1984) Morphology and ultrastructure of the organ of Bellonci in the marine amphipod *Gammarus setosus*. J Morphol 181:97–131
Stephens P, Young J (1976) The statocyst of *Vampyroteuthis infernalis* (Mollusca: cephalopoda). J Zool London 180:565–588
Takahata M, Hisada M (1979) Functional polarization of statocyst receptors in the crayfish *Procambarus clarkii* Girard. J Comp Physiol 130:201–207. doi:10.1007/BF00614606
Wägele JW (1989) Evolution und phylogenetisches System der Isopoda: Stand der Forschung und neue Erkenntnisse [Evolution and phylogeny of isopods. New data and the state of affairs]. E. Schweizerbart'sche Verlagsbuchhandlung, Stuttgart
Wägele JW (1992) Isopoda. In: Harrison FW, Humes AG (eds) Microscopic anatomy of invertebrates, 9th edn. Wiley-Liss, New York, pp 529–618
Wittmann KJ, Schlacher TA, Ariani AP (1993) Structure of recent and fossil mysid statoliths (Crustacea, Mysidacea). J Morphol 215:31–49. doi:10.1002/jmor.1052150103
Wolff T (1962) The systematics and biology of bathyal and abyssal Isopoda Asellota. Galathea Rep 6:1–320
Würzberg L, Peters J, Brandt A (2011) Fatty acid patterns of Southern Ocean shelf and deep sea peracarid crustaceans and a possible food source, foraminiferans. Deep Sea Res Part II 58:2027–2035. doi:10.1016/j.dsr2.2011.05.013
Yoshino M, Takahata M, Hisada M (1980) Statocyst control of the uropod movement in response to body rolling in crayfish. J Comp Physiol 139:243–250. doi:10.1007/BF00657085

Author contributions

The study was designed and conducted by Simon Bober with subsequent contributions of Torben Riehl.

This publication is based on the master thesis of S. Bober, in which the 3D-reconstruction was done. Additional histological preparations were performed by S. Bober. The histological sectioning was done by S. Bober and Sabine Gaude. The EDX analysis was performed by S. Bober with assistance of Renate Walter and S. Gaude. All figures were arranged by S. Bober. The first draft of the manuscript was written by S. Bober with subsequent contributions of T. Riehl and Angelika Brandt.

Chapter 7

Caught in the act:
an abyssal isopod collected while feeding on Komokiaceae

Mar Biodiv
DOI 10.1007/s12526-016-0606-y

SENCKENBERG

OCEANARIUM

Caught in the act: an abyssal isopod collected while feeding on Komokiaceae

Torben Riehl[1] · **Simon Bober**[1] · **Ivan Voltski**[2] · **Marina V. Malyutina**[3] · **Angelika Brandt**[1]

Received: 1 March 2016 / Revised: 10 November 2016 / Accepted: 14 November 2016

Protists such as Komokiaceae represent a huge, unexplored diversity in the abyss (Gooday et al. 1992). They likely play a key role in the food web and structuring of deep-sea benthos (Sokolova 1972), where isopods are abundant and diverse. Deep-sea isopods were initially classified as detritus feeders, but gut-content analyses (e.g. Svavarsson et al. 1993) revealed tests of hard-shelled Foraminifera, suggesting that some isopods, additionally or instead, prey upon protists. Isopod foraminiferivory was inferred also by means of fatty acid biomarkers (Würzberg et al. 2011). However, in a diverse taxon like Isopoda, feeding specialisation and plasticity can be expected, given temporal and spatial variations in food availability in the deep sea (Sokolova 1972). Hence, isopod feeding selectivity is likely complex, although it is not obvious from the often dominant materials in their guts: unidentifiable organic mucus, indicating that important food sources may be overlooked. Nevertheless, in addition to hard foraminiferan shells, some gut contents of *Acanthocope* and *Betamorpha* (Isopoda) were interpreted as remains of Komokiacea (Brökeland et al. 2010), a largely unexplored group of large-sized protists that often dominate the abyssal megabenthos.

Vema-TRANSIT samples from the North Atlantic (see Supplementary material) contained a specimen of *Betamorpha* cf. *profunda* (Menzies & George, 1972) (ZMH K-45805) with parts of a komokiacean (cf. *Lana* Tendal & Hessler 1977) (Fig. 1) projecting out of the oral cavity. Between the mandible incisors, the komokiacean branches had been macerated to a pulp that can be further traced into the oral cavity and oesophagus, and is enriched in the stomach. To our knowledge, this is the first observation of an isopod directly feeding on a komokiacean. This evidence solidifies previous ideas of a komokiacean role in the diets of *Betamorpha* (Brökeland et al. 2010) and isopods in general. Given that both groups are abundant and diverse in abyssal settings, our observation yields the hypothesis that Komokiaceae may be an important food source for isopods.

Communicated by C. Smith

Electronic supplementary material The online version of this article (doi:10.1007/s12526-016-0606-y) contains supplementary material, which is available to authorized users.

✉ Torben Riehl
Torben.riehl@uni-hamburg.de

[1] Zoological Museum, Centre of Natural History, University of Hamburg, Martin-Luther-King-Platz 3, 20146 Hamburg, Germany

[2] Department of Geological and Environmental Sciences, Ben-Gurion University of the Negev, P.O. Box 653, Beer-Sheva 84105, Israel

[3] A.V. Zhirmunsky Institute of Marine Biology, Far Eastern Branch of the Russian Academy of Sciences (FEB RAS), Far Eastern Federal University, 17 Palchevskogo Street, 690041 Vladivostok, Russia

Published online: 24 November 2016

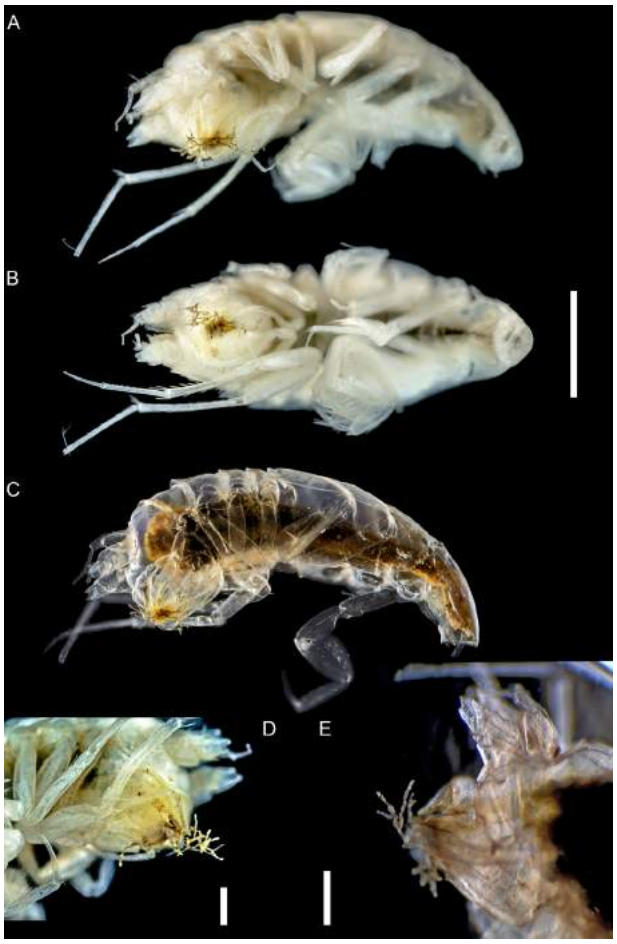

Fig. 1 *Betamorpha* cf. *profunda* feeding on cf. *Lana* sp. Vema-TRANSIT, RV Sonne station SO237-2-7: start trawl: 10°42.891′ N, 25°03.167′ W; 5509 m depth. **A**–**C**, isopod–komokiacean association. **D**, **E**, cephalothorax and komokiacean food fragment. Scale bars: A–C = 1 mm; D, E = 0.3 mm

Acknowledgments Funding: German Federal Ministry of Education and Research (03G0237A). The help of the captain and crew of RV Sonne and sorters is acknowledged. Lidia Lins kindly proofread the initial manuscript. This is Vema-TRANSIT publication #1.

References

Brökeland W, Guðmundsson G, Svavarsson J (2010) Diet of four species of deep-sea isopods (Crustacea: Malacostraca: Peracarida) in the South Atlantic and the Southern Ocean. Mar Biol 157(1):177–187

Gooday AJ, Levin LA, Linke P, Heeger T (1992) The role of benthic foraminifera in deep-sea food webs and carbon cycling. In: Rowe GT, Pariente V (eds) Deep-sea food chains and the global carbon cycle. Springer, Dordrecht, pp 63–91

Sokolova MN (1972) Trophic structure of deep-sea macrobenthos. Mar Biol 16(1):1–12

Svavarsson J, Gudmundsson G, Brattegard T (1993) Feeding by asellote isopods (Crustacea) on foraminifers (Protozoa) in the deep sea. Deep Sea Res Part I Oceanogr Res Pap 40(6):1225–1239

Würzberg L, Peters J, Brandt A (2011) Fatty acid patterns of Southern Ocean shelf and deep sea peracarid crustaceans and a possible food source, foraminiferans. Deep Sea Res Part II Top Stud Oceanogr 58(19–20):2027–2035

Electronic supplement for article:

Caught in the act: An abyssal isopod collected while feeding on Komokiaceae

Torben Riehl, Simon Bober, Ivan Voltski, Marina V. Malyutina, Angelika Brandt

Author affiliations

T. Riehl (Torben.riehl@uni-hamburg.de), Simon Bober, A. Brandt

Zoological Museum, Centre of Natural History (CeNak), University of Hamburg, Martin-Luther-King-Platz 3, 20146 Hamburg, Germany

Ivan Voltski

Department of Geological and Environmental Sciences, Ben-Gurion University of the Negev, P.O. BOX 653, Beer Sheva 84105, Israel

Marina V. Malyutina

A.V. Zhirmunsky Institute of Marine Biology, FEB RAS, 17 Palchevskogo Street, 690041; Far East Federal University, Vladivostok, Russia

Additional Discussion

Many deep-sea organisms from abyssal plain soft sediments, such as isopod crustaceans were initially classified as detritus feeders (Menzies 1962). Later, gut-content analyses revealed tests of hard-shelled Foraminifera and it was suggested that selective feeding on living foraminifers may occur in isopod crustaceans (Menzies 1962; Wolff 1976; Svavarsson *et al.* 1993; Gudmundsson *et al.* 2000; Brökeland *et al.* 2010), suggesting that some isopods prey upon protists, in addition to, or instead of, feeding on detritus. The term for this feeding strategy was coined foraminiferivory (Hickman & Lipps 1983) and was subsequently inferred also by means of fatty-acid and stable-isotope biomarkers that revealed a clear signal of enriched foraminifer fatty acids in selected macro- and megafaunal taxa, and thus suggesting that Foraminifera may be considered a bridge in the energy flow from phytodetritus and sediments to metazoans in the deep sea (Nomaki *et al.* 2008; Würzberg *et al.* 2011). Given spatial and temporal variability of POC (particulate organic carbon) supply to the abyss, a certain plasticity of food choice can be expected for the benthos (Sokolova 1972; Jamieson *et al.* 2012). Besides the isopod crustaceans, further evidence for the importance of Komokiacea and the potentially related Xenophyophoria (Gooday *et al.* 2007) in deep-sea food webs was reported from stomach contents of deposit-feeding holothurians (Sokolova 1972; Khripounoff & Sibuet 1980). These organisms may thus, besides their role as a bridge in the energy flow, also act as a buffer representing a stock upon which certain macro- and megafauna can graze.

Methods for electronic supplement

During the Vema-TRANSIT (Bathymetry of the Vema-Fracture Zone and Puerto Rico TRench and Abyssal AtlaNtic BiodiverSITy Study) expedition, samples were collected along the Vema Fracture Zone with the German research vessel RV Sonne, station SO237-2-7: 20. December 2014; start of trawl: 10°42.891' N, 25°03.167' W; 5,509 m depth (Devey 2015) with a camera-equipped epibenthic sledge (Brandt *et al.* 2013). The sediment samples were treated and fixed onboard as described elsewhere (Riehl *et al.* 2014). After fixation, samples were sorted onboard and targeted isopods were separated individually. From the target taxa, such as *Betamorpha* cf. *profunda* (Menzies & George

1972) (Munnopsidae; Zoological Museum Hamburg: ZMH K-45805), first photographs and then tissue samples were taken for DNA barcoding and other studies (work in progress). The other images (Figure 1A, C–E) were taken using a macro-photo setup before dissection of tissue for DNA (Devey 2015): A Canon EOS 600D was used with a Canon MP-E 65mm f/2.8 macro lens featuring 5x magnification. A Canon MT–24EX II macro flash and additional SPEEDLITE 430EX slave flashes were used to illuminate the specimen from laterally in order to create a black background. Glass chips were used to stabilize the object in any desired position. The camera was mounted on a stand with manual precision focusing drive. To avoid unnecessary vibration, the Canon software EOS Utility was used to trigger the camera shutter from a laptop and to directly store images on the personal computer hard drive. Additional photographs were taken with a Leica M125 stereo microscope equipped with an AX Carrier (for parallax correction) and a MC170 HD camera. The Camera was connected to a PC and photographs were directly saved to the internal hard drive using the software Leica Application Suite (LAS) v.4.5.0 (Build 418). Finally, the specimen was first transferred to 100 % Ethanol and then soaked in methyl salicylate (salicylic acid methyl ester) for 3–4 hours to change the refractive index and to be able to look through the cuticle and inside the specimen. The specimen was again photographed in this translucent condition using the Leica M125 as described above as well as a Passport II Imaging System (http://www.duninc.com/passport-ii.html) with the MP-E 65mm f/2.8 macro lens.

References for electronic supplement

Brandt, A., Elsner, N., Brenke, N., Golovan, O., Malyutina, M. V., Riehl, T., Schwabe, E. & Würzberg, L. (2013) Epifauna of the Sea of Japan collected via a new epibenthic sledge equipped with camera and environmental sensor systems. *Deep Sea Research Part II: Topical Studies in Oceanography*, 86–87, 43–55.

Brökeland, W., Guðmundsson, G. & Svavarsson, J. (2010) Diet of four species of deep-sea isopods (Crustacea: Malacostraca: Peracarida) in the South Atlantic and the Southern Ocean. *Marine Biology*, 157(1), 177–178.

Devey, C. W. (Ed.) (2015) RV SONNE Fahrtbericht / Cruise Report SO237 Vema-TRANSIT. *Geomar Report*, 130 (GEOMAR Report).

Gooday, A. J., Cedhagen, T., Kamenskaya, O. E. & Cornelius, N. (2007) The biodiversity and biogeography of komokiaceans and other enigmatic foraminiferan-like protists in the deep Southern Ocean. *Deep Sea Research Part II: Topical Studies in Oceanography*, 54, 1691–1719.

Gudmundsson, G., von Schmalensee, M. & Svavarsson, J. (2000) Are foraminifers (Protozoa) important food for small isopods (Crustacea) in the deep sea? *Deep Sea Research Part I: Oceanographic Research Papers*, 47(11), 2093–2109.

Hickman, C. S. & Lipps, J. H. (1983) Foraminiferivory; selective ingestion of foraminifera and test alterations produced by the neogastropod Olivella. *The Journal of Foraminiferal Research*, 13(2), 108–114.

Jamieson, A. J., Fujii, T. & Priede, I. G. (2012) Locomotory activity and feeding strategy of the hadal munnopsid isopod Rectisura cf. herculea (Crustacea: Asellota) in the Japan Trench. *The Journal of Experimental Biology*, 215(17), 3010–3017.

Khripounoff, A. & Sibuet, M. (1980) La nutrition d'echinodermes abyssaux I. Alimentation des holothuries. *Marine Biology*, 60(1), 17–26.

Menzies, R. J. (1962) On the food and feeding habits of abyssal organisms as exemplified by the Isopoda. *Internationale Revue der gesamten Hydrobiologie und Hydrographie*, 47(3), 339–358.

Nomaki, H., Ogawa, N. O., Ohkouchi, N., Suga, H., Toyofuku, T., Shimanaga, M., Nakatsuka, T. & Kitazato, H. (2008) Benthic foraminifera as trophic links between phytodetritus and benthic metazoans: carbon and nitrogen isotopic evidence. *Marine Ecology Progress Series*, 357, 153–164.

Riehl, T., Brenke, N., Brix, S., Driskell, A., Kaiser, S. & Brandt, A. (2014) Field and laboratory methods for DNA barcoding and molecular-systematic studies on deep-sea isopod crustaceans. *Polish Polar Research*, 35(2), 205–226.

Sokolova, M. N. (1972) Trophic structure of deep-sea macrobenthos. *Marine Biology*, 16(1), 1–12.

Svavarsson, J., Gudmundsson, G. & Brattegard, T. (1993) Feeding by asellote isopods (Crustacea) on foraminifers (Protozoa) in the deep sea. *Deep Sea Research Part I: Oceanographic Research*, 40(6), 1225–1239.

Wolff, T. (1976) Utilization of seagrass in the deep sea. *Aquatic Botany*, 2(0), 161–174.

Würzberg, L., Peters, J. & Brandt, A. (2011) Fatty acid patterns of Southern Ocean shelf and deep sea peracarid crustaceans and a possible food source, foraminiferans. *Deep Sea Research Part II: Topical Studies in Oceanography*, 58(19–20), 2027–2035.

Author contributions

The idea for this study came from Simon Bober and was realized by Torben Riehl. The experiments were performed by S. Bober. The photographs were taken by S. Bober and T. Riehl. The manuscript was written by T. Riehl with subsequent contributions of S. Bober, Ivan Voltski, Marina V. Malyutina and Angelika Brandt.

Chapter 8

Adding depth to line artwork by digital stippling –a step-by-step guide to the method

Org Divers Evol
DOI 10.1007/s13127-014-0173-7

METHODS AND APPLICATIONS

ORGANISMS DIVERSITY & EVOLUTION

Adding depth to line artwork by digital stippling—a step-by-step guide to the method

Simon Bober · Torben Riehl

Received: 13 February 2014 / Accepted: 21 April 2014

Abstract Vector-based software has revolutionized scientific illustrating and is well established in taxonomy. However, simple line drawings lack depth information. Shading techniques, such as stippling—the application of dots to generate shade—are the methods of choice for simulating shade, structure, shape, and texture. In this paper, a step-by-step guide for digital stippling is presented. Manual stippling offers great flexibility to achieve highly realistic results. A round brush is applied to the line art by tapping. To drastically reduce time consumption and generate homogeneous tinges, a semiautomation was developed: the smallest units of symmetric stippling patterns are stored in a brush library. Using macroinstructions (macros), such stored raw patterns are converted into symmetric repetitive patterns. This way, stippling can be applied quickly and evenly across large areas of the underlying line drawing. These methods come with all the advantages of vector illustrations, such as high scalability, reproducibility and easy correction of strokes that have turned out imperfect.

Keywords Systematics · Stippling · Shading · Digital inking · Illustration

Introduction

Line drawings have gone digital. The use of pen tablets for the creation of biological illustrations is commonly applied across many organism groups, such as predominantly animal taxa (various groups of Arthropoda, but also Digenea, Gastrotricha, Kinorhyncha, Polychaeta, and Vertebrata among others) as well as fungi (Andres and Overstreet 2013; Barber and Keane 2007; Coleman and Sen-Dunlop 2013; Ivanova and Wilson 2009; Kieneke et al. 2008; Reuscher et al. 2009; Salles et al. 2011; Sørensen 2008; Weigmann et al. 2013). Digital illustration techniques have numerous advantages over traditional inking techniques (Bouck and Thistle 1999; Fisher and Dowling 2010). The easy and quick possibility to undo strokes that have turned out imperfect, for instance, is a major time-saving factor. Vector-graphics software allows manipulation of the actual drawing after the completion of the lines (Holzenthal 2008). It further permits compact data files and the possibility to scale an illustration without losing information or changing line weights, if unwanted. Manuals to the basically relevant scientific drawing techniques using a pen tablet and Adobe® Illustrator® (AI) are available (Barber and Keane 2007; Bouck and Thistle 1999; Coleman 2003; Holzenthal 2008). Through the application of macroinstructions (macros) and the brush tool, the illustration of frequently occurring features, such as setae, can be significantly sped up (Coleman 2009).

For transmitting a general impression of the shape and form of an organism or parts of the latter, line drawing is a powerful technique (Honomichl et al. 1982). There are instances where a purely line-based illustration providing a contour and certain important protruding features are fully sufficient. That is especially the case when the illustrated object is flat or has an otherwise even surface. However, a weakness of line drawings in general is the lack of depth.

Most biological objects comprise more than plain surfaces; edges, convex or concave areas, as well as form, and texture may be of significance (Dalby and Dalby 1980). To overcome this shortcoming and even emphasize certain features, shading techniques can be applied. They create the impression of three dimensionality (3D), texture, and to some degree even color

Electronic supplementary material The online version of this article (doi:10.1007/s13127-014-0173-7) contains supplementary material, which is available to authorized users.

S. Bober · T. Riehl (✉)
Biocenter Grindel and Zoological Museum, University of Hamburg, Martin-Luther-King-Platz 3, 20146 Hamburg, Germany
e-mail: t.riehl@gmx.de

Published online: 13 May 2014

(Dalby and Dalby 1980). Stippling is the method of choice to produce shaded line art in science (Briscoe 1996). It is achieved by producing dots into the line drawings and generates the illusion of greyscale within the preferable (Dalby and Dalby 1980) black-and-white (B/W) regime by varying densities of dots (Honomichl et al. 1982; Zweifel 1988). Stippling may be time consuming compared with plain line drawings, but it provides full control over the application of shading and highly realistic results are achievable (Sousa 2003). Stippling is therefore a widely applied method in biological sciences (e.g., Brandt and Wägele 1988; Meißner and Hutchings 2003; Kieneke et al. 2008; Miljutina and Miljutin 2012; Köhler and Criscione 2013; de Zeeuw et al. 2013; Moravec et al. 2014).

In this paper, we describe methods for vector-based stippling. These fulfill all requirements from scientific illustrations, such as reproducibility, clarity, and scalability. They allow shading without compromising the clarity, simplicity, and storage-saving advantages of B/W (e.g., bitmap) images. They are further advantageous over traditional stippling using ink because of the possibilities to electronically manipulate size and orientation. High flexibility in plate preparation as well as easy correction possibilities are further improvements (Bouck and Thistle 1999). Moreover, we describe a significantly time-saving automation technique.

Materials

Any computer with at least 1,300 MHz processor, 1 GB RAM, and USB port can be used. A second monitor is advisable. For this paper, both Apple and Windows operation systems in combination with Wacom Intuos pen tables (models 3 A4 (PTZ930) and 4 A4 (PTK840)) were used. The required hard- and software runs on any of the widely applied operation systems (Microsoft Windows, Macintosh OS, Linux). Throughout the guidelines, we provide keyboard shortcuts in

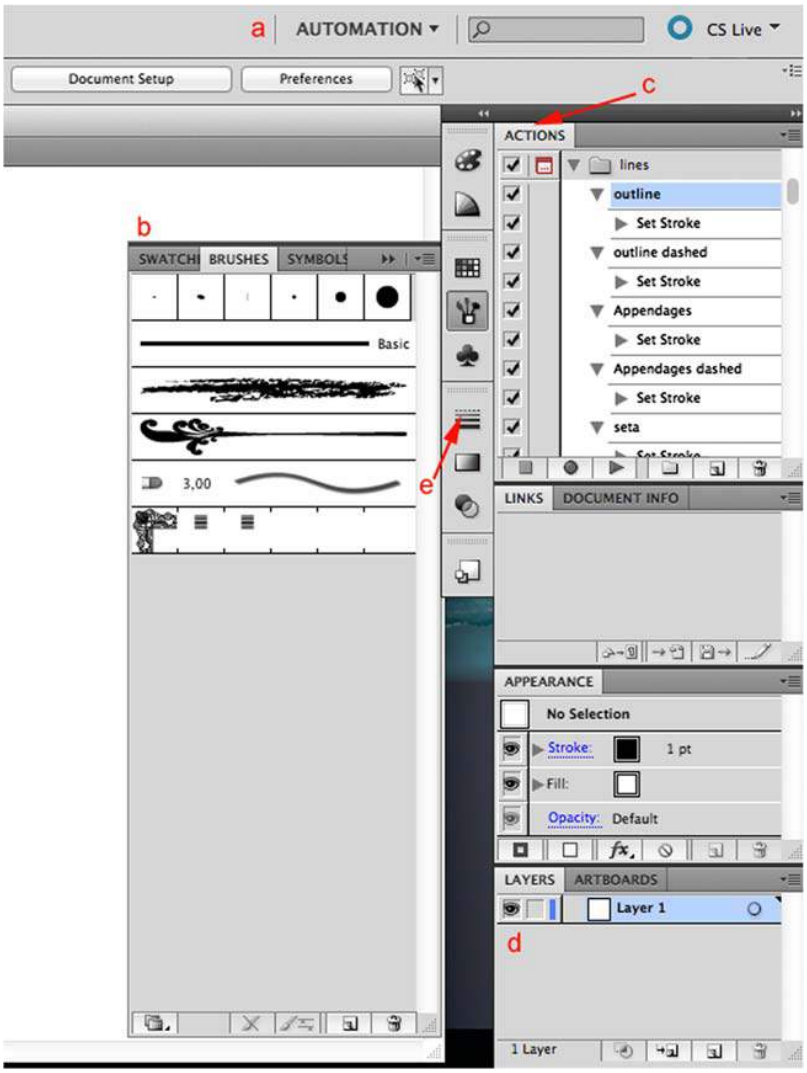

Fig. 1 Overview over the *AUTOMATION* workspace in Adobe Illustrator. **a** The workspace selection panel is located near the top right corner of the window. **b** The *Brushes* menu. **c** The *Actions* panel. **d** The *Layers* menu. **e** The *Stroke* panel

brackets that are applicable for both Apple and Windows systems. The Apple-specific ⌘ key is used synonymously with the Windows Ctrl key. The Shift key is represented by ⇧.

The underlying scientific illustrations were created by following the methods described by Coleman (2003, 2009), and their creation is not part of this documentation. Adobe® Illustrator® (AI) CS5 (version 15.0.0 and 15.0.2) was used during the development of the methods. All methods described herein were successfully tested in the still widely applied AI CS 4 and the latest AI CS 6 version as well. We recommend to use the *Automation* workspace (Fig. 1a) because all necessary menus are found therein.

Manual stippling

1. Open AI and attach the drawing tablet.
2. Load a vector drawing, e.g., one prepared following the guidelines by Coleman (2003, 2009) (File➞ Open; or ⌘ O).
3. Open the *brushes* panel (Fig. 1b) and select the *3 pt. round* brush (*Artistic_Calligraphic* library) (Fig. 2a). Adjust the stroke size to 0.25 pt. (Fig. 2d).
4. Add a row of dots by tapping on the tablet. The dots should evenly distributed (ca. 0.5 mm distance).
5. Add a second similar row of dots parallel and alternating to the first row.
6. Add a third row parallel and alternating to the second row.
7. Etc.

Following this pattern, the shade will look even without any gradation (Fig. 3a–c). If a desaturation is desired for this tone to receive a gradation, the next steps need to be followed (Fig. 3d–g).

8. Add another parallel row of dots with more distance to the previous row.
9. Use the same distance for one or more additional rows.
10. For a stronger desaturation effect, double the distance between the dots in another (set of) row(s)—alternating with every second dot in the previous row.
11. This can be deliberately expanded.

Automated stippling

Stippling can be semi-automated through brushes and an appropriate macro (called "Action" in AI terminology). The latter method is described in this section. We are providing exact values that lead to the example brushes in the Electronic supplementary material.

Creating stippling brushes

1. Open a new document (⌘ N).
2. For easier navigation, activate the ruler (View ➞ Ruler ➞ Activate Ruler; or ⌘ R).

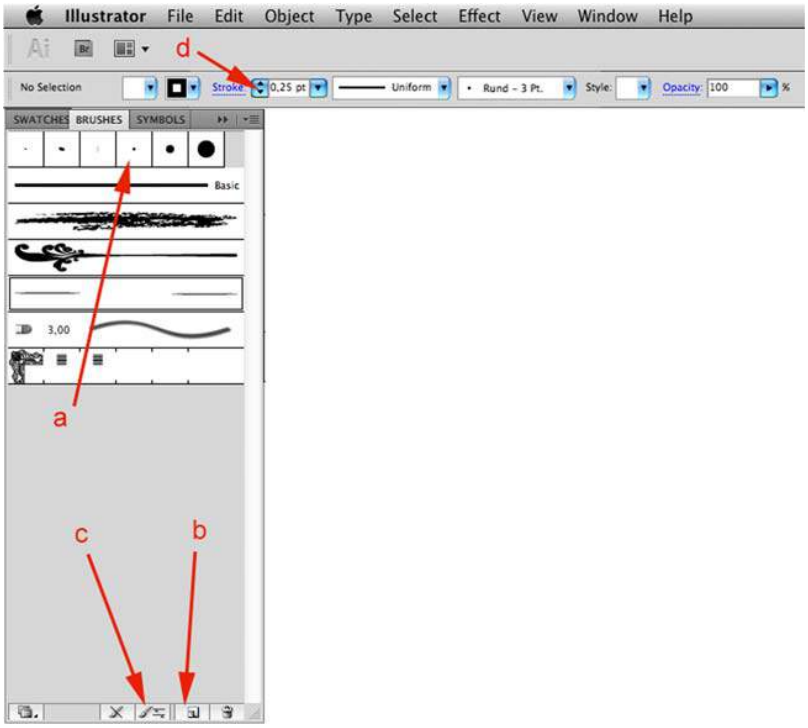

Fig. 2 The *Brushes* panel. **a** *3 pt. Round* brush. **b** *Create New Brush*. **c** *Selected object options*. **d** The suggested size for a single stipple is 0.25 pt

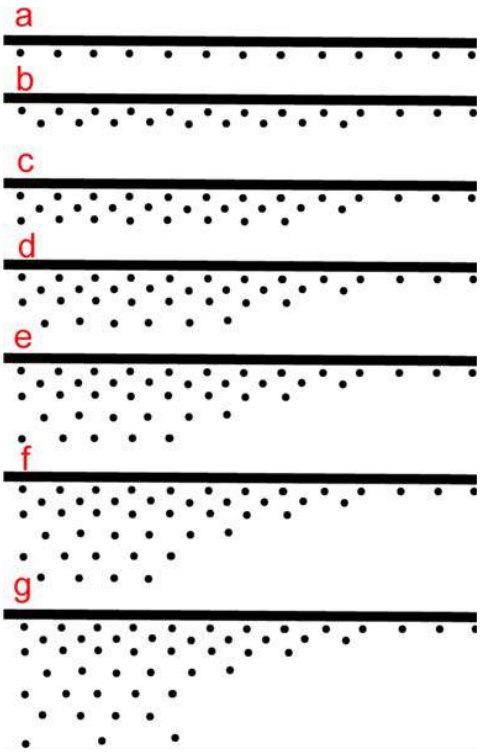

Fig. 3 Example of how to build up shading through manual stippling. **a** Start with one row of equally-spaced dots. **b**, **c** Add second and third rows alternating to the previous row. **d**–**g** For a desaturation effect, add more rows but with increased distance between them. For a stronger desaturation, double the spacing between the dots in another (set of) row(s)—alternating with every second dot in the previous row. This pattern can be deliberately expanded

3. Use the *brush* tool (b) and select the *round-3 Pt* brush. Adjust the stroke size to 0.25 pt. (Fig. 2d).
4. Create a random dot by tapping on the pen tablet and a second one 0.6 mm to the right and 0.7 mm below (Fig. 4a; this is the fundamental fragment of the simplest stippling pattern).
5. Select the pattern by either using the *direct selection* tool (A) or the *lasso* tool (Q).

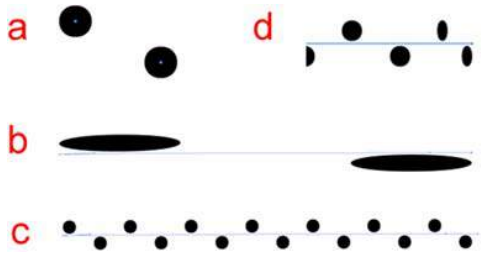

Fig. 4 Steps for creating semi-automated stippling (not to scale). **a** Two stipples are the basis for a simple repetitive pattern, *Stippling basic*. **b** When the stippling brush is applied without using the proper type of dashed line, a stretched stippling brush appears. **c** After application of the corresponding action, the stretched brush is turned into a symmetric, repetitive pattern. **d** The end of the stroke may be distorted. This can be adjusted by extending or shortening the vector at the terminal anchor point

6. Open the *brushes* panel (Fig. 1b) and add a new brush by clicking the *new brush* button on the bottom of the panel next to the *bin* button (Fig. 2b). Select the *art brush* type (Fig. 5a) and name the brush (in this case, *stippling basic*). The *brush scale options* should be set to *stretch to fit stroke length* (Fig. 5b).

Make sure the stroke direction is correct and press *OK* (Fig. 5b).

Following the guideline above produces a rather simple stippling pattern. It is suitable, for example, for slight shadings or to pronounce layer separation (*see*, e.g., antennae and uropods in Fig. 6b). This pattern can become more complex by adding more rows of dots and gradients. Once a pattern is established (e.g., by following steps 1–6 above) this pattern can be used as template to easily produce derivatives. Copies can be made and transformed by up- or down scaling with or without keeping the aspect ratio. A large library of stippling brushes can thus be generated quickly.

We recommend preparing a set of at least four to six stippling brushes. In Table 1 (Electronic supplementary material), coordinates for six further stippling patterns are presented. Pattern no. 7 (*Concavity*) is different to all other patterns in that this special pattern is simulating a concavity (Fig. 6c).

Once a brush library is generated, it can be saved (Fig. 7a) and is then available for further illustrations (Fig. 7b). An exemplary brush library containing those brushes presented here is provided in the Electronic supplementary material.

Creating a stippling action

Stippling brushes have a certain length defined by its underlying pattern fragment. Longer homogeneous stippling is produced by using the *dashed line* function which produces repetition of the pattern fragment. The *dash* length has to be set to equal the length of the pattern fragment and the *gap* length has to correspond to the necessary distance between two such fragments. *Actions* allow quick adjustments of these pattern-specific parameters so the generated stippling pattern is homogeneous. *Actions* are AI-specific macros. Once a brush is saved to the brush library, it is recommended to program a corresponding *action*.

1. In the *actions* panel (Fig. 1c), create a *new set* and name it *stippling* (Fig. 8a).
2. Create a *new action* within this set and name it *stippling basic* (Fig. 8b). Assign the *function key* [⇧ F9]. Click *record* (Fig. 8b).
3. Open the *stroke* panel (Fig. 1e). Set *weight* to 1 pt. and check the *dashed line* box (Fig. 9a). To the right of this

box, check *preserves exact dash and gap lengths* (Fig. 9b).

Set the dash length to 2.5 pt. and the gap length to 0.5 pt. (Fig. 9c).

4. Stop recording by clicking the *stop* button (Fig. 8c) next to the red *record* button on the bottom of the *actions* panel.
5. Use the *brush tool* (B), select the brush *stippling basic* and draw a line; the dots appear stretched (Fig. 4b).
6. Press [⇧ F9] and the stretched line are converted into a repetitive pattern (Fig. 4c).
7. The end of the stippling turns out squeezed when the length of the underlying vector does not exactly equal a multiple of the fragment length (Fig. 4d). If this is the case, the length of the vector should be altered by moving the last *anchor* point.

Once the *action set* is generated, it can be saved and is available for further illustrations (Fig. 8d–f). This *action* corresponds only to the stippling-brush pattern described above as well as derivatives with similar fragment length and spacing between dots. We recommend preparing *actions* corresponding to each individual stippling type (Table 2 of the Electronic supplementary material). The *actions* presented here are available as Electronic supplementary material.

Adding stippling to a drawing

1. Open AI and attach the pen tablet.
2. Load a vector drawing prepared following the guidelines by Coleman (2003, 2009) (File ➜ Open; or ⌘ O).
3. Create a new *layer* in the *layer* panel by clicking *create new layer* next to the *bin* symbol and name it (e.g., *stippling*; Fig. 10a). Working with layers has many advantages. First of all, it helps to organize the document properly. Then, the order of the layers represents an object hierarchy (stacking order). Furthermore, layers can be selectively locked, masked out and dimmed (among many other attributes) to provide great working comfort.
4. Use the *brush tool* (B) and select one of the previously prepared stippling brushes.
5. Activate the corresponding *action*.

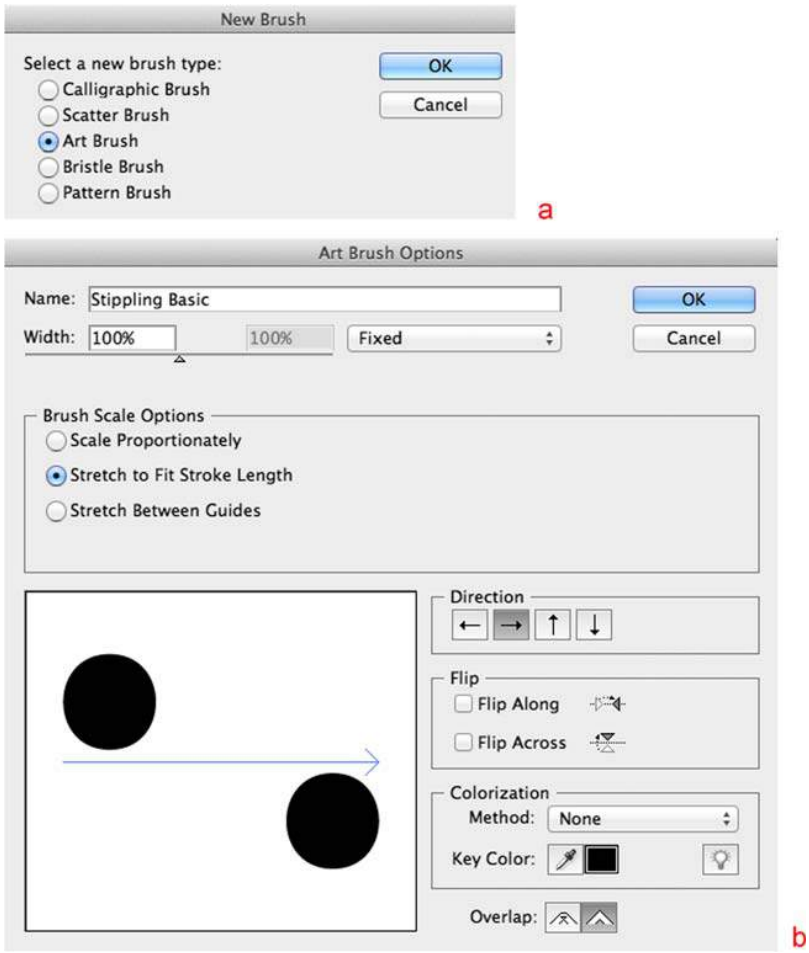

Fig. 5 How to create a brush. **a** The pattern is saved as *Art brush*. **b** The options *Stretch to Fit Stroke Length* and the brush *Direction* are set in the *Art Brush Options* window

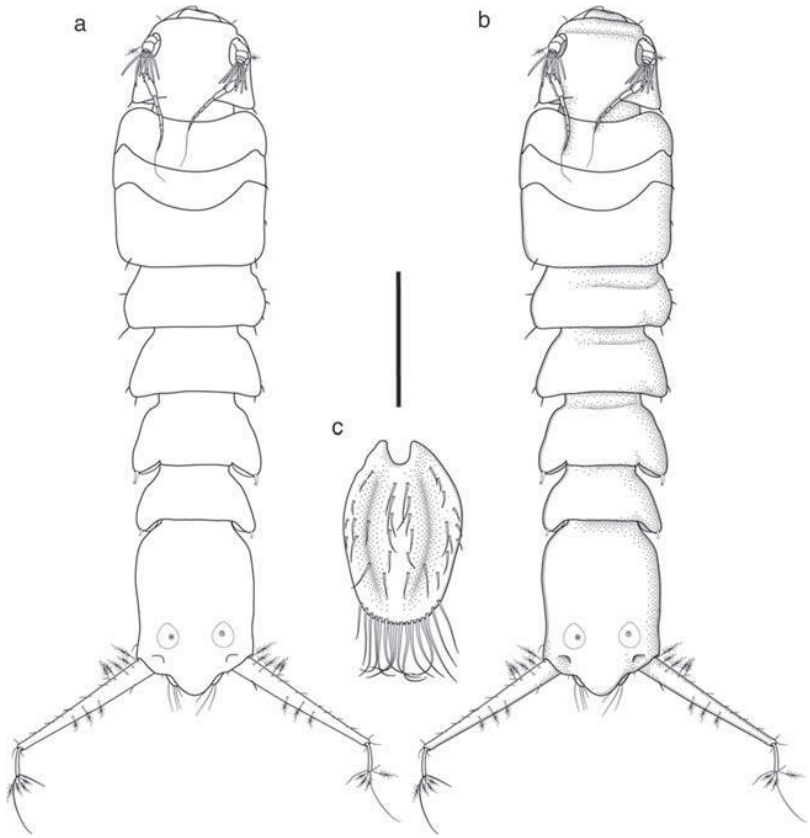

Fig. 6 Plain versus stippled vector illustrations exemplified by the isopod (Crustacea) species *Macrostylis scotti* Riehl and Brandt 2013. **a** Plain illustration without any shading. **b** Same illustration as **a** but with stippling added. Various types of brushed stipplings as well as manual stippling were applied. **c** The second female pleopods (operculum) with concavities (stippling pattern no. 7) on the surface

6. Trace those lines that need stippling.
7. If the stippling pattern is upside down (Fig. 11d), you can either draw the line in the other direction or preferably open the *options for selected object* window (Fig. 2c) by clicking the button on the left to the *create new brush* button. Choose *flip across* (Fig. 11e).
8. Adjust the *anchor* points for optimal coverage and avoiding a compressed end of the vector.

Line-parallel stippling over large areas

In cases where a large area that is parallel to a line needs homogeneous stippling, it may be easier to copy this line and transform it into a stippling pattern.

1. Select the whole line or parts that need stippling with either the *direct selection* tool (A) or the *lasso* tool (Q) (Fig. 12a).
2. Copy this line (⌘ C) and paste it behind the original line (⌘ B).
3. Use the *selection tool* (V) and move the copied line in the preferred position next to the original line (Fig. 12b).
4. Open the *brushes* menu and choose one of the previously prepared stippling brushes (Fig. 12c).
5. Make adjustments if needed (Fig. 12c).
6. Go to the *layers* menu and drag the selection to the stippling layer (Fig. 10b).

Stippling within a closed line

Where roundish structures that are represented in a drawing by closed lines, such as any form of operculum (Fig. 6c) or microfungal conidia (Barber and Keane 2007), stippling may be used to simulate bulge form. To achieve this, parallel stippling on the inside of the closed line is required.

1. Select the whole line with either the direct selection tool (A) or the lasso tool (Q) (Fig. 11a).
2. Copy this line (⌘ C) and paste it behind the first (⌘ B).
3. Scale the selection (Object ➜ Transform ➜ Scale) to ≤99 % depending on the used stippling brush (Fig. 11e) and diameter of the closed line.
4. Open the *brushes* menu and transform the line into a stippling brush (Fig. 11d).

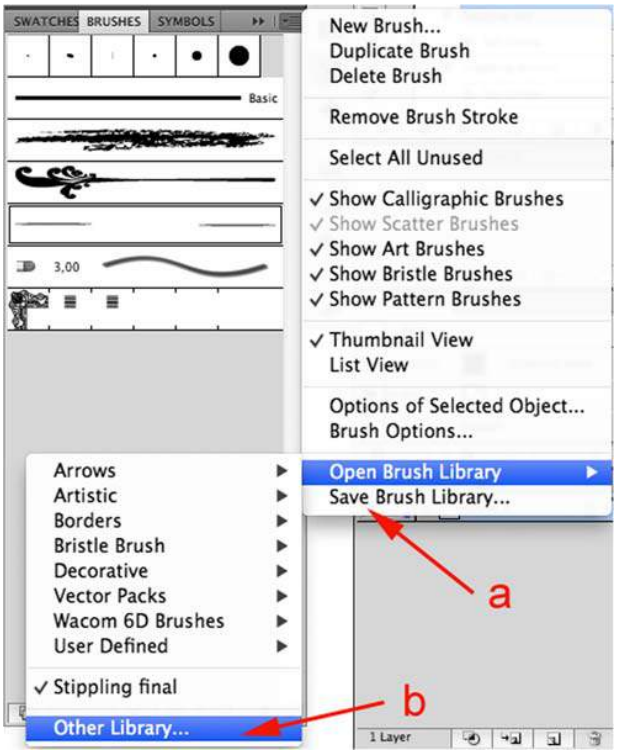

Fig. 7 How to save and load a brush library. A click on the upper right corner of the *Brushes* panel opens a dropdown menu. **a** *Save Brush Library* opens an explorer window to select the proper location for storing the library. **b** Custom-made libraries can be loaded by clicking on *Other Library*

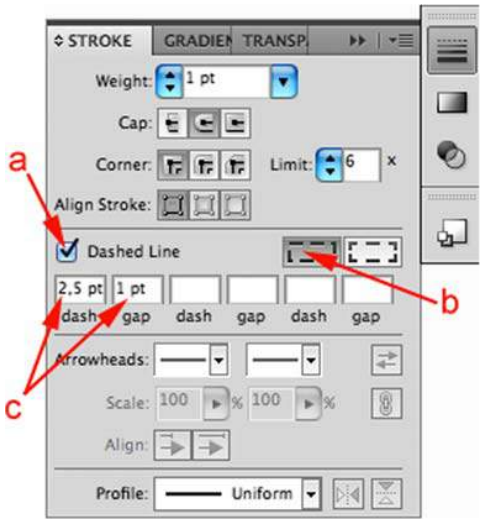

Fig. 9 The *Stroke* panel. **a** Checking this box change a line into a dashed line. **b** For stippling brushes, it is recommended to check *Preserves exact dash and gap lengths*. **c** The dash and gap distance is manually adjustable and proper values depend on the underlying stippling pattern

5. Make adjustments if needed (Fig. 11c, d).
6. Go to the *layers* menu and drag the selection to the stippling layer (Fig. 10b).

Scaling of stippled illustrations

One major advantage of vector-based graphics is its high reproducibility. The final size of the illustration can be adjusted without compromising the quality even after the actual drawing is completed (Object ➜ Transform ➜ Scale) (Fig. 13a). There is a much higher flexibility with regard to adjusting line weights etc. in the process of plate arrangement. Unlike pixel-based graphics, vector graphs can be infinitely enlarged without losing resolution. Moreover, scaling may

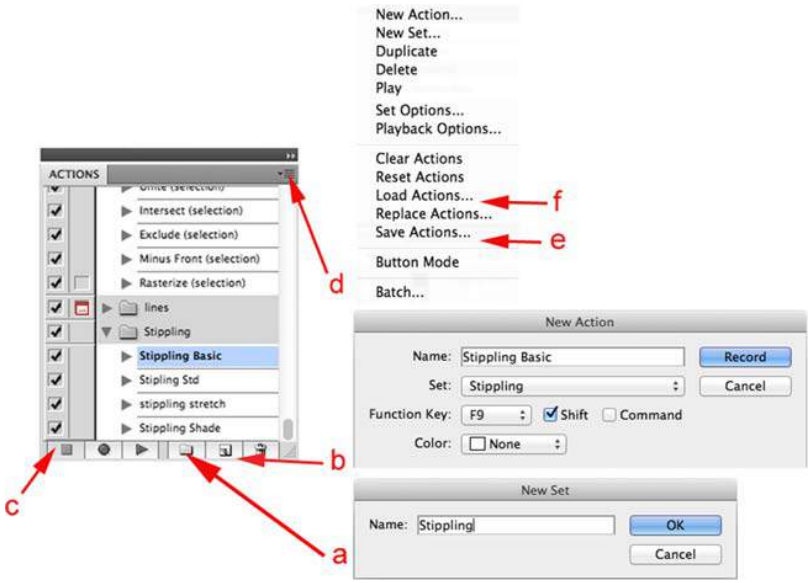

Fig. 8 Every type of stippling brush needs a corresponding *Action*. **a** *Actions* are saved to a *New Set*, which can be called *Stippling*. **b** For every *New action* that is recorded, a unique name and *Function Key* should be assigned. **c** To stop recording, press the *Stop* button. **d** To save or load an *Action*, open the *Actions Options*. **e** Then press *Save Actions* or **f** *Load Action*

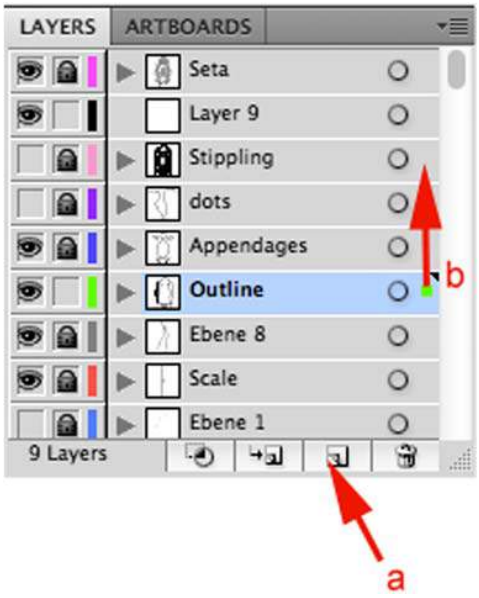

Fig. 10 The *Layers* menu. **a** Create a *New Layer*. **b** Selected paths can be moved to different layers

change the appearance of the illustration, if desired, by selectively excluding strokes and brushes from the scaling process. When the box *scale strokes and effects* in the *scaling* panel is checked (Fig. 13b), lines and brushes change their appearance equivalently to the overall scaling. Thus, when the drawing is scaled down to 50 % of its original size, a 1-pt. outline becomes 0.5 pt. When the box *scale strokes and effects* is unchecked, lines do not change their weight and brushes do not change their appearance during scaling. In the abovementioned case, the line weight would double relative to the size of the drawing. This is also relevant for stippling, because manually applied dots and stippling brushes may behave differently depending on the applied settings. However, we present three ways of scaling artwork that contains stippling:

First of all, checking the box *scale strokes and effects* allows for a straight-forward scaling approach where all relative values remain constant. Using this method, manual and brushed stipples are equally affected.

At the same time, AI provides a tool to change the relative dimensions of the stipples, without changing their relative positions while the overall size of the drawing is altered. The *expand appearance* function (*Object* ➜ *Expand appearance*) converts the stippling brushes as well as manually applied dots into circular paths filled with black color. Thus, the dimensions of the black dots are not defined by a stroke anymore but by the diameter of the circular vector. Given that during scaling the relative positions of the paths and anchor points always stay identical, downscaling in this case means downsizing the stipples and vice versa. This implies that as long as the box *scale strokes and effects* remains unchecked,

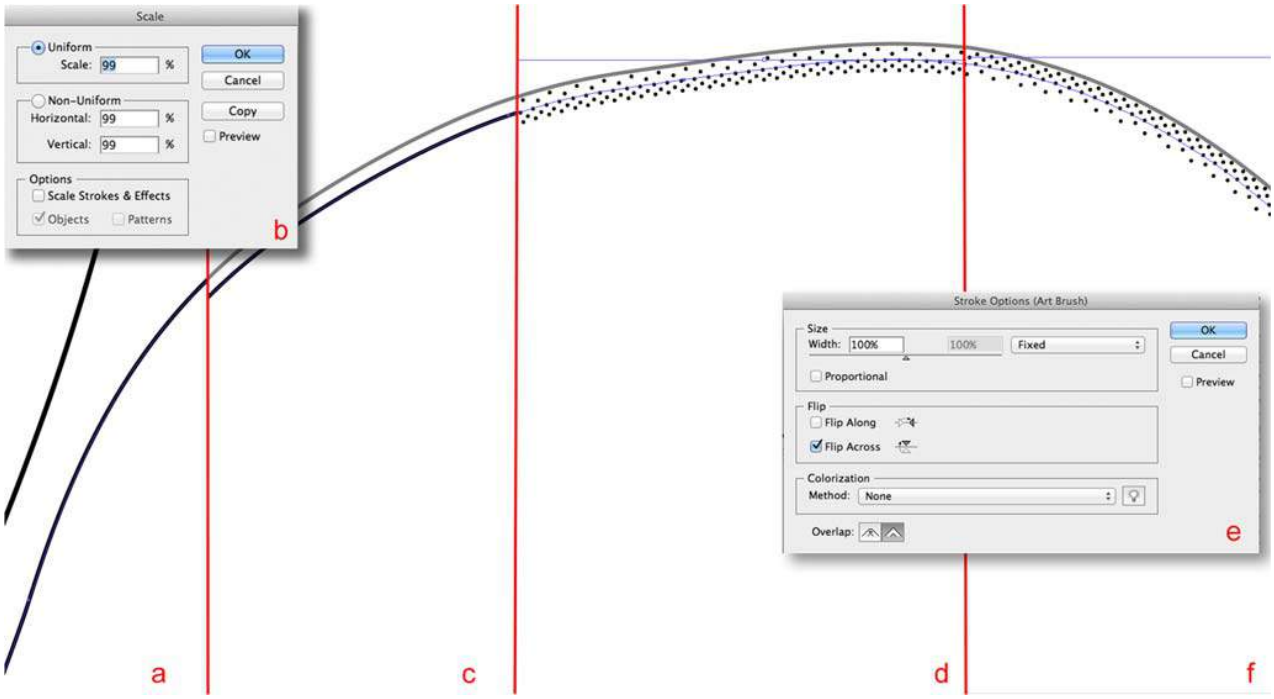

Fig. 11 Excerpt of a round closed line that is supposed to get a stippling. **a** Select a path, create a copy behind the template. **b** Scale selected path to 99% of its original size. **c** The path should now lie within the round structure. **d** Convert path into a stippling brush by selecting an appropriate pattern from the brushes library. **e** To flip over the stippling brush when it has turned out upside down, check the *Flip Across* box in the *Stroke Options* window. **f** The ready stippling

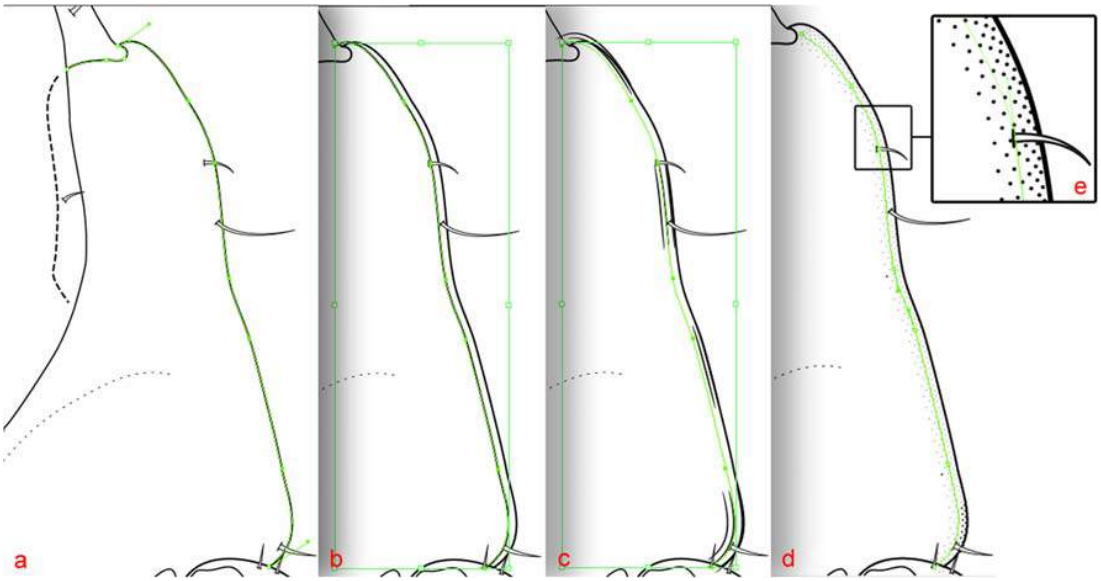

Fig. 12 Automated stippling exemplified on a ventral head drawing of a macrostylid isopod. **a** Select a path. **b** Copy the selected path behind the original template. **c** Move the copied path to be parallel to the template. **c** Convert line into a stippling brush by selecting the desired pattern from the brush library. **d** After applying the corresponding action command this stippling is adjusted. **e** Magnification from **d**

any scaling changes the appearance of the individual dots. Going back to the previous example of the drawing that is scaled down to 50 % of its original size: a 1-pt. outline retains its weight; the dots of the stippling, however, are reduced to 50 % of their original diameter.

As AI may automatically group dots of the brushed stippling when the *expand appearance* function is applied, scaling may cause distortion of the stipple positions. To counteract this, select all stippling patterns (lock all layers, except the stippling layer; then press ⌘ A) and ungroup (*Object* ➜ *Ungroup*; or ⌘ G) the selection. To ensure that also groups nested within groups have ungrouped, the ungrouping may need to be repeated.

Finally, the *Transform each tool* (*Object* ➜ *Transform* ➜ *Transform Each*; or ⌘ ⇧ D) allows altering the intensity of the shading by scaling the selected dots individually. As a prerequisite for this approach, it is necessary to convert all stippling brushes to circular paths beforehand using the *expand appearance* tool.

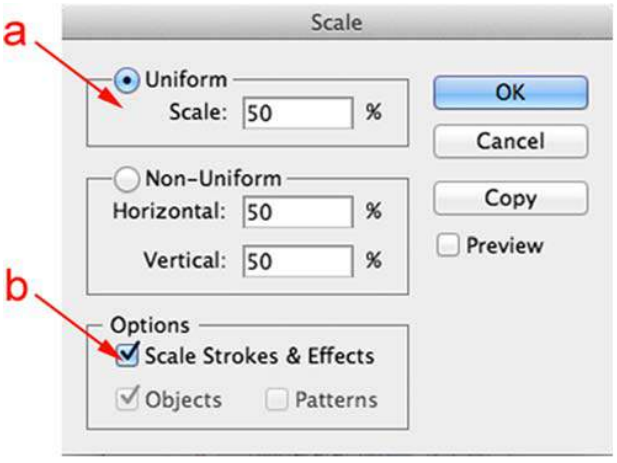

Fig. 13 How to scale vector illustrations that contain stippling patterns. **a** Uniform scaling is required to keep length-width ratios of the illustration. **b** The box *Scale Strokes and Effects* should be checked when lines and brushes are supposed to change their appearance equivalently to the overall drawing

Discussion

Line drawings involve selectiveness and emphasis to certain aspects of the illustrated objects (Dalby and Dalby 1980). Stippling is a method that allows emphasizing structures interpreted as relevant by the scientist. It provides a high degree of freedom and adaptability. By applying a digital approach to stippling (Riehl and Brandt 2013; Riehl et al. 2012, 2014), this technique has been brought up to date concordant with widely applied digital line-drawing methods (Bouck and Thistle 1999; Coleman 2003, 2009).

However, manual stippling can be relatively time consuming. Another general difficulty with manual stippling is to create homogeneous tinges over large areas (Honomichl et al. 1982). We hence developed a method that allows relatively straight contours to be shaded reasonably quick: the automated stippling presented in this paper guarantees both, to significantly speed up the process and to produce homogeneous shades. It however fails to produce satisfactory results where the path underlying the stippling is heavily curved. In particular in broad stippling brushes, the dots of the outer rows

get distorted easily. This may cause accentuating effects that are not desirable. To a certain degree, this might be tolerable. In curved regions, however, it is recommended to link straight sections produced by the automated method with manually applied stipples.

The methods described in this paper provide a general introduction to our new approach. Any values provided in this paper can be changed to fit the individual requirements. The method provides an alternative to another recently described method (Barber and Keane 2007) that applies filters in Adobe® Photoshop® to automatically generate stippling. One disadvantage of the latter method, in contrast to our approach, lies in the computer-generated dot distribution that produces randomly variable distances and often overlapping of the individual dots which is generally not desirable (Sousa 2003). The method described herein allows full control over dot distribution. Likewise, their pixel-based approach does not provide the reproducibility and scalabilities inherent in vector drawings.

It should be noted that the freely available software Inkscape (http://www.inkscape.org; among others; *see*, e.g., Barber and Keane 2007 and references therein) offers a suitable alternative to AI with regard to the manual stippling approach (*see* Riehl et al. 2014) and digital illustrations in general (*see*, e.g., Wilson 2008). However, the methodology differs regarding the tools and settings and possibilities to automate stippling need yet to be explored.

Acknowledgments The authors are thankful for the support of A. Brandt and the helpful and friendly working environment at the Zoological Museum Hamburg. N. Heitland practically tested the methods described in this paper. J. Ruch kindly provided comments on an earlier version which improved this paper. This paper benefitted from discussions about the topic with G.D.F. Wilson. During preparation of this manuscript, TR received funding from the German National Academic Foundation (Studienstiftung des deutschen Volkes). Two anonymous reviewers are thanked for their efforts to critically improve this paper.

References

Andres, M. J., & Overstreet, R. M. (2013). A New Species of *Podocotyloides* (Digenea: Opecoelidae) from the Grey Conger Eel, *Conger esculentus*, in the Caribbean Sea. *The Journal of Parasitology, 99*(4), 619–623.

Barber, P. A., & Keane, P. J. (2007). A novel method of illustrating microfungi. *Fungal Diversity, 27*(1), 1–10.

Bouck, L., & Thistle, D. (1999). A computer-assisted method for producing illustrations for taxonomic descriptions. *Vie et Milieu, 49*(2–3), 101–105.

Brandt, A., & Wägele, J.-W. (1988). *Antarcturus bovinus* n. sp., a new Weddell-Sea Isopod of the family Arcturidae (Isopoda: Valvifera). *Polar Biology, 8*(6), 411–419.

Briscoe, M. H. (1996). *Preparing scientific illustrations: A guide to better posters, presentations, and publications* (2nd ed.). New York: Springer.

Coleman, C. O. (2003). "Digital inking": how to make perfect line drawings on computers. *Organisms Diversity & Evolution, 3*(4), 303–304. doi:10.1078/1439-6092-00081.

Coleman, C. O. (2009). Drawing setae the digital way. *Zoosystematics and Evolution, 85*(2), 305–310. doi:10.1002/zoos.200900008.

Coleman, C. O., & Sen-Dunlop, Y. (2013). *Iphinotus lisae* n. sp. (Crustacea, Amphipoda, Phliantidae) from Western Australia. *Zoosystematics and Evolution, 89*(1), 5–11. doi:10.1002/zoos.201300001.

Dalby, C., & Dalby, D. H. (1980). Biological illustration: a guide to drawing for reproduction. *Field Studies, 5*, 307–321.

De Zeeuw, M., Westbroek, I., van Oijen, M., & Witte, F. (2013). Two new species of zooplanktivorous haplochromine cichlids from Lake Victoria, Tanzania. *ZooKeys, 256*, 1–34. doi:10.3897/zookeys.256.3871.

Fisher, J. R., & Dowling, A. P. (2010). Modern methods and technology for doing classical taxonomy. *Acarologia, 50*(3), 395–409.

Holzenthal, R. W. (2008). Digital illustration of insects. *American Entomologist, 54*(4), 218.

Honomichl, K., Risler, H., & Rupprecht, R. (1982). *Wissenschaftliches Zeichnen in der Biologie und verwandten Disziplinen*. Stuttgart: G. Fischer.

Ivanova, E. S., & Wilson, M. J. (2009). Two new species of *Angiostoma* Dujardin, 1845 (Nematoda: Angiostomatidae) from British terrestrial molluscs. *Systematic Parasitology, 74*(2), 113–124. doi:10.1007/s11230-009-9200-z.

Kieneke, A., Arbizu, P. M., & Ahlrichs, W. H. (2008). Anatomy and ultrastructure of the reproductive organs in *Dactylopodola typhle* (Gastrotricha: Macrodasyida) and their possible functions in sperm transfer. *Invertebrate Biology, 127*(1), 12–32. doi:10.1111/j.1744-7410.2007.00111.x.

Köhler, F., & Criscione, F. (2013). Small snails in a big place: a radiation in the semi-arid rangelands in northern Australia (Eupulmonata, Camaenidae, *Nanotrachia* gen. nov.). *Zoological Journal of the Linnean Society, 169*(1), 103–123. doi:10.1111/zoj.12051.

Meißner, K., & Hutchings, P. A. (2003). *Spiophanes* species (Polychaeta: Spionidae) from Eastern Australia with descriptions of new species, new records and an emended generic diagnosis. *Records of the Australian Museum, 55*(2), 117–140.

Miljutina, M. A., & Miljutin, D. M. (2012). Seven new and four known species of the genus *Acantholaimus* (Nematoda: Chromadoridae) from the abyssal manganese nodule field (Clarion-Clipperton Fracture Zone, North-Eastern Tropical Pacific). *Helgoland Marine Research, 66*(3), 413–462. doi:10.1007/s10152-011-0282-z.

Moravec, J., Lehr, E., Cusi, J. C., Cordova, J., & Gvozdik, V. (2014). A new species of the *Rhinella margaritifera* species group (Anura, Bufonidae) from the montane forest of the Selva Central, Peru. *ZooKeys, 371*, 35–56. doi:10.3897/zookeys.371.6580.

Reuscher, M., Fiege, D., & Wehe, T. (2009). Four new species of Ampharetidae (Annelida: Polychaeta) from Pacific hot vents and cold seeps, with a key and synoptic table of characters for all genera. *Zootaxa, 2191*, 1–40.

Riehl, T., & Brandt, A. (2013). Southern Ocean Macrostylidae reviewed with a key to the species and new descriptions from Maud Rise. *Zootaxa, 3692*(1), 160–203. doi:10.11646/zootaxa.3692.1.10.

Riehl, T., Wilson, G. D. F., & Hessler, R. R. (2012). New Macrostylidae Hansen, 1916 (Crustacea: Isopoda) from the Gay Head-Bermuda transect with special consideration of sexual dimorphism. *Zootaxa, 3277*, 1–26.

Riehl, T., Wilson, G. D. F., & Malyutina, M. V. (2014). Urstylidae—a new family of deep-sea isopods and its phylogenetic implications. *Zoological Journal of the Linnean Society, 170*, 245–296. doi:10.1111/zoj.12104.

Salles, F. F., Boldrini, R., Shimano, Y., & Cabette, H. R. (2011). Review of the genus *Aturbina* Lugo-Ortiz & McCafferty (Ephemeroptera: Baetidae). *Annales de Limnologie-International Journal of Limnology, 47*(1), 21–44.

Sørensen, M. V. (2008). A new kinorhynch genus from the Antarctic deep sea and a new species of *Cephalorhyncha* from Hawaii

(Kinorhyncha: Cyclorhagida: Echinoderidae). *Organisms Diversity & Evolution, 8*(3), 230.e1–230.e18. doi:10.1016/j.ode.2007.11.003.
Sousa, M. C. (2003). Scientific Illustration, Part1: Traditional Techniques and NPR Approaches. *Theory and Practice of Non-Photorealistic Graphics: Algorithms, Methods, and Production Systems*, *10*. http://sites.google.com/site/shankarg73/hand_1.pdf. Accessed 14 April 2014.
Weigmann, S., Stehmann, M. F. W., & Thiel, R. (2013). *Okamejei ornata* n. sp., a new deep-water skate (Elasmobranchii, Rajidae) from the northwestern Indian Ocean off Socotra Islands. *Deep Sea Research Part II: Topical Studies in Oceanography*. doi:10.1016/j.dsr2.2013.09.005.
Wilson, G. D. F. (2008). A review of taxonomic concepts in the Nannoniscidae (Isopoda, Asellota), with a key to the genera and a description of *Nannoniscus oblongus* Sars. *Zootaxa, 1680*, 1–24.
Zweifel, F. W. (1988). *A handbook of biological illustration* (2nd ed.). Chicago: The University of Chicago Press.

Author contributions

The automated stippling process was developed by Simon Bober based on manual stippling, a method established by Torben Riehl. All figures, except for Fig. 6, were made by S. Bober. The first draft of the manuscript was written by S. Bober with subsequent contributions of T. Riehl.

Chapter 9

General Discussion

General Discussion

Cosmopolitan species in the deep sea

In recent history abyssal species were typically considered to be cosmopolitan due to the assumed lack of barriers within the abyssal habitat (Bruun, 1957). And many morphological studies confirmed widespread species in the deep sea (Brandt, 1991; Stockton, 1982; Wägele, 1986). However, due to genetic investigations a high genetic diversity with high genetic differentiation was attested to many taxa in the deep sea (Brasier et al., 2016; Chase et al., 1998; Held, 2003; Janssen et al., 2015; Moura et al., 2008; Quattro J. et al., 2001; Raupach et al., 2007; Vrijenhoek, 2009; Zardus et al., 2006) and cryptic species were repeatedly found in deep sea (Brandt et al., 2014; Brix et al., 2015, 2014, 2011; Brökeland, 2010b; Bucklin et al., 1987; Eustace et al., 2016; France and Kocher, 1996; Held, 2003; Held and Wägele, 2005; Larsen, 2003; Leese and Held, 2008; Miyamoto et al., 2010; Raupach and Wägele, 2006; Schnurr et al., 2018; Wilson et al., 2007). In Chapter 5 a similar case was treated and the *Macrosytlis sabinae-amaliae* complex had to be established for two macrostylid species, which are morphologically identifiable only by their adult males. A comparable problem was also found within the asellote family Haploniscidae Hansen, 1916 by (Brökeland, 2010b). This is a special case of cryptic speciation potentially driven by sex-specific selective forces, in Macrostylidae the males are potentially actively seeking more stationary females (Chapter 5; Heitland, 2015; Kniesz et al., 2017; Riehl et al., 2012). The specimens of the *Macrosytlis sabinae-amaliae* complex are not fully cryptic, but without genetic analyses the females remain virtually indistinguishable to the human eye. In the absence of a better concept, the complex was established, so that we have a taxonomic unit to address the cryptic material now and new material in future.

Cryptic species are so commonly found in deep-sea peracarids that (Raupach et al., 2007) proposed the *patchwork theory*, which says that most if not all widespread peracarids with benthic lifestyle are in reality closely related but distinct species.

This theory is hardly supported by recent revelation on the widespread deep-sea amphipod *Eurythenes gryllus sensu lato* and the data presented here on widespread isopods in Chapter 2, 3 and 4. *Eurythenes gryllus* is an interesting taxon, which has much in common with the here studied *Acanthocope galatheae*. Both species were morphologically considered a cosmopolitan species (Brandt et al., 2012; Ingram and Hessler,

1987; Schmid et al., 2002; Smith et al., 1979) and both species belong to the natatory suprabenthos. The taxonomic status of *E. gryllus* however was dubious, morphologically (Barnard, 1961; Bowman and Manning, 1972; Ingram and Hessler, 1983) and genetically (Bucklin et al., 1987; France and Kocher, 1996; Havermans et al., 2013).
In 1961 Barnard already wrote (p. 25): "*The still cloudy status of giant amphipods assignable to Eurythenes gryllus suggests directions for future science*".
Among multiple morphological investigations there was disagreement regarding the relevance of certain morphological characters (Charmasson and Calmet, 1990; Christiansen et al., 1990; Thurston and Bett, 1995), with some authors assuming the presence of multiple species (Bowman and Manning, 1972; Ingram and Hessler, 1983; Thurston and Bett, 1995). Also specimens of *A. galatheae* sampled at different localities caused controversy: Malyutina (1999) analyzed a specimen from the Southern Atlantic and found the mandibular palp to be reduced to two articles and possibly a different fragmentation of the article five of the antennula, which might have been missed or misjudged in the original description by Wolff (1962) with specimens sampled in the Gulf of Panama. Schmid et al. (2002) described further individuals from the Southern Atlantic and states (p. 5): "*An ultimate decision whether the Caribbean specimens are really conspecific with the ones from the southwest Atlantic is not possible with the available data ... The known morphological differences are small and give no clue (Malyutina 1999*)".
In *E. gryllus* multiple genetic studies rather suggest a species complex, the most recent analyses suggests nine species–level lineages, with partly overlapping geographic ranges (Havermans et al., 2013). All performed molecular analyses agree in a bathymetric distinction between lineages (Bucklin et al., 1987; France and Kocher, 1996; Havermans et al., 2013), which furthermore rejected the previously assigned extensive bathymetric distribution of *E. gryllus*.
The vast geographic distribution of haplotypes in the abyssal Atlantic study and also in the Pacific Ocean of *E. gryllus* (France and Kocher, 1996) is of great relevance to this study. These widespread haplotypes were included in the analyses by (Havermans et al., 2013) and formed the clade *Eg3* which was later described by D'Acoz and Havermans in 2015 and is today accepted as *Eurythenes maldoror*. The species *E. gryllus sensu stricto* is nowadays considered a bathyal species with bipolar distribution (Havermans et al., 2013: Clade *Eg1*).
Eurythenes maldoror is not the only cosmopolitan species of its genus. In 2015 Ritchie

et al. found an individual being genetically identical to *Eurythenes magellanicus* (H. Milne Edwards, 1848) in the Peru-Chile Trench in the Pacific, which was genetically known only from the Brazil Basin in the Atlantic (Havermans et al., 2013: Clade *Eg4*, *Eg5*; see also D'Acoz and Havermans, 2015). This emphasizes that unrestricted gene flow between oceans and across barriers in the abyssal deep sea is possible for benthic Peracarida.

As it is mentioned by Eustace et al. (2016), the lacking variance could also result from incomplete lineage sorting after the formation of the Isthmus of Panama approximately 3.0 million years ago (mya) (Ibaraki, 1997; O'Dea et al., 2016). However, the type locality for this species was described from the Drake Passage off Cape Horn, where the holotype was part of a fish´s gut content. Assuming the holotype and genetically identified *E. magellanicus* belong to the same species, the holotype would close the gap between the Atlantic and Pacific populations in the Southern Ocean. *Eurythenes maldoror* or *E. magellanicus* is possibly the species already mentioned in 1987 by Bucklin et al. Their analyses were based on allozyme assays, where little variation was found within a geographic distance of 4,000 km in the North Pacific.

The population structure of *A. galatheae* in the Atlantic is comparable to that of *E. maldoror*, but in *A. galatheae* the Atlantic populations seem to be separated from the Pacific populations for approximately 3.0–7.0 mya (Chapter 4). The time of divergence coincides with the formation of the Isthmus of Panama. However, as discussed in Chapter 4 in detail, due to the closure of deep passages already 9.2 mya, today's distribution range is most likely not a result of the Isthmus of Panama.

The recent findings on *E. maldoror* and *E. magellanicus* and the herein described distribution range of *A. galatheae* challenges the universality of the *patchwork theory* by Raupach et al. (2007) and confirms the existence of cosmopolitan and widespread species in the abyssal deep sea in rare cases. The *patchwork theory* is based on *Betamorpha fusiformis* (Barnard, 1920), which belongs to the same suprabenthic family Munnopsidae like *A. galatheae*. Therefore, one has to be careful about generalizations. The motile ability of a species is obviously not the only factor relevant for extensive distribution ranges. However, it is most important to emphasize that although such extensive geographic distribution ranges occur, they remain exceptional within deep-sea peracarids. Although *A. galatheae* was shown to be a pan-Atlantic, widespread species in Chapter 4, the previously hypothesized cosmopolitism of *A. galatheae* has to be rejected.

Barriers in the deep sea

The occurrence of true benthic cosmopolitans in the abyssal deep sea shows that there are no definitive barriers in the deep sea. However, dispersal ability and ecological fitness varies between taxa and cosmopolitans are more exceptional than common. The significance of a barrier and the resulting distribution range varies among species. Therefore, a possible barrier effect induced by the Mid-Atlantic Ridge (MAR) was tested on four different isopod families.

Among four families studied in Chapter 2 and 3, three families had at least one species that was distributed across the MAR. But contrary to the previously mentioned cosmopolitism of some deep-sea species, the conclusive results from the sampled animal groups during the VEMA–TRANSIT expedition suggest that the MAR represents a barrier to gene flow for the majority of taxa. The macrofaunal (Brandt et al., 2018) and meiofaunal assemblages (Schmidt et al., 2018) differed significantly in terms of species composition and abundance between eastern and western sampling sites. At the species level a significant difference across the MAR was found in polychaetes (Guggolz et al., 2018), harpacticoid copepods (Schmidt et al., 2018), as well as the isopod families Macrostylidae (Riehl et al., 2018), Desmosomatidae and Nannoniscidae (Chapter 3). In opposite to all other analyzed taxa the nematode study by Lins et al., (2018) found no significant difference across the MAR in genus composition and species distribution of the genus *Acantholaimus* Allgén, 1933. Previous studies attested generally low levels of endemism for deep-sea nematodes (Bik et al., 2010), however, due to few species delimitating characters in nematodes most ecological analyses are performed at genus level (Ingels et al., 2011; Pape et al., 2013; Vanreusel Ann et al., 2010), which lacks resolution for biogeographical analyses. In consequence, this study is difficult to compare to the other analyzed taxa. As stated by Lins et al. (2018) molecular analyses might reveal further cryptic species with reduced distribution ranges each. Genetic analyses can help delimitating species as it is shown in Chapter 3 for Desmosomatidae/Nannoniscidae, in Chapter 4 for *A. galatheae* or by Riehl et al. (2018) for Macrostylidae.

In contrast to the most recent results from the Vema-TRANSIT expedition presented herein, most previous studies on the MAR as a barrier were limited to bathyal depth above 2,800 m (deep-sea fish (Knutsen et al., 2012; Priede et al., 2013; White et al., 2011), bivalves (van der Heijden et al., 2012), holothurians (Shields et al., 2013), polychaetes (Shields et al., 2013; Shields and Blanco-Perez, 2013) and isopods (Brix et al.,

2014)). These studies found no distribution barrier across the MAR.

Merely the studies on bivalves (Etter et al., 2011; Zardus et al., 2006), Foraminifera (Pawlowski et al., 2007), amphipods (France and Kocher, 1996; Havermans et al., 2013) and isopods (Brix et al., 2015) were performed on species from abyssal depth, but these studies furthermore found no distribution barrier in the MAR. However, both analyzed protobranch bivalves *Ledella ultima* (E. A. Smith, 1885) and *Deminucula atacellana* (Schenk, 1939) for instance have a planktotrophic development (Etter et al., 2011; Rhind and Allen, 1992), which is most likely favorable for passive long distance dispersal with currents (Etter et al., 2011). Deep-sea currents are able to penetrate and cross the MAR, and provide means of dispersal for planktonic larvae across such barriers. Trans-MAR currents through fracture zones were repeatedly reported (Eittreim et al., 1983; Fischer et al., 1996; Heezen et al., 1964; McCartney et al., 1991; Mercier and Speer, 1998; Metcalf et al., 1964; Vangriesheim, 1980) and also a theoretical model suggests an insufficient separation of basins when there are breaks, such as fracture zones, within the barrier (Pedlosky and Spall, 1999).

In contrast to a geographic isolation the results on bivalves, foraminifera and amphipods suggest a bathymetrical isolation of species. When genetic differentiation was found it was higher between bathyal and abyssal populations, than among populations within one depth zone, indicating an isolation of the abyssal from the bathyal fauna. Thus depth seems to be a more significant barrier than geological barriers within the abyss.

For the direct developing Peracarida, distribution ranges across the MAR in the deep sea are scarce. Brix et al. (2014) showed that the Reykjanes Ridge, which is the region of the MAR around Iceland, is no barrier to gene flow in the desmosomatid *Chelator insignis* species complex at bathyal depth of 214–305 m. Until recently solely the already mentioned amphipod *Eurythenes maldoror* (France and Kocher, 1996: here still known as *E. gryllus*) and the isopod *Parvochelus russus* Brix and Kihara, 2015 were known to have an abyssal distribution range across the MAR. For *P. russus* a sporadic connectivity through the Romanche Fracture Zone was assumed (Brix et al., 2015).

Due to the sampling effort of the Vema-TRANSIT expedition (see Chapter 2–4 and Riehl et al. (2018)), five additional abyssal isopod species are identified with trans-MAR distributions (*Macrostylis* sp. VTpap, *Macrostylis* sp. ML08, *Acanthocope galatheae sensu stricto*, *Prochelator barnacki* Bober and Brix, 2018, *Whoia sockei* Brix and Kihara, 2018). The preliminary denotation *Macrostylis* sp. VTpap and *M*. sp. ML08

is derived from Chapter 2 and Riehl et al. (2018), due to a lacking formal description of these proposed species.

The suprabenthic species *E. maldoror* and *A. galatheae* have identical haplotypes even across the MAR, suggesting recent and possible ongoing dispersal and gene flow across the MAR. *Eurythenes maldoror* had identical haplotypes in the 16S gene and little divergence (0.8–2.0 % K2P-distance) in the COI gene across the MAR. *Acanthocope galatheae* shared identical haplotypes across the MAR within 16S and COI. It seems as if the MAR has no effect on the distribution range of these two species (Chapter 2–4; France and Kocher, 1996; Havermans et al., 2013). The other three species are either in- or epibenthic and had slightly higher levels of divergence across the MAR. *Parvochelus russus* had a trans-MAR divergence of 1.5–11.9 % uncorrected pairwise-distance (*p*-distance) within the COI gene (Brix et al., 2015). *Macrostylis* sp. MLpap had a *p*-distance of 0.5 %, *P. barnacki* of 1.1 % and *W. sockei* of 3.8 % in the 16S gene. As discussed in Chapter 2 the few mutational steps within *M.* sp. MLpap suggest a recent dispersal event across the MAR. The *p*-distance of *P. barnacki* is comparable to the measured *p*-distance of *P. russus*, therefore a historical dispersal across the MAR has occurred. For *W. sockei* a recent dispersal is unlikely, but both species are morphologically indistinguishable and the barcoding gap detection analyses in Chapter 3 furthermore suggest that both individuals belong to the same species. Only further sampling of that region could reveal the connectivity of this particular species.

However, despite few species being able to cross the MAR successfully and to establish trans-MAR populations, most species are not. The few species seemingly unaffected by the MAR were found to be capable swimmers. This conclusion confirms the hypothesis on natatory species being more effective dispersers in the deep sea.

The overall biogeographical assumptions retrieved from the samples from the Vema Fracture Zone (VFZ) in the Atlantic coincide with studies on the Blanco Transform Fault in the Northeastern Pacific. The connectivity of vent fauna was tested with sessile tube worms *Ridgeia piscesae* Jones, 1985 (Young et al., 2008) and Limpets of the genus *Lepetodrilus* McLean, 1988 (Johnson et al., 2006). Like the VFZ the Blanco Transform Fault is found to be an isolation barrier for species with limited dispersal capabilities. For species with better dispersal capabilities gene flow is reduced but not ceased.

However, barriers in the deep sea appear in very different forms; In Chapter 5 for

instance, the connectivity of the inbenthic *M. sabinae* was tested across the Kuril-Kamchatka Trench (KKT) -a hadal trench. Individuals across the trench had little genetic divergence (0.2 % *p*-distance). Yet, the genetic distance does not correlate with geographic distance (Mantel test, r= 0.191, 9999 replicates, $p > 0.30$). This observation was statistically confirmed by Monmoniers´s algorithm, thus a reduced gene flow across the trench was assumed, what confirms the hypothesis that hadal trenches represent distribution barriers in the abyssal deep sea.

The Greenland-Iceland-Scotland Ridge (GIS-Ridge) is another considerable barrier in the North Atlantic, which separates the Nordic Seas from the North Atlantic. The deepest passage is 840 m deep (Hansen and Østerhus, 2000) and therefore the GIS-Ridge was proposed to be a substantial barrier for the abyssal fauna (Brix et al., 2014; Brix and Svavarsson, 2010; Schnurr et al., 2014). Similar to the results we retrieved from the VFZ, many studies have shown that the GIS-Ridge is a an effective barrier for multiple taxa (Brix and Svavarsson, 2010; Jennings et al., 2018; Negoescu and Svavarsson, 1997; Schnurr et al., 2018, 2014; Stransky and Svarvarsson, 2006; Weisshappel, 2001, 2000) and the connectivity of peracarid crustaceans is at least reduced.
Based on the genetic analyses by Brix and Svavarsson (2010) of 34 desmosomatid and nannoniscid isopod species, only five species were commonly found north and south of the GIS-Ridge and five more were found to be able to cross the ridge ocassionally. Interestingly, the species found only north or south, were found at shallower depth than the actual saddle depth of the GIS-Ridge, thus the authors concluded that the species are most likely bound either to the cold waters north or warm waters south of the ridge and are not physically separated by the ridge. The species that crossed the ridge were either eurybath or distributed at shallower bathyal depth and were able to inhabit waters with a wide temperature range (< 0 to ≥ 6°C), which supports the author's hypothesis.
Jennings et al., (2018) analyzed the distribution of the desmosomatid genus *Oecidiobranchus* Hessler, 1970 across the GIS-Ridge in more detail. The authors found three to four operational taxonomic units (OTU) at species level in the GIS-region. OTU 1 (*Oecidiobranchus* cf *plebejum*) was found exclusively north of the GIS-Ridge and OTU 3 (O. sp. nov.) was only found at shallow depth on the GIS-Ridge. OTU 2 (*O.* cf. *nanseni*) was found north and south of the ridge, but the southern population was separated from the northern population by 22 mutational steps in the COI gene and two mutational steps in 16S gene, indicating an at least reduced gene flow across the ridge.

A pure morphological approach was performed by Brökeland and Svavarsson (2017) on Haploniscidae. Eight of ten species were limited to the southern boundary of the GIS-Ridge. The only two species *Haploniscus bicuspis* (Sars G.O., 1877) and *H. angustus* Lincoln, 1985 occurring on both sides of the ridge were in contrast to the other sampled species occurring at shallower depth than the saddle depth of 840 m. The authors concluded that for this family the physical presence of the GIS-Ridge limits the distribution of most of the haploniscid species towards the Northern Seas.

Schnurr et al. (2014) analyzed the faunal composition of the natatory Munnopsidae in the same region morphologically and genetically (Schnurr et al., 2018). The conclusions based on genetic and morphological analyses differed, which emphasizes the significance of a combination of multiple methods. Based on the more recent genetic analyses only two species (*Eurycope producta* Ep_1, *E. inermis* Ei_B_C) of twelve delimitated species are found north and south of the GIS-Ridge. One of these two species (*E. inermis* Ei_B and EI_C) shows signs of genetic differentiation across the ridge and as stated by the authors might indicate an early stage of allopatric speciation. The GIS-Ridge seems to restrict the distribution range of most, but not all *Eurycope* G.O. Sars, 1864 species. Although munnopsid species do have an enhanced swimming capability, the dispersal ability across the ridge seems comparable to that of Desmosomatidae, Nannoniscidae and Haploniscidae (Brix and Svavarsson, 2010; Brökeland and Svavarsson, 2017). Species at the GIS-Ridge have to cope with extreme environmental challenges across the ridge, such as temperature and salinity changes induced by the differing water masses originating from the Atlantic south and the Arctic Ocean north of the ridge (Hansen and Østerhus, 2000). Specifically in this case the enhanced natatory capabilities might increase the dispersal ability, but do not help to sustain in a habitat with unfavorable environmental conditions. As discussed for the MAR in the next section, the habitat on both sides of a barrier and hence the ecological adaptability of a species is essential for successful colonization and subsequent gene flow across a barrier.

Another prominent ridge in the Atlantic is the Walvis Ridge in the SE Atlantic, which extends from the MAR and separates the Angola Basin from the Cape Basin. This ridge was hypothesized to represent a distribution barrier for benthic deep-sea macrofauna (Brandt et al., 2005), but against expectations Brökeland (2010a) showed for the epibenthic isopod *Haploniscus rostratus* (Menzies, 1962) based on morphological characters and the COI gene that the Walvis Ridge is an insufficient barrier to gene flow This

assumption was later confirmed in a study by Brix et al. (2011).

Based on previous studies and recent data it is impossible to create an universal conclusions regarding the effect of potential barriers for all deep-sea taxa.
Since it was shown in multiple studies that there are always certain species that are not affected by the respectively analyzed barrier, the most general conclusion would be that there are no barriers in the deep sea. A more nuanced conclusion would be that whether a barrier is limiting the distribution range of a species depends on the species´ motility, reproductive strategy and ecological requirements. Previous studies demonstrated that bathyal species with higher bathymetric tolerances and swimming abyssal species such *as A. galatheae* or species with drifting larvae like bivalves are more likely to cross geographic barriers such as ridges. Non-swimming abyssal benthic species on the contrary are more affected by these barriers as shown for Macrostylidae, Desmosomatidae and Nannoniscidae.
However, although there usually are exceptional species that are able to sustain distribution ranges across barriers, most species are not. These barriers are therefore capable of structuring populations, which might even lead to allopatric speciation (Chapter 4; Schnurr et al. 2018).

The Mid-Atlantic Ridge -what else could explain the observed population structure?

The MAR as a physical barrier is perhaps not the only reason to explain the observed faunal divergence across the MAR. The MAR does not just separate one uniform habitat in two regions with identical habitat properties, the basins west and east of the MAR differed in multiple abiotic parameters that might explain the dissimilar faunal assemblages as well.
The sites sampled to the west of the MAR were characterized by either manganese crusts or nodules (Brandt et al., 2018), a disturbance of the typical deep-sea soft sediment, which was for instance found in the eastern sites exclusively (Devey et al., 2018). In the eastern Atlantic elevated particulate organic carbon (POC), total organic carbon (TOC) and total nitrogen (TN) levels were measured and the sediment grain size differed between eastern and western stations (Schmidt et al., 2018).
The sediment grain size was coarser at the western sites (Devey et al., 2018; Lins et al., 2018; Schmidt et al., 2018). Grain size and grain size diversity can directly affect

meiofaunal (Kitahashi et al., 2012; Montagna, 1982) as well as macrofaunal assemblages (Leduc et al., 2012; Wheatcroft, 2003). Especially, burrowing or tube dwelling animals like *Macrostylis* spp. might favor certain sediment types. As shown in Chapter 6 macrostylids are targeting sand grains to build their statoliths and thus are potentially dependent on sandy sediments. The abundance of macrostylids was for instance lower in the west with coarser sediments compared to the east (Riehl et al., 2018). However, these differences are best explained by the hard substrate, which is unsuitable for inbenthic species and furthermore reduces the efficiency of the sampling gear.

The environmental factors, such as POV, TOC, TN, depth and grain size statistically correlate with the increased meiofaunal abundance in the east (Lins et al., 2018; Schmidt et al., 2018) and most likely with the macrofaunal abundance as well. Compared to the east, the west had reduced levels of carbon; but the western sides were by no means free of carbon influx, photographs showed accumulated *Sargassum* debris (Devey et al., 2018). Nevertheless, if food is the most limiting factor in the deep sea (Gooday et al., 1990; McClain et al., 2012; Smith et al., 2008), an increased supply of POC and TOC in the east could explain higher abundances.

The hereby presented divergent abiotic factors could explain different faunal assemblages and impede a successful colonization of species from the respective other habitat even without the MAR being a physical barrier. As mentioned in Chapter 2 and 3, six species were able to establish populations within the Vema Transform Fault (VTF) invading from the eastern and western basins, but trans-MAR distributions are rare. Assuming the populations east and west of the MAR are at equilibrium or near-equilibrium state, niches are occupied and competitive exclusion is furthermore impeding a successful colonization across the MAR (Gillespie and Roderick, 2002; Simberloff and Wilson, 1970, 1969). Moreover, species that are able to occasionally cross a barrier have, due to a low population density a disadvantage in finding a mating partner (Allee effect) (Stephens et al., 1999). Within the VTF however several species from both habitats seem to successfully co-exist. The VTF as intermediate habitat between both sides is possibly easier to colonize due to more similar abiotic parameters to their habitat. Additionally, due to the neighboring position individuals potentially invade the habitat more frequently, what increases the possibility of a successful reproduction.

Another possible explanation is the exceptional location of the VTF within the MAR, which is more prone to disturbances by currents. The *intermediate disturbance hypothesis* by Connell (1978) says that diversity is higher at intermediate levels of distur-

bance, in opposite to a habitat at equilibrium state. The *contemporaneous disequilibrium hypothesis* by Richerson et al. (1970) could furthermore explain the co-existence of competitive species within the VTF. Periodic disturbances combined with proposed slow rates of colonization in the deep sea (Grassle, 1977; Khripounoff Alexis et al., 2006; Miljutin et al., 2011) could create patches of microhabitats in which competing species are able to co-exist. Due to the unbalanced sampling success among sites and the single sampling station within the VTF, assumptions remain highly speculative and sampling bias might have played an important role as well.

The Vema samples were taken along a vast transect (2,776 km) with an average distance of 560 km between sampling sites. The geographic distance one species has to cover to maintain a trans-MAR distribution based on this sampling effort is at least 1,215 km (geographic distance from sampling site 6 to sampling site 9). With such large distances, isolation-by-distance is a further factor one has to consider to explain the observed distribution patterns. Within the Vema samples, a common distribution range of desmosomatid and especially nannoniscid species covers one or two sampling sites (Chapter 3). Thus, species sampled at two stations have a proven distribution range of only ~560 km. In Chapter 2 a Mantel test was further performed on trans-MAR species to test a correlation between Φ_{ST} and geographic distance for *Macrostylis* sp. MLpap and *A. galatheae*. The test was not significant, what indicates that the mere geographic distance is not the reason for the observed population structure in these two widely distributed species. The genetic analyses on the isopod family Macrostylidae of Riehl et al. (2018) found a clear distinction between the three areas East, West and VTF with a conical analysis of principal coordinates. Therefore, geographic distance alone is unlikely the only reason for the observed population structure in Macrostylidae. However, most analyzed species had narrow distribution ranges as shown in Chapter 3 and thus geographic distance in itself has to be considered as barrier for many species. Apart from the geographic distance all other discussed factors are at least induced by the MAR. So even if the MAR is not a physical barrier, the MAR might still induce a barrier effect on the abyssal benthic macrofauna.

Natural history information derived from museum material

Behavioral information of deep-sea isopods is rare as live observations are difficult and usually not possible under laboratory conditions (see also Chapters 1, 6, 7). In Chap-

ters 5–7 it was possible to infer natural history information from fixed material. The assumption by Brökeland et al. (2010) that the soft walled Foraminifera of the superfamily Komokioidea is a valuable food source for munnopsid isopods was confirmed in Chapter 7. One sampled specimen of *Betamorpha* cf. *profunda* was caught while feeding on a Komokioidea. To preserve this unique snapshot of deep-sea asselote behavior, methyl salicylate (Methyl 2-hydroxybenzoate) was used to change the refractive index and to be able to look through the cuticle inside the specimen. This method is reversible and once the specimen is removed from methyl salicylate it will lose its transparency. We were able to show that this specimen was feeding and digesting Komokioidea.
Since Komokioidea are globally abundant (Gooday et al., 2004; Tendal and Hessler, 1977) and Foraminifera considerably contribute to the deep-sea biomass (Altenbach and Sarnthein, 1989; Gooday et al., 1992), Foraminifera would represent a sustainable food source for benthic macrofauna. For instance, Komokioidea were found in all Vema-TRANSIT samples (pers. observation) and, therefore, food availability was most likely not a restrictive factor for foraminiferivory species along the sampled transect. This knowledge is an important insight into the difficult to access deep-sea food web.

The statocysts of Macrostylidae were anatomically analyzed in Chapter 6, an organ already mentioned with the erection of the family Macrostylidae by Hansen in 1916. The function of this organ however remained unclear (Wägele, 1989). Only the isopod families Anthuridae and Leptanthuridae of the superfamily Anthuroidea have one or two statocysts in the telson (Poore, 2001; Wägele, 1989, 1981), of which the paired statocyst is the plesiomorphic state (Wägele, 1989, 1981). Statocysts as organs of equilibrium in isopods are presumed to be present especially in burrowing species and irrelevant for swimming and walking locomotion (Langenbuch, 1928; Wägele, 1981). Experiments show that once the statocyst is removed in *Cyathura carinata* (Krøyer, 1847) the individuals are no longer able to dig vertical burrows (Langenbuch, 1928). Furthermore, it was suggested that the statocysts of Paranthuridae Menzies and Glynn, 1968 were lost because members of this family no longer live within the sediment but rather climb on algae (Langenbuch, 1928).
The statocysts of *Cyathura polita* Stimpson, 1886 and *C. carinata* of the family Anthuridae were morphologically described within Isopoda (Langenbuch, 1928; Rose and Stokes, 1981). As already suggested by Wägele in 1989 the assumption of a convergent development of statocysts within Isopoda in Anthudridae and Macrosrylidae is con-

firmed based on their differing anatomy, and unlikely relatedness of both taxa. Furthermore it was possible to demonstrate that the statoliths of Macrostylidae are in contrast to those of Anthuridae made of SiO_2 and not calcium salts. Thus, the hypothesis that Macrostylidae as deep-sea family are, potentially due to the carbonate compensation depth, not building their statoliths from calcium salts was confirmed.

Although Macrostylidae are thought to be obligatory inbenthic (Harrison, 1989; Hessler and Strömberg, 1989; Hessler and Wilson, 1983; Wägele, 1989), recent studies on Macrostylidae assumed a shift to a rather epibenthic lifestyle in adult males (Chapter 2 and 5; Kniesz et al., 2017; Riehl et al., 2012). A shift to an epibenthic lifestyle in males was especially presumed in sexual dimorphic species. A range of morphological adaptations in adult males support this hypothesis. Some males of sexually dimorphic species such as *M*. sp. MLpap have dramatically elongated posterior pereopods (unpublished drawings of *M*. sp MLpap: Heitland, 2015). The function of these elongated pereopods is unknown, but an advantage within the sediment is unlikely. *Echinozone* sp. was observed to use the elongated pereopods III–IV specifically for walking, which is also the case in other Munnopsidae (Hessler and Strömberg, 1989). Furthermore, the elongated pereopods could be used similar to the observation in Munnopsidae, in which animals swim up in the water column and the elongated pereopods serve as non-locomotory stabilizers, the authors call it a “hanging or parachuting posture” to prevent sinking (Marshall and Diebel,1995). An effective “walking” in the water column as observed for *Munneurycope* sp. 1 is probably unlikely due to the lack of suitable setation. Thus, the elongated pereopods are most likely used for walking on the sediment.
Kniesz et al. (2017) presented data on infestation rates with filter feeding ciliate epibionts on Macrostylidae, which showed that 64.3 % of the adult males were infested compared to 10.4 % of adult females, 12.5 % of juvenile females and 5.0 % of juvenile males. Ólafsdóttir and Svavarsson (2002) detected a higher infestation rate of epibenthic isopods compared to inbenthic isopods, which indicates that the macrostylid adult males are rather epibenthic. In addition, it seems that males of the sexually dimorphic species are more likely and heavier infested by epibionts (pers. observation).
As already stated by Riehl et al. (2012) the increased number of aesthetascs in adult males suggests a dependency on a chemosensory organ to find a mating partner. In Chapter 5 it was possible to show that in some species the adult males develop an additional type of aesthetasc (Chapter 5, Fig. 20G, 21), which is not found in females or

juvenile males. Since the common type of aesthetasc is preserved in low numbers in these males (possibly for general chemoreception), it is assumed that the diverged aesthetasc is specialized for long-range perception of female pheromones.

These observations among others suggest that it is not unlikely that macrostylid males are leaving the sediment for an epibenthic lifestyle and are actively searching for a mating partner.

These conclusions have an impact on biogeographical analyses. In Chapter 2 it was hypothesized that swimming, suprabenthic isopods are more likely to cross barriers compared to non-swimming, inbenthic species. We were able to show that the swimming Munnopsidae *A. galatheae* had the widest distribution range of all analyzed species, but the inbenthic Macrostylidae did not differ in their distribution patterns from the epibenthic facultative swimming Desmosomatidae. The analyzed desmosomatid genus *Prochelator* is known to have natatory adaptations (Hessler and Strömberg, 1989) and, therefore, we assumed an enhanced dispersal ability and thus increased distribution range for this species. Macrostylid isopods as inbenthic group may therefore not be as restricted geographically as previously hypothesized. It was for instance also shown in shallower waters for inbenthic Cumacea Krøyer, 1846 that they are regularly leaving the sediment and swim up in the water column (Anger and Valentin, 1976), a behavior found in many Peracarida (Dauvin and Zouhiri, 1996). As a result, also inbenthic Peracarida might leave the sediment regularly. The long-range connectivity of populations in Macrostylidae comparable to that of epibenthic isopods is furthermore interpretable by an epibenthic phase in adult males. However, for an enhanced distribution range, also the females should be able to overcome such geographic distance and barriers.

These morphological studies show that classic morphology is a powerful tool to retrieve behavioral data even from difficult to access habitats like the deep sea.

Phylogenetic and taxonomic implications on Macrostylidae

The asellote family Macrostylidae was due to its high abundance, and its inbenthic life style and hence reduced dispersal ability, an important deep-sea model taxon for this thesis. Three new species from the Northwest Pacific were described and for two of which, the *Macrostylis sabinae-amaliae* complex had to be established due to cryptic females. Including the three herein described species the family Macrostylidae now comprises 90 accepted species (including two species *nomina dubia*).

New characters were assigned for species delimitation and the relevance of commonly

used characters was tested in Chapter 5. Interestingly, the anatomy of the statocysts differed slighlty among six species studied in detail (Chapter 6). Therefore, the statocyst might comprise a valuable character for macrostylid phylogeny and systematics.

During the KuramBio expedition 247 individuals of the *Macrostylis sabinae-amaliae* complex were sampled. This species complex was in numbers the most abundant macrostylid morphospecies during the expedition. However, due to the cryptic females and subadult males only 30 individuals were distinguishable on species level by genetic analyses. The female and juveniles of these species are distinguishable with genetic analyses only, solely the adult males can be morphologically differentiated on species level. Therefore the hypothesized morphological uniformity of these two species is rejected. The males of both species have multiple characters to distinguish both species, with the male antennule being the most striking character. The aspect ratio of the articles varies between both species. Furthermore, both species have two different kinds of aesthetascs (Chapter 5, Fig. 22), with *Macrostylis sabinae* exhibiting a unique type not observed in any other macrostylid species before. Within both species a sexual-size dimorphism was statistically confirmed. The males were significantly smaller compared to the females (Chapter 5, Fig. 39A), a trend observable for the whole species complex (Fig. 39B, D). Within the Asellota, a sex biased size dimorphism was previously found within the families Ischnomesidae (Kavanagh et al., 2015) and Haploniscidae (Brökeland, 2010a) and was now discovered in Macrostylidae as well. Since no morphological difference was detected among females, the whole complex was treated as one morphospecies and tested for size dimorphism. The size of ovigerous females varied considerably among stations (1.50–2.39 mm) indicating that the body size is only vaguely linked to the developing stage (but these size differences were not associated with the proven presence of a specific species of this complex), which questions the utility of body size as taxonomic character. A strong variation among ovigerous and non-ovigerous females was further obvious and found to be consistent among all available specimens. The pereonal collum 4 and to some extent 5 are distinct within non-ovigerous females, but is almost absent in ovigerous females (for details see Chapter 5). This results in a more squat body shape when the ovigerous females are marsupium bearing (Chapter 5, Fig. 34). For future taxonomic work within this group it was proposed to measure pereonite 4 excluding the collum.

The previously described method of Congo Red staining as fluorescence marker for confocal laser scanning miscroscopy (CLSM) (Michels and Büntzow, 2010) was commonly used to obtain surface scans (Brix et al., 2014; Kihara and Arbizu, 2012; Kottmann et al., 2013). In Chapter 5 this method was found to be useful for rare and delicate material, which deep-sea material often is. The specimen preparation for a SEM scan is irreversible and thus not advisable for holotypes and similarly valuable specimens. Therefore, the CLSM combined with *Congo Red* staining proved to be a valuable non-invasive method to obtain micrographs in a near SEM quality.

Digital inking, a hybrid process

In taxonomy accurate drawings are essential. Nowadays the use of pen tablets to create a digital line drawing is very common (Coleman, 2003). In Chapter 8 an automated shading method for digital line drawings is presented. Here an additional method is shown, which was developed to equalize taxonomic drawings of multiple authors in Chapter 3.

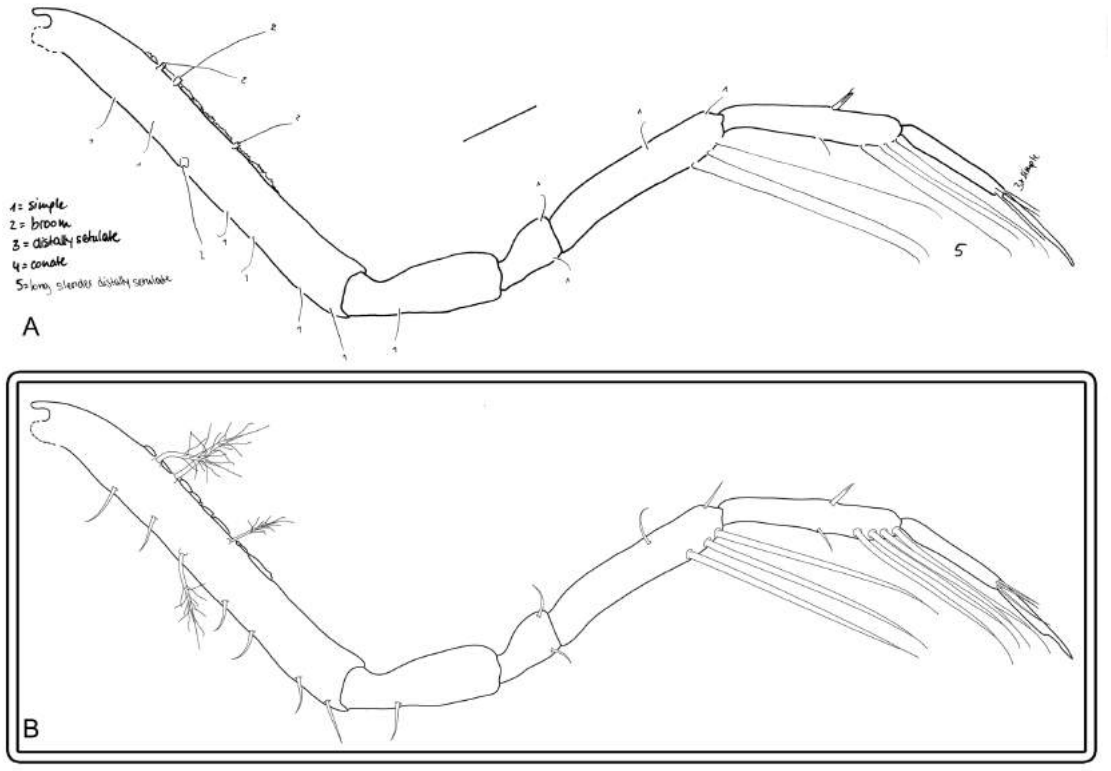

Fig. 2: A. outline sketch with simplified setation. The type of seta is simplified and only indicated by numbers. B. the final image, now converted into a digital vector graphic. The previously indicated setation was added accordingly

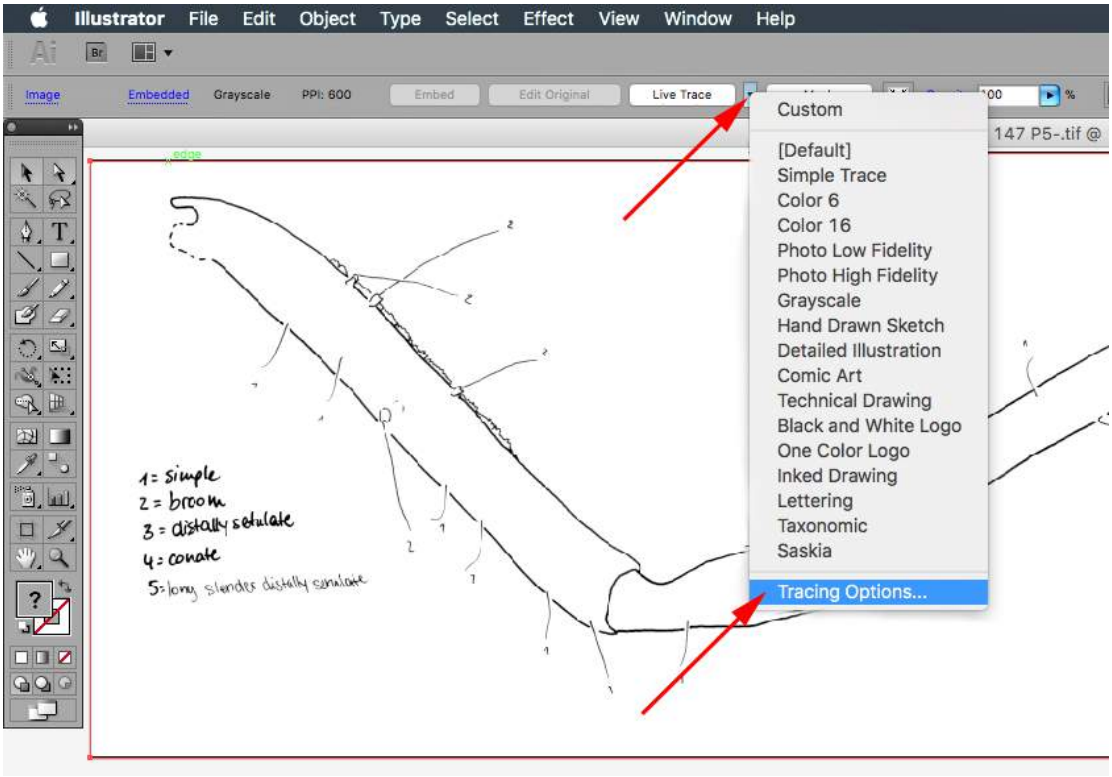

Fig. 3: This is where you find the *Live Trace* tool. For good results the *Tracing Options* need few adjustments

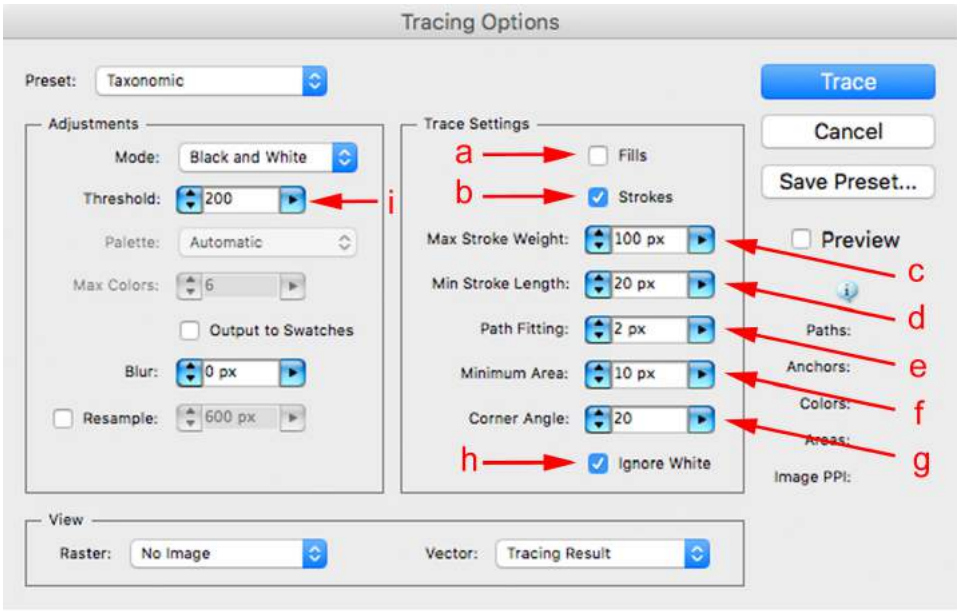

Fig. 4: *Tracing Options* window and the necessary adjustments.

This method can quickly transform pencil drawings into digital drawings in Adobe Illustrator using the *Live Trace* tool. The advantage of this method is that sketching the illustration on paper is still possible, but the tedious process of applying setation (Coleman, 2009) and shading (Chapter 8) is digitally simplified. Thus we have a hybrid process of both methods. A further advantage is that illustrations from multiple authors are equalized to match the same style and a pen tablet is not mandatory since corrections are easily made with the mouse.

For the here presented hybrid method a clean outlined sketch is sufficient (Fig. 2A). For each seta only the basis to distal tip and a note on type of seta are needed (Fig. 2A), the final seta is applied in Adobe Illustrator as described by Coleman (2009). The following step-by-step guide was written for Mac OS X with Adobe Illustrator CS5.

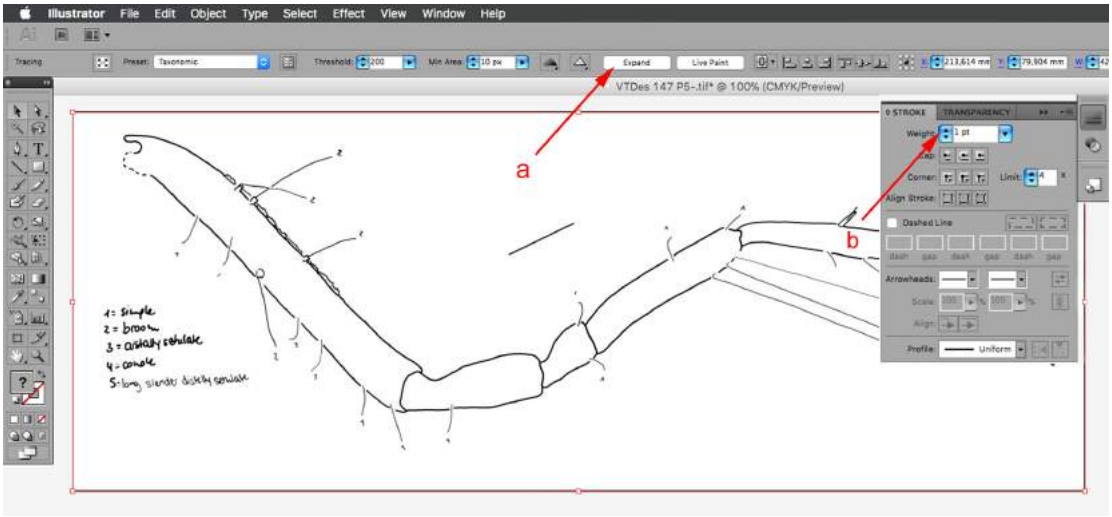

Fig. 5: If you are satisfied with the *Life Trace* result, click *Expand*. After conversion, the line weight is adjusted to 1 pt.

Step-by-step guide:

1. Prepare a simplified taxonomical drawing (Fig. 2A)
2. Scan the drawing and open the file in Adobe Illustrator
3. Click on the imported scan to have an activate selection and then click on the *Live Trace -> Tracing Options*... (Fig. 3)
4. Change the *Trace Settings* (Fig. 4):
    a. Deselect *Fills*
    b. Select *Strokes*
    c. *Max Stroke Weight*: 100 px
    d. *Min Stroke Length*: 20 px
    e. *Path Fitting*: 2 px
    f. *Minimum Area*: 20 px
    g. *Corner Angle*: 20
    h. Select *Ignore White*
    i. Set the *Threshold* to 200 (this setting is variable; sometimes a different *Threshold* delivers better results.)
5. Click on Trace, if you are satisfied with the result click Expand (Fig. 5a)
6. Select all (⌘A) and set the stroke weight to 1 pt (Fig. 5b)
7. Usually the selection is joined in a Group, for further adjustments a ungrouping is necessary (Object ➔ *Ungroup* or press ⇧⌘G).
8. Adjust the resulting paths as needed. The most powerful tool here is Delete Anchor Points to flatten lines.
9. As described by Coleman (2009) the suitable setae are added to the illustration.

The method is time saving when drawings are already available or for people who are not comfortable with pen tablets. For a trained person, however, the conventional method of digital inking with a pen tablet is faster and more convenient. The drawing has to be near perfect and corrections are still necessary after the conversion, therefore the conversion method is only an optional method and unsuitable to replace the digital inking method as described by Coleman (2003).

Conclusions and Outlook

Whether a barrier is affecting the distribution range of a species is related to the species´ motility, reproductive strategy and ecological adaptability. As presented in multiple previous studies bathyal eurybathic species seem to be more likely to cross barriers in the deep sea than abyssal stenobathic species.

The hypothesis that swimming isopods have an advantage over non-swimming species was confirmed, however the facultative swimming species of Desmosomatidae for instance had no advantage over the non-swimming inbenthic Macrostylidae.

Conclusions derived from the Vema-TRANSIT project suggest that most analyzed taxa were affected by the Mid-Atlantic Ridge (MAR) as a distribution barrier, only few species were found to have a distribution range through the Vema Transform Fault across the MAR. As a result, the hypothesis that the Vema Fracture Zone is due to its topology a continuous pathway across the MAR for the abyssal benthic fauna has to be rejected for the majority of species.

To obtain a more accurate understanding of the MAR as a barrier in the abyss, it is necessary to sample more transects across the MAR, near other fracture zones as well as areas without nearby fracture zones. Furthermore, a more comprehensive sampling in a smaller region would be beneficial for detailed population studies. As shown for *Acanthocope galatheae* in the Atlantic, mtDNA is for some species not sufficient to resolve a population structure. For future analyses other methods, such as RAD sequencing should be considered to obtain a higher resolution.

Swimming species such as the herein investigated *A. galatheae* or species with drifting larvae like polychaetes or bivalves are less affected by barriers and can have more extensive distribution ranges. The hypothesis that natatory species are more effective dispersers and that there are widespread and cosmopolitan benthic peracarids in the abyssal deep sea was confirmed. Nevertheless, *A. galatheae* was not verified to be a cosmopolitan species. *A. galatheae sensu stricto* is a pan-Atlantic species with seemingly persistent gene flow among populations, but a historic isolation of Atlantic and Pacific lineages is assumed. This study however suffered undersampling of non-Atlantic populations. To understand the pan-oceanic relatedness of populations more sampling of other populations is required.

In the course of this thesis three species of Macrostylidae were formally described using integrative taxonomy, thus the family Macrostylidae comprises 90 species by

the completion of this thesis (including two species *nomina dubia*). The *Macrostylis sabinae-amaliae* complex had to be established due to cryptic females in the herein described species *M. sabinae* and *M. amaliae*. Moreover, previously accepted morphological characters for Macrostylidae (body size, collum present/absent on fourth pereonite) were found to be misleading for species delimitation and should be avoided in future taxonomy. Furthermore, the importance to include ovigerous as well as non-ovigerous females for taxonomic descriptions was demonstrated.

An unknown type of aesthetasc was discovered in adult males of *M. sabinae*. Future taxonomist should carefully investigate the aesthetascs as worthwhile delimitating character in Macrostylidae. Within macrostylid statocysts, the composite statolith was found to be made from silicon dioxide particles (sand grains) in all investigated specimens and thus the hypothesis that the deep-sea living Macrostylidae are not building their statoliths from calcium salts as they live below the carbonate compensation depth was approved. However, the immediate fixation in ethanol after sampling, what is preferred for genetic studies rendered the material useless for many morphological studies and it was impossible to visualize the innervation of the macrostylid statocyst with immunohistochemistry. For future studies, it will be necessary to pick specimens from the samples before ethanol fixation, to store these samples in a fixative more suitable for morphological studies like Bouin´s solution.

Acknowledgements

First of all I want to thank my supervisor Prof. Dr. Angelika Brandt, who gave me the opportunity to execute this thesis and of course for her comprehensive knowledge and continuing support and trust.
Furthermore, I want to express my gratitude to Dr. Martin Schwentner for his profound expertise and thorough help during my final phase of this thesis.
Many thanks go to Dr. Torben Riehl for introducing me into the world of deep-sea biology, back when everything started with a master project on macrostylid statocysts. I am also very grateful to Dr. Saskia Brix for supporting me all this time and making many things possible.
Dr. Inmaculada Frutos deserves extended thanks aswell, she accompanied me through the whole process and was always available and shared so much knowledge on deep-sea peracarids
I want to especially thank Dr. Terue Cristina Kihara for introducing me into her lab routine and sharing her comprehensive knowledge about CLSM and staining techniques with me. Further I would like to thank Dr. Marina Malyutina for the introduction to the Munnopsidae.
Very special thanks go to the GRG: Theresa Guggolz, Klaas Gerdes, Dr. Stephan Henne, Lena Schwinger and Kathy Gebauer for their professional and especially non-professional support in the past years.
I highly appreciated that Sarah Schnurr shared her *R* knowledge with me and I want to thank Karen Jeskulke for her support in the lab and Kathrin Phillips Bussau and Petra Wagner for their technical support, as well as the working groups Wirbellose 2 and Biodiversität der Tiere and the DZMB Hamburg. Very special thanks go to Renate Walter and Dr. Frank Friedrich who always keep the SEM and other tools running and Sabine Gaude who helped me preparing histological sections.
Additionally, I owe thanks to everyone involved in the Vema-TRANSIT expedition (SO237), especially Dr. Nils Brenke, Ann-Christine Zinkann, Enrico Schwabe and Dr. Kathrin Linse. Off course I also want to thank all the editors and anonymous reviewers.
My deepest gratitude goes to my wife Daniela Bober who now probably knows just as much about deep-sea crustaceans as I do.

This thesis was realised within the project Vema-TRANSIT, which received funding from the German Ministry for Science and Education (BMBF), grant 03G0227A.

Eidesstattliche Versicherung

Hiermit erkläre ich an Eides statt, dass ich die vorliegende Dissertationsschrift selbst verfasst und keine anderen als die angegebenen Quellen und Hilfsmittel benutzt habe.

Affirmation in lieu of oath

I hereby declare, on oath, that I have written the present dissertation on my own and have not used other than the acknowledged aids.

Signature / Unterschrift

SENCKENBERG
world of biodiversity

Senckenberg | Senckenberganlage 25 | 60325 Frankfurt

To whom it may concern!

3.7.2018

Publications of Simon Bober

Simon Bober hat in seiner Dissertationsschrift die Beteiligung der Autoren an den einzelnen Veröffentlichungen dargelegt. Ich bestätige hiermit, dass seine Beteiligung der tatsächlichen Arbeitsverteilung entspricht.

SENCKENBERG FORSCHUNGSINSTITUT UND NATURMUSEUM FRANKFURT

Prof. Dr. Angelika Brandt | Abteilungsleiterin | Abteilung Marine Zoologie

T +49 (0) 69 7542 - 1249 F +49 (0) 69 746238 angelika.brandt@senckenberg.de www.senckenberg.de

SENCKENBERG Gesellschaft für Naturforschung | Senckenberganlage 25 | 60325 Frankfurt am Main
Direktorium: Prof. Dr. Dr. h.c. Volker Mosbrugger, Prof. Dr. Andreas Mulch, Stephanie Schwedhelm, Prof. Dr. Katrin Böhning-Gaese, Prof. Dr. Uwe Fritz, Prof. Dr. Ingrid Kröncke

Frankfurter Sparkasse | IBAN DE15500502010000760157 | SWIFT HELADEF1822 | USt/DNr. DE114235295

Mitglied der Leibniz-Gemeinschaft

References

Altenbach, A.V., Sarnthein, M., 1989. Productivity record in benthic foraminifera, in: Berger, W.H., Smetacek, V.S., Wefer, G. (Eds.), Productivity of the Oceans: Present and Past. New York, pp. 255–279.

Anger, K., Valentin, C., 1976. In situ studies on the diurnal activity pattern of *Diastylis rathkei* (Cumacea, Crustacea) and its importance for the "hyperbenthos." Helgoländer Wissenschaftliche Meeresuntersuchungen 28, 138–144. https://doi.org/10.1007/BF01610349

Armstrong, C.W., Foley, N.S., Tinch, R., van den Hove, S., 2012. Services from the deep: Steps towards valuation of deep sea goods and services. Ecosystem Services 2, 2–13. https://doi.org/10.1016/j.ecoser.2012.07.001

Bader, R.G., Gerard, R.D., Benson, W.E., Bolli, H.M., Hay, W.W., Rothwell Jr., W.T., Ruef, M.H., Riedel, W.R., Sayles, F.L., 2007. Deep Sea Drilling Project -Introduction. DSDP IV, 1–15. https://doi.org/10.2973/dsdp.proc.4.1970

Baldwin, R.J., Smith, K.L., 1987. Temporal variation in the catch rate, length, color and sex of the necrophagous amphipod, *Eurythenes gryllus*, from the central and eastern North Pacific. Deep Sea Research Part A. Oceanographic Research Papers 34, 425–439. https://doi.org/10.1016/0198-0149(87)90146-4

Barnard, J.L., 1961. Gammaridean Amphipoda from depth of 400 to 6000 meters. Galathea Report 5, 23–128.

Beron, P., 1997. On the High Mountain Isopoda Oniscidea in the Old World. Historia naturalis bulgarica. 8, 85–100.

Bik, H.M., Thomas, W.K., Lunt, D.H., Lambshead, P.J.D., 2010. Low endemism, continued deep-shallow interchanges, and evidence for cosmopolitan distributions in free-living marine nematodes (order Enoplida). BMC Evolutionary Biology 10, 389. https://doi.org/10.1186/1471-2148-10-389

Blazewicz-Paszkowycz, M., Bamber, R., Anderson, G., 2012. Diversity of Tanaidacea (Crustacea: Peracarida) in the World's Oceans – How Far Have We Come? PLOS ONE 7, e33068. https://doi.org/10.1371/journal.pone.0033068

Bober, S., 2014. 3D reconstruction of the macrostylid (Crustacea: Isopoda) statocysts based on a new species from the deep sea (Master Thesis). Universität Hamburg, Hamburg.

Bouchet, P., 2006. The Magnitude of Marine Biodiversity, in: Duarte, C.M. (Ed.), The Exploration of Marine Biodiversity: Scientific and Technological Challenges. Fundación BBVA, pp. 33–64.

Bowman, T.E., Manning, R.B., 1972. Two Arctic Bathyal Crustaceans: the Shrimp *Bythocaris cryonesus* New Species, and the Amphipod *Eurythenes gryllus*, With *in situ* Photographs From Ice Island T-3. Crustaceana 23, 187–201. https://doi.org/10.1163/156854072X00363

Brandt, A., 2012. Southern Ocean Deep-Sea Isopod Biodiversity Research: From Census to Ecosystem Functioning, in: di Prisco, G., Verde, C. (Eds.), Adaptation and Evolution in Marine Environments, Volume 1. Springer Berlin Heidelberg, Berlin, Heidelberg, pp. 21–34.

Brandt, A., 2004. Abundance, diversity, and community patterns of Isopoda (Crustacea) in the Weddell Sea and in the Bransfield Strait, Southern Ocean. Antarctic Science 16, 5–10. https://doi.org/10.1017/S0954102004001749

Brandt, A., 1991. Zur Besiedlungsgeschichte des antarktischen Schelfes am Beispiel der Isopoda (Crustacea, Malacostraca) = Colonization of the Antarctic shelf by the Isopoda (Crustacea, Malacostraca). Berichte zur Polarforschung (Reports on Polar Research) 98. ISSN 0176-5027

Brandt, A., Błażewicz-Paszkowycz, M., Bamber, R., Mühlenhardt-Siegel, U., Malyutina, M., Kaiser, S., De, B.C., Havermans, C., 2012. Are there widespread peracarid species in the deep sea (Crustacea: Malacostraca)? Polish Polar Research 33, 139–162. https://doi.org/10.2478/v10183-012-0012-5

Brandt, A., Brenke, N., Andres, H.-G., Brix, S., Guerrero-Kommritz, J., Mühlenhardt-Siegel, U., Wägele, J.-W., 2005. Diversity of peracarid crustaceans (Malacostraca) from the abyssal plain of the Angola Basin. Organisms Diversity & Evolution 5, Supplement 1, 105–112. https://doi.org/10.1016/j.ode.2004.10.007

Brandt, A., Brix, S., Brökeland, W., Choudhury, M., Kaiser, S., Malyutina, M., 2007a. Deep-sea isopod biodiversity, abundance, and endemism in the Atlantic sector of the Southern Ocean—Results from the ANDEEP I–III expeditions. Deep Sea Research Part II: Topical Studies in Oceanography, ANtarctic benthic DEEP-sea biodiversity: colonisation history and recent community patterns (ANDEEP-III) 54, 1760–1775. https://doi.org/10.1016/j.dsr2.2007.07.015

Brandt, A., Brix, S., Held, C., Kihara, T.C., 2014. Molecular differentiation in sympatry despite morphological stasis: deep-sea *Atlantoserolis* Wägele, 1994 and *Glabroserolis* Menzies, 1962 from the south-west Atlantic (Crustacea: Isopoda: Serolidae): Deep-Sea Serolidae. Zoological Journal of the Linnean Society 172, 318–359. https://doi.org/10.1111/zoj.12178

Brandt, A., Frutos, I., Bober, S., Brix, S., Brenke, N., Guggolz, T., Heitland, N., Malyutina, M., Minzlaff, U., Riehl, T., Schwabe, E., Zinkann, A.-C., Linse, K., 2018. Composition of abyssal macrofauna along the Vema Fracture Zone and the hadal Puerto Rico Trench, northern tropical Atlantic. Deep Sea Research Part II: Topical Studies in Oceanography, Bathymetry of the Vema-Fracture Zone and Puerto Rico TRench Abyssal AtlaNtic BiodiverSITy Study (Vema-TRANSIT) 148, 35–44. https://doi.org/10.1016/j.dsr2.2017.07.014

Brandt, A., Gooday, A.J., Brandão, S.N., Brix, S., Brökeland, W., Cedhagen, T., Choudhury, M., Cornelius, N., Danis, B., De Mesel, I., Diaz, R.J., Gillan, D.C., Ebbe, B., Howe, J.A., Janussen, D., Kaiser, S., Linse, K., Malyutina, M., Pawlowski, J., Raupach, M., Vanreusel, A., 2007b. First insights into the biodiversity and biogeography of the Southern Ocean deep sea. Nature 447, 307–311. https://doi.org/10.1038/nature05827

Brasier, M.J., Wiklund, H., Neal, L., Jeffreys, R., Linse, K., Ruhl, H., Glover, A.G., 2016. DNA barcoding uncovers cryptic diversity in 50% of deep-sea Antarctic polychaetes. Royal Society Open Science 3. https://doi.org/10.1098/rsos.160432

Brix, S., Leese, F., Riehl, T., Kihara, T.C., 2015. A new genus and new species of Desmosomatidae Sars, 1897 (Isopoda) from the eastern South Atlantic abyss described by means of integrative taxonomy. Marine Biodiversity 45, 7–61. https://doi.org/10.1007/s12526-014-0218-3

Brix, S., Riehl, T., Leese, F., 2011. First genetic data for species of the genus *Haploniscus* Richardson, 1908 (Isopoda: Asellota: Haploniscidae) from neighbouring deep-sea basins in the South Atlantic. Zootaxa 2838, 79–84.

Brix, S., Svavarsson, J., 2010. Distribution and diversity of desmosomatid and nannoniscid isopods (Crustacea) on the Greenland–Iceland–Faeroe Ridge. Polar Biology 33, 515–530. https://doi.org/10.1007/s00300-009-0729-8

Brix, S., Svavarsson, J., Leese, F., 2014. A multi-gene analysis reveals multiple highly divergent lineages of the isopod *Chelator insignis* (Hansen, 1916) south of Iceland. Polish Polar Research 35, 225–242.

Brökeland, W., 2010a. Redescription of *Haploniscus rostratus* (Menzies, 1962)(Crustacea: Peracarida: Isopoda) with observations on the postmarsupial development, size ranges and distribution. Zootaxa 2521, 1–25.

Brökeland, W., 2010b. Description of four new species from the *Haploniscus unicornis* Menzies, 1956 complex (Isopoda: Asellota: Haploniscidae). Zootaxa 2536.

Brökeland, W., Guðmundsson, G., Svavarsson, J., 2010. Diet of four species of deep-sea isopods (Crustacea: Malacostraca: Peracarida) in the South Atlantic and the Southern Ocean. Marine Biology 157, 177–187. https://doi.org/10.1007/s00227-009-1308-9

Brökeland, W., Svavarsson, J., 2017. Distribution of haploniscids (Isopoda, Asellota, Haploniscidae) in Icelandic waters, with description of *Haploniscus astraphes* n. sp. from the Iceland basin and the Southeast Atlantic Ocean. Zootaxa 4231, 301–326. https://doi.org/10.11646/zootaxa.4231.3.1

Bruun, A.F., 1957. Chapter 22: Deep Sea and Abyssal Depths, in: Geological Society of America Memoirs. Geological Society of America, pp. 641–673.

Bucklin, A., Wilson Jr, R.R., Smith Jr, K.L., 1987. Genetic differentiation of seamount and basin populations of the deep-sea amphipod *Eurythenes gryllus*. Deep Sea Research Part A. Oceanographic Research Papers 34, 1795–1810.

Charmasson, S.S., Calmet, D.P., 1990. Scavenging amphipods *Eurythenes gryllus* from the north-east Atlantic and radioactive waste disposal. Oceanic processes in marine pollution.

Chase, M.R., Etter, R.J., Rex, M.A., Quattro, J.M., 1998. Bathymetric patterns of genetic variation in a deep-sea protobranch bivalve, *Deminucula atacellana*. Marine Biology 131, 301–308.

Christiansen, B., Pfannkuche, O., Thiel, H., 1990. Vertical distribution and population structure of the necrophagous amphipod *Eurythenes gryllus* in the West European Basin. Marine Ecology Progress Series 66, 35–45.

Clark, M.R., Consalvey, M., Rowden, A.A., 2016. Biological Sampling in the Deep Sea. John Wiley & Sons.

Cohen, M.J., 1955. The function of receptors in the statocyst of the lobster *Homarus americanus*. The Journal of Physiology 130, 9–34. https://doi.org/10.1113/jphysiol.1955.sp005389

Coleman, C.O., 2009. Drawing setae the digital way. Zoosystematics and Evolution 85(2), 305–310. https://doi.org/10.1002/zoos.200900008

Coleman, C.O., 2003. "Digital inking": how to make perfect line drawings on computers. Organisms Diversity & Evolution 3, 303–304. https://doi.org/10.1078/1439-6092-00081

Connell, J.H., 1978. Diversity in Tropical Rain Forests and Coral Reefs. Science 199, 1302–1310. https://doi.org/10.1126/science.199.4335.1302

D'Acoz, C. d'UDEKEM, Havermans, C., 2015. Contribution to the systematics of the genus *Eurythenes* S.I. Smith in Scudder, 1882 (Crustacea: Amphipoda: Lysianassoidea: Eurytheneidae). Zootaxa 3971, 1. https://doi.org/10.11646/zootaxa.3971.1.1

Danovaro, R., Gambi, C., Dell'Anno, A., Corinaldesi, C., Fraschetti, S., Vanreusel, A., Vincx, M., Gooday, A.J., 2008. Exponential Decline of Deep-Sea Ecosystem Functioning Linked to Benthic Biodiversity Loss. Current Biology 18, 1–8. https://doi.org/10.1016/j.cub.2007.11.056

Dauvin, J.-C., Zouhiri, S., 1996. Suprabenthic crustacean fauna of a dense *Ampelisca* community from the English Channel. Journal of the Marine Biological Association of the United Kingdom 76, 909. https://doi.org/10.1017/S0025315400040881

Devey, C.W., Augustin, N., Brandt, A., Brenke, N., Köhler, J., Lins, L., Schmidt, C., Yeo, I.A., 2018. Habitat characterization of the Vema Fracture Zone and Puerto Rico Trench. Deep Sea Research Part II: Topical Studies in Oceanography, Bathymetry of the Vema-Fracture Zone and Puerto Rico TRench Abyssal AtlaNtic BiodiverSITy Study (Vema-TRANSIT) 148, 7–20. https://doi.org/10.1016/j.dsr2.2018.02.003

Dijkgraaf, S., 1956. Structure and functions of the statocyst in crabs. Experientia 12, 394–396. https://doi.org/10.1007/BF02157289

Edney, E.B., 1968. Transition from Water to Land in Isopod Crustaceans. Integrative and Comparative Biology 8, 309–326. https://doi.org/10.1093/icb/8.3.309

Eittreim, S., Ewing, J., 1975. Vema fracture zone transform fault. Geology 3, 555–558.

Eittreim, S.L., Biscaye, P.E., Jacobs, S.S., 1983. Bottom-water observations in the Vema fracture zone. Journal of Geophysical Research: Oceans (1978–2012) 88, 2609–2614. https://doi.org/10.1029/JC088iC04p02609

Elsner, N.O., Malyutina, M.V., Golovan, O.A., Brenke, N., Riehl, T., Brandt, A., 2015. Deep down: Isopod biodiversity of the Kuril–Kamchatka abyssal area including a comparison with data of previous expeditions of the RV Vityaz. Deep Sea Research Part II: Topical Studies in Oceanography 111, 210–219. https://doi.org/10.1016/j.dsr2.2014.08.007

Emelyanov, E.M., 2005. The Barrier Zones in the Ocean. Springer-Verlag, Berlin Heidelberg.

Etter, R., Rex, M.A., Chase, M.R., Quattro, J.M., 2005. Population differentiation decreases with depth in deep-sea bivalves. Evolution 59, 1479–1491.

Etter, R.J., Boyle, E.E., Glazier, A., Jennings, R.M., Dutra, E., Chase, M.R., 2011. Phylogeography of a pan-Atlantic abyssal protobranch bivalve: implications for evolution in the Deep Atlantic: EVOLUTION IN THE DEEP ATLANTIC. Molecular Ecology 20, 829–843. https://doi.org/10.1111/j.1365-294X.2010.04978.x

Eustace, R.M., Ritchie, H., Kilgallen, N.M., Piertney, S.B., Jamieson, A.J., 2016. Morphological and ontogenetic stratification of abyssal and hadal *Eurythenes gryllus sensu lato* (Amphipoda: Lysianassoidea) from the Peru–Chile Trench. Deep Sea Research Part I: Oceanographic Research Papers 109, 91–98. https://doi.org/10.1016/j.dsr.2015.11.005

Fischer, J., Rhein, M., Schott, F., Stramma, L., 1996. Deep water masses and transports in the Vema Fracture Zone. Deep Sea Research Part I: Oceanographic Research Papers 43, 1067–1074. https://doi.org/10.1016/0967-0637(96)00044-1

France, S.C., Kocher, T.D., 1996. Geographic and bathymetric patterns of mitochondrial 16S rRNA sequence divergence among deep-sea amphipods, *Eurythenes gryllus*. Marine Biology 126, 633–643.

Frutos, I., Brandt, A., Sorbe, J.C., 2016. Deep-Sea Suprabenthic Communities: The Forgotten Biodiversity, in: Rossi, S., Bramanti, L., Gori, A., Orejas, C. (Eds.), Marine Animal Forests. Springer International Publishing, Cham, pp. 1–29. https://doi.org/10.1007/978-3-319-17001-5_21-1

Fujii, T., Kilgallen, N.M., Rowden, A.A., Jamieson, A.J., 2013. Deep-sea amphipod community structure across abyssal to hadal depths in the Peru-Chile and Kermadec trenches. Marine Ecology Progress Series 492, 125–138. https://doi.org/10.3354/meps10489

Gage, J.D., Tyler, P.A., 1991. Deep-sea biology: a natural history of organisms at the deep-sea floor. Cambridge University Press, UK.

Gillespie, R.G., Roderick, G.K., 2002. ARTHROPODS ON ISLANDS: Colonization, Speciation, and Conservation. Annual Review of Entomology 47, 595–632. https://doi.org/10.1146/annurev.ento.47.091201.145244

Glover, A.G., Smith, C.R., 2003. The deep-sea floor ecosystem: current status and prospects of anthropogenic change by the year 2025. Environmental Conservation null, 219–241. https://doi.org/10.1017/S0376892903000225

Glover, A.G., Smith, C.R., Paterson, G.L.J., Wilson, G.D.F., Hawkins, L., Sheader, M., 2002. Polychaete species diversity in the central Pacific abyss: local and regional patterns, and relationships with productivity. Marine Ecology Progress Series 240, 157–170.

Gooday, A.J., Hori, S., Todo, Y., Okamoto, T., Kitazato, H., Sabbatini, A., 2004. Soft-walled, monothalamous benthic foraminiferans in the Pacific, Indian and Atlantic Oceans: aspects of biodiversity and biogeography. Deep Sea Research Part I: Oceanographic Research Papers 51, 33–53. https://doi.org/10.1016/j.dsr.2003.07.002

Gooday, A.J., Levin, L.A., Linke, P., Heeger, T., 1992. The Role of Benthic Foraminifera in Deep-Sea Food Webs and Carbon Cycling, in: Deep-Sea Food Chains and the Global Carbon Cycle, NATO ASI Series. Springer, Dordrecht, pp. 63–91. https://doi.org/10.1007/978-94-011-2452-2_5

Gooday, A.J., Turley, C.M., Allen, J.A., 1990. Responses by Benthic Organisms to Inputs of Organic Material to the Ocean Floor: A Review [and Discussion}. Philosophical Transactions of the Royal Society A: Mathematical, Physical and Engineering Sciences 331, 119–138. https://doi.org/10.1098/rsta.1990.0060

Grassle, J.F., 1977. Slow recolonisation of deep-sea sediment. Nature 265, 618–619. https://doi.org/10.1038/265618a0

Grassle, J.F., Maciolek, N.J., 1992. Deep-sea species richness: regional and local diversity estimates from quantitative bottom samples. The American Naturalist 139, 313–341.

Gudmundsson, G., Schmalensee von, M., Svarvarsson, J., 2000. Are foraminifers (Protozoa) important food for small isopods (Crustacea) in the deep sea? Deep Sea Research Part I: Oceanographic Research Papers 47, 2093–2109.

Guggolz, T., Lins, L., Meißner, K., Brandt, A., 2018. Biodiversity and distribution of polynoid and spionid polychaetes (Annelida) in the Vema Fracture Zone, tropical North Atlantic. Deep Sea Research Part II: Topical Studies in Oceanography, Bathymetry of the Vema-Fracture Zone and Puerto Rico TRench Abyssal AtlaNtic BiodiverSITy Study (Vema-TRANSIT) 148, 54–63. https://doi.org/10.1016/j.dsr2.2017.07.013

Hansen, B., Østerhus, S., 2000. North Atlantic–Nordic Seas exchanges. Progress in Oceanography 45, 109–208. https://doi.org/10.1016/S0079-6611(99)00052-X

Hansen, H.J., 1916. Crustacea Malacostraca: The order Isopoda. Danish Ingolf Expedition 3, 1–262.

Harris, P.T., Macmillan-Lawler, M., Rupp, J., Baker, E.K., 2014. Geomorphology of the oceans. Marine Geology, 50th Anniversary Special Issue 352, 4–24. https://doi.org/10.1016/j.margeo.2014.01.011

Harrison, K., 1989. Are deep-sea asellote isopods infaunal or epifaunal. Crustaceana (Leiden) 56, 317–319.

Havermans, C., Sonet, G., d'Udekem d'Acoz, C., Nagy, Z.T., Martin, P., Brix, S., Riehl, T., Agrawal, S., Held, C., 2013. Genetic and Morphological Divergences in the Cosmopolitan Deep-Sea Amphipod *Eurythenes gryllus* Reveal a Diverse Abyss and a Bipolar Species. PLoS ONE 8,

e74218. https://doi.org/10.1371/journal.pone.0074218

Heezen, B.C., Gerard, R.D., Tharp, M., 1964. The Vema fracture zone in the equatorial Atlantic. J. Geophys. Res. 69, 733–739. https://doi.org/10.1029/JZ069i004p00733

Heitland, N., 2015. Genetic allocation of sexual dimorphic individuals in a new deep sea isopod species (*Macrostylis papandreas* sp. n.) (Master Thesis). Universität Hamburg, Hamburg.

Held, C., 2003. Molecular evidence for cryptic speciation within the widespread Antarctic crustacean *Ceratoserolis trilobitoides* (Crustacea, Isopoda). Antarctic biology in a global context 135–139.

Held, C., 2000. Phylogeny and Biogeography of Serolid Isopods (Crustacea, Isopoda, Serolidae) and the Use of Ribosomal Expansion Segments in Molecular Systematics. Molecular Phylogenetics and Evolution 15, 165–178. https://doi.org/10.1006/mpev.1999.0739

Held, C., Wägele, J.-W., 2005. Cryptic speciation in the giant Antarctic isopod *Glyptonotus antarcticus* (Isopoda: Valvifera: Chaetiliidae). Scientia Marina 69, 175–181.

Hertwig, I., Schneider, H., Hentschel, J., 1991. Light- and electron-microscopic analysis of the statocyst of the American crayfish *Orconectes limosus* (Crustacea, Decapoda). Zoomorphology 110, 189–202. https://doi.org/10.1007/BF01633003

Hessler, R.R., Sanders, H., 1967. Faunal diversity in the deep-sea. Deep Sea Research and Oceanographic Abstracts 14, 65–78. https://doi.org/10.1016/0011-7471(67)90029-0

Hessler, R.R., Strömberg, J.-O., 1989. Behavior of janiroidean isopods (Asellota), with special reference to deep sea genera. Sarsia 74, 145–159.

Hessler, R.R., Thistle, D., 1975. On the place of origin of deep-sea lsopods. Marine Biology 32, 155–165.

Hessler, R.R., Wilson, G.D.F., 1983. The origin and biogeography of malacostracan crustaceans in the deep sea, in: Sims, R.W., Price, J.H., Whalley, P.E.S. (Eds.), Evolution, Time, and Space: The Emergence of the Biosphere. Academic Press, London, pp. 227–254.

Hessler, R.R., Wilson, G.D.F., Thistle, D., 1979. The deep-sea isopods: A biogeographic and phylogenetic overview. Sarsia 64, 67–75. https://doi.org/10.1080/00364827.1979.10411365

Hopf, J.K., Kingsford, M.J., 2013. The utility of statoliths and bell size to elucidate age and condition of a scyphomedusa (*Cassiopea* sp.). Marine Biology (Berlin) 160, 951–960.

Hult, J., 1941. On soft-bottom Isopods of the Skager Rak. Zoologiska Bidrag fran Uppsala 1–236.

Ibaraki, M., 1997. Closing of the Central American Seaway and Neogene coastal upwelling along the Pacific coast of South America. Tectonophysics, Neogene Evolution of the Pacific: Tecton-

ics of Gateways and Associated Responses 281, 99–104. https://doi.org/10.1016/S0040-1951(97)00161-3

Ingels, J., Tchesunov, A.V., Vanreusel, A., 2011. Meiofauna in the Gollum Channels and the Whittard Canyon, Celtic Margin—How Local Environmental Conditions Shape Nematode Structure and Function. PLOS ONE 6, e20094. https://doi.org/10.1371/journal.pone.0020094

Ingram, C.L., Hessler, R.R., 1987. Population biology of the deep-sea amphipod *Eurythenes gryllus*: inferences from instar analyses. Deep Sea Research Part A. Oceanographic Research Papers 34, 1889–1910. https://doi.org/10.1016/0198-0149(87)90090-2

Ingram, C.L., Hessler, R.R., 1983. Distribution and behavior of scavenging amphipods from the central North Pacific. Deep Sea Research Part A. Oceanographic Research Papers 30, 683–706. https://doi.org/10.1016/0198-0149(83)90017-1

Jamieson, A., 2015. The Hadal Zone: Life in the Deepest Oceans. Cambridge University Press.

Jamieson, A.J., Fujii, T., Priede, I.G., 2012. Locomotory activity and feeding strategy of the hadal munnopsid isopod *Rectisura* cf. *herculea* (Crustacea: Asellota) in the Japan Trench. Journal of Experimental Biology 215, 3010–3017. https://doi.org/10.1242/jeb.067025

Janssen, A., Kaiser, S., Meißner, K., Brenke, N., Menot, L., Martínez Arbizu, P., 2015. A Reverse Taxonomic Approach to Assess Macrofaunal Distribution Patterns in Abyssal Pacific Polymetallic Nodule Fields. PLoS ONE 10, e0117790. https://doi.org/10.1371/journal.pone.0117790

Jennings, R.M., Brix, S., Bober, S., Svavarsson, J., Driskell, A., 2018. More diverse than expected: distributional patterns of *Oecidiobranchus* Hessler, 1970 (Isopoda, Asellota) on the Greenland-Iceland-Faeroe Ridge based on molecular markers. Marine Biodiversity. https://doi.org/10.1007/s12526-018-0857-x

Johnson, S.B., Young, C.R., Jones, W.J., Warén, A., Vrijenhoek, R.C., 2006. Migration, isolation, and speciation of hydrothermal vent limpets (Gastropoda; Lepetodrilidae) across the Blanco Transform Fault. The Biological Bulletin 210, 140–157. https://doi.org/10.2307/4134603

Jumars, P.A., 1976. Deep-sea species diversity: does it have a characteristic scale. Journal of Marine Research 34, 217–246.

Kavanagh, F.A., Frutos, I., Sorbe, J.C., 2015. *Ischnomesus harrietae* sp. nov., a new benthic asellote (Crustacea: Isopoda: Ischnomesidae) from bathyal bottoms of the southern Bay of Biscay. Zootaxa 3911, 201. https://doi.org/10.11646/zootaxa.3911.2.3

Khripounoff Alexis, Caprais Jean-Claude, Crassous Philippe, Etoubleau Joël, 2006. Geochemical and

biological recovery of the disturbed seafloor in polymetallic nodule fields of the Clipperton-Clarion Fracture Zone (CCFZ) at 5,000-m depth. Limnology and Oceanography 51, 2033–2041. https://doi.org/10.4319/lo.2006.51.5.2033

Kihara, T.C., Arbizu, P.M., 2012. Three new species of *Cerviniella* Smirnov, 1946 (Copepoda: Harpacticoida) from the Arctic. Zootaxa 3345, 1–33.

Kitahashi, T., Kawamura, K., Veit-Köhler, G., Danovaro, R., Tietjen, J., Kojima, S., Shimanaga, M., 2012. Assemblages of Harpacticoida (Crustacea: Copepoda) from the Ryukyu and Kuril Trenches, north-west Pacific Ocean. Journal of the Marine Biological Association of the United Kingdom 92, 275–286. https://doi.org/10.1017/S0025315411001536

Kniesz, K., Brandt, A., Riehl, T., 2017. Peritrich epibionts on the hadal isopod species *Macrostylis marionae* n. sp. from the Puerto Rico Trench used as indicator for sex-specific behaviour. Deep Sea Research Part II: Topical Studies in Oceanography. https://doi.org/10.1016/j.dsr2.2017.10.007

Knutsen, H., Jorde, P.E., Bergstad, O.A., Skogen, M., 2012. Population genetic structure in a deepwater fish *Coryphaenoides rupestris*: patterns and processes. Marine Ecology Progress Series 460, 233–246. https://doi.org/10.3354/meps09728

Kottmann, J., Kihara, T.C., Glatzel, T., Veit-Köhler, G., 2013. A new species of *Wellsopsyllus* (Copepoda, Harpacticoida, Paramesochridae) from the deep Southern Ocean and remarks on its biogeography. Helgoland Marine Research 67, 33–48. https://doi.org/10.1007/s10152-012-0302-7

Krapp-Schickel, T., De Broyer, C., 2014. Revision of *Leucothoe* (Amphipoda, Crustacea) from the Southern Ocean: a cosmopolitanism concept is vanishing. European Journal of Taxonomy 0. https://doi.org/10.5852/ejt.2014.80

Langenbuch, R., 1928. Ueber die Statocysten einiger Crustaceen. I. Cyathura. II. Ampelisca. Zoologische Jahrbuecher Jena Allgemeine Zoologie 575–622.

Larsen, K., 2003. The Tanaidacean Fauna (Peracarida) from a Deep-Sea Cold-Seep in the Gulf of Mexico. Journal of Crustacean Biology 23, 777–794. https://doi.org/10.1651/C-2395

Leduc, D., Rowden, A.A., Probert, P.K., Pilditch, C.A., Nodder, S.D., Vanreusel, A., Duineveld, G.C.A., Witbaard, R., 2012. Further evidence for the effect of particle-size diversity on deep-sea benthic biodiversity. Deep Sea Research Part I: Oceanographic Research Papers 63, 164–169. https://doi.org/10.1016/j.dsr.2011.10.009

Leese, F., Held, C., 2008. Identification and characterization of microsatellites from the Antarctic isopod *Ceratoserolis trilobitoides*: nuclear evidence for cryptic species. Conservation Genetics 9,

1369–1372. https://doi.org/10.1007/s10592-007-9491-z

Lins, L., da Silva, M.C., Neres, P., Esteves, A.M., Vanreusel, A., 2018. Testing deep-sea biodiversity paradigms on abyssal nematode genera and *Acantholaimus* species. Deep Sea Research Part II: Topical Studies in Oceanography, Bathymetry of the Vema-Fracture Zone and Puerto Rico TRench Abyssal AtlaNtic BiodiverSITy Study (Vema-TRANSIT) 148, 208–222. https://doi.org/10.1016/j.dsr2.2016.12.005

Linsenmair, K.E., 1984. Comparative studies on the social behaviour of the desert isopod *Hemilepistus reaumuri* and of a *Porcellio* species.Symposia of the zoological Society of London 53, 423–453.

Linsenmair, K.E., LinsenMair, C., 1971. Paarbildung und Paarzusammenhalt bei monogamen Wüstennassel *Hemilepistus reaumuri* （Crustacea, Isopoda; Oniscoidea). Zeitschrift für Tierpsychologie 29, 134–155.

Lynn, R.J., Reid, J.L., 1968. Characteristics and circulation of deep and abyssal waters. Deep Sea Research and Oceanographic Abstracts 15, 577–598. https://doi.org/10.1016/0011-7471(68)90064-8

Malyutina, M.V., 1999. New Species of *Acanthocope* (Isopoda, Munnopsidae). Russian Journal of Marine Biology 25, 320–329.

Malyutina, M.V., Frutos, I., Brandt, A., 2017. Diversity and distribution of the deep-sea Atlantic *Acanthocope* (Crustacea, Isopoda, Munnopsidae), with description of two new species. Deep Sea Research Part II: Topical Studies in Oceanography. https://doi.org/10.1016/j.dsr2.2017.11.003

Mantyla, A.W., Reid, J.L., 1983. Abyssal characteristics of the World Ocean waters. Deep Sea Research Part A. Oceanographic Research Papers 30, 805–833. https://doi.org/10.1016/0198-0149(83)90002-X

Marshall, N., Diebel, C., 1995. “Deep-sea spiders” that walk through the water. Journal of experimental biology 198, 1371–1379.

Martínez Arbizu, P., Schminke, H.K., 2005. DIVA-1 expedition to the deep sea of the Angola Basin in 2000 and DIVA-1 workshop in 2003. Organisms Diversity & Evolution 5, 1–2. https://doi.org/10.1016/j.ode.2004.11.009

McCartney, M.S., Bennett, S.L., Woodgate-Jones, M.E., 1991. Eastward Flow through the Mid-Atlantic Ridge at 11°N and Its Influence on the Abyss of the Eastern Basin. Journal of Physical Oceanography 21, 1089–1121. https://doi.org/10.1175/1520-0485(1991)021<1089:EFTTMA>2.0.CO;2

McClain, C.R., Allen, A.P., Tittensor, D.P., Rex, M.A., 2012. Energetics of life on the deep seafloor. Proceedings of the National Academy of Sciences 109, 15366–15371. https://doi.org/10.1073/pnas.1208976109

McClain, C.R., Schlacher, T.A., 2015. On some hypotheses of diversity of animal life at great depths on the sea floor. Marine Ecology, 1–24. https://doi.org/10.1111/maec.12288

Menzies, R.J., 1962. On the Food and Feeding Habits of Abyssal Organisms as Exemplified by the Isopoda. Internationale Revue der gesamten Hydrobiologie und Hydrographie 47, 339–358. https://doi.org/10.1002/iroh.19620470303

Menzies, R.J., 1956. New bathyal Isopoda from the Caribbean with observations on their nutrition. Breviora 63, 1–10.

Mercier, H., Speer, K.G., 1998. Transport of Bottom Water in the Romanche Fracture Zone and the Chain Fracture Zone. Journal of Physical Oceanography 28, 779–790. https://doi.org/10.1175/1520-0485(1998)028<0779:TOBWIT>2.0.CO;2

Metcalf, W.G., Heezen, B.C., Stalcup, M.C., 1964. The sill depth of the mid-atlantic ridge in the equatorial region. Deep Sea Research and Oceanographic Abstracts 11, 1–10. https://doi.org/10.1016/0011-7471(64)91078-2

Mezhov, B., 1993. Three new species of Macrostylis GO Sars, 1864 (Crustacea Isopoda Asellota Macrostylidae) from the Pacific Ocean. Arthropoda Selecta 2, 3–9.

Michels, J., Büntzow, M., 2010. Assessment of Congo red as a fluorescence marker for the exoskeleton of small crustaceans and the cuticle of polychaetes. Journal of Microscopy 238, 95–101. https://doi.org/10.1111/j.1365-2818.2009.03360.x

Miljutin, D.M., Miljutina, M.A., Arbizu, P.M., Galéron, J., 2011. Deep-sea nematode assemblage has not recovered 26 years after experimental mining of polymetallic nodules (Clarion-Clipperton Fracture Zone, Tropical Eastern Pacific). Deep Sea Research Part I: Oceanographic Research Papers 58, 885–897. https://doi.org/10.1016/j.dsr.2011.06.003

Miyamoto, H., Machida, R.J., Nishida, S., 2010. Genetic diversity and cryptic speciation of the deep sea chaetognath *Caecosagitta macrocephala* (Fowler, 1904). Deep Sea Research Part II: Topical Studies in Oceanography 57, 2211–2219. https://doi.org/10.1016/j.dsr2.2010.09.023

Montagna, P.A., 1982. Morphological Adaptation in the Deep-Sea Benthic Harpacticoid Copepod Family Cerviniidae. Crustaceana 42, 37–43.

Moura, C.J., Harris, D.J., Cunha, M.R., Rogers, A.D., 2008. DNA barcoding reveals cryptic diversity in marine hydroids (Cnidaria, Hydrozoa) from coastal and deep-sea environments. Zoologica Scripta 37, 93–108. https://doi.org/10.1111/j.1463-6409.2007.00312.x

Murray, J., Appellöf, J.J.A., Gran, H.H., Helland-Hansen, B., Hjort, J., 1912. The depths of the ocean : a general account of the modern science of oceanography based largely on the scientific researches of the Norwegian steamer Michael Sars in the North Atlantic / by Sir John Murray and Dr. Johan Hjort; with contributions from Professor A. Appellöf, Professor H. H. Gran and Dr. B. Helland-Hansen. Macmillan, London

Negoescu, I., Svavarsson, J., 1997. Anthurideans (Crustacea, isopoda) from the North Atlantic and the Arctic Ocean. Sarsia 82, 159–202. https://doi.org/10.1080/00364827.1997.10413650

Neil, D.M., 1975. The Mechanism of Statocyst Operation in the Mysid Shrimp Praunus Flexuosus. Journal of Experimental Biology 62, 685–700.

O'Dea, A., Lessios, H.A., Coates, A.G., Eytan, R.I., Restrepo-Moreno, S.A., Cione, A.L., Collins, L.S., de Queiroz, A., Farris, D.W., Norris, R.D., Stallard, R.F., Woodburne, M.O., Aguilera, O., Aubry, M.-P., Berggren, W.A., Budd, A.F., Cozzuol, M.A., Coppard, S.E., Duque-Caro, H., Finnegan, S., Gasparini, G.M., Grossman, E.L., Johnson, K.G., Keigwin, L.D., Knowlton, N., Leigh, E.G., Leonard-Pingel, J.S., Marko, P.B., Pyenson, N.D., Rachello-Dolmen, P.G., Soibelzon, E., Soibelzon, L., Todd, J.A., Vermeij, G.J., Jackson, J.B.C., 2016. Formation of the Isthmus of Panama. Science Advances 2, e1600883–e1600883. https://doi.org/10.1126/sciadv.1600883

Ólafsdóttir, S.H., Svavarsson, J., 2002. Ciliate (Protozoa) Epibionts of Deep-Water Asellote Isopods (Crustacea): Pattern and Diversity. Journal of Crustacean Biology 22, 607–618. https://doi.org/10.1163/20021975-99990273

Pape, E., Bezerra, T.N., Jones, D.O.B., Vanreusel, A., 2013. Unravelling the environmental drivers of deep-sea nematode biodiversity and its relation with carbon mineralisation along a longitudinal primary productivity gradient. Biogeosciences Discussions 9(12), 19019–19052.

Pawlowski, J., Fahrni, J., Lecroq, B., Longet, D., Cornelius, N., Excoffier, L., Cedhagen, T., Gooday, A.J., 2007. Bipolar gene flow in deep-sea benthic foraminifera. Molecular Ecology 16, 4089–4096. https://doi.org/10.1111/j.1365-294X.2007.03465.x

Pedlosky, J., Spall, M., 1999. Rossby Normal Modes in Basins with Barriers*. Journal of physical oceanography 29, 2332–2349.

Pfenninger, M., Schwenk, K., 2007. Cryptic animal species are homogeneously distributed among taxa and biogeographical regions. BMC Evolutionary Biology 7, 121. https://doi.org/10.1186/1471-

2148-7-121

Poore, G.C.B., 2001. Families and genera of Isopoda Anthuridea, in: Isopod Systematics and Evolution, Crustacean Issues. Rotterdamm, pp. 63–173.

Priede, I.G., Bergstad, O.A., Miller, P.I., Vecchione, M., Gebruk, A., Falkenhaug, T., Billett, D.S.M., Craig, J., Dale, A.C., Shields, M.A., Tilstone, G.H., Sutton, T.T., Gooday, A.J., Inall, M.E., Jones, D.O.B., Martinez-Vicente, V., Menezes, G.M., Niedzielski, T., Sigurðsson, Þ., Rothe, N., Rogacheva, A., Alt, C.H.S., Brand, T., Abell, R., Brierley, A.S., Cousins, N.J., Crockard, D., Hoelzel, A.R., Høines, Å., Letessier, T.B., Read, J.F., Shimmield, T., Cox, M.J., Galbraith, J.K., Gordon, J.D.M., Horton, T., Neat, F., Lorance, P., 2013. Does Presence of a Mid-Ocean Ridge Enhance Biomass and Biodiversity? PLOS ONE 8, e61550. https://doi.org/10.1371/journal.pone.0061550

Pytkowicz, R.M., 1970. On the carbonate compensation depth in the Pacific Ocean. Geochimica et Cosmochimica Acta 34, 836–839. https://doi.org/10.1016/0016-7037(70)90034-7

Quattro J., Chase M., Rex M., Greig T., Etter R., 2001. Extreme mitochondrial DNA divergence within populations of the deep-sea gastropod *Frigidoalvania brychia*. Marine Biology 139, 1107–1113. https://doi.org/10.1007/s002270100662

Ramirez-Llodra, E., Brandt, A., Danovaro, R., De Mol, B., Escobar, E., German, C.R., Levin, L.A., Martínez Arbizu, P., Menot, L., Buhl-Mortensen, P., Narayanaswamy, B.E., Smith, C.R., Tittensor, D.P., Tyler, P.A., Vanreusel, A., Vecchione, M., 2010. Deep, diverse and definitely different: unique attributes of the world's largest ecosystem. Biogeosciences 7, 2851–2899. https://doi.org/10.5194/bg-7-2851-2010

Raupach, M.J., Held, C., Wägele, J.-W., 2004. Multiple colonization of the deep sea by the Asellota (Crustacea: Peracarida: Isopoda). Deep Sea Research Part II: Topical Studies in Oceanography 51, 1787–1795. https://doi.org/10.1016/j.dsr2.2004.06.035

Raupach, M.J., Malyutina, M., Brandt, A., Wägele, J.-W., 2007. Molecular data reveal a highly diverse species flock within the munnopsoid deep-sea isopod *Betamorpha fusiformis* (Barnard, 1920) (Crustacea: Isopoda: Asellota) in the Southern Ocean. Deep Sea Research Part II: Topical Studies in Oceanography 54, 1820–1830. https://doi.org/10.1016/j.dsr2.2007.07.009

Raupach, M.J., Wägele, J.-W., 2006. Distinguishing cryptic species in Antarctic Asellota (Crustacea: Isopoda) - a preliminary study of mitochondrial DNA in *Acanthaspidia drygalskii*. Antarctic Science 18, 191. https://doi.org/10.1017/S0954102006000228

Rex, M.A., Etter, R.J., 2010. Deep-sea Biodiversity: Pattern and Scale. Harvard University Press.

Rhind, P.M., Allen, J.A., 1992. Studies on the deep-sea Protobranchia (Bivalvia): the family Nuculidae. Bulletin of the British Museum, Natural History. Zoology 58, 61–93.

Richerson, P., Armstrong, R., Goldman, C.R., 1970. Contemporaneous Disequilibrium, a New Hypothesis to Explain the "Paradox of the Plankton." Proceedings of the National Academy of Sciences 67, 1710–1714.

Riehl, T., 2014. A phylogenetic approach to the classification of macrostylid isopods and faunal linkages between the deep sea and shallow-water environments. Unpublished Dissertation, University of Hamburg.

Riehl, T., Lins, L., Brandt, A., 2018. The effects of depth, distance, and the Mid-Atlantic Ridge on genetic differentiation of abyssal and hadal isopods (Macrostylidae). Deep Sea Research Part II: Topical Studies in Oceanography, Bathymetry of the Vema-Fracture Zone and Puerto Rico TRench Abyssal AtlaNtic BiodiverSITy Study (Vema-TRANSIT) 148, 74–90. https://doi.org/10.1016/j.dsr2.2017.10.005

Riehl, T., Wilson, G.D.F., Hessler, R.R., 2012. New Macrostylidae Hansen, 1916 (Crustacea: Isopoda) from the Gay Head-Bermuda transect with special consideration of sexual dimorphism. Zootaxa 1–26.

Riehl, T., Wilson, G.D.F., Malyutina, M.V., 2014. Urstylidae - a new family of abyssal isopods (Crustacea: Asellota) and its phylogenetic implications: A New Family of Higher Janiroidea. Zoological Journal of the Linnean Society 170, 245–296. https://doi.org/10.1111/zoj.12104

Ritchie, H., Jamieson, A.J., Piertney, S.B., 2015. Phylogenetic relationships among hadal amphipods of the Superfamily Lysianassoidea: Implications for taxonomy and biogeography. Deep Sea Research Part I: Oceanographic Research Papers 105, 119–131. https://doi.org/10.1016/j.dsr.2015.08.014

Rose, R.D., Stokes, D.R., 1981. A crustacean statocyst with only three hairs: Light and scanning electron microscopy. Journal of Morphology 169, 21–28. https://doi.org/10.1002/jmor.1051690103

Schmid, C., Brenke, N., Wägele, J.W., 2002. On abyssal isopods (Crustacea: Isopoda: Asellota) from the Angola Basin: *Eurycope tumidicarpus* n. sp. and redescription of *Acanthocope galathea* Wolff, 1962. Organisms Diversity & Evolution 2, 87–88. https://doi.org/10.1078/1439-6092-00030

Schmidt, C., Escobar Wolf, K., Lins, L., Martínez Arbizu, P., Brandt, A., 2018. Meiofauna abundance and community patterns along a transatlantic transect in the Vema Fracture Zone and in the

hadal zone of the Puerto Rico trench. Deep Sea Research Part II: Topical Studies in Oceanography, Bathymetry of the Vema-Fracture Zone and Puerto Rico TRench Abyssal AtlaNtic BiodiverSITy Study (Vema-TRANSIT) 148, 223–235. https://doi.org/10.1016/j.dsr2.2017.12.021

Schmidt, C., Lins, L., Brandt, A., 2018. Harpacticoida (Crustacea, Copepoda) across a longitudinal transect of the Vema Fracture Zone and along a depth gradient in the Puerto Rico trench. Deep Sea Research Part II: Topical Studies in Oceanography, Bathymetry of the Vema-Fracture Zone and Puerto Rico TRench Abyssal AtlaNtic BiodiverSITy Study (Vema-TRANSIT) 148, 236–250. https://doi.org/10.1016/j.dsr2.2017.12.024

Schnurr, S., Brandt, A., Brix, S., Fiorentino, D., Malyutina, M., Svavarsson, J., 2014. Composition and distribution of selected munnopsid genera (Crustacea, Isopoda, Asellota) in Icelandic waters. Deep Sea Research Part I: Oceanographic Research Papers 84, 142–155. https://doi.org/10.1016/j.dsr.2013.11.004

Schnurr, S., Osborn, K.J., Malyutina, M., Jennings, R., Brix, S., Driskell, A., Svavarsson, J., Arbizu, P.M., 2018. Hidden diversity in two species complexes of munnopsid isopods (Crustacea) at the transition between the northernmost North Atlantic and the Nordic Seas. Marine Biodiversity 1–31. https://doi.org/10.1007/s12526-018-0877-6

Shields, M.A., Blanco-Perez, R., 2013. Polychaete abundance, biomass and diversity patterns at the Mid-Atlantic Ridge, North Atlantic Ocean. Deep Sea Research Part II: Topical Studies in Oceanography, ECOMAR: Ecosystems of the Mid-Atlantic Ridge at the Sub-Polar Front and Charlie-Gibbs Fracture Zone 98, Part B, 315–325. https://doi.org/10.1016/j.dsr2.2013.04.010

Shields, M.A., Glover, A.G., Wiklund, H., 2013. Polynoid polychaetes of the Mid-Atlantic Ridge and a new holothurian association. Marine Biology Research 9, 547–553. https://doi.org/10.1080/17451000.2012.749992

Simberloff, D.S., Wilson, E.O., 1970. Experimental Zoogeography of Islands. A Two-Year Record of Colonization. Ecology 51, 934–937. https://doi.org/10.2307/1933995

Simberloff, D.S., Wilson, E.O., 1969. Experimental Zoogeography of Islands: The Colonization of Empty Islands. Ecology 50, 278–296. https://doi.org/10.2307/1934856

Smith, C.R., De Leo, F.C., Bernardino, A.F., Sweetman, A.K., Arbizu, P.M., 2008. Abyssal food limitation, ecosystem structure and climate change. Trends in Ecology & Evolution 23, 518–528. https://doi.org/10.1016/j.tree.2008.05.002

Smith, C.R., Demopoulos, A.W., 2003. The deep Pacific ocean floor. Ecosystems of the World 179–218.

Smith, K.L., Baldwin, R.J., 1984. Vertical distribution of the necrophagous amphipod, *Eurythenes gryllus*, in the North Pacific: spatial and temporal variation. Deep Sea Research Part A. Oceanographic Research Papers 31, 1179–1196. https://doi.org/10.1016/0198-0149(84)90057-8

Smith, K.L., White, G.A., Laver, M.B., McConnaughey, R.R., Meador, J.P., 1979. Free vehicle capture of abyssopelagic animals. Deep Sea Research Part A. Oceanographic Research Papers 26, 57–64. https://doi.org/10.1016/0198-0149(79)90085-2

Snelgrove, P.V.R., Smith, C.R., 2003. A riot of species in an environmantal calm: the paradox of the species-rich deep-sea floor, in: Oceanography and Marine Biology, An Annual Review, Volume 40: An Annual Review: CRC Press, pp. 311–342.

Sokolova, M.N., 1972. Trophic structure of deep-sea macrobenthos. Marine Biology 16, 1–12.

Stephens, P., Young, J., 1976. The statocyst of *Vampyroteuthis infernalis* (Mollusca: Cephalopoda). Journal of Zoology London 180, 565–588.

Stephens, P.A., Sutherland, W.J., Freckleton, R.P., 1999. What Is the Allee Effect? Oikos 87, 185. https://doi.org/10.2307/3547011

Stockton, W.L., 1982. Scavenging amphipods from under the Ross Ice Shelf, Antarctica. Deep Sea Research Part A. Oceanographic Research Papers 29, 819–835. https://doi.org/10.1016/0198-0149(82)90048-6

Stransky, B., Svarvarsson, J., 2006. *Astacilla boreaphilis* sp. nov. (Crustacea: Isopoda: Valvifera) from shallow and deep North Atlantic waters. Zootaxa 1259, 23.

Svavarsson, J., Gudmundsson, G., Brattegard, T., 1993. Feeding by asellote isopods (Crustacea) on foraminifers (Protozoa) in the deep sea. Deep Sea Research Part I: Oceanographic Research 40, 1225–1239.

Sye, C.G., 1887. Beiträge zur Anatomie und Histologie von *Iaera marina*. Kiel.

Takahata, M., Hisada, M., 1979. Functional polarization of statocyst receptors in the crayfishProcambarus clarkii Girard. J. Comp. Physiol. 130, 201–207. https://doi.org/10.1007/BF00614606

Tendal, O.S., Hessler, R.R., 1977. An introduction to the biology and systematics of Komokiacea. Galathea Report 14, 94.

Thistle, D., 2003. Chapter 2: The Deep-Sea Floor: An Overview, in: Tyler, P.A. (Ed.), Ecosystems of the Deep Oceans. Elsevier.

Thistle, D., Hessler, R.R., 1976. Origin of a Deep-Sea Family, the Ilyarachnidae (Crustacea: Isopoda). Systematic Biology 25, 110–116. https://doi.org/10.2307/2412736

Thistle, D., Wilson, G.D.F., 1987. A hydrodynamically modified, abyssal isopod fauna. Deep-Sea Research Part A Oceanographic Research Papers 34, 73–87.

Thurston, M.H., Bett, B.J., 1995. Hatchling Size and Aspects of Biology in the Deep-Sea Amphipod Genus *Eurythenes* (Crustacea: Amphipoda). Int. Revue ges. Hydrobiol. Hydrogr. 80, 201–216. https://doi.org/10.1002/iroh.19950800209

Thurston, M.H., Petrillo, M., Della Croce, N., 2002. Population structure of the necrophagous amphipod Eurythenes gryllus (Amphipoda: Gammaridea) from the Atacama Trench (south-east Pacific Ocean). Journal of the Marine Biological Association of the UK 82, 205–211. https://doi.org/10.1017/S0025315402005374

Van Andel, T.H., Von Herzen, R.P., Phillips, J.D., 1971. The Vema fracture zone and the tectonics of transverse shear zones in oceanic crustal plates. Marine Geophysical Researches 1, 261–283.

van der Heijden, K., Petersen, J.M., Dubilier, N., Borowski, C., 2012. Genetic Connectivity between North and South Mid-Atlantic Ridge Chemosynthetic Bivalves and Their Symbionts. PLoS ONE 7, e39994. https://doi.org/10.1371/journal.pone.0039994

Vangriesheim, A., 1980. Antarctic bottom water flow through the Vema fracture zone. Oceanologica Acta 3, 199–207.

Vanreusel Ann, Fonseca Gustavo, Danovaro Roberto, Da Silva Maria Cristina, Esteves André M., Ferrero Tim, Gad Gunnar, Galtsova Valentina, Gambi Cristina, Da Fonsêca Genevois Veronica, Ingels Jeroen, Ingole Baban, Lampadariou Nikolaos, Merckx Bea, Miljutin Dmitry, Miljutina Maria, Muthumbi Agnes, Netto Sergio, Portnova Daria, Radziejewska Teresa, Raes Maarten, Tchesunov Alexei, Vanaverbeke Jan, Van Gaever Saskia, Venekey Virág, Bezerra Tania Nara, Flint Hannah, Copley John, Pape Ellen, Zeppilli Daniela, Martinez Pedro Arbizu, Galeron Joelle, 2010. The contribution of deep-sea macrohabitat heterogeneity to global nematode diversity. Marine Ecology 31, 6–20. https://doi.org/10.1111/j.1439-0485.2009.00352.x

Vinogradova, N.G., 1997. Zoogeography of the Abyssal and Hadal Zones, in: Gebruk, A.V., Southward, E.C., Tyler, P.A. (Eds.), The Biogeography of the Oceans, Advances in Marine Biology. Academic Press, San Diego, Calif, pp. 325–387.

Vrijenhoek, R.C., 2009. Cryptic species, phenotypic plasticity, and complex life histories: Assessing deep-sea faunal diversity with molecular markers. Deep Sea Research Part II: Topical Studies in Oceanography 56, 1713–1723. https://doi.org/10.1016/j.dsr2.2009.05.016

Wägele, J.W., 1989. Evolution and phylogenetisches System der Isopoda: Stand der Forschung und neue Erkenntnisse. E. Schweizerbart'sche Verlagsbuchhandlung, Stuttgart.

Wägele, J.-W., 1986. Polymorphism and distribution of *Ceratoserolis trilobitoides* (Eights, 1833) (Crustacea, Isopoda) in the Weddell Sea and synonymy with *C. cornuta* (Studer, 1879). Polar Biology 6, 127–137. https://doi.org/10.1007/BF00274875

Wägele, J.W., 1981. Zur Phylogenie der Anthuridea (Crustacea, Isopoda). Zoologica 132.

Weisshappel, J.B., 2001. Distribution and diversity of the hyperbenthic amphipod family Calliopiidae in the different seas around the Greenland-Iceland-Faeroe-Ridge. Sarsia 86, 143–151. https://doi.org/10.1080/00364827.2001.10420469

Weisshappel, J.B., 2000. Distribution and diversity of the hyperbenthic amphipod family Eusiridae in the different seas around the Greenland-Iceland-Faeroe-Ridge. Sarsia 85, 227–236. https://doi.org/10.1080/00364827.2000.10414575

Wheatcroft Robert A., 2003. Experimental tests for particle size-dependent bioturbation in the deep ocean. Limnology and Oceanography 37, 90–104. https://doi.org/10.4319/lo.1992.37.1.0090

White, T.A., Fotherby, H.A., Stephens, P.A., Hoelzel, A.R., 2011. Genetic panmixia and demographic dependence across the North Atlantic in the deep-sea fish, blue hake (*Antimora rostrata*). Heredity 106, 690–699. https://doi.org/10.1038/hdy.2010.108

Wilson, G.D.F., 1999. Some of the deep-sea fauna is ancient. Crustaceana 72, 1019–1030. https://doi.org/10.1163/156854099503915

Wilson, G.D.F., 1998. Historical influences on deep-sea isopod diversity in the Atlantic Ocean. Deep Sea Research Part II: Topical Studies in Oceanography 45, 279–301.

Wilson, G.D.F., Hessler, R.R., 1987. Speciation in the deep sea. Annual Review of Ecology and Systematics 185–207.

Wilson, G.D.F., Thistle, D., 1985. *Amuletta*, a New Genus for Ilyarachna Abyssorum Richardson, 1911 (Isopoda: Asellota: Eurycopidae). Journal of Crustacean Biology 5, 350–363. https://doi.org/10.2307/1547885

Wilson, N.G., Hunter, R.L., Lockhart, S.J., Halanych, K.M., 2007. Multiple lineages and absence of panmixia in the “circumpolar” crinoid *Promachocrinus kerguelensis* from the Atlantic sector of Antarctica. Marine Biology 152, 895–904. https://doi.org/10.1007/s00227-007-0742-9

Wittmann, K.J., Schlacher, T.A., Ariani, A.P., 1993. Structure of recent and fossil mysid statoliths (Crustacea, Mysidacea). Journal of Morphology 215, 31–49. https://doi.org/10.1002/jmor.1052150103

Wolff, T., 1962. The systematics and biology of bathyal and abyssal Isopoda Asellota. Galathea Report 6, 1–320.

Wolff, T., 1956. FROM DEPTHS EXCEEDING 6000 METERS. Galathea Report: Scientific Results of the Danish Deep-Sea Expedition Round the World 1950-1952 2, 85.

Young, C.R., Fujio, S., Vrijenhoek, R.C., 2008. Directional dispersal between mid-ocean ridges: deep-ocean circulation and gene flow in *Ridgeia piscesae*. Molecular Ecology 17, 1718–1731. https://doi.org/10.1111/j.1365-294X.2008.03609.x

Zardus, J.D., Etter, R.J., Chase, M.R., Rex, M.A., Boyle, E.E., 2006. Bathymetric and geographic population structure in the pan-Atlantic deep-sea bivalve *Deminucula atacellana* (Schenck, 1939): GENETIC STRUCTURE IN A DEEP-SEA BIVALVE. Molecular Ecology 15, 639–651. https://doi.org/10.1111/j.1365-294X.2005.02832.x

Adding depth to line-artwork by digital stippling

A step-by-step guide to the method

SIMON BOBER & TORBEN RIEHL

Zoological Institute and Zoological Museum, Biocenter Grindel, University of Hamburg

Background

Vector-based software has revolutionized scientific illustrating and is well established in taxonomy. Simple line drawings, however, lack depth information. Shading techniques, such as stippling, are the method of choice for simulating shade, structure, shape and texture.

The illusion of greyscale within the black-and-white regime is achieved by varying densities of dots (Fig. 1).

New Method

Create a minimal fragment of a stippling pattern (Fig. 2) with the brush tool by tapping on the pen tablet (manual stippling). Select the pattern and save it as a brush.

Detailed instructions:

Use the created brush to add stippling to a drawing (Fig. 3a). Trace the region to be shaded with the pencil tool (Fig. 3b). Convert the stroke into the brush by first selecting the line drawing and then the brush from the library. The stippling pattern will appear stretched (Fig. 3c). Convert the stroke into a dashed line and a repetitive homogeneous stippling pattern will form (Fig. 3d-e).

Advantages

- High reproducibility, clarity, and scalability
- Shading without compromising the clarity or simplicity.
- Storage-saving advantages of B/W (e.g., bitmap) images.
- Possibilities to electronically manipulate size and orientation.
- High flexibility in plate preparation.
- Easy correction possibilities.

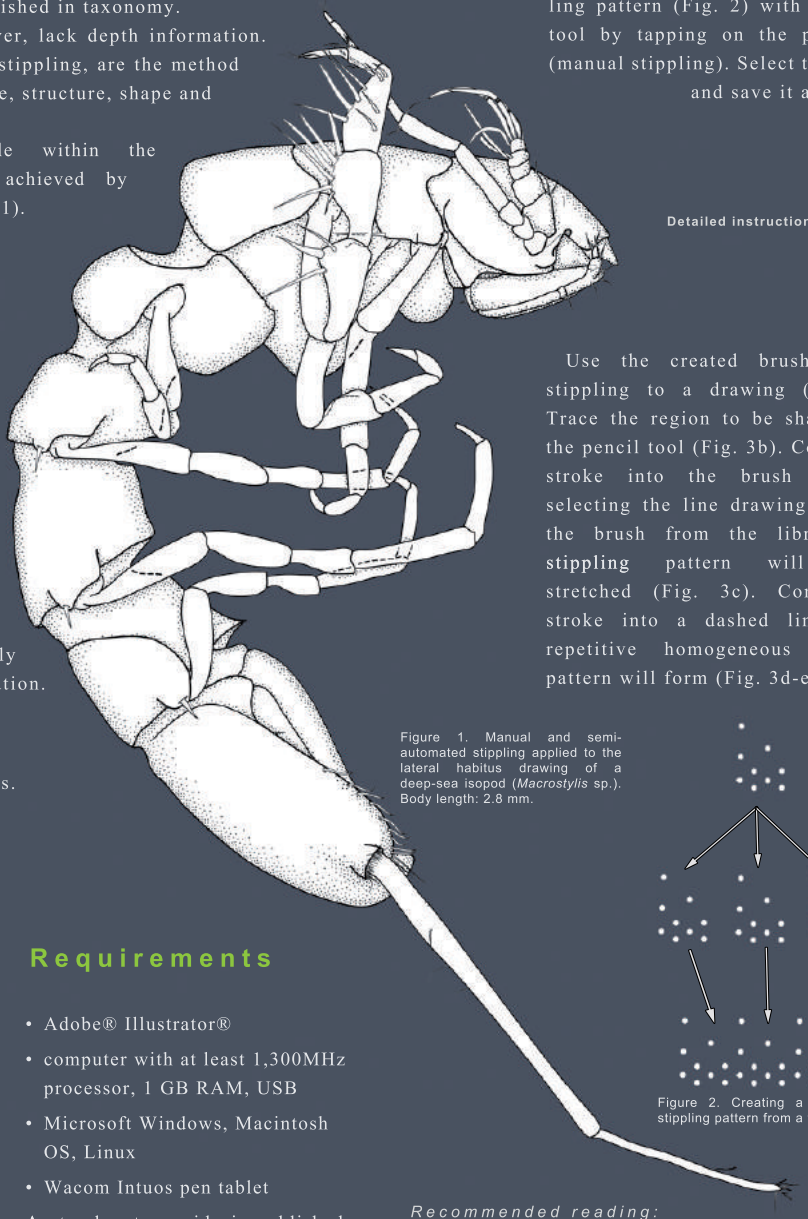

Figure 1. Manual and semi-automated stippling applied to the lateral habitus drawing of a deep-sea isopod (*Macrostylis* sp.). Body length: 2.8 mm.

Figure 2. Creating a repeated stippling pattern from a fragment.

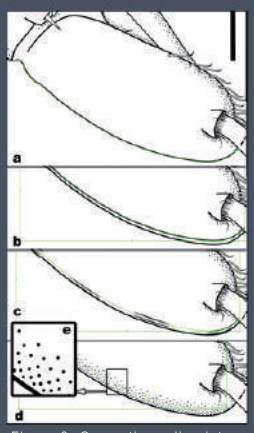

Figure 3. Converting a line into a repetitive stippling pattern.

Requirements

- Adobe® Illustrator®
- computer with at least 1,300MHz processor, 1 GB RAM, USB
- Microsoft Windows, Macintosh OS, Linux
- Wacom Intuos pen tablet

A step-by-step guide is published in Organisms, Diversity and Evolution (Bober & Riehl 2014).

Recommended reading:

Bober, S. & Riehl, T. (2014) Adding depth to line-artwork by digital stippling – A step-by-step guide to the method. Organisms Diversity & Evolution, [online].

Bouck, L. & Thistle, D. (1999) A computer-assisted method for producing illustrations for taxonomic descriptions. Vie et milieu, 49(2-3), 101–105.

Coleman, C. O. (2003) "Digital inking": how to make perfect line drawings on computers. Organisms Diversity & Evolution, 3(4), 303–304.

Coleman, C. O. (2009) Drawing setae the digital way. Zoosystematics and Evolution, 85(2), 305–310.

The support of Angelika Brandt is kindly acknowledged.

contact@simon-bober.de

Poster presentation:
ICC8 (Eighth International Crustacean Congress) -Frankfurt, 2014
DSBS (14th Deep-Sea Biology Symposium) -Aveiro, 2015
17. Crustaceologentagung -Bremerhaven, 2015

Does the Mid-Atlantic Ridge affect the distribution of abyssal benthic crustaceans across the Atlantic Ocean?

Simon Bober[1], Saskia Brix[2], Torben Riehl[3], Martin Schwentner[1] and Angelika Brandt[3]

[1]Universität Hamburg (CeNak) [2]Senckenberg am Meer (DZMB) [3]Senckenberg

Introduction

The general perception of the abyssal deep sea is that of a homogeneous habitat, free of dispersal barriers, which theoretically allows cosmopolitan distributions of species. In fact, the abyss accounts for 84.7% of the ocean, but the abyssal seafloor is subdivided by topographical challenges in form of seamounts, ocean ridges and hadal trenches forming various habitats.

A trans-Atlantic transect along the Vema Fracture Zone was sampled during the Vema-TRANSIT expedition in 2014/15 (Fig. 1). During this study we investigated whether the Mid-Atlantic Ridge (MAR) isolates the abyssal fauna of the western and eastern abyssal basins.
Based on two genetic datasets we found that most of the Macrostylidae and Desmosomatidae/Nannoniscidae species were found at only one side of the MAR.
We analysed those species of Macrostylidae and Desmosomatidae that were sampled across the MAR and complemented these with one species of a third family: Munnopsidae. With these datasets we were further able to consider the effect of different niche adaptations: Macrostylidae are inbenthic (burrowing), Munnopsidae are considered suprabenthic with pronounced swimming capabilities and Desmosomatidae and Nannoniscidae are epibenthic and partly able to swim, but are not as well adapted to swimming as Munnopsidae.

We hypothesize that swimming species have an enhanced capability to cross barriers either by active swimming or by passive drifting as "facultative plankton".

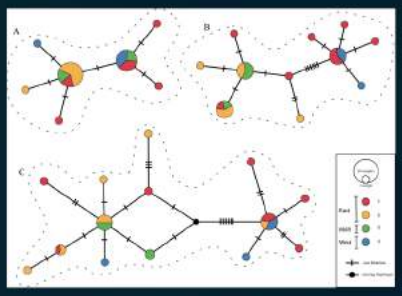

Fig. 2 Haplotype network (Median Joining): Each circle corresponds to a sampled haplotype and the size of the circle to the number of samples. A. *Acanthocope galatheae* Wolff, 1962 (Munnopsidae) haplotype network for the 16S gene fragment. B. *A. galatheae* haplotype network for the COI gene. C. *A. galatheae* haplotype network of the concatenated COI + 16S alignment.

Material and Methods

Samples were obtained using a camera-epibenthic sledge (C- EBS) along 11° N across the Atlantic Ocean (Fig. 1). For this study 24 Munnopsidae were genetically analysed for the 16 S and COI genes. The complete datasets of Macrostylidae and Desmosomatidae / Nannoniscidae were treated by Riehl et al. (2018) (in total 221 macrostylid specimens) and Brix et al. (2018) (in total 195 desmosomatid and nannoniscid specimens).

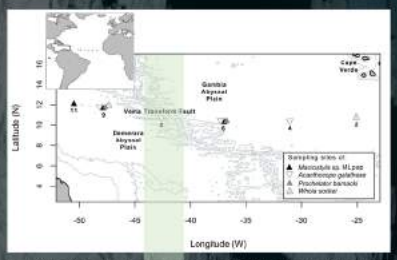

Fig. 1 Map of the sampling locations along the Vema Fracture Zone during the Vema-TRANSIT expedition in the Atlantic Ocean. 3000 m and 4000 m depth lines were plotted.

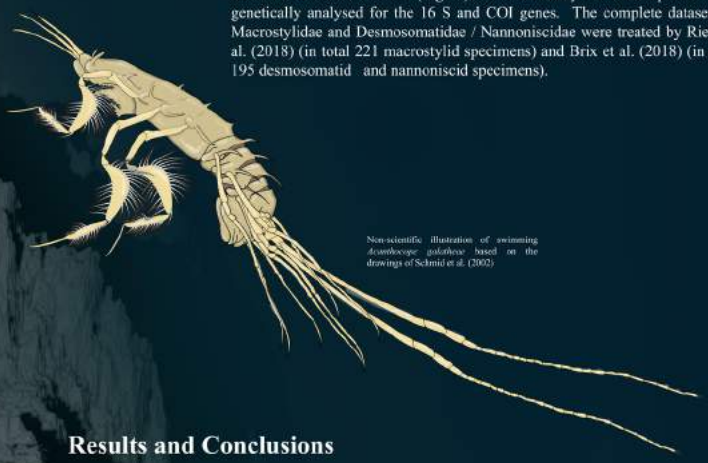

Non-scientific illustration of swimming *Acanthocope galatheae* based on the drawings of Schmid et al. (2002)

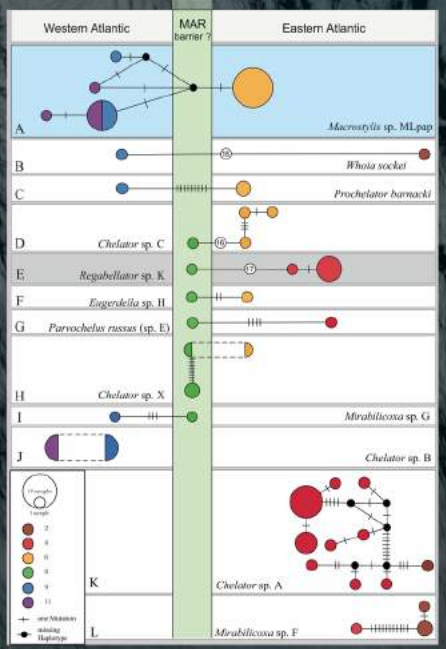

Fig. 2 Haplotype networks of the inbenthic Macrostylidae (blue background), epibenthic Desmosomatidae (white) and Nannoniscidae (grey). We selected only those species that occurred at more than one station and we prepared haplotype networks (Median Joining) for each species and plotted these roughly on the sampled transect. All networks are based on COI sequences except for *Chelator* sp. X and *Macrostylis* sp. MLpap, for which only the 16S gene was available.

Results and Conclusions

- The MAR is a considerable dispersal barrier for most of the non-swimming Macrostylidae and facultative-swimming Desmosomatidae / Nannoniscidae (only two out of 19 macrostylid species and two out of 53 desmosomatid species were found across the MAR. No Nannoniscidae was found with a ttrans-MAR distribution)
- The genetic structure observed in the inbenthic and epibenthic trans-MAR species *Macrostylis* sp. MLpap, *Whoia sockei* Brix & Kihara, 2018 and *Prochelator barnacki* Bober & Brix, 2018 shows genetic variance between eastern and western populations (Fig. 2A, B, C)
- The population structure of the suprabenthic, swimming munnopsid species *Acanthocope galatheae* Wolff, 1962 is seemingly unaffected by the MAR (Fig. 3).

(Individuals from the eastern and western basins as well as from the connecting Vema Transform Fault in the MAR share identical haplotypes (Fig. 2). Thus we assume a persistent gene flow across tthe MAR over a vast geographic distance of 1,843 km for this species.)

References

Brix, S., Bober, S., Tschesche, C., Kihara, T.C., Driskell, A., Jennings, R.M., 2018.Molecular species delimtation and its implications for species descriptions using desmosomatid and nannoniscid isopods from the VEMA fracture zone as xexample taxa. Deep Sea Res. Part II: Top. Stud. Oceanogr. DOI: 10.1016/j.dsr2.2018.02.004

Riehl, T., Lins, L., Brandt, A., 2018. The effects of depth, distance, and the Mid-Atlantic Ridge on genetic differentiation of abyssal and hadal isopods (Macrostylidae). Deep Sea Res. Part II: Top. Stud. Oceanogr. DOI: 10.1016/j.dsr2.2017.10.005.

Schmid, C., Brenke, N., Wägele, J.W., 2002. On abyssal isopods (Crustacea: Isopoda: Asellota) from the Angola Basin: *Eurycope tumidicarpus* n. sp. and redescription of *Acanthocope galathea* Wolff, 1962. Organisms Diversity & Evolution 2(1).

simon.bober@uni-hamburg.de

Poster presentation: ICC9 (Ninth International Crustacean Congress) Washington D.C., 2018